Synthesis of Advanced Hybrid Polymeric Nanomaterials and Characterization of Novel Silsesquioxanes with Desirable Superhydrophobic Coating Properties

Thesis

Synthesis of Advanced Hybrid Polymeric Nanomaterials and Characterization of Novel Silsesquioxanes with Desirable Superhydrophobic Coating Properties

A Thesis submitted for the Degree of Doctor of Philosophy in Chemistry and Nanotechnology

Delphine Oben

December 2016

Department of Chemical and Material Science

The Open University, Walton Hall, Milton Keynes, MK7 6AA, UK

Author's declaration

I declare that the work outlined in this thesis was carried out by the author between February 2012 and January 2016 under the supervision of Prof Peter Taylor, Dr James Bruce and Prof Alan Bassindale at the Open University, Milton Keynes and Dr Alan Taylor and Dr Geraldine Durand from TWI Cambridge.

The work contains no material that has been accepted for the award of any other degree or diploma. To the best of my knowledge, no material in this work has been previously published or written by another person other than I have presented some of the materials at conferences I have attended namely; 6th European Silicon Days in Lyon 2012, 7th European Silicon days in Berlin 2014, 17th International Symposium on Silicon Chemistry (ISOS2014 Berlin), Young polymer chemist conference (Durham UK 2014) and the Silicon polymer conference organised by the American Chemical Society (ACS; San Diego USA 2014). Publications are in progress.

Delphine Oben

Acknowledgement

My sincere gratitude goes to my Supervisors Professor Peter Taylor, Doctor James Bruce, Professor Alan Bassindale, Doctor Alan Taylor and Doctor Geraldine Durand for their continuous guidance and encouragement throughout.

A special thanks goes to The Open University, EPSRC and TWI for providing a safe working environment and the special CASE AWARD to financially support me throughout my research.

I particularly want to thank my brother Cletus Oben for his never ending financial and moral support. Without this man, I will never be who I am today. I equally thank particularly his wife Cynthia Oben who has always been in favour of every support her husband provided. I thank my family too especially my mother and my older sister Constance Oben and her husband Adalbert Ebot.

I equally thank the EPSRC for MALDI-ToF and ESI-MS analysis, Swansea, University of Kent for DLS analysis and Dr Mel Euerby from Hichrom for providing HPLC-MS training and support.

Special thanks also goes to the Christian community in Milton Keynes especially to pastor Olajide, Colins Manna, Yoffie and wife, Genevoix Nana, Mr Chris Nasah, Dr Wilfred Mahmah and family for their moral support.

Finally, a very special thanks to my research group members especially Dr Sergey Bylikin and Dr Yousef Elaziz for some insightful chemistry discussions and for their support in the lab. Also, Dr Allen Bowden for NMR support, Dr Satheesh Krishnamurthy for XPS support, Dr Heather Davies for TEM support and training, Gordon Imlach for DSC and SEM support and the entire Life Health and Chemical Science staff for their invaluable support in various ways.

Abstract

Understanding and controlling the hydrolysis and condensation of trialkoxy and tetraalkoxy silanes in acidic medium **(Figure A)** has not been fully realised. In this research study, both the understanding and control has been achieved using methods developed from the Vitolane™ process invented by TWI Ltd[1] our industrial collaborators. The Vitolane™ process involves the synthesis of 3-methacryloxypropylsilsesquioxane resin from the hydrolytic condensation of 3-methacryloxy-propyltrimethoxysilane (MPTMS) in the presence of methanol, water and an acid catalyst (A-system). The reaction was repeated with two starting materials; 3-methacryloxy-propyltrimethoxysilane (MPTMS) and n-propyltrimethoxysilane (nPTMS) to form the AZ-system. It was found that with certain compositions, the reaction quickly reaches a pseudo equilibrium hence the hydrolysis rate constant could be determined. The instrumental analysis using Maldi-ToF-MS, HPLC, GPC, TGA, GCMS, DLS, DSC, FTIR and CHN analysis of both types of resins gave results that suggested the organic-inorganic hybrid silsesquioxanes obtained had the expected chemical composition and unique physical properties.

This study was further extended to Stöber sphere silica nanoparticles aimed at extending our understanding from the above hydrolysis and condensation mechanistic study to the synthesis of Stöber silica nanoparticles [2] of various sizes **(Figure B)**. The synthesis follows a similar pattern as the Vitolane™ process but using TEOS as starting material and ammonium hydroxide base instead of acid as in the original Vitolane™ process.

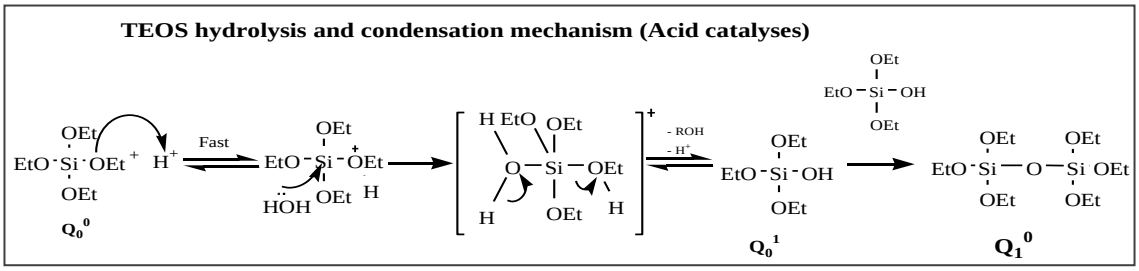

Figure A

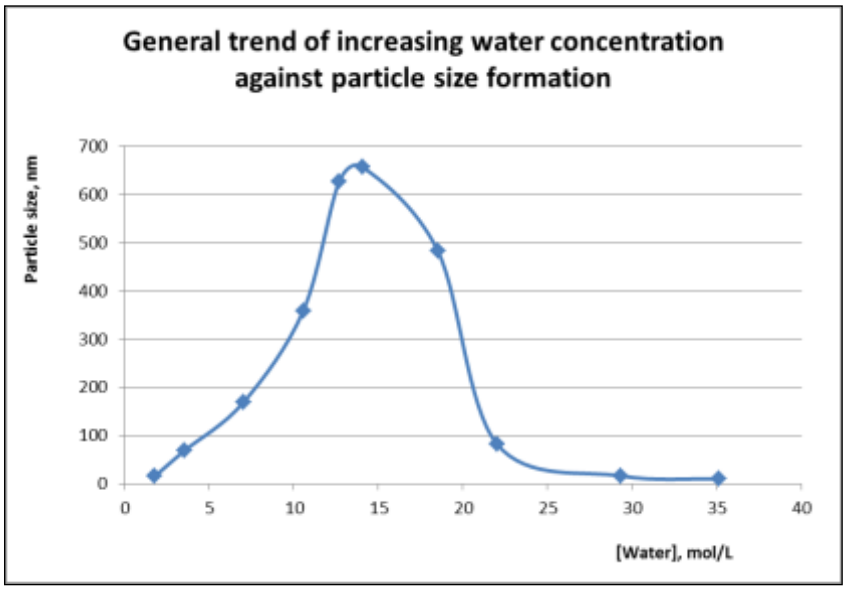

Figure B

The Stöber spheres study was carried out so we could add them to Vitolane in order to give rough (on the nanoscale) surfaces that would be superhydrophobic. The Stöber spheres were characterized using transmission electron microscopy (TEM), X-ray photoelectron spectroscopy (XPS) and dynamic light scattering (DLS) to investigate the particle size formation. The Stöber spheres obtained were of varied sizes depending upon the way they were prepared (**Figure B**).

ABBREVIATIONS AND SYMBOLS

^{13}C NMR - Carbon nuclear magnetic resonance spectroscopy

^{1}H NMR - Proton nuclear magnetic resonance spectroscopy

^{29}Si NMR – Silicon nuclear magnetic resonance spectroscopy

AFM – Atomic force microscopy

AMSi – APTES modified silicon

AMSiO – APTES modified silica

APTES - Aminopropyltriethoxysilane;

A-System - Single component-system

AZ-System – Two component-system

BAM - Brewster angle microscopy

CHN – Carbon, hydrogen and nitrogen

DCM – Dichloromethane

CP-MAS NMR - Cross-polarization magic angle spinning nuclear magnetic resonance spectroscopy

DLS – Dynamic Light Scattering

DRIFT – Diffuse reflectance fourier transform spectroscopy

DSC - Differential Scanning Calorimetry

DTA - Differential thermal analysis;

ES-DMA - Electrospray-differential mobility analysis

ESI-MS - Electrospray Ionization-mass spectrometry

FTIR - Fourier Transform Infrared Spectroscopy

GC-MS - Gas Chromatography-Mass Spectrometry

GPC – Gel permeation chromatography

HPLC - High performance liquid chromatography

ICP-OES - Inductively coupled plasma optical emission spectrometry

LDA – Linear discriminant analysis

MALDI-ToF MS - Matrix-assisted laser desorption/ionization-time of flight mass spectrometry

MeCN - Acetonitrile

MPTES – 3-Methacryloxypropyltriethoxysilane

MPTMS – 3-Methacryloxypropyltrimethoxysilane

NMR - Nuclear magnetic resonance spectroscopy

nPTMS – n-propyltrimethoxysilane

PDA - Photodiode Array detector

PDI – Polydispersity Index

POSS – Polyhedral oligomeric silsesquioxane

SANS- Small-angle neutron scattering

SAXS - Small-angle X-ray scattering

SEM – Scanning Electron Microscopy

TEM – Transmission Electron Microscopy

TEOS – Tetraethoxysilane

TGA – Thermogravimetric analysis

TG-DTA - Thermogravimetric-Differential thermal analysis

TMOS – Tetramethoxysilane

TWI-Vit B – Silsesquioxane resin before quenching in water

TWI-Vit AQ – Silsesquioxane resin after quenching in water

UV-Vis - Ultraviolet–visible spectroscopy

Vitolane™ – Vitolane technology

Vitolane – Vitolane resin

XPS – X-ray Photoelectron Microscopy

TABLE OF CONTENT

Chapter 1: Introduction

This chapter provides a background of materials manufactured by sol-gel chemistry. It describes some of the work undertaken by other researchers so far and their findings. It discusses silsesquioxanes and how they can be made and characterized. The chapter finishes by discussing Stöber silica nanoparticles; explaining what they are, how they are synthesized, functionalised and characterized. These together will provide why the approach adopted in this research has been used and sets the scene for the chemistry developed in the thesis.

1.1 A brief introduction to organosilicon chemistry

Silicon (Si) is the second most abundant element in the earth's crust (8th most abundant in the Universe) after oxygen. It is present in the earth's crust in several different forms and it is always found combined with oxygen as in silica or hydroxides as in silicic acid [3, 4,5,]. About 78% of the earth's crust is made up of silicon and oxygen compounds such as quartz, opal and silicates [6, 7,8,9]. It is also found in the oceans as dissolved salts and in living organisms such as grass and algae. Diatoms are the

most abundant organism that transports silica [10]. 200-280 gigatons of silica are processed every year in the oceans.

Organosilicon chemistry is a very broad field and includes various areas of chemistry and involves silicones, silanes[11], silicates, silsesquioxanes and silicon nanomaterials[12, 13,14,15, 16]. These compounds play important chemical and physical roles in material science and other fields such as biomaterials, electronics, medical dental nanocomposites and cosmetics. Organosilicon chemistry is therefore a very fast growing area of chemistry because of its wide applications and low toxicity. In the area of coatings covered by this research, it has been extensively used and there is a growing expectation that organosilicon hybrid materials will open up new opportunities to the coatings industry.

Water adheres to surfaces leading to for example; rust on the material, decolouration and causing the coating to flake off the material exposing it to corrosion. This can also lead to a short circuit which can cause technology to malfunction causing electrical and material damage. There is a significant need for coatings to protect components from harsh and aggressive environments including water, outer space, very low temperatures, heat and chemical agents such as hydrocarbons, lubricating oils or salt fog.

1.2 Nanocomposite coatings

Coatings are materials that are applied as a thin continuous layer on a surface [17,18]. Nanocomposite coatings involve the addition of inorganic nanoparticles to organic coatings to increase the scratch, abrasive resistance as well as super hydrophobicity as is the case in this study[19,20]. In this research, new building blocks for coatings and coating precursor sol (the solution) involving hybrid organic-inorganic materials have been prepared using sol-gel and polymerization approaches. These new approaches meet new legislations which discourages the use of highly volatile organic solvents (VOCs) in coatings which was the case previously[21,4]. Also, improved performance (thermal protection), functionality(reflective) and durability are some of the advantages of these new coatings [1, 22]. For example, better coatings that exhibit high water and oil repellency are one area of this research focus, with considerable industrial potential for applications across a wide range of vehicles such as ships, cars, planes and spacecraft [4].

Some of the limitations of conventional silicones based coatings include: poor durability, flakiness of the coat and high hydrocarbon VOCs solvent content which are toxic hence detrimental to health and the environment[23,24,25]. Silsesquioxanes are therefore a family of organic-inorganic compounds which offer coatings the potential to overcome the limitations of conventional silicone and simple silane based coating approaches[26,27,27b,28,29]. Silicone oils or elastomers are based on linear polysiloxanes mainly consisting of the D-units (two oxygen substituting the silicon atom) with empirical formula R_2SiO with little 3-dimensional bonding. Silicone resins on the other hand are network polymers consisting of mainly T and Q units (three and four oxygen substituting the silicon atom respectively). However,

Silsesquioxane resins refers to silicones with only the T-units ($RSiO_{1.5}$) consisting of more complex networks. [30,31, 32].

Another important way to make coatings with high potential is to include Stöber nanoparticles. Nanoparticles in coatings increase the surface roughness of the coat thereby reducing direct contact between surfaces hence reducing wear. Adding about 10% nanoparticles to coatings increases their mechanical and chemical nanocomposite properties. These properties includes; increasing the corrosion resistance and hardness of the coat, decreasing the wear and friction possibility of coats as well as increasing the superhydrophobicity of the coating. One example of this is when silanes or silsesquioxanes are functionalised on the surfaces of silica nanoparticles so that they become miscible with Vitolane to create an uneven surface at the nano scale that exhibits superhydrophobicity [33,34,35,36]. This happens only if the silane reduces the surface energy. These coatings have very high contact angles[37,38, 39,40, 41].

1.3 Sol-gel chemistry

Sol-gels are gel-like materials formed from the sol-gel process. It is formed by polymerisation.

Sol-gel refers to a process of formation of a solid phase dispersed in a liquid (sol) which sticks together to form a continuous three-dimensional network throughout the liquid (gel)[42]. During the sol-gel process of silanes especially tetraalkoxysilanes, hydrolysis reactions occur leading to silanols, which later condenses and form silica particles[43,44]. **Figure 1.1** shows the polymerisation process from the monomer up to the formation of the particles. During the particle formation process, the monomer

hydrolyses and condenses to form, linear and cyclic molecules, which react to form several branched and crosslinked networks before finally aggregating as sol-gels[45].

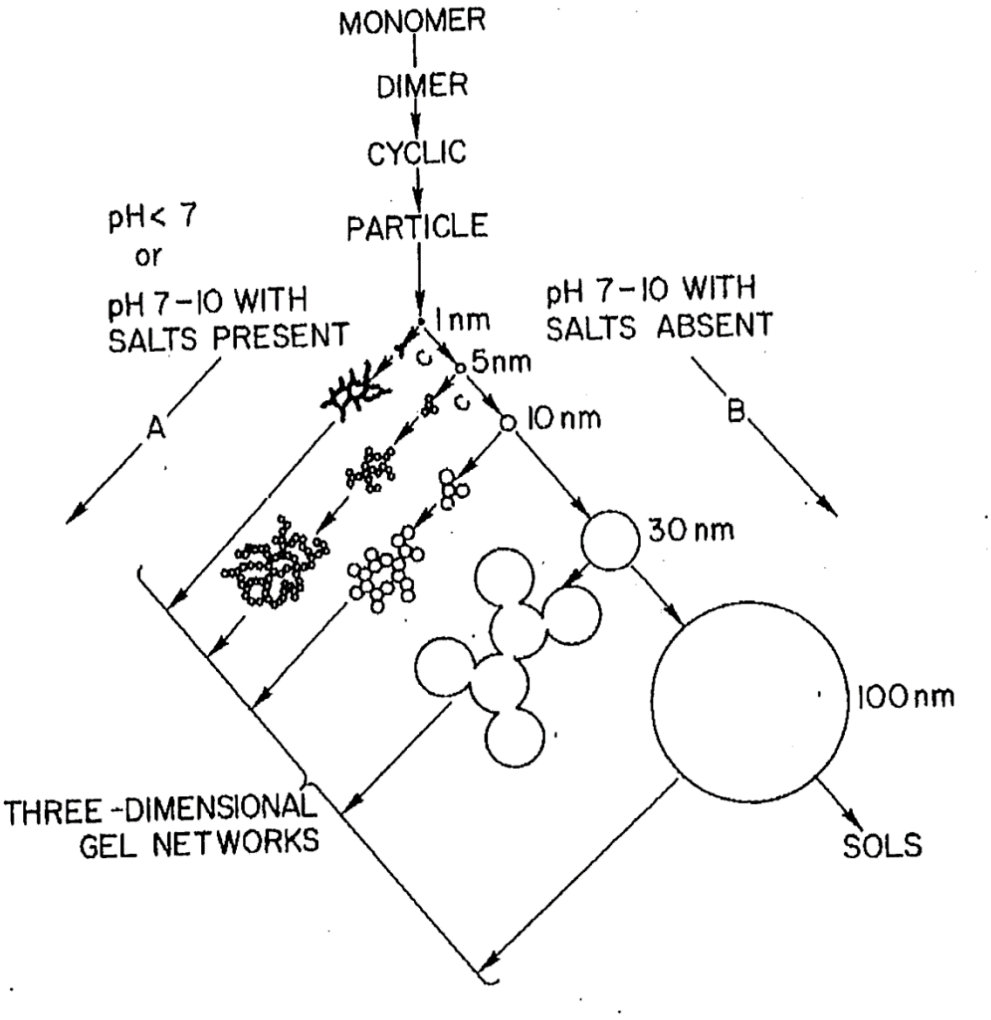

Figure 1.1 Polymerisation of silanes from the monomeric solution to the sol-gel network of silica adapted from Iler[46].

1.1.1 The sol-gel process

The synthesis of silsesquioxane resins that can be used as coatings through the sol-gel process is simple and fast, making it ideal for large scale industrial application.

In the sol-gel process, alkoxysilanes ($RSi(OEt)_3$, $RSi(OMe)_3$) and tetraalkoxysilanes (TEOS, TMOS) react with water in a solvent and either an acid or a base is used as the catalyst to speed up the reaction [1, 47, 48, 49]. Heat is sometimes applied to speed up the rate of hydrolysis and condensation of the alkoxysilanes. Hydrolyzed species are formed during the reaction which condense to form oligomers, polymers and Stöber nanoparticles (**Figure 1.1**) depending on the silane and combination of the reagents used[50,51,52, 2 ,53, 54,55,56,57]. The polymers can grow until they reach a size where a transition (liquid to gel) occurs and a solid-like gel is formed [3,48,27,58, 59, 60, 6,8,30, 61, 62, 63] .

The sol-gel process is controlled by several factors namely; pH, solvent, temperature, time, catalyst and agitation. The pH is quite important as it controls the process from silanol formation through to the process of particle formation. At low pH (<7, acid) the collision of particles will increase due to a decrease in ionic charges. This enhances the formation of aggregated silica chains and gel networks. At high pH (>7, basic), there is repulsion of the negatively charged particles and this limits aggregation thereby leading to the formation of larger particles. See **Figure 1.2a and b** for the acid and based catalysed product formed.

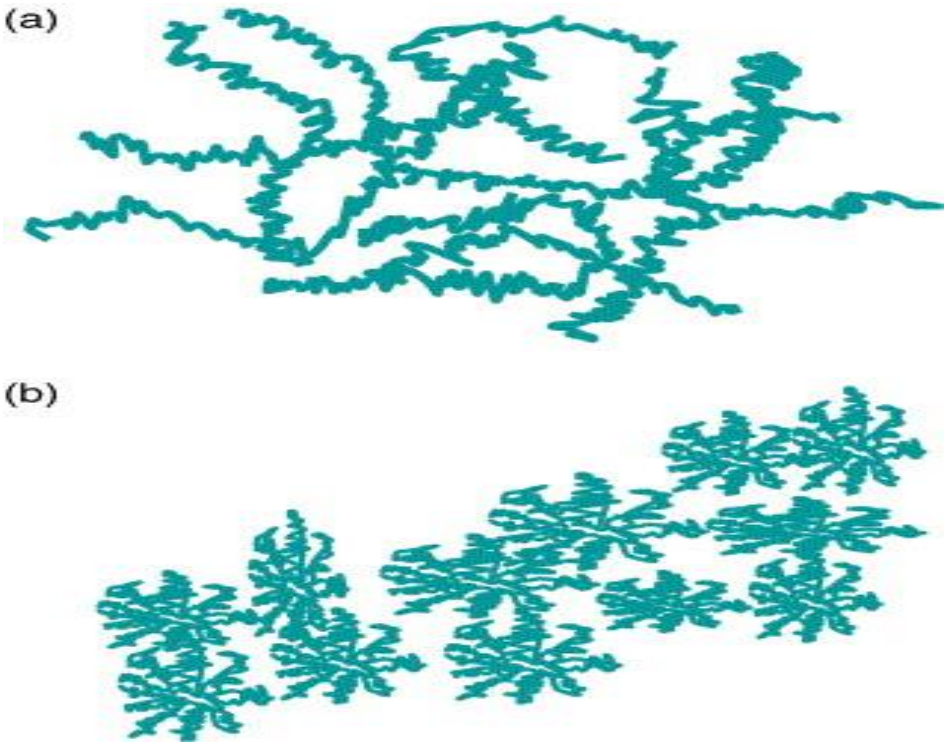

Figure 1.2 (a) Acid catalysis produces linear or randomly branched polymers. (b) Base catalysis yields highly branched polymer clusters[61].

1.4 Mechanism of hydrolysis and condensation leading to the siloxane (Si-O-Si) bond formation

The mechanisms of base and acid catalysed hydrolysis and condensation of alkoxysilanes is shown in **Figure 1.3 and Figure 1.4** respectively. The mechanism of sol-gel hydrolysis and condensation has been studied by Stöber *et al.*[2] and Sanchez *et al*[25,25, 64,65]. The formation of the siloxane bond from the silsesquioxane follows a multistep hydrolysis and condensation reaction. The general equation for trifunctionalsilanes hydrolysis and condensation is shown in **Equation 1.1.**

$$nRSiX_3 + 1.5nH_2O \longrightarrow ((RSiO)_{1.5})_n + 3nHX$$

(R= A chemically stable substituent (methyl, phenyl, vinyl) and X = A highly reactive substituent (Cl, H, OEt))

Equation 1.1 Hydrolysis and condensation reaction equation of trifunctional silanes.

The reaction process starts with hydrolysis to form silanols (Si-OH). Condensation follows involving the silanol groups reacting to form siloxane bonds (silsesquioxane oligomers) (**Figure 1.3**) [66,67,68,69]. This has been proven in the literature using ^{29}Si NMR and other techniques[70,71,72,73,74]. The hydrolysis and condensation mechanism is by nucleophilic attack. Ethanol provides a homogenized environment to allow hydrolysis to take place while also promoting depolymerisation reactions[75,67, 76, 77].

Base hydrolysis

In the case of base hydrolysis, the hydroxyl anion directly attacks the electropositive silicon to form a pentacordinate transition state or intermediate (**Figure 1.3**). A partial negative charge developes on the silicon atom causing a redistribution of charge which is then accomodated by the alkoxy group. The alkoxyl group then leaves the reactive intermediate and picks up a proton from the readily available water or ethanol molecule [78, 79,]. This mechanism is very sensitive to inductive effects of the R group due to the formal negative charge being acquired by the silicon.

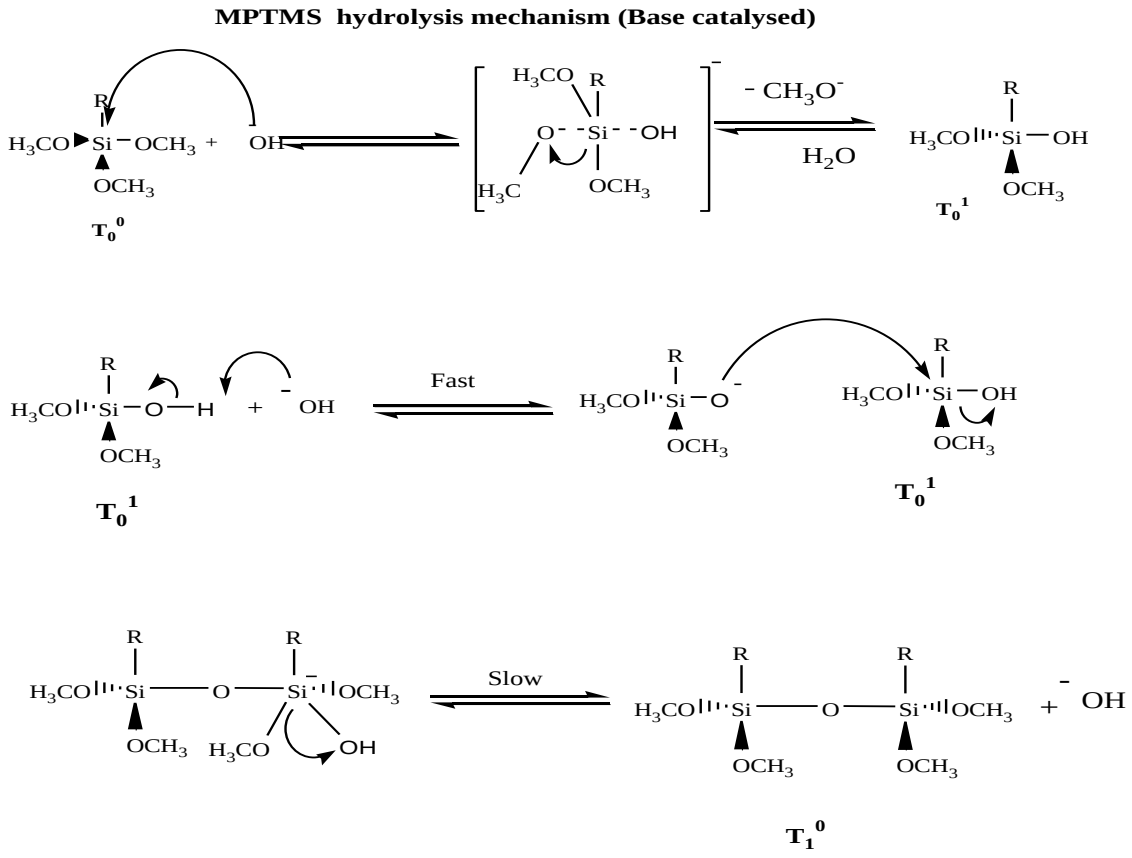

Figure 1.3 Proposed mechanism of base-catalysed hydrolysis and condensation of (3-methacryloxypropyl)-trimethoxysilane adopted from Peng *et al* [80].

Analogues of the pentacoordinate intermediates can be isolated and have been characterized by Bassindale, Taylor and coworkers[27b] with several X-ray structures determined. Notice that the pentacordinated species in **Figure 1.3** can be either transition states or intermediates and not observed species.

Acid hydrolysis

Acid catalysed hydrolysis proceeds generally via substitution of an alkoxy group for a hydroxyl group. Both the three and five coordination silicon species transition state intermediates have been proposed though the five coordinate is the most reasonable results from a bimolecular SN_2 nucleophilic substitution reaction[81]. In the reaction, the acid protonates the alkoxide first making the central silicon atom more susceptible to attack by a nucleophile as the silicon becomes more electrophilic. The protonated alkoxy group can then leave as a neutral molecule (**Figure 1.4**, top). Generally, when hydrolysis and condensation takes place via the sol-gel process, three reactions are possible; hydrolysis, water and/or alcohol condensation as shown in the reaction mechanisms in **Figure 1.4** top, middle and bottom respectively.

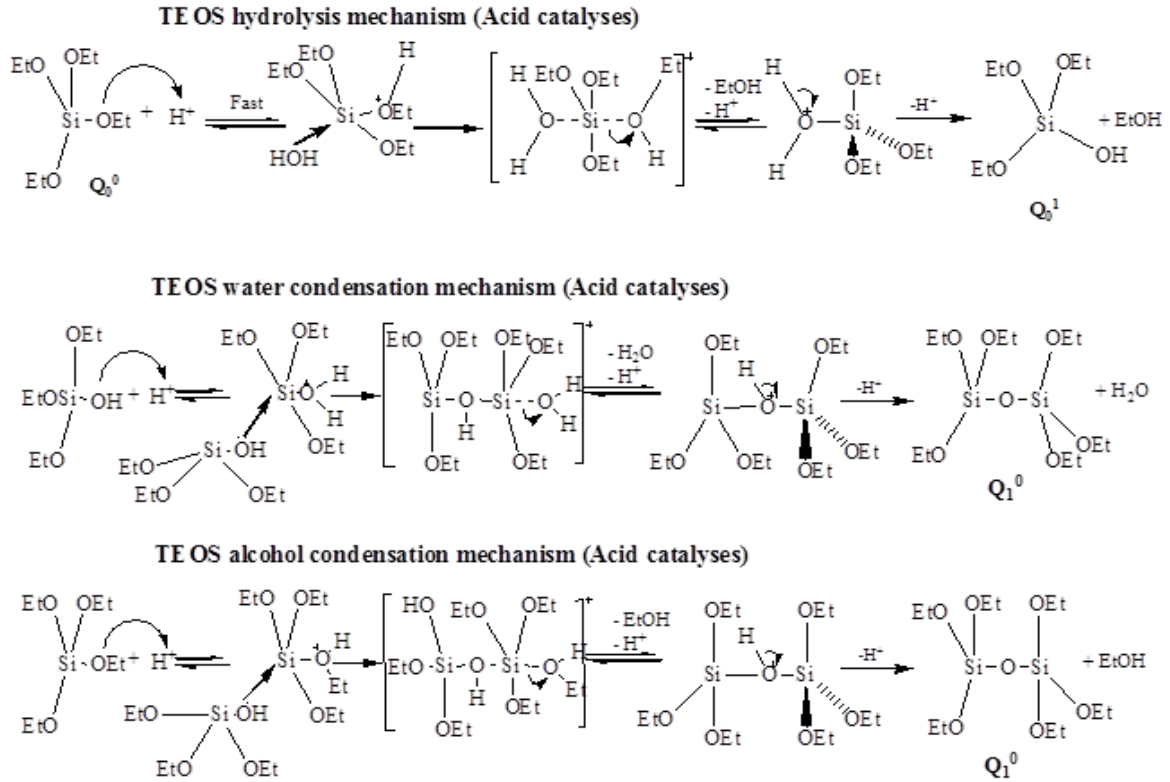

Figure 1.4. Acid catalyzed mechanism of hydrolysis and condensation of TEOS showing normal hydrolysis (top), water condensation (middle) and alcohol condensation (bottom).

This multi-step mechanism has been understood for a number of years but the detailed mechanism of resin formation has not been well understood because the products formed depend on the conditions of the reactions. That is, the Si-O bond formation is well understood. It is the further composition of the mixture of oligomers and polymers species that is not so well understood.

1.1.2 Previous study of the hydrolysis and condensation of alkoxysilanes and Vitolane™ technology

The products formed from the hydrolysis and condensation of alkoxysilanes range from simple siloxane dimers, through tetramers and then larger oligomers such as polyhedral oligomeric silsesquioxane (POSS)[82] as identified by Bassindale, Taylor and coworkers[27b], Taylor *et al.*[23], Ervithayasuporn *et al.* [83] and Peng *et al* (2014)[80]. Taylor *et al.*[23] and Assink and Kay[84] has equally given us a new method for controlling these structures by controlling the water and pH content of the reaction which has been demonstrated practically.

TWI our industrial collaborators did some initial research on the hydrolysis and condensation of alkoxysilanes and found that these processes can be controlled by controlling the amounts of water and pH in the reaction. They have used the tudy of sol-gel to develop different materials such as aerogels, other advanced materials as well as super hydrophobic coatings. Gelation, aging and the drying of these materials have also been exploited. They equally found out that the mixing pattern of the reagents equally produces different coating materials.

TWI Ltd then devised and patented (US7910216) a method called the Vitolane™ technology which is based on the sol-gel process to produce most of its materials[23]. This technology follows the use of one or two starting materials known as the A and AZ-system respectively. This has been described in the patent and discussed in chapters two and five in this thesis. Hence, most of the research in this thesis follows the Vitolane™ technology with variation of the reaction conditions in order to achieve different coatings of varied properties. The Vitolane™ technology will be described later in chapter 2 of this thesis.

1.5 The chemistry of the formation of nanocoating sol-gel materials

In this thesis, two classes of materials have been used to develop the chemistry of the sol-gel process to form advanced hybrid polymeric coating materials. These two classes of materials are based around Silsesquioxane resin formation and Stöber silica nanoparticles preparations.

1.6 Silsesquioxanes

Silsesquioxanes are hybrid organic-inorganic molecules or materials [85, 86, 87, 88,89]. They are compounds of the general formula $(RSiO_{3/2})_n$, where R is a hydrogen atom or an organic group and n is an integer (n=1, 2, 3, 4….)[21, 90,91,92]. They are of various shapes and sizes from linear, random and cyclic to cage structures as shown in **Figure 1.5**[1,93, 94,95].

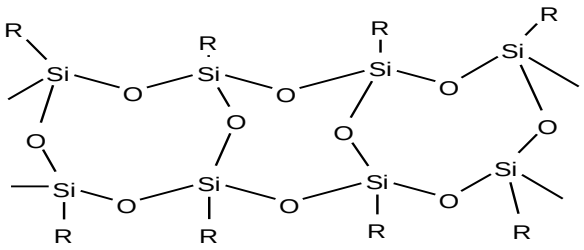

Ladder structure

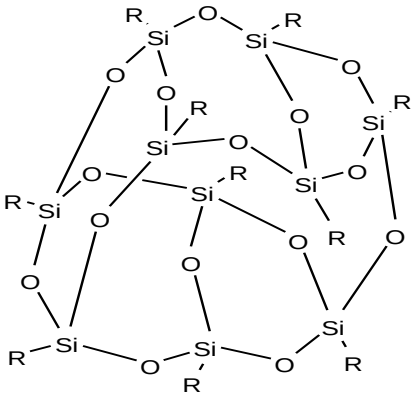

Larger cage

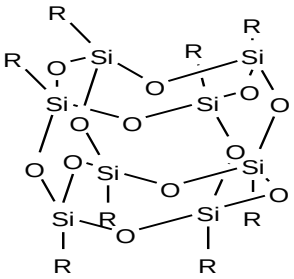

Smaller cage

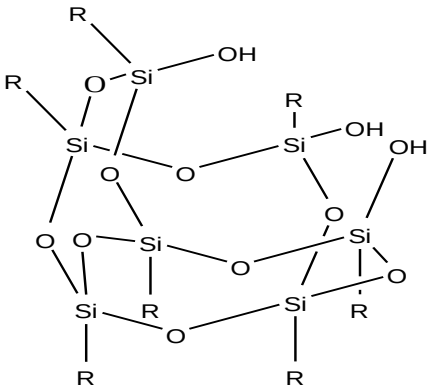

Partial cage

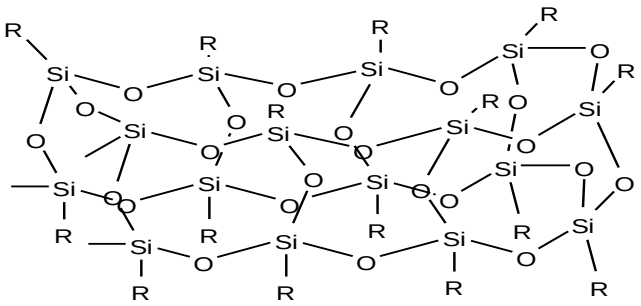

Random structure

Figure 1.5. Representation of silsesquioxanes as random, ladder, cage and partial cage structures.

The synthesis of a condensed silsesquioxane resin starts with the controlled hydrolysis and condensation of trifunctional organosilicon monomers (That is; $RSiX_3$, where R = alkyl groups such as c-C_6H_{11}, c-C_5H_9)[94, 96, 97, 98]. R can also be a

reactive group (epoxy, acrylate, hydroxy). X is a highly reactive functional group (OH, OMe, OEt). It is now possible to prepare a wide range of $RSiO_{1.5}$ framework silsesquioxanes from relatively low cost starting materials[99, 99, 100]. Silsesquioxanes with one or more covalently bonded reactive functionalities (such as: epoxy, acrylate) are as represented in **Figure 1.6** [27a, 101]. These functionalities impart various properties to the silsesquioxanes.

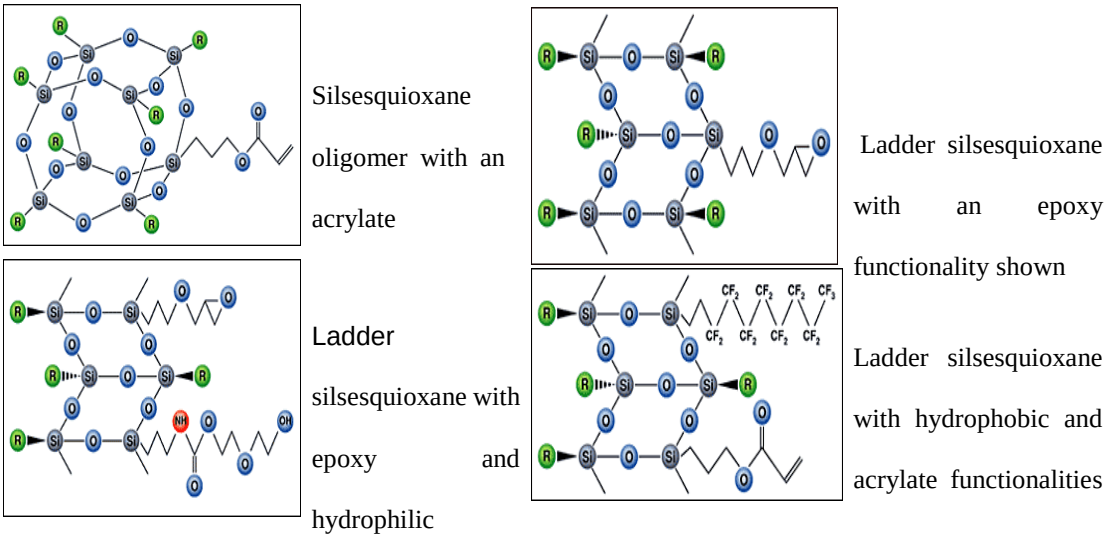

Figure 1.6. Some silsesquioxanes with different reactive functionalities made by TWI Ltd[102].

It has been shown by previous researchers such as Arguello *et al*[90] that the structural composition of the silsesquioxane mixture formed from a reaction will determine the properties of the resin[4, 21, 103]. That is, silsesquioxane based coatings with a flexible network gives low density materials with poor mechanical strength. For example, a coating for wood is different from a coating for glass because these materials have different surfaces and hence requires coatings of different properties. High density materials are achievable with closed network silsesquioxane coatings,

that is, silsesquioxane based on less flexible networks [90,91]. **Figure 1.7a** shows the flexible and closed network connectivity of silsesquioxane materials.

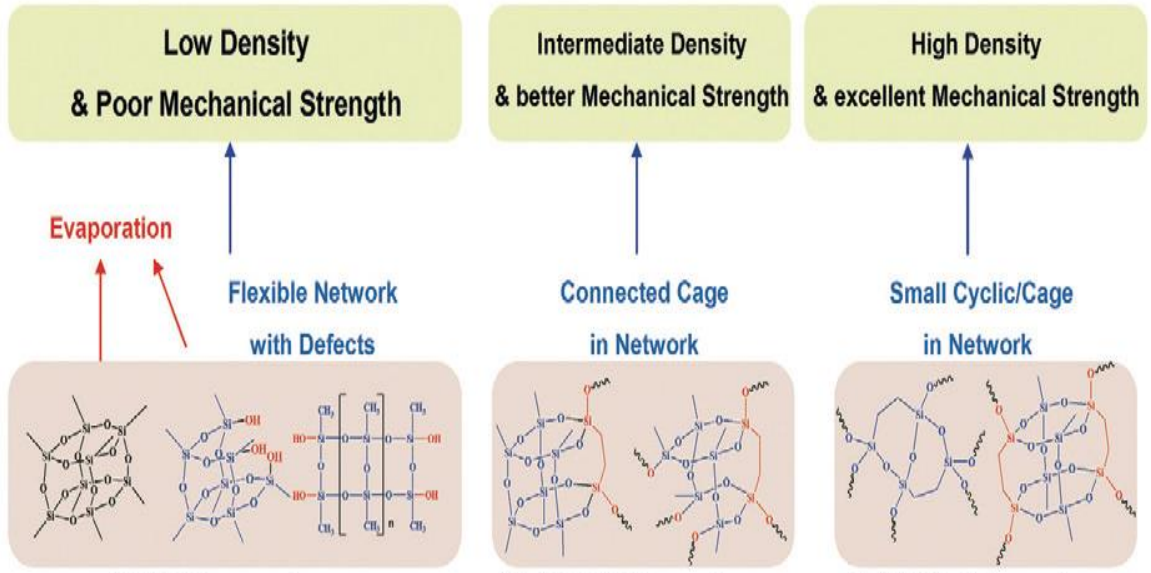

Figure 1.7a. A scheme describing the structure-property relationship for silsesquioxane materials [90]**.**

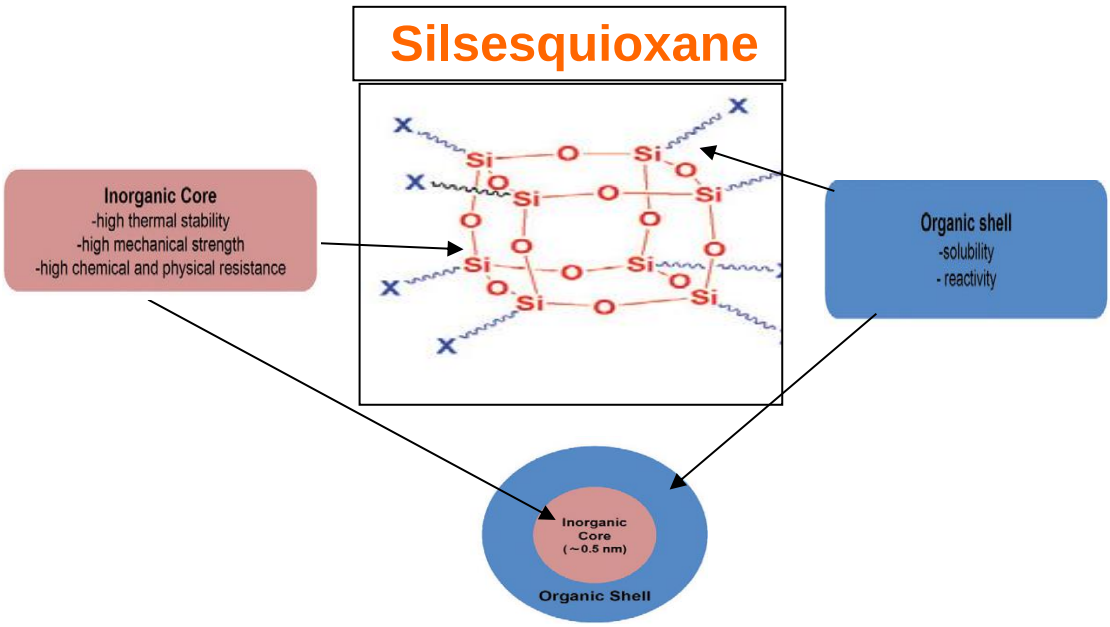

Figure 1.7b. Structure-property relationship of the organic and inorganic framework of a silsesquioxanes. X can be any functional group.

One type of silsesquioxane, the caged polyhedral oligomeric silsesquioxane (POSS) are structured silsesquioxanes and contain an inner inorganic framework covered by inert and/or reactive organic substituents [104, 91, 105] (**Figure 1.7b**). The different properties of the R (X) are used to enhance miscibility with polymeric host materials[106,107,108]. Making one or more of a POSS R groups reactive, permits bonding of the cages to polymers by copolymerisation [109] or grafting[110,111]. Incorporating such silsesquioxane cages into polymeric materials by sol-gel polymerization has shown useful physical and chemical property enhancements, decomposition temperatures and mechanical strength[112,107, 113,91]. The type of functional group (R) it contains will determine the properties of that particular silsesquioxane coating. Silsesquioxanes also have a number of useful physical properties such as, thermal stability and their solubility in organic solvents like tetrahydrofuran (THF), toluene, chloroform and hexane[114,98].

POSS silsesquioxanes were first discovered in 1946 by Scott [26,106, 98,115]. Research in this field has since been developed by others including researchers at the Open University, Bassindale, Taylor and coworkers[27a], Feher[116], Lickiss[94] and Kawakami[117]. They have derived many methods for silicon cage synthesis and how they can be chemically modified. They have equally focussed on the use of distinct silsesquioxanes in polymer-related applications such as coatings.

1.1.3 Nomenclature of Silsesquioxanes

Naming silsesquioxanes can be a little difficult especially with naming large polyhedral oligosilsesquioxanes (POSS). To begin with, siloxanes and silicones[42] are sometimes used interchangeably yet certain distinctions are maintained in other cases. The term 'silicone' generally denotes an organosilicon polymer with a repeating silicon oxygen backbone and attached organic groups (R) on the silicon atoms (R_2**Si-O**)$_n$ [2, 3,17, 118]. On the other hand, the term 'siloxane' describes the silicon oxygen silicon units (**Si-O-Si**). See **Figure 1.8.**

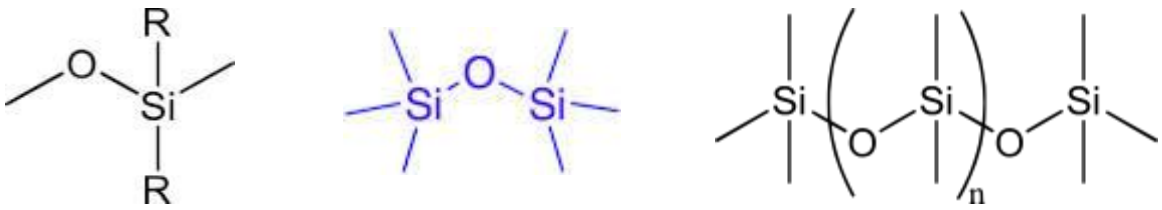

Silicone | Siloxane | Silicone (siloxane)

Figure 1.8 (a) silicone (b) siloxane (c) siloxane in a silicone environment

Silicon-oxygen frameworks can be built from different building blocks; M(mono), D(di), T(tri) and Q(tetra). Those that are important to this research are what are commonly referred to as the T and Q units (**Figure 1.9**) [119] because of their ability to form complex hydrolysable and condensed species. A 'T' unit denotes a silicon atom with three oxygen atoms attached to it and an alkyl or aryl group attached. An 'M' unit describes a silicon atom that is bound to one oxygen atom and three alkyl or aryl groups attached, 'D' denotes a silicon atom bound to two oxygen atoms with two alkyl or aryl groups attached and 'Q' is when a silicon atom is bonded to four oxygen atoms, as in the case of silicates (SiO_4), (F**igure 1.9a**) [3,18,19] .

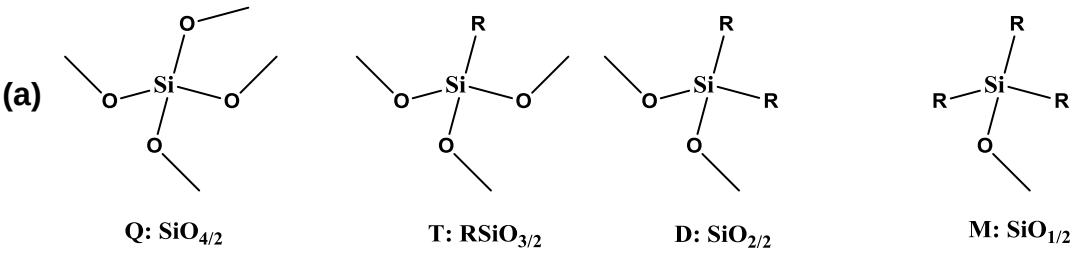

R = Alkyl, aryl, epoxy or amino functional group

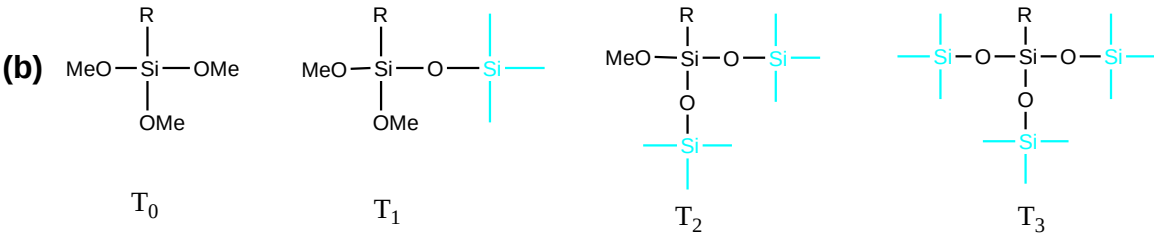

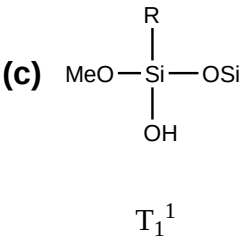

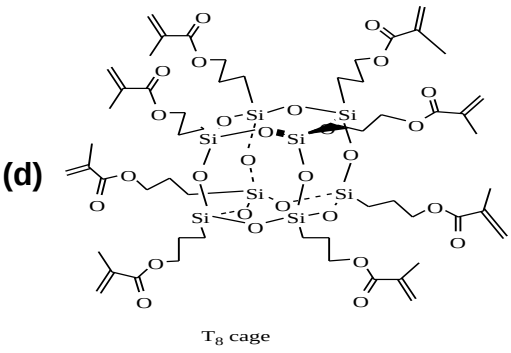

Figure 1.9. (a) The structure of siloxane species [20], (b) structure of $\mathbf{T_n}$ units [21] and (c) Structure of $\mathbf{T^m}$ units (d) Structure of a $\mathbf{T_8}$ silsesquioxane cage.

Another aspect of silsesquioxane nomenclature is based on the number of silicon-oxygen-silicon attachments. For example (T-subscripts T_n) T_0, T_1, T_2 and T_3 is where the numbers 0, 1, 2 and 3 represent the number of silicon-oxygen (Si-O) bonds/units

attached to a single silicon atom (**Figure 1.9b**). An extended definition (T-superscripts T^m) refers to the number of OH groups attached to a silicon atom (Si-OH). Both definitions together give (T_n^m) (**Figure 1.9c**). An additional way to name symmetrical cage silsesquioxanes is according to the number of T silicon atoms in a cage molecule (Ts). For example T_6, T_8, T_{10}, T_{12}.The smallest closed-cage T's are T_4's which are very reactive and therefore difficult to isolate. The most important T-species with a wide range of applications are the T_8's which are very convenient to synthesise and easy to handle because they are slightly less reactive and can be easily isolated [2,3,4,20]. See **Figure 1.9d** above for an example of a T_8 cage.

Another group of silicon-oxygen compounds of interest to this research are called the 'Q' type **(Figure 1.10).** Sugahara *et al.* (1992)[120], Schmidt *et al.* (1984)[121], Sanchez *et al.*[122] and many other scientists have also described and carried out research on this class of compound.

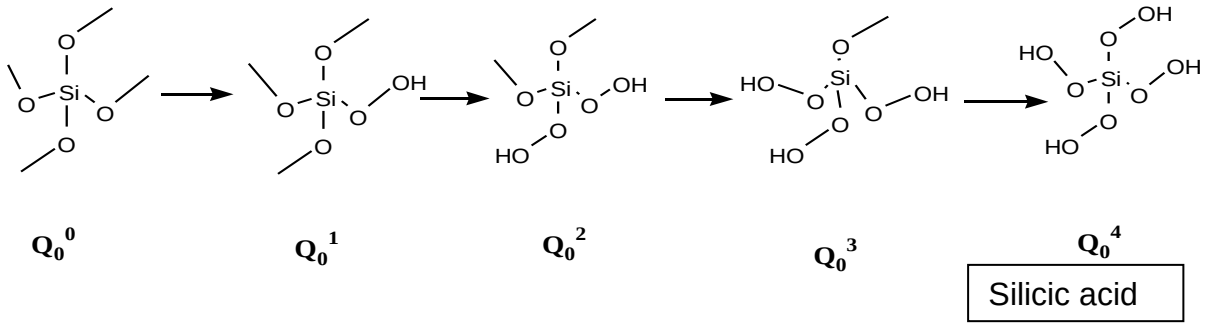

Figure 1.10 Structures of 'Q' units[123]

The various silicon species are distinguished by their degree of hydrolysis (number of OH groups) which is the superscript (a), and condensation (number of other silicon atoms attached via an oxygen atom to the main silicon) which is the subscript (b) leading to Q_b^a (**Figure 1.10**).

1.1.4 Characterisation of Silsesquioxanes

Due to the range of structures and the types of silsesquioxanes present in a resin mixture, they cannot precisely be identified using NMR, FTIR, MALDI-ToF and HPLC-MS. However, by using these techniques together the most reasonable generic structures and the type of silsesquioxanes may be determined [79].

1.1.4.1 Nuclear magnetic resonance (NMR)

A range of techniques have been used in the past to study the detailed mechanism of hydrolysis and condensation of silsesquioxanes leading to polymerisation. One of the most appropriate techniques used for kinetic studies involves ^{29}Si NMR. Kinetic studies using ^{29}Si NMR have been very useful to understand the mechanism of the reaction in order to be able to control the structure of the species formed for different application purposes[124].

The ^{29}Si NMR shows the type of silicon environments generated during the sol-gel polymerization process. For example, the ^{29}Si NMR of the initial trimethoxysilanes ($RSi(OMe)_3$) (T_O) generally shows a sharp single peak at around -40 to -42 ppm in a ^{29}Si NMR spectrum.

Condensation of silanols (Si-OH) to form siloxane bonds (Si-O-Si) generate silicon environments that resonate further upfield from the parent monomer. The greater the number of siloxane bonds attached to a silicon, the further upfield the corresponding resonance will appear. The degree of hydrolysis and condensation

of the trimethoxysilane leads to different silicon environments and hence, different resonance peaks separated from the parent monomer.

The first group of peaks adjacent to the monomer signal (T_0) arise from silicon species with a single siloxane bond and varying states of hydrolysis denoted T_1. They are about 8ppm upfield from the parent monomer (T_0) in the ^{29}Si NMR spectrum. The second groups of peaks arise from silicon species with two siloxane bonds and lies a further 8ppm upfield. These are called T_2 compounds (**Figure 1.11**). The third group of peaks arises from silicon species with three siloxane bonds, T_3; and will be a further 8ppm upfield and may sometimes appear fairly broad especially when the degree of condensation is high and there are a lot of different T_3 environments present (**Table 1.1**).

Table 1.1. ^{29}Si NMR chemical shift ranges for trimethoxysilane and its oligomers.

Monomer (T_0)	T_0	T_1	T_2	T_3
$RSi(OMe)_3$	-40 to -42	-49 to -52	~ -57 to -61	~ -63 to -70

A very detailed study of the mechanism was carried out by Green[125], Brinker[126] and more extensively by Sanchez *et al* [25]. Some of their findings of the hydrolysis of trialkoxysilanes are shown in **Figure 1.11** showing the various T species.

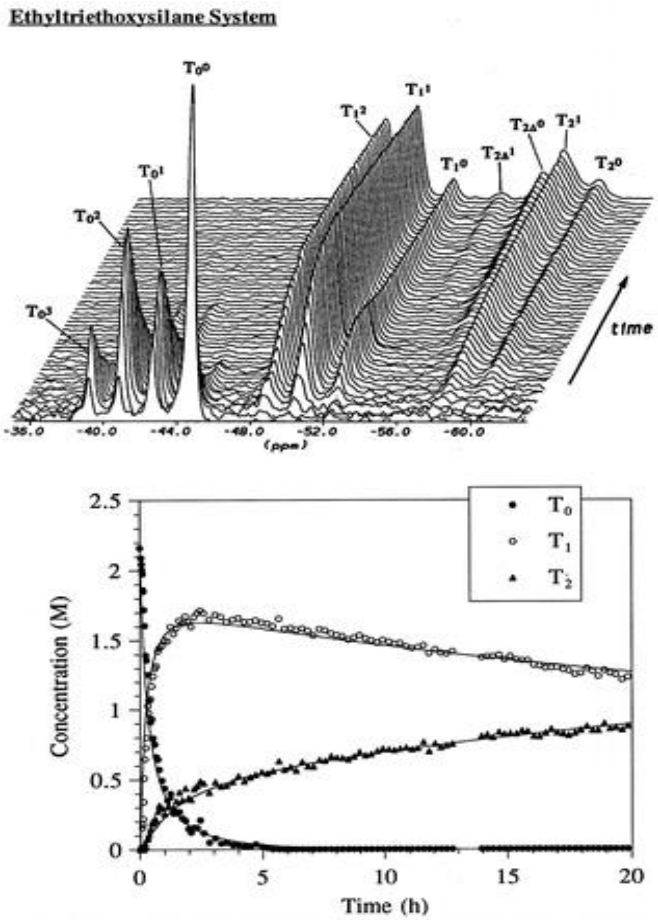

Figure 1.11 [29]Si CP-MAS NMR spectra for the polymerization of ethyltriethoxysilane (top) and experimental (points) and fit (lines) concentration curves (bottom) taken from Sanchez[25] (see license at appendix 25).

Sanchez[25] found that the hydrolysis of silicon units in trialkoxysilanes can be very rapid under high acid concentration. Chromium(III) acetylacetonate $Cr(acac)_3$ which is paramagnetic was added because this compound helps with the relaxation in the NMR hence making it easy to analyze the silicon peaks. The monomer was completely reacted (T_0^0) and disappeared within 5 hours as one can see in **Figure 1.11** top and bottom figures. The starting material (T_0^0) peak is seen to decrease over time as more hydrolysed species T_0^1, T_0^2 and T_0^3 are being formed. Condensation is seen to increase over time as hydrolysis reduces leading to the formation of T_1 and T_2 peaks. Their results were very consistent with those of

Schmidt[121] and Sugahara *et al*[120]. The first process identified was the hydrolysis of the monomer to give the corresponding silanols (T_0^1, T_0^2 and T_0^3). This was followed by condensation to form various T_1's, that is, (T_1^0, T_1^1 and T_1^2). This is further followed by condensation to give T_2 sites. This again agrees with the work of Sugahara. The message here is that hydrolysis is fast and occurs more readily at the beginning of the reaction than condensation.

Sanchez also investigated the hydrolysis and condensation of tetraalkoxysilanes (TEOS for example). See (**Figure 1.12** below).

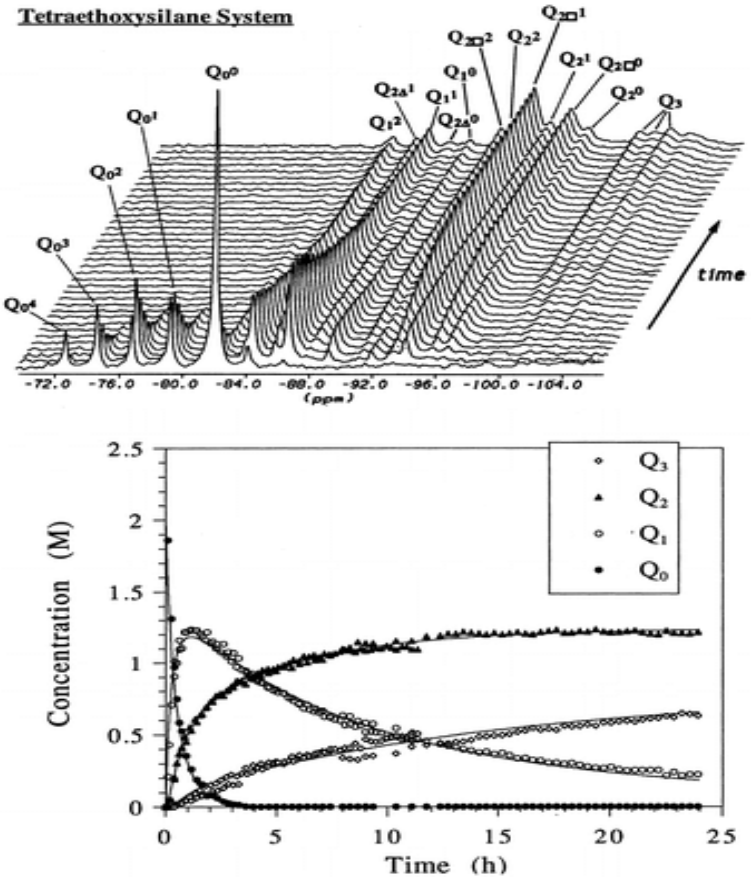

Figure 1.12 ^{29}Si NMR spectra for the polymerization of tetraethoxysilane (TEOS) (top) and experimental (points) and fit (lines) concentration curves (bottom) from Sanchez[25] (license at the appendix 25).

From the investigation using TEOS (**Figure 1.12**), Sanchez *et al.* found out that hydrolysis followed the same pattern as with the trialkoxysilanes but this time with a little more complex polycondensation taking place leading to a greater range of peaks, as seen in the top spectra of **Figure 1.12**. Sanchez *et al.* also found that monomer hydrolysis quickly reaches a pseudoequilibrium (a point at which no further reaction is happening regardless of the reactants present) and that no Q_4 peaks were detected during the time (24hrs) of his investigation. These findings also agreed with the findings of Kelts and Armstrong[127].

Sanchez *et al.* also observed that the rate of hydrolysis increases (for the same catalyst concentration) as one goes from trialkoxysilanes ($R\text{-}Si(OEt)_3$) to tetra-alkoxysilanes ($Si(OEt)_4$) as expressed in **Figure 1.13**. This is as a result of electronic and steric effects. The silicon in tetraalkoxysilane is more electropositive because of the four electron withdrawing groups (OEts) it is bonded to compare to the silicon in trialkoxysilane which is only bonded to three electron withdrawing groups. This makes tetraalkoxysilanes more electrophilic and open to nucleophilic attacks hence more reactive than trialkoxysilanes. On the other hand, tetraalkoxysilanes are less sterically hindered compare to the trialkoxysilanes with more bulky R groups hence making tetraalkoxysilanes more reactive than trialkoxysilanes.

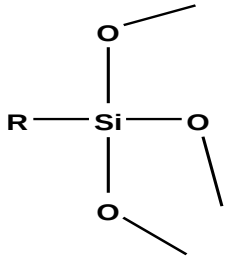

Trialkoxysilane

(Hydrolysis favoured)

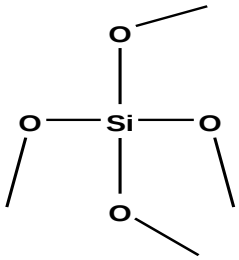

Tetraalkoxysilane

(Condensation favoured)

Figure 1.13. MPTMS and TMOS structures showing which is favoured by hydrolysis and which favours condensation.

1.1.4.2 Chromatographic techniques

Chromatography is the separation of a mixture of compounds. Some chromatographic techniques include: gel permeation chromatography (GPC) and combined techniques such as gas chromatography-mass spectrometry (GCMS). GPC and GCMS were used in these studies to determine the molecular size of the species formed and to monitor the fragmentation patterns and molecular masses of the silane fragments [128, 129,130] respectively.

Gel Permeation Chromatography

GPC is a very important technique for the analysis of silsesquioxanes because the masses of the individual fragments can be estimated. It is very important, to know the molecular mass of the polymer or resin components being made and how to control the distribution of masses [129,131]. The rest of the instrumental techniques used have been described in the instrumental section in **Chapter 2.2** and some described in the next section of this chapter (Stöber spheres).

1.7 Stöber sphere silica nanoparticles

1.1.5 Introduction

Stöber sphere silica nanoparticles are silica nanoparticles that are made by the hydrolysis and condensation of TEOS using the Stöber process[2,132,131, 133, 134]. The process was invented by Stöber in 1968[2] hence the name of the particles. Stöber spheres are used in coatings to improve the properties such as those mentioned in section 1.2 as well as the durability of the coatings. The Stöber process is used for the preparation of monodispersed silica particles by means of hydrolysis of tetraalkoxysilanes and subsequent, condensation of silicic acid in alcoholic solutions using ammonia as catalyst as described by Stöber *et al* [2,135, 136,137,131, 138]. The addition of Stöber spheres of between 1-10nm to coatings leads to a surface roughness which is similar to that of the lotus leaf effect as discussed in Section 6.1 leading to superhydrophobic type properties.

It is often important for applications to use silica nanoparticles with a specified particle size and extremely narrow distribution [139]. This is because the quality and type of products is greatly dependent on the size and size distribution of the particles[140]. Functionalising silica nanoparticle surface is advantageous because it allows for specific and unique applications of silica nanoparticles than would otherwise be possible[141]. The diameter of the silica particles from the Stöber process is controlled by the relative nucleation and growth processes. During the hydrolysis reaction, the ethoxy groups of TEOS are displaced by the water molecules to form the intermediates [Si $(OC_2H_5)_{4-X}$ $(OH)_X$] [125,142,143,144] . Ammonia works as a basic catalyst to speed up the rate of the reaction. The mechanism of the reaction is shown in **Figure 1.14**.

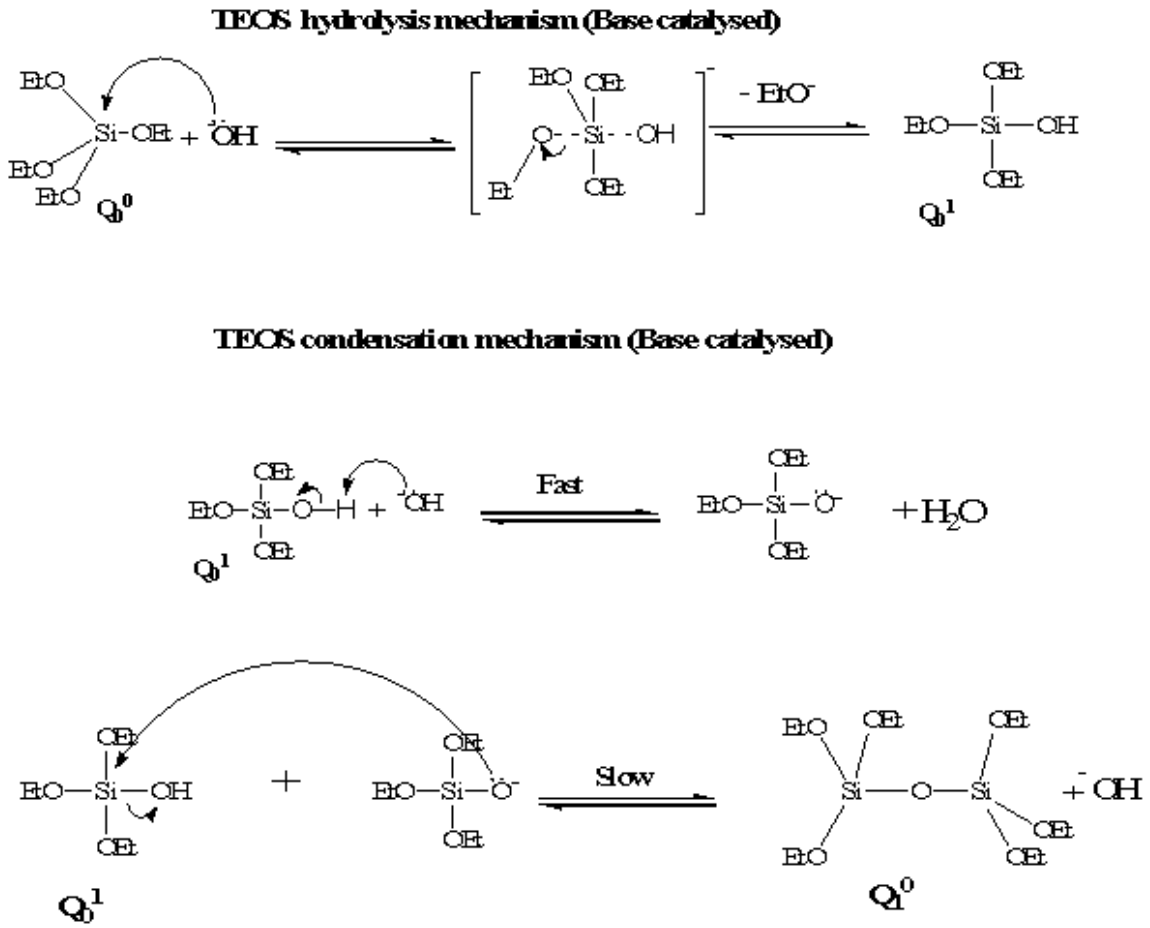

Figure 1.14 The mechanism of TEOS hydrolysis and condensation leading to silica nanoparticles formation.

The mechanism in **Figure 1.14** shows that hydrolysis occurs before condensation. The availability of both water and base catalyst is more likely to facilitate hydrolysis as earlier stated and therefore is more likely to result in highly condensed species. The above figure simply shows the initial process up to Q_1^0 formation.

1.1.6 Synthesis of silica nanoparticles

A number of experimental methods have been published in the literature which has been used to synthesise small silica nanoparticles of diameter ~ 5-10nm. These small silica nanoparticles can be made using the Stöber process [2, 145, 146, 147, 148]. In this review, two of the methods (Stöber and microwave) will be mentioned although only one, the Stöber method, is particularly important to us to make Stöber silica nanoparticles because it is cheaper, safer and easily applicable for large scale commercial use.

The Stöber method of synthesising silica nanoparticles results in monodispersed and uniformly sized particles[2]. The process involves the hydrolysis of TEOS in ethanol in the presence of ammonia and water (**Figure 1.15)**. This method has also been used by Plumere [149]**.**

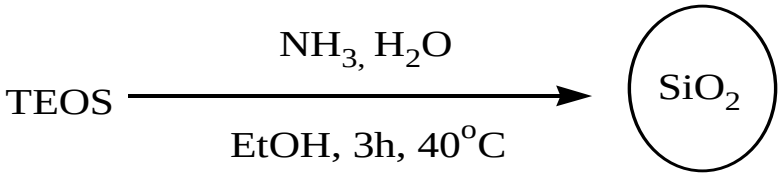

Figure 1.15. Classical Stöber nanoparticles synthetic route by Stöber**[2]**.

In a representative Stöber process[2], first an ethanol (1.7mol, 100ml) – water (0.1mol, 1.8ml) mixture is made and TEOS (0.011mol) added to it and stirred for almost an hour[2]. Ammonium hydroxide 25 wt. % (7ml) is added as the catalyst to speed up the rate of hydrolysis and condensation. The mixture is stirred for another 4 hours at room temperature. The transparent liquid obtained contains the Stöber silica

nanoparticles (35-100 nm diameters). The diameter can be varied by changing the reaction conditions [67,2,150,148,151,152,153,154,155].

The product mixture is kept stirring constantly for 24 hours at room temperature. Finally, the dispersed particles are centrifuged, washed with ethanol to remove any starting material left in solution and then dried on a Petri dish at 50°C [156].

The Stöber process has been modified by several scientists to make different sized Stöber silica nanoparticles. For example, Rao *et al*. [140] made a few modifications of reagent concentrations and achieved the same size distribution as Stöber. Bogush[157] also developed and improved the Stöber method and achieved particles having a maximum diameter of 1-10nm. More recently, by varying reagent concentrations, Wang *et al.*[132] also prepared particles of various sizes using the Stöber process. Flory-Huggins [158] and Tanaka and co-workers [159] proposed that the primary particle size is smaller when a different or non-organic solvent is used.

1.1.7 The effects of the concentration of TEOS, alcohol, water, ammonia and temperature on Stöber silica particle size

The amount of TEOS, water, ammonia, ethanol and temperature all affect the size of the silica nanoparticles formed [7,160,82]. Understanding the effects of these enabled the sizes of the particles formed to be controlled. This is because as the rates of hydrolysis and condensation increases, particles grow in two ways: by monomer addition (nucleation) or by controlled aggregation. Monomer addition takes place from nucleation formation leading to growth of particles. More detail of this is discussed on page 283-284 and **Figure 6.11**. Controlled aggregation occurs when particles grow by clumping of smaller particles. As hydrolysis rate increases, the

rate of conversion of the silyl ether to silanol increases leading to condensation. This in turn leads to faster nucleation and aggregation and hence the growth rates of the particles. Hydrolysis reactions lead to nucleation and condensation reactions leads to growth.

1.1.7.1 Effect of TEOS concentration

Stöber *et al*.[2] reported that size does not increase with increasing TEOS concentration. However, Bogush *et al*.[157] and Raman *et al*[148] discovered that the particle size gets larger as the TEOS concentration increases. By contrast, Van Helden *et al.* [161] reported that the size gets smaller as the TEOS concentration increases. Other studies have also said that size increases with an increase in TEOS concentrations. More recently, studies have shown that size decreases with increasing TEOS concentration by Rao *et al*[140]. These discrepancies is one of the reason for this research to understand clearly what actually happens with increase or decrease in TEOS concentration. As TEOS concentration increases, the rate of nucleation and growth increases hence the particle size increases as shown in **Figure 1.16**.[152]

On the other hand, increasing the [TEOS] excessively leads to a reduction in conversion of TEOS to Stöber nanoparticles because the amount of water becomes deficient with very high TEOS concentration. This leads to a decrease in particle size presumably because the rate of growth stops (**Figure 1.16**).

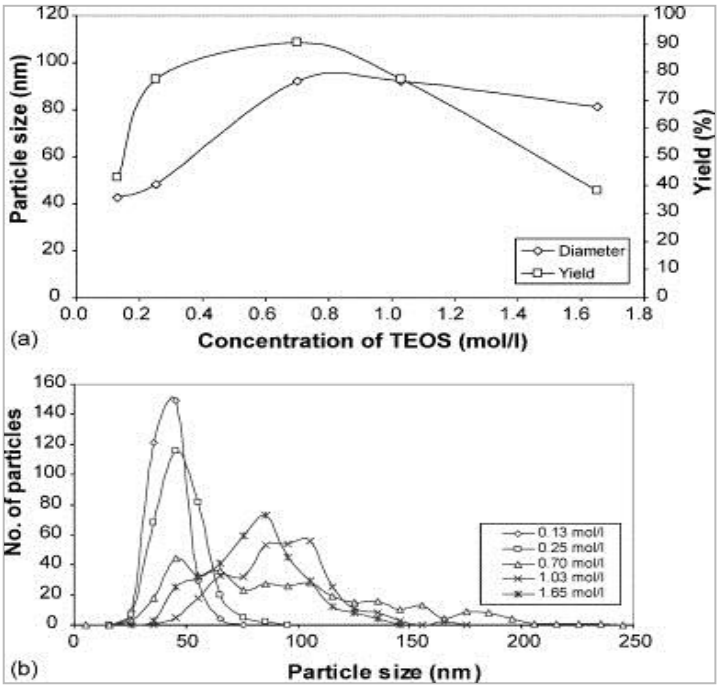

Figure 1.16. The effects of [TEOS] on particle size and yield adapted from Rahman *et al* [152]. Copyright @ licence 1-Appendix 24.

The TEM images from Rahman *et al.*[152] in **Figure 1.17** clearly shows the increase in particle size with higher concentrations of TEOS.

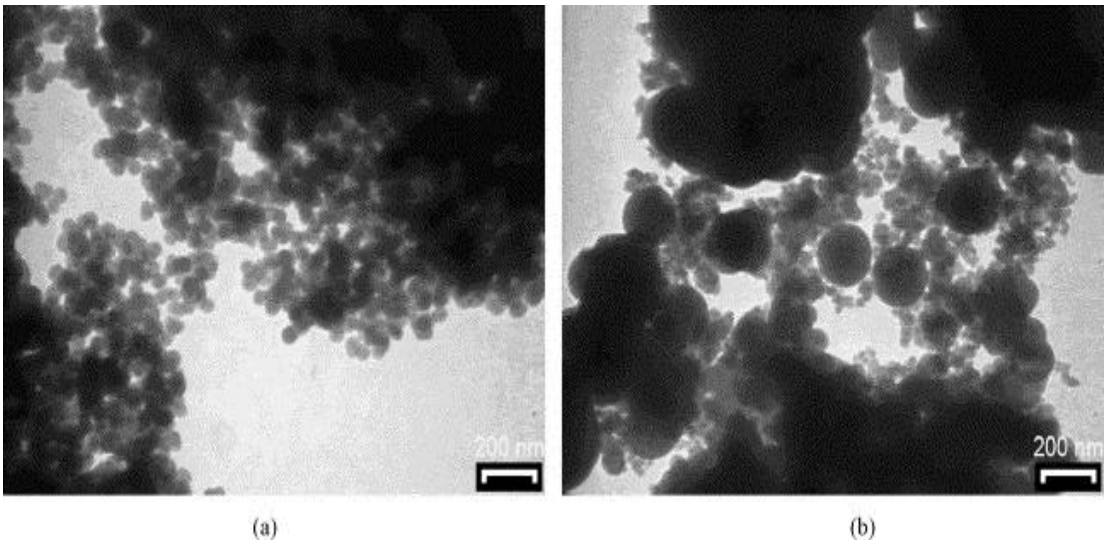

Figure 1.17.TEM images of silica nanoparticles synthesized at different [TEOS]: (a) 0.13 mol l^{-1} and (b) 1.65 mol l^{-1} under fixed conditions[152]. Licensed appendix 24.

1.1.7.2 Effect of water concentration

Matsouka *et al*. [155] initially found that increasing the amount of water leads to an increase in particle size. However, in recent studies the authors found that increasing the amount of water leads to a decrease in size of the particles formed. Park *et al.* [162] reported later that increasing the amount of water leads to an increase in the sizes of particles. Park's conclusion was backed up by the fact that, increasing water concentration leads to agglomeration of the particles hence larger sizes are observed. However, Park *et al.* concluded that with excess water, the particles become smaller which is surely the bit that Matsouka *et al.* missed out. They did not study and hence did not observe the excess water scenario. More recently, Wang *et al.* [132] suggested that more water accelerates TEOS hydrolysis and condensation and contributes to the formation of larger particles. With excess water above a 2:1 molar ratio (water:TEOS), the water dilutes the oligomers in the reaction solution leading to the formation of smaller particles.

It can also be noted that, higher amounts of water lead to more hydrolysis and hence more hydrolysable species (nucleation). That is, high water retards the condensation process (growth) because condensation leads to the formation of more water which is contrary to the Le Chatelier's principle. Therefore, at high water concentration, hydrolysis reactions (nucleation) is favoured more than condensation reactions (growth) leading to the formation of smaller silica particles and vice versa with less water[163]. This implies water and hence hydrolysis is the rate limiting process in the formation of silica nanoparticles.

1.1.7.3 Effect of ammonia concentration

It has been reported that an increase in ammonia concentration leads to a proportional increase in the sizes of the particles [148,125]. Ammonia acts as a catalyst thus speeding up the rate of the reaction. The faster the rate of hydrolysis and condensation, the faster the particles nucleate and grow as there are sufficient amounts of water and TEOS hence the larger the particles become (**Figures 1.18** and **Figure 1.19)**. This was confirmed by Stöber *et al.* [2] but disagree with the findings of Rahman *et al*[148]. However, recent studies by *Rao et al.* [140] have reported the opposite, that is, an increase in [NH_3] leads to a decrease in particle size. His reason to disagree was based on the fact that the acidity of the silane (silanols groups) is responsible for the growth of the silica particles. The more the ammonia, the more the protonation from the water in ammonium hydroxide and hence the more the silanols formed. This leads to a more negative particle surface and hence repulsion leading to smaller particles. Rahman *et al*. [148] reported that particles prepared at higher concentrations of ammonia are smooth, spherical and also very dispersed and are obtained in greater yield. However, both groups could be correct because the particles could actually be small but look bigger as a result of agglomeration (particles sticking to one another). Another reason could be because increasing the amounts of ammonia leads to increase in water in the solution hence the bigger the sizes of the particles formed.

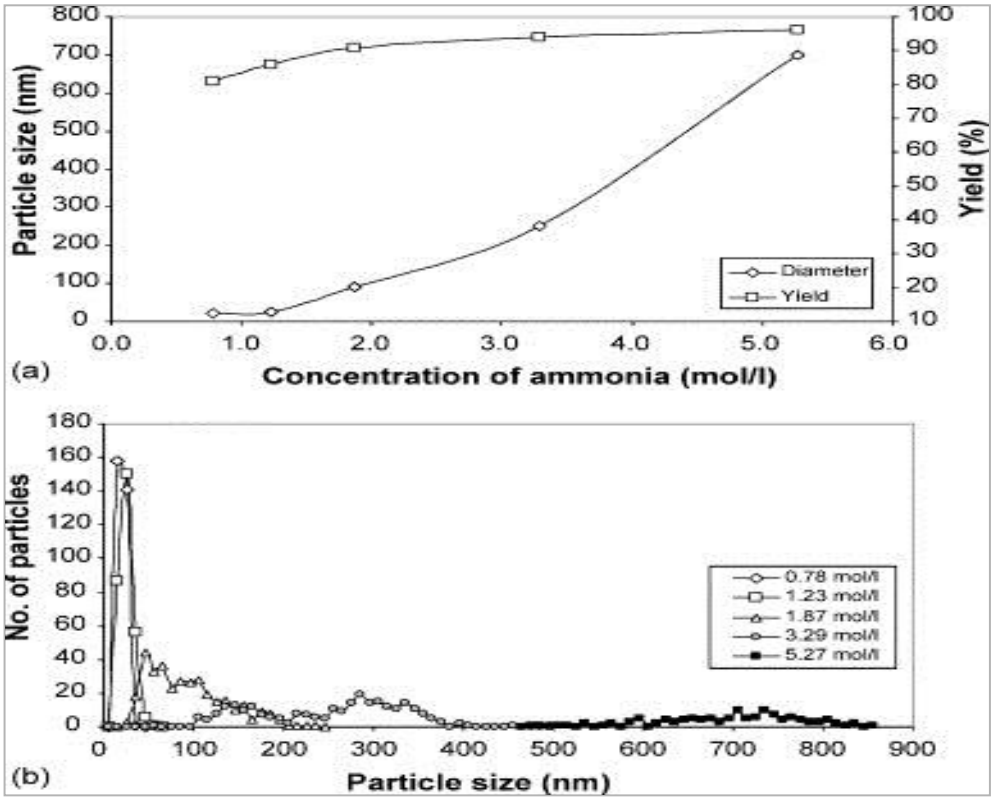

Figure 1.18. The effect of ammonia concentration on (a) particle size and yield, and (b) size distributions of silica prepared at fixed initial [TEOS]; (0.08 mol l^{-1}) and H_2O (1.09 mol l^{-1}) [148].

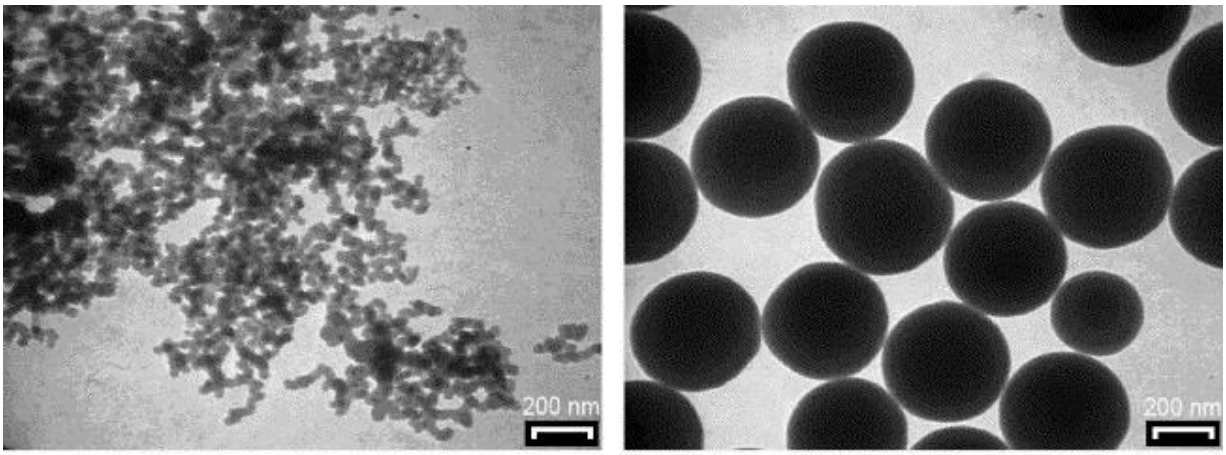

Figure 1.19. TEM images of silica nanoparticles that were synthesized at different [ammonia]: (a) 0.78 mol l^{-1} and (b) 5.27 mol l^{-1} under fixed conditions as reported by Rahman *et al* [152].

1.1.7.4 Effect of temperature

Particles are generally seen to increase in size as temperature increases according to Rao *et al*[140]. This can be explained as follows: silica particles are stabilized by electrostatic repulsion. The charges originate from silanol groups which are relatively acidic and dissociate in the presence of ammonia. Temperature effects therefore is directly related to the saturation concentration of ammonia[140]. When temperatures are high, ammonia evaporates easily leaving a high concentration of water in the reaction mixture which will increase therefore causing particle size to increase [140]. This conclusion by Rao is wrong because more water should lead to smaller particles.

Rahman *et al.*[152] suggest the opposite of the Rao's findings. Particle size decreases as temperature increase. Rahman predicted that particle size is related to nucleation rate. He suggested that as temperature increases, the nucleation rate will rise and this will lead to a small particle size. Particle size and distribution are seen to decrease as temperature increases (**Table 1.2**). **Table 1.2** shows the change in particle size with respect to changes in temperature. At 55°C and 65°C, there are no major changes in particle size but the standard deviation of the particle size reduces. 45^0C can be assumed to be the optimum temperature (**Figure 1.20**, **Table 1.2** below).

Table 1.2. The effect of temperature on silica nanoparticle size formation [152]

Temperature (^{0}C)	Particle size (nm)	Standard deviation
45	92.3	43.6
55	35.2	11.3
65	32.6	7.1

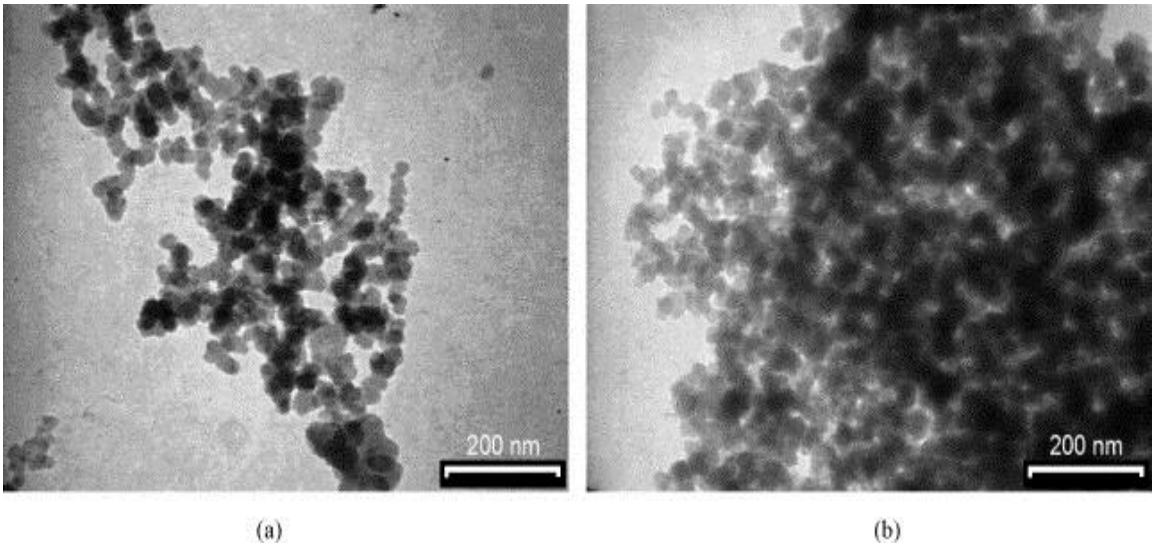

Figure 1.20. The TEM images of silica nanoparticles prepared at (a) 45 °C and (b) 65 °C using fixed conditions [152].

1.1.7.5 Variation of ratios of concentration of all species

The variation of concentration plays a big role in particle size. Recent studies have reported that the final size of silica nanoparticles is dependent on the molar ratio [TEOS]/[NH_3] and a fixed ratio of [TEOS] = 0.71 $moll^{-1}$ and [NH_3] = 1.90 $moll^{-1}$ is advised by Rahman *et al*[152]. The higher this ratio the smaller the nanoparticles obtained and the smaller the yield [152]. If the [EtOH]/ [TEOS] ratio is maintained, an increase in the amount of water will lead to an increase in particle size and later a decrease. Rahman *et al.* mentioned it will lead to a decrease in particle growth and

hence the particle size will decrease as the hydrolysis and condensation rate reduce (incomplete hydrolysis). What is important is the fact that the reaction system does change from a non-aqueous to an aqueous mixture when the ratio of water to TEOS is increased (Ratio=[H_2O]/[TEOS])[152, 2, 154, 164]. (See **Figure 1.21** and **Figure 1.22**).

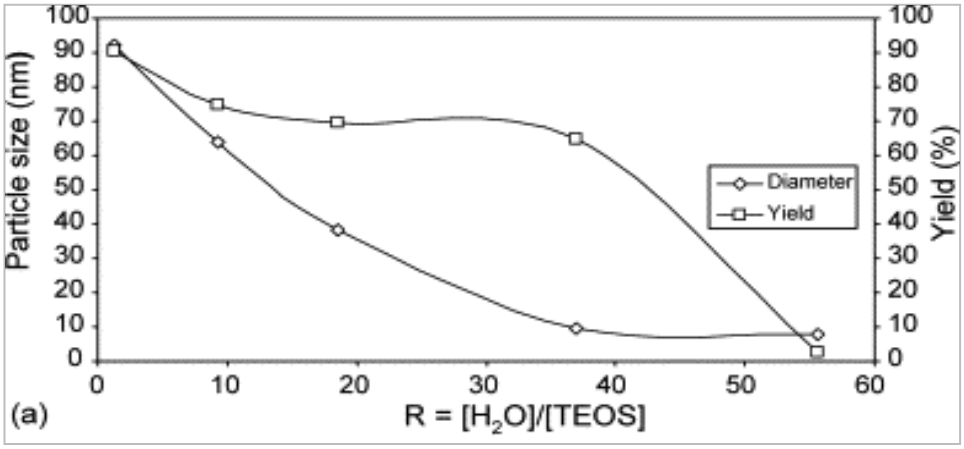

Figure 1.21 The effect of ratio(R) of [H_2O]/[TEOS] on the size and yield of silica particle [152]

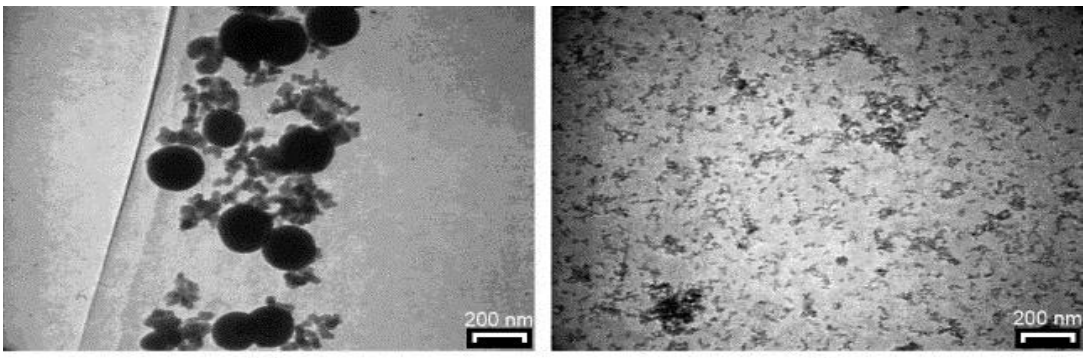

Figure 1.22 TEM images of silica nanoparticles prepared at different *R* ([H_2O]/[TEOS]) values: (a) 1.3, (b) 37.0 [152]. Copyright-see Appendix 24.

1.1.7.6 Effect of ultra-sonication versus magnetic stirring

An experiment to investigate the effect of ultra-sonication versus magnetic stirring under standard conditions by Rahman *et al.* showed that both procedures gave an equal yield. They found that particles aggregate more under magnetic stirring compared to ultra-sonication (**Figure 1.23**). The difference could be due to the differences in contact modes caused by using two different methods of mixing. This again goes to explain how several factors affect the synthesis of nanoparticles and the variation in the size formation.

Figure 1.23. TEM images of silica nanoparticles prepared at fixed conditions using

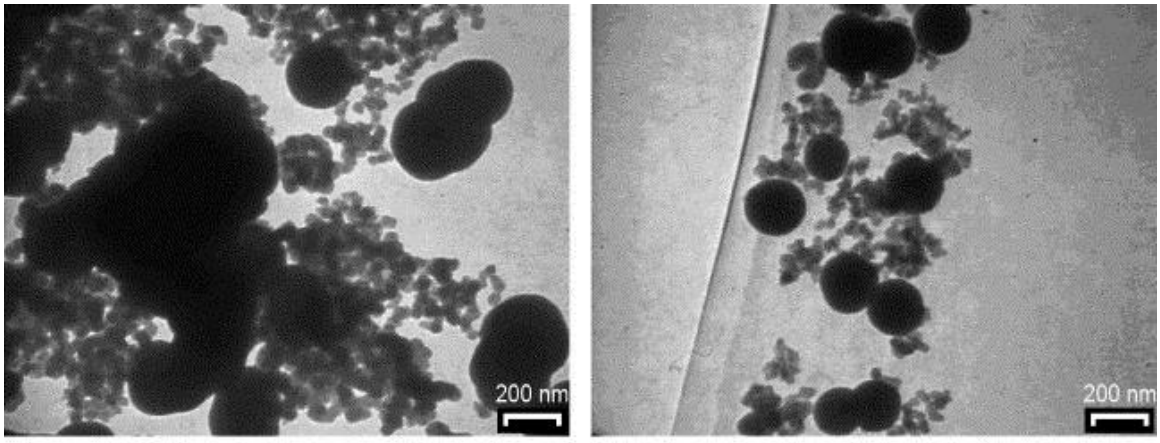

(a) magnetic stirrer and (b) ultra-sonication as reported by Rahman *et al* [152].

1.1.8 Functionalization of silica nanoparticles

There are several methods of functionalising silica nanoparticles including: Click chemistry and sol-gel hydrolysis and condensation [165,166,167,168,169,170]. We will only consider sol-gel Chemistry in this thesis because it is cheap, reliable and the method that was used in the original research by TWI.

Stöber nanoparticles can be functionalised using silanes or other functionalization agents[171, 172, 173]. The lengths of the alkyl chains in the silanes used to functionalise

the particles also matters as long chain silanes hinder the coverage of silica nanoparticles because their steric effect prevents close packing of the ligands to surfaces [171,174, 175] . Silanes such as trialkoxy or tetralkoxysilanes (TEOS) on the surface of Stöber nanoparticles introduce charges on the surface. The increase of the charges give rise to a repulsive electrostatic force between the particles hence stabilising the particle dispersion in solution[176, 119, 177]. The wettability of Stöber silica particles can be controlled by attaching hydrophilic or hydrophobic silanes on its surface (**Figure 1.24**).

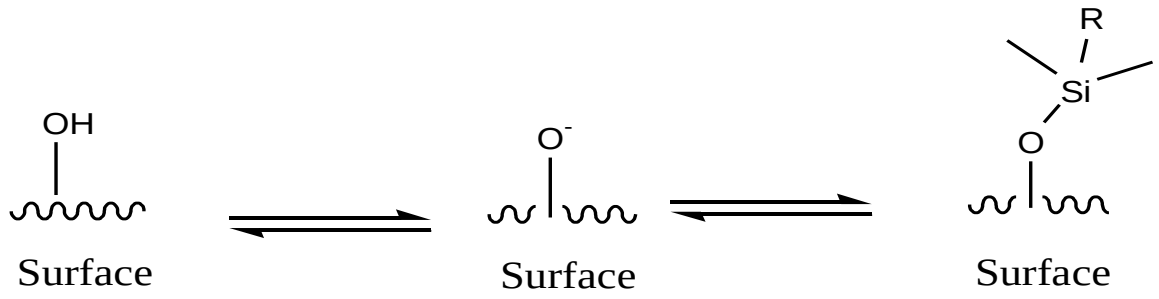

Figure 1.24. Schematic of ligand functionalization on the surfaces of Stöber nanoparticles.

1.1.8.1 Functionalization using the sol-gel method

The approach used here by Arantes *et al.*[156] is similar to the functionalization method used in this thesis. Functionalization of silica nanoparticles has been performed by using a silane functionalising agent such as: 3(trimethoxysilyl) propyl methacrylate (MPTMS). The MPTMS is added in excess (20 mmol/g SiO_2) directly to the alcohol dispersion containing the particles (including ammonium hydroxide). The mixture is stirred continuously for 24hrs at room temperature. After 24 hours, the functionalised silica MPTMS nanoparticles were purified by repeated

centrifugation and washing with dry ethanol (6000 rpm for 20mins) to remove any excess ammonia and MPTMS. The functionalised sample obtained were dried in a petri dish at 50^{o}C [156], **Figure 1.25**.

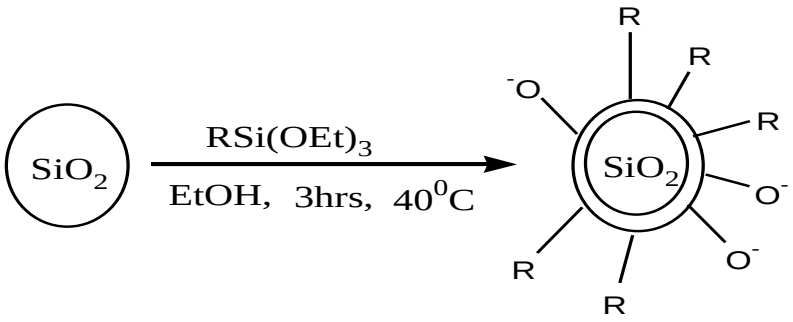

Figure 1.25. Functionalization of silica nanoparticles

The number of reactive sites on a surface area and the type of silane bonding (monolayer, bilayer, multilayer or bulk layer) can be used to calculate the number of moles of silane necessary to populate a surface [7,178,179]. For mono layer silane deposition, the particles should be predried at 150^{o}C for about four hours [171,180,181].

1.1.9 Factors that affect functionalization of silanes onto the surfaces of silica nanoparticles

1.1.9.1 The silane functionalising agent

The nature of the silane functionalising agent is one of the main factors that affect the bonding of a silane onto the surface of silica particles. The number of hydrolysable groups on the coupling agent matters [36,16, 182,182b]. Traditional silane coupling agents had three hydrolysable groups which made it more hydrolytically stable but then made it more hygroscopic [182b, 183,33]. On the other hand, a silane with one hydrolysable group produces the most hydrophobic properties but with the least

long term hydrolytic stability. Silanes with two hydrolysable groups form less rigid interfaces than silanes with three hydrolysable groups.

1.1.9.2 The silane thermal stability

Thermal stability is another useful factor. Silanes have moderate thermal stability; hence they are suitable for plastics processing of below 350^{o}C. However, silanes with an aromatic core have higher thermal stability, as shown in **Table 1.3** below:

Table 1.3. Class of silanes vs their thermal stability[156]

Class Example	**Thermal Limit**
$ZCH_2CH_2SiX_3$	< 150°C
$ZCH_2CH_2CH_2SiX_3$	390°C
$ZCH_2AromaticCH_2CH_2SiX_3$	495°C
Aromatic SiX_3	550°C

Where Z = Functional groups

Different classes of silanes attached on the surface have different thermal stability because of the differences in the silane chemical composition.

1.1.10 Characterisation of Stöber sphere silica nanoparticles

A wide variety of different techniques have been used in characterising silica nanoparticles, as mentioned above (**Section 1.4.1**) which have been very useful in looking at various aspects of the particle surface, the properties and the amount of silane bonded on the surface. Some of these techniques include: NMR, MALDI-ToF MS, GPC, FTIR, SEM, DLS, XPS and TGA.

A problem that is associated with characterising functionalised Stöber sphere silica particles is aggregation[184,157]. This problem can be avoided using different functionalization techniques such as atom transfer radical polymerisation (ATRP) and reversible addition-fragmentation chain-transfer (RAFT). For example, a long silane chain stabilises aggregation by steric repulsion. Controlling aggregation helps improve the mechanical properties of the coatings[7,174] and also affects the properties of the final formulation and coatings. In the Stöber process, aggregation can be avoided by repeated cleaning of the Stöber nanoparticles once formed to remove left over base (ammonia).

Some of the techniques used in this research for the analysis of the Stöber sphere silica nanoparticles are reviewed below.

1.1.10.1 Spectroscopic techniques

Spectroscopic techniques such as (NMR, XPS FTIR, DRIFT, Maldi-ToF MS, ESI MS, and XRD) have been used to study the sizes of the particles, the morphology, the distribution and the presence and thickness of any silane functionalization on silica surfaces.

1.1.10.1.1 Nuclear magnetic resonance

Nuclear magnetic resonance spectroscopy (NMR) is one of the most important techniques used in the literature. NMR is simple to use and it is fairly straightforward to analyse the results. It gives detailed information and it is a non-destructive technique.

Silicon NMR (^{29}Si NMR) has been used in most published journals by other researchers such as; Tanaka *et al.*[159], Stöber *et al.*[2] and many others. The ^{29}Si isotope is the only naturally occurring NMR-active isotope. Due to the issues of long relaxation times and low abundance which made the technique insensitive, it was not used in the early days of NMR. However, as a result of the introduction of Fourier transform spectroscopy (FT) and the development of new pulse sequences, silicon NMR has now been routinely used for the last 40 years.

For example, NMR; CP-MAS (CP, cross-polarization-magic angle spinning) [185] spectroscopy have been widely used to study the immobilization of the initiator layers on the silica particle by Song *et al* [185, 186, 187] **(Figure 1.26).**

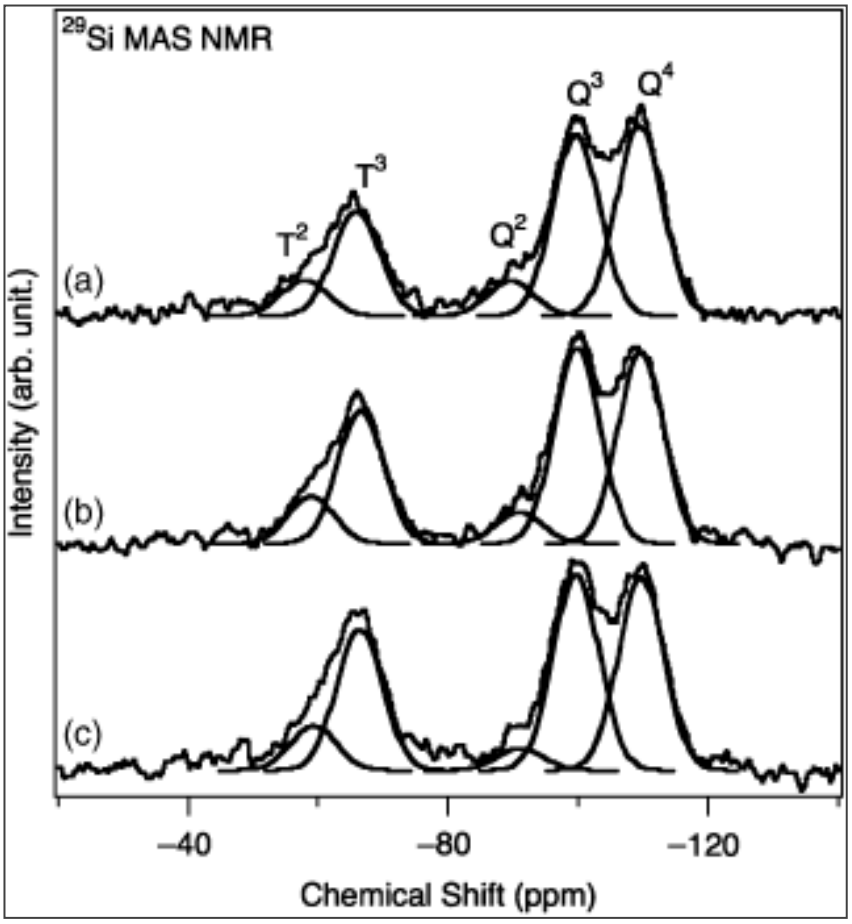

Figure 1.26. ^{29}Si MAS NMR spectra of amino-functionalised silica nanoparticles of: (a) AMSi0$_{45}$, (b) AMSi$_{45}$ and (c) AMSi$_{90}$ [185]. Where AM means APTES-modified (APTES, aminopropyltriethoxysilane) and AMSiO$_{45}$, AMSi$_{45}$ and AMSi$_{90}$ are silica particles with 0.45, 4.5 and 9.0mmol APTES content respectively.

The ^{29}Si MAS NMR spectrum in **Figure 1.26** shows specific structural information of the silicate network of the particles prepared by Song *et al*[185]. The NMR profiles extend in two regions; -80 to -120 ppm and -40 to -80 ppm which corresponds to units Q and T regions respectively.

Song *et al.*[185] identified here, T_1^2, T_2^1, and T_3^0 to be R–Si(–O–Si)(OH)$_2$, R–Si(–O–Si)$_2$(OH) and R–Si(–O–Si)$_3$ (Where R is the organic skeleton of the APTES monomer), respectively. While Q_2^2, Q_3^1 and Q_4^0 equally represents Si(–O–

$Si)_2(OH)_2$, $Si(–O–Si)_3(OH)$ and $Si(–O–Si)_4$ respectively. This result confirms the presence of the functionalising group APTES (T-units) on the particles. So it confirms the functionalization was successful [188].

1.1.10.1.2 XPS

X-ray photoelectron spectroscopy (XPS) is used to examine changes in the particle surface chemistry. XPS also measures the surface composition and chemical state. The presence and nature of functional groups on the surface of nanoparticles can also be measured. Attachment of silane on the silica particle surface is by covalent bonding [166]. SiO_2 and SiO_x signals are slightly shifted to about 3.45 eV (binding energy) for the functionalised silica as compared to the unfunctionalised. XPS in particular is useful for monitoring the presence of different oxidization states of atoms, relative abundance of atomic species and the silica core itself. Elemental and chemical information on the surface composition of the unfunctionalised silica particle and the silane bonded functionalised silica particles can be studied by XPS. An example where XPS has been used to study the surface of silica particles is as shown in **Figure 1.27** by Robert *et al* [174].

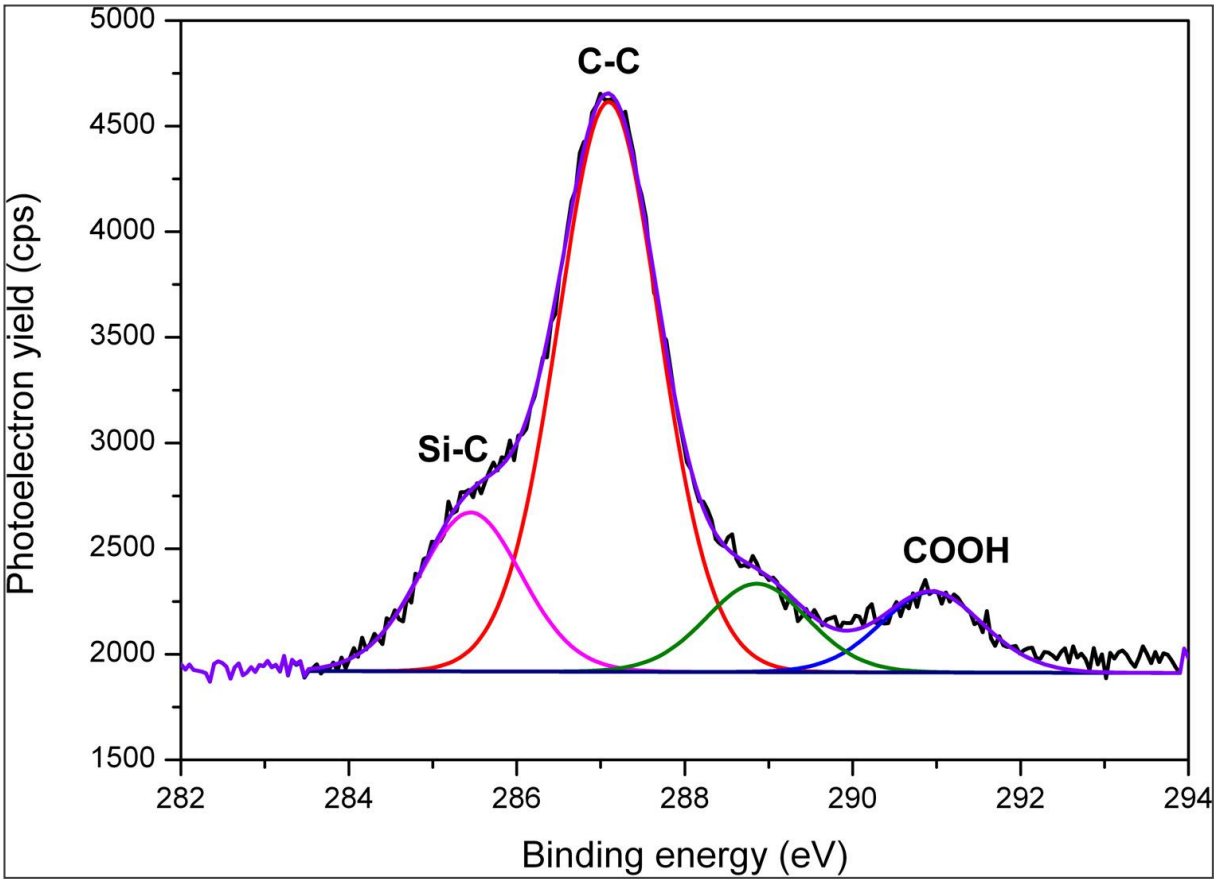

Figure 1.27. XPS C 1s spectra of acrylic acid-functionalized nanoparticles.

The maximum of the C-C peak is lying at 287.1 eV, and the Si-C peak is centred at 285.4 eV, displaying a shift of 1.7eV. The peak attributed to the carboxyl group is located at 291 eV [174]. This spectrum confirms the presence of acrylic acid on the silica surface by identifying some of the key bonds that exist. XPS has also been used by Perruchot *et al*.[166] to characterise signals for silicon, oxygen, carbon and nitrogen in order to confirm the presence of different polymer chains bonded on the silica surface (**Figure 1.28**).

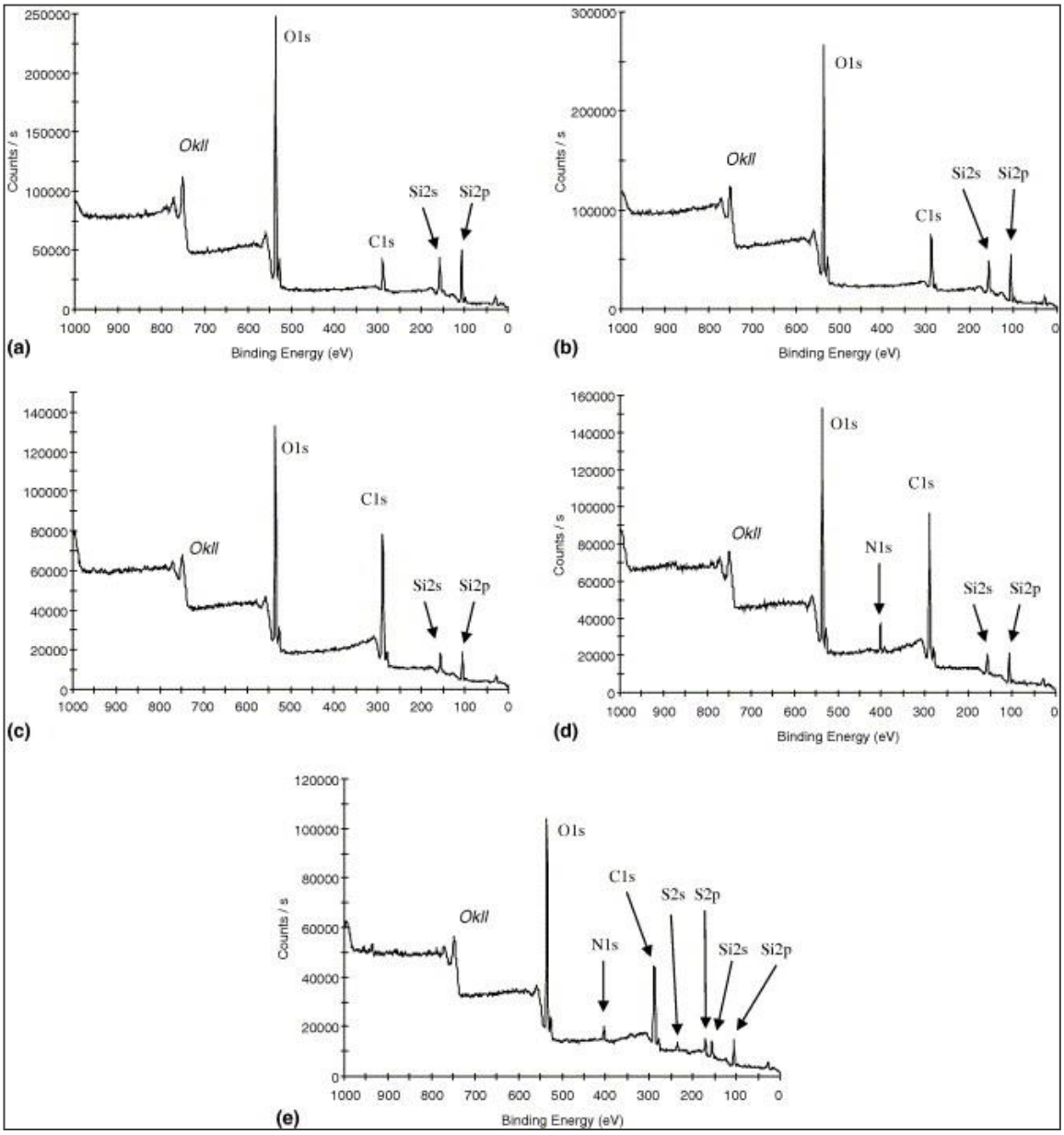

Figure 1.28. The XPS spectra of the following: (a) the bare silica sol, (b) the initiator-functionalised silica particles, (c) silica-init-OEGMA(500), (d) silica-init-MEMA(500) and (e) silica-init-SEM(500) particles, respectively. Where OEGMA, MEMA and SEM are initials of undisclosed functionalising agents [166].

The findings of Perruchot *et al.*[166] are as described below. In the unfunctionalised silica particle (**Figure 1.28a**) signals for silicon (Si2p at 103 eV and Si2s at 155 eV) and oxygen (O1s at 533 eV and oxygen Auger OkII at 740 eV) are detected. Also,

an additional weak carbon signal is being detected (C1s at 285 eV). This C1s could probably be an indication of incomplete hydrolysis of the alkoxide precursor used for the synthesis of the silica nanoparticles.

Figure 1.28b is the initiator-functionalised silica particles. It has strong silicon, oxygen and carbon signals which are also detected in the bare silica. However, the carbon signal is noticeably stronger compared to bare silica; this is because of the additional carbon atoms in the bromosiloxane-based initiator that was used.

Moving onto the polymer-functionalised silica nanoparticles (**Figure 1.28c-e**), the distinctive silicon and oxygen signals from the bare silica are still being seen, but with a reduced intensity. The carbon C1s signals are more intense compared to the initiator-functionalised silica nanoparticles. Moreover, in the case of the silica-I-MEMA(500) (**Figure 1.28d)** and silica-I-SEM(500) (**Figure 1.28e**) polymer functionalised silica particles, additional weak signals are seen with nitrogen N1s at 400 eV, as well as sulphur S2p and S2s signals (at 169 and 230 eV, respectively) for the silica-I-SEM(500) compound. These elements are typical of the functionalised polymer chains used but not of the inorganic particles. This result confirms XPS to be an important tool to identify grafting onto surfaces and is a very important technique for this study to confirm functionalization success.

1.1.10.1.3 FTIR/DRIFT

Infrared techniques such as fourier transform IR (FTIR) and Diffuse reflectance IR Fourier transform spectroscopy (DRIFTS) are also used to study silica particle surfaces[174, 189]. An example can be seen in **Figure 1.29** below studied by Robert *et al*. Robert and co-workers used FTIR to identify the presence of a bond of a ligand attached to the silica particle surface (surface functionalization).

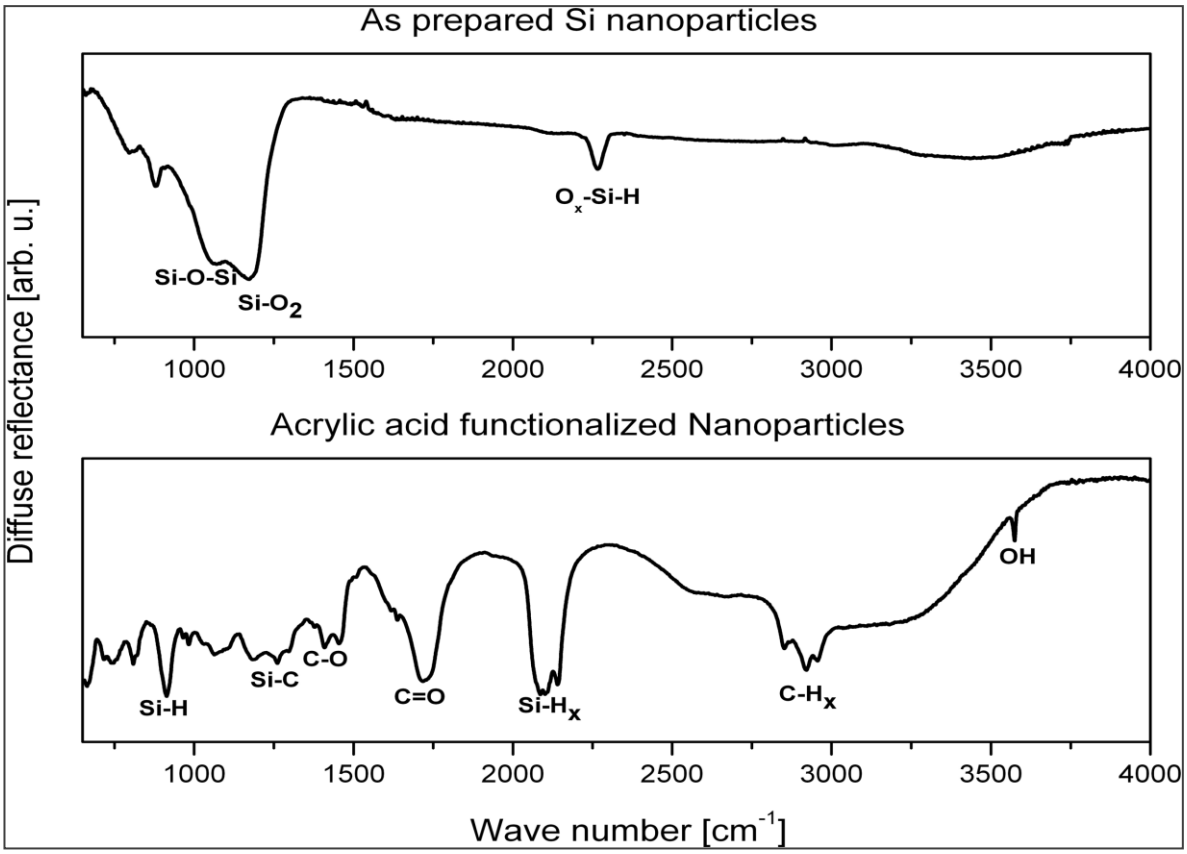

Figure 1.29.DRIFT spectra of as-prepared nanoparticles (top), and acrylic acid-functionalized nanoparticles (bottom) with the appointed functional groups [174].

This technique gives similar results to the XPS. In fact, it can be used as confirmatory evidence when XPS is not present. Just as with XPS, IR also gives different peaks for the different functional groups (such as Si-C, C-O, C=O in **Figure 1.29**) present in order to confirm the presence of an organic group on the surface.

For example, the difference in the peak intensities of the Si-C and C-O signals can stress the presence of surface functionalization of the acrylic acid (Figure 1.29 bottom).

1.1.10.2 Light scattering techniques

Light scattering techniques such as; DLS, SANS, SAXS, LDA and ES-DMA gives the size and size distribution of the particles.

1.1.10.2.1 DLS

Dynamic Light Scattering (DLS) like other light scattering techniques is used to measure the stability of the dispersion of the silica particles and whether there is degradation occurring with time [174]. Scientists have studied size and size distribution of functionalised and the unfunctionalised particles by DLS from when they were initially made compared to months afterwards. If the sizes / distribution remain the same after months of testing, then the particles will be said to have long term dispersion stability.

DLS works by determining the weighted mean nanoparticle size and the range of the particle size distribution (PolyDispersity Index, PDI). The particle size and PDI are then calculated by the instrument from a cumulant analysis. This calculates both the mean particle size and the PDI. The PDI indicates the variance of the sample and is given in the range of between zero and one [0,1]. Low PDI is normally less than 0.3. This means that the samples are monodisperse. Large PDI means the distribution is broader and this could be as a result of agglomeration. A PDI that is greater than 0.5 are usually unreliable.

Measurements of DLS are performed by first carrying out a dilution versus concentration screening to find the right dilution in which the particle size is not dependent on concentration. This is done to make sure multiple scattering and particle-particle interactions are being minimised. For every sample, 3-5 sets of measurements of 13 scans each are taken. These are then averaged to give the

average particle diameter of the particles. The temperature of the analysis can be maintained at 25^{o}C or varied depending upon the investigation.

1.1.10.3 Microscopic techniques

Microscopic techniques such as; SEM, TEM, AFM and BAM are used to study size and nature of the Stöber silica particles as described in the experimental section [148, 166].

1.1.10.3.1 Scanning Electron Microscopy (SEM)

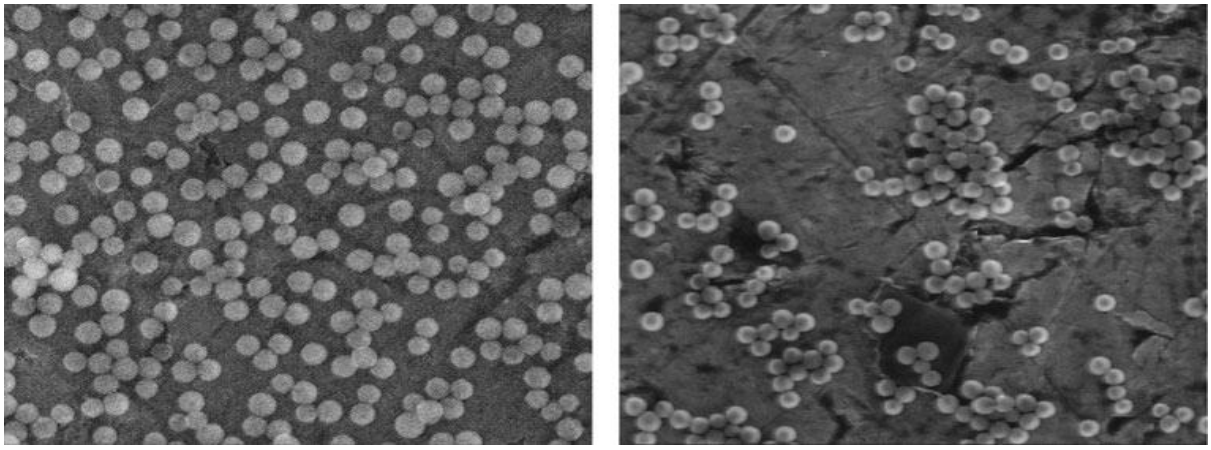

Figure 1.30. Scanning electron micrographs of unfunctionalised silica (left), and functionalised silica particles (right)[188].

The above figure (**Figure 1.30**) was used to study the morphological changes that occurred when a particle is functionalised. From the SEM image, Ruff *et al.*[188] confirmed that functionalization has no significant influence on the shape and size of particles.

1.1.10.3.2 Transmission Electron Microscopy (TEM)

TEM is a microscopic technique used to examine morphology changes, size and the shapes of silica particles. It works in a very similar fashion to SEM but TEM has higher energy that can penetrate particles more deeply than SEM hence it is used especially for small sized particle analysis and detailed characterisation as for example in the case of functionalised particles, A description of how the TEM works is explained in Chapter 2.1.11. TEM show agglomerates which are highly unchanged with respect to time. Also, about 1nm size is added to the original particles surface as a result of silane coating[190].

1.1.10.3.3 Atomic Force Microscopy (AFM)

Atomic force microscopy (AFM) is used to determine the size and nature of silica nanoparticles, before and after each stage of functionalization. AFM can also determine the shape, texture and roughness of individual particles and their distribution for an aggregation of particles. This method provides a visual image of the formation of the silane chains on particles and the aggregation properties. AFM images can show the surface structure and can specify whether the silane on the surface has a constant spacing or not [191].

1.1.10.4 Gravimetric techniques

Gravimetric techniques such as: TGA (e.g. TG-DTA) are generally used to study weight changes as a result of temperature before and after functionalization.

1.1.10.4.1 Thermo Gravimetric Analysis (TGA)

TGA is used to measure changes in weight before and after functionalization of the silica particle surface. The TGA in **Figure 1.31** has been used to study the weight loss of three different samples a, b and c.

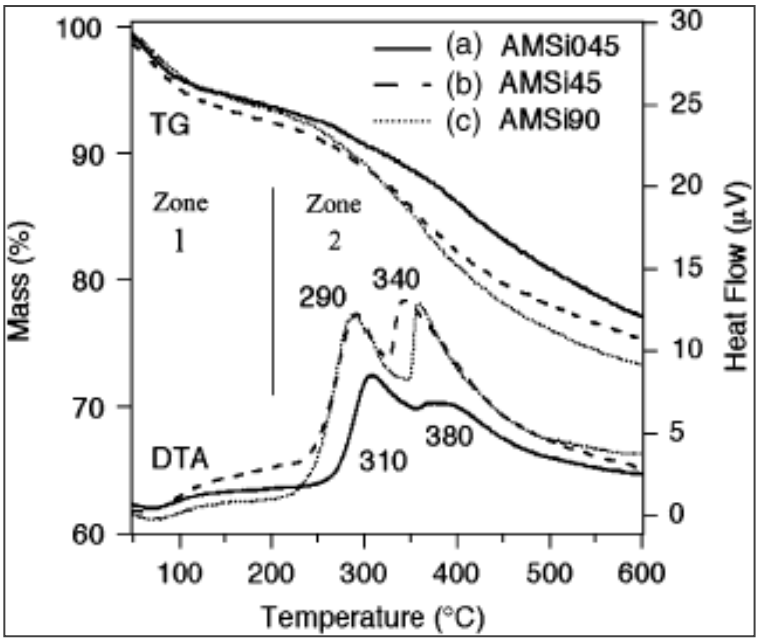

Figure 1.31. The TGA-DTA curves of the particles of: (a) $AMSi0_{45}$, (b) $AMSi_{45}$ and (c) $AMSi_{90}$. Zone 1 shows the elimination of physically adsorbed water and zone 2 is for ignition of the APTES fixed on the particle surface. (AM=APTES-modified; APTES=aminopropyltriethoxysilane; DTA=differential thermal analysis; TGA= thermogravimetric analysis) [185].

Figure 1.31 Shows the TGA-DTA curves of particles (a) $AMSi0_{45}$, (b)$AMSi_{45}$ and (c) $AMSi_{90}$ which are all different functionalised silica. Their TGA and DTA profiles are divided into two temperature zones (zone 1: 40–200 represent an endothermic DTA peak at 50^0C and Zone 2: 200–600 consisting of two distinct DTA exothermic peaks). The mass loss around 100^0C is most usually due to the loss of water physically adsorbed on the surface, and the exothermic peaks at higher

temperatures are as a result of organic components burning off or crystallisation. According to Song *et al.*[185], the DTA profile for zone 1 shows no difference between the particles. The results obtained showed a total loss from 40 to 600 and that was about 25%. This was as a result of water loss of about 6-7%. In zone 2, the loss was as a result of the burning off of the silane functional groups. Two peaks were observed in this zone which indicated that the decomposition of the organic group took place in two steps. This could have been due to the silane bonded on the silica surface decomposing first before those bonded inside close to the silica surface.

1.7.1.2 DSC-DTA

DSC-DTA is a thermos-analytical technique that can be used to study the effect of tethering and chain mobilization on the glass transition temperature of the silane of the functionalised particles.

1.7.1.3 Elemental analysis

Elemental analysis like ICP-OES (inductively coupled plasma-optical electron spectroscopy) is used to study the surface composition of silica nanoparticles as reported in literature[192,193] .

1.1.11 Defunctionalisation of silanes from the surface of silica nanoparticles

Stöber silica nanoparticles have a high surface to volume ratio[178]. Silanes on the surface of the Stöber silica particles can be removed by dissolving the functionalised Stöber particles in diluted hydrofluoric acid (HF) or other acids. The silane obtained can be characterised to understand its structure and chemistry [173, 194].

1.8 Aim and Scope of Thesis

This research project was instigated by our industrial sponsor and collaborator TWI Ltd based in Cambridge, United Kingdom[23] and then further developed by myself. TWI, have patented and developed a two-step hydrolysis/condensation method of synthesizing organosilsesquioxane resins [22,195, 196, 197]. This technology has been named Vitolane™ and is being scaled up to industrial level[23]. The coating department of TWI has been developing and supplying coating ideas for many years to its customers. However, to create technologies that suits the current changing market and environment [93,198, 103], they have therefore focused their attention to develop their research and development (R&D) further. During an initial study, they found out that water and pH plays an important role in the structural formations of resin products hence they needed further indepth research to understand the chemistry. This is where I as a researcher along with the research team of experts (my supervisors) come in with the right instrumentation to understand and further develop the research. Based upon this background, goals were set into place by both TWI Ltd[23] and my university supervisors and the research aims were set as below.

Mains research aims are:

1. To study the mechanism of hydrolysis and condensation of trialkoxysilanes, tetraalkoxysilanes and silsesquioxanes
2. To control the reactions of tetraalkoxysilane hydrolysis and condensation to obtain Stöber silica nanoparticles of various sizes.
3. To control the functionalization of Stöber silica nanoparticles

4. To develop the analysis of complex polymeric mixtures using various instrumentation techniques
5. To characterize and improve current silsesquioxane coating precursors (resins).
6. To control the process of production of Vitolane resin and to optimize its performance and durability.
7. To synthesize and characterize new advanced coating resin materials using Stöber Sphere silica nanoparticles.

1.9 The structure of the thesis

The main subject of this thesis is the hydrolysis and condensation of trialkoxysilanes and tetraalkoxysilanes and how they can be controlled to synthesise different silsesquioxane resins for coating applications. The second aspect involves the synthesis and surface functionalization of Stöber sphere nanoparticles, and how the sizes of the particles can be varied by varying different amounts of reagents used. The different parts have been sectioned into chapters as below:

Chapter 1: This chapter of the thesis contains the introduction. It also includes the overall introduction to silicon and silicon compounds[199, 200]. It introduces the main chemistry in the thesis which is sol-gel chemistry. It also touches on advanced materials and how these can be made using silsesquioxanes and how these materials could be enhanced using functionalized silica nanoparticles to acquire different properties for the coatings[77, 78, 201,76]. The later parts of this chapter talks about the literature findings of different functionalizing agents used as this is crucial in understanding the process of functionalization[202, 201, 203]. Finally, this chapter talks about the different techniques which have been used to study silsesquioxanes and

nanoparticles. These techniques are important because these substances are complex and it is important to understand what they are in order to understand the chemistry[204, 205, 206].

Chapter 2: This is the experimental section and it also includes the instruments used, where the chemicals used were obtained and it discusses the various characterization techniques use in the thesis.

Chapter 3: This chapter focuses on the kinetics of the hydrolysis and condensation of TEOS. The sol-gel reaction route has been applied by varying the ratios of reagents; TEOS, water and the concentration of acid, the mechanism and rate of hydrolysis and condensation have been studied. Solution silicon nuclear magnetic resonance (^{29}Si NMR) was used to measure the silicon species formed with respect to time and the ratio of reagents. ^{29}Si NMR and Matrix-assisted laser desorption/ionization time of flight mass spectrometry (MALDI-ToF-MS) was also used to investigate the hydrolysis and condensation processes occurring during the reaction by measuring the molecular weights and the detailed structure of the species formed.

Chapter 4: Here, the hydrolysis and condensation of trialkoxysilanes precisely; 3-Methacryloxypropyltriethoxysilane (MPTES),
3-methacryloxypropyltrimethoxysilane (MPTMS) and n-propyl trimethoxysilanes (nPTMS) have been studied. The study also included monitoring the effects of altering each reagent (silane, water and acid) on the composition of the silsesquioxane resin formed. This section also includes understanding what happens when excess reagents are being added to the reaction after equilibrium,

this gives an understanding of the durability or shelf-life of the materials formed[23]. The mixing pattern of the reactants, alcohol exchange and some equilibrium studies were also carried out. Finally, just as the in the case of Chapter 3, various instrumentation has been used to monitor the reaction and the final product formed.

Chapter 5: This chapter sets the scene for this research. The understanding of the silsesquioxane resin product is the origin for the need to find out what is going on in the reaction process and what products are being formed. The study of the hydrolysis of trialkoxysilanes in Chapter 4 have been applied in various case scenarios in this chapter such as; silsesquioxane hydrolysis and condensation in order to understand resin formation and other advanced materials [207]. The synthesis, purification, characterization and optimization study have also been carried out.

Two systems of synthesis have been described in Chapter 5: The single component-system (A-system) and the two component-system (AZ-system) of making Silsesquioxanes resin mixture. The single component-system involves the preparation of a silsesquioxane resin using a single monomer, 3-methacryloxypropyltrimethoxysilane (MPTMS) as the starting material. The AZ-system involves the use of two monomers; 3-methacryloxypropyltrimethoxy silane (MPTMS) and n-propyltrimethoxy silane (nPTMS) as starting materials. The mechanism of these reactions has been followed by characterization using various instrumental techniques some of which include: MALDI-ToF MS, ESI-MS, ^{29}Si NMR, FT-IR, DSC and HPLC-MS. The results, discussion, summary of the resin structures from the A and AZ-systems have been discussed based on the findings of each of these techniques.

Chapter 6: This chapter is similar to Chapter 5 as it involves the application of the research findings in Chapter 3 to develop advanced coating materials. Here, the hydrolysis and condensation of TEOS (Chapter 3) have been applied to Stöber nanoparticle study. In this chapter, we have used the understanding of the mechanism studied in chapter 3 to make Stöber nanoparticles, functionalize and characterize them. Chapter 3 findings were also used to further study the control of particle size which is an important parameter to understand when designing new advanced materials for super hydrophobic coating application[208, 209, 210].

Chapter 7: This chapter comprises the general conclusion of all the above chapters. It gives a general summary and then the conclusion. Future work has also been provided here.

In conclusion, the research aims have been achieved while some proposals have been made for future work. In each chapter, abbreviations are defined when first used and they are also defined in **Page v** (abbreviations and symbols). The appendices are given at the end and are numbered throughout the thesis. References are given at the very end followed by the appendices.

Chapter 2 – Experimental, materials and instruments

This is the experimental section. It includes where the chemicals used were obtained and it discusses the various characterization techniques use in the thesis.

2.1 Experimental

2.1.1 Hydrolysis and condensation of TEOS – Kinetic study

TEOS (>99%), water (deionised), ethanol (>99.7%) and an acid catalyst, in this case trifluoromethanesulphonic acid (CF_3SO_3H) were used in the proportions shown in **Table 3.2** (varying the molar ratio of water to TEOS by keeping the [H_2O] constant and changing the [TEOS]). This acid was used because it contains no water hence the amounts of water in the reaction can be measured accurately. The mixing procedure follows the original sol gel process.

In a typical procedure, tetraethyl orthosilicate (TEOS; 2.60g, $1.25x10^{-2}$mol) was added to a mixture of absolute ethanol (4.89g, 0.1061mol) and deionized water (0.45g, $2.50x10^{-2}$mol). Then, a stock solution (A) was made of 50g ethanol (EtOH) and 0.059g ($3.96X10^{-4}$mol) of trifluoromethanesulfonic acid to give an acid concentration of $6.2x10^{-3}$mol/L. From the stock solution **A**, 1.0g was used and further diluted with 9.5g EtOH to obtain an acid concentration of $5.9x10^{-4}$mol/L. 5.06g of the final acid stock solution was added to the TEOS-EtOH-water mixture and shaken for about 5 minutes at room temperature to give a final acid concentration of $2.3x10^{-4}$mol/L. The reaction was monitored by ^{29}Si NMR in a 5mm NMR tube using an insert containing tetramethylsilane (TMS) and chloroform-d. NMR spectra were acquired using 79.4 MHz ^{29}Si NMR every 20 hours (depending on the $[H^+]$) for a total of about 500 hours. 20 hours was used for the 1 molar ratio of water to 2 mol silane because of the very low $[H^+]$ used and for an extensive study of the complete reaction. Fresh stock solutions were made for each of the experiments and the results presented in **Table 3.2**. In all cases, the amount of water was kept constant as well as the final volume of the reaction mixture by topping up with ethanol.

In the case of the acid studies, the same amounts of other substances (**Table 3.2**) were used (1:2 molar ratio) but the concentration of the acid was varied as shown in **Table 3.3**

2.1.2 Hydrolysis and condensation of MPTES - Kinetic study

The hydrolysis and condensation of MPTES is similar to that of TEOS (Chapter 2.1 above) apart from different silanes and quantities that are used, as will be explained. MPTES (>99%), water (deionised), ethanol (>99.7%) and an acid catalyst, in this case trifluoromethanesulphonic acid (CF_3SO_3H) were used in the proportions shown in **Table 2.1** (varying the molar ratio of water with respect to MPTES by keeping the water concentration constant and changing the [MPTES]. The mixing procedure follows the original sol-gel process[2, 211].

In a typical procedure, 3-methacryloxypropyltrimethoxysilane (MPTES; 4.85g, $1.67x10^{-2}$mol) was added to a mixture of absolute ethanol (7.64g, $1.66x10^{-1}$mol) and deionized water (0.45g, $2.50x10^{-2}$mol). Then, a stock solution (A) was made from 50g ethanol (EtOH) and 0.059g ($3.96x10^{-4}$mol) trifluoromethanesulfonic acid to give a final concentration of 0.0025M. From the stock solution A, 1.0g was used and further diluted with 9.5g EtOH to obtain an acid concentration of $2.3x10^{-4}$M. 5.06g of the final acid stock solution was added to the MPTES-EtOH-water mixture and shaken for about 5 minutes at room temperature. The reaction was monitored by ^{29}Si NMR in a 5mm NMR tube using an insert containing TMS and chloroform-d. NMR spectra were acquired the same way as in the TEOS hydrolysis. Fresh stock solutions were made for each of the experiments in **Table 2.1**. In the case of the acid studies, the same amounts as above (typical procedure, 1:2 mol ratio) were used but the concentration of the acid was varied as shown in **Table 2.2**.

Table 2.1: Reactant compositions by varying the molar ratio of water to MPTES

MPTES:water ratios	**[CF_3SO_3H], mol/L (catalyst)**	**[Water], mol/L**	**[MPTES], mol/L**	**[EtOH] mol/L**	**Timescale for data collection**
1MPTES:0.5H_2O	$2.3x10^{-4}$	1.66	3.13	7.90 in excess	1–7 hr. 2hr scan 8-20 hr. 4hr scan >20 4-7hr scan
1MPTES:1H_2O	$2.3x10^{-4}$	1.66	1.66	7.60	1–7 hr. 2hr scan 8-20 hr. 4hr scan >20 4-7hr scan
1MPTES:1.5H_2O	$2.3x10^{-4}$	1.66	1.11	11.07	1–7 hr. 2hr scan 8-20 hr. 4hr scan >20 4-7hr scan
1MPTES:2H_2O	$2.3x10^{-4}$	1.66	0.83	12.87	1–7 hr. 2hr scan 8-20 hr. 4hr scan >20 4-7hr scan
1MPTES:2.5H_2O	$2.3x10^{-4}$	1.66	0.67	13.87	1–7 hr. 2hr scan 8-20 hr. 4hr scan >20 4-7hr scan
1MPTES:3.0H_2O	$2.3x10^{-4}$	1.66	0.53	14.53	1–7 hr. 2hr scan 8-20 hr. 4hr scan >20 4-7hr scan

NB: Where MPTES:water represents molar ratios of MPTES:water.

Table 2.2: Varying the concentration of the acid (CF_3SO_3H) to determine the rate of MPTES hydrolysis and condensation.

MPTES:water ratios	**[CF_3SO_3H]mol/L (catalyst)**	**[Water], mol/L**	**[MPTES], mol/L**	**[EtOH], mol/L**	**Timescale for data collection**
1MPTES:1.5H_2O	$4.81x10^{-5}$	1.66	1.11	11.07	1–5hr 1hr scan 6-9 hr. 2hr scan
1MPTES:1.5H_2O	$9.62x10^{-5}$	1.66	1.11	11.07	1–5hr 1hr scan 6-9 hr. 2hr scan
1MPTES:1.5H_2O	$1.44x10^{-4}$	1.66	1.11	11.07	1–5hr 1hr scan 6-9 hr. 2hr scan
1MPTES:1.5H_2O	$1.92x10^{-4}$	1.66	1.11	11.07	1–5hr 1hr scan 6-9 hr. 2hr scan
1MPTES:1.5H_2O	$2.29x10^{-4}$	1.66	1.11	11.07	1–5hr 1hr scan 6-9 hr. 2hr scan

2.1.3 Synthesis of 3- methacryloxypropyltrimethoxysilane dimer

3-methacyloxypropyltrimethoxysilane; MPTMS (20.0g, 0.08mol, M = 248.35g/mol, 1eq) was added to a container containing a mixture of methanol (20g, 0.6mol, M = 32.04g/mol, 8eq (excess)), water (0.8g, 0.04mol, M = 18.0g/mol, 0.5eq) and conc. hydrochloric acid (0.10g, 0.0003mol, M = 37.5g/mol, 3 drops). The mixture was shaken for a few minutes and left at room temperature for 2 hours in a sealed container. After 2 hours, the reaction was monitored using GCMS to see if any product had been formed (**Figure 5.12**). The product formed was then evaporated to remove solvent using a rotary evaporator. The product was purified by distillation at 0.01mbar pressure and over a temperature range of 0-162^{O}C. The dimer was isolated at 159^{0}C. A transparent clear liquid product was obtained (4.1g, 11.4%) and

the product characterised using the appropriate techniques (**Chapter 5.3.2.2**) and results recorded below and discussed in Chapter 5.

^{1}H NMR (99.98MHz, $CDCl_3$)/ppm: δ = 1.2 (=CH_2, Ha), 1.7 (=CH_2, Hb), 3.2 (2(Si-CH_2), 3.6 (4(-OCH_3), 5.4 (2(=CH_3), 5.5 (2(O-CH_2), 6.6 (2(-CH_2)).**^{13}C NMR** (75.4MHz, $CDCl_3$)/ppm: δ= 167.4 (C=O, 136.5 (C=CH_2), 125.2 (=CH_2), 66.5(OCH_3), 50.3 (OCH_3)x4, 22.2 (CH_3), 18.3 (CH_2CH_2), 6.8 ($SiCH_2$). **^{29}Si NMR** (99.3MHz, $CDCl_3$)/ppm: δ -50.3421. **MS** (**MALDI-ToF MS**): m/z (%): $C_{18}H_{34}O_9Si_2Na^+$: Found 473.1(100% dimer), 675.2(25% trimer). **MS (HPLC-MS):** $C_{18}H_{34}O_9Si_2NH_4^+$: Found 468.13(100%).**MS (GCMS**): $C_{18}H_{34}O_9Si_2NH_4^+$: Found 468.13(100%). **GPC**: Mn = 369, Mw = 382.

2.1.4 Synthesis of 3- methacryloxypropyltrimethoxysilane tetramer

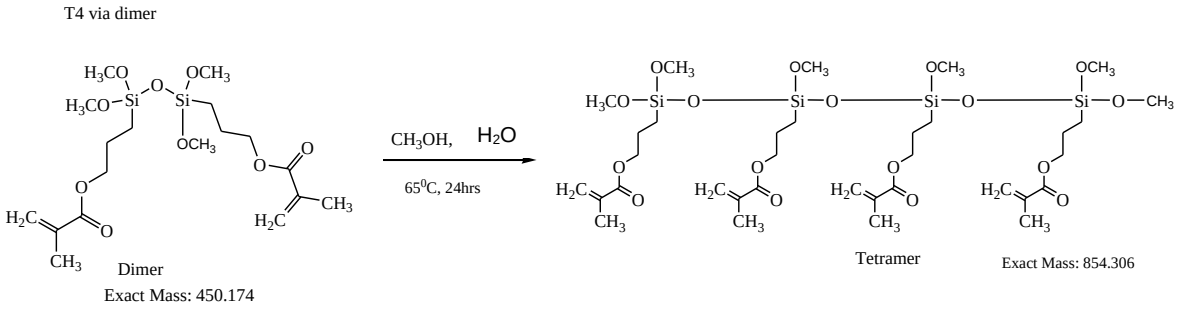

3-methacyloxypropyltrimethoxydisiloxane; dimer (0.57g, 0.001mol, M = 450.17/mol, 1eq) was added to a flask containing a mixture of methanol (0.103g, 0.003mol, M = 32.04g/mol, 3eq), water (0.043.0g, 0.002mol, M = 18.0g/mol, 2eq) and conc. hydrochloric acid (0.10g, 0.0003mol, M = 37.5g/mol, 3 drops). The mixture was shaken for a few minutes and allowed to react at room temperature for four hours in an NMR tube while reaction progress was monitored using ^{29}Si NMR for 3 hours. After 3 hours, the reaction was stopped. DCM was added to dissolve the product while magnesium sulphate was used to remove any water that was left in the reaction. Magnesium sulphate was removed by filtration and the DCM removed using a rotary evaporator. The product was further dried under high vacuum to

remove any moisture. A transparent liquid product was obtained (0.32g, 49%).The product contained mostly tetramers though it could not be fully purified because of the presence of some impurities of larger oligomers. Instrumental results are shown in **Chapter 5.3.3.2** and interpreted below.

^{29}Si NMR (99.3MHz, $CDCl_3$)/ppm: δ -57.4691, -57.4996**. MS** (**MALDI-ToF MS**): m/z (%):$C_{22}H_{46}O_{15}Si_4$: Found 816.276(100%), 973.257(20% pentamers), 1143.293 (10% hexamers). **MS (LC-MS**): $C_{22}H_{46}O_{15}Si_4NH_4^+$: Found 812.259(100% linear), 826.3(100% cyclics). **GPC**: Peak 1 - Mn = 2953, Mw = 3437; Peak 2 – Mn = 1327, Mw = 1365. (See GPC conditions at section 2.2.13). This product has been partially characterized because of its reactive and unstable nature since it prefers the cubic form otherwise it forms larger Silsesquioxanes units.

2.1.5 Synthesis of the T_8 Cage

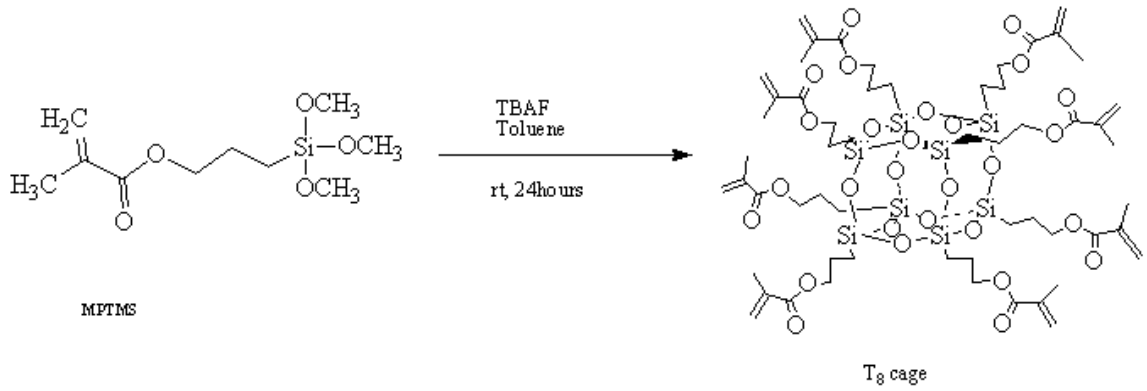

3-methacyloxypropyltrimethoxysilane (1.24g, 5mmol, MW = 248.35g/mol, 2eq) was dissolved in dry toluene (20ml) in a 250ml round bottom flask. Tetra n-butyl ammonium fluoride (2.5ml of the 1M solution in THF with 5% water, 1eq) was added. The mixture was stirred at room temperature over 24 hours under argon. After 24 hours, the reaction was stopped and solvent removed on a rotatory evaporator at 40^0C under vacuum. The product obtained was a light brown oil and contained both T_8 and T_{10} as seen on TLC. The crude product was purified by column

chromatography on silica using a solvent mixture of hexane: ethyl acetate; 100ml (80:20), 100ml (70:30), 100ml (60:40), 60ml (50:50) and 40ml of 100% ethyl acetate. One of the fractions gave rise to tiny crystals of T_8 which were sent off for characterisation by X-ray crystallography. Proton and silicon NMR are shown in **Figure 5.43** and interpreted below:

^{1}H NMR (99.98MHz, $CDCl_3$)/ppm: δ = 0.68 (15H), 1.93 (34H), 4.11 (13H), 5.5 (=CH_2, Ha), 6.1 (=CH_2, Hb). **^{29}Si NMR** (99.3MHz, $CDCl_3$)/ppm: δ -66.8326. This product has also been characterized using X-ray crystallography and reported in **Chapter 5.4.3.2.** The compound has also been fully characterised and X-ray data reported in El Aziz thesis, 2010.

2.1.6 Vitolane Resin Synthesis (A and AZ-systems)

2.1.6.1 Via the mono or A-System (MPTMS)

Figure 5.2 shows the equation of the synthesis of vitolane resin via the A-system. The samples were prepared as described below.

3-Methacryloxypropyltrimethoxysilane; MPTMS (20.0g, 0.08mol, M = 248.35g/mol, 1eq) was added to a container containing a mixture of methanol (3.61g, 0.1mol, M = 32.04g/mol, 1eq), water (1.45g, 0.080mol, M = 18.0g/mol, 1eq) and conc. hydrochloric acid (0.10g, 0.0003mol, M = 37.5g/mol, 3drops). The mixture was shaken for a few minutes and left in the oven at 65^{o}C for 4 hours in a sealed container. After 4hours, the container was opened and mixture left in oven for 24 hours (part 1). After 24 hours, the mixture was cooled, poured into a container of deionised water (25g), shaken and allowed to settle for an hour. The product was extracted after an hour and dried in the oven for another 24 hours (part 2). A

transparent liquid polymer product (yield: 5.81g, 23.3%) was obtained. This product being a mixture (gel) could not be characterized fully. However, a lot of attempt was made to characterize the gel-like product as recorded below with more results details reported in Chapter 5 instead due to the debt of identifying each compound.

^{29}Si NMR (99.3MHz, $CDCl_3$)/ppm: δ = – 40 to -45ppm (T_0), -48 to -52ppm (T_1), -59 to -61 (T_2), -65 to -71 (T_3). **TGA** (air, 1000ºC) 320ºC-380ºC. **DSC**; 300ºC - 400ºC. **GPC:** Peak 1-Mn = 2165, Mw = 2420, Peak 2 -Mn = 1053, Mw = 1076, Peak 3 -Mn = 726, Mw = 729, Peak 4-Mn = 544, Mw = 547, Peak 5-Mn = 366, Mw = 369. **FTIR (post DSC**) – No C=O at 1720cm^{-1}). **CHN (Elemental analysis)** post DSC (char): CH_3SiO_x as graphite or silicon carbide. **UV-Vis** (180-240 nm) wavelength

2.1.6.2 Via the two component or AZ-system (nPTMS and MPTMS)

The AZ-system resin was synthesized as below:

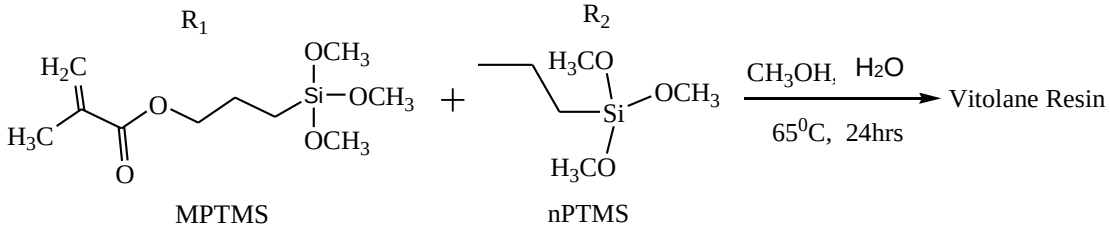

3-Methacryloxypropyltrimethoxysilane; MPTMS (7.5g, 0.03mol, M = 248.35g/mol, 1eq) was added to a container containing a mixture of methanol (1.4g, 0.04mol,

M = 32.04g/mol, 1eq), water (0.5g, 0.03mol, M = 18.0g/mol, 1eq) and conc. hydrochloric acid (0.10g, 0.003mol, M = 37.5g/mol, 3drops). The mixture was shaken for ten minutes. At the same time, a mixture of *n*-propyl trimethoxysilane; nPTMS (5.0g, 0.03mol, M = 164.09g/mol, 1eq), methanol (1.4g, 0.04mol, M = 32.04g/mol, 1eq), water (0.5g, 0.03mol, M = 18.0g/mol, 1eq) and hydrochloric acid

(0.10g, 0.003mol, M = 37.5g/mol, 3drops) was prepared the same way as the MPTMS and shaken for ten minutes. The two mixtures were then added together and shaken for four minutes and then placed into the oven at 65^{O}C for 4 hours in a sealed container. After 4hrs, the container was opened and mixture left in an oven for 24 hrs (part 1). After 24 hrs, the mixture was cooled, poured into a container of deionised water (25g), shaken and allowed to settle for an hour. The product was extracted after an hour and dried in the oven for another 24 hours (part 2). A transparent liquid product was obtained. This product was also very similar to the A-system resin above hence also could not be characterized fully but more detail characterization is in chapter 5. However, a lot of attempt was made to characterize the gel-like product as recorded below with more details reported in Chapter 5. **Yield**: (38g, 38.8%).

^{29}Si NMR (99.3MHz, $CDCl_3$)/ppm: δ = – 40 to -45ppm (T_0), -48 to -52ppm (T_1), -59 to -61 (T_2), -65 to -71 (T_3). **TGA** (air, 1000^{o}C) 320^{o}C, 480^{o}C. **DSC**; 350^{o}C, 530^{o}C. **GPC:** Peak 1-Mn = 1610, Mw = 2112, Peak 2 -Mn = 744, Mw = 716, Peak 3 -Mn = 420, Mw = 341, Peak 4-Mn = 147, Mw = 148. **CHN (Elemental analysis)** post DSC (char): CH_3SiO_x as graphite or silicon carbide

2.1.7 Distillation of the A-system silsesquioxane resin

50g of methanol was mixed with 2g of water and shaken together. 2g of this stock solution was mixed with 2g of the 3-methacryloxypropyltrimethoxysilane starting material and a few drops of hydrochloric acid added. That was allowed to stand for about 2 hours, which is just enough time to make sure some reaction has taken place.

After 2 hours, a silsesquioxane reaction sample was taken and analyzed by GC-MS to determine the fractions present (GC-MS spectra in **Figure 5.14**). A dimer, a trimer of the silsesquioxane resin mixture and a small amount of the starting material (monomer) were seen. From these results, the reaction was stopped and the resin formed was distilled under high vacuum (0.01mbar pressure) at a temperature of 159^0C. Three fractions were individually obtained, only one of which was the pure dimer (third fraction). Results are shown and discussed in Chapter 5.1.4.2.

2.1.8 Column chromatography to separate silsesquioxane resin

1.0g of synthesized silsesquioxane resin was dissolved in hexane (1.0ml). 20g of silica slurried in hexane was used to fill the column for column chromatography. Several solvents/solvent mixtures were used to run the column and the collection volume was 1-2ml per vial. A pasteur pipette was also used for smaller volume separation. For the Pasteur pipette, 0.3g of sample was used. Prior to doing the column chromatography and during the separation, several TLC plates were run to determine which solvent or solvent mixture best separates the resin components. Various TLC solvents/solvent mixtures were used and their success rates are shown in **Table 5.2**. The best of the TLC solvent mixture was a 1:1 ratio hexane: ethyl acetate.

2.1.9 Synthesis of Stöber silica nanoparticles by the sol-gel process

In these experiments, TEOS (>99%), water (deionised), ethanol (>99.7%) and a basic catalyst, in this case ammonium hydroxide (25% NH_3 in H_20, 99.99%) were used in the proportions shown in **Table 2.3** (varying the molar ratios of TEOS to

H_2O). The mixing procedure follows the original Stöber process. In a typical procedure, an ethanol (4.83g, 0.1048mol) – water (0.5g, 0.028mol) mixture is made. Then a TEOS (2.60g, 0.0125mol) – ethanol (5.0g, 0.1085mol) mixture is also made and added to the first mixture followed by vigorous mixing. Aqueous ammonia (25 wt. %, 7ml) is then added as the catalyst to speed up the rate of condensation. The mixture is further mixed for another 10 minutes. The transparent/opaque liquid contained the Stöber silica nanoparticles[67,2,150,148,151,152,153,154,155].

The resulting systems were left in the oven at 65^0C for 24 h to evaporate off the solvents. Finally, the colloidal dispersion of silica nanoparticles obtained is ready and the particles cleaned as described below before being characterized by dynamic light scattering (DLS) for suspensions and /or transmission electron microscopy (TEM) for dried particles. The particles were not centrifuged and washed with ethanol to eliminate initial reactants during the size measurement study. This was to maintain uniformity in the measurements since some of the particle sizes were extremely fine and could not be separated by centrifugation.

Cleaning and drying Stöber Spheres

Some particles were washed and dried either for the purpose of size measurements by TEM or for functionalization. For such particles, after 1h gelation, the gel was centrifuged and then washed 3 times (7min, 6,000rpm) each with ethanol (30ml). To obtain dried solid particles instead, the cleaned Stöber spheres were dried under vacuum for 24h (overnight). Some of the particles were dried in the oven for 24h at atmospheric pressure for comparison purposes with the vacuum dried samples.

To obtain completely dried particles, some samples were dried by calcination. That is, the samples were placed in enamel vials made from silicon oxide and aluminum,

covered using another enamel pan and placed in an oven. The oven was programmed as follows; Temperature set as: 110°C at 5°C/min to 600°C. Then kept (hold) at 600°C for 2h before cooling back to 110°C (overnight).

Fresh stock solutions were made for each of the experiments in **Table 2.3**. In all cases, the amount of water was kept constant as well as the final volume of the reaction mixture.

When the amounts of base were varied, the same amounts as above (typical procedure) were used. However, the concentration of the base was varied as shown in **Table 2.4.** The same conditions were used for varying the amount of water as shown in **Table 2.5**.

Table 2.3: Reactant compositions varying the amount of TEOS

Molar ratios of TEOS:water (mol)	**[NH_4OH],M (catalyst)**	**[Water],M**	**[TEOS],M**	**[EtOH],M**
0TEOS:1H_2O(blank)	0.6	18.7	-	14.0 (excess)
0.5TEOS:1H_2O	0.6	18.7	3.3	9.9
1TEOS:1H_2O	0.6	18.7	1.8	10.0
1.5TEOS:1H_2O	0.6	18.7	1.1	12.6
2TEOS:1H_2O	0.6	18.7	0.8	13.9
3.01TEOS:1H_2O	0.6	18.7	0.6	15.1
4.0TEOS:1H_2O	0.6	18.7	0.4	15.8
10TEOS:1H_2O	0.6	18.7	0.2	16.8

NB: these are stoichiometric molar ratios

Table 2.4 Reactant compositions varying the amount of ammonium hydroxide

Molar ratios of TEOS:NH_4OH	**[NH_4OH],M (catalyst)**	**[Water],M**	**[TEOS],M**	**[EtOH],M**
1TEOS:0NH_4OH, blk	0.0	18.7	0.8	14.4
1TEOS:20.7NH_4OH	0.1	18.7	0.8	14.3
1TEOS:9.2NH_4OH	0.2	18.7	0.8	14.2
1TEOS:6.9NH_4OH	0.3	18.7	0.8	14.2
1TEOS:4.6NH_4OH	0.4	18.7	0.8	14.1
1TEOS:2.3NH_4OH	0.8	18.7	0.8	13.8
1TEOS:2.1NH_4OH	1.0	18.7	0.8	13.7
1TEOS:1.6NH_4OH	1.1	18.7	0.8	13.5
1TEOS:0.9NH_4OH	1.9	18.7	0.8	13.0

NB: since NH_4OH is a catalyst, its stoichiometric ratio is irrelevant.

Table 2.5: Reactant compositions varying the amount of water

Molar ratios of TEOS:water	**[NH_4OH],M (catalyst)**	**[Water],M**	**[TEOS],M**	**[EtOH],M**
1TEOS:0H_2O	0.53	-	0.67	14.40
1TEOS:0.5H_2O	0.53	1.78	0.67	14.00
1TEOS:1.0 H_2O	0.53	3.54	0.67	13.30
1TEOS:2.0 H_2O	0.53	7.03	0.67	12.00
1TEOS:3.0 H_2O	0.53	10.56	0.67	10.67
1TEOS:3.5 H_2O	0.53	12.67	0.67	10.00
1TEOS:4.0 H_2O	0.53	14.05	0.67	9.30
1TEOS:5.0 H_2O	0.53	18.51	0.67	7.71
1TEOS:6.0 H_2O	0.53	22.0	0.67	6.00
1TEOS:8.0 H_2O	0.53	29.3	0.67	4.00
1TEOS:10.0 H_2O	0.53	35.13	0.67	0.47

NB: [Water] includes that from NH_3 solution.

2.1.10 Synthesis by microwave

TEOS (1ml, 0.58mol) was dissolved in dry ethanol 99.9% (6ml). 0.2ml of distilled water was added drop wise (rate 0.2ml/min^{-1}) into the reaction mixture to facilitate hydrolysis of TEOS. Ammonium hydroxide 25% (0.4 ml, 0.6 mol) was added to the reaction mixture at a rate of 0.01 ml/min^{-1}.

Microwave Conditions

Temperature: 50°C

Power: 200W

Time: 2 minutes

2.1.11 Functionalization of Stöber Silica nanoparticles

The procedure used followed the sol-gel method of Chi-Hwan *et al.* [212] and

Jafarzadeh *et al* [213].

Amino-functionalization of powdered (dried) Stöber SiO_2 nanoparticles

SiO_2 nanoparticles (0.5g) were dispersed in toluene (10ml) in a 50ml two-necked flask equipped with a refluxing condenser and a stirrer. Aminopropyltriethoxysilane (APTES) (0.015g) functionalizing agent ~1 drop was added with continuous stirring. The mixture was refluxed for 6h after which the product was filtered off, washed with toluene and ethanol and dried at 60°C for 6h. Results are shown in Figure 6.4 and 6.5. N.B. The above procedure can also be carried out at room temperature for 8h instead of 60°C for 6h and the product obtained was the same. The above procedure was applied to functionalization using different functionalizing agents and quantities

as tabulated in **Table 2.6** and characterized as described in **Chapter 6** with main focus on APTES functionalized nanoparticles.

Table 2.6. Functionalizing agents and quantities used

Silanes	**Mass (g)**	**Molar amounts**
Propyltrimethoxysilane (nPTMS)	0.015	9.131×10^{-5}
3,3,3-Trifluoropropyl)trimethoxysilane	0.015	6.873×10^{-5}
3-(Methacryloxy)propyl]trimethoxysilane (MPTMS)	0.015	6.040×10^{-5}
(3-Aminopropyl)triethoxysilane (APTES)	0.015	6.776×10^{-5}
3-Mercaptopropyltrimethoxysilane*	0.015	7.640×10^{-5}

*=carried out by industrial partner (TWI)

An alternative functionalization method was used in a case where functionalization is carried out through an intermediate[214]. An example is where imidazole is used to catalyze the functionalization process of a ligand onto a silica particle surface. imidazole (0.015g) was used. This is particularly useful in cases where the functionalizing silane does not bind firmly on the surface of the particle. A typical example is where fluorofunctionalised SiO_2 nanoparticles (0.220g) were dispersed in ethanol (5ml). 0.015g of imidazole was added and the mixture allowed to stir at room temperature for 48h and then dried.

Propyltrimethoxysilane (nPTMS)-functionalization of powdered (dried) Stöber SiO_2 nanoparticles

SiO_2 nanoparticles (0.220g) were dispersed in ethanol (5ml). 0.015g of imidazole was added and the mixture allowed to stir at room temperature for 48h and then dried. The dried SiO_2 nanoparticles (0.2g) were dispersed in toluene (5ml) in a 20ml

two-necked flask equipped with a refluxing condenser and a stirrer. Propyltrimethoxysilane (nPTMS) - (0.015g) functionalizing agent ~1 drop was added with continuous stirring. The mixture was refluxed for 6h after which the product was filtered off, washed with toluene and ethanol and dried at 60°C for 6h. Results shown in Figure 6.2.ii.

3,3,3-Trifluoropropyl)trimethoxysilane-functionalization of powdered (dried) Stöber SiO_2 nanoparticles

SiO_2 nanoparticles (0.220g) were dispersed in ethanol (5ml). 0.015g of imidazole was added and the mixture allowed to stir at room temperature for 48h and then dried. The dried SiO_2 nanoparticles (0.2g) were dispersed in toluene (5ml) in a 20ml two-necked flask equipped with a refluxing condenser and a stirrer. 3,3,3-Trifluoropropyl)trimethoxysilane (0.015g) functionalizing agent ~1 drop was added with continuous stirring. The mixture was refluxed for 6h after which the product was filtered off, washed with toluene and ethanol and dried at 60°C for 6h. Results recorded in Figure 6.2.iii.

3-(Methacryloxy)propyl]trimethoxysilane (MPTMS)-functionalization of powdered (dried) Stöber SiO_2 nanoparticles

SiO_2 nanoparticles (0.220g) were dispersed in ethanol (5ml). 0.015g of imidazole was added and the mixture allowed to stir at room temperature for 48h and then dried. The dried SiO_2 nanoparticles (0.2g) were dispersed in toluene (5ml) in a 20ml two-necked flask equipped with a refluxing condenser and a stirrer. Methacryloxy)propyl]trimethoxysilane (MPTMS) (0.015g) functionalizing agent ~1 drop was added with continuous stirring. The mixture was refluxed for 6h after which

the product was filtered off, washed with toluene and ethanol and dried at 60°C for 6h. Results recorded in Figure 6.2.iv.

2.1.12 Back titration to determine particle surface coverage

APTES functionalized Stöber sphere silica back titration experiment

An APTES functionalized Stöber sphere silica sample (0.15g, 6.776×10^{-5}mol/L) was suspended in acetonitrile (4.09g, HPLC grade, see Note 1), then aqueous HCl (5.00mL, 0.100M) added. The mixture was stirred at room temperature (RT) for 1.5hours in a sealed vial and allowed to settle (2 hrs). Alternatively, the mixture could be centrifuged to save time. A sample of the supernatant solution (4.55g, which is exactly 5.00mL) was taken, diluted with 5.00mL of water, and the unreacted HCl was titrated with aqueous KOH (0.05–0.06M) using 2 drops of saturated aqueous solution of Bromocresol Green until the solution turns light-blue. Note; the volume of KOH used was compared with the volume of the blank experiment (4.09g of acetonitrile + 5.00mL of 0.100M HCl stirred for 1.5 hrs. without silica).

Calculation of the amounts of KOH and $-NH_2$ used[215]

The following points noted below need to be considered

Note 1: 4.09g of acetonitrile was used because a mixture of 4.09g of acetonitrile and 5.00 ml of 0.100 M HCl has a volume of exactly 10.0mL.

Note 2: since only 5 out of 10mL of the supernatant is titrated, the volume difference (ΔV) needs to be doubled.

Note 3: if bare silica is titrated, the surface coverage might appear slightly negative. This is a result of the residual acidity of silanol groups — they react with the titrant

(KOH) and slightly increases the volume of KOH needed for the neutralization of the acid in the mixture.

In this titration, we used 4.30 mL of 0.058M KOH (from titration), and the blank experiment (no silica) used 4.40 mL of the same KOH solution. The difference was 0.10 mL, which was due to HCl reacting with NH_2 groups on silica. The amount of KOH in 0.10 mL of its 0.0575M solution was 0.0001 L x 0.0575 mol/L = 0.00000575 mol = 0.00575 mmol. The equations are as shown below:

$$-NH_2 + HCl \longrightarrow -NH_3Cl$$

$$KOH + HCl \longrightarrow KCl + H_2O$$

Since we used only half of the supernatant for the titration (5.00ml out of 10.00ml), the amount of HCl reacted with the total amount of silica was twice as large, i.e., 0.00575mmol x 2 = 0.0115mmol.

This implies there was 0.0115mmol of NH_2 groups on 133mg (actual mass weighed out) = 0.133g of silica. This implied the amount of $–NH_2$ used was 0.0115mmol / 0.133g = 0.0865mmol/g, or approximately 0.09mmol/g.

2.2 Instrumental techniques

When analyzing mixtures and Stober silica nanoparticles there is no single technique that can be applied, so it is useful to use a variety of techniques. Some of the instruments and procedures used for this thesis are briefly described below.

2.2.1 Nuclear magnetic resonance - NMR (^{1}H, ^{13}C, and ^{29}Si)

^{29}Si NMR spectra were performed in a $CDCl_3$ medium using a JEOL EX 400 NMR spectrometer at 79.3 MHz (^{29}Si) at a temperature of about $25^{0}C$. Tetramethylsilane $(CH_3)_4Si$) (TMS) and deuterated chloroform ($CDCl_3$) were used as the standard substance for the chemical shifts (δ) obtained in each spectrum. Carbon and proton NMR were analyzed with a JEOL Lambda 300 NMR spectrometer using; ^{13}C NMR (75.4 MHz, $CDCl_3$) and ^{1}H NMR (99.98MHz, $CDCl_3$) respectively. The pulse delay for ^{29}Si NMR spectra were standardized at 20 seconds in order to minimize (negative) nuclear Overhauser effects unless stated otherwise. The spectral data point position of these compounds was accurately located before acquisition. Coupling constants for all spectra are reported in Hertz (Hz).

2.2.1.1 Carbon NMR Analysis

The most abundant carbon isotope ^{12}C has no overall nuclear spin, having an equal number of protons and neutrons. The ^{13}C isotope however does have spin 1/2, but is only 1% abundant. ^{13}C NMR has a chemical shift range of about 220 ppm, normally expressed relative to the ^{13}C resonance of TMS corresponding to a frequency range of 20-100 MHz, for typical spectrometers. About 5-20 mg of the resin sample was taken and dissolved in 0.4 - 2 ml of solvent (normally $CDCl_3$); a good spectrum was obtained with between 64 - 6400 scans.

2.2.1.2 Proton NMR analysis

In contrast to carbon, proton spectra tend to be much more complicated in appearance due to the smaller chemical shift range found for typical compounds (20 ppm at most), and the wide variation in the magnitude of the coupling constants [115].

2.2.1.3 Silicon ^{29}Si NMR analysis

^{29}Silicon is a low sensitivity NMR nucleus which has spin ½ and yields sharp lines. Silicon has a wide chemical shift range between -346 to 173ppm. It is therefore good for determining the chemical environment in silicon compounds such as: Silicon, Silicates, Silanes and many more. ^{29}Si NMRs were recorded as solution and as solids. The instrument used was a Jeol DX400, the Probe was a Doty Scientific 609 with 4mm zirconium rotors, Mode: MAS-GHD (Magic angle spinning gate proton decoupling) and CP-MAS (cross-polarization magic angle spinning) with a frequency field strength of 99.3MHz.

2.2.2 FT-IR analysis

FT-IR analyses were carried out using a modern Perkin Elmer 1710 and a Nexus FTIR spectrometer instrument with an ATR (attenuated total reflectance) model embedded in the range 400-4000 cm^{-1}. For liquid and solid samples, a small drop of the liquid or powder of the solid compound was placed on the diamond crystal surface and then analyzed [96].

2.2.3 TGA analysis

Thermogravimetric analysis involves heating a sample in an inert or oxidizing atmosphere and measuring the weight. The weight change over a specific temperature range provides indications of the composition of the sample and thermal stability. Between 20 - 40 mg and 50-100mg of the sample was placed in a platinum crucible and analyzed under a nitrogen atmosphere at a heating rate of 10^0C/min over the range 100–1000^0C using a STA 1500 rheometric scientific

instrument. The TGA curve indicates the percentage weight loss as a function of increasing temperature [216, 217].

2.2.4 DSC analysis

Differential Scanning Calorimetry (DSC) measures the temperatures and heat flow associated with transitions in materials as a function of time and temperature. It provides qualitative and quantitative information about physical and chemical changes in heat capacity using minimal amounts of sample. DSC samples were analyzed using a Toledo DSC 822. A small amount of sample of about 10-15mg was placed into an aluminum pan with a sealed lid. This pan was then placed into the DSC unit and heated from -25^{o}C to 150^{o}C at 10^{o}C/min and between 200-600^{o}C at 20^{o}C/min using argon gas at a flow rate of 80ml/min [218, 219, 220].

2.2.5 UV-Vis analysis

UV/Vis spectroscopy was used in this research for the quantitative determination of different organic and inorganic analytes. The UV-Vis instrument used was a UV-310PC spectrophotometer with a reflectance attachment. 4μl of each sample was dissolved (using the GC syringe) into 2 mL of hexane. The solution was mixed with a new and clean pipette to dissolve the analyte and obtain a homogeneous solution. This was then placed into a transparent micro-cuvette and analyzed in the spectrophotometer. The UV-Vis spectra of the samples were measured in the 200-650 nm wavelength range [221, 97].

2.2.6 HPLC MS and HPLC UV

HPLC is a chromatographic technique used to separate a mixture of compounds with the purpose of identifying, quantifying and purifying the individual components of the mixture [222,223]. 4μl of the sample was dissolved (using a micro-pipette) into 2 mL of acetonitrile. The solution was mixed with a new and clean pipette to dissolve the analyte and obtain a homogeneous solution. Following method development, the sample was placed into an HPLC vial and analyzed in the autosampler at a flow rate of 0.2ml/min using a mass spectrometer and a photo diode array (PDA) detector for one system. The two HPLC systems used were:

an Agilent Technologies 1260 Infinity equipped with 1260 binary pump, 1260 ALS auto sampler, 1260 TCC oven and 1260 DAD detector along with OpenLab CDC and Chemstation software.

HPLC-UV were performed on a SCI-TEK 2695 chromatographic instrument using a photodiode array (PDA) detector 996.

HPLC-MS, An autotune was performed prior to use and the software was Xcaliber.

2.2.7 MALDI-TOF MS and ESI-MS analysis

Two types of Mass Spectrometric analysis have been used in this research: MALDI-ToF and ESI-MS. In this research, the Mass Spectrometric analyses of silsesquioxane resins has been carried out by the EPSRC National Mass Spectrometry Service Centre at University of Wales in Swansea.

In **MALDI-ToF** most of the laser energy is absorbed by the matrix, which prevents unwanted fragmentation of the molecule [224, 225]. The method is used for detection and characterization of small and large molecules such as my polymeric samples which tend to be fragile and fragment when ionized by more conventional ionization

methods. MALDI-ToF MS and ESI-MS are very similar in character in their relative softness and the ions produced [226]. The samples were analyzed by MALDI in DCM/MeCN solvent, LiCl and $AgNO_3$ additives, and in positive-reflectron mode. The samples were solubilized in THF and analyzed by +ve MALDI using a Dithranol matrix with an additive of either LiCl or NaI.

ESI-MS were also carried out by the EPSRC National Mass Spectrometry Service Centre at University of Wales in Swansea. The samples were analyzed by positive nano-electrospray MS. The instrument used was a LTQ Orbitrap XL which runs routinely at a resolution of 100,000 and is calibrated before each analysis set to be accurate to <3ppm. Sample were solubilized in DCM/MeCN and analyzed with minimal exposure to air/moisture.

2.2.8 GC-MS

GC-MS is a method that combines the features of gas-liquid chromatography and mass spectrometry to identify different substances within a test sample. Gas chromatography separates the components of a mixture, and mass spectrometry characterizes each of the components individually.

The GC-MS system used was an Agilent Technologies 6890N gas chromatography system fitted with a thermo Sc TG-5MS 15mx0.25um column with an Agilent 5973 mass selective detector. The GC injector was operated in a split mode (20:1) at a temperature of 250^0C and with a column flow rate of 1.1ml/min. The oven temperature was held at 30^0C for 2 min and then programmed to rise to 250^oC at 5^oC/min. An autotune was performed prior to being used. About 4μl of the sample was dissolved (using a micro-pipette) into 2 mL of hexane before analysis.

2.2.9 Viscometer

The viscosity measurements were carried out by myself at TWI Ltd; our industrial collaborators. The viscosity was measured using a Brookfield Model DV-11 viscometer, using spindle number 61. A viscometer measures the viscosity of liquids. The liquid, in this case the silsesquioxane resin, remains stationary and the spindle moves through it. Different spindles are used according to the thickness of the resin/fluid. As the spindle rotates, the drag caused by relative motion of the fluid and a surface is a measure of the viscosity.

2.2.10 Dynamic Light Scattering (DLS)

Dynamic light scattering experiments were carried out at the University of Kent. DLS experiments were performed to determine the weighted mean particle size and the breadth of the particle size distribution (polydispersity index, PDI) [227]. This was achieved using a Zetasizer Nano (Nano-ZS) supplied by Malvern UK instruments. The z-average, number average and polydispersity were measured at 25^{o}C and at temperatures between 5°C and 70°C at a height of 0.85 cm when varied temperature analysis were needed [228].

The particle size and PDI were calculated by the instrument from a cumulant analysis. The PDI indicates the variance of the sample (dispersity) and is given in the range of between zero and one [0,1]. Low PDIs are normally less than 0.3. This means that the samples are monodisperse. Large PDIs mean the distribution is broader and this could be as a result of agglomeration. A PDI that is greater than 0.5 is usually unreliable.

Measurements using the DLS involved first carrying out a dilution versus concentration screening to find the dilution in which the particle size is not dependent on concentration. This concentration and dilution is determine by the instrument based on its internal calculations. This was done to make sure multiple scattering and particle-particle interactions are being minimized. For every sample, 3-5 sets of measurements of 12-15 scans were taken. Measurements were taken over a period of 90 seconds. Multiple videos were recorded and analyzed in batch mode to obtain good statistical data. These were then averaged to give the average particle diameter of the particles.

2.2.11 TEM-EDX

TEM is a widely used physical technique to examine materials under high magnification. It provides morphological information regarding the size and shape as well as the particle size distribution of the nanoparticles in this study. EDX was used together with the TEM to obtain the elemental composition of the particles.

TEM works by first producing beams of electrons by the electron gun. These beams are accelerated by a high voltage and then focused onto the thin sample specimen by two condenser lenses. This beam is allowed to strike the sample surface producing electrons which will be scattered by collision of the electrons with atoms in the sample. An image of the sample is formed by electrons which penetrate and pass through the sample. The various detectors connected to the TEM then take the images and this is what we see and measure using different imaging software.

Particle size measurements using transmission electron microscopy energy dispersive X-ray spectroscopy (TEM-EDX) were carried out on the unfunctionalised

and functionalized Stöber nanoparticles using a JEOL, JEM 2100, TEM running a LaB_6 (lanthanum hexaboride crystal) emitter [229, 190b]. This has a high tilt Objective polepiece. The point resolution is 0.25nm at 200kV. During the analysis, silica particles were put on a carbon grid and allowed to dry. TEM images were then obtained and the results processed using image-j software.

2.2.12 SEM

Scanning electron microscopy (SEM) was carried out using a Zeiss Supra 55VP Analytical FEG-SEM that was equipped with an Everhart-Thornley Secondary Electron Detector, variable pressure secondary electron detector mode (VPSE) and HKL electron backscattered diffraction system (EBSD). The samples were coated with gold prior to analysis to enhance the image[230].

2.2.13 GPC

GPC is a size exclusion chromatography that separate compounds or analytes according to size. In GPC, separation occurs on porous beads packed in a column (stationary phase). Smaller analytes enter the pores through a mobile phase containing solvent and stay in it causing a lengthy retention time[131]. Larger analytes go through the column quickly and elute first.

GPC was carried out on an Agilent Technologies 1260 Infinity instrument equipped with a 1260 binary column. This was the same system as the HPLC UV which was enhanced by myself (bought new refractive index detector, columns and calibration standards) to be used as a GPC. THF was used as the mobile phase, at 1 ml/min flow rate, at 30^{o}C, with a refractive index detector and OpenLab Agilent GPC/SEC software. The instrument was calibrated with PMMA standards between 2540 and

936000, the columns were 2 x 10µm mixed-hydrogel Waters HR1 and HR4 columns (300 mm x 7.8 mm) connected in series with a 5 µm guard column (50 mm x 7.8 mm) [231].

2.2.14 XPS

X-ray photoelectron spectroscopy (XPS) is a spectroscopic technique used to measure elemental composition of a surface of a material. XPS works by irradiation of a material with X-rays while measuring the kinetic energy and the number of electrons that escapes from the top layer (0-10nm) of the material that is being analyzed. The energy of an X-ray of each element has a particular wavelength. For example, for aluminum it is; K_α X-rays, E_{photon} = 1486.7 eV. Therefore, due to the fact that the emitted electrons' kinetic energies are measured, the electron binding energy for each emitted electron could be determined using the Ernest Rutherford's equation[232, 233].

$$E_{binding} = E_{photon} - (E_{kinetic} + Ø)$$

Where $E_{binding}$ is the electron binding energy (BE),

E_{photon} is the energy of the X-ray photons being used,

$E_{kinetic}$ is the kinetic energy of the electron as measured by the instrument (photoelectron) and Ø is the work function of the spectrometer and the material.

Silica particles were put on a carbon grid and allowed to dry on a stud. The stud was then inserted into the chamber. X-ray photoelectron spectroscopy (XPS) spectra were recorded on load-locked Kratos XSAM 800 apparatus equipped with a dual anode X-ray source, a hemispherical electrostatic electron energy analyzer and a

channeltron electron multiplier [234, 235]. The spectra were obtained using Mg Kα (1253.6 eV) radiation in the medium pass energy and fixed analyzer transmission (FAT) mode, also known as a constant analyzer energy (CAE). The entry slits of the spectrometer were set to 4mm giving a resolution of approximately 1.1eV. The high magnification analyzer mode was chosen to collect electrons from the smallest possible area on the specimen, approximately 4 mm^2. The X-ray gun was operated at 12 kV and 10 mA. The pressure in the sample analysis chamber was 10^{-9} mbar. The XPS results were then obtained and the data processed using casaXPS software.

We expect carbon contamination on the surface of all samples due to exposure to the atmosphere. We consider this contamination as adventitious carbon. We refer to this carbon peak at 285 eV and adjust the other peaks accordingly.

2.2.15 AFM

Atomic force microscopy (AFM) has been used to determine the size and nature of the silica particles, before and after each stage of modification. AFM can also determine the shape, texture and roughness of individual particles and their distribution for an aggregation of particles. This method provides a visual image of the aggregation properties. AFM images shows surface structure and can specify whether the silane on the surface has a constant spacing or not [191].

2.2.16 X-Ray Crystallography

X-ray crystallographic analysis were performed by the EPSRC X-ray crystallography service at the University of Southampton.

2.3 Materials

2.3.1 Solvents

Hexane, Toluene, Acetonitrile, THF, Methanol, Ethyl Acetate and Diethyl ether were obtained from Sigma Aldrich and dried using molecular sieve. For instrumental solvent, HPLC solvent grades were used.

2.3.2 Chemicals

All Chemicals and reagents were obtained from Sigma Aldrich Chemical Company, Gelest, ABCR and Fluorochem. Some reagents and silanes were stored in the fridge and under nitrogen.

2.3.3 Flash column chromatography

Flash column chromatography was performed using silica gel 60 (230-400 mesh) from EM Science using different solvent mixtures as those mentioned above.

Chapter 3: Understanding the mechanism of TEOS hydrolysis and condensation

This chapter focuses on the kinetics of the hydrolysis and condensation of TEOS. It includes the rate of the reaction and the overall order of the hydrolysis of TEOS. The sol-gel reaction route has been applied by varying the ratios of reagents; TEOS, water and the concentration of acid, the mechanism and rate of hydrolysis and condensation have been studied. Solution silicon nuclear magnetic resonance (^{29}Si NMR) was used to measure the silicon species formed with respect to time and the ratio of reagents. ^{29}Si NMR and Matrix-assisted laser desorption/ionization time of flight mass spectrometry (MALDI-ToF-MS) was also used to investigate the hydrolysis and condensation processes occurring during the reaction by measuring the molecular weights and the detailed structure of the species formed. Finally, a computer model was deduce and used to validate the result findings and to further extrapolate TEOS hydrolysis and condensation to compare with other literature predictions.

3.1 **Introduction**

An understanding of the effects of water and acid on the hydrolysis and condensation of tetraethyl orthosilicate (TEOS) is important in the development of different sol-gel materials for coating applications. This chapter focuses on the effects of varying the ratio of water to TEOS and the concentration of acid on the hydrolysis and condensation of TEOS, and also interprets any trends in the structural properties of the product formed [236,237,] . The sol-gel route has been applied here and by varying the ratios of water to TEOS and the concentration of acid added, the rate of hydrolysis and condensation have been studied. Acid acts as a catalyst as hydrolysis is most rapid and complete only when a catalyst is being used. Solution silicon nuclear magnetic resonance (^{29}Si NMR) was used to measure the silicon environments formed with respect to time and the ratio of reagents. Matrix-assisted laser desorption/ionization time of flight mass spectrometry (MALDI-ToF-MS) was used to investigate the hydrolysis and condensation processes occurring during the reaction by measuring the molecular weights and the detailed structure of the species formed[122,238,239,240, 241].

Hydrolysis and condensation can occur simultaneously if a high molar amount of water, acid and high temperatures are used [122,152,242, 241b]. To reduce the rate of the reaction to make it easier to monitor the hydrolysis rate, a very low concentration of acid or base catalyst needs to be used[243,240,198,185]. Similarly to slow the hydrolysis rate to monitor the reaction, less water and low temperatures or room temperature are to be used[75, 25,244] .

Although hydrolysis is generally fast, there can be a large amount of unhydrolysed or partially hydrolyzed species present; depending on the reaction conditions used,

especially the amounts of water. Therefore, the hydrolysis of TEOS does not only produce fully hydrolyzed intermediates ($Si(OH)_4$), even if the stoichiometric molar amounts of water to TEOS are being used. This has been demonstrated by Sanchez, Stöber and Hsu [122,2, 230]. Tingli and Fuxing[114a] also demonstrated that as hydrolysis occurs, the TEOS concentration decreases and other intermediate hydrolyzed TEOS species develop [24, 243, 242,240,245,].

Sakka, Schaefer and Green *et al.*[125] have reported more recently that varying the amounts of the reagents including the catalyst, leads to a substantial variation in the structure and properties of the polymer formed from linears, to cyclics, ladders and cages. These results are consistent with earlier results reported in the Stöber sol-gel process[2] and also consistent with the findings of this research. However, my work disagrees with the proposal that when the water to TEOS ratios are greater than two, the product solutions are not spinnable as reported by Brinker and Kamiya. In this research, between 1-2 molar ratios of water to TEOS, the solution is viscous but becomes less viscous at ratios of water to TEOS greater than two where the TEOS becomes deficient.

In our experiments TEOS, water and ethanol were used in high concentrations in order to get a good ^{29}Si NMR signal to noise ratio by producing sharper peaks so as to follow how the ^{29}Si NMR changes with time. Long accumulation times are needed because the presence of so many species leads to many silicon peaks with low signal to noise ratios. The acid concentration was adjusted to make the rates appropriate with long accumulation times, but also to make the rates quick enough to be measurable. The ^{29}Si NMR peak heights do not correlate directly with silicon concentration so there is a degree of approximation. The silicon environments on

individual compounds are measurable and a single compound may have many silicon environments [246].

The silicon environments from the NMR have been assigned based on the chemical shift correlation data of Sugahara *et al.* (1992)[120] and Schmidt *et al.* (1984)[121] as referenced by Sanchez et al.[122], and as predicted in this study (**Table 3.1**). The reason for the slight difference in chemical shift of about 1ppm could be as a result of using different solvent systems and higher stock concentrations. Quantification was achieved by measuring peak heights and then comparing the ratios as a percentage of the total sum of the peak heights. The various silicon environments are distinguished by their degree of hydrolysis (number of OH groups) which is the superscript (a), and condensation (number of other silicon atoms attached to the main silicon) which is the subscript (b) leading to Q_b^a. Q indicating a tetrahedral central silicon bonded to four oxygen atoms.

Table 3.1: Chemical shift assignments

chemical shift of peak as in literature (ppm)	Chemical shift as observed (ppm)	Proposed species/environments
-74	-73	Q_0^3
-76	-75	Q_0^2
-78	-78	Q_0^1
-82	-81	Q_0^0
-84	-83	Q_1^2
-86	-85	Q_1^1
-89	-87	Q_1^0
-91	-92	Q_2^2
-93	-93	Q_2^1
-95	-94	Q_2^0
-100	-100	Q_3^1
-102	-102	Q_3^0

Assignment based on Sugahara[120] and Schmidt[121] *et al.* as shown in Sanchez *et al.* [122] and new assignments that originate from this research.

If TEOS is Q_o^0, the TEOS intermediate species formed go from Q_o^1 which is TEOS with one hydroxyl group, followed by Q_o^2, Q_o^3 and Q_o^4 with subsequent increase in the number of OH groups attached to the central Si atom[121, 186, 247, 185] **(Figure 3.1).** In the ^{29}Si NMR, the peaks arising from Q_o^0 to Q_o^3 appear from -81 to -73 respectively[248, 230, 243]. Low concentrations of acid enable the accumulation of enough scans to be able to get a reasonably good signal to noise ratio, repeated over a given amount of time.

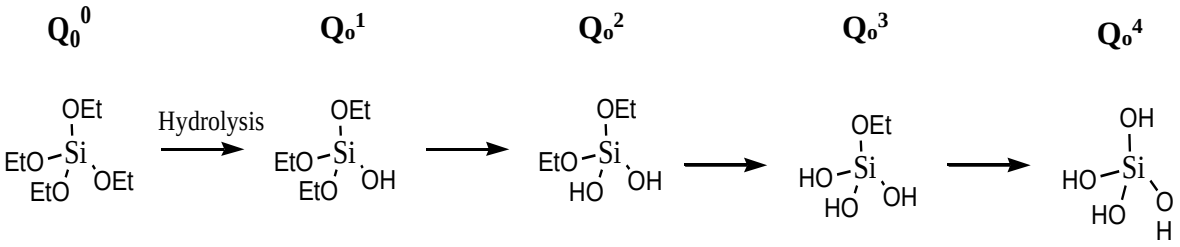

Figure 3.1. Q-environments of silicon species formed from hydrolysis of TEOS.

The aim of this study was to understand the processes of TEOS hydrolysis and condensation and hence study the various species that are formed. This approach uses very low amounts of acid and hence the process could be slowed down such that each step of the process could be understood and followed through using different instrumentation.

3.2 The process and mechanism of hydrolysis and condensation of TEOS

A kinetic study of TEOS hydrolysis using ^{29}Si solution NMR shows that hydrolysis occurs before condensation[249,250,213,251,252]. In other words, initially hydrolysis is faster than condensation[253,172, 153,254]. A pseudo equilibrium is reached which is the point where no further hydrolysis nor condensation appear to take place[255, 256, 29, 70, 257]. To understand this kinetic behavior, different molar ratios of TEOS, water and acids have been used in this study.

Generally and as observed, with very low amounts of reactants (for example water), one can go from Q_o^0 to Q_o^1 as shown in the equation below.

$$Q_o^0 + H_2O \longrightarrow Q_o^1 + ROH$$

With slightly more water, Q_o^1 is further hydrolyzed through to Q_o^2 and then to Q_o^3.

$$Q_o^1 + H_2O \longrightarrow Q_o^2 + ROH$$

$$Q_o^2 + H_2O \longrightarrow Q_o^3 + ROH$$

As the molar ratio of water to TEOS is continuously increased more Q_1, Q_2 and Q_3 species are observed over time [70, 71, 72, 73].

From this experiment and literature findings (Sanchez *et al.*[25] and other scientists), the hydrolysis of TEOS leads to partially hydrolyzed intermediates [243,172,258]. However, further condensation of the partially hydrolyzed intermediates leads to the formation of complex species involving Q_1^1, Q_1^2 and Q_2^2 environments [259, 260, 261]. See the **Experimental section 2.1** for details of the reaction procedure. **Appendix 1** shows the raw data for the hydrolysis and condensation of TEOS. That is, the ^{29}Si NMR results of all the TEOS kinetics together with the plots corresponding to the conditions shown in **Tables 3.2 and 3.3**.

Table 3.2: Reactant compositions by varying the molar ratio of TEOS to water

TEOS:water ratios	**[Water] mol/L**	**[TEOS], mol/L**	**[CF_3SO_3H], mol/L (catalyst)**	**[EtOH], mol/L**	**Timescale for data collection**
1TEOS:0.5H_2O	1.66	3.13	$2.29x10^{-4}$	10.31 in excess	1–7 hr. 2hr scan 8-20hr. 4hr scan >20 4-7hr scan
1TEOS:1H_2O	1.66	1.66	$2.29x10^{-4}$	10.53	1–7 hr. 2hr scan 8-20 hr. 4hr scan >20 4-7hr scan
1TEOS:1.5H_2O	1.66	1.13	$2.29x10^{-4}$	13.07	1–7 hr. 2hr scan 8-20 hr. 4hr scan >20 4-7hr scan
1TEOS:2H_2O	1.66	0.78	$2.29x10^{-4}$	13.41	1–7 hr. 2hr scan 8-20 hr. 4hr scan >20 4-7hr scan
1TEOS:2.5H_2O	1.66	0.66	$2.29x10^{-4}$	15.33	1–7 hr. 2hr scan 8-20 hr. 4hr scan >20 4-7hr scan
1TEOS:3.0H_2O	1.66	0.53	$2.29x10^{-4}$	15.60	1–7 hr. 2hr scan 8-20 hr. 4hr scan >20 4-7hr scan
1TEOS:3.5H_2O	1.66	0.47	$2.29x10^{-4}$	15.93	1–7 hr. 2hr scan 8-20 hr. 4hr scan >20 4-7hr scan
1TEOS:4.0H_2O	1.66	0.40	$2.29x10^{-4}$	16.20	1–7 hr. 2hr scan 8-20 hr. 4hr scan >20 4-7hr scan

NB: Where TEOS:water ratio represents the molar amounts of TEOS:water.

Table 3.3: Varying the concentration of the acid (CF_3SO_3H) to determine the rate of TEOS hydrolysis and condensation.

TEOS:water ratios	**[CF_3SO_3H],M (catalyst)**	**[Water],M**	**[TEOS],M**	**[EtOH],M**	**Timescale for data collection**
1TEOS:2.0H_2O	$4.81x10^{-5}$	1.66	0.78	13.41	1–5hr 1hr scan 6-9 hr. 2hr scan
1TEOS:2.0H_2O	$9.62x10^{-5}$	1.66	0.78	13.41	1–5hr 1hr scan 6-9 hr. 2hr scan
1TEOS:2.0H_2O	$1.44x10^{-4}$	1.66	0.78	13.41	1–5hr 1hr scan 6-9 hr. 2hr scan
1TEOS:2.0H_2O	$1.92x10^{-4}$	1.66	0.78	13.41	1–5hr 1hr scan 6-9 hr. 2hr scan
1TEOS:2.0H_2O	$2.29x10^{-4}$	1.66	0.78	13.41	1–5hr 1hr scan 6-9 hr. 2hr scan

3.3 Results from the hydrolysis and condensation of TEOS

Different experimental techniques have been used to monitor and analyze the reactions from **Table 3.2** and **Table 3.3**. The disappearance of the TEOS peak and the formation of various silicon environments were monitored using two of the most applicable techniques; ^{29}SiNMR and MALDI-ToF-MS. The ^{29}Si NMR results are shown in **Figures 3.3** (a, b, c, d, e, f, g, h). MALDI-ToF-MS was also used to analyze molar masses of some of the species formed during the reaction and the results are shown in **Figure 3.4**. These results are further discussed in the discussion section.

3.3.1 ^{29}Silicon NMR results

^{29}Si NMR results monitoring the effects of increasing the ratio of TEOS to water on the hydrolysis and condensation of TEOS and the trend of the species formed are shown in **Figure 3.3** (a, b, c, d, e, f, g, h). The insets show trends at pseudo equilibrium.

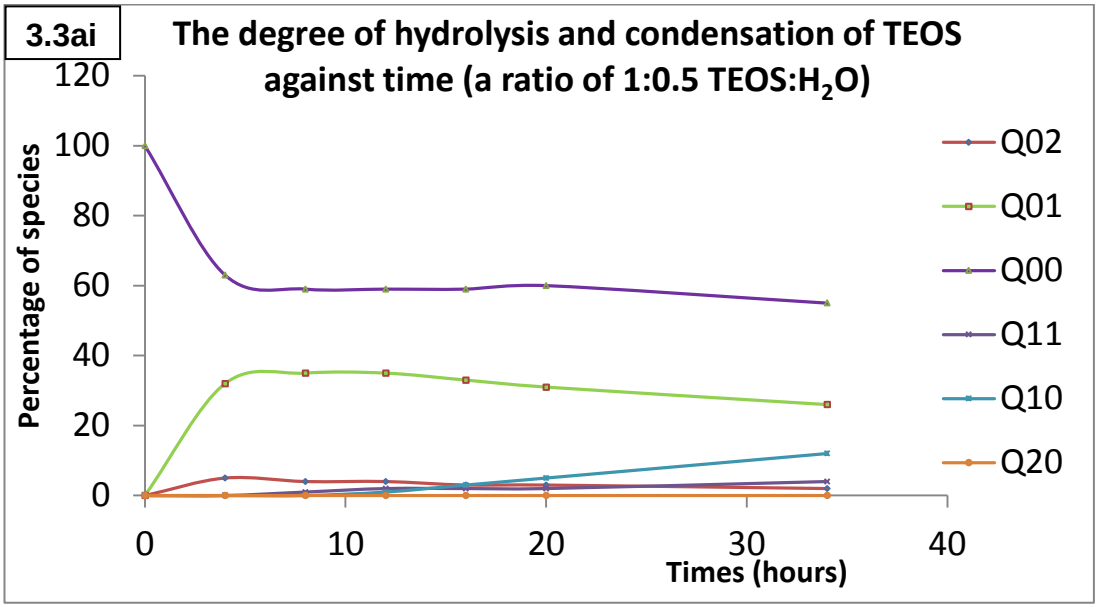

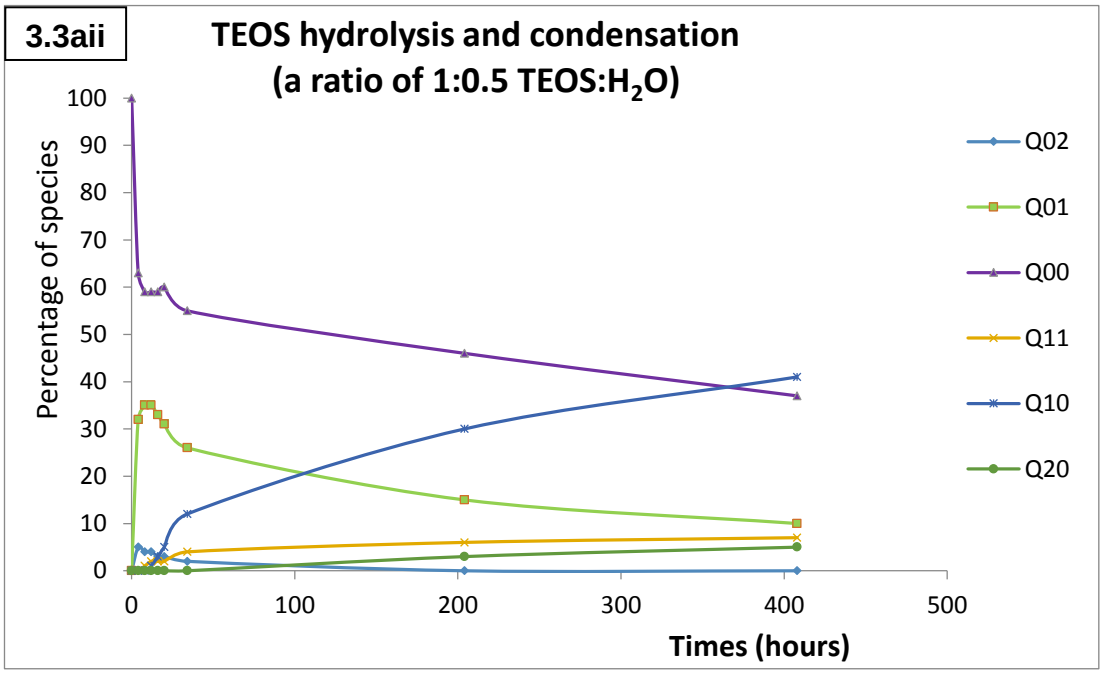

A ratio of TEOS:H_2O of 1:0.5 (Appendix 1)

In **Figure 3.3a**, 50% hydrolysis of the TEOS is quickly observed to give mainly Q_0^1 species with some Q_0^2. The Q_0^1 condenses to give Q_1^0 as does Q_0^2 to give Q_1^1. No Q_0^3 is observed in this reaction. This implies that there is no water remaining otherwise this species would be present. Finally, the Q_1^0 and Q_1^1 species are fairly stable and Q_1^1 do not condense further on this timescale.

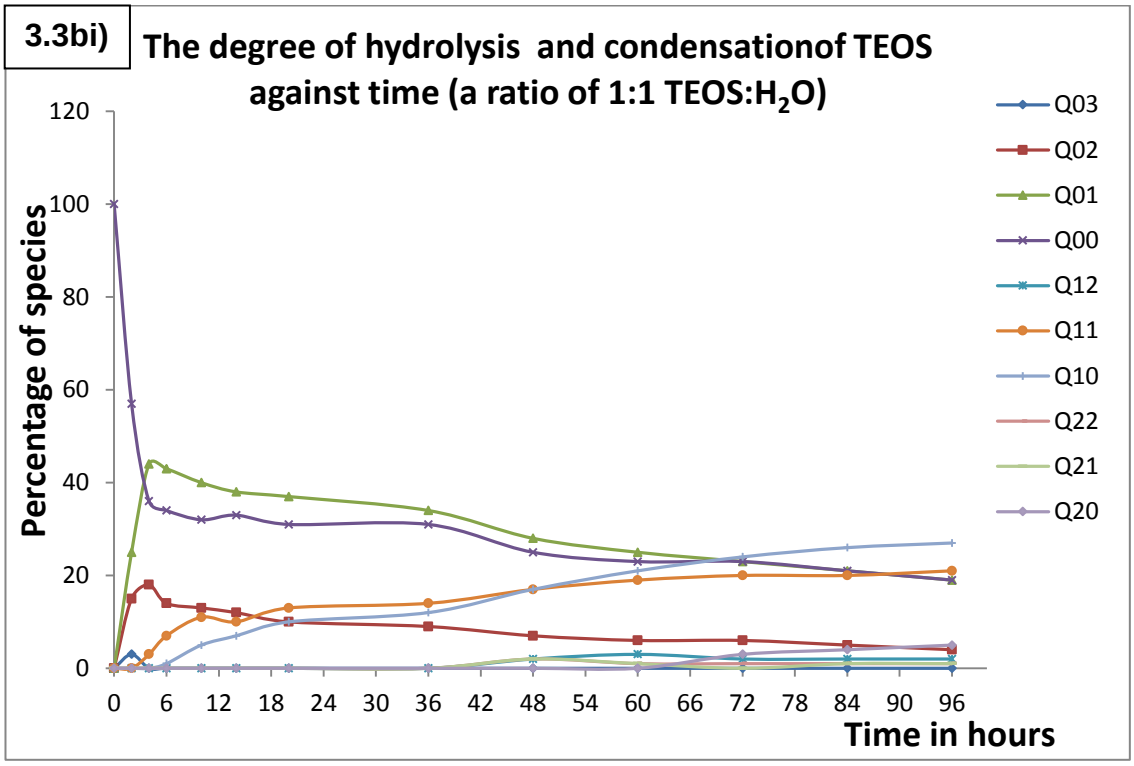

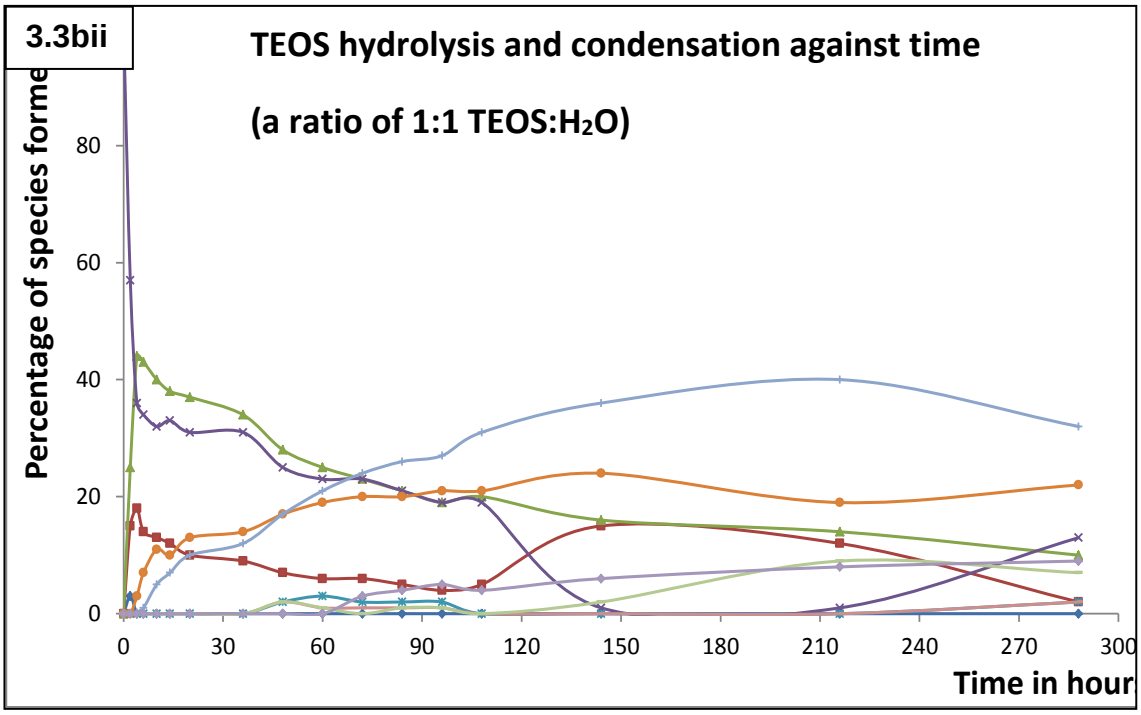

A ratio of TEOS:H_2O of 1:1 (Appendix 1)

In this case there is greater hydrolysis than when using a 0.5 mol water equivalent. Q_0^1 is formed quickly but then, it slowly decreases. Q_1^0 begins to rise really quickly. Q_0^2 Increases but then it plateaus afterward. That is, its formation from Q_1^0 is matched by the formation of Q_1^1. Q_1^1 increases and does not undergo further

condensation on this timescale. Q_0^3 begins to appear. Finally, TEOS is nearly 75% used up.

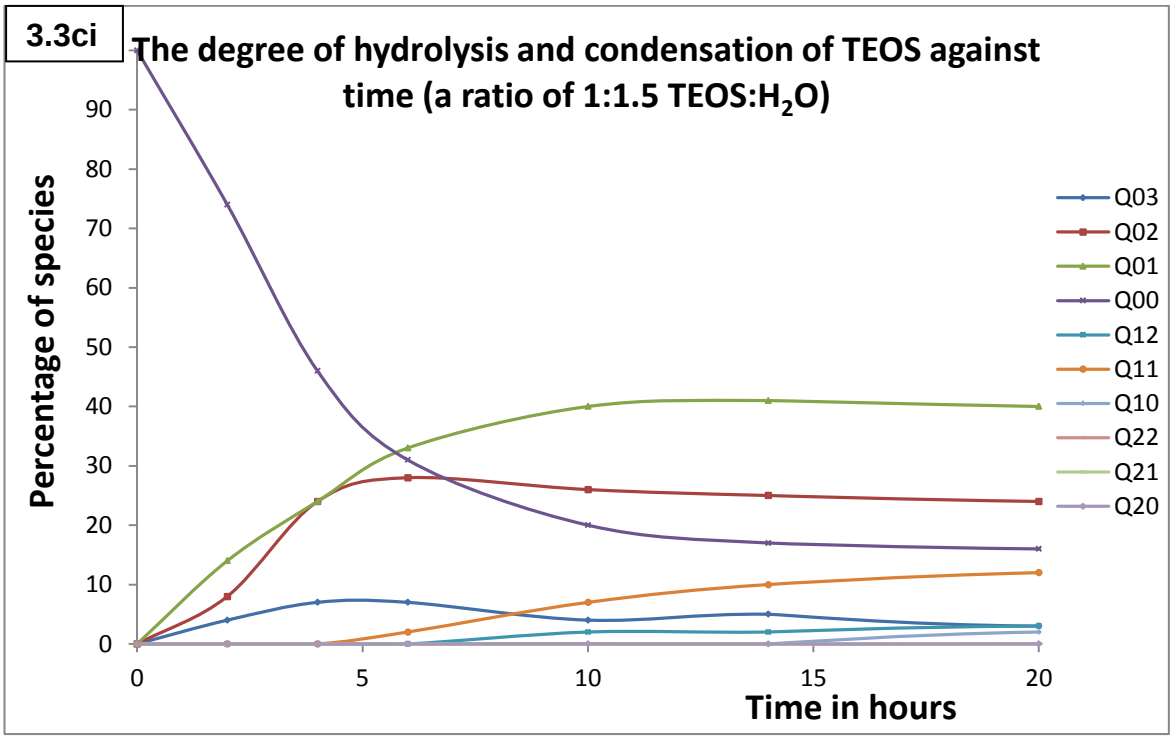

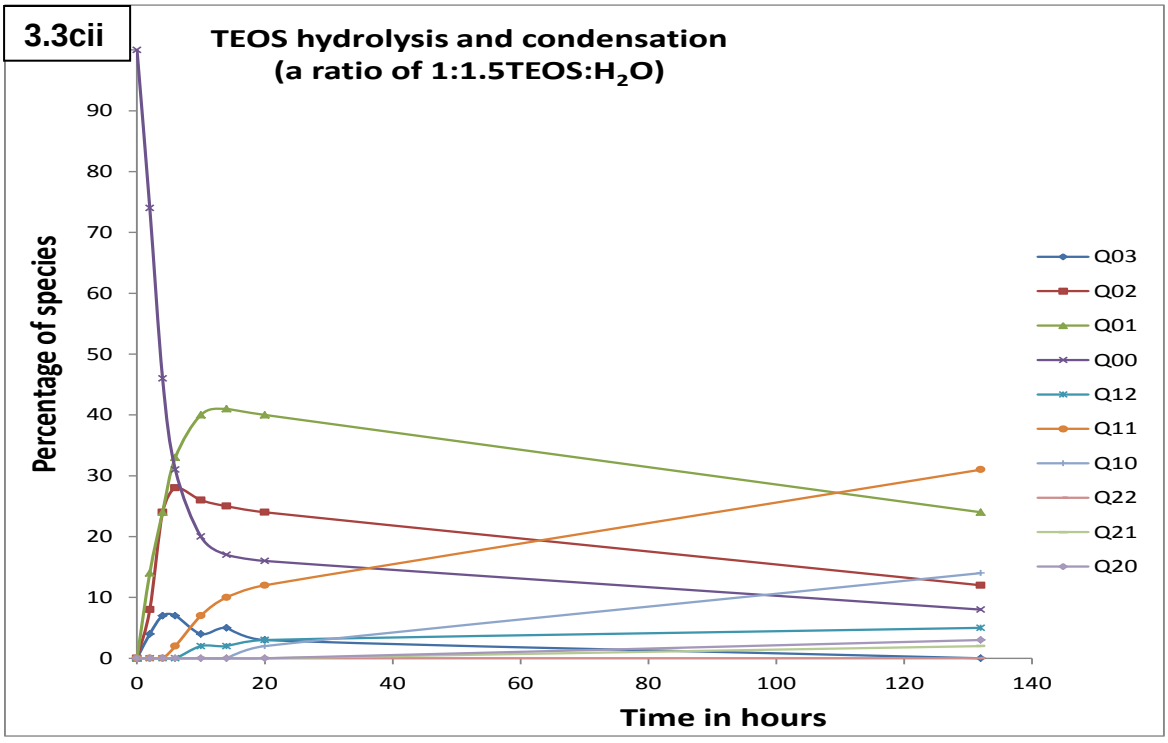

A ratio of TEOS:H_2O of 1:1.5 (Appendix 1)

First, TEOS is almost completely used up. Q_0^1 is formed quickly but then it slowly decreases. Q_0^1 is the dominant hydrolysis species. Q_1^0 is not formed a lot presumably because the hydrolysis to Q_0^2 occurs more readily as there is more water for the second hydrolysis. It is also observed that Q_0^2 increases but then decreases, i.e. its formation from Q_0^1 is not as fast as the formation of Q_1^1. Q_1^1 increases consistently but because of its stability it does not react further, although a little Q_2^0 is seen. Q_0^3 increases a little more but then decreases as the Q_1^2 increases. Finally, Q_2's are observed for the first time.

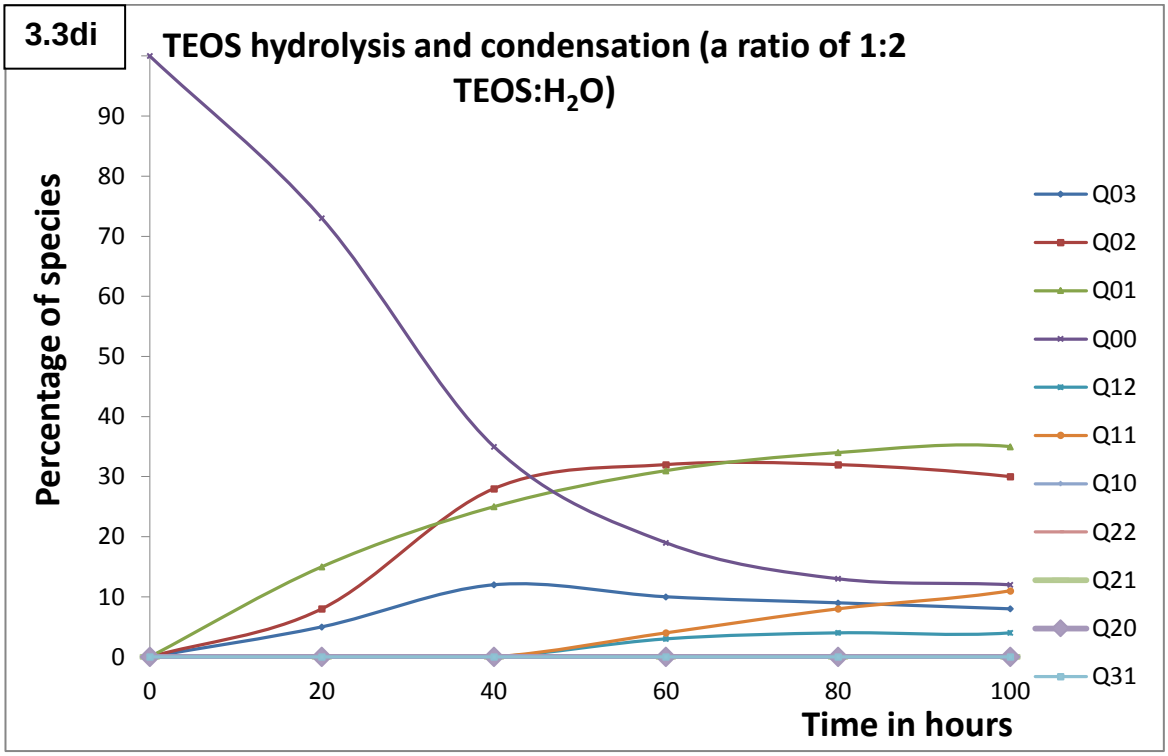

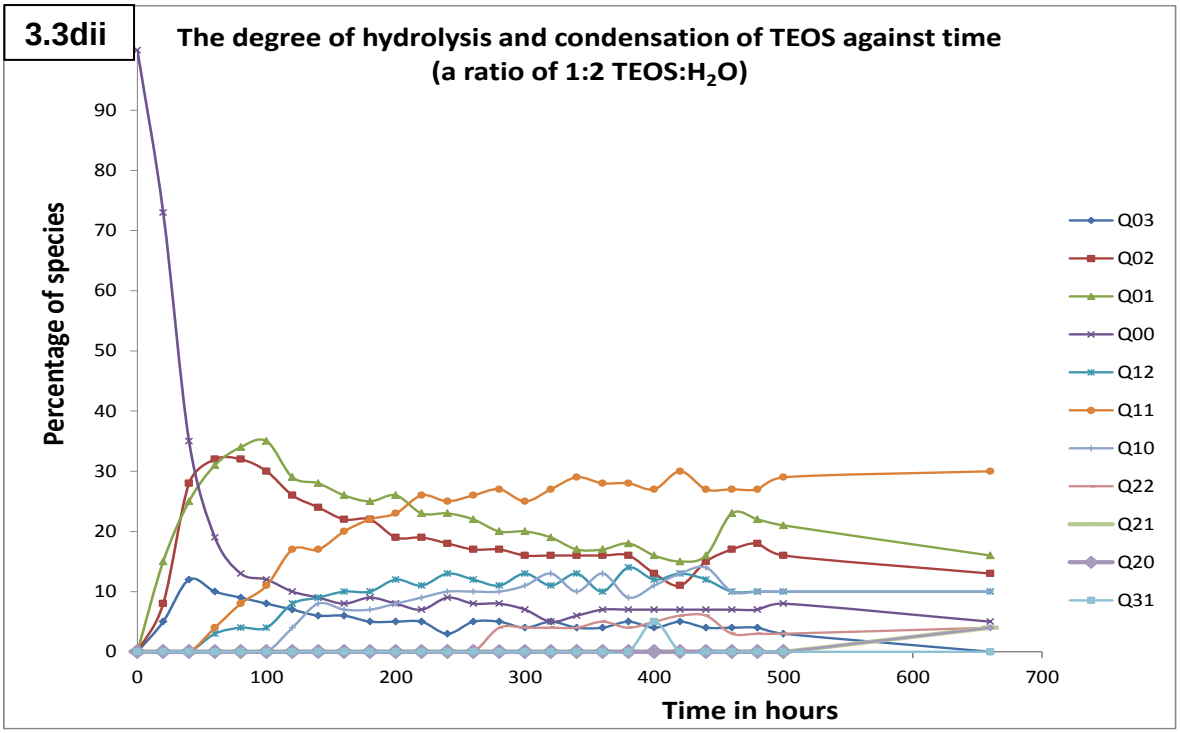

A ratio of TEOS:H_2O of 1:2 (Appendix 1)

There is clear evidence of the pseudo-equilibrium being achieved. TEOS is almost completely used up. Q_0^1 is formed quickly but then slowly decreases to the same extent as before. Less amount of Q_1^0 than previously because of the greater concentration of water. Q_0^1 is preferentially hydrolyzed to Q_0^2. Q_0^2 increases but then decreases – that is, its formation from Q_0^1 is not as fast as the formation of Q_1^1. The amount of Q_0^2 now peaks at about the same point as Q_0^1, as a result of the extra water (previously the reaction ran out of water). There is more Q_0^3 which increases but then it decreases as Q_1^2 increases. In the long term, Q_1^1 becomes the dominant species suggesting it is a particularly stable species. Again Q_2's are observed and also Q_3 are observed for the first time.

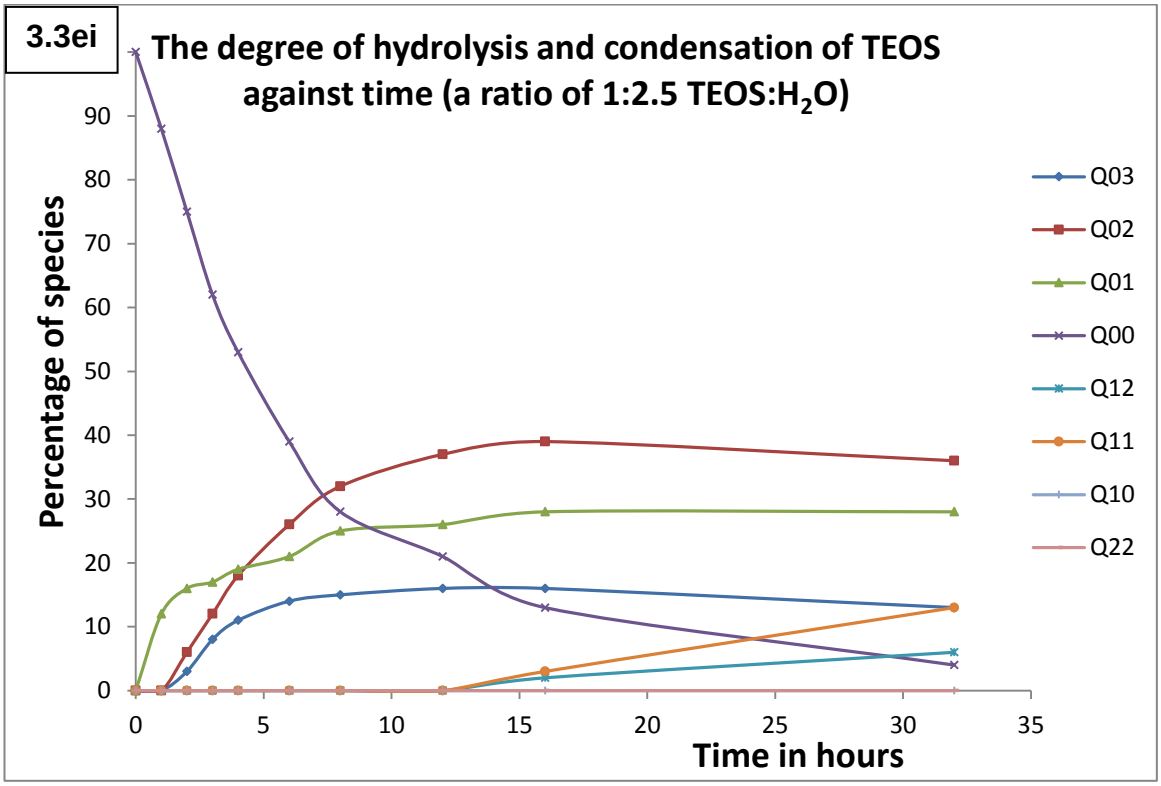

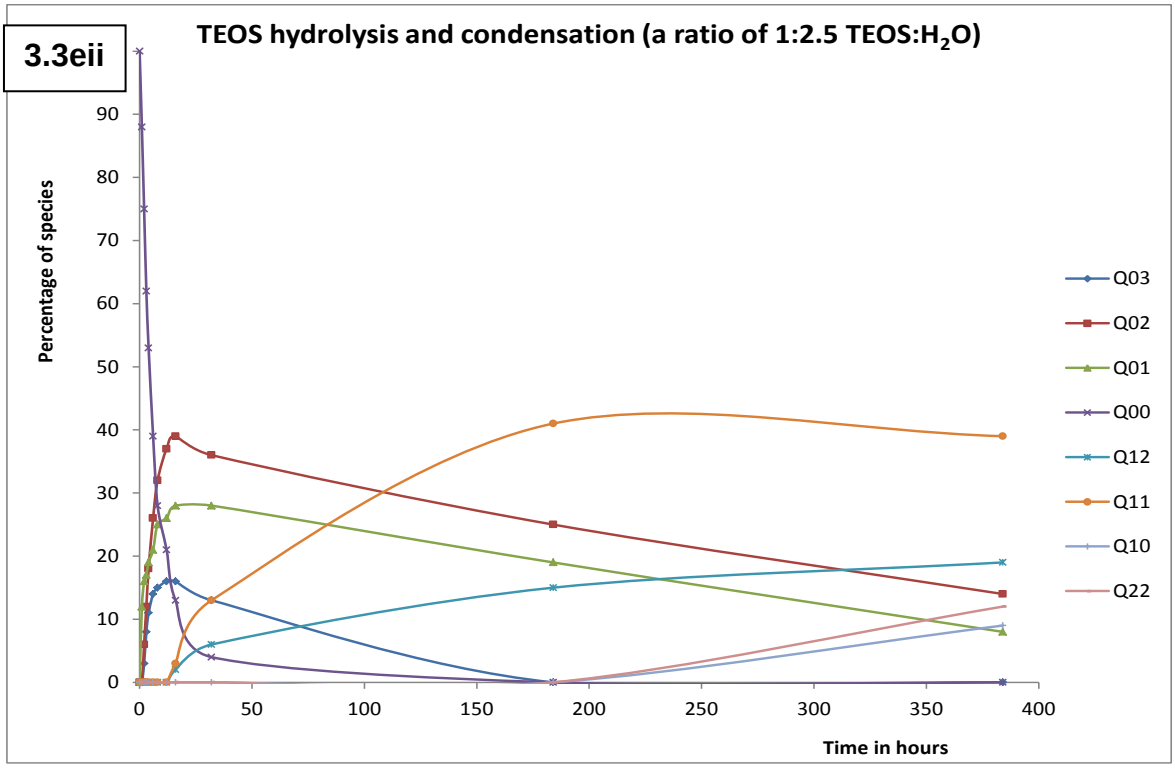

A ratio of TEOS:H_2O of 1:2.5 (Appendix 1)

TEOS is reduced to 5%. Out of the Q_0 species, Q_0^2 is now the dominant species for the first time and not Q_0^1 with a little more Q_0^3 observed. On the longer timescale,

Q_1^1 becomes the overall dominant species in the long term with more Q_1^1 and Q_1^2.

More condensation is taking place such that Q_2^2 starts to become more prominent.

3.3fi

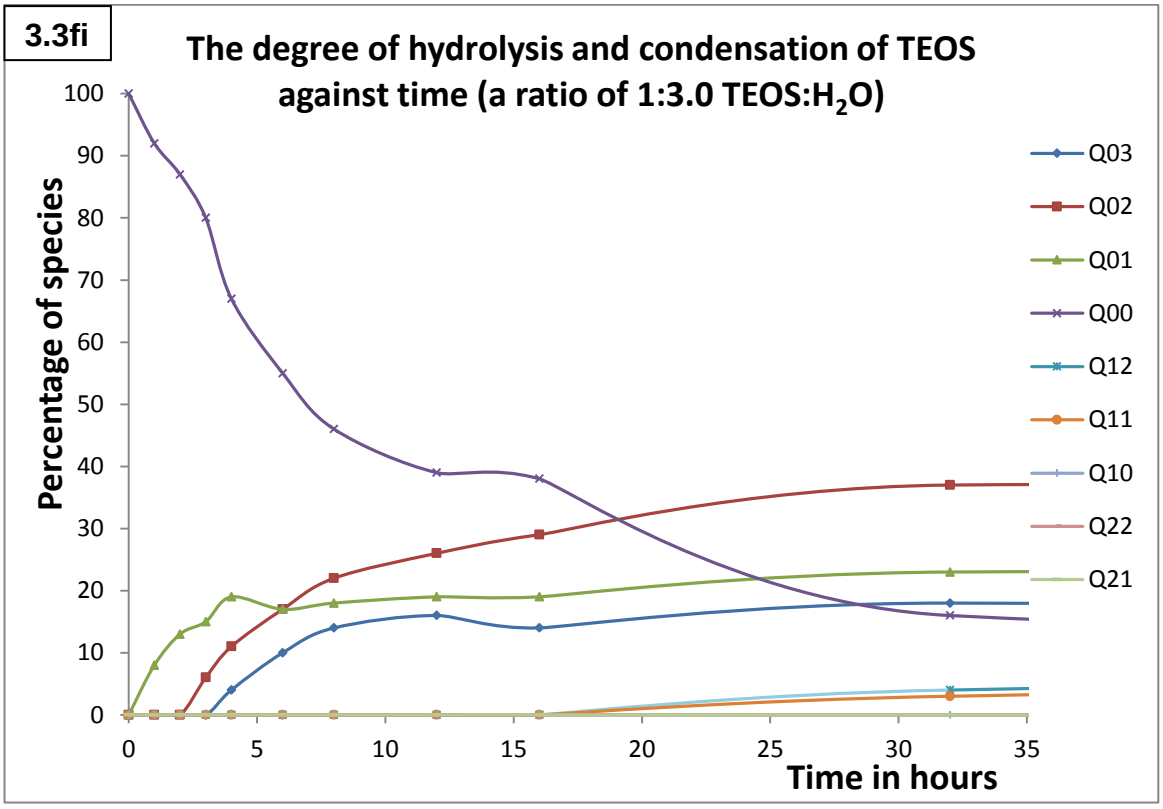

3.3fii

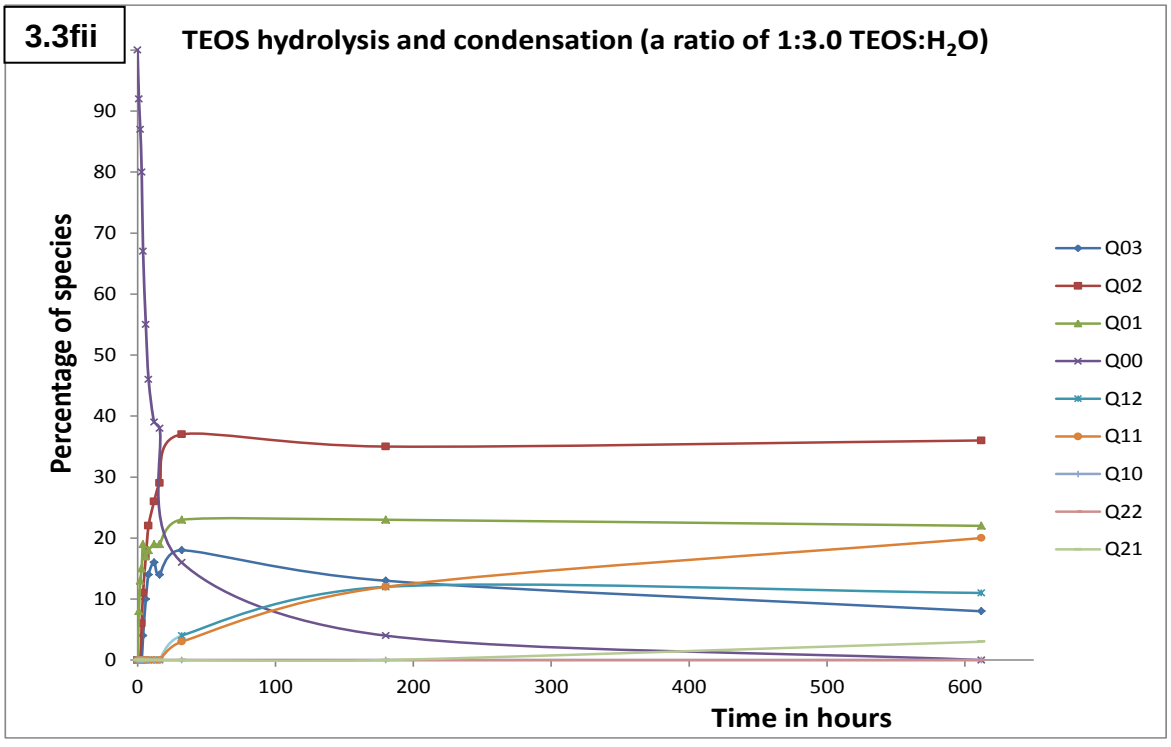

A ratio of TEOS:H_2O of 1:3.0 (Appendix 1)

Here, TEOS is completely used up very quickly. Of the Q_0 species Q_0^2 is very much the dominant species and now with levels of Q_0^3approaching those of Q_0^1. On the longer timescale condensation seems to be slowing down with less Q_1^1 and Q_1^2 formed. Less condensation seems to be occurring hence less Q_2 species. This is possibly because with excess water the back reaction starts to become favored.

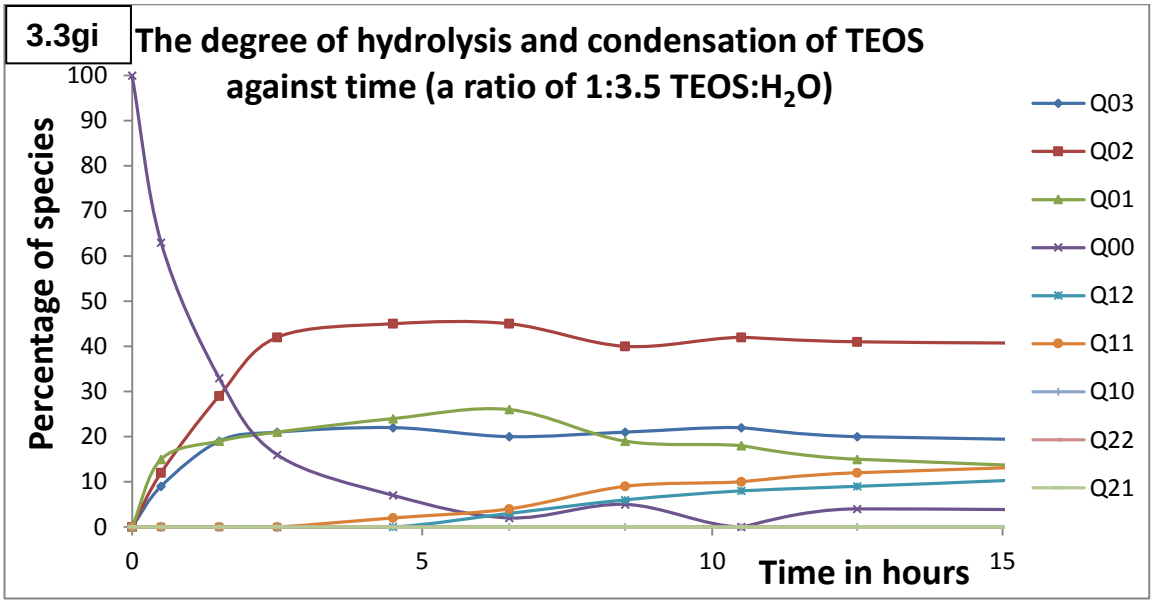

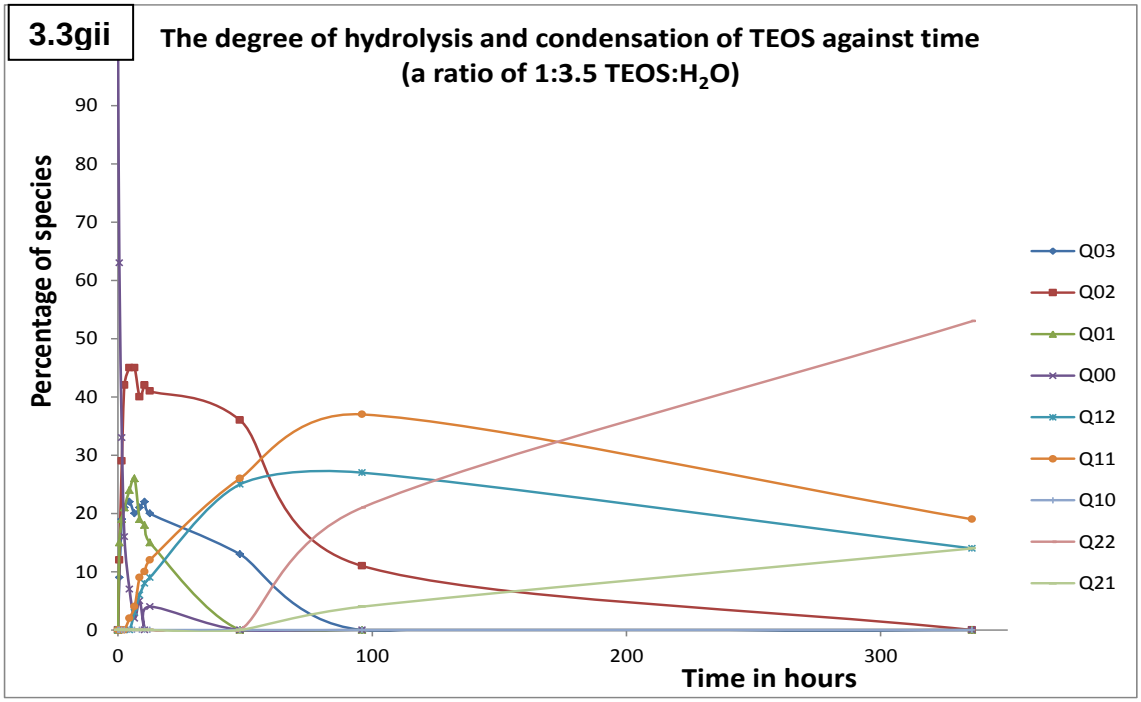

A ratio of TEOS:H_2O of 1:3.5 (Appendix 1)

This has a similar pattern to the previous 1:3.0 TEOS:H_2O. The rate of hydrolysis is fast and reaches equilibrium very quickly. Q_0^2 prevails initially with more water. However, as the TEOS gets completely saturated or used up, condensation set in with Q_2^2 becoming the dominant species in the long term for the first time, indicating more condensation occurring.

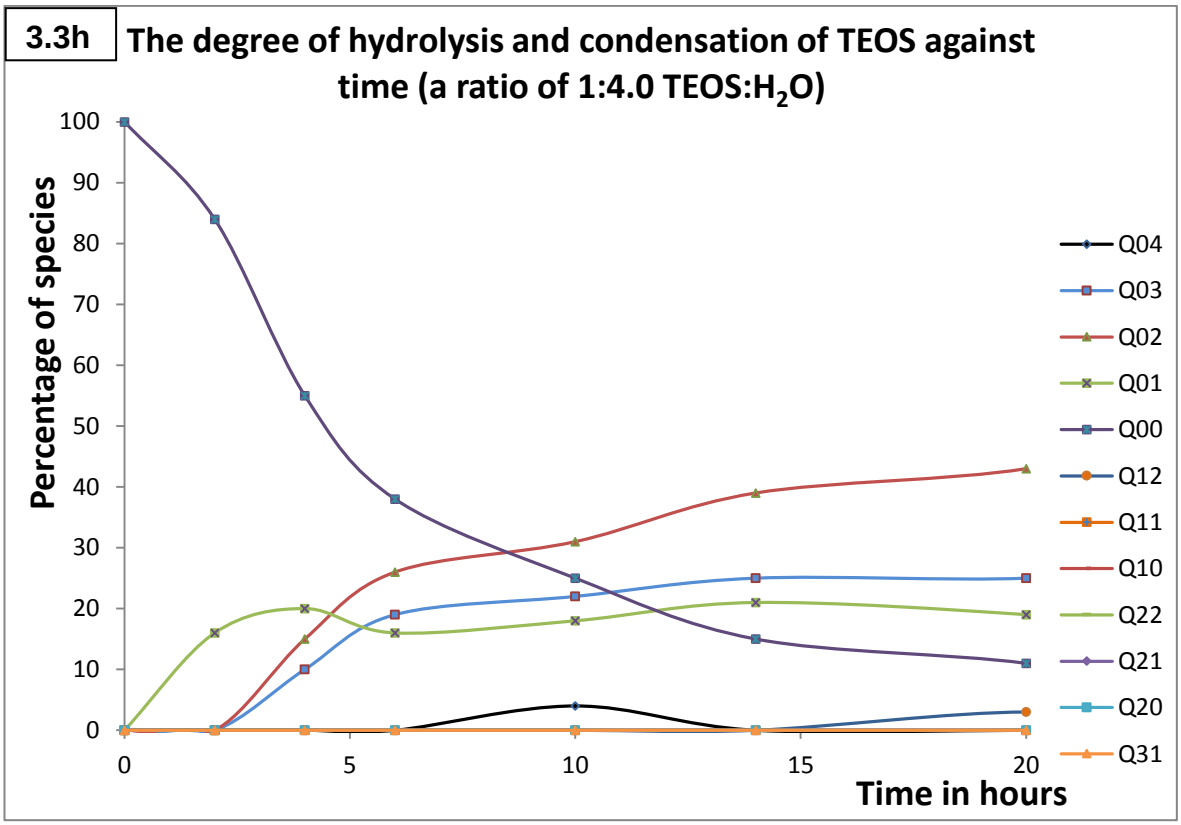

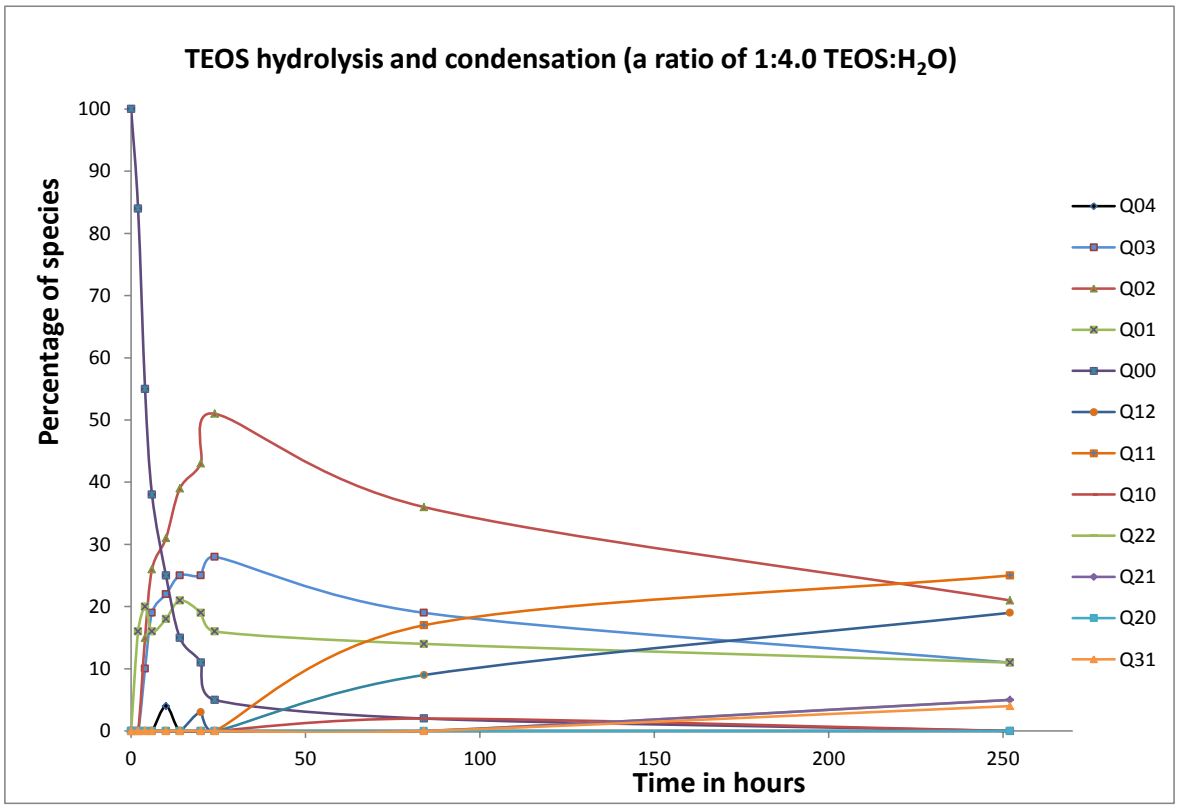

A ratio of TEOS:H_2O of 1:4:0 (Appendix 1)

Similar to 2.5 in terms of TEOS hydrolysis of the Q_0 species. Q_0^2 is now the dominant species and not Q_0^1 with a little more Q_0^3 observed. Q_1^1 is not such a dominant species here. Q_2^2 is present but in a reduced amount compare to Figure 3.3g. Q_3^1 species observed again and Q_0^4 species appeared for the first time. In the long term, Q_1^1 and Q_1^2 become dominant.

As a result of varying the ratios of the TEOS:water, hydrolysis/condensation was faster at some points so data had to be captured more frequently to accurately monitor every step of the process. Hence, the reason some plots have more data points than others.

3.3.2 MALDI-ToF MS of TEOS hydrolysis

The mass spectrometry results from the MALDI-ToF-MS shows the different species formed following complete hydrolysis using a 2 mol ratio of water to TEOS after equilibrium (X Hours) and at room temperature. The proposed species and silicon environments are shown in **Table 3.4** with their corresponding ^{29}Si NMR chemical shifts.

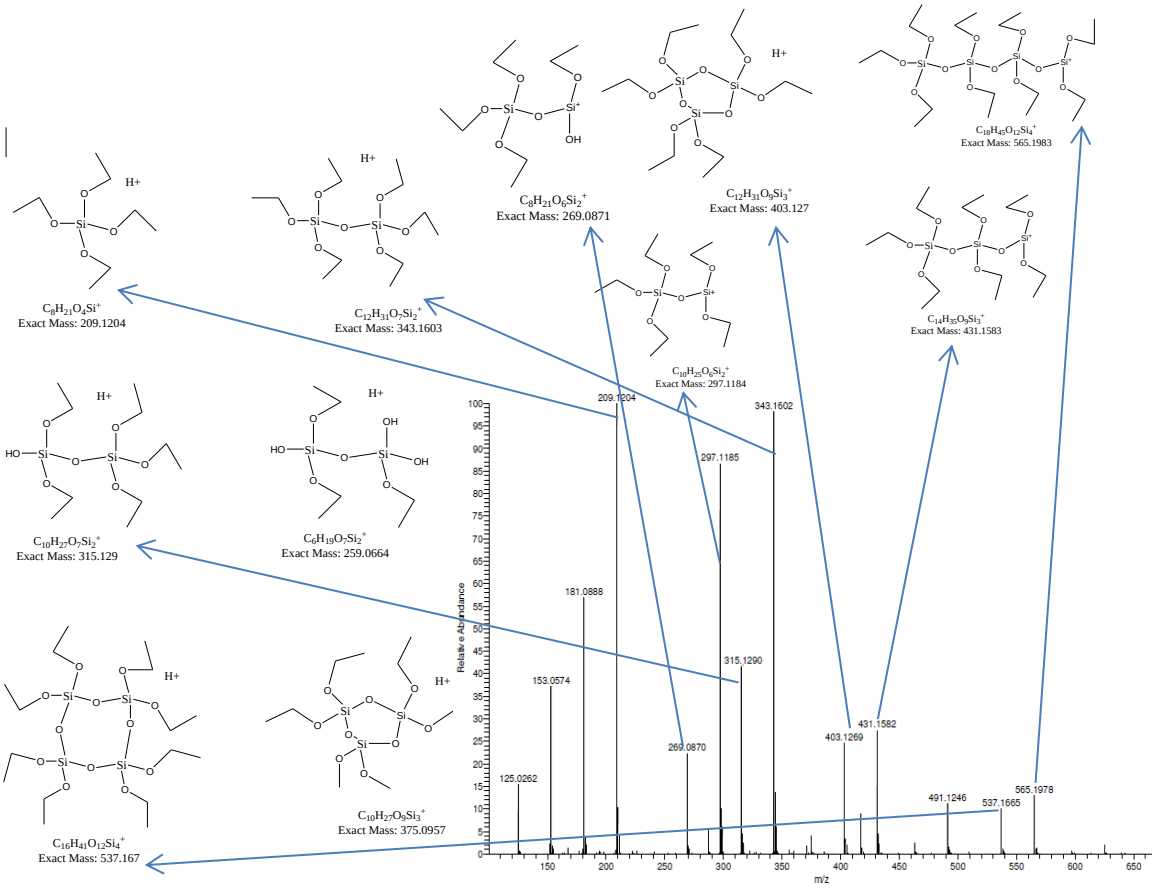

Figure 3.4. The MALDI-ToF-MS of the species formed following the hydrolysis and condensation of TEOS using 1:2 molar equivalents of TEOS and water (other isomers are not included).

From the MALDI-ToF-MS spectra in **Figure 3.4**, the ionic species were identified to correspond to the neutral species in **Table 3.4** based on the molecular masses of the molecular ion. The environments and structures of the silicon species (as in

Figure 3.4) matches the chemical shifts observed in the ^{29}Si NMR shown in **Table 3.1**.

Table 3.4. Predicted MALDI results of the different silicon environments formed using 1:2 (TEOS:H_2O) ratio in relation to the ^{29}Si NMR chemical shifts.

NMR Chemical shifts	Proposed neutral species/ environments	Ions	Mass Spectrometry (m/z of ions)
-73	Q_0^3 = $(EtO)Si(OH)_3$	Q_0^3 = $(EtO)Si(OH)_3H^+$	125.0262
-75	Q_0^2 = $(EtO)_2Si(OH)_2$	Q_0^2 = $(EtO)_2Si(OH)_2$ H^+	153.0574
-78	Q_0^1 = $(EtO)_3Si(OH)$	Q_0^1 = $(EtO)_3Si(OH)$ H^+	181.0888
-81	Q_0^0(TEOS)= $Si(OEt)_4$	Q_0^0(TEOS)= $Si(OEt)_4$ H^+	209.1204
-83	Q_1^2=$(EtO)_3Si$-O-Si$(OH)_2$ (OEt)		
-85	Q_1^1=$(EtO)_3Si$-O-Si(OH) $(OEt)_2$	Q_1^1=$(EtO)_3Si$-O-Si^+(OH) (OEt) Q_1^1=$(EtO)_3Si$-O-Si(OH) $(OEt)_2$ H^+	269.087 315.129
-87	Q_1^0 = $(EtO)_3Si$-O-Si$(OEt)_3$	Q_1^0 =$(EtO)_3Si$-O-$Si^+(OEt)_2$ Q_1^0 = $(EtO)_3Si$-O-Si$(OEt)_3$ H^+	297.1185 343.1602
-94	Q_2^0=$(EtO)_3Si$-O-Si$(OEt)_2$-O-Si$(OEt)_3$	Q_2^0=$(EtO)_3Si$-O-Si$(OEt)_2$-O-Si$(OEt)_3$ H^+ Q_2^0=$(EtO)_3Si$-O-Si$(OEt)_2$-O-$Si^+(OEt)_2$	403.1269 431.1582
-102	Q_3^0=$((EtO)_3Si$-O$)_3$-Si(OEt)	Q_3^0=$((EtO)_3Si$-O$)_3$-Si(OEt)	565.1978

NMR and MALDI-ToF MS using 1molTEOS:2mol water. NB: Only one of the possible isomers are shown.

Table 3.5 gives a general summary of the species observed on the NMR using different molar ratios of TEOS to water.

Table 3.5 ^{29}Si NMR results summarizing the silicon species formed using different ratios of water to TEOS via hydrolysis and condensation after equilibrium.

Chemical shift	Proposed species/ environments	0.5 H_2O	1.0 H_2O	1.5 H_2O	2.0 H_2O	2.5 H_2O	3.0 H_2O	3.5 H_2O	4.0 H_2O
-72	Q_0^4								√
-73	Q_0^3		√	√	√	√	√	√	√
-75	Q_0^2	√	√√	√√	√√√	√√√	√√√	√?	√√√
-78	Q_0^1	√√√	√√√	√√√	√√√	√√?	√√√	√	√√
-81	Q_0^0	√√√	√	√	√	√	√	√	√
-83	Q_1^2		√	√	√	√√√	√√	√√√	√√√
-85	Q_1^1	√	√√√	√√√	√√√	√√√	√√√	√√√	√√√
-87	Q_1^0	√√√	√√√	√√	√√	√	√	√	√
-92	Q_2^2				√	√√	√	√√√	√
93	Q_2^1			√	√	√	√	√√	√
94	Q_2^0	√		√	√	√	√	√	√
-100	Q_3^1				√	√	√	√	
-102	Q_3^0				√ ?				
-109	Q_4				√ ?				

NB: Where the mol water represent molar ratio of water to TEOS. √√√ = good amount, √√ = average, √ = small amount of species.

The spectral progress of one of the reactions (1TEOS:2H_2O as in **Experiment 2.1** is as shown below (**Figure 3.5**). This figure shows the evolution of the species with time as the reaction progresses.

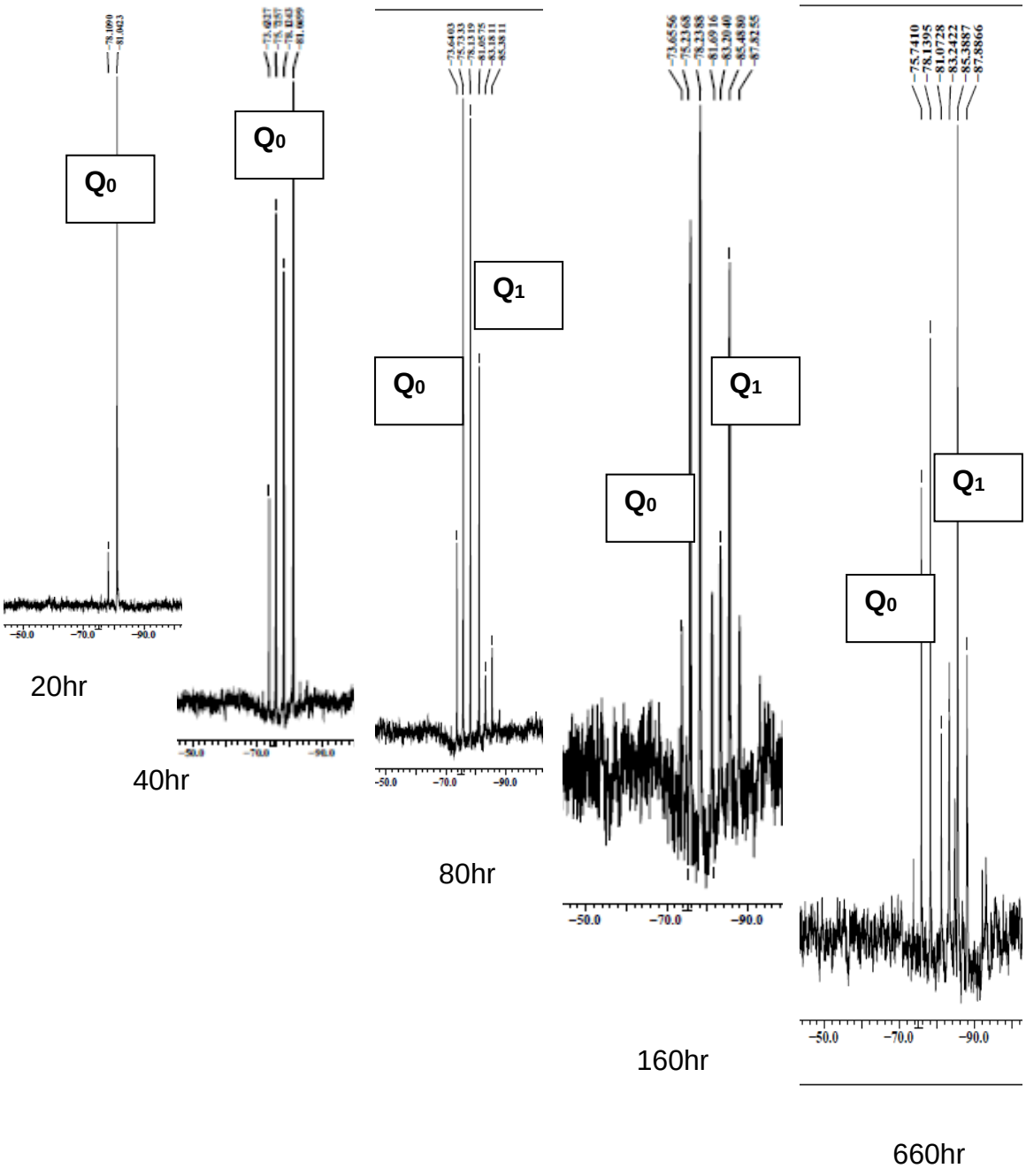

Figure 3.5. Changes in the ^{29}Si NMR spectra with time due to the hydrolysis and condensation of TEOS. The full set of ^{29}Si NMR spectra for the other ratios can be found in **Appendix 1 and 2 usb.**

3.3.3 Determining the rate constant for TEOS hydrolysis

3.3.3.1 Order of reaction with respect to [TEOS]

From the previous graphs in **Figure 3.3**, the initial rate for the loss of TEOS is expected to be as expressed below.

TEOS + H_2O + H^+ = Products (Oligomeric species)

The proposed theoretical rate equation for the loss of TEOS is;

Initial rate = k [TEOS] [H_2O] [H^+]

The [H^+] is a catalyst and was held constant

Initial rate = d[TEOS]/dt= - k'[TEOS][H_2O]

[H^+] and [H_2O] were effectively constant at the very beginning of the reaction. In each experiment, the [H_2O] was same but [TEOS] was varied. Therefore,

Initial rate = *k"* [TEOS]

So for rate equation, we plot the initial rate of loss of TEOS from **Figure 3.3a-h** graphs against [TEOS] as shown below (**Figure 3.6**).

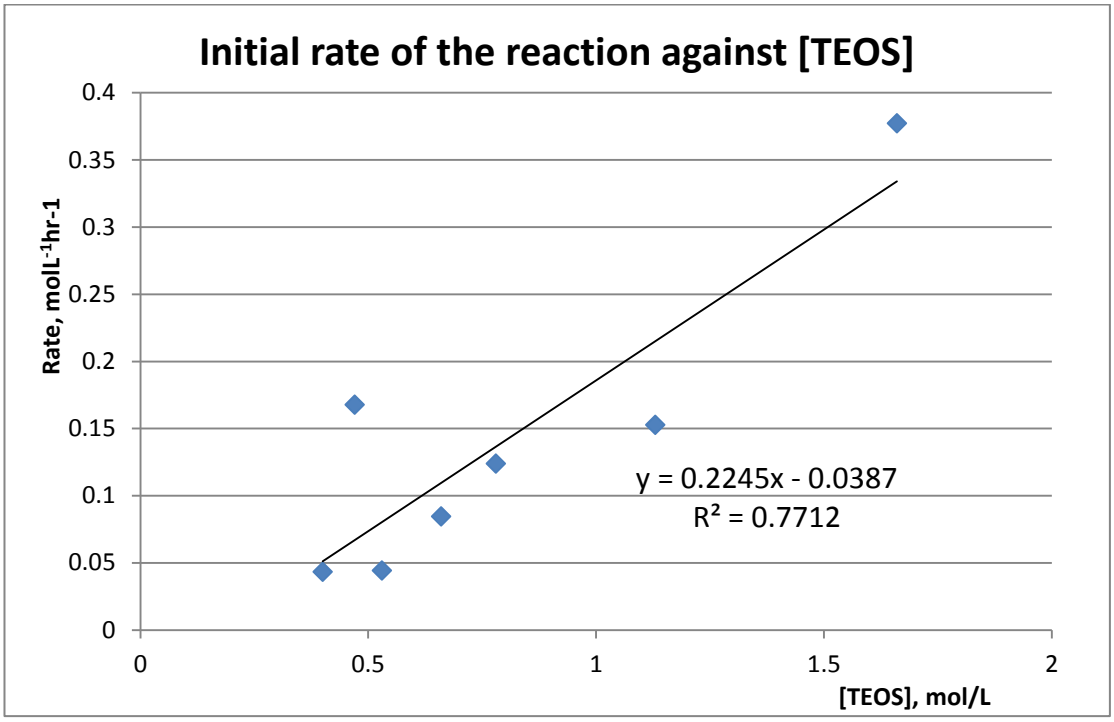

Figure 3.6 Initial reaction rate against [TEOS] for the hydrolysis of TEOS. Raw data in **Appendix 2**.

Although one point appears to be an outlier, **Figure 3.6** suggest the order of the reaction with respect to [TEOS] is first order. That is, as [TEOS] increases, the rate of the reaction increases giving a reasonably straight line. Notice the line does not go through zero although the cause of this is not immediately obvious.

So, Rate = k[TEOS], where k is the rate constant

The relative rate constant with respect to [TEOS] from the slope of the graph, **k", is 0.22hr^{-1}**.

Since k" = k[H_2O][H^+]

k = k"/ [H_2O][H^+]

k = 0.22hr^{-1}/1.66mol/l. 2.4X10^{-4}mol/l

The absolute rate constant, **k=553 hr^{-1} mol^{-2} l^2**

3.3.2.2 Order of reaction with respect to the [H^+]

To calculate the relationship between the initial rate of hydrolysis of TEOS and the acid concentration, we vary the concentrations of acid in five different analysis having constant water and TEOS concentrations. The ^{29}Si NMR results of monitoring the effects of increasing the concentration of acid on the hydrolysis and condensation of TEOS are recorded in **Appendix 3 USB** and the graphs are plotted in **Figure 3.6**.

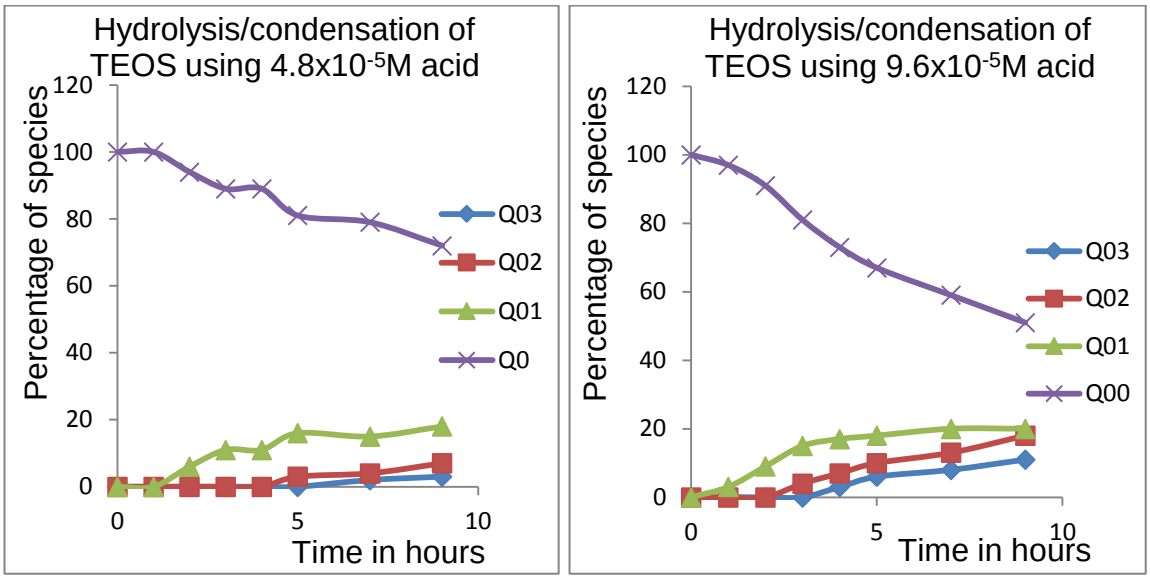

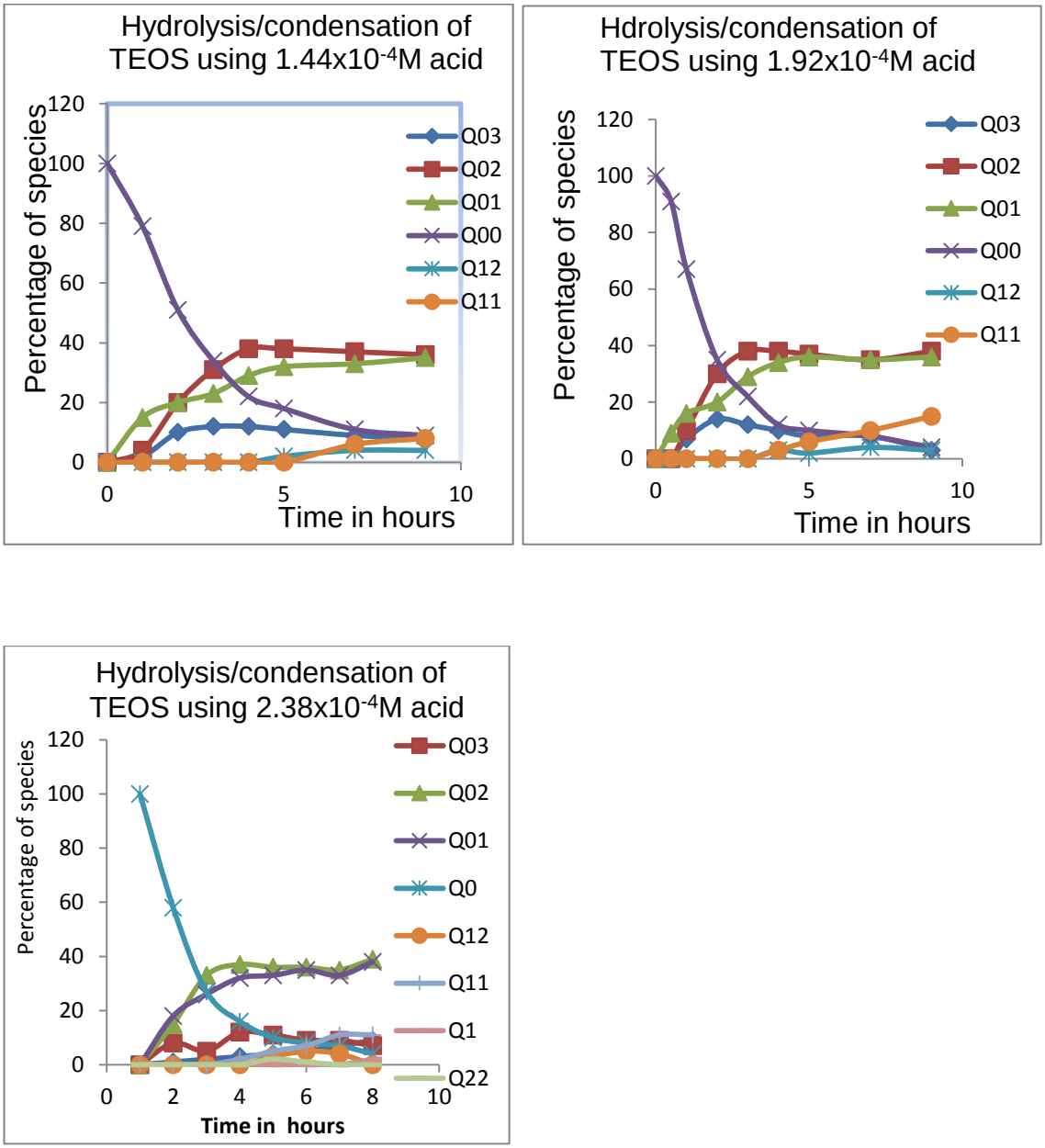

Figure 3.6. The hydrolysis and condensation of TEOS using different amounts of acid.

Based on the reaction profiles above, the initial rate of reaction is plotted below (**Figure 3.7**).

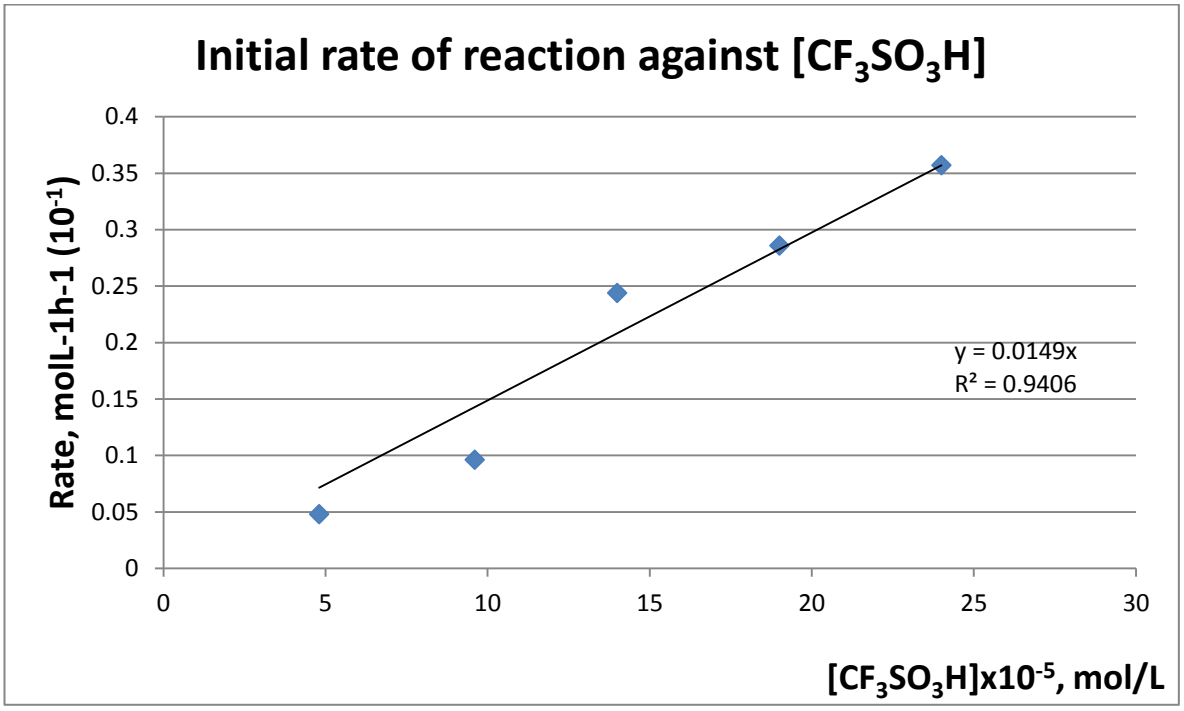

Figure 3.7. Initial rate of the reaction against $[H^+]$ for the hydrolysis of TEOS (Raw data in **Appendix 4**).

From **Figure 3.7**, when $[H^+]$ doubles, the initial rate doubles too. This implies the rate with respect to $[H^+]$ is first order.

Notice the line does not go through zero. This may be because working with extremely low amounts of acid meant that any basic impurities in the glassware or solvents would have consumed some of the acid.

From these predictions, therefore the overall rate equation for the hydrolysis of TEOS is;

$$\text{Rate} = k[\text{TEOS}][H^+]$$

From **Figure 3.7**, the slope of the line, k", is 0.01 ~ $\mathbf{0.01/10^{-5}hr^{-1}}$.

$k'' = k[H_2O][\text{TEOS}] = 1000hr^{-1}$.

Absolute rate constant, $k = 1000hr^{-1}/1.66mol/L \times 0.78mol/L = \mathbf{775hr^{-1}mol^{-2}}l^2$

So TEOS and acid influence the rate of the hydrolysis and condensation. Other researchers found the reaction rates difficult to predict using ^{29}Si NMR because it is difficult to maintain a high spectral resolution to identify individual rate coefficients[25].

The concentration of species resulting from the hydrolysis and condensation of TEOS at pseudo equilibrium

Measuring the amounts of species at pseudo equilibrium gives an indication of the trend of the species formed using different amounts of TEOS. From the ^{29}Si NMR spectra in **Figure 3.3a-h,** the species were recorded at pseudo-equilibrium (around 450-500hrs). The results are as shown in **Figure 3.8** and discussed later in the chapter.

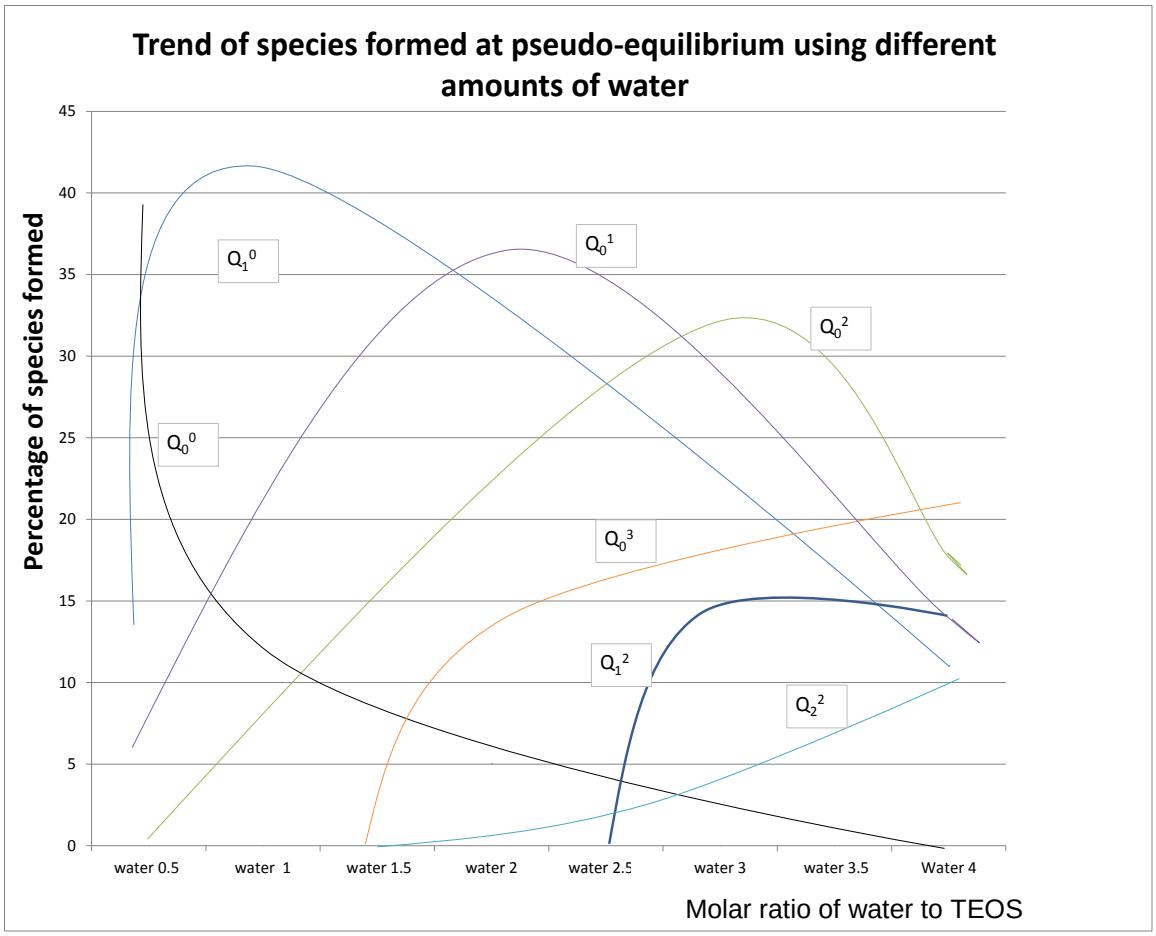

Figure 3.8. Trends for hydrolysis and condensation of TEOS at pseudo-equilibrium after smoothing the original curves

3.4 Discussion of TEOS hydrolysis and condensation

Beginning with **Figure 3.3a-h**, the reaction profiles in all cases indicate that pseudo equilibrium occurred where the reaction comes to a stop regardless of whether there are still starting materials left in the reaction mixture. This suggests a certain amount of the water is tied up as silanols and because of their concentration and/or stability, the silanol species do not further condense. The amount of water refers to the molar amount relative to that of TEOS. A 2.0 molar equivalent of water is needed to completely hydrolyze a TEOS molecule. From the observations of each spectra, it

can be confirmed that with less water (<1.5mol equivalent), more hydrolyzed species are favored. This is also confirmed by the results in **Table 3.5.** On the other hand, with higher amounts of water (>1.5mol equivalent), more condensed species are observed. However, even with excess water where we might produce maximum condensation, there are still Si-OH groups that is, condensation is not complete.

3.4.1 Computer modelling designed to understand the hydrolysis and condensation of TEOS

This section describes a computational model used to understand the pattern of hydrolysis and condensation of tetralkoxysilanes without necessarily carrying out all the experiments in the laboratory. By so doing, extra time and money can be saved from running laboratory experiments. It is also a good way to check or validate our experimental findings of the hydrolysis and condensation of TEOS. The model was designed using parameters based on the actual laboratory experiments and also based on some assumptions (mentioned in the paragraphs below). The literature describes several other methods to perform this such as temperature and virtually using computer modelling without basing it on actual experiments and they found a similar pattern to this results. More on the different literature modelling methodologies are described below.

3.4.1.1 Understanding the trends of TEOS hydrolysis and condensation

To interpret the concentration data for TEOS hydrolysis and condensation, a kinetic model was devised. Though other kinetic models have been devised and used in the past such as that of Sanchez *et al.*[122], Kay and Assink[84], Pouxviel *et al.*[262], Yang *et al.*[154] and Ro *et al.*[263], our model is a useful tool because we can use it to interpret

the behavior at low amounts of water which the other researchers have not achieved in the past. This gives a more accurate understanding of the process of TEOS hydrolysis and condensation and hence, allows us to achieve a clear knowledge of the mechanism of reaction. Yang[264], Pouxviel[262] and Ro[263] obtained a series of rate constants although they did not determine these by direct measurement but rather by computer modelling the reaction. Also, their acid concentration was higher and so their monomer hydrolysis rates proceeded faster than in this research. Their kinetic profiles included a large number of condensation reactions[122].

It is useful to note that the values of the rate constant obtained by Yang and the others were all different to one another and likewise the trends of the species formed. These differences were due to the different systems and conditions used as well as the different models and assumptions made as reported by Sanchez *et al*[122]. However, many of these researchers came to a similar conclusion that it is difficult to analyze hydrolysis rate constants alone without factoring in condensation and back reactions that may be occurring. This is where our model is better because it analyses hydrolysis in consideration of condensation and all the forward and reversible reactions which Assink and Kay as well as other researchers from **Table 3.6** did not consider in their model. **Table 3.6** shows a summary of the literature rate constants published for the hydrolysis of TEOS and TMOS adapted from Sanchez *et al*[122].

Table 3.6. Summary of literature rate constant for TEOS and TMOS hydrolysis

Source	Limitations	System composition	Rate constants for the monomer hydrolysis
Sanchez *et al.*[122]	Assumes irreversible hydrolysis overall	TEOS:1.03M H_2O: 4.15M EtOH: 11.93M HCl : $5.04x10^{-4}$M	k_1/k_{-1} (K_1) =0.1/->50 L/mol h^{-1} k_2/k_{-2} (K_2) =0.28/->50 L/mol h^{-1} k_3/k_{-2}(K_3) =0.91/0.06(15) L/mol h^{-1} k_4/k_{-4} (K_4) =4.3/1.3 (3.3) L/mol h^{-1}
Yang *et al.*[264]	irreversibility pseudo-first-order	TEOS:1.89M H_2O: 7.57M EtOH: HCl : $9.6x10^{-4}$M	k_1 = 0.86 L/mol h^{-1} k_2 = 3.84 L/mol h^{-1} k_3 = 17.4 L/mol h^{-1} k_4 = 78 L/mol h^{-1}
Kay and Assink[84].	Statistical model irreversibility	TMOS:2.24M H_2O: variable MeOH HCl : $1.6x10^{-3}$M	k_1 = 48 L/mol h^{-1} k_2 = 36 L/mol h^{-1} k_3 = 24 L/mol h^{-1} k_4 = 12 L/mol h^{-1}
Pouxviel *et al.*[262]	Assumes a particular set of reactions	TEOS:1.28M H_2O: 12.8M EtOH:8.5M HCl : $7.9x10^{-4}$M	k_1/k_{-1}(K_1) = 0.8/0.11 L/mol h^{-1} k_2/k_{-2}(K_2) = 4.02/0.26 L/mol h^{-1} k_3/k_{-3}(K_3) =16.05/1.46 L/mol h^{-1} k_4/k_{-4}(K_4) =29.18/7.3 L/mol h^{-1}
Ro *et al.*[263]	Statistical model irreversible condensation	TEOS:9.3M H_2O: 1.6M EtOH : 7M HCl : 10^{-3}M	k_1/k_{-1}(K_1)=0.328/0.014 L/mol h^{-1} k_2/k_{-2}(K_2)=0.282/0.026 L/mol h^{-1} k_3/k_{-3}(K_3)=0.164/0.042 L/mol h^{-1} k_4/k_{-4}(K_4)=0.082/0.056 L/mol h^{-1}

NB: in all cases, hydrolysis and condensation proceeded for a sufficient length of time during the kinetic measurements to achieve suitable results. K_1, K_2, K_3 and K_4 are different rate constants for TEOS hydrolysis as defined below:

The difference in the rate constants from the k_1 – k_4 hydrolysis are due to:

The more OHs, the faster the rate constant because of the lack of steric hindrance. The more OEts, the more likelihood of getting protonation and more likely to loose ethanol and hence the faster the reaction. The difference in the electron withdrawing

power between the OEt and an OH. The contribution of each of these factors may differ depending upon the conditions such as solvent and hence the differences observed in the literature.

$Q_0^0 + H_2O = Q_0^1 + ROH \quad k_1/k_{-1}$

$Q_0^1 + H_2O = Q_0^2 + ROH \quad k_2/k_{-2}$

$Q_0^2 + H_2O = Q_0^3 + ROH \quad k_3/k_{-3}$

$Q_0^3 + H_2O = Q_0^4 + ROH \quad k_4/k_{-4}$

According to **Table 3.6**, Sanchez *et al.*[122], Yang *et al.*[264] and Pouxviel *et al.*[262] all proved that the trend in rate constants of TEOS hydrolysis and condensation goes from $k_4 > k_3 > k_2 > k_1$ which is contrary to my results (see later). On the Other hand, Kay and Assink *et al.*[84] and Rao *et al.*[140] found that their results trend is the same as those of this thesis which is $k_1 > k_2 > k_3 > k_4$.

3.4.1.2 The kinetic model

The hydrolysis and condensation of TEOS prepared using the normal Vitolane™ technology route (chapter 2.1.10.1) using 1:1 molar ratio of TEOS:water instead (Table 3.2) can be modelled using the mechanism in **Figure 3.9** and making some assumptions as described below.

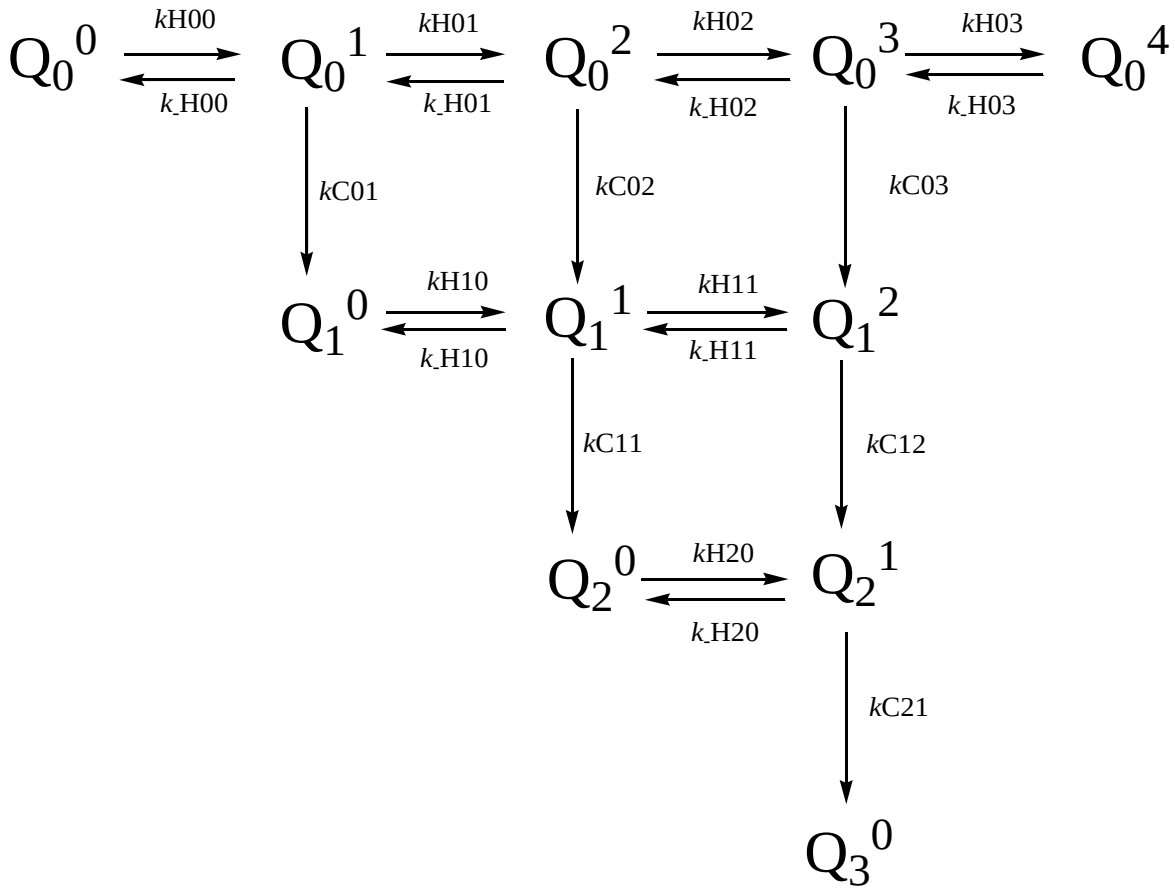

Figure 3.9. Scheme showing TEOS (Q_0^0) hydrolysis and condensation

Notice from **Figure 3.9** that the other species have been ignored (Q_1^3, Q_2^2, Q_3^1 and Q_4^0) because they were not seen in our spectral analysis. The terms in **Figure 3.9** are explained below together with how they have been used in the model. Note that the kinetic data were obtained using an excel computational model designed following a set of equations and assumptions.

Q_0^0 has the usual meaning with the subscript identifying the number of OSi linkages and the superscript identifying the number of OH linkages as defined in the introduction (Chapter 1).

*k*H01 refers to a rate constant ***k*** for ***H***ydrolysis of a Q silicon with ***0*** OSi linkages but ***1*** OH linkage. *k*C01 refers to the condensation of Q_0^1.

The back reactions for hydrolysis, *k*-H01 have been included because it is known that given the large excess of ethanol the reaction goes to about 90% completion, The back reaction for condensation have not been included because the concentration of water is low and besides, the back reaction for condensation is unlikely as it involves breaking the strong Si-O-Si bonds.

The assumptions made were:

It was assumed that room temperature was the same everyday which could not have been the case throughout the kinetic study.

Also, it was assumed that the reactions were occurring in the same way, this could not have been the case on different days and on different experiments.

The rate equations for the model

For each individual process given by an arrow a rate equation can be written;

So for the hydrolysis reactions (*J* is the rate of the individual reaction). See model spreadsheet data in **Appendix 5 "USB**".

H00 $J = k\text{H00}[Q_0^0][H_20]$ (assume the $[H^+]$ is constant and subsumed in kH00)

H01 $J = k\text{H01}[Q_0^1][H_20]$

H02 $J = k\text{H02}[Q_0^2][H_20]$

H03 $J = k\text{H03}[Q_0^3][H_20]$

H10 $J = k\text{H10}[Q_1^0][H_20]$

H11 $J = k\text{H11}[Q_1^1][H_20]$

H20 $J = k\text{H20}[Q_2^0][H_20]$

For the back reaction of hydrolysis (ethanolysis or re-esterification reactions)

-H00 $J = k\text{-H00}[Q_0^1]$ (assume the $[H^+]$ is constant together with [EtOH] and subsumed in k-H00)

-H01 $J = k\text{-H01}[Q_0^2]$

-H02 $J = k\text{-H02}[Q_0^3]$

-H03 $J = k\text{-H03}[Q_0^4]$

-H10 $J = k\text{-H10}[Q_1^1]$

-H11 $J = k\text{-H11}[Q_1^2]$

-H20 $J = k\text{-H20}[Q_2^1]$

For the condensation reactions

C01 $J = k\text{C01}[Q_0^1]$[Si-OH] (assume the $[H^+]$ is constant and subsumed in kC01)

C02 $J = k\text{C02}[Q_0^2]$[Si-OH]

C03 $J = k\text{C03}[Q_0^3]$[Si-OH]

C11 $J = k\text{C11}[Q_1^1]$[Si-OH]

C12 $J = k\text{C12}[Q_1^2]$[Si-OH]

[Si-OH] represents the total silanol concentration in the mixture that a single silanol can react with i.e.

$$[Si\text{-}OH] = [Q_0^1] + 2[Q_0^2] + 3[Q_0^3] + 4[Q_0^4] + [Q_1^1] + 2[Q_1^2] + [Q_2^1]$$

The numbers 1,2, 3, 4…..n refers to the number of OH's in each species. In this equation, an assumption has been made that all silanol groups react similarly irrespective of environment. That is, there is no steric effect occurring.

Therefore, the rate equation for each of the species in the scheme above can be written as;

$$d[Q_0^0]/dt = -kH00[Q_0^0][H_20] + k\text{-}H00[Q_0^1]$$

$$d[Q_0^1]/dt = kH00[Q_0^0][H_20] - k\text{-}H00[Q_0^1] - kH01[Q_0^1][H_20] + k\text{-}H01[Q_0^2] - kC01[Q_0^1][Si\text{-}OH]$$

$$d[Q_0^2]/dt = kH01[Q_0^1][H_20] - k\text{-}H01[Q_0^2] - kH02[Q_0^2][H_20] + k\text{-}H02[Q_0^3] - kC02[Q_0^2][Si\text{-}OH]$$

$$d[Q_0^3]/dt = kH02[Q_0^2][H_20] - k\text{-}H02[Q_0^3] - kH03[Q_0^3][H_20] + k\text{-}H03[Q_0^4] - kC03[Q_0^3][Si\text{-}OH]$$

$$d[Q_0^4]/dt = kH03[Q_0^3][H_20] - k\text{-}H03[Q_0^4]$$

$$d[Q_1^0]/dt = - kH10[Q_1^0][H_20] + k\text{-}H10[Q_1^1] + kC01[Q_0^1][Si\text{-}OH]$$

$$d[Q_1^1]/dt = kH10[Q_1^0][H_20] - k\text{-}H10[Q_1^2] – kH11[Q_1^1][H_20] + k\text{-}H11[Q_1^2] + kC02[Q_0^2][Si\text{-}OH] – kC11[Q_1^1][Si\text{-}OH]$$

$$d[Q_1^2]/dt = kH11[Q_1^1][H_20] - k\text{-}H11[Q_1^2] + kC03[Q_0^3][Si\text{-}OH] – kC12[Q_1^2][Si\text{-}OH]$$

$$d[Q_2^0]/dt = - kH20[Q_2^0][H_20] + k\text{-}H20[Q_2^1] + kC11[Q_1^1][Si\text{-}OH]$$

$$d[Q_2^1]/dt = kH20[Q_2^0][H_20] - k\text{-}H21[Q_2^1] + kC12[Q_1^2][Si\text{-}OH]$$

$$d[H_2O]/dt = -kH00[Q_0^0][H_20] + k\text{-}H00[Q_0^1] - kH01[Q_0^1][H_20] + k\text{-}H01[Q_0^2] - kH02[Q_0^2][H_20] + k\text{-}H02[Q_0^3] - kH03[Q_0^3][H_20] + k\text{-}H03[Q_0^4] – kH10[Q_1^0][H_20] + k\text{-}H10[Q_1^1] – kH11[Q_1^1][H_20] + k\text{-}H11[Q_1^2] \; kH20[Q_2^0][H_20] - k\text{-}H20[Q_2^1] + ½(kC01[Q_0^1][Si\text{-}OH] + kC02[Q_0^2][Si\text{-}OH] + kC03[Q_0^3][Si\text{-}OH] + kC11[Q_1^1][Si\text{-}OH] + kC12[Q_1^2][Si\text{-}OH] + kC21[Q_2^1][Si\text{-}OH])$$

In the above reactions, it is important to note that the water concentration is changing at each of the 19 stages of the process hence the long equation for the rate of change of water. Also note that the positive and negative signs in all the equations refer to the formation (+) and consumption (-) of a species respectively.

Also, the factor of a half arises because two silanols give rise to one water molecule

Si-OH + Si-OH ⟶ Si-O-Si + H_2O

So, half of a water molecule comes from condensation of one Si-OH.

3.4.1.2 Computational model - Calculations

The numerical integration in the excel spreadsheet (**Appendix 5** USB) is explained as follows;

$$X + Y = A + B$$

Suppose the experimental rate equation for the above reaction is $d[X]/dt = -k[X][Y]$

For numerical integration we can write;

$$\Delta[X]/\Delta t = -k[X][Y]$$

Where Δt is a small time increment. The change in concentration of X over this time increment is;

$$\Delta[X] = -k[X][Y]\,\Delta t$$

By starting off with a specific concentration of species (since the concentrations here are relative, 100% or 0% can be used normally), the change in each concentration was calculated over the first time increment and the concentrations adjusted accordingly. The change in each concentration over the second time increment was calculated and again the concentrations adjusted accordingly. By repeating the process again and again over the total reaction time, a picture of how the species change with time was built. See details in **Appendix 5**.

3.4.1.3 Using the computer model to determine the rate constants of TEOS hydrolysis/condensation

The starting concentration of water was varied. It was assumed that at the start the Q_0^0 concentration was 100% and the other species were 0%. These can be altered if needed to but in this case it was not necessary.

For complete hydrolysis of TEOS (Q_0^0) two moles of water is needed

$$Si(OEt)_4 + 2H_2O = SiO_2 + 4EtOH$$

So for this condition the starting water concentration was set at 200%. Then from this the various time curves as on the spreadsheet were reproduced with different concentrations of water. The curves were fitted with the experimental results (dotted lines) by choosing appropriate rate constants. See **Figure 3.10** for some of the curve fits and **Appendix 5** for the rest.

The fitting was done as described below; the disappearance of TEOS and the appearance of other species such as: Q_0^1, Q_0^2 ….Q_3^0 were monitored from time zero. Using different concentrations of TEOS to water, the disappearance of TEOS was measured at different times and plotted to give the initial rate. In the model, the rate expression for the change in concentration of each species were multiplied by small changes in time (numerical integration) for each of the species formed (see the different rate equations above). The time looked at for each TEOS disappearance or other species formation was from 1-8000 seconds to achieve 50 minutes in total to be compared with literature of Sanchez *et al.*[25] for validation of the model. Fittings were carried out using our kinetic data for each species where

possible and using literature data where possible, considering their forward and backward reaction in some cases. It was found that for very small amounts of water (and large amounts of ethanol), the back reaction becomes very important.

a)

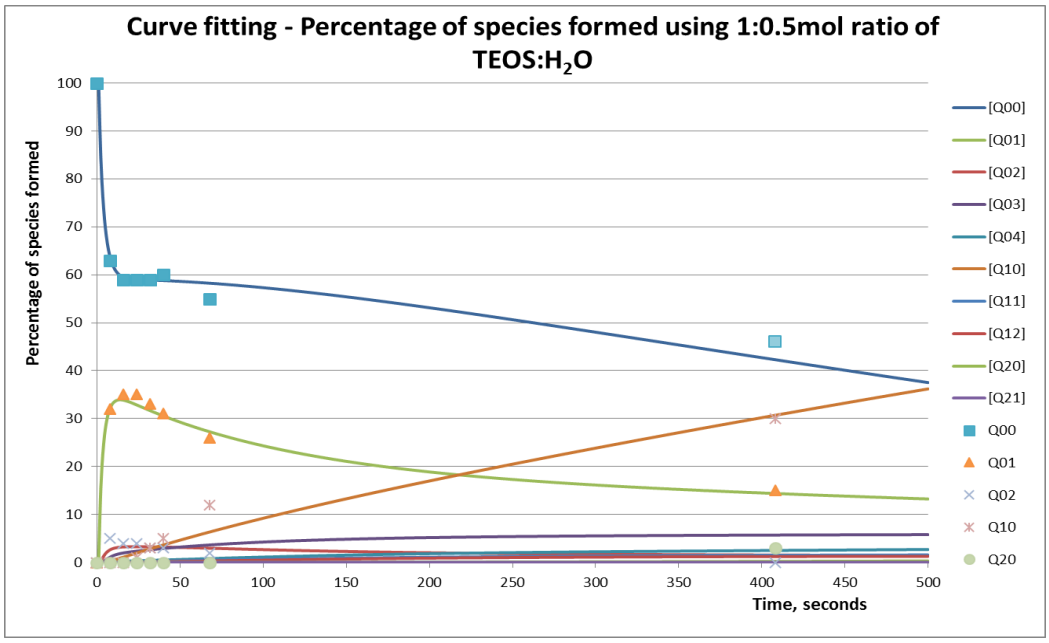

b)

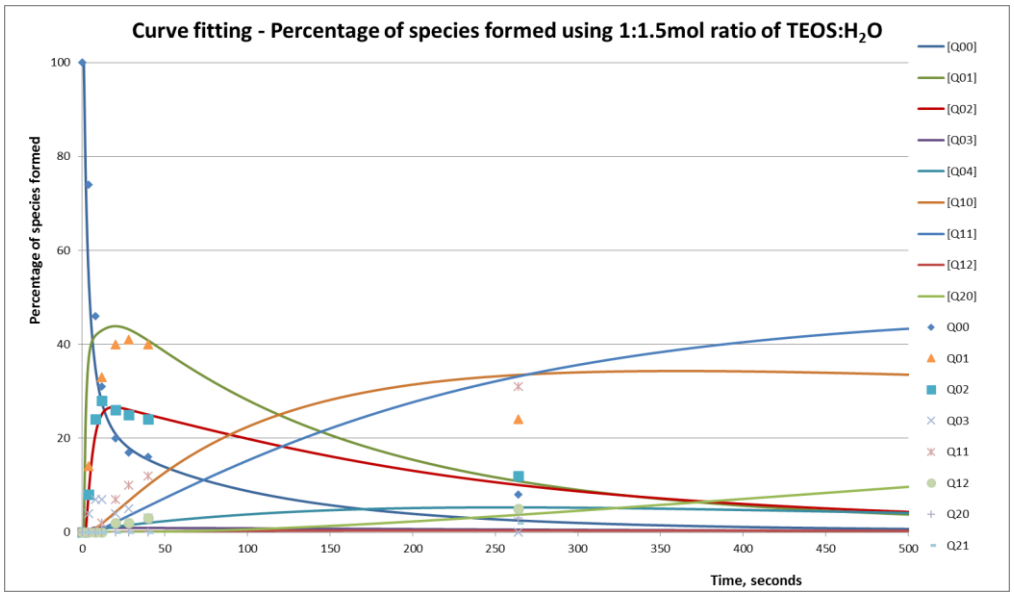

c)

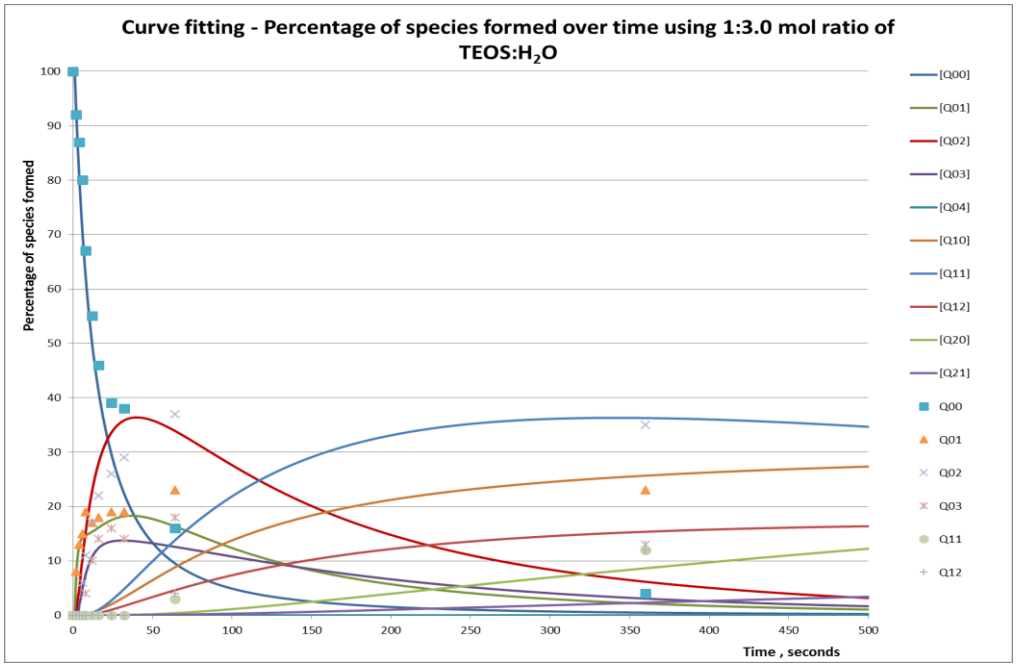

Figure 3.10. Model and experimental curves showing the degree of hydrolysis of TEOS as a function of time using a) 1:0.5mol ratio of TEOS:H_2O, b) 1:1.5mol ratio and c) 1:3.0mol ratio

There are a total of ten concentration terms and 19 variable rate constant terms, so to simplify the scheme there was a need to look in the literature for the relative rates of hydrolysis of TEOS i.e. the relative sizes of *k*H01, *k*H02, *k*H03 and *k*H04. See **Table 3.6** for findings. The ratio of *k*H (forward hydrolysis) to *k*-H (reversible hydrolysis) were included in the model and were set to be the same for all pairs of *k*H and *k*-H since the forward and back reaction was expected to behave the same irrespective of the silicon environment. Sanchez and other researchers[25,84] have reported the relative sizes of *k*C (rate constant for condensation) so this provided a starting point for these values. The relative sizes of *k*H and *k*C were adjusted since these were the biggest unknowns.

Finally, we had to bear in mind that the same set of rate constants should model all the water concentrations and so we aimed at having enough data to get a reasonable set of relative rate constants.

Using the same procedure and information recorded from literature in **Table 3.6**, we were able to determine the relative rate constants of our sol-gel systems using the data points (concentrations, time, forward and backward reactions and so on) from our excel spreadsheet and model (**Figure 3.10** and **Appendix 5**), the relative rate constants were determined and recorded in **Table 3.7** below.

Table 3.7. Relative rate constants in (L $(mol)^{-1}$ h^{-1}) for eight different ratios of [TEOS]:[H_2O] with the same starting amounts of water (1.66M) and acid [CF_3SO_3H]= $2.29x10^{-4}$M.

	Composition TEOS/EtOH (M)	***k_1/k_{-1}* (K_1)**	***k_2/k_{-2}* (K_2)**	***k_3/k_{-2}*(K_3)**	***k_4/k_{-4}* (K_4)**
1TEOS:0.5H_2O	3.13/10.31 excess	22/0.01	12/0.01	4/0.001	1/1
1TEOS:1H_2O	1.66/10.53	22/0.01	12/0.01	4/0.001	1/0.0001
1TEOS:1.5H_2O	1.13/13.07	12/0.01	10/0.001	6/0.01	1/0.0001
1TEOS:2H_2O	0.78/13.41	4/0.01	12/0.1	8/1.6	8/0.0001
1TEOS:2.5H_2O	0.66/15.33	4/0.01	12/0.1	8/1.6	8/0.0001
1TEOS:3.0H_2O	0.53/15.60	2/0.01	12/0.1	4/1.6	8/0.0001
1TEOS:3.5H_2O	0.47/15.93	5/0.01	12/0.1	8/1.6	8/0.0001
1TEOS:4.0H_2O	0.40/16.20	3/0.01	10/0.1	4/1.6	1/0.0001

Note that the different TEOS/EtOH (M) refers to the different sol-gel systems

From **Table 3.7**, the trend from k_1 to k_4 is not uniform. Some literature (Sanchez *et al.*[25], Yang *et al.*[164] and Pouxviel *et al.*[262]) predicts that $k_4>k_3>k_2>k_1$. Other researchers like; Kay and Assink[84] and Ro *et al.* predicted the opposite which is what the findings in this research also predicts ($k_1>k_2>k_3>k_4$). Varying the ratios of TEOS and water varies the polarity of the solvent. Secondly, because the amounts of TEOS were varied, the amounts of water consumed varied from one reaction to the next. Another aspect is that very small amount of acids were used hence it was difficult to get a consistent amount of acid. Finally, some of the species were only formed in small amounts so measuring their peak heights based on their signal to noise ratios meant that these calculations were more in-precise than those were the species appeared in large amounts. This is similar to the findings of Hook [265] as well as the other researchers mentioned above.

3.4.1.4 Validation of our model

Our model was validated using the data from Sanchez *et al*[122]. They published the following graph (**Figure 3.11a**) and we obtained a similar graph based on their calculated rate constants (**Figure 3.11b**). This proves our model is valid as we get a perfect match for the change in concentration in the trends observed.

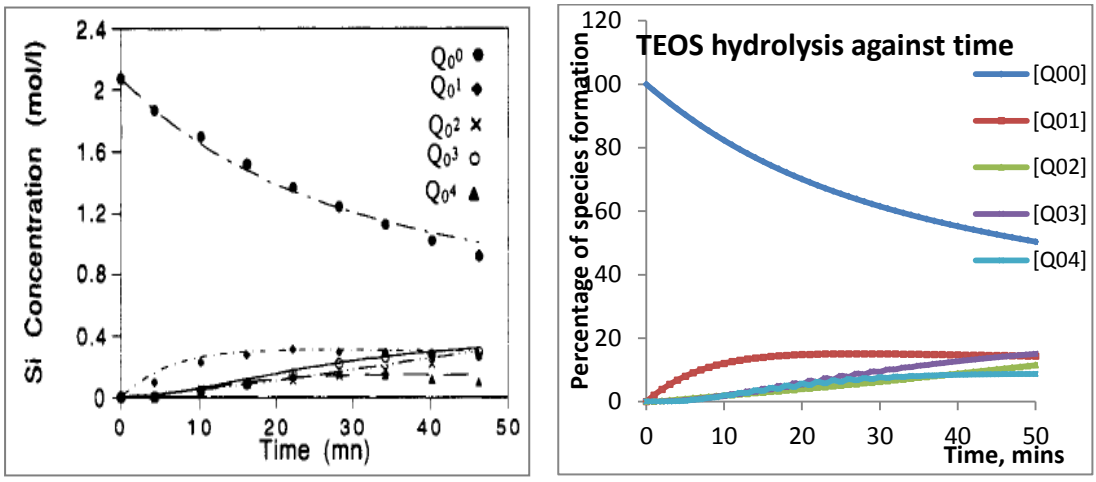

(a) **(b)**

Figure 3.11. Validation of our model based on the similarity in the results (a) Sanchez *et al.*[122] and (b) Our model @ 5°C using the published rate constants.

3.4.2 **Trend of the effects of varying the TEOS:water concentration ratio on the hydrolysis and condensation of TEOS**.

There is a trend in the way the rate profiles change from 0.5mol to 4.0mol ratio of water to TEOS - though not constant **(Figure 3.3a-h).** This agrees with the findings of Takeda *et al.*[67] and English *et al*[69]. At 0.5mol of water (a), there is more hydrolysis taking place than condensation, at 2mol water (d), there is more condensation where two species come together. There is even more condensation when 4mol of water (h) is used leading to even more highly condensed species.

Each reaction seems to reach a pseudo-equilibrium. The pseudo-equilibrium does not correspond to complete condensation. There is still a substantial amount of uncondensed silanols present. **Figure 3.3a-h, Table 3.5** and other results suggest

there are more Q_0^1, Q_0^2 and Q_1^1 species at equilibrium than the rest of the other species.

As the amount of water increases so the amount of hydrolysis increases. Hydrolysis leads to silanols but at lower concentrations of water the concentration of silanol is relatively low such that condensation is slow. As the amount of water increases we see more hydrolysis and more silanol being formed leading to more condensation. The Q_0^1 species is fairly stable at low water concentrations. At higher water concentrations, the Q_1^1 becomes the overall dominant species which suggests it is more stable to hydrolysis than thought.

With excess water, more condensation is observed but the mixture becomes stable with little further condensation happening regardless of the amount of water added. That is, there are free O-Hs but they do not condense.

The question to ask here is, does the composition of the mixture depend on the way the water is added and how long it's added for? For example if the water was metered in would the balance of hydrolysis and condensation reactions lead to a different composition from if the water is added all at the beginning? This is something to investigate in future work on the hydrolysis of TEOS.

The ^{29}Si NMR and mass spectrum show a fair amount of hydrolyzed and condensed species at equilibrium **(Figure 3.4 and Table 3.4).** A lot more hydrolyzed species were noticed when relatively small amounts of water were employed and vice versa when more water was used (**Table 3.5**). This agrees with the findings of Sanchez *et al.*[25] about the former but his group did not vary the ratio of TEOS:water.

3.4.3 Effects of acid concentration on hydrolysis and condensation of TEOS

The rate plot **(Figure 3.7)** shows that the initial rate of the reaction increases with an increase in the $[H^+]$. This is exactly as expected because the acid acts as a catalyst hence speeding up the rate of the reaction. So the rate depended upon the $[H^+]$ in a linear fashion since the concentration of water and TEOS were held constant.

The trend in **Figure 3.10** is not very smooth. The slight variations could be due to slight changes in room temperature and random errors in measured amounts and volumes of the acid. This is particularly true because in a standard reaction using acid, at low concentration, small changes will make a noticeable impact, whereas at high concentration of the acid, small changes are almost negligible.

3.4.4 Balance of TEOS hydrolysis and condensation at pseudo-equilibrium

Figure 3.8 shows that at pseudo-equilibrium, there are still some hydrolyzed species present (Q_o^1,Q_0^2). This is because, condensation is slow and a large number of hydrolyzed species are formed. Sanchez *et al*[25] also predicted this but explained that it is as a result of the slow condensation as the connectivity of the condensed species increases. That is, steric factors increase and so rate of condensation decreases (not factored into our model).

3.5 Summary and Conclusion

The initial rate of the reaction could be determined by varying both the [TEOS] and the $[H^+]$. From the results, the initial rate of TEOS hydrolysis is first order with respect to $[H^+]$ and with respect to [TEOS]. In both of the rate profiles obtained by varying

[TEOS] and [H^+], some of the data points were slightly away from the straight line. This was due to experimental errors that may have occurred from the glassware solvents or slight differences in the measurement times.

Our experiments confirmed that, at low ratios of water to TEOS (0.5mole equivalent), the concentration of free silanol species are relatively low such that condensation is slow. As the ratio of water to TEOS increases (1.0 -1.5 mole equivalents), we see more hydrolysis and more silanols formed leading to more condensation. Condensation is faster at higher water/TEOS ratios above two mole equivalent. With excess amounts of water (>2.5 mole equivalent), more condensation is observed but the system quickly becomes stable with little further condensation happening regardless of the amount of water added.

This study is particularly useful for industrial application showing that the product mix and thus its properties depend on the relative amount of water added. Only the necessary amounts of water will be used to avoid excess water in the product which may need removing afterwards leading to a waste of material, time and energy. On the other hand, excess water can be added to the reaction if the target is to achieve a more complex and more condensed composition. That is, the properties of the final product can be fine-tuned by modifying the amount of water and the way in which it is added.

Figure 3.3 shows that increasing the relative amounts of water leads to the formation of more complex species and **Figure 3.5** shows that as time increases,

even more complex species are formed. Therefore, time, [H_2O] and [TEOS] all need to be considered in controlling the product mixture.

From **Figure 3.3a-f,** one can confirm that a pseudo equilibrium is reached whereby the reaction comes to a stop. That is, no more hydrolysis nor condensation occurring this may be particularly useful for understanding shelf life of intermediates.

Most other authors [262,264] assumed irreversible hydrolysis reactions in their kinetic study models. In our systems, when we attempted to assume irreversible reactions. This resulted in good fits initially with lower amounts of water (**Figure 3.10**). We obtained poor fits in systems where higher amounts of water were being used. This finding that the back reaction of hydrolysis needs to be included agrees with Sanchez *et al*[122]*.*

The mass spectrometer provides a suggestion that the hydrolysis of TEOS leads to mostly linears.

Other conclusions to draw from the model are that; the model works and proves some predictions in the literature such as; hydrolysis occurring faster than condensation. Generally the curve fits are fine for lower ratios of [H_2O] to [TEOS]. Some curves do not fit very accurately especially when using higher [H_2O] above 2 molar ratios to TEOS. High [H_2O] leads to complex mixtures. Lots of small peaks in the ^{29}Si NMR are difficult to measure and have a higher percentage of error, so there is more uncertainty over the percent values of high [H_2O].

Chapter 4: A kinetic study of trialkoxysilane hydrolysis and condensation to gain insight into the mechanism of reaction

This chapter explores different methods of syntheses and characterization of POSS (polyhedral oligomeric silsesquioxane) compounds. It also attempts at the design of crystalline and polymeric silsesquioxane materials. The hydrolysis and condensation of trialkoxysilanes precisely; 3-Methacryloxypropyltriethoxysilane (MPTES), 3-methacryloxypropyltrimethoxysilane (MPTMS) and n-propyl trimethoxysilanes (nPTMS) have been discussed. The study also included monitoring the effects of altering each reagent (silane, water and acid) on the composition of the silsesquioxane resin precursor formed. This section also includes the understanding of what happens when excess reagents are being added to the reaction mixture after equilibrium, this gives an understanding of the durability or shelf-life of the resin materials formed[23]. The mixing pattern of the reactants, alcohol exchange and some equilibrium studies were also carried out. Finally, this chapter

also exploits to use of various instrumentation to monitor the reaction mixture and the final products formed.

4.1 Introduction

The reaction conditions are the same as described in Chapter 3 except that trialkoxysilanes are used here. However, unlike chapter three, the research here goes a little further to understand other areas such as alcohol exchange, what happens after the pre-equilibrium when additional reagents are added and the mixing pattern of the reagents. This will provide more insight into the materials that are developed and allow the enhancement of their properties even further. Finally, a comparison of the degree of hydrolysis of tri and tetra-alkoxysilanes will be made.

Understanding the effects of water and acid on the hydrolysis and condensation of 3-methacryloxypropyltrimethoxysilane (MPTES) is vital in the development of different sol-gel materials for diverse application[266]. In this research, it was particularly important to help us understand silsesquioxane resin formation which will be discussed in a later chapter (Chapter 5). This study focuses on the effects of varying water and acid concentration on the hydrolysis and condensation of MPTES, and it also interprets any trends in the composition of the product mixtures. Solution silicon-29 nuclear magnetic resonance (^{29}Si NMR) was used to measure the silicon environments formed with respect to time and the amount of water. Matrix-assisted laser desorption/ionization time of flight mass spectrometry (MALDI-ToF-MS) was used to investigate the hydrolysis and condensation processes occurring during the reaction by measuring the molecular masses of the species formed.

A careful study of the hydrolysis and condensation of MPTES is therefore very important for understanding the mechanism of hybrid material formation [122, 264,98, 238,108,240]. Hydrolysis and condensation can occur simultaneously if a high molar amount of water, acid and high temperatures are used [122,152, 108, 242, 112]. A relatively small amount of acid or basic catalyst is used to speed up the rate of the reactions. However, in this work a very low concentration of acid was used to slow the reaction enough to monitor the front end of the reaction [243,240,198] . As in chapter 3, we are interested in studying the reaction using stoichiometric and sub stoichiometric amounts of water [75].

As discussed in the previous chapter, although hydrolysis is generally fast, there can be a large amount of unhydrolysed or partially hydrolyzed species formed, depending on the reaction conditions used. Therefore, the hydrolysis of MPTES does not only produce fully hydrolyzed intermediates ($RSi(OH)_3$), even if the right equivalent molar amount of water is being used[122,91,230].

As hydrolysis occurs, MPTES concentration decreases and other intermediate hydrolyzed MPTES species develop[26,24, 243,242,240,245] . As the molar ratio of water to MPTES is continuously increased, more condensed T_1^0, T_2^0 and T_3^0 species are observed over time[70, 71, 72,73]. If MPTES is T_o^0, MPTES intermediate environments formed go from T_o^1 which is MPTES with one hydroxyl group, followed by T_o^2 and T_o^3 with a subsequent increase in the number of OH groups on the central Si atom (**Figure 4.1b**)[121,106,186,247,185]. Further condensation lead to the species in Figure 4.1 as in the ^{29}Si NMR, the peaks from T_o^0 to T_2^0 go from -40 to -60ppm respectively. Using a low concentration of acid ($4.8x10^{-4}M$) as in this study, one can monitor the amounts of T_o species formed[248,230,243]. See **Table 4.1** for the full assignment of chemical shifts based on the literature and on this research.

a)

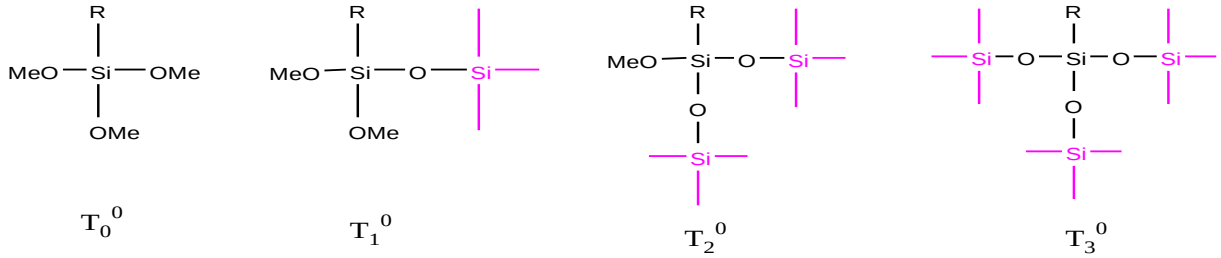

b)

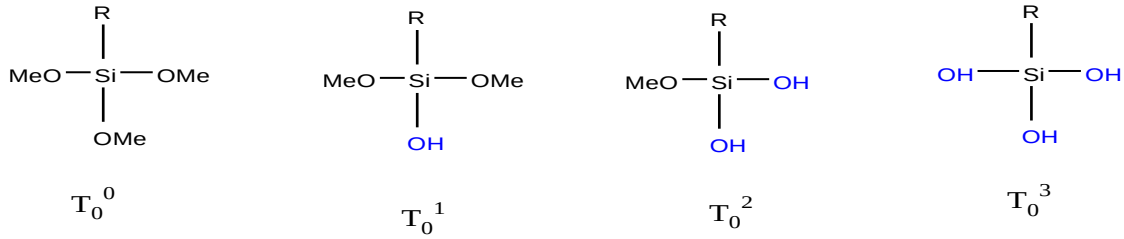

Figure 4.1. (a) T-silicon species formed from trialkoxysilane hydrolysis and condensation and (b) T-environments of silicon species formed from hydrolysis.

Table 4.1: Chemical shift assignments

chemical shift of peak as in literature	Chemical shift as observed	Proposed species
-39.2	-40.7	T_0^3
-40.8	-42.1	T_0^2
-42.6	-43.7	T_0^1
-44.7	-45.7	T_0^0
-48.5	-50.0	T_1^2
-50.2	-51.3	T_1^1
-52.1	-53.1	T_1^0
-54.7	-56.0	T_2^2
-57.0	-58.0	T_2^1
-60.1	-60.0	T_2^0

Assignment based on Sugahara[120] and Schmidt[121] *et al.* as shown in Sanchez *et al.* [122] and new assignments that originates from this research (observed).

A kinetic study of MPTES hydrolysis using ^{29}Si liquid NMR shows that hydrolysis occurs before condensation[249,250,213,251,252]. In other words, initially hydrolysis is faster than condensation[253,172,153,254]. A pseudo equilibrium is reached just as in the case of TEOS in chapter 3 [255, 256, 29, 70, 257]. To understand this behaviour, different molar ratios of water and acids have been used in this study with respect to MPTES.

With very small amounts of water in the presence of an acid catalyst, one can go from T_o^0 to T_o^1 as shown below.

$$T_o^0 + H_2O \longrightarrow T_o^1 + ROH$$

With slightly more water, T_o^1 is further hydrolyzed through to T_o^2 and then T_o^3.

$$T_o^1 + H_2O \longrightarrow T_o^2 + ROH$$

$$T_o^2 + H_2O \longrightarrow T_o^3 + ROH$$

4.2 Mechanism of hydrolysis and condensation of MPTES

The hydrolysis and condensation follows the same mechanism as in **Figure 1.10** except that trialkoxysilane is used instead of tetraalkoxysilane. **Figure 4.2** shows the stepwise hydrolysis and condensation process leading to the formation of the siloxane bond. Ethanol provides a homogenous environment to facilitate hydrolysis to take place while also promoting depolymerisation reactions[75]. The acid speeds up the rate of the reaction hence act as a catalyst [67].

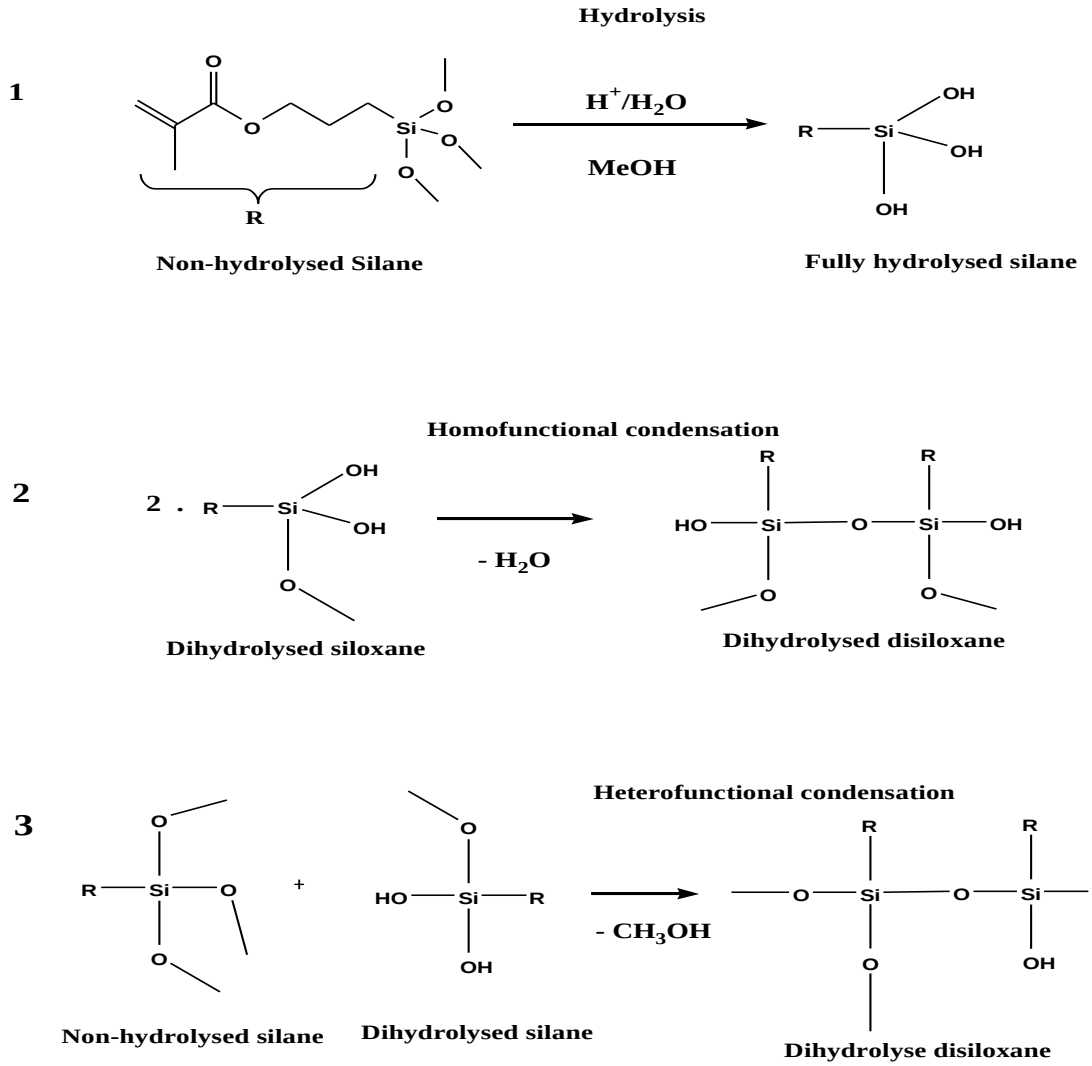

Figure 4.2. Stepwise process for the hydrolysis and condensation of MPTES leading to siloxane bond formation[82]

The experimental details for this hydrolysis and condensation reaction are described in **Chapter 2.1.2**. From the experiment and literature findings [66,67, 68,69], the hydrolysis of MPTES leads to partially hydrolyzed and condensed intermediates [243, 112, 172, 187, 258,259, 260,261,45, 27a, 267, 114b].

4.3 Results of the kinetic study of MPTES hydrolysis and condensation

Solution ^{29}Si NMR was used to monitor the hydrolysis and condensation of MPTES and the results are shown in **Figures 4.3** followed by the interpretation in **Table 4.2** and discussion afterwards**.** The rest of the 29-SiNMR results can be found in **Appendix 6**. MALDI-ToF-MS **Figure 4.4** was used to study some of the species formed from MPTES hydrolysis and condensation. The results are further discussed in the discussion section.

Using different ratios of water to MPTES by varying the concentration of MPTES **(Table 2.3),** the disappearance of the MPTES peak and the formation of various species was monitored using ^{29}Si NMR and the results can be seen in **Figure 4.3** below (**4.3**; a, b, c, d, e, f). The assignment of the peaks is same as mentioned in **Table 4.1**.

4.3.1 ^{29}Si NMR results from monitoring the effects of increasing the ratio of MPTES to water on the hydrolysis and condensation of MPTES

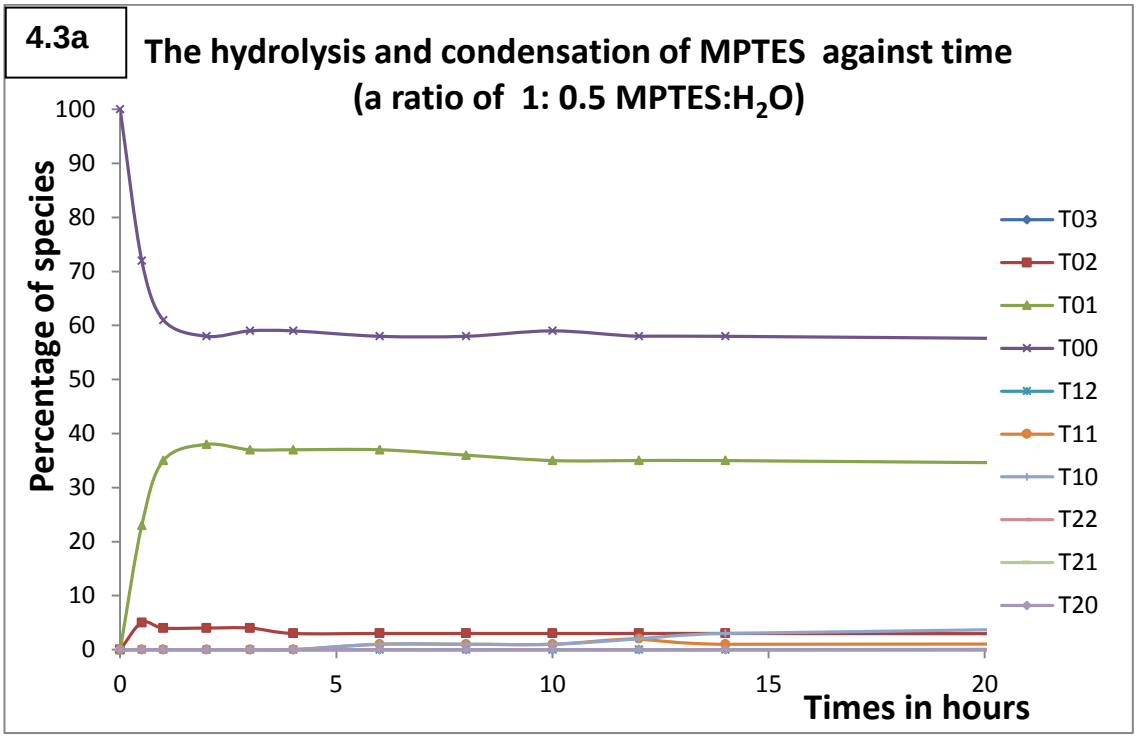

A ratio of MPTES:H_2O of 1:0.5 (Appendix 1)

In **Figure 4.3a**, 50% hydrolysis of the MPTES is quickly observed to give mainly T_0^1 species with some T_0^2. No T_0^3 is observed in this reaction. This implies that there is no water remaining otherwise this species would be present. Condensation is also observed slightly with some T_1 peaks being seen on the graph.

bi

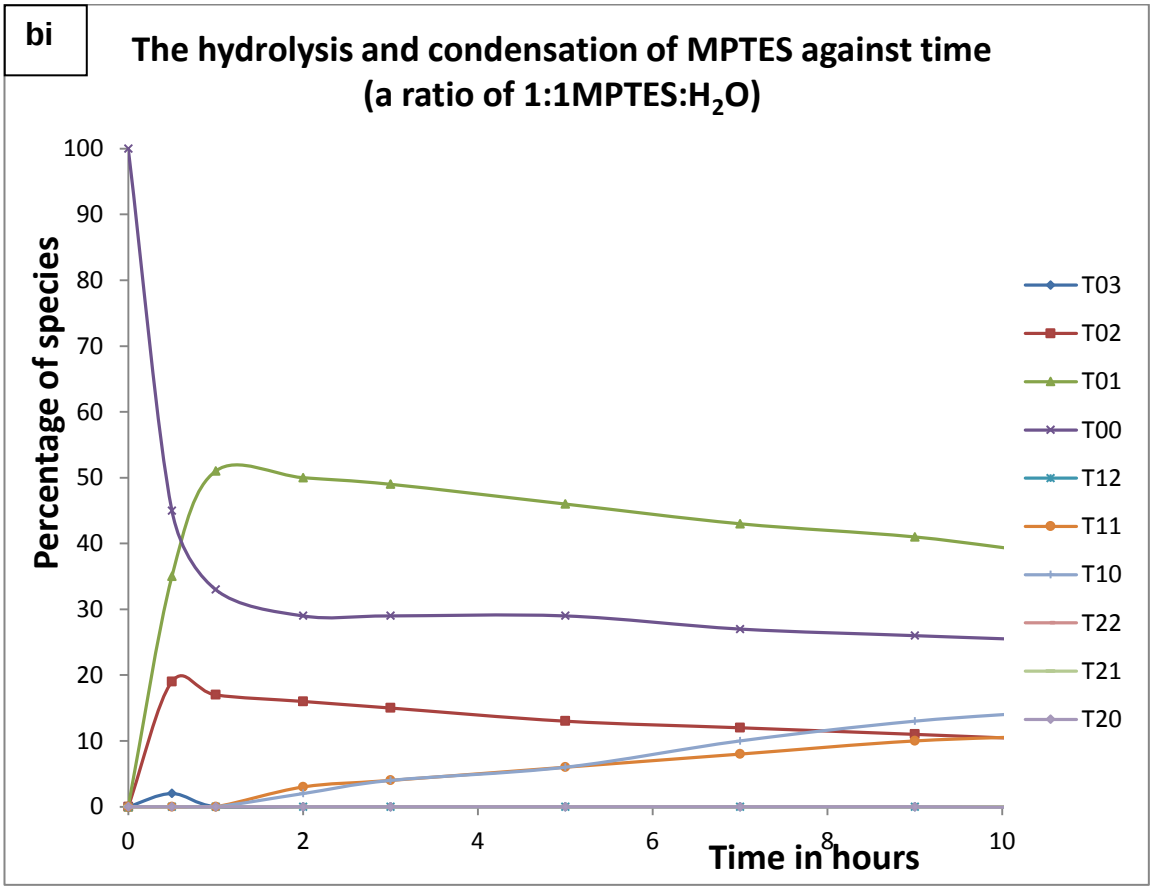
The hydrolysis and condensation of MPTES against time
(a ratio of 1:1MPTES:H2O)
Percentage of species
Time in hours
T03
T02
T01
T00
T12
T11
T10
T22
T21
T20

bii

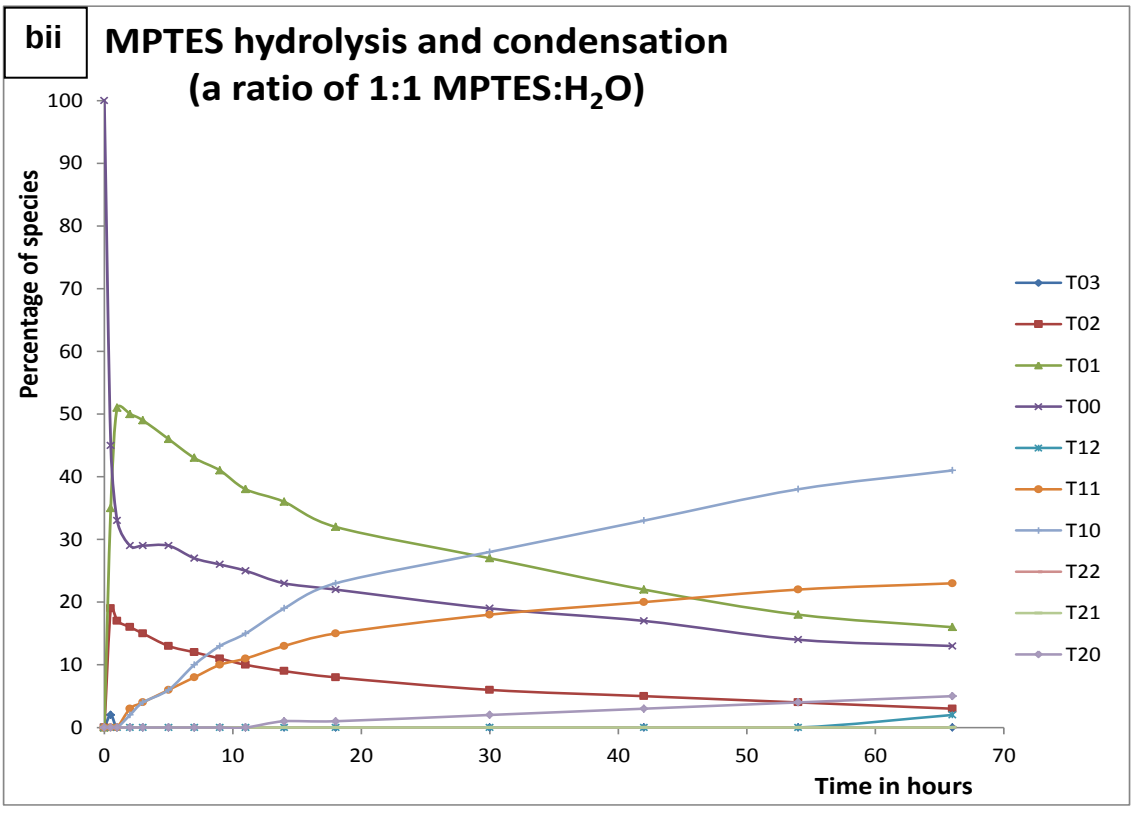
MPTES hydrolysis and condensation
(a ratio of 1:1 MPTES:H2O)
Percentage of species
Time in hours
T03
T02
T01
T00
T12
T11
T10
T22
T21
T20

A ratio of MPTES:H_2O of 1:1 (Appendix 1)

In this case there is greater hydrolysis than when using a 0.5 mol water equivalent. T_0^1 is formed quickly but then, it slowly decreases. T_1^0 begins to rise really quickly. T_0^2 Increases but then it plateaus afterward. T_1^1 increases and does not undergo further condensation on this timescale.

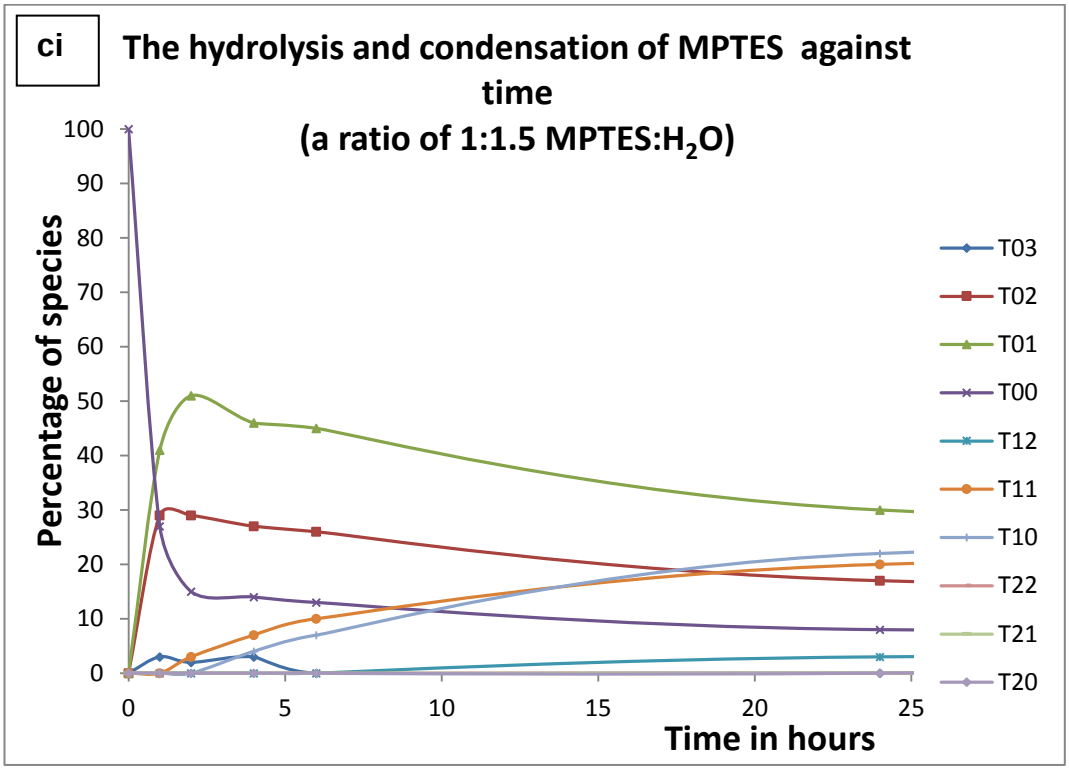

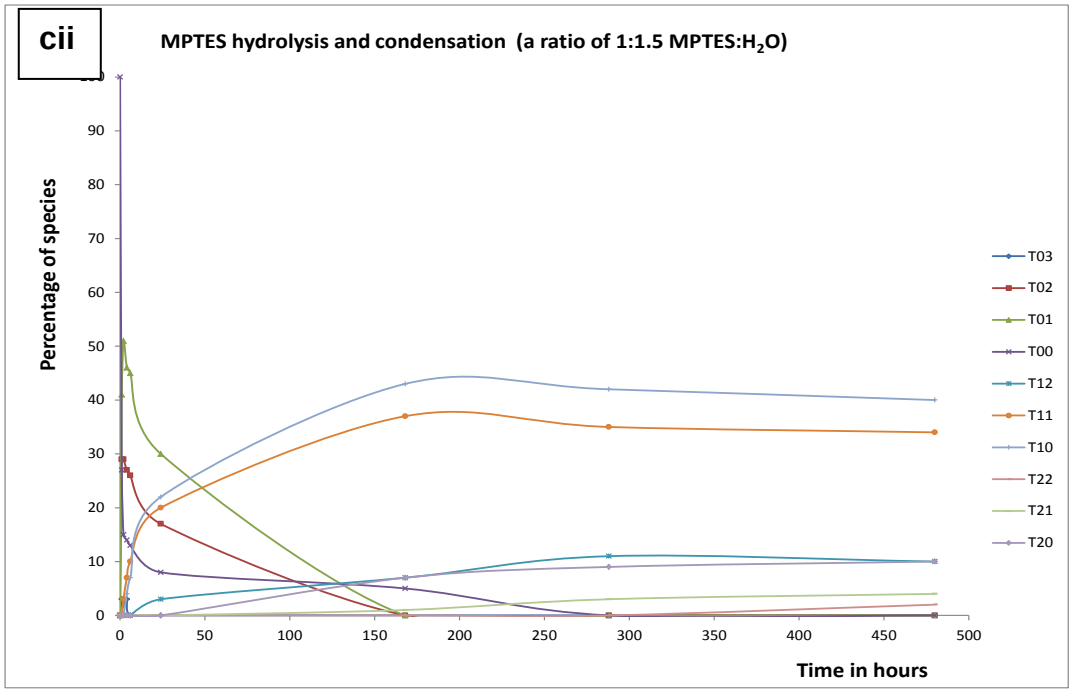

A ratio of MPTES:H_2O of 1:1.5 (Appendix 1)

There is clear evidence of the pseudo-equilibrium being achieved. MPTES is almost completely used up. T_0^1 is formed quickly but then slowly decreases. T_1^0 is seen to be rising as well. T_0^2 increases but then decreases – that is, its formation from T_0^1 is not as fast as the formation of T_1^1. T_1^0 is dominant followed by T_1^1 after a longer run time beyond 25 hours.

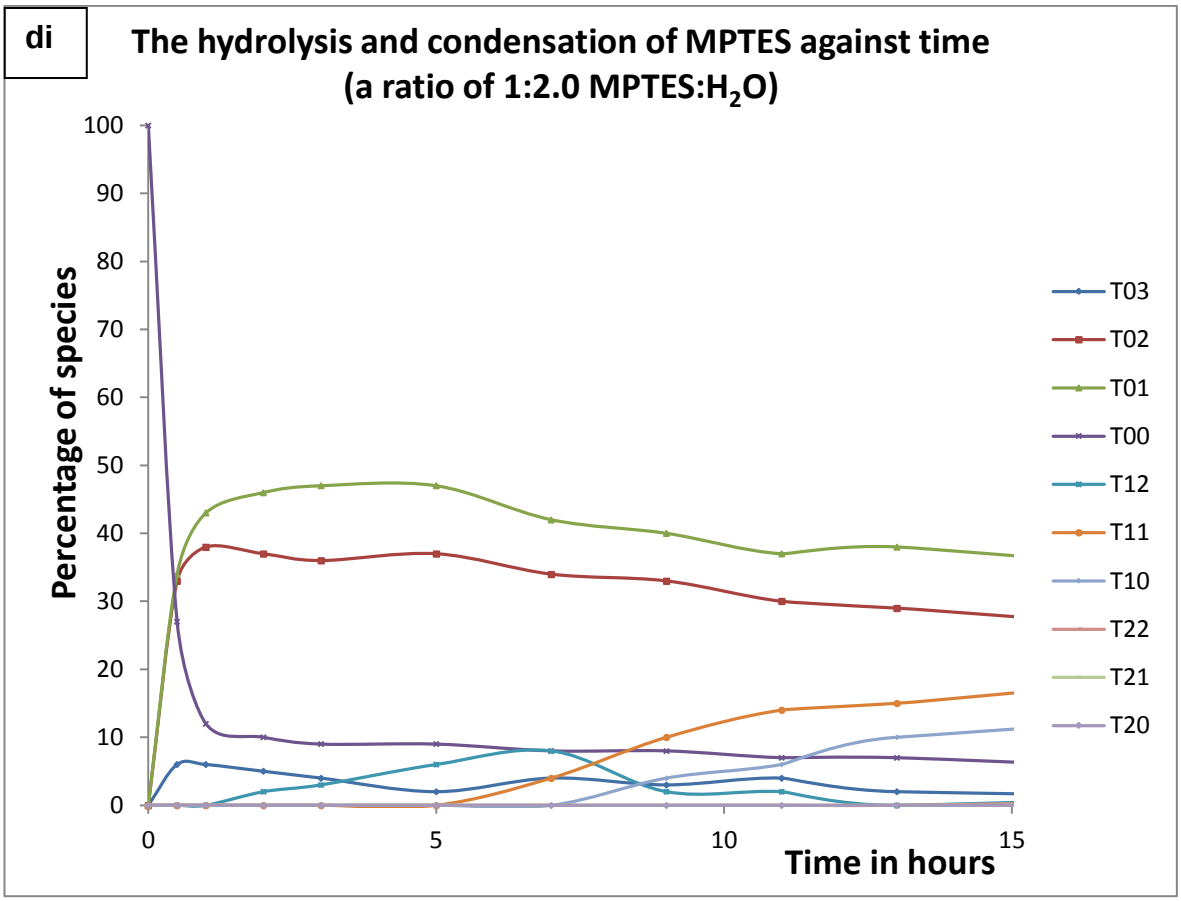

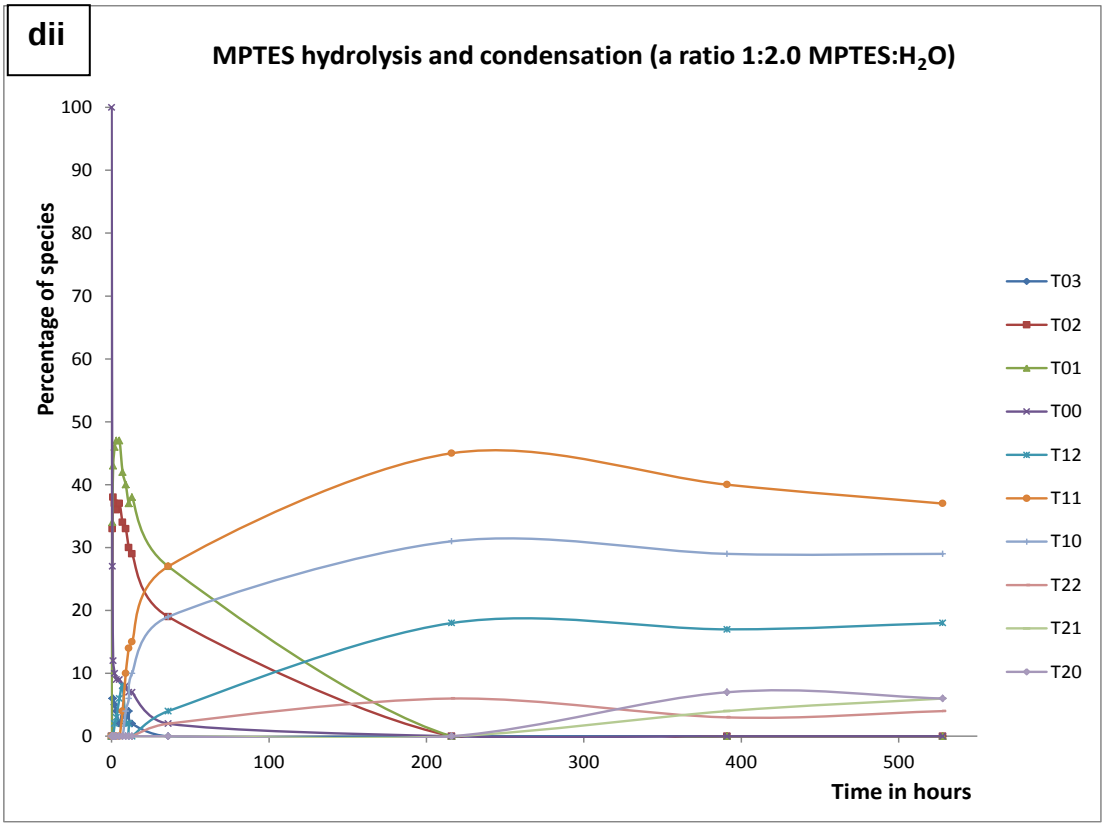

A ratio of MPTES:H_2O of 1:2.0 (Appendix 1)

MPTES is completely used up very quickly. T_1^1 is now the dominant species. On the longer timescale, T_1^1 becomes the overall dominant species followed by T_1^0 and then T_1^2. This implies more condensation is taking place and can be confirmed by the presence of T_2's also which starts to become more prominent.

ei

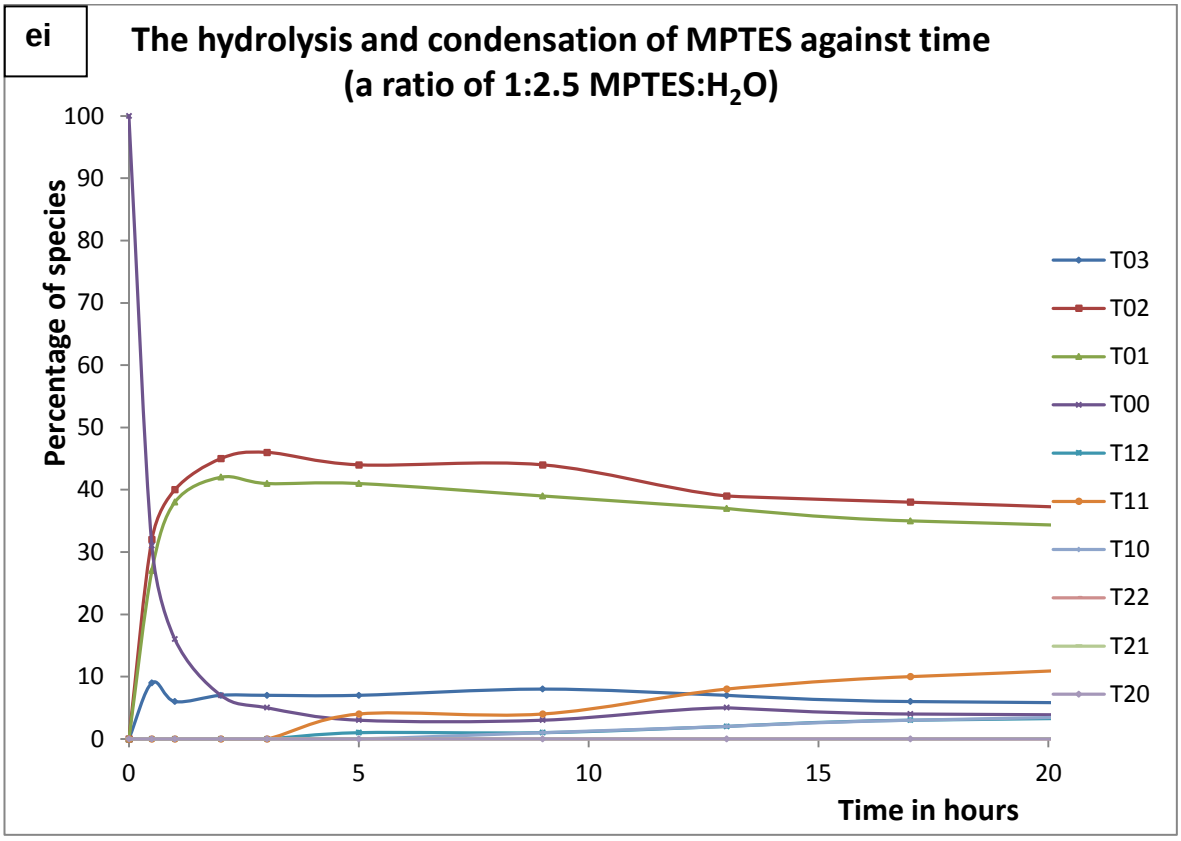
The hydrolysis and condensation of MPTES against time
(a ratio of 1:2.5 MPTES:H2O)
Percentage of species
Time in hours
T03
T02
T01
T00
T12
T11
T10
T22
T21
T20

eii

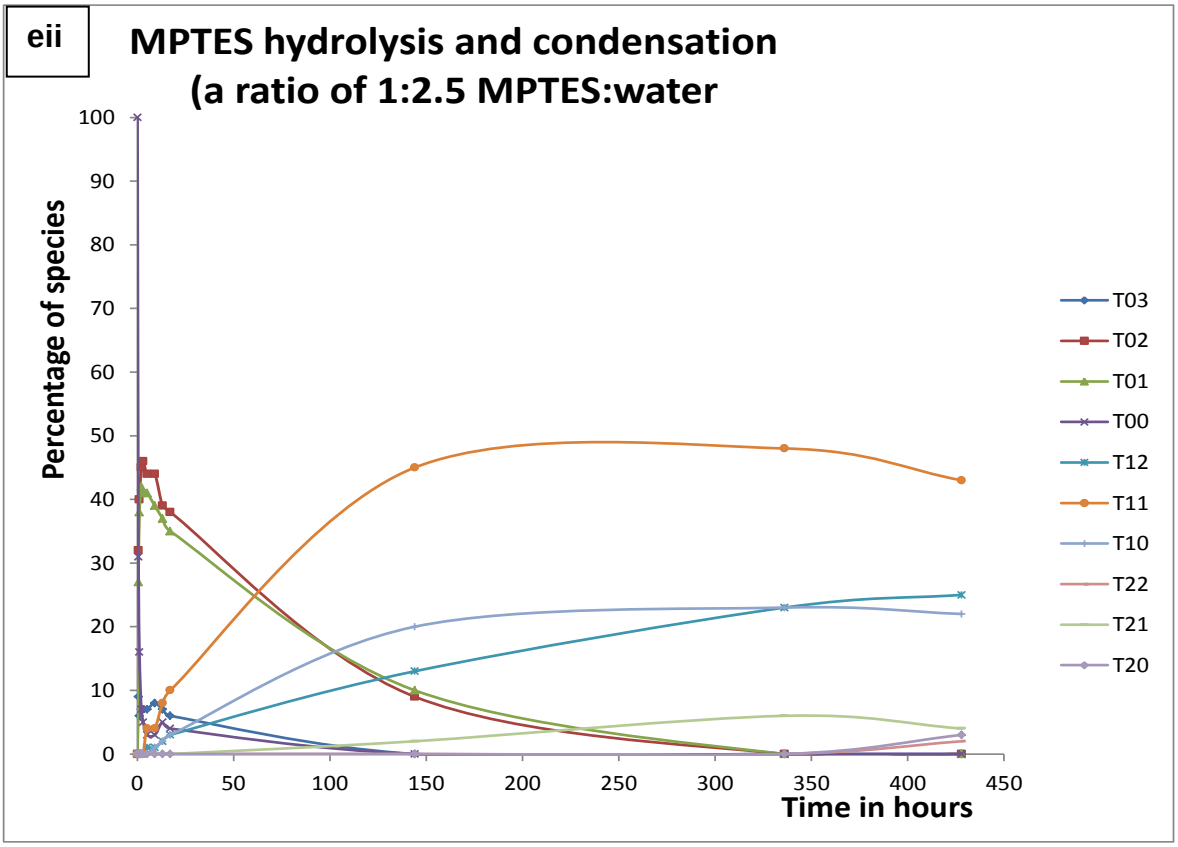
MPTES hydrolysis and condensation
(a ratio of 1:2.5 MPTES:water
Percentage of species
Time in hours
T03
T02
T01
T00
T12
T11
T10
T22
T21
T20

A ratio of MPTES:H_2O of 1:2.5 (Appendix 1)

MPTES is completely used up very quickly. T_1^1 is very much the dominant species and T_1^2 and T_1^0 follows. This finding is similarly to the 1:2.0 MPTES:H_2O molar ratio above. The amount of condensation of is high though slightly less than the previous case with less T_2 species being formed. This is possibly because with excess water the back reaction starts to become favored.

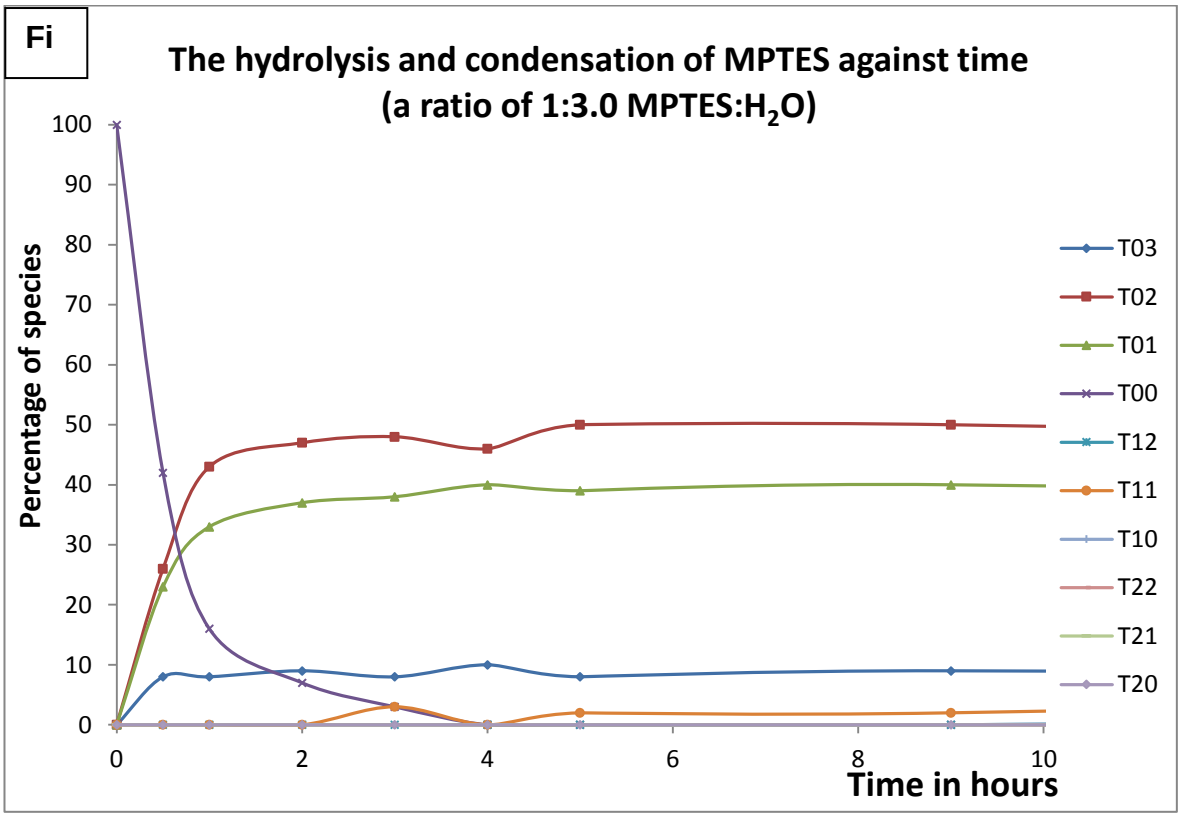

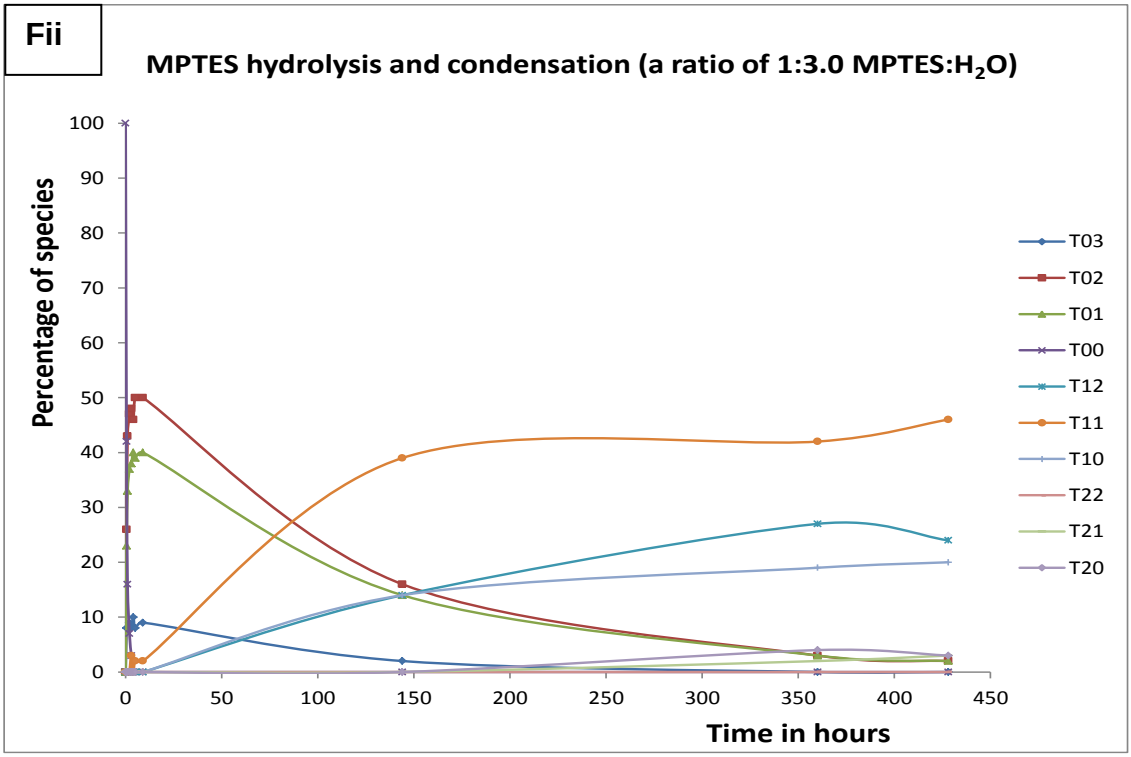

Figure 4.3(a-f). Comparison of experimental plots from the ^{29}Si NMR spectra using different molar ratios of MPTES:H_2O**.** a) 1:0.5, b)1:1, c) 1:1.5, d) 1:2, e) 1:2.5, f)1:3

A ratio of MPTES:H_2O of 1:3.0 (Appendix 1)

This is similar to the 2.5 ratio in terms of MPTES hydrolysis of the T_0 species. T_1^1 is still the dominant species with T_1^2 and T_1^0 following.

4.3.1.1 Interpretation of the MPTES kinetic results

From **Figure 4.3a-f** above, the following summary can be made about the trend of the species formed using different ratios of water as shown in **Table 4.2**.

Table 4.2 ^{29}Si NMR results summarizing the silicon species formed using different ratios of water to MPTES via hydrolysis and condensation after equilibrium.

Chemical shift, ppm	Proposed species/ environments	0.5H_2O	1.0H_2O	1.5H_2O	2.0H_2O	2.5H_2O	3.0H_2O
-40.7	T_0^3			√	√	√	√
-42.1	T_0^2	√	√	√	√√	√	√
-43.7	T_0^1	√√	√	√	√	√	√
-45.7	T_0^0	√√	√				
-50.0	T_1^2	√	√	√	√√	√√	√√
-51.3	T_1^1	√	√√	√√√	√√√	√√√	√√
-53.1	T_1^0	√√√	√√√	√√√	√√√	√√	√√
-56.0	T_2^2		√	√√	√	√	√
-58.0	T_2^1		√	√	√	√	√
-60.0	T_2^0		√√	√	√	√	√

NB: Where the mol water represents molar ratios. (√√√ = good amount, √√ = average, √ = small amount).

4.3.1.2 Interpretation of the ^{29}Si NMR results

From **Figure 4.3 a-f**, once again as in the case of TEOS, some plots have more data points in order to provide a more detailed analysis of the process since the hydrolysis rate was faster in some reactions than others. As predicted for the case of TEOS in chapter 3, the same pattern is experienced here regarding the formation and disappearance of the different species. From the NMR spectra (**Figures 4.3a-f and Figure 4.5**), the extent of hydrolysis and condensation are seen to increase with increasing amounts of water. **Table 4.2** shows that T_1^1, T_1^2 and T_1^0 are the dominant species with T_1^1 being the most dominant and prevailing. This is a very similar pattern to that of TEOS which showed, Q_1^1, Q_1^0 and Q_0^2 to be the dominant species and Q_1^1 being the most dominant. This confirms the literature findings of Sanchez *et al.*[25] who also reported that tri and tetraalkoxysilanes have a similar pattern of hydrolysis and condensation. Overall, with very little amounts of T_2 relative to T_1, only dimers are mostly seen. With more T_2 relative to T_1, longer linear chain length oligomers are seen. Only when T_3 starts to appear will branched and cyclic species will be seen.

The above results are also confirmed in the Maldi-Tof-MS in **Figure 4.9** on page 161. Here with increasing amounts of water from 0.5 to 3.0 molar equivalents, the sizes of the species are seen to increase. With low amounts of water, hydrolysis is favored and occurs slowly leading to smaller and fewer species/silicon environments as seen in **Figure 4.9** (0.5mol H_2O). Larger species and more silicon environments are seen with increased amounts of water as condensation is favored, seen in **Figure 4.9** (3.0 mol H_2O). Larger species means more T_1^x, T_2^x and T_3^x. Yang[264] actually states that the sol-gel reaction initially proceeds by more hydrolysis and then later by more condensation.

Figure 4.4 below shows a stacking of a sequence of ^{29}Si NMR spectra from the kinetic study of MPTES hydrolysis and condensation using a 1.5 molar ratio of water: MPTES corresponding to **Figure 4.3c**.

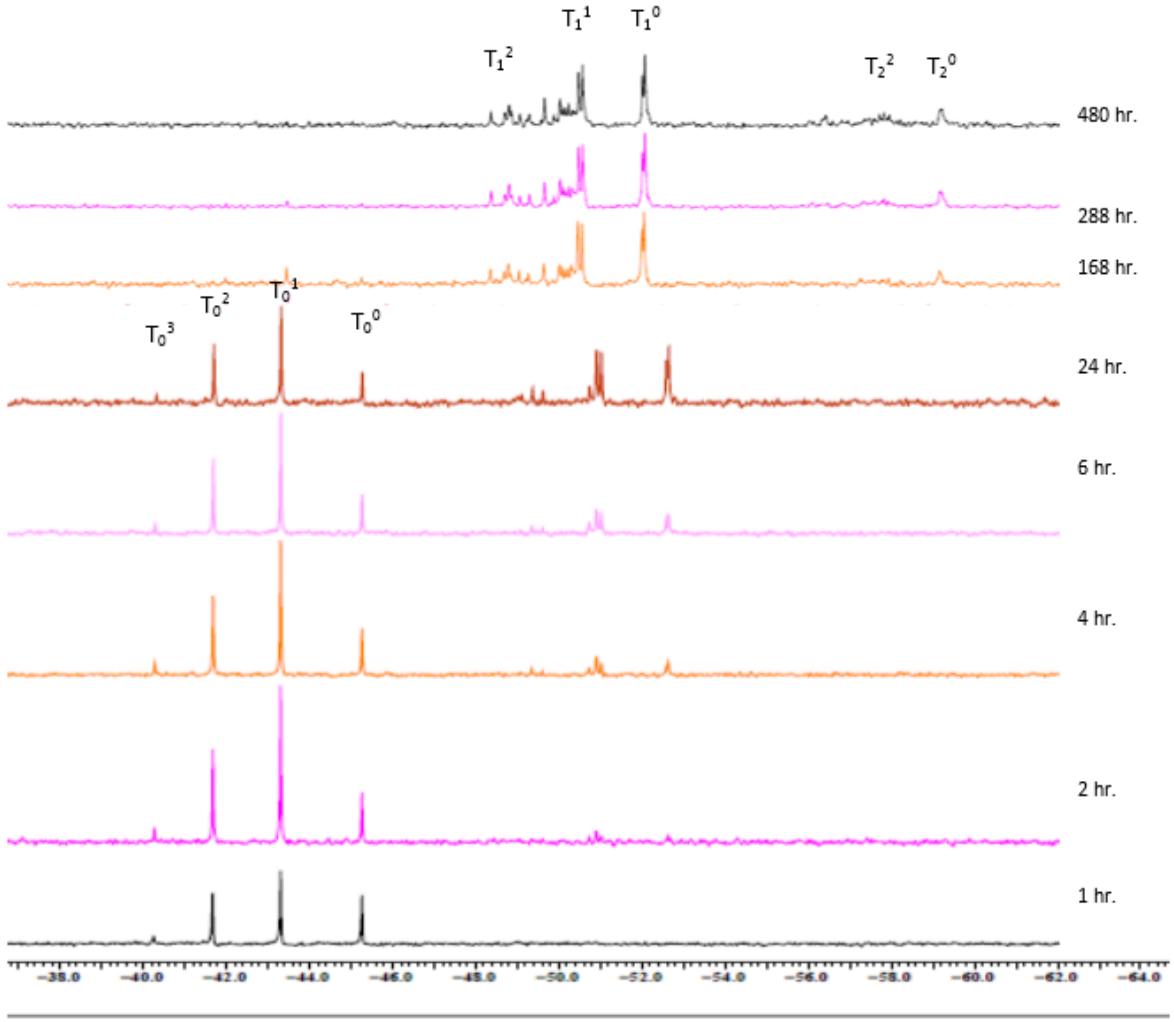

Figure 4.4. Stacks of ^{29}Si NMR spectra at different times using 1.5 molar equivalence water to MPTES ratio.

Trend of species formed at pseudo-equilibrium following the hydrolysis and condensation of MPTES

From the ^{29}Si NMR plots (**Figure 4.3a-f)** obtained from the spectra (reported in **Appendix 6 - usb)**, the species at equilibrium found around 400-500 hours were plotted against the ratio of water to MPTES. The **Figure 4.5** shows the distribution of species using different concentrations of water.

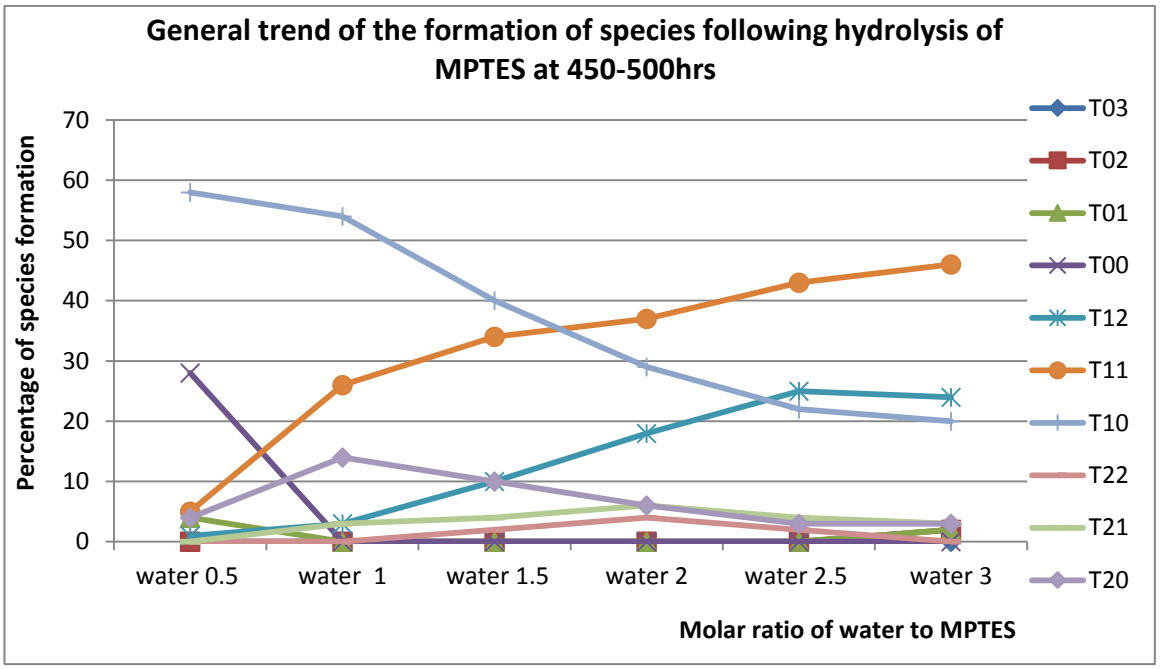

Figure 4.5. Trend of species formed using different molar ratios of water:MPTES.

This figure shows that at pseudo equilibrium as the relative amount of water increased with respect to MPTES at pseudo-equilibrium, there is both more hydrolysis and more condensation. Also, the higher the amounts of water, the more condensed the species formed. For example, T_1^1 is low at 0.5mol water but rises very quickly as the amount of water rises up to 3.0molar equivalent.

4.3.2 Determining the rate constant of MPTES hydrolysis

4.3.2.1 Rate constant of MPTES hydrolysis with respect to [MPTES]

From the previous graphs in **Figure 4.3a-f**, the initial rate for the loss of MPTES can be calculated and plotted against the [MPTES] as shown in **Figure 4.6** (^{29}SiNMR spectra data in **Appendix 7**).

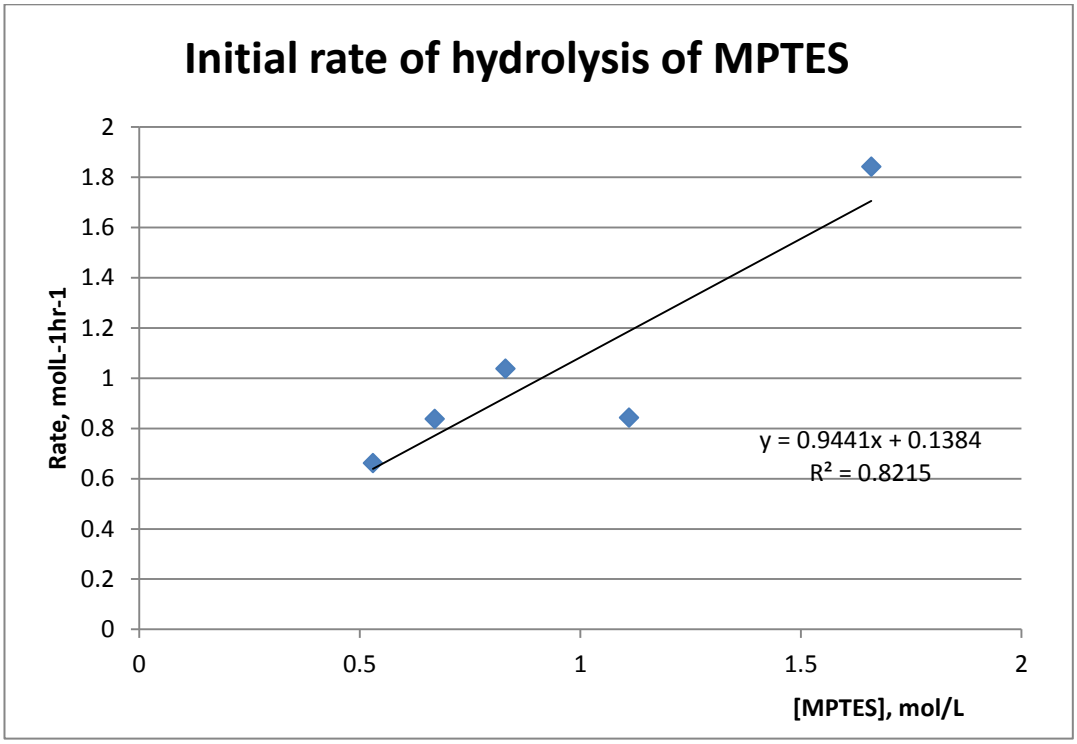

Figure 4.6. Initial rate of MPTES hydrolysis against [MPTES]

Given the equation for hydrolysis of MPTES;

MPTES + H_2O + H^+ = products

The proposed theoretical rate equation is;

Rate = k[MPTES][H_2O][H^+]

The initial concentration of [MPTES], [H_2O] and [H^+] are effectively constant because the initial rate was measured right at the beginning where we know what they were.

Since [H^+] and [H_2O] were effectively constant at the very beginning of the reaction throughout the six experiments where the [MPTES] was varied, we can write

Rate = $-k'$[MPTES]

The straight line in **Figure 4.6** confirms the reaction is first order with respect to MPTES.

Rate constant (from the slope of the graph) k' is =0.94 = **0.94hr^{-1}** from **Figure 4.6**.

Since k' = k[H_2O][H^+]

k = k'/ [H_2O][H^+]

k = 0.94hr/1.66mol/l. 2.29x10^{-4}mol/l

The absolute rate constant, **k=2361hr^{-1}mol^{-2}l^2**

4.3.2.2 Rate constant of MPTES hydrolysis with respect to [H^+]

The rates of the reaction were also determined as a function of the concentration of acid [H^+] used. The reaction was carried out using a 1.5 molar ratio of MPTES to water. The same reaction procedure as described in **Chapter 2.1.2** was applied and the spectra recorded in **Appendix 7** and graphs plotted in **Figure 4.7**. The initial rates determined from **Figure 4.7** were plotted against the [H^+] (**Figure 4.8)** to give the rate constant for the reaction.

^{29}Si NMR results monitoring the effects of increasing the concentration of acid on the hydrolysis and condensation of MPTES

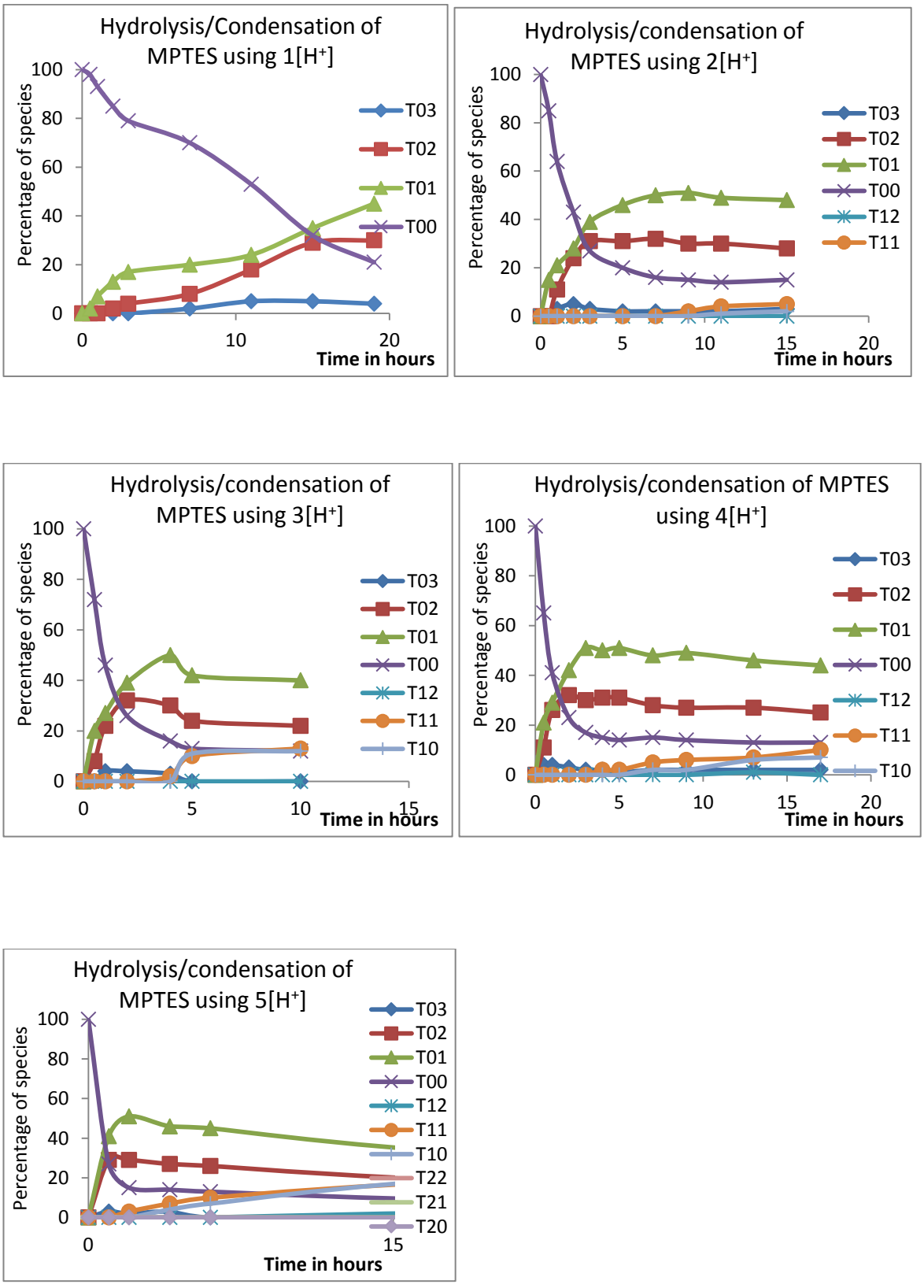

Figure 4.7. Hydrolysis and condensation of MPTES with varied amounts of acid.

Figure 4.7 shows the rate profiles for the hydrolysis of MPTES with respect to increasing acid concentration. From the graphs, the rate of hydrolysis is seen to increase as the amounts of acid increases. The initial rate for the consumption of acid can be calculated and plotted in **Figure 4.8**.

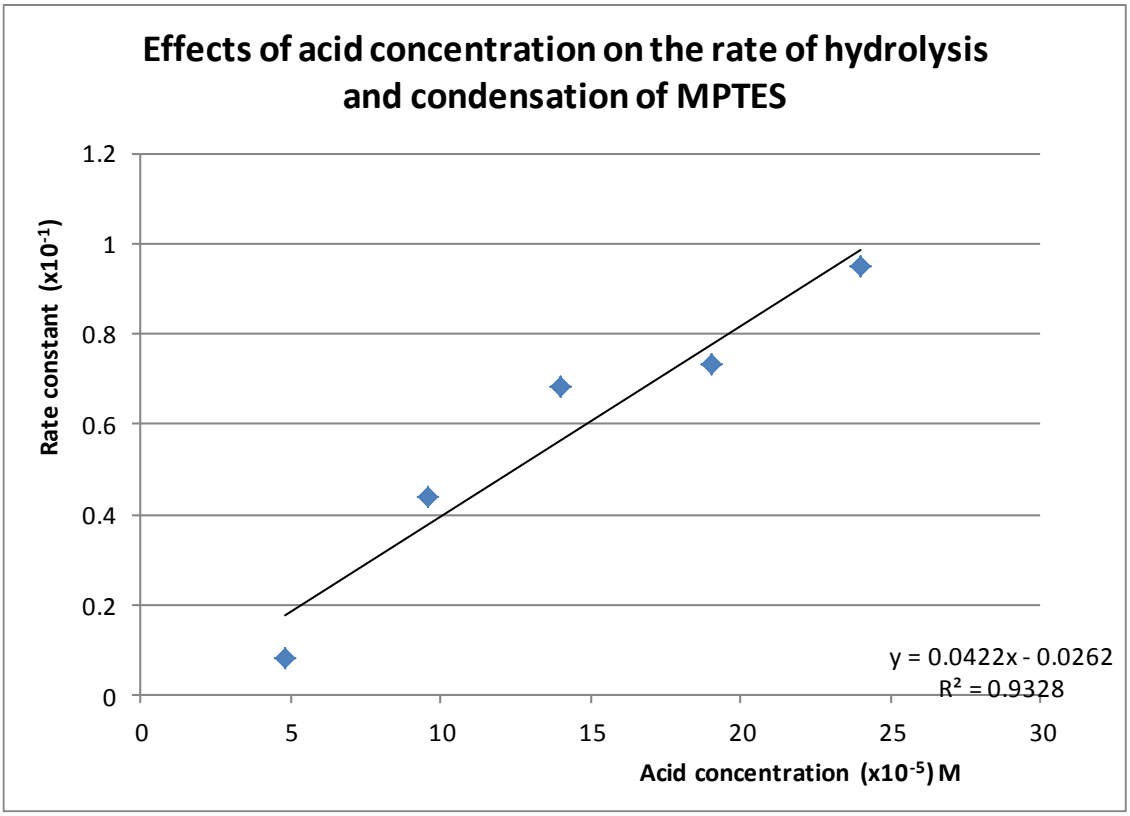

Figure 4.8. Initial rate of the reaction for the hydrolysis of MPTES with respect to acid concentration**.**

The reaction rate is directly proportional to the amount of acid added. As the concentration of acid increases, the reaction rate also increases indicating a first order reaction. Therefore;

Rate = k $[H^+]$ where k is the rate constant.

Rate constant k" = $0.042/10^{-5}$ = **4200hr^{-1}** from the slope of the graph in **Figure 4.8**.

We know [H_2O] and [MPTES] so we can calculate the actual rate constant and compare it with the previous value and data in the literature.

From these predictions, therefore the overall rate equation for the hydrolysis of MPTES is;

Rate = k[MPTES][H_2O][[H^+]

k" = k[H_2O][MPTES]

k = k"/ [H_2O][MPTES]

k = 4200hr^{-1} /1.66mol/l.1.11mol/l = **2282hr^{-1}** $mol^{-2}l^2$

This rate constant is very close to the previous rate constant with respect to [MPTES] of 2361 $hr^{-1}mol^{-2}l^2$.

4.3.3 Maldi-ToF-MS of MPTES hydrolysis and condensation using different mole ratios of water:MPTES

The mass spectrometry results from the MALDI-ToF-MS shows the different species formed (**Figure 4.9**). The proposed species are shown in **Table 4.3** with their corresponding ^{29}Si NMR chemical shifts in **Appendix 14** for MPTMS hydrolysis. The MALDI-ToF-MS results provide us with structural information of the species or Si-environments formed and how it differs using different ratios of MPTES to water. This goes to confirm the previous findings by other scientists and to confirm my earlier NMR results above (**Chapter 4.3.1 and 4.3.2**) about varying the molar ratios of MPTES to water. That is, the greater the relative amounts of water, the more condensed the species formed. **Figure 4.9** show increasing molar masses formed as one goes from 0.5 mol water to 1.5 molar water to MPTES.

Using 0.5mol H_2O

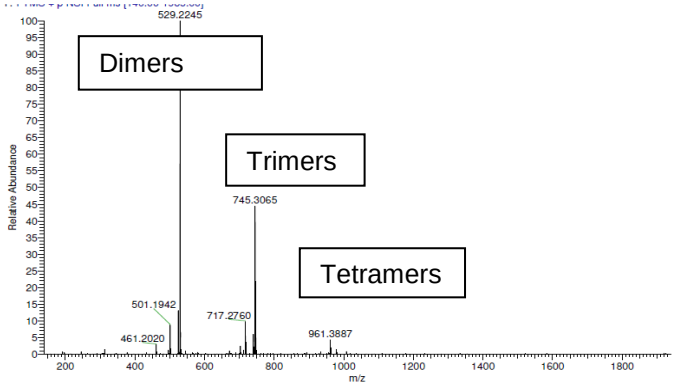

Using 1.5mol H_2O

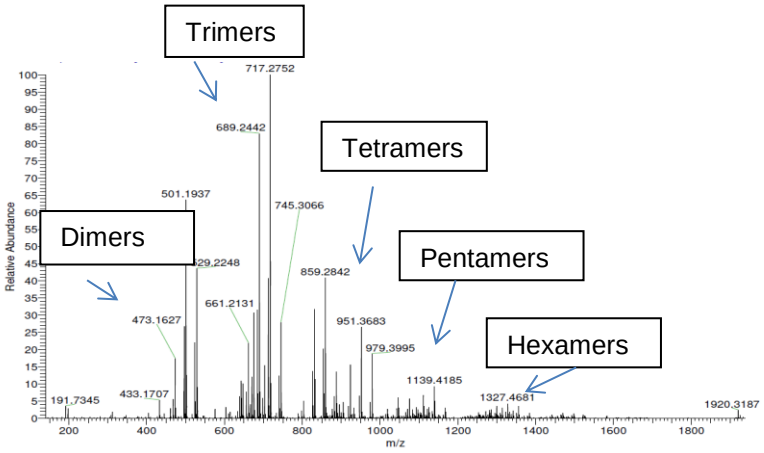

Using 3.0mol H_2O

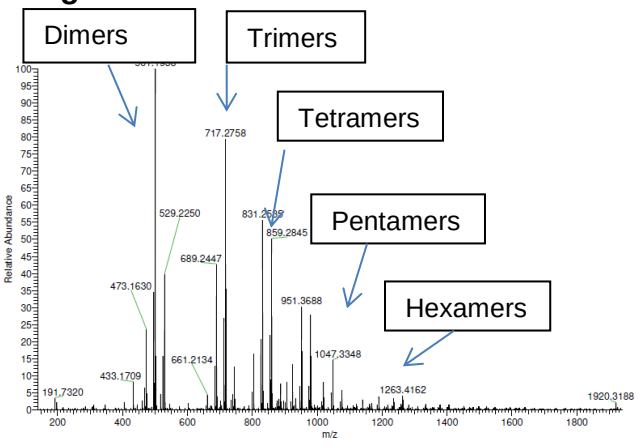

Figure 4.9. The MALDI-ToF-MS of the species formed following the hydrolysis and condensation of MPTES using different molar ratios of water: MPTES 0.5mol, 1.5mol and 3.0mol of water respectively.

As the water ratio to MPTES increases, the abundance of the peaks changes. For example, peak m/z 501 (corresponding to a dimer with silanols in a sodium ion positive mode) becomes larger with increasing amounts of water, whereas peak m/z 529 which corresponds to the dimer decreases. This implies as the amount of water increases, hydrolysis rate increases and hence more silanol species are being formed. Likewise, peak m/z 717 (trimer with silanol with sodium ion positive mode) increases with increasing amounts of water and then decrease again as silanol becomes less abundant. Peak m/z 745 (trimer in sodium ion positive mode) decreases as m/z 717 increases. This confirms the previous findings which say; hydrolysis increases with increasing amounts of water and agrees with the results in **Figure 4.3**.

Table 4.3. Predicted MALDI results of the different silicon environments formed in the polymerization of triethoxysilanes using 1:1.5 (MPTES:H_2O) ratio in relation to the ^{29}Si NMR chemical shifts.

NMR Chemical shifts	Proposed neutral species/ environments	Ions	Mass Spectrometry (m/z of ions)
-40.7	T_0^3 = RSi$(OH)_3$	T_0^3 = RSi$(OH)_3NH_4^+$	224.094
-42.1	T_0^2 = RSi(OEt)$(OH)_2$	T_0^2 = RSi(OEt)$(OH)_2Na^+$	243.066
-43.7	T_0^1 = RSi$(OEt)_2$(OH)	T_0^1 = RSi$(OEt)_2$(OH)Na^+	257.082
-45.7	T_0^0 = RSi$(OEt)_3$	T_0^0 = RSi$(OEt)_3Na^+$	271.098
-50.0	T_1^2=SiOSiR$(OH)_2$	T_1^2=SiOSiR$(OH)_2Na^+$	445.132
-51.3	T_1^1= SiOSiR(OEt)(OH)	T_1^1= SiOSiR(OEt)(OH)Na^+	459.148
-53.1	T_1^0 = SiOSiR$(OEt)_2$	T_1^0 = SiOSiR$(OEt)_2Na^+$	473.1634
-58.0	T_2^1= $(SiO)_2$ SiR(OH)	T_2^1= $(SiO)_2$ SiR(OH)NH_4+	656.258
-60.0	T_2^0= $(SiO)_2$ SiR(OEt)	T_2^0= $(SiO)_2$ SiR(OEt)Na^+	675.230

NMR and MALDI-ToF MS using 1molMPTES:1.5mol water. NB: Only one of the possible isomers are shown.

Table 4.3 gives a general summary of the species observed on the NMR using different molar ratios of MPTES to water.

4.4 Discussion of MPTES hydrolysis and condensation

Generally the discussion is the same as that of TEOS in chapter three since the findings are similar to those of Sanchez *et al.*[25] and Robert *et al*[265]. From **Table 4.3,** more silanol species are seen compared to fully condensed species. This is a similar observation with the TEOS species in **Table 3.4** confirming the similarity in the hydrolysis and condensation of these two groups of compounds (tri and teraalkoxysilanes).

4.4.1 Effects of acid concentration on hydrolysis and condensation of MPTES

Figures 4.7 and **4.8** are good indications of the effects of increasing the $[H^+]$. The acid acts as a catalyst, the higher the concentration of the acid, the faster the reaction and hence the faster the rate of hydrolysis and condensation. This agrees with the findings of Yang *et al.*[264] who predicted that increasing the $[H^+]$ leads to a proportional increase in polymerization. Yang also found that the rate of hydrolysis is directly proportional to the $[H^+]$.

4.4.2 Computer model to understand the kinetic behaviour of MPTES (T_0^0) hydrolysis and condensation

This section applies a similar model to that described in **Chapter 3.4.5** except that it is for MPTES instead of TEOS. The MPTES hydrolysis and condensation scheme is shown in **Figure 4.10**. The curve fits obtained are as shown in **Figure 4.11** and **Appendix 6** for the rest of the curves.

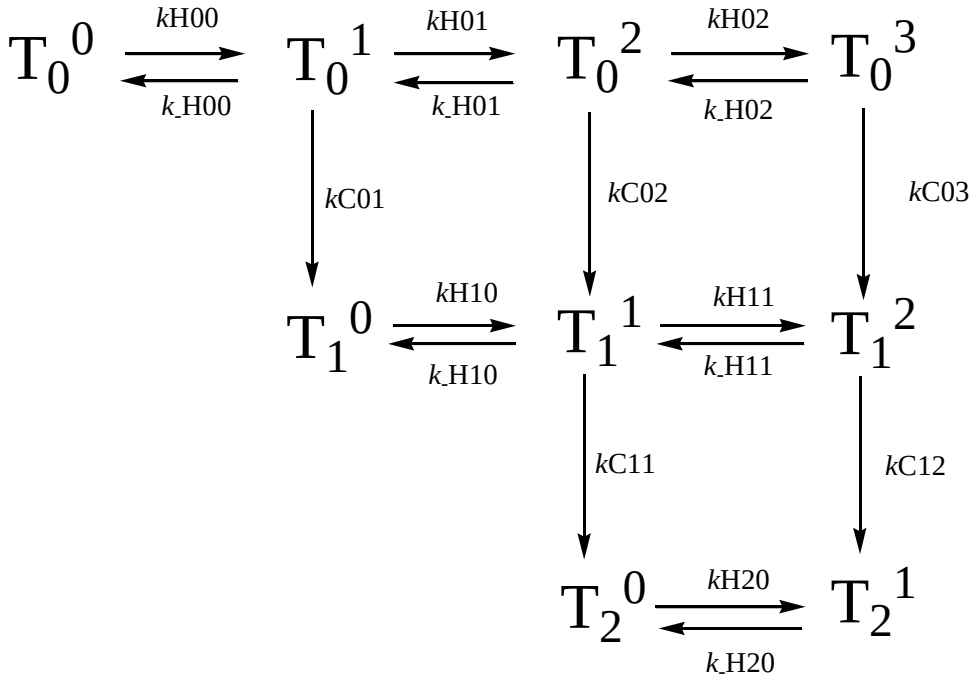

Figure 4.10. Schematic representation of MPTES hydrolysis and condensation

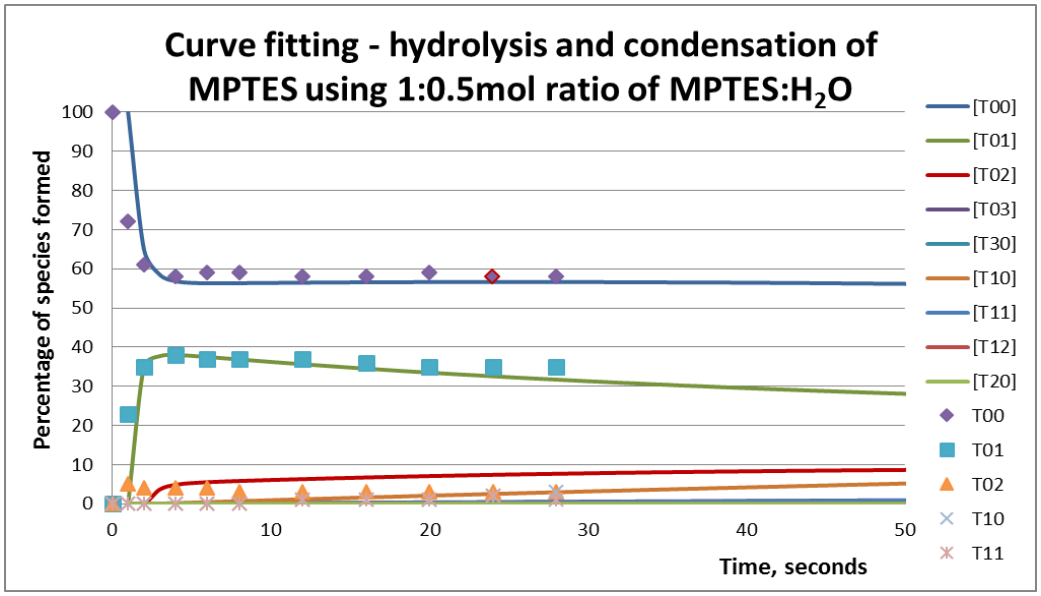
Curve fitting - hydrolysis and condensation of MPTES using 1:0.5mol ratio of MPTES:H2O
Percentage of species formed
Time, seconds
[T00]
[T01]
[T02]
[T03]
[T30]
[T10]
[T11]
[T12]
[T20]
T00
T01
T02
T10
T11

a)

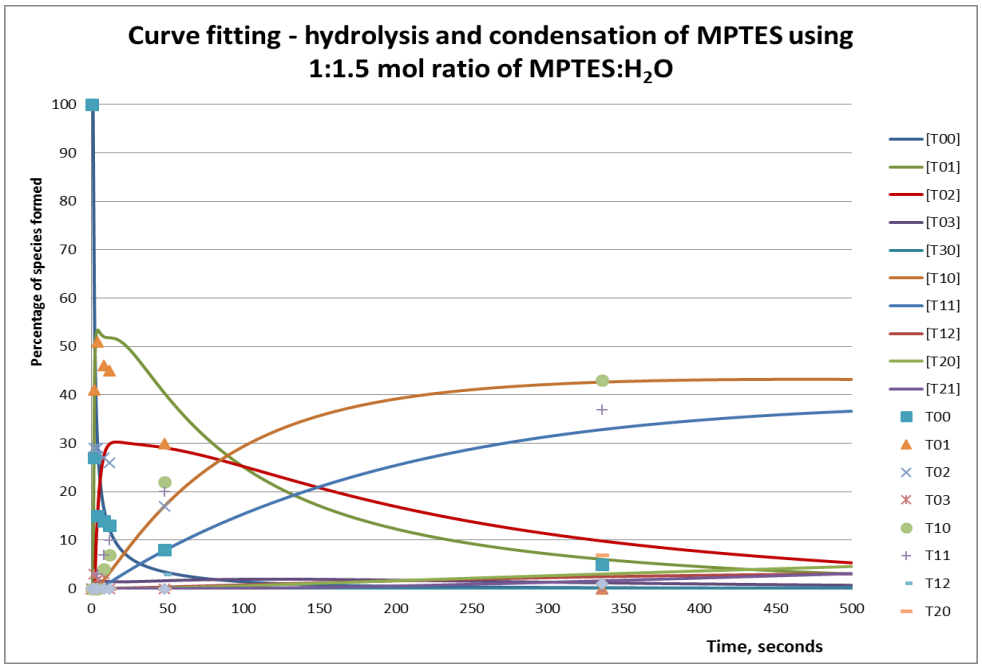
Curve fitting - hydrolysis and condensation of MPTES using 1:1.5 mol ratio of MPTES:H2O
Percentage of species formed
Time, seconds
[T00]
[T01]
[T02]
[T03]
[T30]
[T10]
[T11]
[T12]
[T20]
[T21]
T00
T01
T02
T03
T10
T11
T12
T20

b)

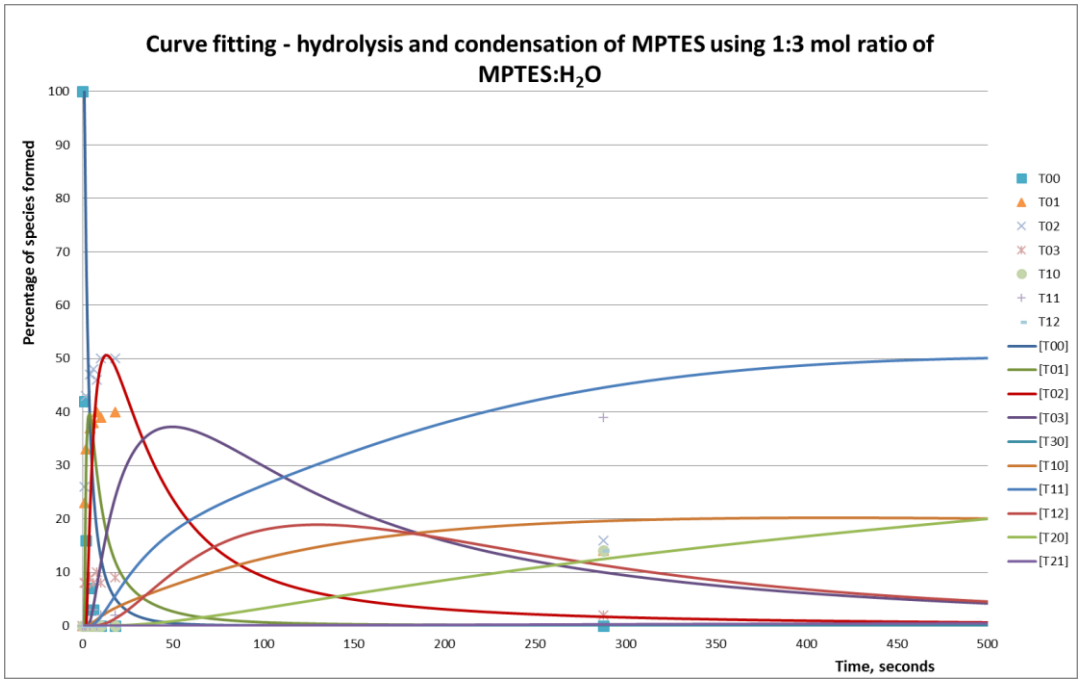

c)

Figure 4.11. Model and experimental curves showing the degree of hydrolysis of MPTES as a function of time using a) 0.5mol ratio of water: MPTES, b) 1.5mol ratio and c) 3.0mol ratio.

Table 4.4. Rate constants in (L (mol)$^{-1}$ h^{-1}) for six different hydrolysis reactions with the same amounts of water (1.66M) and acid [CF_3SO_3H] = 2.29x10^{-4}M.

	Composition MPTES/EtOH (M)	***k_1/k_{-1}* (K_1)**	***k_2/k_{-2}* (K_2)**	***k_3/k_{-2}*(K_3)**
1MPTES:0.5H_2O	3.13/7.90 excess	70/0.01	70/0.01	40/0.01
1 MPTES:1H_2O	1.66/7.60	25/0.1	12/0.1	30/0.1
1MPTES:1.5H_2O	1.11/11.07	30/0.008	20/0.1	15/1
1 MPTES:2H_2O	0.83/12.87	30/0.008	20/0.1	35/1
1MPTES:2.5H_2O	0.67/13.87	16/0.008	20/0.1	4/0.1
1MPTES:3.0H_2O	0.53/14.53	10/0.008	12/0.01	3/0.01

From **Table 4.4**, $k_1 > k_2 > k_3$ though not in a similar trend according to some literature results. However, Sanchez *et al.* predicts a similar trend of $k_1 > k_2 > k_3$.

The variation here is the same as that in TEOS, again this could in part be due to steric effects of the structures involved in hydrolysis and condensation not being accounted for as previously discussed in the TEOS case.

4.5 Developments and other findings following trialkoxysilane hydrolysis and condensation.

4.5.1 Alcohol exchange of MPTMS and nPTMS in ethanol

Since advanced coating materials using the Vitolane^{TM} methodology were initially made using methanol instead of ethanol, this section of the research aims at understanding the difference between using the same alcohol as solvent versus using different alkoxy groups to those contained in the starting material. Here, trimethoxysilanes (nPTMS and MPTMS) were hydrolyzed using ethanol as opposed to methanol (with a ratio of 1.5 H_20).

When the same MPTES reaction as above was repeated using MPTMS (**Appendix 9**) and nPTMS (**Appendix 8**) as starting materials, the result is an alcohol exchange reaction. We therefore get mixed methoxy and ethoxy peaks in the NMR. See **Figure 4.12** and **Appendix 13** for NMR spectra of the alcohol exchange reactions. The work is novel and has not been reported inliterature.

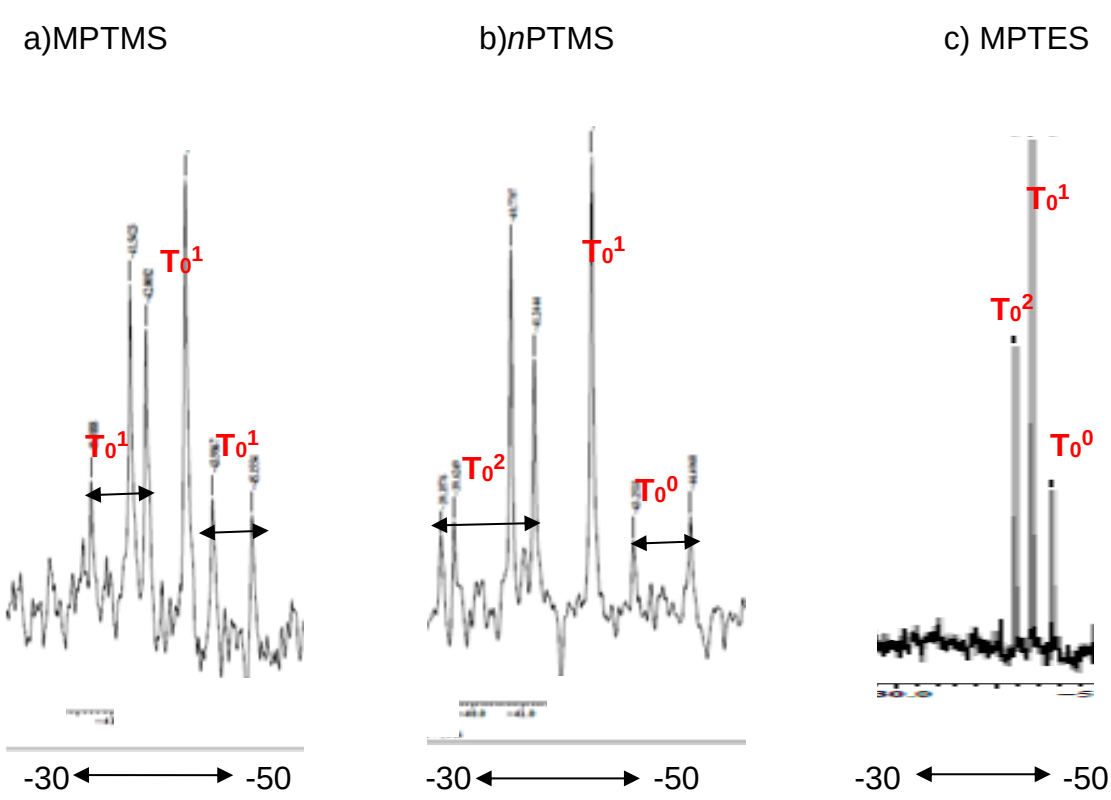

Figure 4.12. Comparing alcohol exchange in the hydrolysis of a) MPTMS in ethanol, b) nPTMS in ethanol and c) MPTES in ethanol.

Comparison of the same region between a), b) and c) shows greater complexity in a) and b) due to alcohol exchange leading to a greater variety of T_0^x species compared to the less complex c) spectra.

A full alcohol exchange peak assignments/interpretation has been done (See **Figure 4.13**) on an expanded diagram with peaks identified using the assumptions below:

- MeO to EtO leads to about a +1.14ppm shift
- EtO to OH leads to about a +1.5-2ppm shift and
- MeO to OH leads to about a +0.86ppm shift.

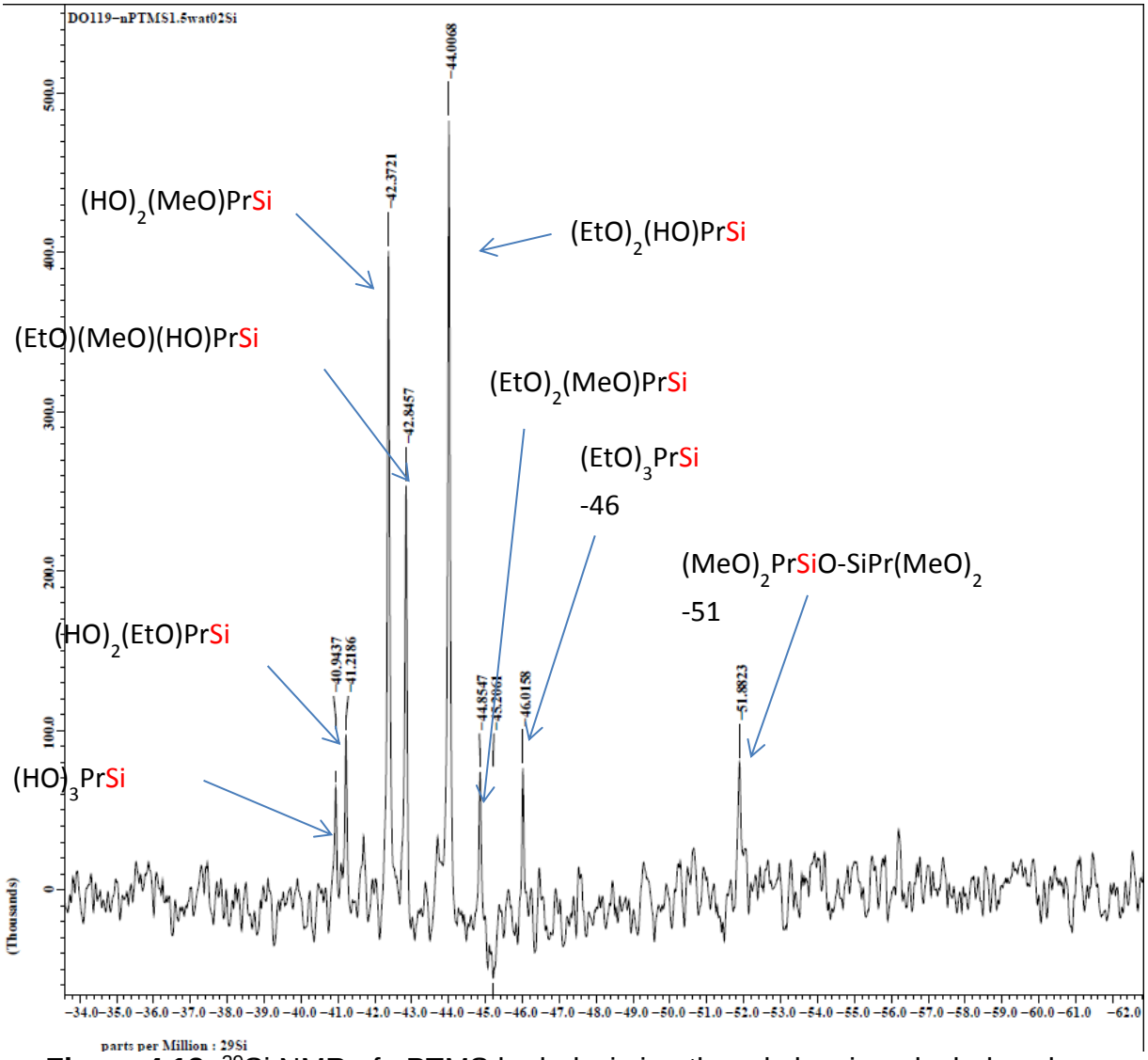

Figure 4.13. ^{29}Si NMR of nPTMS hydrolysis in ethanol showing alcohol exchange.

From the alcohol hydrolysis, one of the conclusions that can be reached is that due to greater [EtOH], ethanol exchange happens faster than hydrolysis.

Another conclusion to draw from this study is that alcohol exchange will lead to a slight change in the rates of hydrolysis for T_o^x species and thus affect the overall outcome and distribution of the products.

4.5.2 Co-hydrolysis of two trialkoxysilanes (nPTMS+MPTMS) plus the effect of variation in mixing pattern

In the case of a mixed system, that is, using two silanes within the same reaction, alcohol exchange does occur giving a complex mixture of products as shown in **Figure 4.14a**. Most importantly, it is realized that depending on the pattern of mixing the reagents, different products are formed as shown in **Figure 4.14b** and **Appendix 12**. In both cases, the same volume of reactants was being used. In **Figure 4.14a**, silanes were reacted individually in the ratios of 1.0mol MPTMS to 1.5molH_2O (**Table 4.1above**), with acid and ethanol and then finally mixed together and shaken for about a minute before being analyzed. The silanes each had the chance to hydrolyze individually before mixing together. In the case of **Figure 4.14b**, the same proportions of reactants were used but here, water, ethanol and both silanes (nPTMS+MPTMS) were added to one pot followed by acid addition. The silanes did not get the chance to hydrolyze independently but rather compete to hydrolyze against each other in the mixture. See **Figure 4.14a** and **Figure 4.14b** below for the different result patterns.

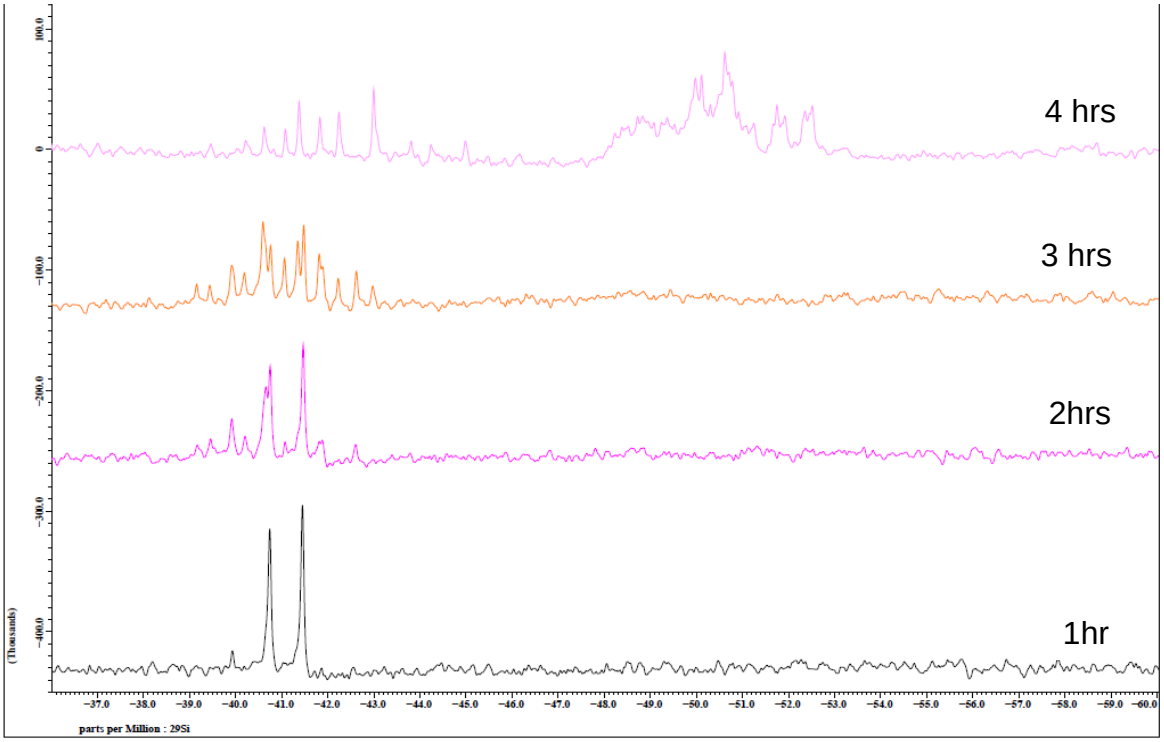

Figure 4.14a Hydrolysis of the individual silanes before mixing together (1hr, 4hr, 6hr, 218hrs).

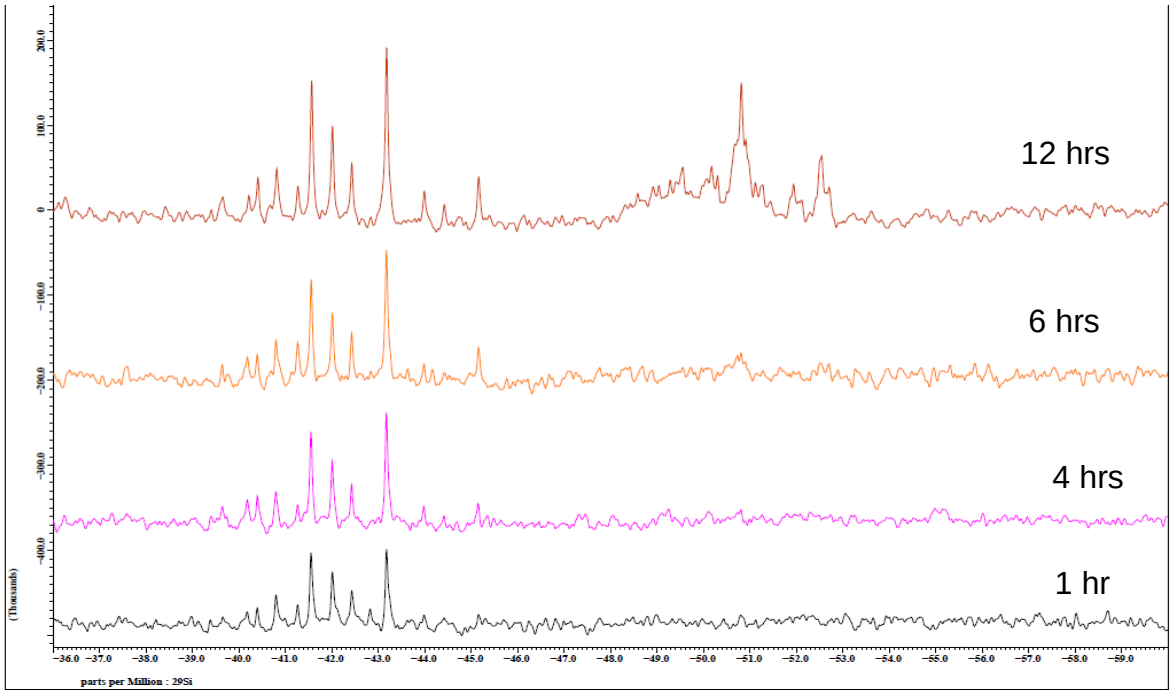

Figure 4.14b After mixing both silanes together and hydrolyzing (1hr, 4hr, 6hr, 12hr).

The two cases seem to yield a similar product, but when the silanes were independently hydrolyzed (**Figure 4.14a**), there appear to be slightly fewer peaks observed especially at the onset of the reaction compared to when they were mixed and then hydrolyzed together (**Figure 4.14b**). It appears once independently mixed, they each had the time to hydrolyze and condense to produce homo oligomers such that once mixed together, b) gave rise to block copolymers. In the second scenario when they were mixed together and then hydrolyzed, more random copolymers were made. However, because of the difference in reactivity between MPTMS and nPTMS, a certain extent of block copolymers were formed. nPTMS hydrolyses before MPTMS. This is because MPTMS is bulky hence steric effect leading to slightly slower hydrolysis than nPTMS. Chapter five will give more insight into the product mixture formed from such a combination of hydrolysis of two silanes (AZ-system).

4.5.3 Equilibrium studies to determine product life span.

What happens to the hydrolysis of MPTES once it reaches pseudo equilibrium when more silane, water and acid are added independently separately after every 24 hours? The results are shown in **Figure 4.15** A, B, C and D and **Appendix 11**. Using the same reaction mixture 1:1.5water (**Table 4.1**), a study was carried out after equilibrium had been reached. New reagents (silane, water and then acid) were added separately every 24hrs followed by NMR analysis in each case.

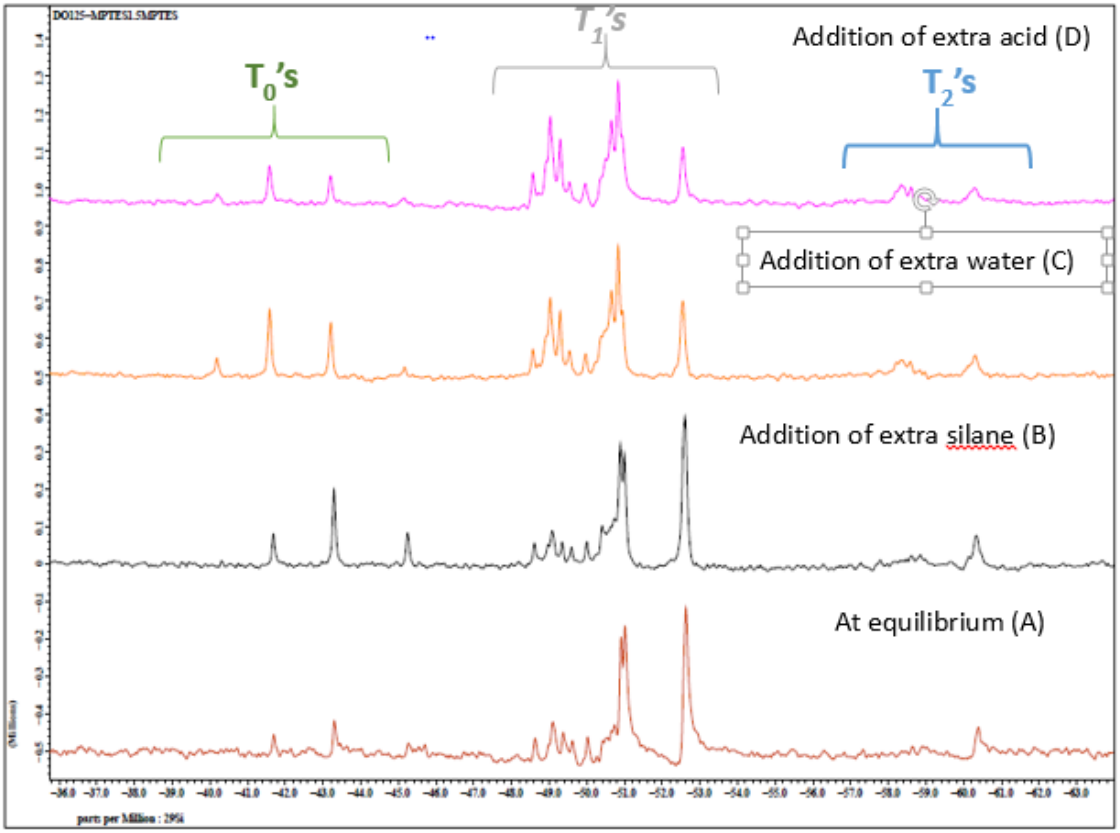

Figure 4.15 A, B, C, D: kinetic equilibrium studies following the hydrolysis of MPTES using 1:1.5 ratio of silane to water. A) at equilibrium, B) after addition of silane, C) after addition of water and D) after addition of acid.

4.5.4 Discussion of the equilibrium study

4.5.4.1 At equilibrium (Figure 4.15A),

There are more T_1 and T_2 species present and less T_0 than at the start.

4.5.4.2 After addition of more silane at equilibrium (Figure 4.15B).

After equilibrium, upon addition of more silane (MPTES), the equilibrium shift to the left as more T_0 peaks are observed (T_0^1, T_0^2). Not just a greater T_0^0 peaks were

observed but also some of it hydrolyzed to T_0^X species confirming there is still acid and water present at equilibrium. This result indicates that the acid has not been consumed so therefore pseudo equilibrium is not as a result of the loss of acid.

4.5.4.3 After addition of more water at equilibrium (Figure 4.15C)

More T_0^X hydrolyzed species are observed. More condensation is also observed. This indicates that there is still some acid left at equilibrium and that it has not been consumed. Some T_2 peaks are also being observed.

4.5.4.4 After addition of more acid at equilibrium (Figure 4.15D)

Slight changes are observed on the other silicon environments such as more T_2 environments increasing. However, there is not such a big change as acid is a catalyst and will not affect the position of the pseudo equilibrium.

4.5.5 Comparing the hydrolysis and condensation of MTPES vs TEOS

Sanchez *et al.* [25] studied the hydrolysis and condensation using ^{29}Si NMR and concluded that tri (T) and tetra (Q) alkoxysilanes hydrolyse at a similar rate. According to the data in this thesis, the hydrolysis rate constants (k) for MPTES is (2361 $hr^{-1}mol^{-2}L^2$) from section 4.3.2.1 and that of TEOS is (553$hr^{-1}mol^{-2}L^2$, section 3.3.3.1). This implies the rate of hydrolysis of trialkoxysilanes is greater than the rate of tetraalkoxysilanes by a magnitude of about four times. This disagrees with the findings of Arkles *et al.*[268] and Sanchez *et al*[25].

Furthermore, comparing the rates of hydrolysis of one silane over the other by varying the acid concentration shows that the rates with respect to MPTES (2282 $hr^{-1}mol^{-2}L^2$, **Figure 4.8**) is again faster than the rates with respect to TEOS (775 $hr^{-1}mol^{-2}L^2$, **Figure 3.7**). This equally disagrees with the discussions which suggested that TEOS is more reactive than MPTES. One reason for this is that acid can more easily protonate the TEOS compared to MPTES.

Looking at the electron donating and withdrawing effect of the groups around the silicon atoms in TEOS and MPTES in **Figure 4.16** below:

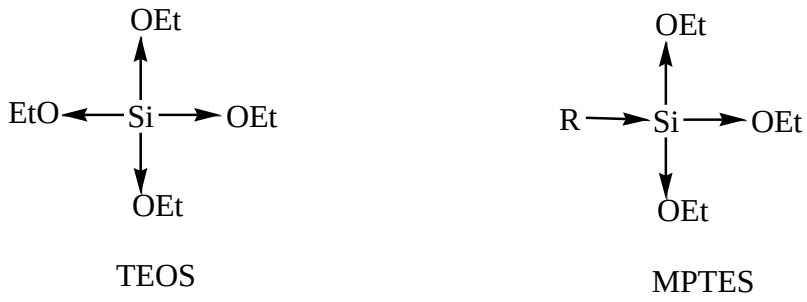

Figure 4.16. Showing electronic effect of the groups around the silicon atom in TEOS and MPTES

The silicon atom will be more positively charged in the TEOS than MPTES and thus if nucleophilic attack on the silicon atom is the rate limiting step, the TEOS should react faster than the MPTES. However, if the extent of protonation determines the rate of hydrolysis it could be argued that the lone pair on the oxygen will be more available in MPTES than in TEOS because the silicon is less positive. On the other hand, if steric effects prevail it might be expected that the bulky R group makes MPTES less reactive than TEOS.

Finally, the rate of condensation decreases with more alkyl groups attached to the central silicon atom. This is probably due mainly to the steric effect of the more bulky alkyl group on the various condensation reactions. What is certain is that the trend for the degree of condensation is opposite to the degree of hydrolysis for both the tri and tetra alkoxysilanes. This has also been confirmed by Schmidt and Sanchez *et al*.

4.5.6 Comparing the model results of both TEOS and MPTES hydrolysis and condensation

The model provides the following insights from the kinetic studies of TEOS and MPTES hydrolysis and condensation:

Overall, the model helped us to understand the process of hydrolysis and condensation of tri and tetraalkoxysilanes.

The model tells us that the back reaction is important for hydrolysis for both Q and T species because a single silicon site can go from Si-O-R to Si-OH and then back to

Si-O-R. However, the back reaction is not important for condensation because once Si-O-R or Si-OH goes to Si-O-Si, it cannot easily go back to Si-O-R again. (See **Figure 4.17** with illustrations of the various processes as noticed with most or all curves for TEOS and MPTES).

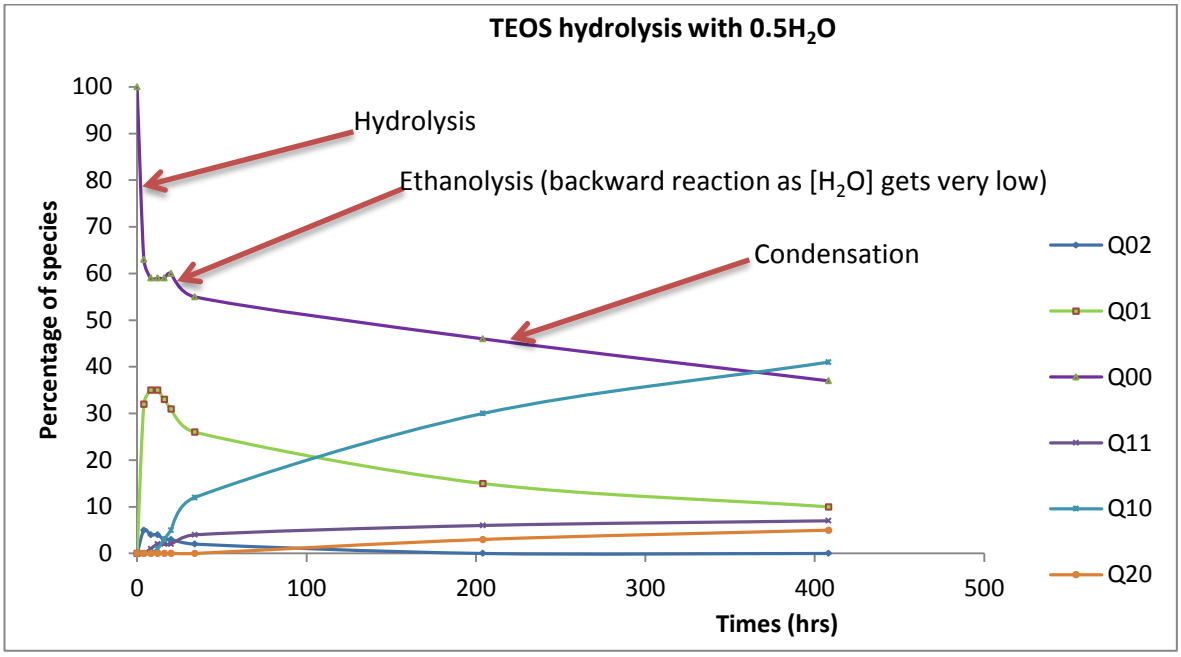

Figure 4.17. Graph showing the different processes with very low amounts of water. Initially TEOS quickly gets hydrolyzed to form Q_0^1, Q_0^2, Q_0^3, then there is a drop or small plateau which indicates no more water available. The backward reaction leads to the formation of Q_0^0, as condensation starts to become more important, water is formed and more hydrolysis slowly takes place. Towards the end of the reaction, the graph slopes, indicating condensation is beginning to become the predominant process (Q_1^0, Q_1^1, Q_1^2 etc).

- In both cases the model gives us the predictability of hydrolysis and condensation. That is, one can explore reactions that have not been done yet hence avoiding unnecessary reactions in the laboratory.
- The model also concluded that with higher [H_2O], Q_1^0 disappears quickly to other species Q_1^1 and Q_1^2. Also, Q_1^0 condenses very quickly to Q_1^1 . These suggest that both hydrolysis and condensation happens much faster with higher amounts of water.
- Finally, the model suggests that some control of hydrolysis and condensation of both TEOS and MPTES can be achieved with small amounts of water.

With larger amounts of water, hydrolysis and condensation becomes almost uncontrollable to manage.

4.6 Summary and Conclusion

The initial rate of hydrolysis and condensation is first order with respect to the [H^+] and [MPTES]. A pseudo equilibrium is achieved where the reaction stops regardless of the presence of any hydroxyl groups in the solution mixture.

The experiments confirmed that, at lower water to MPTES ratios (0.5H_2O:1MPTES), the concentration of the free silanol species are relatively low such that condensation is slow. As the ratio of MPTES to water increases (1.0 -1.5 mole equivalents), more hydrolysis and more silanols formed leading to more condensation. Condensation is faster at higher water to MPTES ratios above 1.5 mole equivalent. With excess amounts of water (>2.0 mole equivalent), more condensation is observed but this quickly becomes stable with little further condensation happening. On the other hand, increasing the concentration of acid leads to a proportionate increase in the rate of the reaction.

This study is particularly useful for industrial application depending on the nature of the target products. Only the necessary amounts of water will be used to avoid excess water in the product which may need removing afterwards and this will be a waste of material, time and energy. On the other hand, excess water can be added to the reaction if the target is to achieve a fully condensed composition. That is, the properties of the final product can be fine-tuned by modifying the amount of water.

The result also shows that, the mixing pattern, the type of solvent used and the type of trialkoxysilane can offer slight changes in the environment of the species formed.

Also, the study confirms that at pseudo equilibrium, the reaction virtually comes to a stop, important for shelf life of intermediates.

Finally, the kinetic study has been incorporated into a polymerization model in chapter 5 used to understand the structure development and properties of silsesquioxanes and other advanced hybrid materials.

CHAPTER 5 Silsesquioxane-based Resins

The chapter is one of the main reason for this research. The aim here is to understand silsesquioxane resin products for the need to find out what is going on in the reaction process and what products are being formed in the complex product mixture. The study of the hydrolysis of trialkoxysilanes in Chapter 4 have been applied in various case scenarios in this chapter in order to understand resin formation and other advanced materials [207]. The synthesis, purification, characterization and optimization study of advanced silsesquioxane materials have also been carried out.

5.1 Introduction

As defined in chapter one, silsesquioxanes are hybrid organic-inorganic nanostructured materials. They have the general formula $(RSiO_{3/2})_n$, where R is a hydrogen atom or an organic group and n is an integer (n=1, 2, 3,4)[21, 90,91,92]. They have various shapes and sizes from linear, random and cyclic to cage structures as shown in **Figure 1.5** [23,93, 94,95]. Silsesquioxanes act as suitable base materials for

coatings as mentioned in Chapter 1 section 1.6. **Figure 5.1** shown below is a picture of an aerogel developed from silsesquioxanes by our research counterpart TWI Ltd, which serves as a good coating material with insulating properties.

Figure 5.1. Aerogel on a Bunsen burner. This aerogel was made by our collaborators TWI Ltd following this research work. TWI copyright[23]

In this chapter, silsesquioxane resins will be discussed in detail. Their synthesis, purification, characterisation and optimisation of the silsesquioxane products will be studied following the knowledge gained in chapters three and four for the mechanism of hydrolysis and condensation of tri and tetra-alkoxysilanes. Such a study is very important for the optimisation of coating materials for various applications such as: antifouling, antimicrobial, aerogels and other advanced coatings [269,270, 271, 272, 273].

In this chapter, two types of synthesis have been described: The single component-system (A-system) and the two component-system (AZ-system) for making

silsesquioxane resin mixtures. The single component-system involves the preparation of a silsesquioxane resin using a single monomer, 3-methacryloxypropyltrimethoxysilane (MPTMS) as the starting material. The AZ-system involves the use of two monomers; methacryloxypropyltrimethoxy silane (MPTMS) and n-propyltrimethoxy silane (nPTMS) as starting materials as discussed in Chapter 4.5.2. The mechanisms of these reactions have been followed by characterization using various instrumental techniques which include: MALDI-ToF MS, ESI-MS, ^{29}Si NMR, FT-IR, DSC and HPLC-MS.

Furthermore, some smaller model compounds such as the MPTES functionalised dimer, tetramer and T_8 cage have been synthesised, isolated and characterised using various different techniques to use as models for further structural analysis of silsesquioxanes.

Single component-system of silsesquioxane synthesis

5.2.1 Introduction

The single component-system for synthesising silsesquioxane resins refers to using only one starting material, 3-methacryloxypropyl trimethoxysilane (MPTMS) along with methanol, water and acid. This synthesis follows the vitolane^{TM} method designed by TWI Ltd[23].

In this initial work, the aim was to synthesise silsesquioxane resins using the quickest and cheapest route possible, yet leading to optimised coating properties for industrial applications as mentioned in the introduction. Another reason was to meet the government regulations of coatings with low volatile organic compounds

(VOCs). So, using a single starting material (MPTMS) was an appropriate place to start, especially since it met most, if not all, of our requirements of robustness, cheapness and low VOCs as discussed in the introduction. This chapter describes how the silsesquioxane resin was made and its structural composition.

The hydrolysis and condensation of MPTMS leading to the formation of the resin follows the same reaction as described in Chapter 2.1.2 and studied in Chapter 4 of this thesis. The product of the hydrolysis and condensation was characterized using ^{29}Si NMR spectroscopy, also studied in Chapter 4. Column chromatography, preparative thin layer chromatography and distillation were used to separate/isolate some of the smaller fragments of the silsesquioxane resin mixture.

The effects of varying some of the reaction conditions such as water, methanol, acid and time were also examined.

5.2.2 Synthesis and mechanism of (3-methacryloxypropyl) silsesquioxane resin formation by the single component-system (A-System)

The synthesis of this methacrylate functionalised silsesquioxane resin follows a process called the Vitolane™ Technology [1]. This involves reaction of a silane precursor, 3-methacryloxypropyl trimethoxysilane (MPTMS) with water, methanol and a few drops of concentrated hydrochloric acid (HCl). The process has two stages, the first product is recovered after 24hrs in an oven to remove all the volatile components by evaporation (before quenching).The second and final Vitolane product is recovered after the first product has been quenched in water to remove

excess solvents before further drying in an oven for 24 hours at 65^{0}C (after quenching). The silsesquioxane resin formed (Vitolane) is a mixture and could contain linear, ladder, cubic and random structures. The synthetic scheme is shown in **Figure 5.2** below.

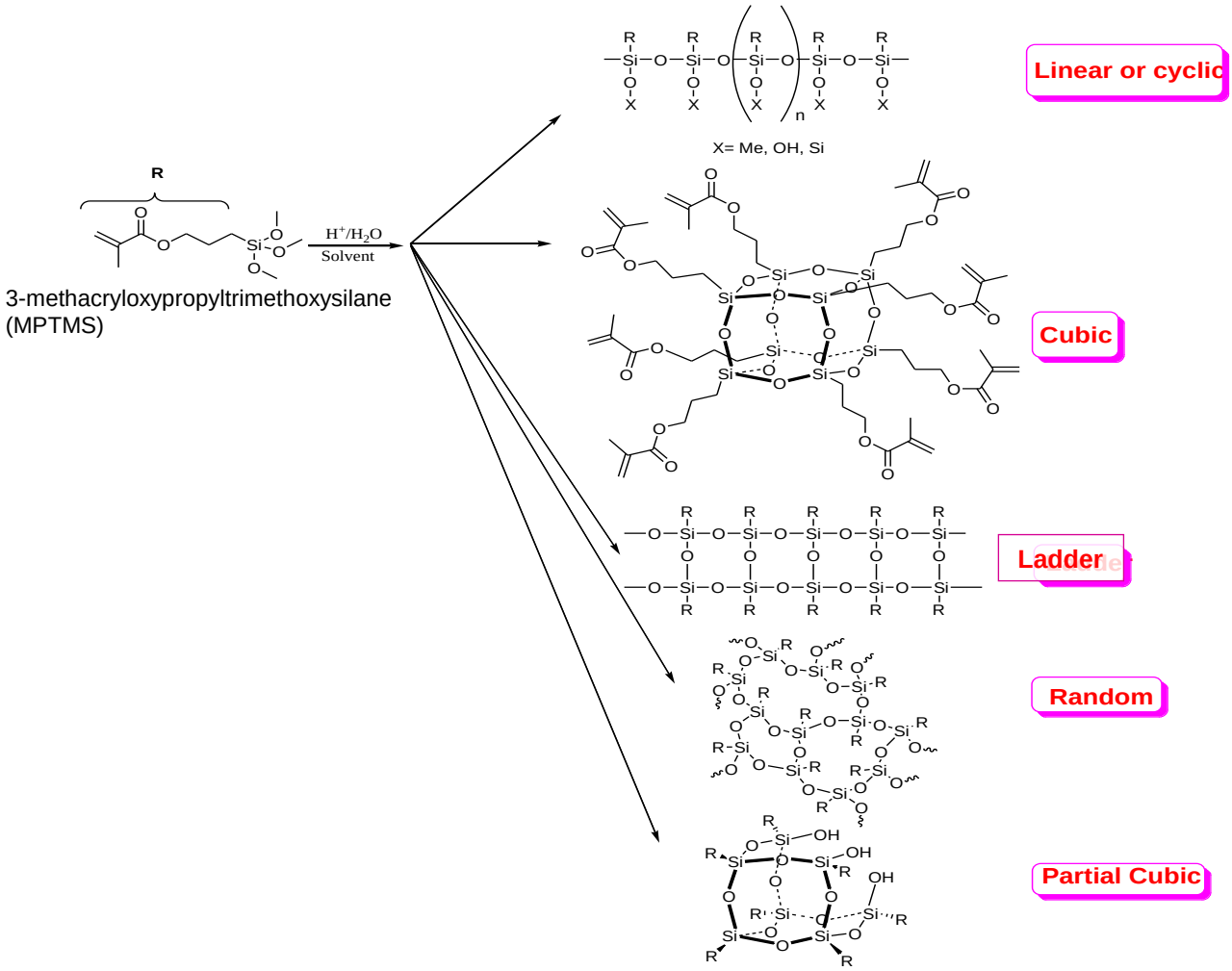

Figure 5.2. Possible composition of Vitolane resin formed from the reaction of 3-methacryloxypropyl-trimethoxysilane monomer with water.

The above reaction has been repeated more than twelve times, yet the product obtained remains the same (mixture) and is obtained in high yield. This implies the synthesis of silsesquioxane resins is very repeatable. Also, previously it was done

in 24 hours but in this study, after four hours the product was obtained hence reducing the reaction time. The mechanism of the silsesquioxane formation is the same as that described in the sol-gel process in Chapter 4.2. The structure of the silsesquioxane resin that evolves depends on the degree of hydrolysis and condensation reactions that takes place[203, 206, 274].

5.2.3 Results and discussion of the silsesquioxane resin formed by the single component-system (A-system).

The silsesquioxane resin formed from the polymerization of 3-methacryloxypropyl-trimethoxysilane resin was characterized using different instrumentation as below.

5.2.3.1 ^{29}Si NMR Results of the A-system silsesquioxane resin

The solution 29-silicon NMR shows the type of silicon species formed following the sol-gel polymerization process. The different silicon environments in the resin are identified according to the conventional T_m^n notation as earlier defined in Chapters 1, 3 and 4. Where T refers to the trifunctional units and m corresponds to the number of neighboring silicon atoms interconnected through oxygen atoms of the first sphere of coordination [15, 17]. T_0^0, T_1^0 and T_2^0 are monomeric and dimeric silicon environments, while T_3^0 represents completely condensed silicon atoms. The ^{29}Si NMR of organotrimethoxysilanes such as the starting material, MPTMS ($RSi(OMe)_3$) generally show a sharp single peak at around -40 to -42 ppm (T_0).

The first groups of peaks at -49 to -52 ppm corresponds to T_1 silicon environments with a single siloxane bond (**Figure 5.3**) and varying states of hydrolysis, for example; T_1^2 [$RSi(OSi)(OH)_2$]. They are about 8ppm upfield from the parent

monomer (T_0^0) in the ^{29}Si NMR spectrum. They represent mostly dimers or the end groups of oligomers and other linear structures of the silsesquioxane resin mixture. The second groups of peaks at (-57 to -61) ppm form silicon species with two siloxane bonds and lie a further 8ppm downfield. These are called T_2 silicon environments e.g. T_2^1 [$RSi(OSi)_2(OH)$] (**Figure 5.3**) and corresponds to mostly linear portions of the compounds. The third group T_3 at peaks (-63 to -70) ppm are silicon species with three siloxane bonds [$RSi(OSi)_3$]. They are a further 8ppm upfield and appear broad. These can range from branched, random, cyclic or cage-like structures.

The proportions of T_0 (monomeric species), T_1 (dimers and end groups) and T_2 (linears) suggest a fairly simple mixture of short chain oligomers are formed. The absence of T_3 species suggest little branching.

A reaction of the hydrolysis and condensation of MPTMS was carried out in ethanol and this led to a mixture of products due to alcohol exchange between the methanol and ethanol as earlier discussed in section 4.5.1.The reaction was carried out on a 1:1 molar ratio of MPTMS:water which is the proposed original Vitolane™ methodology apart from the different acid and acid concentration used here. **Figure 5.3** below shows the products formed and their corresponding species/environments assigned. Where X, Y and Z represent OH, OMe and OEt respectively.

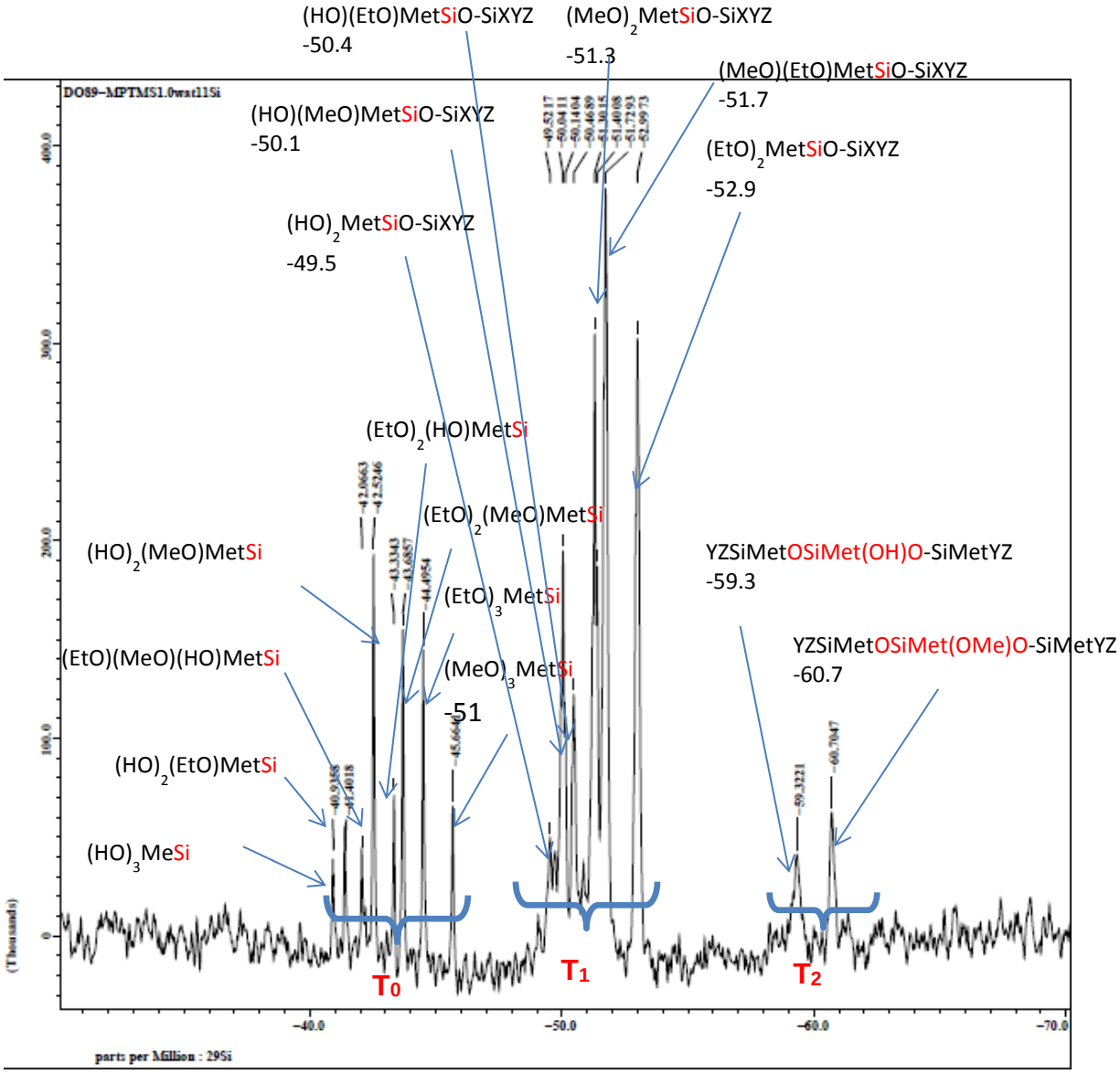

Figure 5.3 ^{29}Si NMR spectrum of 3-methacryloxypropyltrimethoxysilane silsesquioxane resin prepared using trifluoromethanesulphonic acid (2.3×10^{-4}mol/L) in a 1:1 molar ratio of MPTMS:water. The spectrum shows T_0,T_1 T_2 silicon species or environments.

The above assignments were based on findings from Chapter 4 and also based upon the assumptions below in the case of alcohol system such as this.

Assumptions/approximations in analysis

The methanol-ethanol exchange is assumed to lead to some changes in the chemical shifts on the ^{29}Si NMR as stated in chapter 4.5.1 on page 167.

In the T_1 region of the spectra in **Figure 5.3**, there are more peaks than can be accounted for based on first shell effects (i.e. the immediate environment around the silicon atom in question) so the shift depends on the nature of XYZ in (MeO)(EtO)MetSiO-SiXYZ where Met means methacryloxypropyl.

Figure 5.4 shows the peaks in the A-system resin prepared using Vitolane's solgel method. From **Figure 5.3** and other ^{29}Si NMR spectra in Chapter 4, these peaks can be identified where X, Y, Z represent OMe, OEt, and OH respectively.

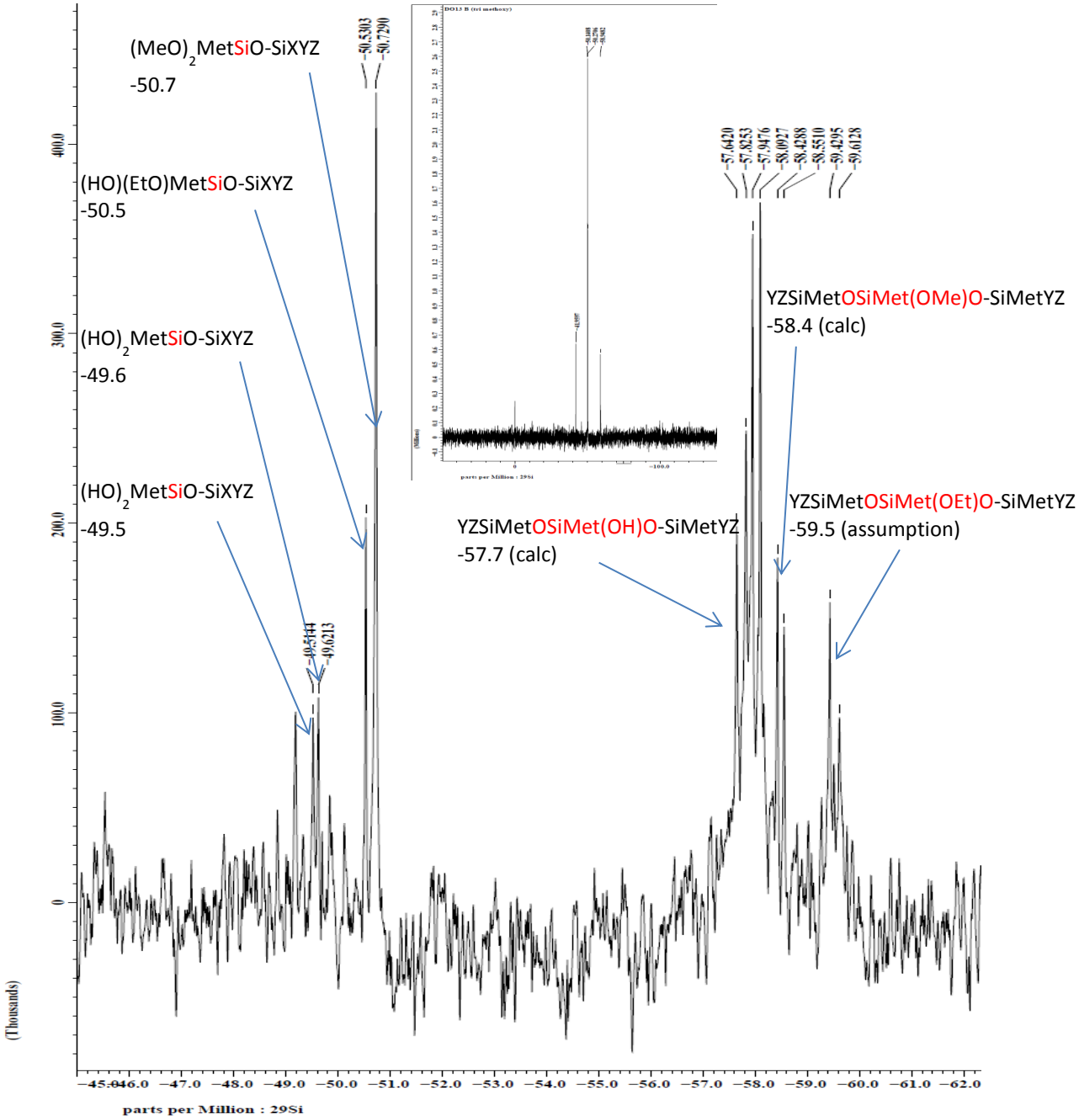

Figure 5.4. ^{29}Si NMR spectrum of 3-methacryloxypropyltrimethoxysilane silsesquioxane resin using the Vitolane-solgel approach (1MPTMS:1H_2O) in ethanol.

Notice that the peak assignments are speculations only because of the complexity of the peaks analysis. In **Figure 5.4,** there is no peak at -45 indicating there is no

starting material or T_0^X species left in the resin product mixture. There are more T_2 peaks implying larger oligomers.

There are mainly T_1^X (dimers and end groups) and T_2^X (linear portions) species although the amounts of T_2^X is greater than T_1^X. It can therefore be concluded that vitolane consists of mainly short chain oligomers (cyclics and linears) with little branching. Although the extent of oligomer formation is greater than that shown in **Figure 5.3** when methane sulphonic acid was used.

To conclude, it has been noted from previous work by the industrial partners, TWI Ltd[23] that hydrolysis/condensation of MPTMS to silsesquioxane resin resulted in a significant increase in the fraction of T_1 and T_2 environments but less of the proportion of T_3 species. This implies little branching occurs and the products are mainly linears and cyclics. Presumably condensation to form T_3 species is slow as a result of steric hindrance. The presence of so many free silanols suggests the hydrolysis of the methoxy groups of the MPTMS occurs first, but condensation of these hydroxyl groups is relatively slow. This finding by TWI has been confirmed in this research with even more in-depth identification of the individual/group of the peaks. Moreover, more silanol (Si-OH) peaks are seen than first suggested by TWI.

5.2.3.2 FT-IR of the A-system silsesquioxane resin

FT-IR was used to study the product of the hydrolysis and condensation process, and to identify the silanol content in the silsesquioxane resin mixture. The FT-IR spectrum (**Figure 5.5**) shows the presence of the Si-OH stretch with a peak at 3021.01cm^{-1} which was not present in the starting material, MPTMS (**Figure 5.5a**).

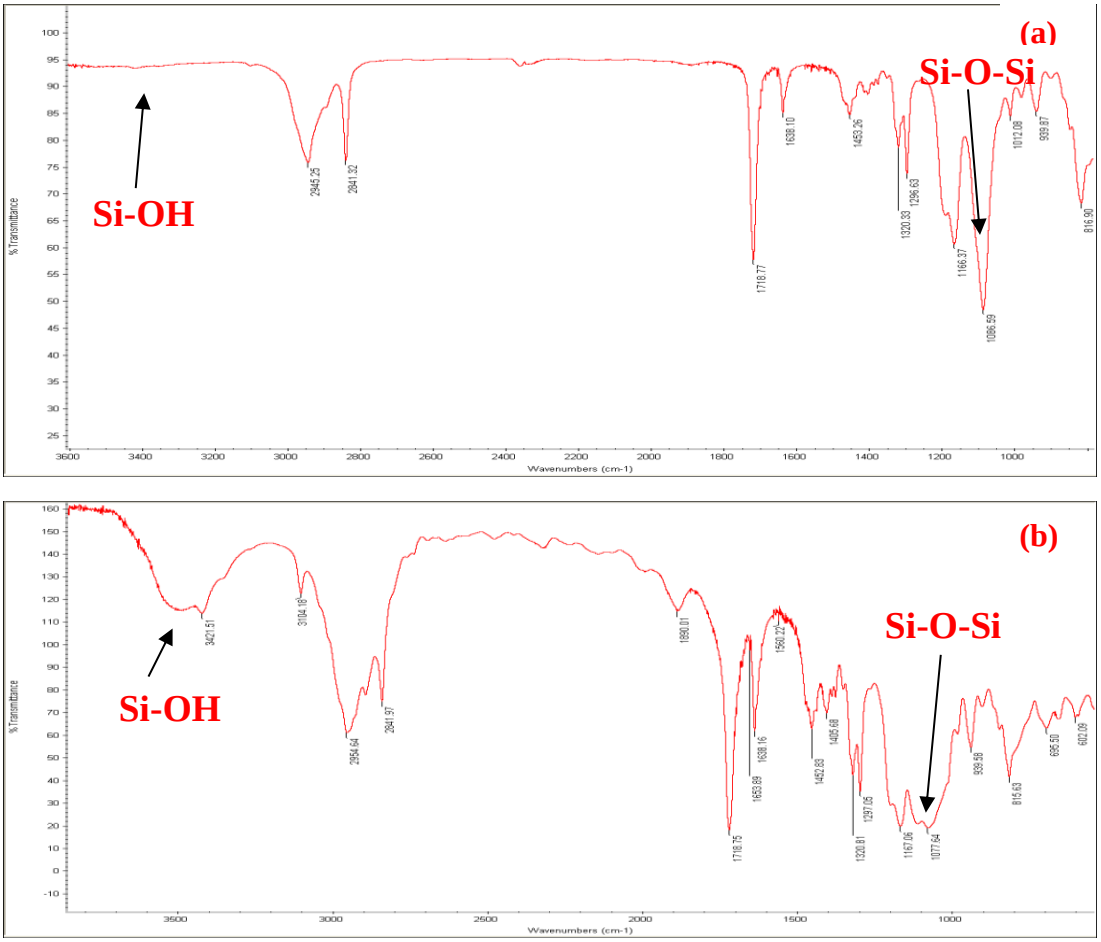

Figure 5.5. (a) FT-IR spectra of MPTMS silane and **(b)** FT-IR spectra of the A-system silsesquioxane resin measured using ATR (attenuated total reflectance).

The broad Si-OH peak in the FT-IR spectrum of the resin indicates a good degree of hydrolysis taking place compared to condensation which would have led to fewer less Si-OH bonds. This agrees with the conclusion from the ^{29}Si NMR spectra above. This suggests condensation is not complete although the broad O-H peak could also be due to some extent from the ethanol/methanol or residual water still present in the product mixture.

5.2.3.3 TGA of the A-system silsesquioxane resin

The thermal stability of the resin was investigated by TGA at a heating rate of 10^0C/min. The resin exhibited a high thermal stability under nitrogen. The TGA results of the resin (**Figure 5.6)** shows a minor weight loss between 180-300^{0}C, which indicates that moisture and solvents (water, methanol) are lost through evaporation. The endothermic peak at 320-330^{o}C arises from polymerization of the resin. There is a weight loss of a major fragment at about 380-600^{o}C. At this temperature, it is tentatively assigned that the resin begins to polymerize and we are also losing the organics (R-groups). That is, product loss by the cleavage of silicon-R bonds. After oxidation, 40% of the component remains as residue on heating up to 1000^{o}C (**Figure 5.6).** This means that the resin is a very suitable coating material because up to 40% of it is retained after heating or oxidation at high temperatures making the coating durable.

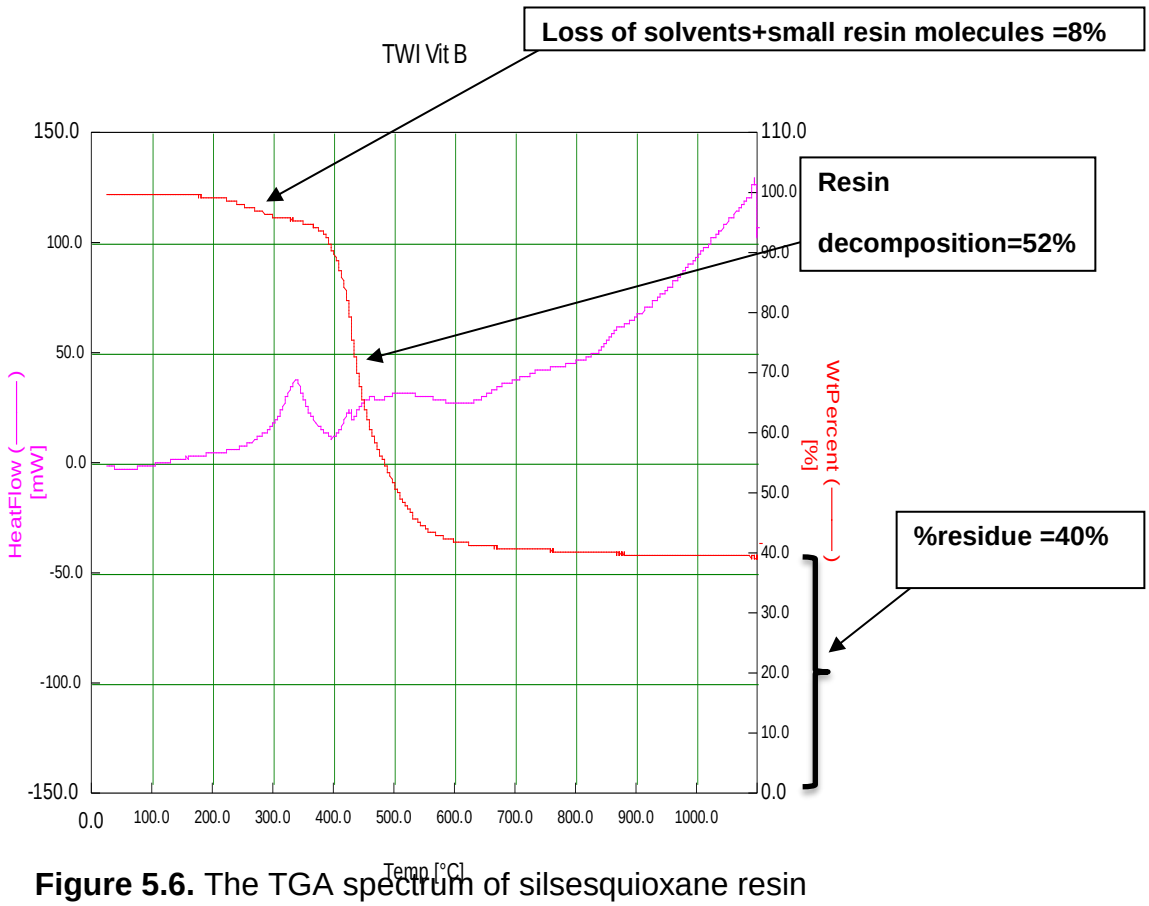

Figure 5.6. The TGA spectrum of silsesquioxane resin

5.2.3.4 DSC of the A-system silsesquioxane resin

DSC is similar to TGA. DSC measures the thermal behavior of the resin at different temperatures. When applications of these polymers are considered, such as highly temperature-resistant insulating materials for use in space craft and computer chip fabrication technology, the materials require very high thermal stability

The DSC reflects the heat flow graph shown in the TGA in **Figure 5.6**. The DSC trace shows a heat gain peak between 300^0C to 400^0C corresponding to the polymerization of the acrylic groups. This is followed by some heat changes above 400^0C corresponding to the cleavage of Si-C bonds and loss of the ligand. The

reaction requires an exceptionally wide temperature range to achieve the conversion.

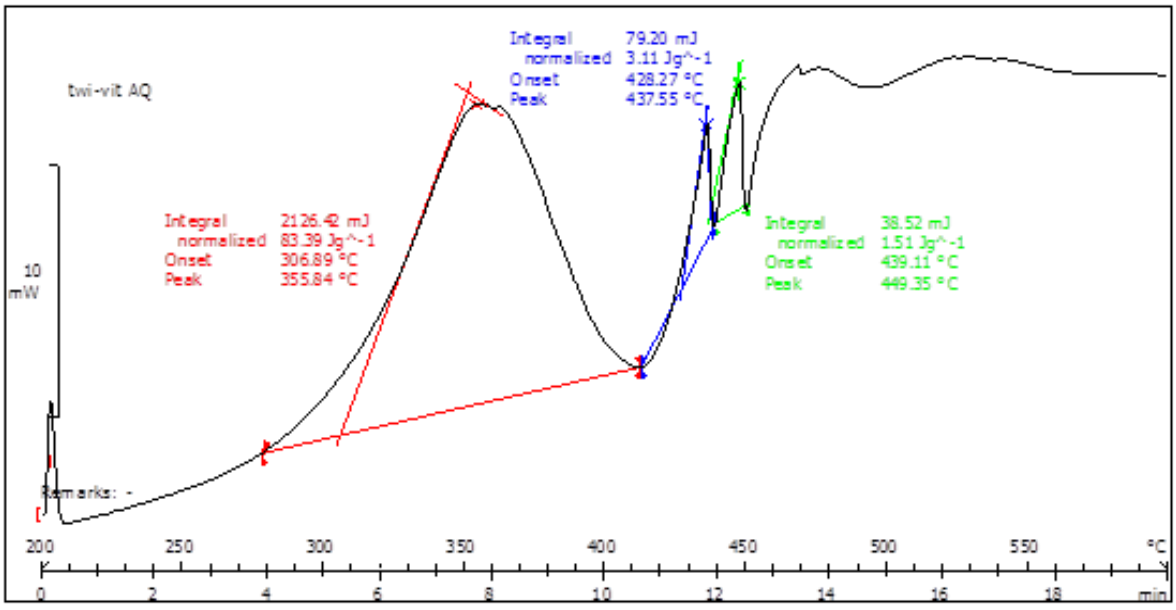

Figure 5.7. The DSC spectrum of Silsesquioxane resin measured between 0-600^{o}C at 20^{o}/mins

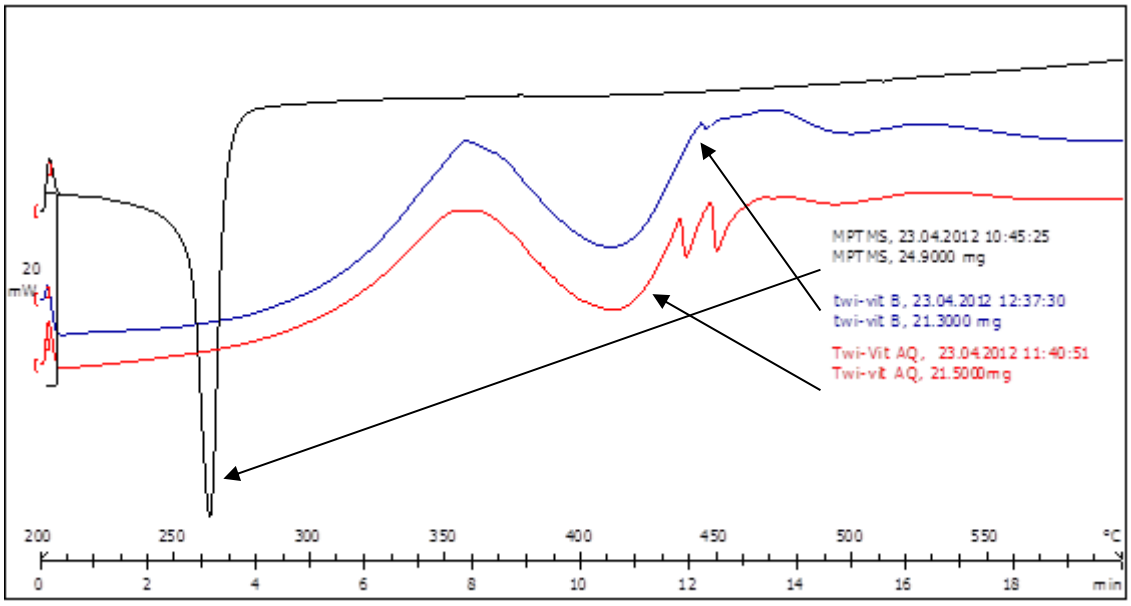

Figure 5.8. The DSC spectrum of three materials; starting material (black, MPTMS), silsesquioxane resin before quenching (blue) and silsesquioxane resin after quenching in oven (red). Where vit B = Vitolane before quenching in water, vit AQ = After quenching in water.

Figure 5.8 shows a comparison of all three materials (MPTMS), silsesquioxane resin before quenching (TWI-Vit B) and after quenching and drying (TWI-Vit AQ). With MPTMS, evaporation occurs at about 262^0C. In the resins, the broad peak between 300-410^{o}C is polymerisation, there are two more peaks in the spectrum in red (Twi-vit AQ). This suggests that in the final Vitolane^{TM} process after further quenching in water, more condensation takes place leading to the formation of some slightly larger structures such as cyclics or even ladders. Loss of ligands from these larger structures occur at higher temperatures around 420 and 450^{o}C on the DSC. These structures could be included in the major fragment loss on the TGA in **Figure 5.6** between 380-600^{o}C (Twi vit B) which is very similar to TWI vit AQ TGA. Such similarity in the TGA results indicates the DSC peaks around 420^{o}C are not real peaks, they could be simply noise.

5.2.3.5 Surface morphology and CHN analysis of the A-system resin chars following DSC

In order to classify a coating precursor such as a silsesquioxane resin as a good fire retardant, it is important to not only rely on the results of DSC, but also to gain an insight into the composition of the chars obtained from the pyrolysis. The chemical composition of the chars was studied by FT-IR and the results are shown in **Figure 5.10**. Carbon, Hydrogen and Nitrogen (CHN) analysis was also carried out to obtain elemental information (**Table 5.1**).The char of the silsesquioxane resin obtained in nitrogen from a viscous liquid, ended up as hard black substances that was difficult to break (**Figure 5.9**).

Figure 5.9. (a) Pure silsesquioxane resin and (b) the product of the silsesquioxane resin after being exposed to a high temperatures of 600ºC by DSC.

5.2.3.5.1 FTIR analysis of samples before and after DSC

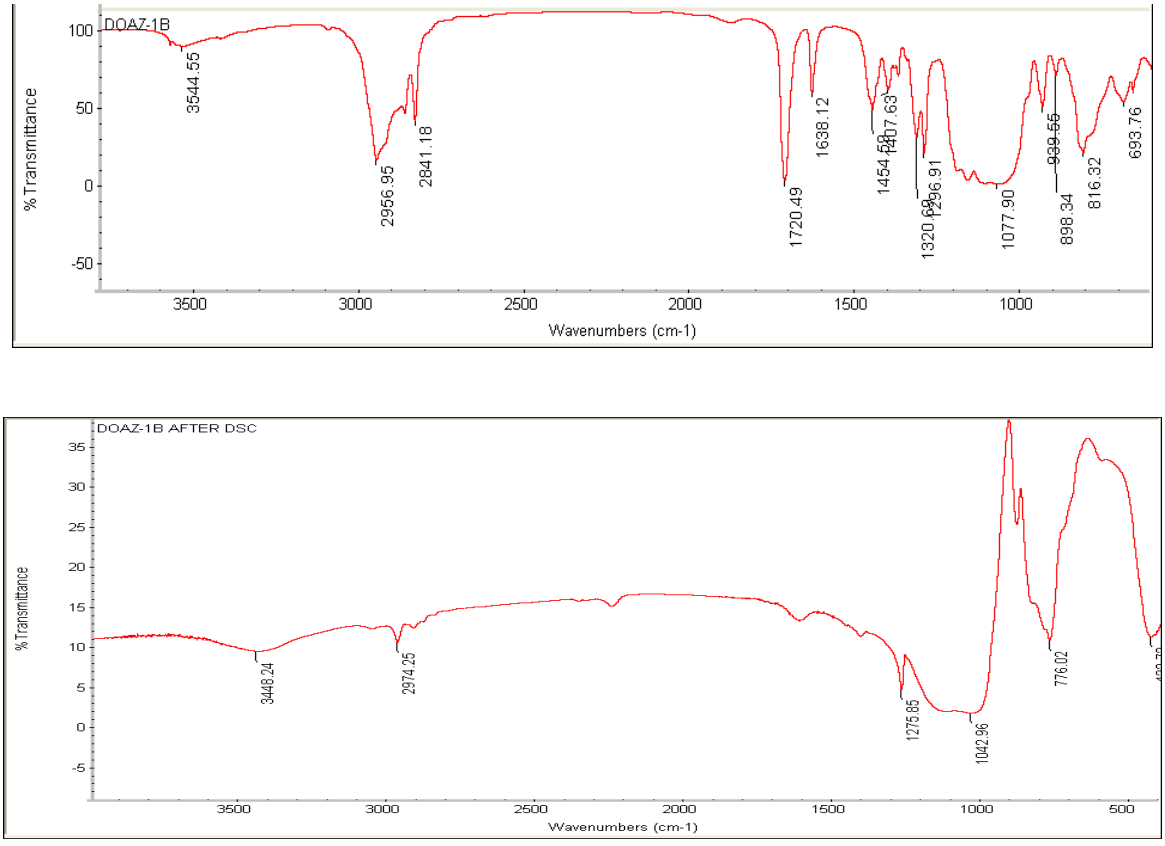

Figure 5.10. FTIR of top) starting material MPTMS versus vitolane silsesquioxane before DSC and bottom) vitolane after DSC.

After DSC as in **Figure 5.10b)**, no C=O peaks are observed (~1720cm^{-1}) suggesting most of the methacrylate groups have been burnt off and there is very little of the C-H still left (~3000cm^{-1}).

5.2.3.5.2 CHN analysis of samples before and after DSC

Table 5.1. CHN results of the char after DSC analysis @600^{o}C

Element	**C**	**H**	**N**
% Found 1	23.69	2.74	<0.10
% Found 2	23.21	2.72	<0.10

The elemental information in **Table 5.1** shows that carbon is still present even after burning at such a high temperature. This result indicates that silicon could have formed a protective layer engulfing and retaining some of the carbon at this temperature.

Based on the results in **Table 5.1**, one can calculate the estimated percentage of each atom left in the char to be:

In 100g of sample there is:

23.7g of carbon =23.7/12.0 = 2mols

2.74g of Hydrogen = 2.74/1.01 =2.7mols

73.6g (rest is $SiO_{1.5}$) = 73.6/52 = 1.4mols

The hydrogen in the mixture left is likely to be part of CH_3SiO_x suggesting the structure following the decomposition of the silsesquioxane from the A-system is likely to be a polysiloxane (CH_3SiO_x), together with carbon as graphite or silicon carbide and Q silica.

5.1.3.4 UV-Vis of the A-system silsesquioxane resin

UV-vis was used to study the absorbance of the silsesquioxane resin as well as the starting material (MPTMS). This information was needed to decide whether the materials would be suitable for HPLC analysis using a UV detector, and to know in what region the samples will absorb in the UV. The UV-Vis results showed that the resin absorbed near the ultra-violet region at a wavelength of 180-240nm.

5.1.3.5 HPLC of the A-system silsesquioxane resin

HPLC is a chromatographic technique used to separate a mixture of compounds with the purpose of identifying, quantifying and purifying the individual components of the mixture. This technique was used in this research to identify some of the components in the silsesquioxane resin mixture.

The HPLC results of the resin (**Figure 5.11**) using a UV detector demonstrates that the synthesized resin is made up of a mixture of compounds (linear, branched, cyclic and maybe some partial cages). The small peak at 1.5 minutes is noise from the injections. There are different peaks at different retention times (**Figure 5.11**). These peaks clearly indicate that there are compounds of different structural types present in the resin. The earlier peaks are possibly due to some linear and/or branched

structures. The later peaks could be due to few larger molecules. The heights indicate the abundance of the species in the resin mixture.

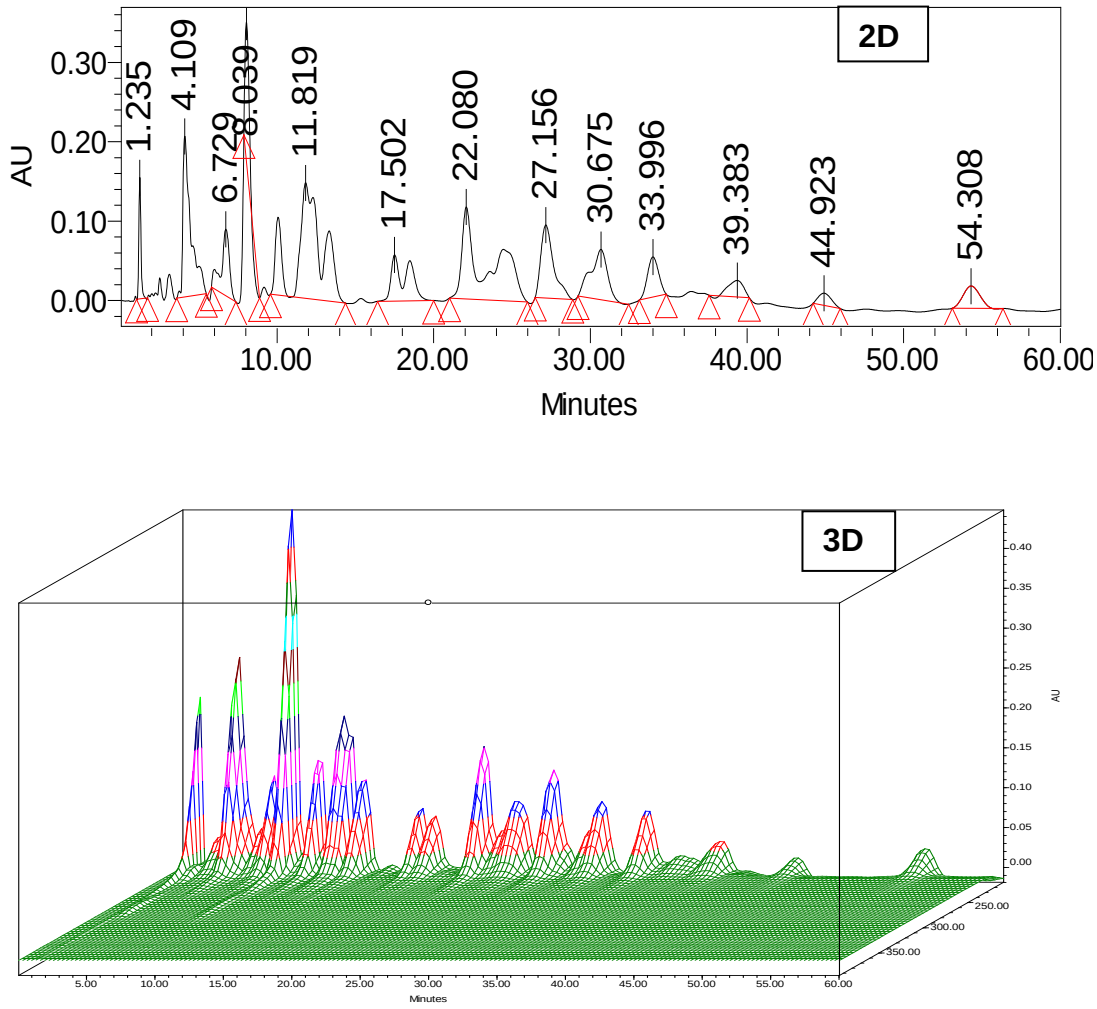

Figure 5.11. HPLC chromatogram of vitolane silsesquioxane resin (a) 2D, (b) 3D image

The GPC results as will be seen in **Figure 5.17a** suggest the average molecular mass of the vitolane are between 2000-3000 which is about an average of ten monomer units in the chain length. Vitolane is a relatively simple mixture of linears, branched and some cyclic oligomers.

5.1.3.6 Mass spectrometry of the A-system silsesquioxane resin

The above HPLC peaks can be assigned using HPLC-MS which has been largely used from chapter 5.3.3.8 to 5.4.4 to identify components of the vitolane resin.

MALDI-ToF MS and ESI-MS are used for the detection and characterization of small and large components in the resin which tends to be fragile and fragment when ionized by conventional ionization methods [275]. ESI-MS and MALDI-ToF have been used to study the larger molecular mass components in the resin mixture that would otherwise be destroyed by other techniques such as electron ionization.

5.1.3.5.1 ESI-MS of vitolane silsesquioxane

ESI-MS which is Electrospray ionization mass spectrometry allows the identification of each of the silsesquioxane components, each component to be identified by its molecular ion. See **Figure 5.12** below for the mass spectrum together with some peak identification (more on peak identification is described in **Appendix 14).**

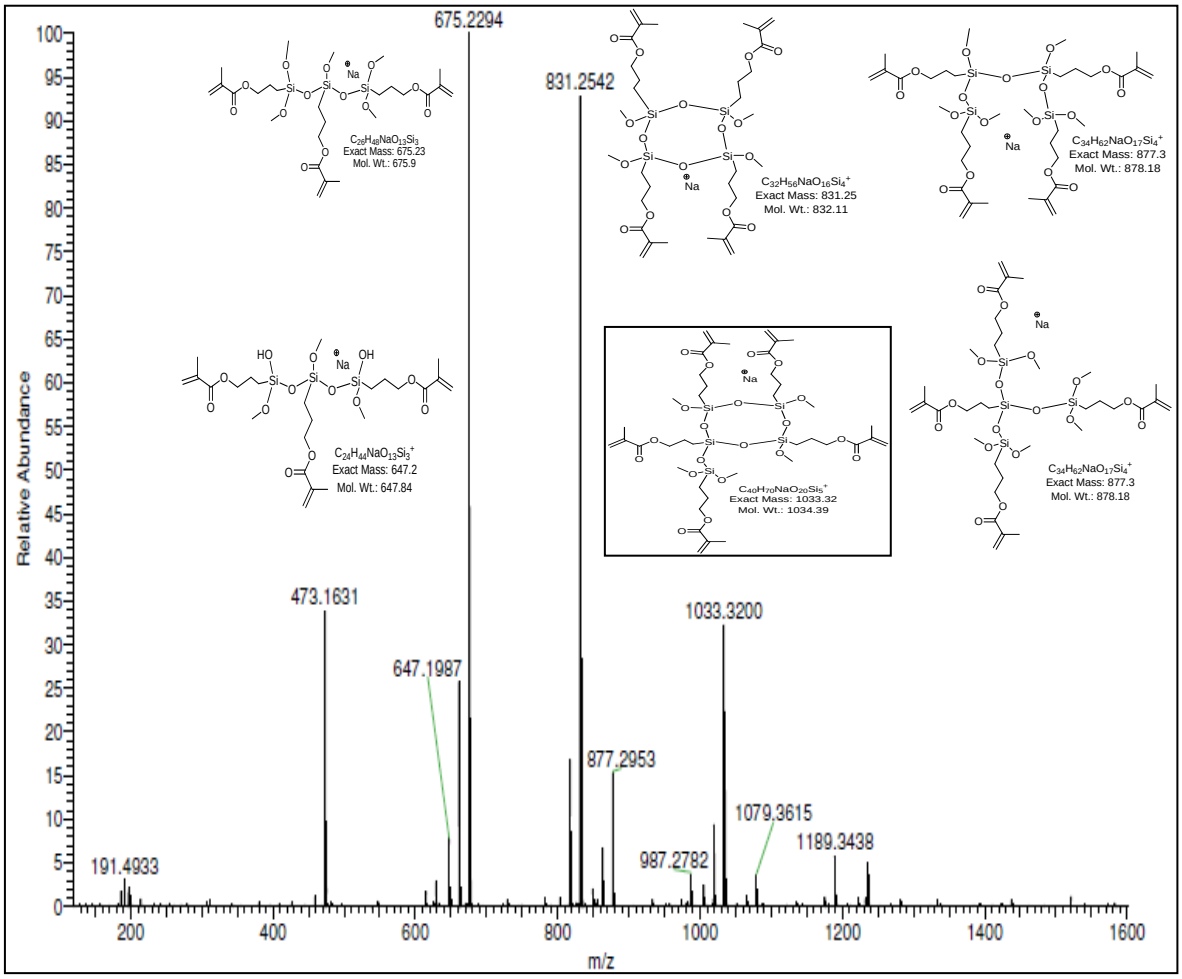

Figure 5.12: The ESI mass spectrum of the A-system vitolane silsesquioxane resin.

The ESI-MS result in **Figure 5.12** confirms the product composition of the peaks as earlier described (linears, branched and some cyclics).

5.1.3.5.2 Maldi-Tof-MS of vitolane silsesquioxane resin

Maldi-ToF-MS allows the separation of silsesquioxane components by time of flight. Therefore, the Maldi-Tof mass spectrum in **Figure 5.13** shows peaks of the components in the vitolane silsesquioxane resin mixture. See **Appendix 14** for peaks identification.

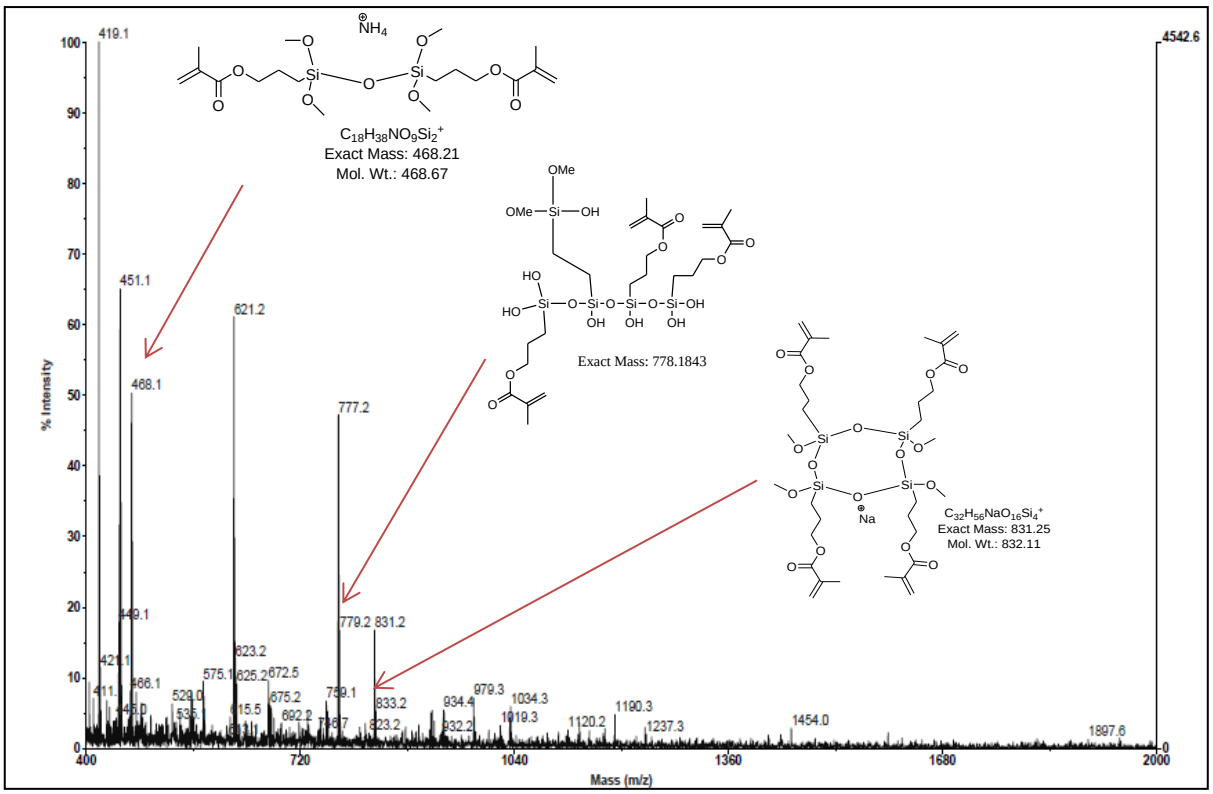

Figure 5.13. MALDI-ToF-MS spectrum of the A-system vitolane silsesquioxane resin.

From the above results **(Figure 5.12 and 5.13**), It can be seen that the resin consist mainly of linear, branched and cyclic structures. The peaks at 473 (**Figure 5.12**) and 468 (**Figure 5.13)** are the methacrylate dimer with different numbers of OH and OEt groups or different ionizing agents. The peaks 647 and 675 are linear trimers (**Figure 5.12 and 5.13**) with different numbers of OH and OEt groups. The peak at 777 (**Figure 5.13**) corresponds to tetramer of the silsesquioxane resin formed during the ionization process. The peak at m/z 831 (**Figure 5.12**) is a cyclic pentamer. The rest of the peaks have been drawn out structurally in **Appendix 14**.

The ESI and Maldi-Tof-MS results confirm the complex structural mixture of the silsesquioxane resin. They both show that the dimers, trimers, tetramers and pentamers formed both linears and cyclics. Larger oligomers may be present but do not fly so well in the Maldi nor picked up well in the electrospray experiment.

5.1.3.6 GC-MS of the A-system silsesquioxane resin

GC-MS is used to separate mixtures of compounds into individual components. Though it is a destructive technique and can cause decomposition of the resin, it has been used to study the species present in the silsesquioxane resin mixture (**Figure 5.14**).

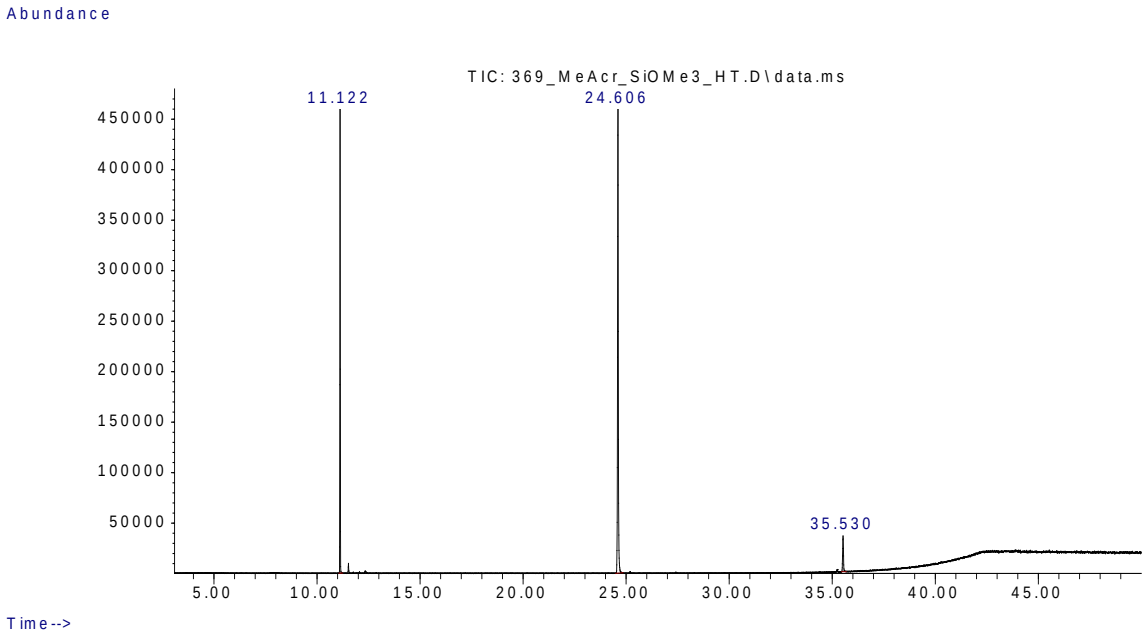

Figure 5.14. GC-MS chromatogram of silsesquioxane resin

The GC-MS results above show some species present in the silsesquioxane resin. The peaks at 11.122, 24.606 and 35.530 minutes corresponds to monomeric, dimer and trimer structures respectively. This was the initial stage of the reaction (about

20 minutes) hence capturing just the low molecular weight species. On the other hand, some higher molecular weights species could have been present but do not evaporate into the GC column hence not seen in the mass spectrum. These results again confirm the complex nature of the silsesquioxanes resins.

Other results such as GPC is shown at **Appendix 17.**

5.2.4 Isolation of the silsesquioxane resin components

5.1.4.1 Purification of silsesquioxane resin using column chromatography.

The separation of the resin was attempted using both normal flash column chromatography and micro-pasteur pipette [276, 277] column chromatography in order to isolate individual components of the silsesquioxane resin mixture [278].

Column chromatography to separate silsesquioxane resin

The separation experiment is outlined in chapter 2.1.12 in the experimental section. **Table 5.2** below shows the different solvent variations that were carried out before the final separation was achieved.

Table 5.2. Column and TLC solvent mixtures used to attempt to separate components of silsesquioxane resin.

Entry	Solvent mixtures	Column solvent ratios	TLC solvent ratio for analysis	Results (including retention values (rf) values)
1	Hexane/ Ethyl Acetate	9:3	Hexane/ Ethyl Acetate. 1:1	No separation T_1, T_2 and T_3 (rf)= 0.47
2	Hexane/ Ethyl Acetate	7:3	Hexane/ Ethyl Acetate	No separation T_1, T_2 and T_3 (rf)= 0.47
3	Hexane/ Ethyl Acetate	8:2	Hexane/ Ethyl Acetate: 8:2	No separation T_1, T_2 and T_3 (rf)= 0.47
4	Hexane/ Ethyl Acetate	9:1	Hexane/ Ethyl Acetate: 1:1	Good separation. T_1, T_2 and T_3 (rf)= 0.43, 0.45, 0.49
5	Hexane/ Ethyl Acetate	9.9:0.1	Hexane/ Ethyl Acetate. 6:4	Better separation T_1, T_2 and T_3 (rf)= 0.43 and 0.45
6	Hexane / Diethyl ether	9.9:01	Hexane/ Ethyl Acetate. 1:1	Better separation T_1, T_2 and T_3 (rf)= 0.43 and 0.45
7	Hexane / Diethyl ether	6:4	Diethyl ether/DCM. 1:1	No separation T_1, T_2 and T_3 (rf)= 0.47
8	Hexane / Diethyl ether	7:3	Hexane / Diethyl ether. 6:4	Product stick to tlc plate. T_1, T_2 and T_3 (rf)= 0
9	Hexane / Diethyl ether	1:1	Hexane / Diethyl ether. 6:4	Separate but spots too close together. T_1, T_2 and T_3 (rf)= 0.43, 0.45, 0.49
10	Hexane / Diethyl ether	2:8	Hexane / Diethyl ether. 7:3	No separation T_1, T_2 and T_3 (rf)= 0.47
11	Hexane / Diethyl ether	8:2	Hexane / Diethyl ether. 1:1	No separation T_1, T_2 and T_3 (rf)= 0.47
12	Hexane/Toluene	6:4	Toluene/Hexane. 6:4	Product stuck to tlc plate. T_1, T_2 and T_3 (rf)= 0
13	Hexane	100%	Hexane/Diethyl ether. 1:1	No separation. Stuck to plate. T_1, T_2 and T_3 (rf)= 0
14	Diethylether	100%	Hexane/Diethyl ether. 1:1	Product did not move at all. T_1, T_2 and T_3 (rf)= 0

5.1.4.1.1 Results and interpretation of the column chromatography

After carrying out several column and TLC chromatographic experiments using different solvents/solvent mixtures, it was realized that, though some of the separations showed single spots on the TLC and gave a good separation (e.g. entry 4 from **Table 5.2**), the NMR spectra of the samples collected from the column showed several peaks, especially the ^{29}Si NMR spectra, suggesting a poor separation. Presumably, the different components could be a result of overlapping peaks due to the complex mixture including linear diastereoisomers (Meso (RS: SR), RR and SS) of some of the species.

5.1.4.1.2 Summary and Conclusion of the column chromatography results

Column chromatography has not proven to be a good separation method so far for this silsesquioxane resin. Even when a separation on TLC does occur, the subsequent analysis of the samples from the column using NMR spectroscopy shows there is no apparent separation. The product probably degrades in the column. Even when a separation is seen, the mixture contains compounds that are too similar to be successfully characterized spectroscopically.

5.1.4.2 Separation using Preparative thin layer chromatography (TLC)

Introduction

Preparative TLC was used to isolate preparative quantities of the materials from the resin. Since a better separation was observed in the column chromatography using solvent mixtures as in entries 4, 5 and 6 in **Table 5.2**, the same procedure was repeated using preparative TLC to obtain larger quantities of the separate fractions.

5.1.4.2.1 Experiment using preparative TLC to separate silsesquioxane resin

0.2g of the resin sample was dissolved in about 0.5ml of hexane and spotted on a preparative TLC plate. The TLC solvents used were those of entries 4, 5 and 6 in **Table 5.2**. Several sample weights were used, some of which gave too concentrated mixtures which were not suitable for separation. The separate bands were scraped off the preparative TLC plate, put into separate vials, hexane added to dissolve the resin components from the silica and then evaporated to dryness. By trial and error, some preparative TLC gave good separation and others did not. Some gave very little yield which could not be collected after removing solvent using the rotary evaporator. For this reason, the 5:5 and 9:1 solvent mixture, as in **Table 5.2,** were used to separate some of the resin components.

5.1.4.2.2 ***Results and interpretation of preparative TLC separation of the resin***

One of the silsesquioxane resin samples from the preparative TLC gave ^{29}Si NMR spectra that showed peaks at **-**57 ppm indicating the presence of T_2 type silicones. However, the peaks were very close to the background noise. When this was repeated on a larger scale (0.8g), there was no apparent separation as the sample was too concentrated. Further repetitions (0.4g) gave acceptable results but revealed the presence of a single peak -50 ppm (T_1 silicon) and several T_2 peaks at -57 ppm which could be due to other silicon environments on the polymer chain. The presence of only T_1 and T_2 peaks suggest it is a linear chain mostly.

5.1.4.2.3 ***Conclusion of preparative TLC results***

This method did not give a good separation of the silsesquioxane resin. With only a small amount of the resin used to perform this analysis, and also due to the similar chemical properties of the resin species to be separated, one can conclude that this method is not suitable to isolate the resin fragments.

5.1.4.3 **Separation of the silsesquioxane resin using distillation**

Introduction

After the many attempts to separate the silsesquioxane products using the above separation techniques but to no avail, a different technique, distillation was tried.

5.1.4.3.1 ***Distillation of the A-system silsesquioxane resin***

In order to study the components produced at the beginning of the reaction, half the amount of MPTMS was used in an excess of methanol. Half the ratio of water to MPTMS was used to minimize the degree of hydrolysis taking place in the reaction of MPTMS and water. With less water, less hydrolysis/condensation will occur and hence only the simple structures of the resin will be formed. To accurately control the amount of water, the resin was prepared as described in Chapter 2.1.10 and results shown and discussed below:

5.1.4.3.2 ***Results from the distillation of the silsesquioxane resin***

The proton and silicon NMR spectra of the pure dimer (4.1g, 11.4%); disiloxane distilled from the resin are shown in **Figure 5.15a and 5.15b** showing the characteristic peaks. The ^{13}C NMR and GC-MS results are also shown in Appendix **11 and 12**.

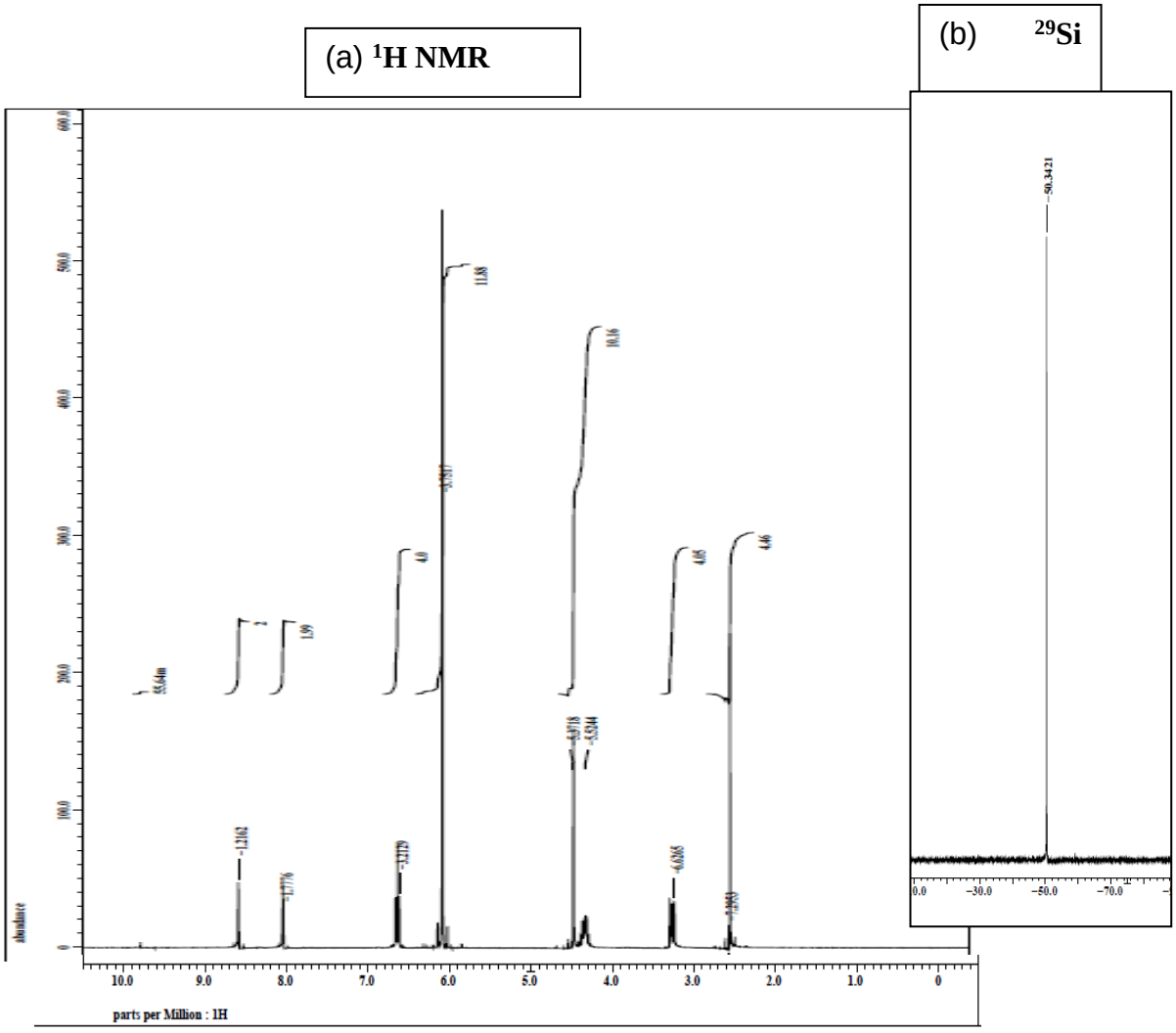

Figure 5.15. (a) ^{1}H NMR of disiloxane and **(b)** ^{29}Si NMR of disiloxane

The ^{29}Si NMR spectrum above (**Figure 5.15b**) displayed a single sharp peak at -50 ppm. This peak corresponds to the condensation of silanols to form the siloxane bond (-Si-O-Si-) in the disiloxane dimer.

5.1.4.3.3 ***Conclusion of distillation results***

The distillation was very successful although only for the separation of the dimer. The trimer could not be distilled because of it is very high boiling point which a normal laboratory distillation cannot attain.

5.1.4.4 Variation of the starting material leading to silsesquioxane resin formation.

In this section we varied the starting materials and followed the hydrolysis /condensation to see what insights this provided on the process for making the vitolane silsesquioxane.

5.1.4.4.1 Reaction using 3-acryloxypropylmethyl dimethoxysilane (MPDMS)

The reaction of 3-methacryloxypropyl dimethoxysilane (MPDMS) with water, ethanol and acid was carried out to find out which intermediates are formed first, since the current starting material (MPTMS), the trimethoxysilane, gave a complicated spectrum under the same conditions (see **Figure 5.1 and 5.2**). The dimethoxysilane was thought to likely produce a simpler spectrum which could be studied more easily. Therefore, a silsesquioxane resin was synthesized using the dimethoxysilane starting material (MPDMS) following the same procedure as above (**Chapter 5.1.2**) and the various spectra were analyzed.

The results of the resin obtained here did not show a simpler pattern but actually reflected some of the complications observed with the trimethoxysilane. It reacts very fast just like the trimethoxysilane producing a complex ^{29}Si NMR spectra pattern of D_1, and D_2 peaks very similar to the results of the one component system resin (**Figure 5.2**). The trial was abandoned because it did not improve the situation of producing a simpler spectrum.

5.1.4.4.2 Reaction using 2,2,2-trifluoroethyl methacryloxypropylsilane

The reaction using 2,2,2-Trifluoroethyl methacryloxypropylsilane (tris(trimethylsiloxy)methacryloxypropylsilane) using the same method as the silane resin in Chapter 2 produced the following results using ^{19}F NMR (**Figure 5.16**). The 2,2,2-Trifluoroethyl methacryloxypropylsilane was used because the fluorine NMR should be simpler as they are not complicated by coupling. Although the fluorine is at a distance from the reaction centre, it has quite a large ppm range.

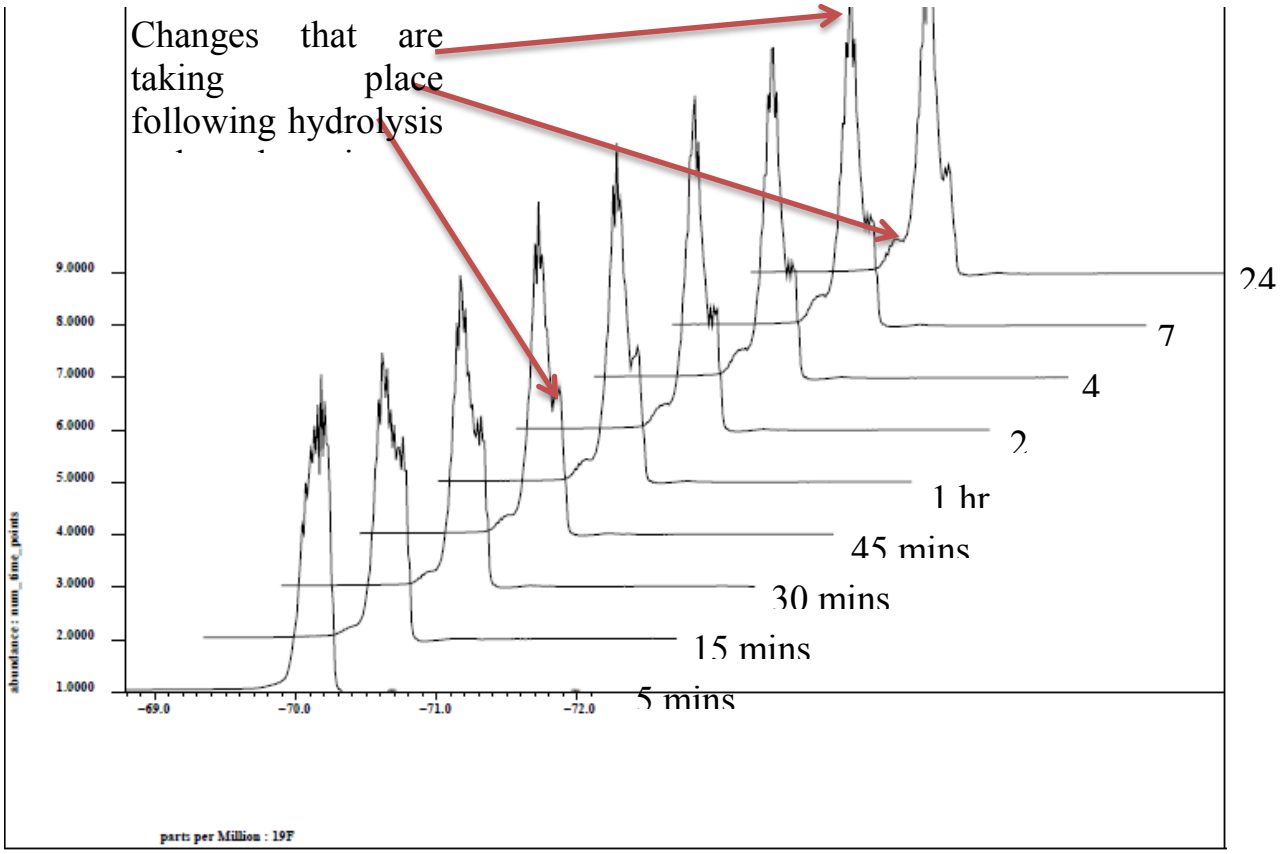

Figure 5.16. F NMR Kinetic study to understand the rate of hydrolysis and condensation in tris(trimethylsiloxy)methacryloxypropylsilane silsesquioxane formation.

Unfortunately the fluorine atoms were too far from the reaction centre**. Figure 5.16** shows the peaks overlap and became more complex with time and difficult to analyse, hence this method was abandoned.

5.2.5 Changing the reaction conditions for the vitolane synthesis

5.2.5.1 Reaction using half (1:0.5 molar ratio of MPTMS:H_2O) the amount of water

This study was carried out to verify the effect of using less water on the hydrolysis and condensation of MPTMS to form a complex methacryloxypropyl silsesquioxane resin. The synthesis of this resin using half the amount of water (as described in Chapter 4) gave a very fluid product which is not suitable as a coating material as it will wash off easily. The reaction does not go to completion and there is usually a lot of starting material remaining. Although this material is not a suitable coating resin, it has been very useful in the study of the initial components formed during a normal silsesquioxane resin synthesis. From the results in Chapter 4, using half the amount of water leads to less degree of hydrolysis and condensation and hence the formation of less complex silsesquioxane resin structures which are linear and some cyclic species with low molecular weights as seen in the GPC results in **Figure 5.17b** using 0.5 moles of H_2O.

5.1.4.4.3 Reaction using twice (1:2.0 molar ratio of MPTMS:H_2O) the amount of water

This study was carried out to verify the effect of using twice the amount of water on the hydrolysis and condensation process of the formation of the silsesquioxane resin. This is the same process that was done in Chapter 4 whereby a 1:2 molar ratio (MPTES: water) was used and analyzed by ^{29}Si NMR.

Reaction of trimethoxysilane with twice the amount of water gave a very speedy reaction which led to a very thick product which was not suitable as a base resin for

coating as it will crack easily. The resin formed from this type of mixture will age quickly and form a gluey/gummy mixture. The ^{29}Si NMR spectra obtained for this type of mixture showed a more complex mixture as reported in Chapter 4. The GPC result is also reported in **Figure 5.17c** (x2H_2O) below and there are larger molecular weight products observed which possibly suggest more cage-like resins.

GPC results of all three water variation scenarios

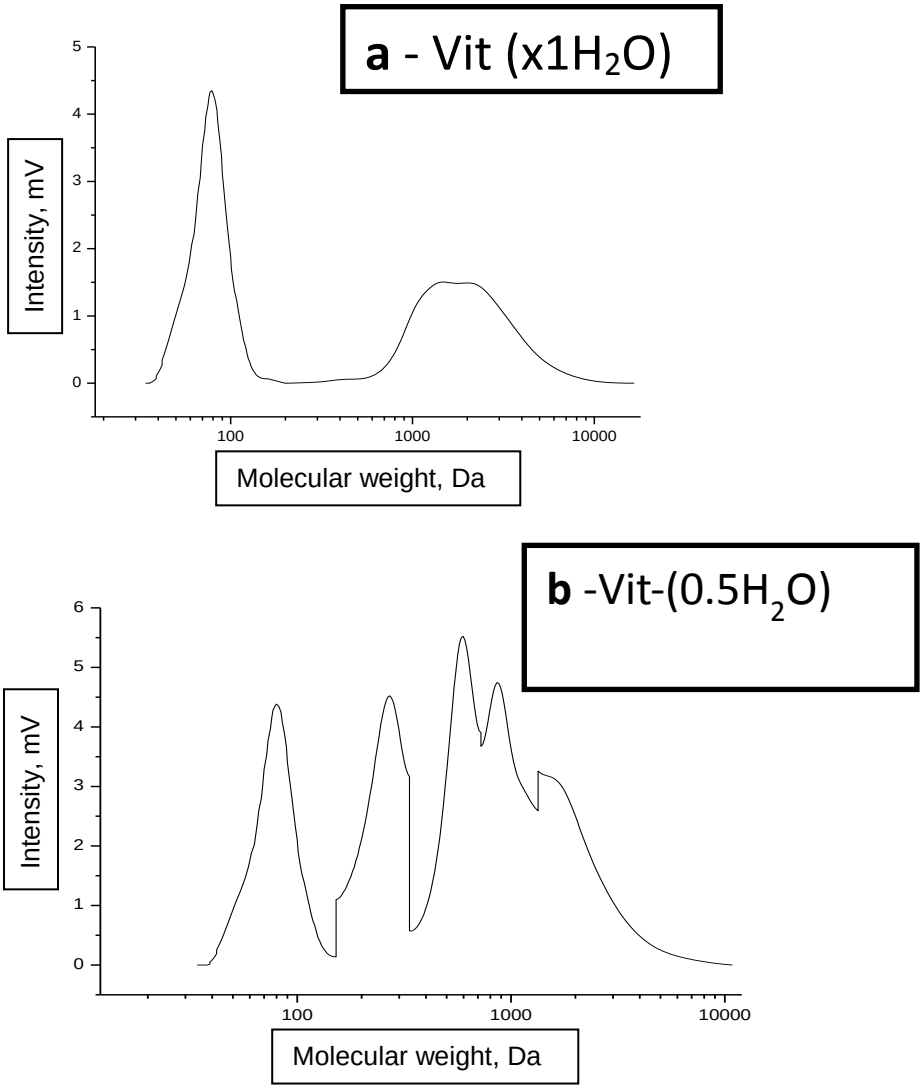

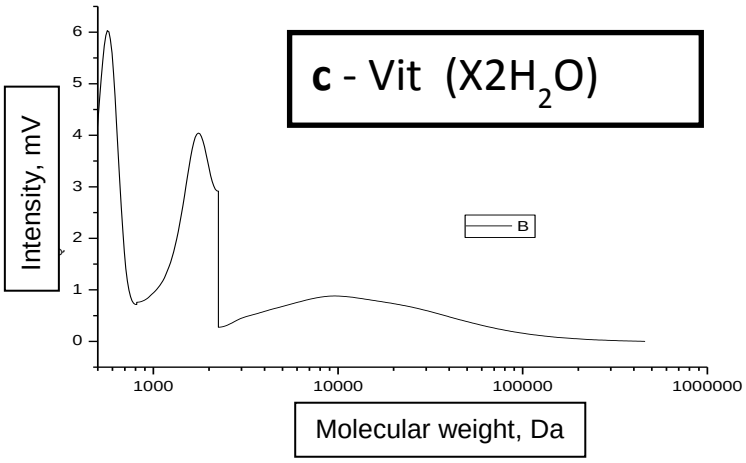

Figure 5.17. GPC chromatograms of **a**) pure Vitolane resin using 1:1 molar ratio of MPTMS:water, **b**) Vitolane resin using 1:0.5 molar ratio of MPTMS:water and **c**) vitolane resin 1:2 molar ratio of MPTMS:water. With mV(millivolts) and Da(Daltons).

The GPC results suggest the molecular weights of the species formed ranges from 500-50,000 (**Figure 5.17**) with **Figure 5.17c** having molecular weights of up to 100,000 (~400 connected monomer units). The first peak around 100 dalton is ignored as it is mostly the solvent front. The pure vitolane (**Figure 5.17a**) is monomodal averaging about 3000 daltons (12 monomer units). Using half the amounts of water as in **Figure 5.17b** gives multiple small sized species averaging ~1000 daltons (4 monomer units). Doubling the amounts of water (**Figure 5.17c**) produces a bimodal peak with the majority of the species formed comprising of higher molecular weights up to MW of between 2000-100 000 (8- 400 monomer units).

Therefore, the higher the amounts of water while holding every other reagent constant, the higher the molecular weights of the species formed.

5.1.4.5 Summary of the silsesquioxane resin obtained from the A-system

We have successfully synthesized silsesquioxane resin several times with good reproducibility. According to MALDI-ToF MS, ESI-MS, HPLC, DSC and TGA analysis shown earlier in this chapter, the silsesquioxane resin possibly contains a mixture of various structures: linears mostly and some cyclics though the ^{29}Si NMR shows very little of T_3^X species. The broad Si-OH peak in the FT-IR spectra of the single component- system (A-system) indicates that the condensation is incomplete provided it is not ethanol and also according to findings in **Chapters 3 and 4**. This is also supported by the MALDI-Tof MS, ESI-MS, HPLC spectra.

Also, it has been shown that using less or more water gives different composition of the resin formed. Less water leads to a fluid resin (less hydrolyzed structures) which will easily be washed off. Too much water produces a very thick gluey resin (more condensed structures) which will age and crack off easily. Therefore, water plays a vital role in the quality of the silsesquioxane resin product. DSC and TGA results show no weight loss until around 300^0C. This indicates the synthesized silsesquioxane resin has a high thermal stability. Finally, according to the kinetic studies, the time of the synthesis can be reduced from 24 hours to about 4-5 hours, hence reducing the resin production time. This is therefore the first step in optimizing the reaction conditions of the Vitolane^{TM} process.

Two component-system (AZ-system) for synthesising silsesquioxane resin.

5.2.6 Introduction

In section 5.2 above, the single component system (A-system), we have seen how a single starting material MPTMS gave silsesquioxane resins with particular properties. The A-system gave a resin with presumably more hydrolyzed than condensed linear and cyclic species with thermal stability of about 300^{o}C. This type of resin is suitable for some materials but not all. For very harsh conditions such as ocean water bodies, high altitudes as required for planes and space craft, enhancing some of these already existing coating properties will be vital. Hence, the reason for the two component-system (AZ-system) is to get more improved physical and chemical properties from the silsesquioxane resins. The A-Z system of synthesizing silsesquioxane resins refers to using two starting materials, 3-methacryloxypropyltrimethoxysilane (MPTMS=A) and n-propyltrimethoxysilane (nPTMS=Z) along with methanol, water and acid (**Figure 5.18**).

5.2.7 Synthesis of silsesquioxane resin by the AZ-system

The reaction follows the same scheme as the A-system described in **Chapter 5.1** above. But on this occasion, the two starting materials were mixed independently with methanol and acid in the proportions shown in **Table 5.3**. The two separate mixtures were then mixed together after 10 minutes to obtain the desired silsesquioxane resin. The reaction scheme is represented below in **Figure 5.18.** Notice that the structures below are a random selection. There could be several different sets of species formed in different combinations of *n*-propyl and MPTMS.

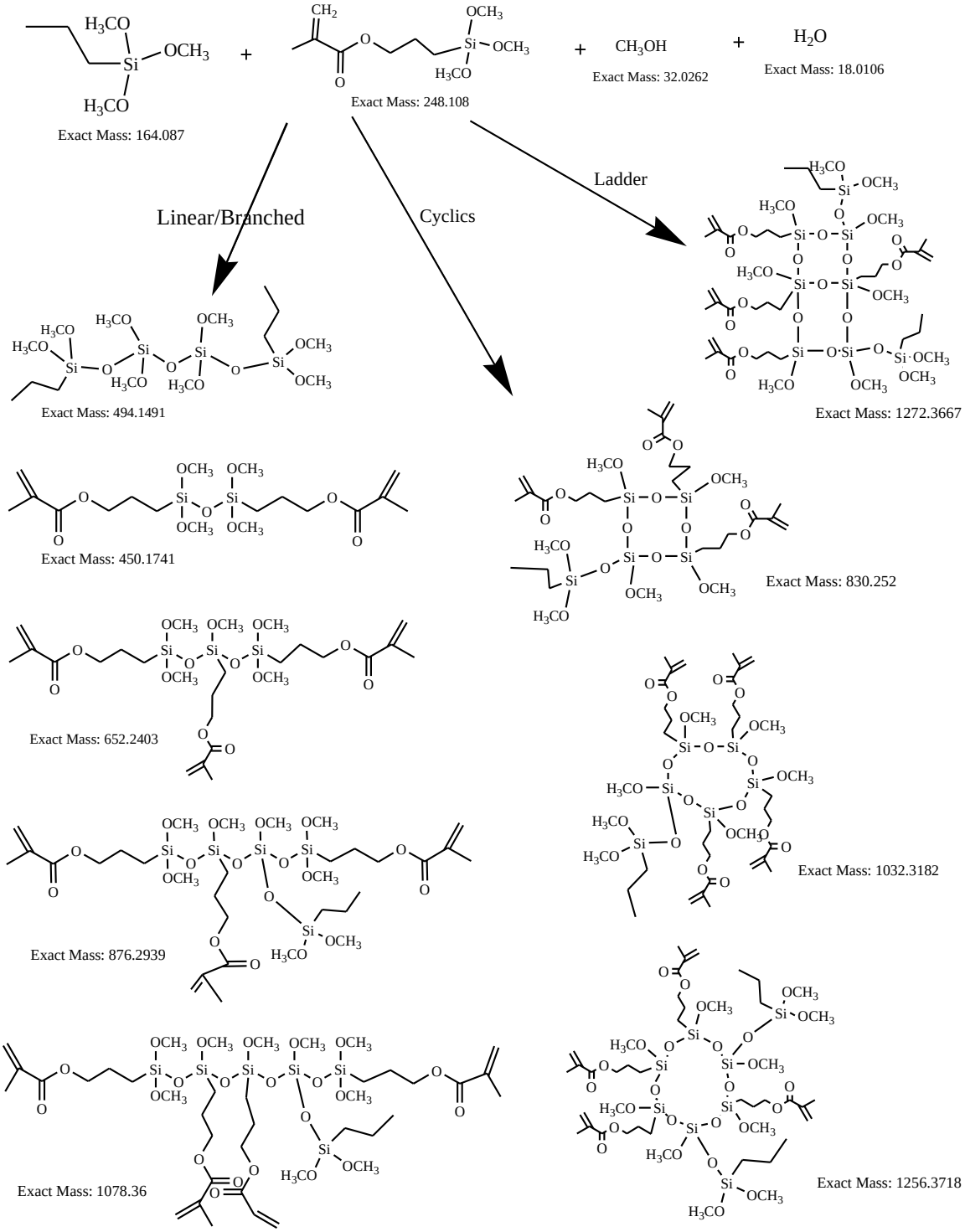

Figure 5.18. Possible composition of silsesquioxane resin formed from reacting 3-methacryloxypropyl-trimethoxysilane and n-propyltrimethoxysilane.

The table below (**Table 5.3**) shows the formation of silsesquioxane resin by varying the starting material (MPTMS and nPTMS) concentrations, and also by changing the solvent (water) ratio. The row in pink (DOAZ-1) represents the original silsesquioxane resin mixture and the rest of the reactions DOAZ 2-9 are variations of the original. In the Table: m=MPTMS and n=NPTMS, colour: pink= Standard AZ vitolane mixture, light yellow means time variation, dark yellow means H_2O molar ratio variation. .Notice that the viscosity measurements were carried out as described in section 2.2.9.

Table 5.3. The different AZ reaction conditions

Sample Codes	**m mixture shaken time (mins)**	**n mixture shaken time (mins)**	**m (H_2O molar ratio added)**	**n (H_2O molar ratio added)**	**Resin viscosity (cP)**
DOAZ-1	10.0	10.0	1.0	1.0	65.7
DOAZ-2	1.0	1.0	1.0	1.0	63.8
DOAZ-3	1.0	10.0	1.0	1.0	68.9
DOAZ-4	10.0	1.0	1.0	1.0	57.3
DOAZ-5	10.0	10.0	1.1	1.0	69.7
DOAZ-6	1.0	1.0	1.1	1.0	88.9
DOAZ-7	10.0	10.0	1.2	1.0	102.4
DOAZ-8	1.0	1.0	1.2	1.0	120.4
DOAZ-9	1.0	1.0	1.0	1.1	120.4

5.2.8 Characterisation, results and discussion of the silsesquioxane resin formed from the two component-system (AZ-system).

The results of the characterisation of the AZ-system resin are as discussed below:

5.2.8.1 ^{29}Si NMR results of the AZ-system silsesquioxane resin

Based on the analysis of the MPTMS hydrolysis and condensation in **Figure 3.5** above, and the nPTMS characterisation of the species/environments in **Figures 5.19, 5.20** and **5.21** below, the ^{29}Silicon NMR of the AZ-system silsesquioxane has been characterised as in **Figure 5.22**. Peak assignments were based on the assumptions as in chapter 4.3.2 on page 167.

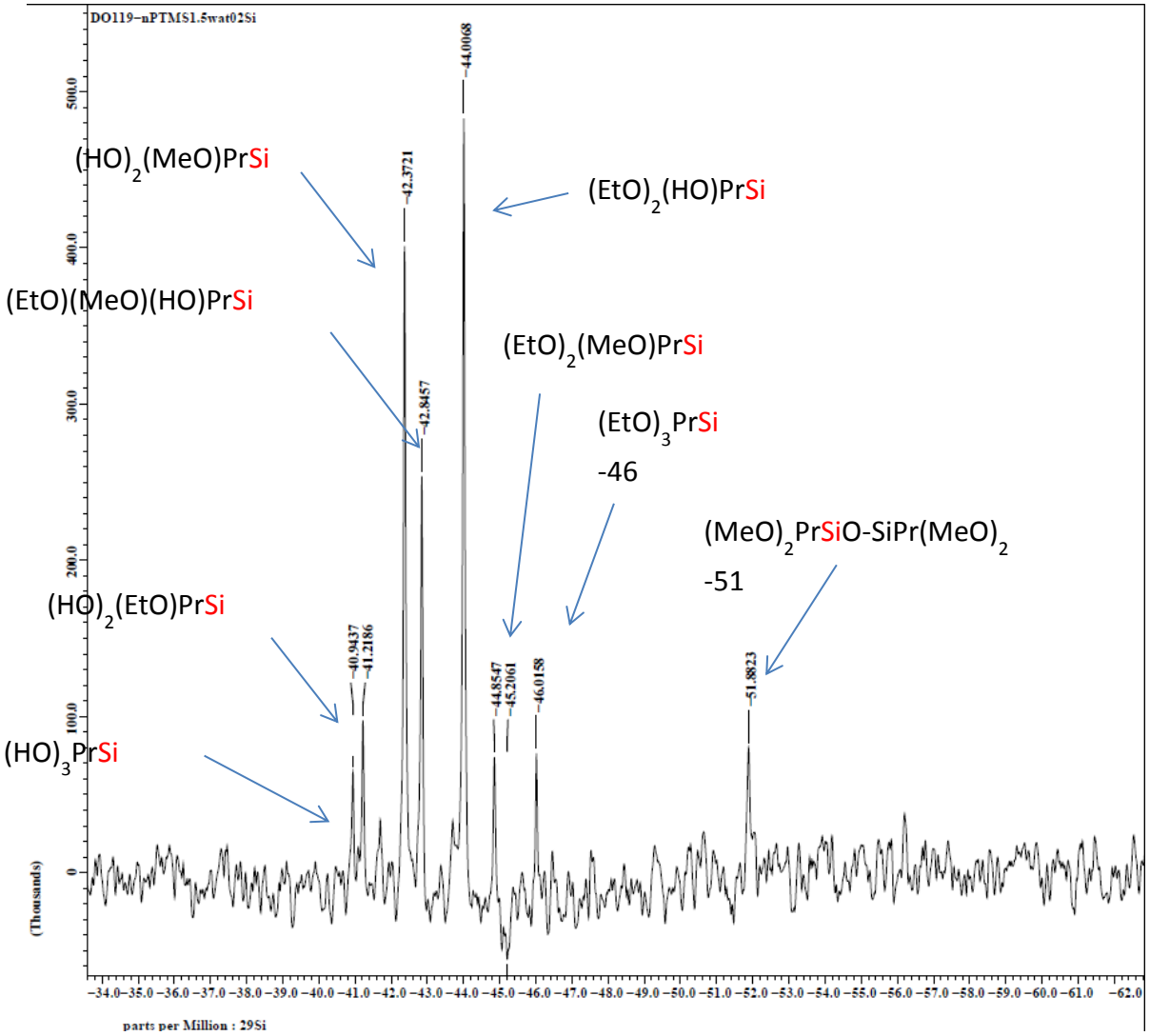

Figure 5.19. ^{29}Silicon NMR analysis of nPrSi(OMe)$_3$ hydrolysis - T_0 region after 1hr of reaction time using 1:1.5 molar ratio of nPTMS:water.

The peaks in **Figure 5.19** represent the hydrolysis and condensation of nPTMS at the initial stages of the reaction. Hydrolysis is seen to be favored here (more silanols) compared to condensation as one can see more hydrolysed peaks (-40 to -46ppm). Alcohol exchange is also seen to occur between the ethoxy and methoxy as seen on the bracketed terms; EtO and MeO. The next stage of the reaction was captured as seen in **Figure 5.20**.

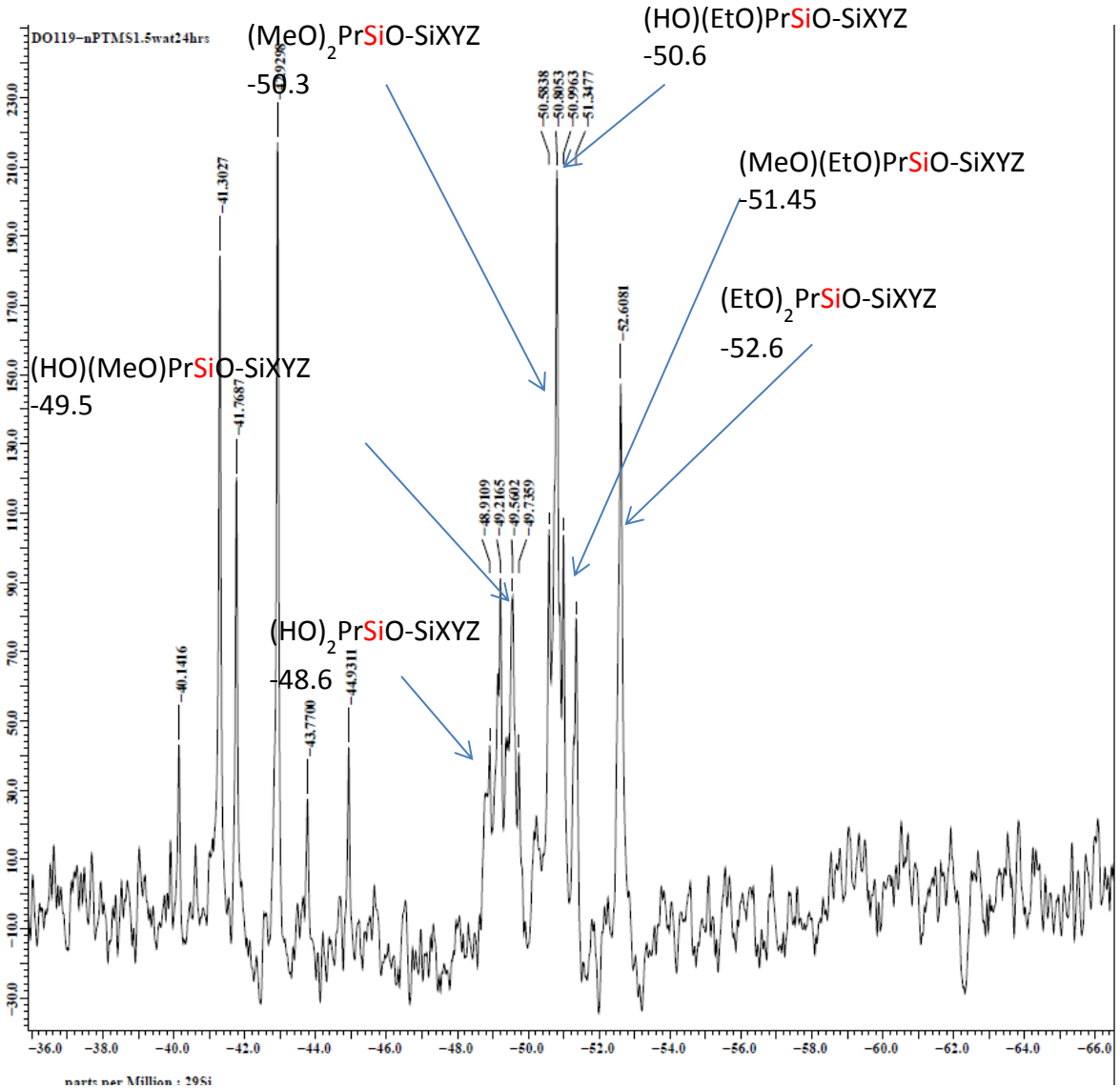

Figure 5.20. ^{29}Silicon NMR analysis of nPrSi(OMe)$_3$ hydrolysis - T_1 region at 24 hr reaction time using 1:1.5 molar ratio of nPTMS:water.

This next stage in **Figure 5.20** shows both hydrolysed T_0 (-40 to -44ppm) and condensed peaks T_1 (-48 to -52ppm) of the hydrolysis and condensation of nPTMS. More condensed peaks T_1 (siloxanes bonds) are present here compared to **Figure 5.19** which is a result of mainly hydrolysis (silanols) with only one condensed T_1 peak (-51ppm) observed. The next stage of the reaction process after extended analysis time of 744hrs is seen in **Figure 5.21.**

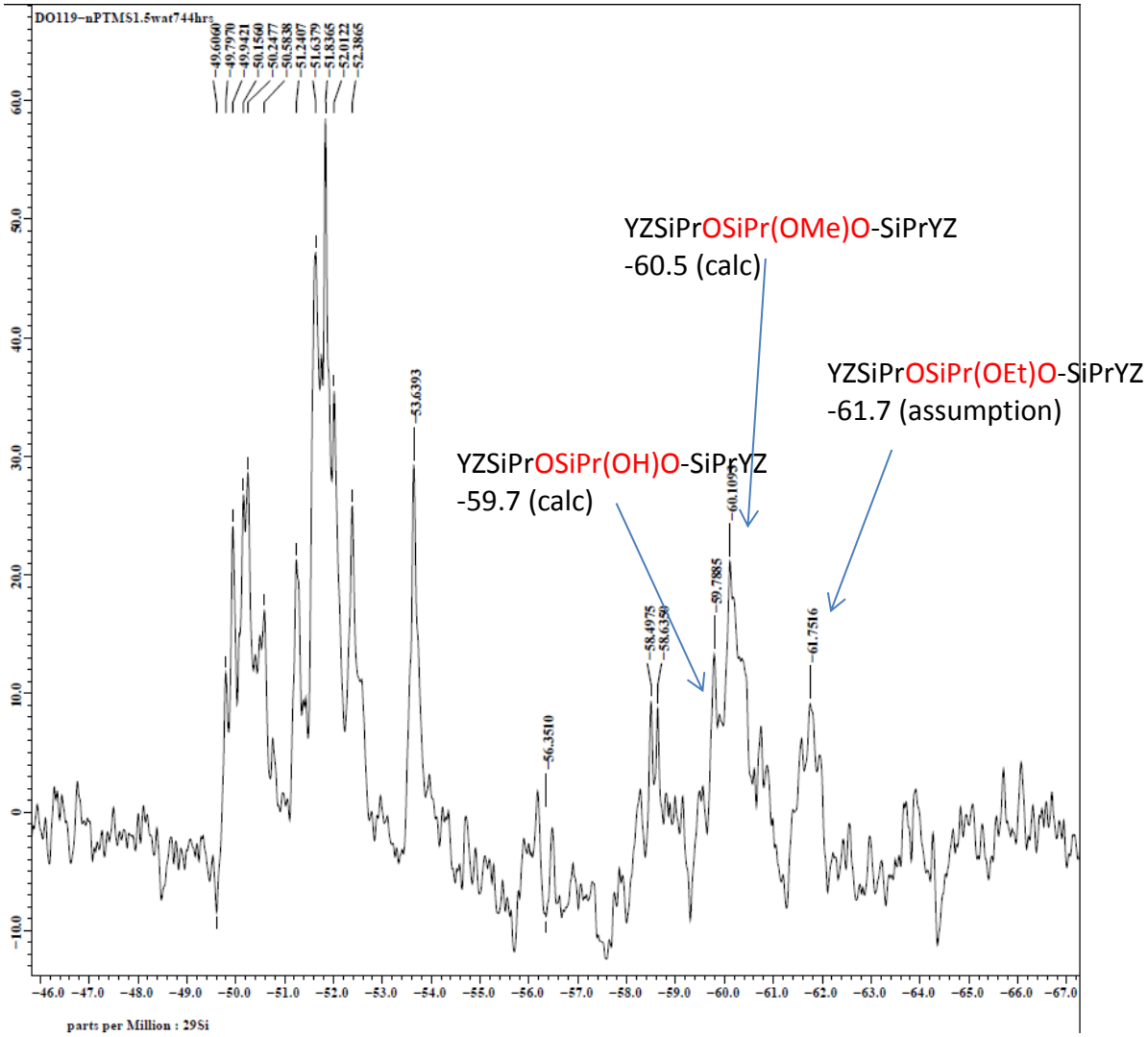

Figure 5.21. ^{29}Silicon NMR analysis of nPrSi(OMe)$_3$ hydrolysis - T_2 region at 744 hr reaction time using 1:1.5 molar ratio of nPTMS:water.

At this stage of the reaction (**Figure 5.21**), condensation is fully favoured compared to hydrolysis leading to T_1 and T_2 peaks. The final stage (**Figure 5.22**) is the vitolane resin (AZ-system) using starting materials; nPTMS and MPTMS. The T_3 peaks appear although you can't see them in the figure and thus we are starting to get branching.

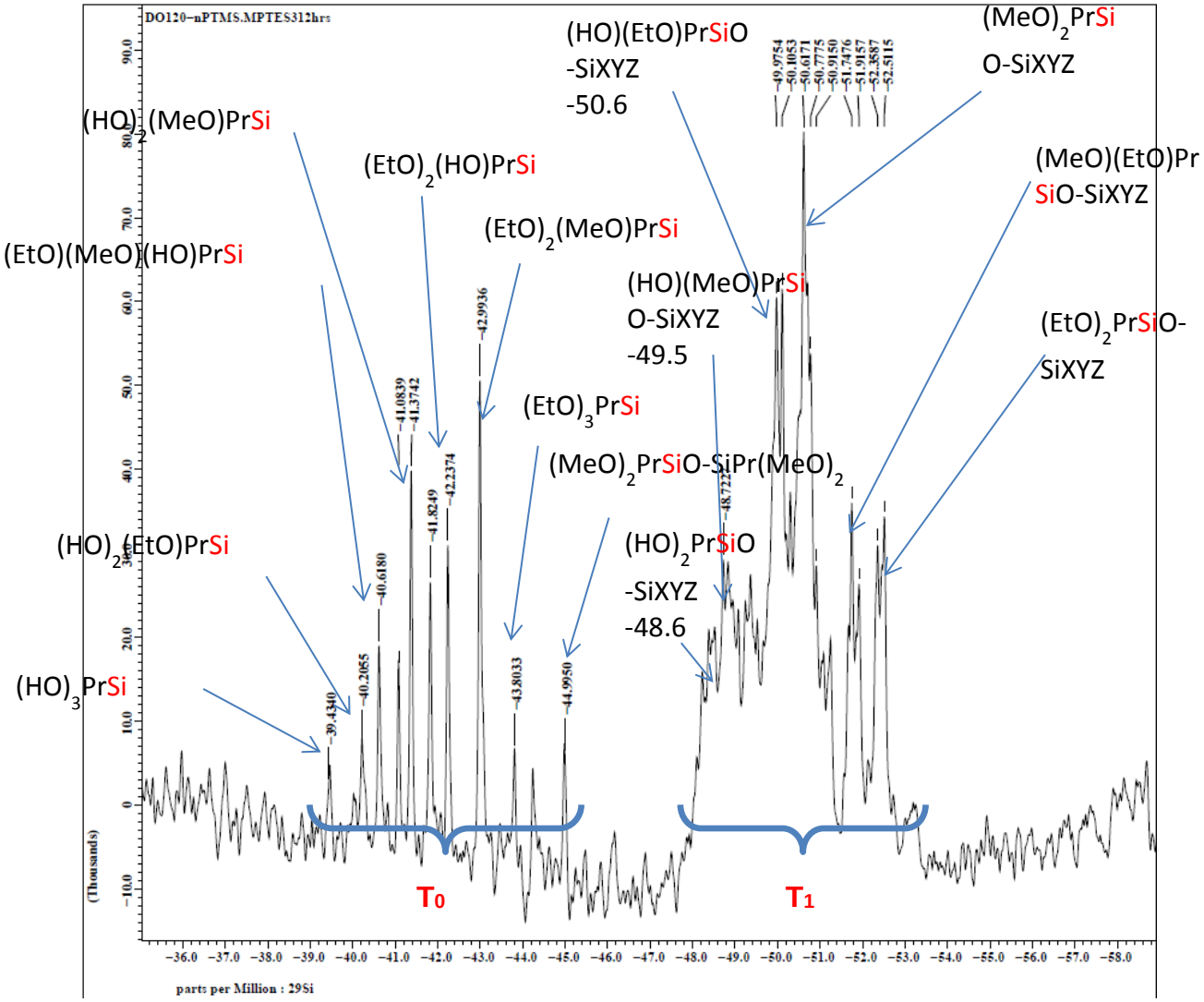

Figure 5.22 The ^{29}Si NMR of the silsesquioxane resin formed from the AZ-system (DOAZ-1b) after 312 hours reaction time. T_0 and T_1 is a mixture of nPTMS and MPTMS hydrolysed/condensed species or environments.

Figure 5.22 shows the AZ-system resin under the conditions used (original Vitolane conditions as in the experimental, section 2.1.10.2) after 312 hours using low amounts of acid. Once full hydrolysis and condensation is attained up to the point of pseudo-equilibrium, the T_0 peaks disappear and T_1, T_2 and some T_3 peaks are formed and remained predominant as seen in the ^{29}Si NMR spectra in **Figure 5.23**

below. The presence of T_3 peaks indicates that branching is beginning to be observed.

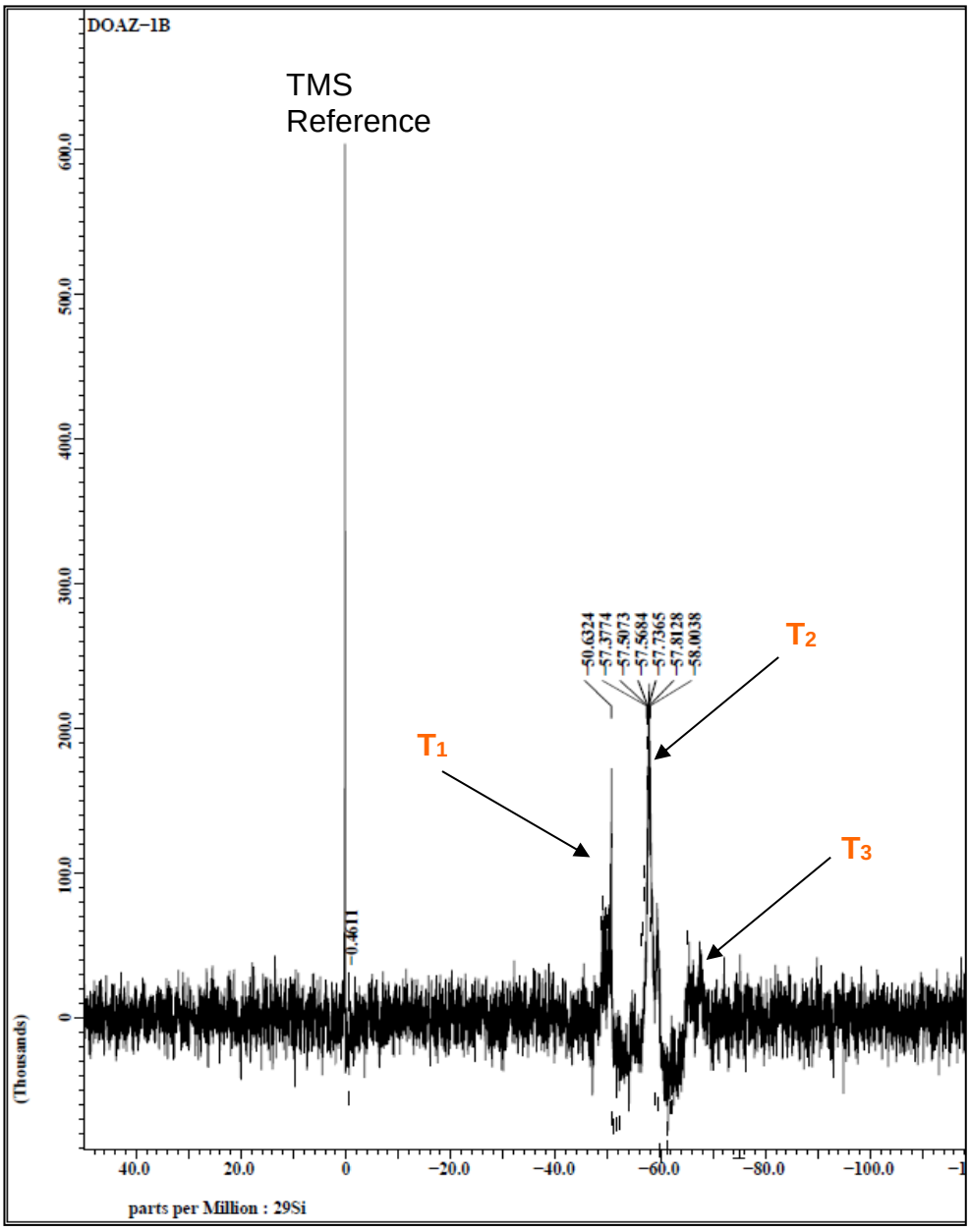

Figure 5.23. The ^{29}Si NMR of the silsesquioxane resin formed from the AZ-system (DOAZ-1) after attaining pseudo-equilibrium.

The 29-silicon NMR in **Figure 5.23** is the spectrum obtained from the resin formed from the AZ system using conditions 1 in **Table 5.3** (DOAZ-1). Notice two main silicon environments are present, T_1 (-50) and T_2's (-57 to -70ppm) and a small amount of T_3 peaks are also being observed. This suggest the reaction went to completion as there are no peaks from the starting materials (-42ppm) present. The presence of T_1, T_2 and a small amount of T_3 peaks suggest the species are not much different from those in the A-system. That is, predominantly oligomeric linears and cyclics.

Below (**Figure 5.24**) is a comparison of the ^{29}Si NMR of the silsesquioxane resin formed from DOAZ-1 with some of the other AZ resins (DOAZ-6 and DOAZ-9), as well as the silsesquioxane resin obtained from the single component-system

(A-system). This show similar peaks and peak heights and allows some understanding of the composition of the silsesquioxane resin formed from each of the A and AZ-systems as well as the variations.

AZ-systems

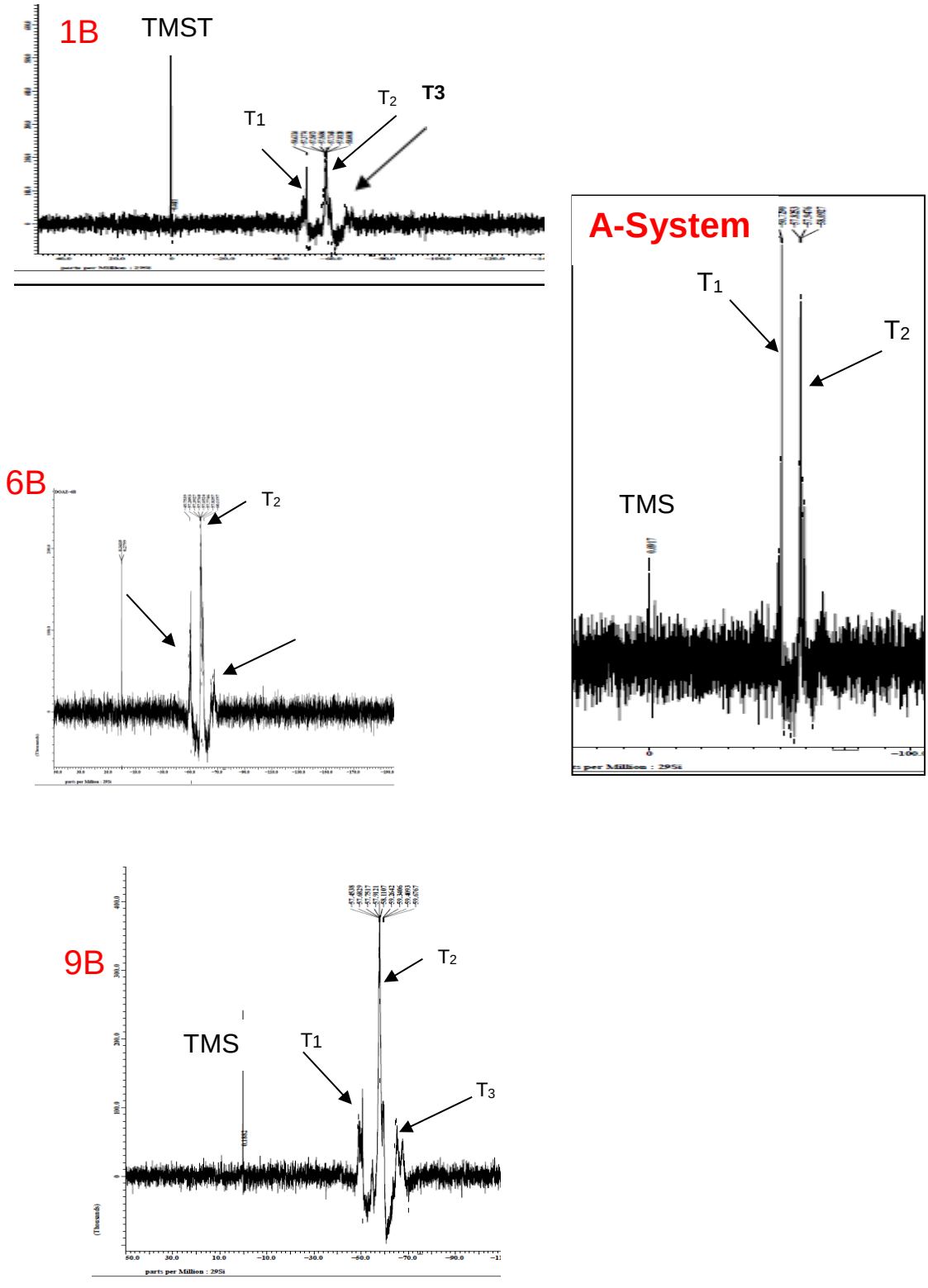

Figure 5.24. ^{29}Si NMR showing the comparison between the AZ-systems (DOAZ-1, 6B and 9 B) and the single component system (A-system).

The AZ-systems DOAZ-1, 6 and 9B (**Figure 5.24**) show an almost 1:2:1 ratio pattern of T_1^x:T_2^x:T_3^x whereas the A-system shows almost a 1:1 ratio pattern with more T_1 type resin structures than the T_2's and very little T_3. One explanation is that with the AZ-systems the *n*-propyl will react more readily because of its simpler/smaller structure and thus reacts further to give T_3 structures which is more difficult with the methacrylate structure. Also, in the AZ-system there are two different monomers (MPTMS and nPTMS). This implies two different silicon environments will be formed and this will affect the regions of the T_2 and T_3 peaks in the ^{29}Si NMR spectra leading to a broader range of peaks.

From the ^{29}Si NMR spectra, one can conclude that the AZ-system leads to the formation of similar types of species although with more branching than the A-system. Further analysis has been done subsequently to see if there are any changes to the types of structure of the species within these two systems.

5.2.8.2 GPC results of the AZ system resin compared to A-system resin

GPC results of the A and AZ-system resin are as shown in the chromatograms below. The straight line of the calibration was carried out using polystyrene standards which was used to calibrate the instrument. Polystyrene standards are long chain polymers made from the monomers 'styrene' These standards were bought from the supplier 'Agilent' and two sets were bought (Easi Vial kits – 100-10million g/mol) to use as reference to cover the full range of the expected molecular

weight of the A and AZ system resins. Polystyrene was used because it was the closest in property to the type of silsesquioxane long chains. The GPC analysis was carried out to determine the molecular weights of the two resins using the different conditions (A and AZ-system resins). This will give an indication of the different species that exist in the two resins.

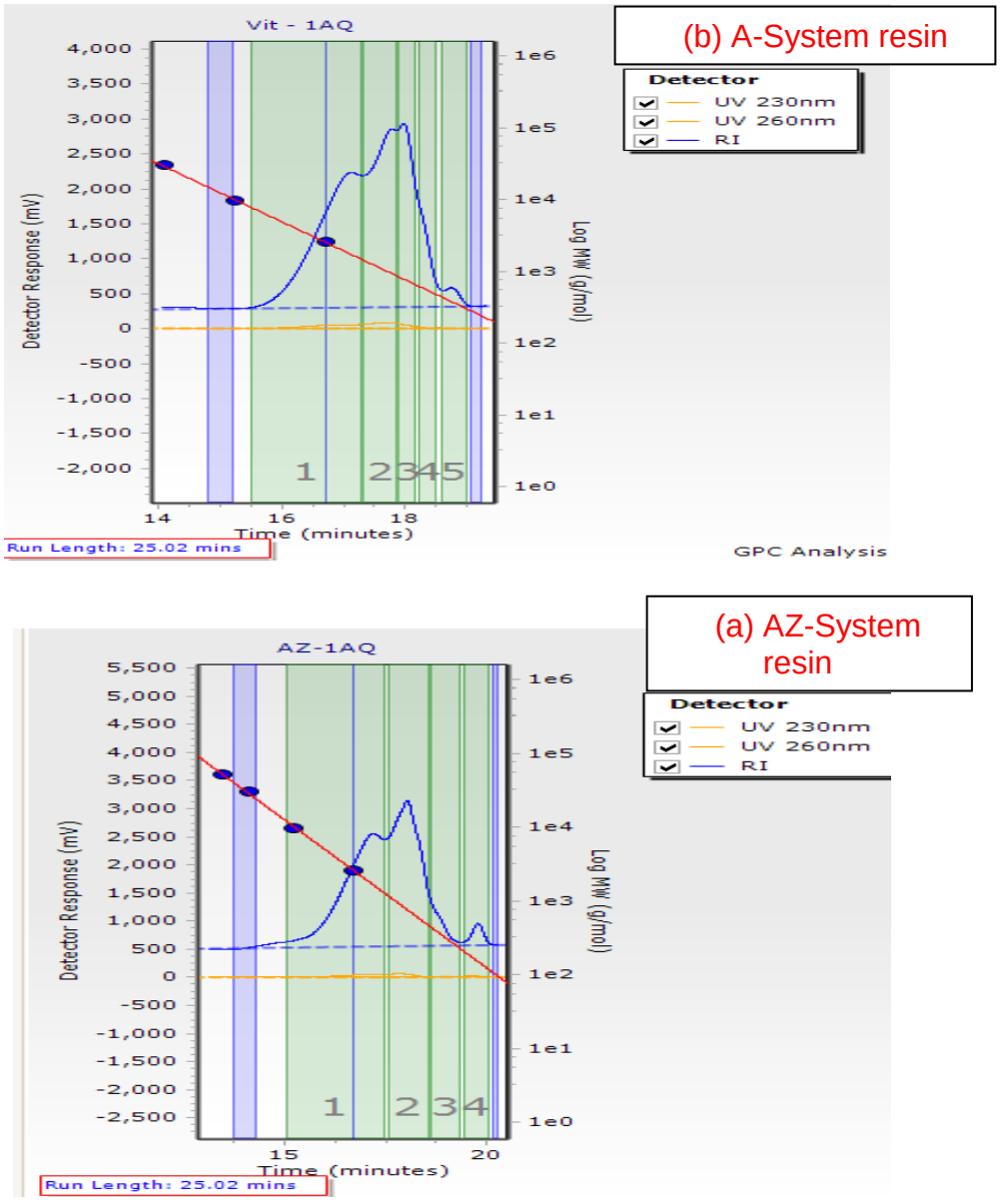

Figure 5.25 GPC results of (a) One-component system (A) and (b) two component system (AZ) resin

The GPC result of the two system resins (**Figure 5.25a and b**) show a trimodal peak for both systems with a close range of molecular weights. These GPC results agree with the ^{29}Si NMR findings again suggesting the two systems are not very different. The average molecular weight of both systems is about 2000g/mol. Even a GPC result of these two systems from another instrument suggests the same. See **Appendix 17 and 18** of the A and AZ chromatograms and the table of Mn and Mr results.

5.2.8.3 Mass spectroscopy (ESI-MS) of the AZ-system silsesquioxane resin compared to the A-system.

One of the aims of this research is also to use different instruments to characterize the resins. ESI-MS has therefore been used as one of the instruments to study the components in the resin that would otherwise be destroyed by harsh techniques such as gas chromatography-mass spectrometry (GC-MS)[275]. Below are the ESI-MS and chromatograms of the A-systems resin and the AZ-system resin (**Figures 5.26a and b**) put together for comparison purpose.

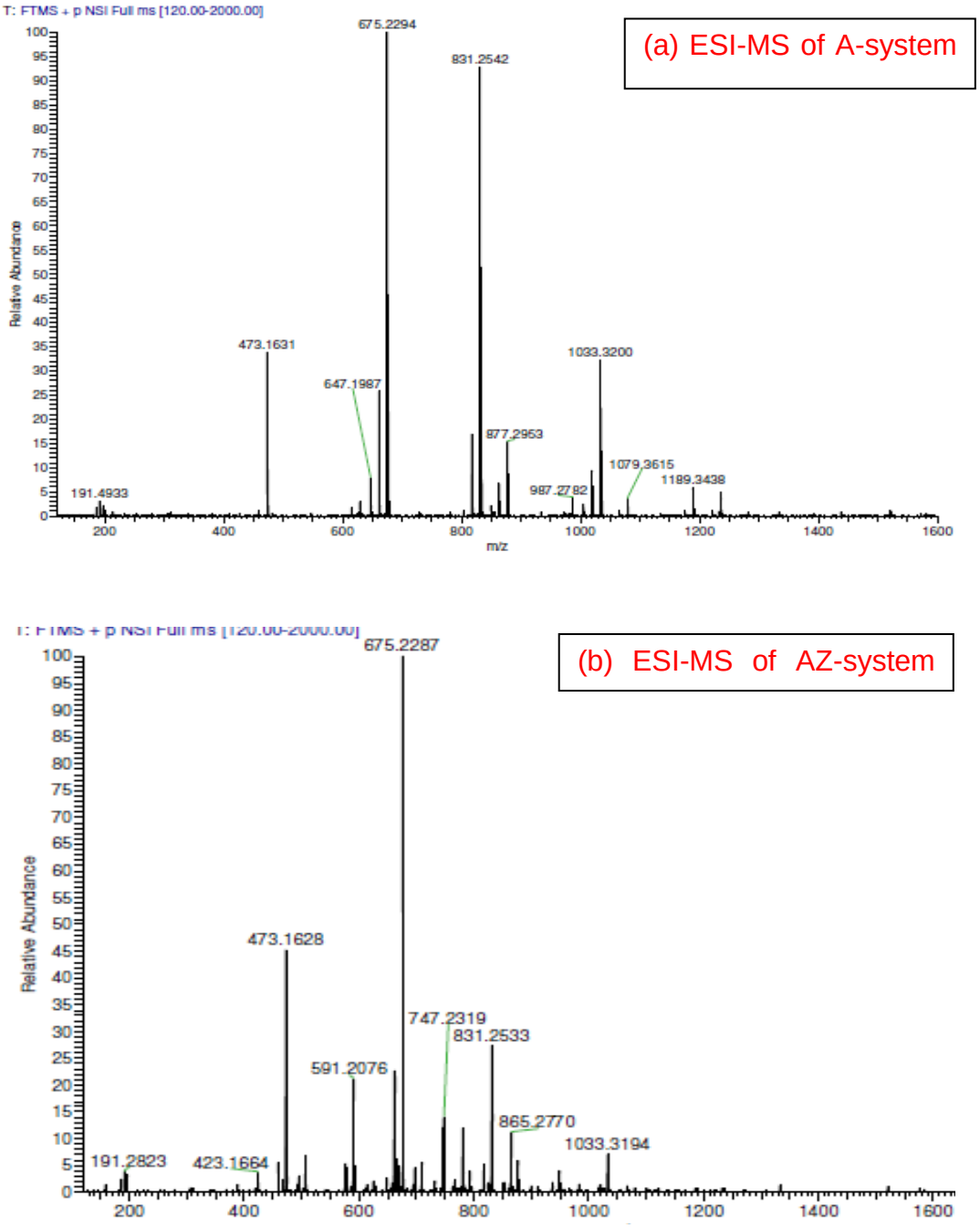

Figure 5.26. (a) ESI-MS of the A-system resin and **(b)** ESI-MS of the AZ-system resin (DOAZ-1)

Looking at the ESI-MS spectra (**Figures 5.26a and b**), some of the peaks in the A-system appear in the AZ-system. This suggests they are formed in the initial hydrolysis before mixing. For example, the *n*-propyl condenses very quickly such

that the MPTMS effectively condenses with itself. Also, there is a similarity in many of the peaks though the abundance is different in some. For example, peak m/z 675 is common in both spectra and the most abundant in both cases. It is an MPTMS trimer with no silanol groups hence confirms the presence of small amount of trimer in the NMRs in **Figure 5.24** above. From the spectra (**Figure 5.26a and b**), it can be said that the A-system and AZ-system resins have very similar types of species. The molecular mass of species ranges from 191 – 1199g/mol. This almost tie in with the GPC results of the molecular weights averaging about 2000g/mol. However, the average from the MS was ~800. This suggests there are heavier species which do not fly in the MS.

On the other hand, comparing the AZ-system to its alternatives (DOAZ-6 and 9) in **Figure 5.27** and in **Appendix 19** which correspond to variation in the water quantities, the conclusion can be made that more water increases the number of condensed structures. This conclusion was reached because there are higher molecular weight peaks present in DOAZ-6 and 9 and in greater abundance compared to the others. The NMRs in Figure 5.27 and appendix 19 also showed more T_3 species.

DOAZ-6

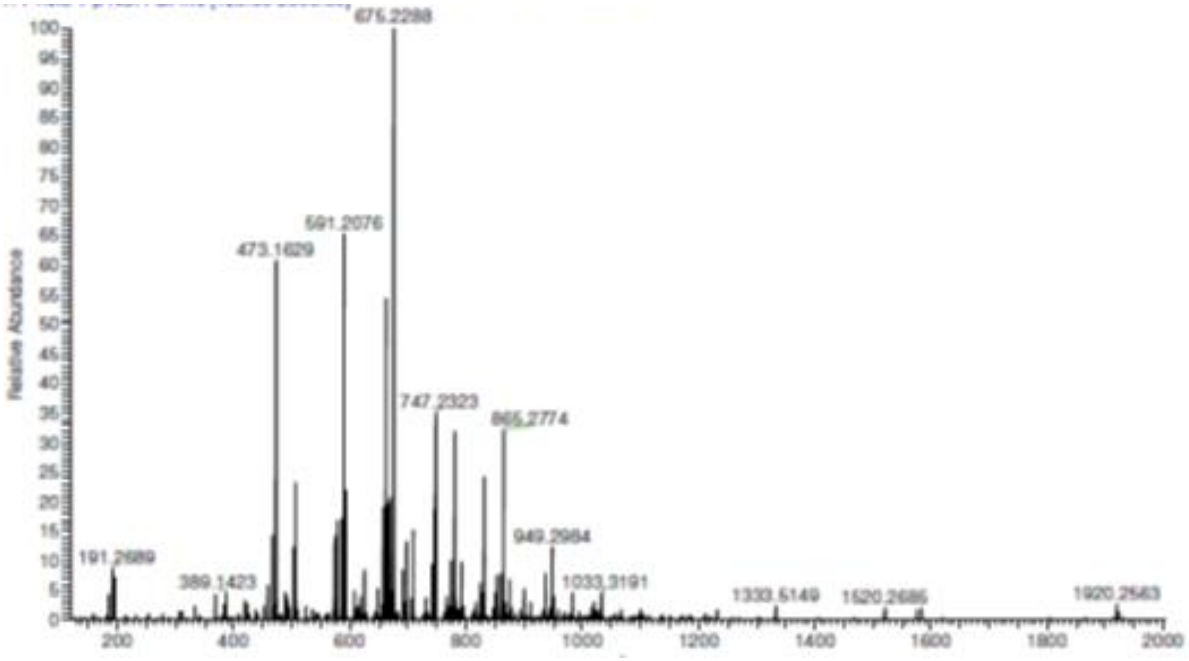

DOAZ-9

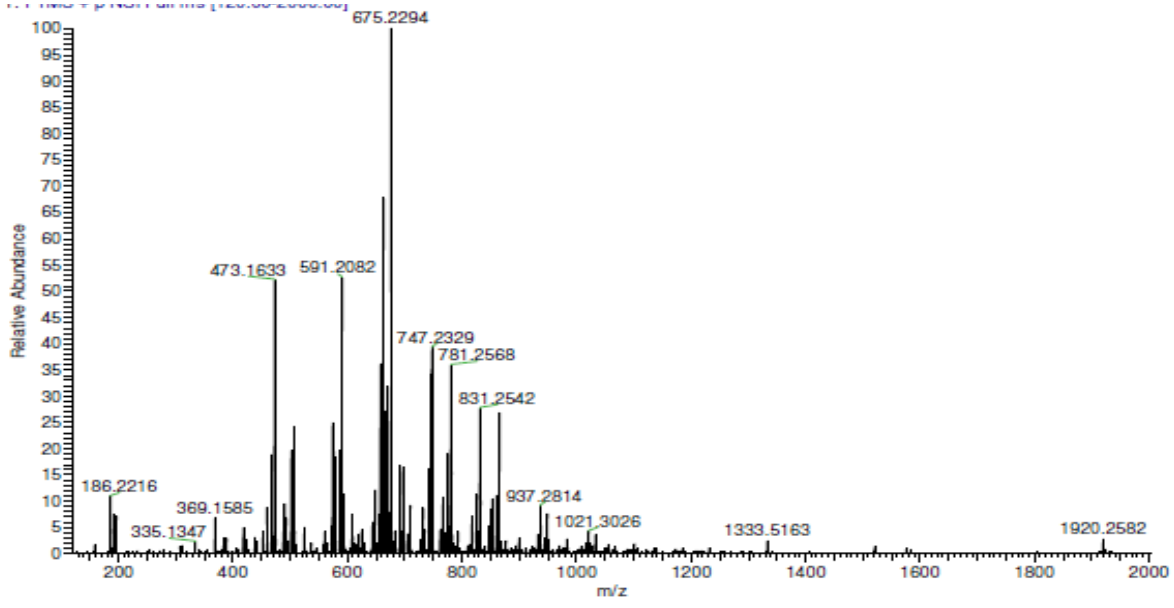

Figure 5.27– Maldi-ToF MS of the two-components system resin (DOAZ-6 and DOAZ-9)

The determination of the molecular weights of the products of hydrolysis and condensation of the MPTMS/nPTMS reaction (AZ-system) was carried out by ESI-MS. **Table 5.4** shows the experimental molecular weights and the assignment of the peaks appearing in the mass spectra. In the table, P equals nPTMS and M is MPTMS.

Table 5.4. Assignment of the ESI- MS peaks for silsesquioxanes prepared using the two component system (AZ-system.) showing the propyl (P) and methacrylate (M) exchange.

m/z exp.	**Assigned structure (H^+, Na^+, NH_4^+)**	**m/z calc.**	**m/z exp.**	**Assigned structure (H^+, Na^+, NH_4^+)**	**m/z calc.**
191	-	-	**831**	Si_4Na^+ (M)	**831.25**
423	Si_3Na^+ (P) Or $Si_2(OH)_2H^+$ (M)	**423.17** **423.15**	**865**	$Si_4(OH)Na^+$ (M)	**863.28**
473	Si_2Na^+ (M)	**473.16**	**1033**	Si_5Na^+ (M)	**1033.32**
591	Si_3Na^+ (1P+2M)	**591.21**			
675	Si_3Na^+ (M)	**675.23**			
747	Si_4Na^+ (1P+3M)	**747.23**			

Where P=nPTMS and M=MPTMS. All the other silicon valences are OEts.

From **Table 5.4**, there is a good agreement between the experimental molar masses and the predicted or calculated values found.

Matching the molecular weights in **Table 5.4** and **Figures 5.26** and **5.27**, there appear to be more MPTMS and MPTMS+nPTMS species observed than isolated nPTMS. It is either the nPTMS is not being detected by the instrument or there isn't an abundance of it in the final resin product formed. That is, it is evaporated off during the isolation stage. This is a similar finding shown by the NMR above.

5.2.8.4 DSC results of the AZ-system silsesquioxane resin

Figure 5.28 shows the DSC results of the silsesquioxane resin formed from the AZ-system. The DSC result is necessary to determine the melting points or thermal stability (phase transition) of the resins.

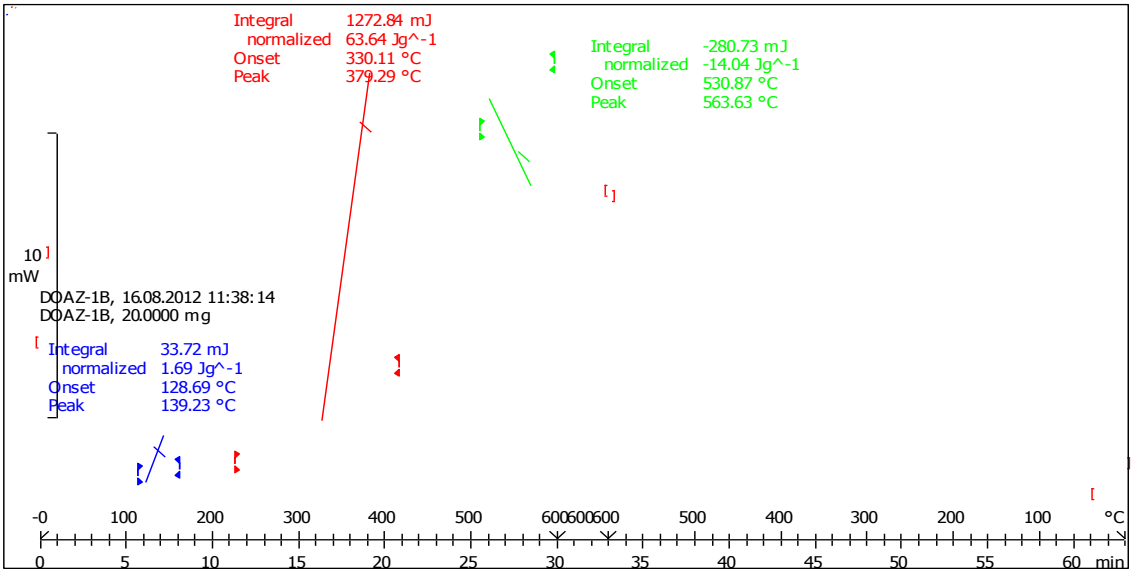

Figure 5.28. DSC of silsesquioxane resin formed from the AZ-system

The small peak (blue) at 128^{o}C came from the loss of water and methanol by evaporation. There is a significant heat flow up to 350^{o}C (red) with a strongly exothermic reaction. The reaction requires a wide temperature range to achieve a complete conversion. This may be a result of further polymerization of the

methacrylate double bonds that led to higher molecular weight oligomers in the resin. Notice this heat flow range is similar to the resin formed from the A-system (**Figure 5.7**) but the decomposing temperature here (**Figure 5.28**) is higher than that of the A-system resin. There is an endothermic peak at about 530^{o}C (green). This could possibly be an artifact or the peak could suggest that heat is absorbed as the resin goes from viscous oil to a crystalline solid, requiring higher temperatures for the transition.

5.2.8.5 TGA of the AZ-system silsesquioxane resin

TGA measures the thermal degradation of the resin by measuring weight loss from the resin over a range of temperatures at a set rate under a nitrogen atmosphere. This investigation by TGA was done at a heating rate of 20^{o}C/min, **Figure 5.29**. The comparative TGA results of silsesquioxane resin from the A-system and the AZ system (DOAZ-1, 6, 7 and 9) are shown below.

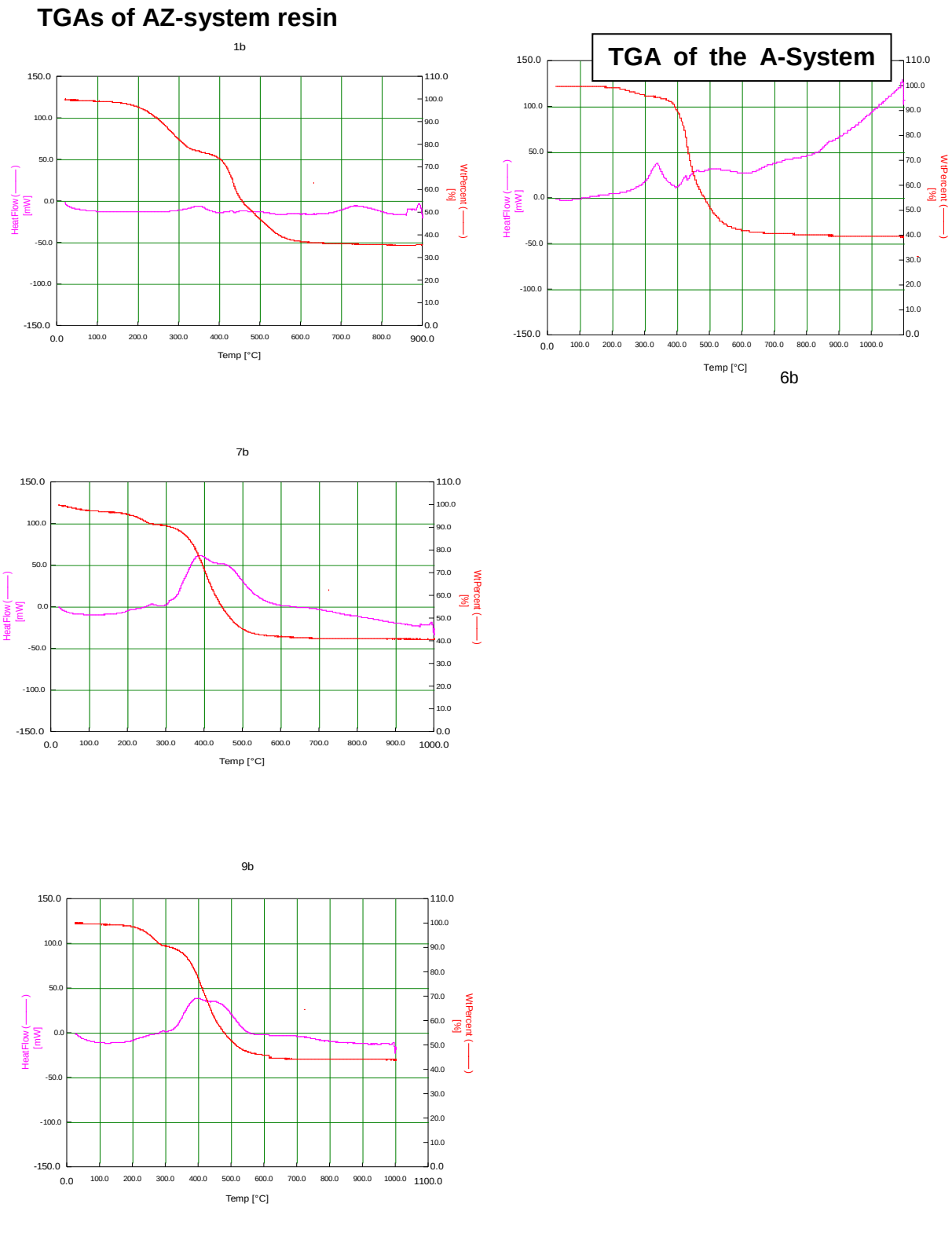

Figure 5.29. Variation in TGA results between the AZ-system (DOAZ-1b, 6b, 7b and 9b) and the A-system silsesquioxane resins**.**

Looking at **Figure 5.29**, there is a noticeable difference between the AZ-system (1b) and the A-system results. The graph from the DOAZ-1b resin (AZ-system) show two major transition temperatures or weight losses compare to the A-system resin with one main and one small weight loss at the beginning.

Comparing the AZ-systems (traces DOAZ-1B to the others, DOAZ 7 and 9) graphs between each other, there are no significant differences. The weight percent of samples retained after burning in all systems is about 40%, again confirming the thermal stability of the silsesquioxane resin. There are two processes occurring; condensation/polymerization at ~350^{o}C and ligand loss at ~450^{o}C. In 7 and 9, the ligand loss occurs earlier (~400^{o}C) so the two peaks merge giving a more broad peak.

5.2.8.6 FT-IR of the AZ-system silsesquioxane resin

FT-IR was used to study the hydrolysis and condensation processes to identify the silanol content in the silsesquioxane resin mixture. This will tell us the chemical difference between the starting material (MPTMS) and the resin formed. The FT-IR spectrum (**Figure 5.30**) shows the presence of the Si-OH stretch at 3544nm of

the resin (red). Again, this peak was absent in the starting material, MPTMS (purple).

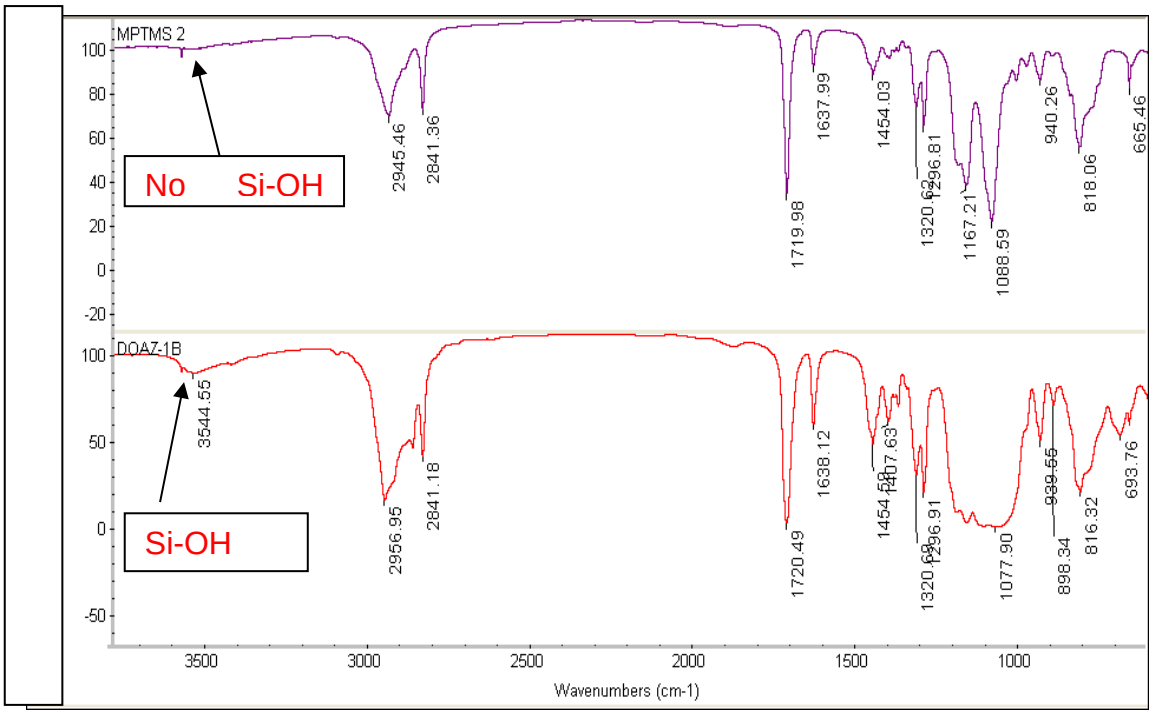

Figure 5.30. FT-IR of the AZ-system's vitolane resin (AZ-1B), compared to MPTMS starting material

Looking at the resin FT-IR spectra in **Figure 5.30**, the acrylate is not changing significantly (see C=O region ~1720cm^{-1}) in both spectra. That is, there is no polymerization of the methacrylate. The difference is the hydrolysis/condensation taking place in the AZ vitolane resin (Si-OH) which is not present in the starting material. Again, this OH peak could come from the solvent methanol or it could be residual water. The Si-OH peak of the AZ-system's resin is less broad compared to the A-system's resin (**Figure 5.5**); this implies there is more condensation in the AZ-system as the silanols (Si-OH) have been reduced forming complex siloxane structures. The broadness of the Si-OH peak of the A-system could be due to more hydrolyzed components in the resin, but this could also be due to more water or methanol.

Below is the FTIR of the AZ-system resin char after DSC (**Figure 5.31**) and the CHN analysis results (**Table 5.5**) of DOAZ 1 (AZ -1B, vitolane) to understand the elemental composition of the AZ-resin after exposure to high temperature of 650ºC.

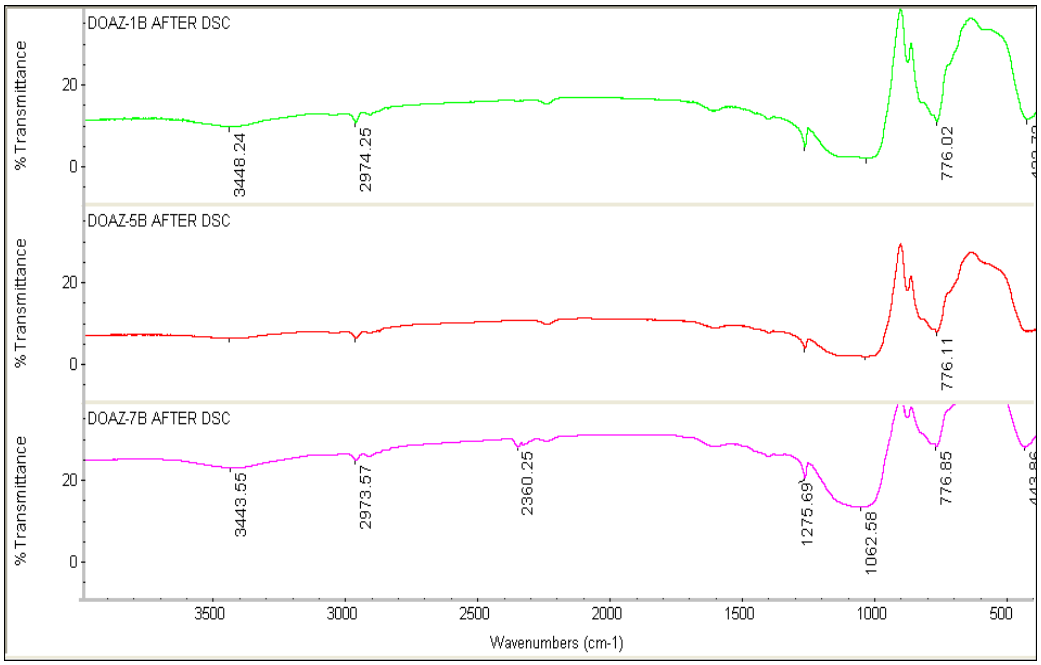

Figure 5.31. FTIR spectra of the silsesquioxane resin after DSC analysis (DOAZ-1, 5 and 7).

Comparatively, the FT-IRs before DSC (**Figure 5.30**) and after DSC (**Figure 5.31**) show completely different peaks. Many of the peaks in the FT-IR before DSC have disappeared and a few new ones have appeared. There are no longer any carbonyl, C=C and C-H bonds present. What is left is probably just silica. This suggests the chemical composition of the resin has been greatly altered.

5.2.8.7 CHN elemental analysis of the AZ-system silsesquioxane resin after DSC (char)

A CHN analysis was carried out to determine the elemental composition (carbon, hydrogen and nitrogen) of the resin's char after heating the resin to about 600^{o}C. This result will give an indication of compositional changes once the resin is exposed to high temperatures.

Table 5.5. CHN results of the char (AZ-1B vitolane) after DSC analysis @600^{o}C

ELEMENTs	**C (carbon)**	**H (hydrogen)**	**N (nitrogen)**
% Found 1	25.74	3.10	<0.10
% Found 2	25.63	3.10	<0.10

From **Table 5.5**, the results are similar to those found in the A-system. As before, one can calculate the estimated percentage of each atom left in the char to be:

Assuming that in 100g of sample there is:

25.74g of carbon = 25.75/12= 0.257 or 2mols

3.10g of Hydrogen =3.10/1.01= 0.031 or 3.0mols

71.16g (rest is SiO_x) = 71.16/52 = 1.4mols

Therefore, this suggests the structure following the decomposition of the silsesquioxane from the AZ-system is likely to be a polysiloxane (CH_3SiO_x) with carbon as graphite or silicon carbide as found from the A-system.

5.2.8.8 LCMS of the AZ-system silsesquioxane resin

This technique was used to enable the identification of the different species in the silsesquioxane resin mixture in order to understand its structure.

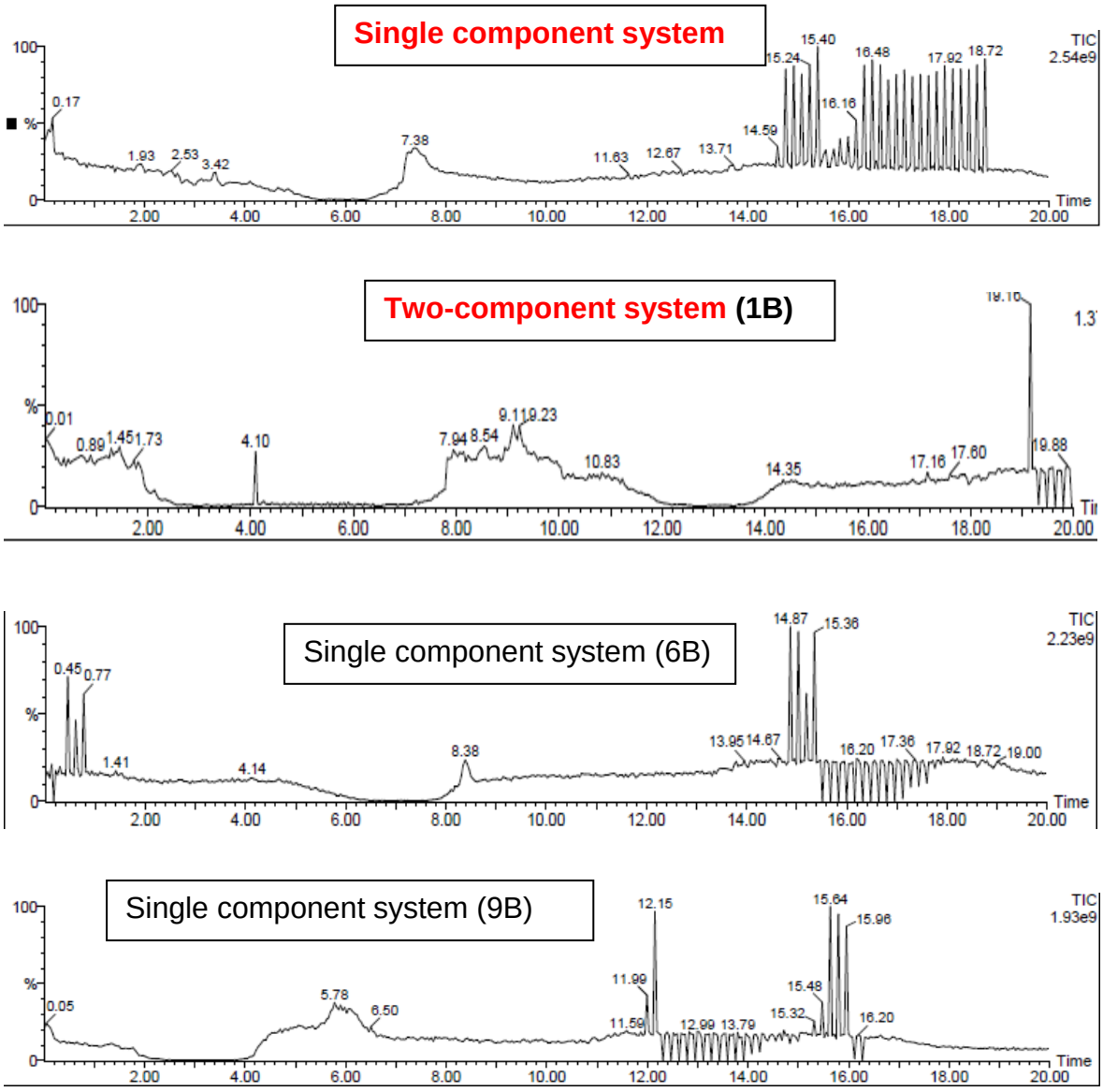

Figure 5.32. Comparing the LCMS chromatograms of the A-system to the AZ-system's resin (DOAZ1, 6 and 9B).

From the above LCMS chromatogram in **Figure 5.32**, the mass spectrum is as shown in **Figures 5.33**. The molecular ion is the peak at 860 with the base peak being the peak at 186. Comparison of the single component system with the two component-system can be seen on the same figure. This mass spectrum show different peaks present in the silsesquioxane resin from the A and AZ-systems. This allows a comparison of the resin composition between the two systems within the first ten minutes of scanning time. The masses are as identified in **Table 5.6** that follows. The chromatograms of the DOAZ-6B and DOAZ-9 can be found in **Appendix 20**.

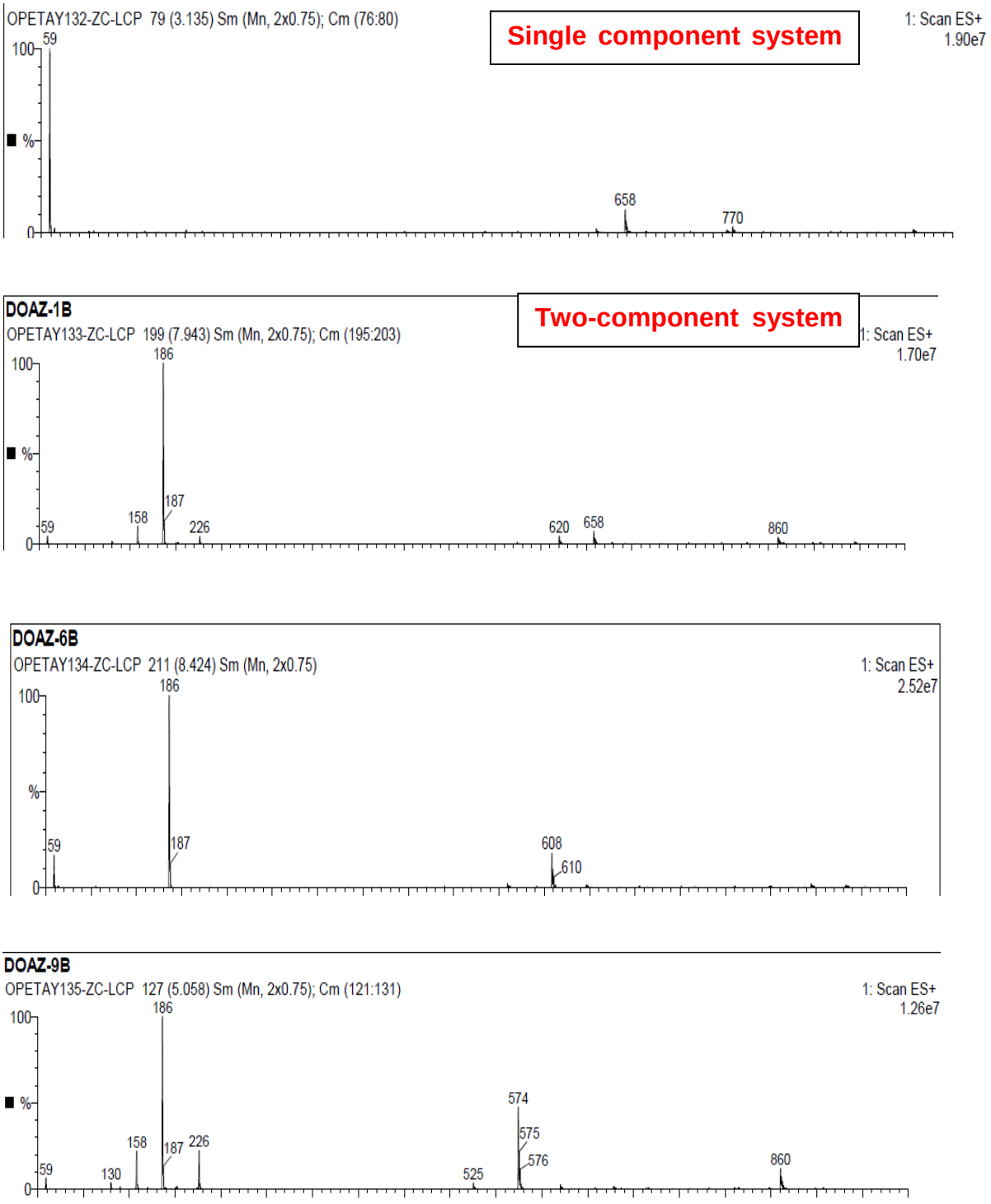

Figure 5.33. Comparing the LCMS mass spectrum of the A-system to the AZ-system's resin (DOAZ1, 6 and 9B).

Although the MS were done at different retention times, (3.1, 7.9, 8.4 and 5.1 minutes respectively), it did not affect the results as the reactions had all come to

completion already. There is a common base peak ion at 186 which is the npropyl staring material complexed to a sodium ion. This is only seen in the AZ system resins. Also, the ion at 59 is seen in both systems but much reduced in abundance in the AZ system resins. It is most likely a fragment off the main species or a common impurity in the instrument. The highest molecular ion of the single component-system has a m/z ratio of 770 which corresponds to MPTMS with four silicon atoms bonded to four hydroxyl groups and an ammonium ion, and sufficient MeO groups. See **Table 5.6** below for other corresponding peaks. The AZ system's resin has a molecular mass of 860. Note that in the table: P represents Si environment from nPTMS and (M) from MPTMS.

Table 5.6. Assignments of AZ- system's Silsesquioxane predicted structures based on LC-MS data

m/z exp.	**Assigned structure (H^+, Na^+, NH_4^+)**	**m/z calc.**	**m/z exp.**	**Assigned structure (H^+, Na^+, NH_4^+)**	**m/z calc.**
59	-	**-**	**608**	$Si_3(OH)_3NH_4^+$ (M) Or T_3^+ (M)	**610.22** **606.20**
130	$Si_1(OH)_3Na^+$ (P)	**131.01**	**620**	$Si_3(OH)_4Na^+$ (M)	**619.17**
158	$Si_1(OH)_1Na^+$ (P)	**159.14**	**658**	$Si_4(OH)_2$ (2P+2M)	**658.23**
186	Si_1Na^+ (P)	**187.08**	**770**	$Si_4(OH)_4NH_4^+$ (M) or Si_4 (1P+3M)	**770.23** **770.29**
226	$Si_2(OH)_4$ (P)	**226.07**	**860**	$Si_4(OH)NH_4^+$ (M)	**858.33**
574	$Si_3NH_4^+$ (M)	**574.21**	**-**	-	-

Where P=nPTMS and M=MPTMS. Other components attach to silicon are OMes and OEts.

Table 5.6 above shows the assigned structures based on the silicon environment (T), degree of hydrolysis (OH) and the fragment ion that the structure is present as (H^+, NH_4^+ and Na^+). Some of the structures are found in **Appendix 14**. The species that were detected in the AZ-system silsesquioxane resin ranged from the monomer to the tetramer and then other larger oligomers. The assigned molecular ions show various -Si- environments from the MPTMS and nPTMS. Comparison of the A-system resin with the DOAZ-1 of the AZ-system resin reveals some similarities. The peaks m/z 59 and m/z 658 occurred in both spectra (not in 6B and 9B) with the molecular ions occurring at m/z 770 and m/z 860 respectively for the A and AZ-system. Species 186 is present in each of the AZ-systems resin and in high abundance but absent in the A-system resin.

5.3 Model compounds used to characterise silsesquioxane resin products

To further understand the results of the silsesquioxane resin both from the A- and AZ-systems, individual compounds had to be synthesised, purified and characterised to be used as models. The model compounds were synthesized because the silsesquioxane resin produced complex spectra and chromatograms and hence it was difficult to identify the peaks. The model compounds will enable us to identify the complex silsesquioxane resin. Some of the individual species synthesised and modelled were, T_2, T_4 and T_8.

5.3.1 Methacryloxypropyl trimethoxysilane dimer

This is the dimer obtained from the sol-gel reaction of MPTMS to produce a disiloxane.

5.3.1.1 Dimer synthesis

The methacrylate dimer was synthesised following the synthetic method described in **Chapter 2.1.7**. In the case of the dimer, instead of 24 hours for full hydrolysis to have occurred, the reaction mixture was stopped after 2 hours when the dimer would have been formed but not undergone further reaction to form larger oligomers.

5.3.1.2 Dimer characterisation

The isolated dimer was characterised to identify the compound using the techniques below.

5.3.1.2.1 MALDI-ToF MS: m/z (%) of the MPTMS dimer after distillation

MALDI-ToF MS positive ion mode has been used to investigate the identity of the dimer (**Figure 5.34**) by identifying the ions based on the m/z ratio.

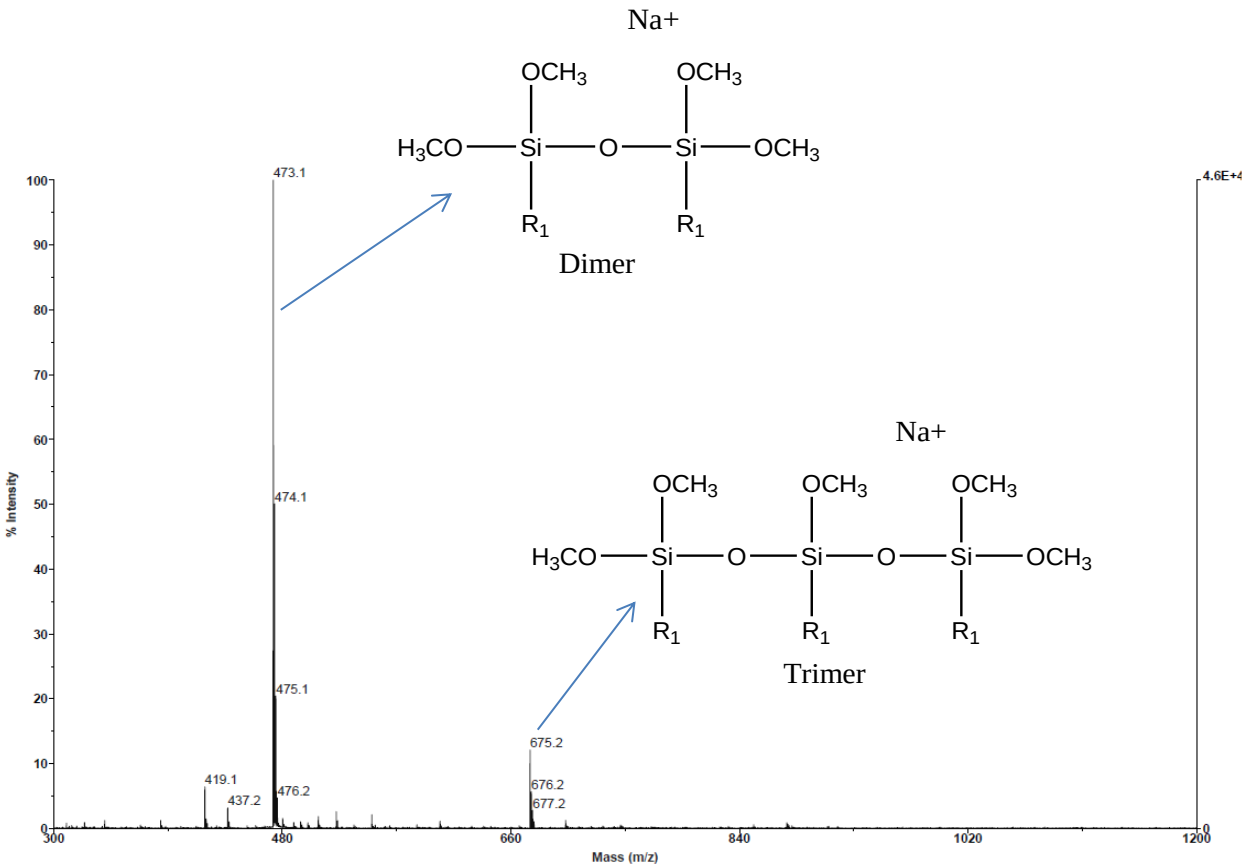

Figure 5.34. MALDI-ToF MS (positive ion mode) of MPTMS dimer

The formation of the MPTMS dimer has been confirmed by MALDI-ToF MS (**Figure 5.34**). The molecular weight of the dimer is 473.1g/mol with sodium forming the MALDI positive ion. The trimer peak at 675.2g/mol was not expected but could have occurred as a result of further hydrolysis occurring in the Maldi instrument (moisture), the dimer being a very reactive species. However, the HPLC (**Figure 5.35**), the GC-MS **(Figure 5.36a)** and ^{29}Si NMR (**Figure 5.36b)** all confirmed a pure dimer was isolated.

5.3.1.2.2 HPLC-MS of the MPTMS dimer

HPLC MS was also used to confirm the identification of the dimer.

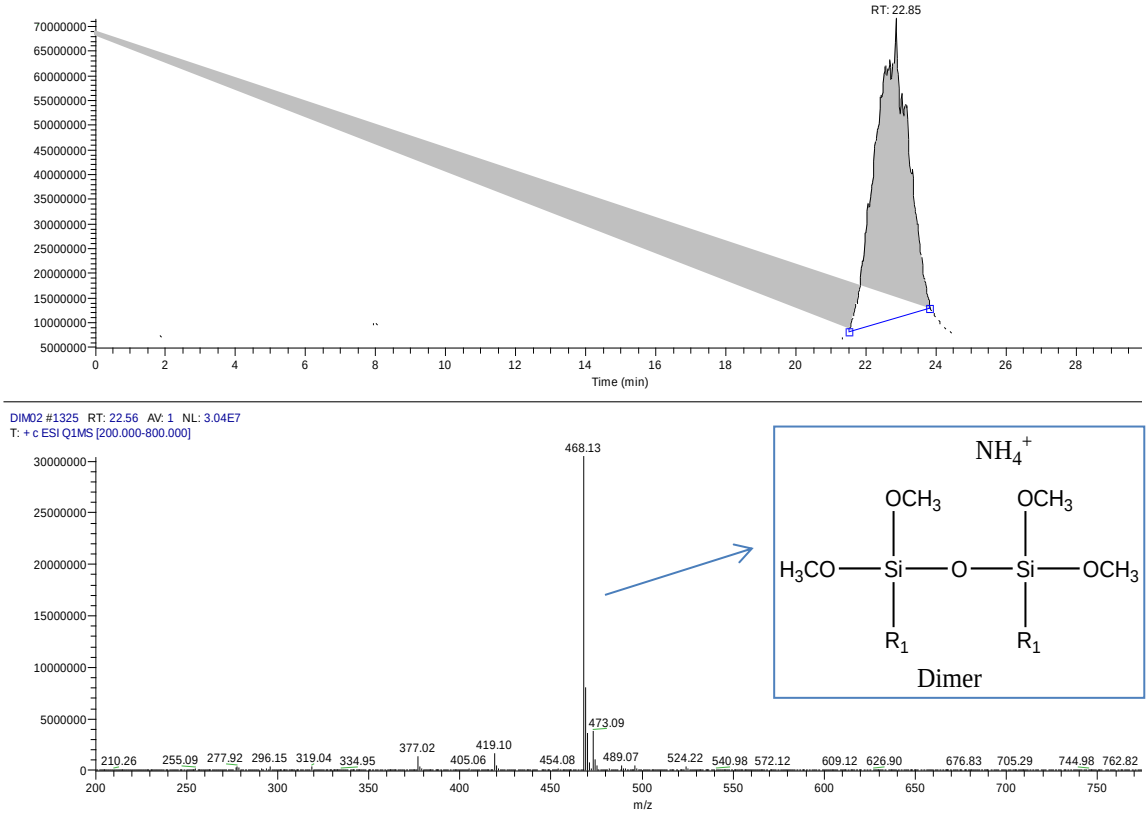

Figure 5.35. HPLC-MS of MPTMS disiloxane

The ion at m/z = 468.13 mass units corresponds to the parent ion whose peak and structure are shown in **Figure 5.35**.

5.3.1.2.3 ^{1}HNMR and ^{29}Si-NMR of MPTMS dimer

The ^{1}H and ^{29}Si NMR in **Figure 5.36a and b** finally confirm the identity of the dimer.

a)

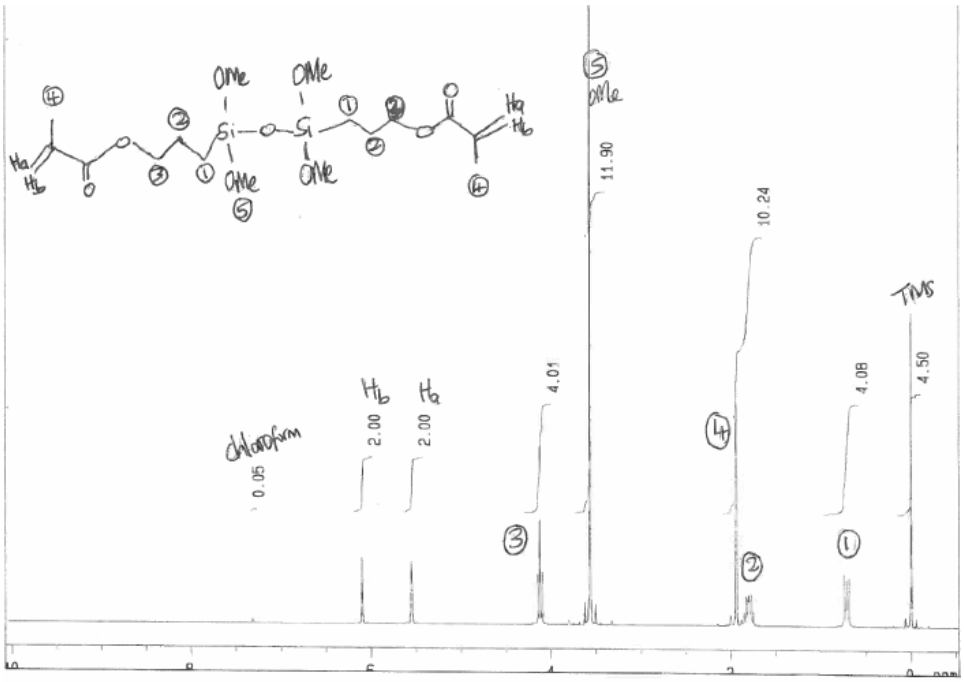

b)

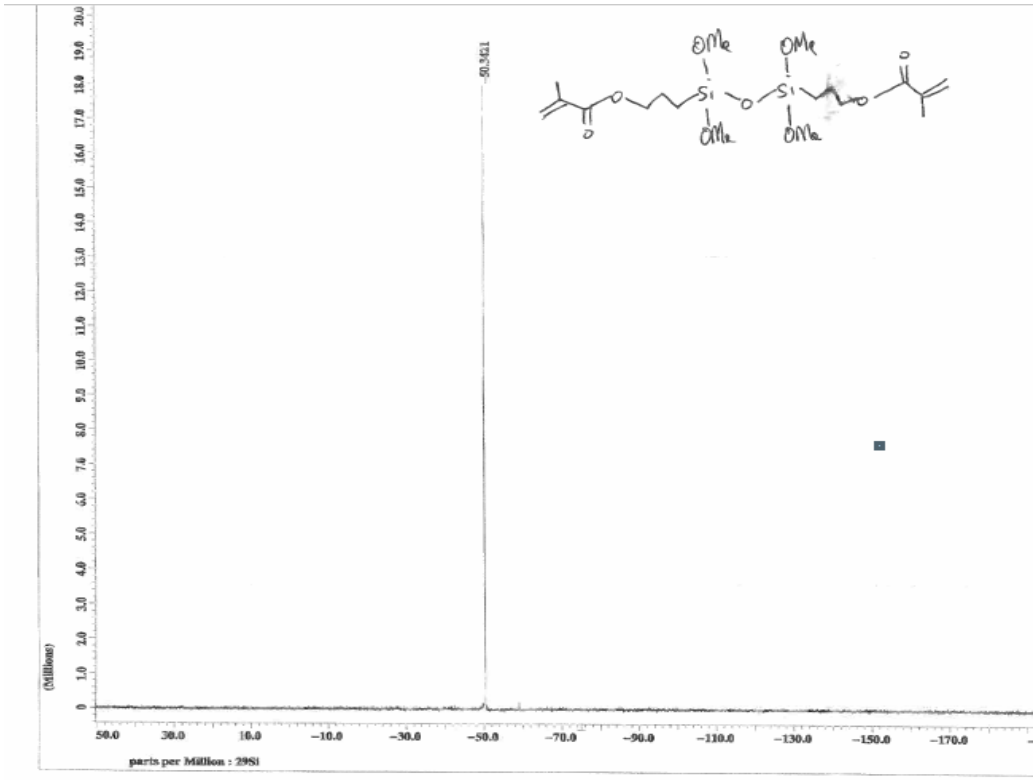

Figure 5.36. ^{1}H NMR (a) and ^{29}Si-NMR (b) of MPTMS dimer

The ^{1}HNMR (**Figure 5.36a**) of the pure dimer recorded in $CDCl_3$ confirms the compound is a pure dimer. See the corresponding carbon NMR in appendix 15. The peak exhibited at -50.3421ppm on the ^{29}Si NMR spectrum (**Figure 5.36b**) is the dimer.

This product being very unstable and hence difficult to isolate has not been reported in literature hence a very unique and novel finding. This compound has been fully characterized and confirms it is the obtained product. With the above being said, other similar larger molecular dimers have been reported in the past by Antonucci *et al*[279].

5.3.2 Methacryloxypropyl trimethoxysilane (MPTMS) tetramer

After isolating the dimer, several trials were carried out to isolate other species to confirm if they will be present in the silsesquioxane resin mixture. Other routes were studied to find out if the tetramers (linears) in any form were present in the mixture. The phenyl route was carried out as it is easier to isolate and characterise and thus provided a useful model for the synthesis.

5.3.2.1 Tetramer synthesis

The synthesis was carried out using two approaches although the phenyl route was not successful (**Scheme 5.2 and 5.3**)**.** The second route using the dimer product approach as the starting material was successful. See the equation for the synthesis in **Scheme 5.4** and the synthesis described in **Chapter 2.1.8.** The characterization follows in **Figures 5.37, 5.38, 5.39,**

a) Using Iodophenyltrimethoxysilane

This was applied as a trial to see how successful it could be. If the cyclic tetramer was obtained, it could be characterised and also used to investigate the presence of cyclic tetramers in the vitolane resin. This reaction was not pursued because whilst step one was successful obtaining products from the last step was not possible despite several trials using various reactants including; iodophenyl, methyl and vinyl methacrylate intermediates (**Scheme 5.2**) and changing the starting material (**Scheme 5.3**).

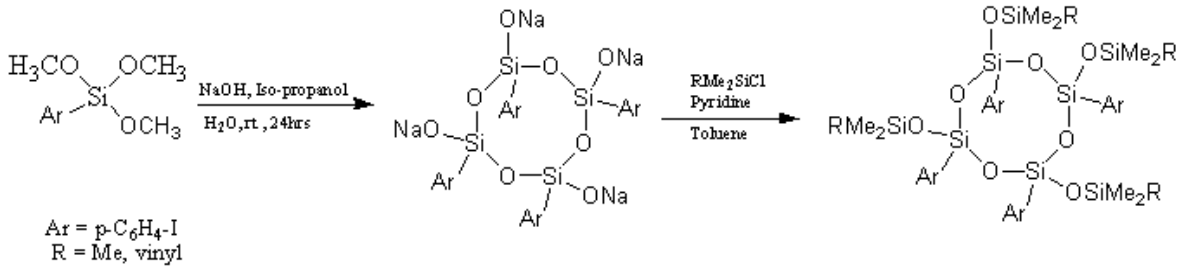

Scheme 5.2. Equation for the proposed synthesis of the iodophenyl tetramer

b) Using MPTMS

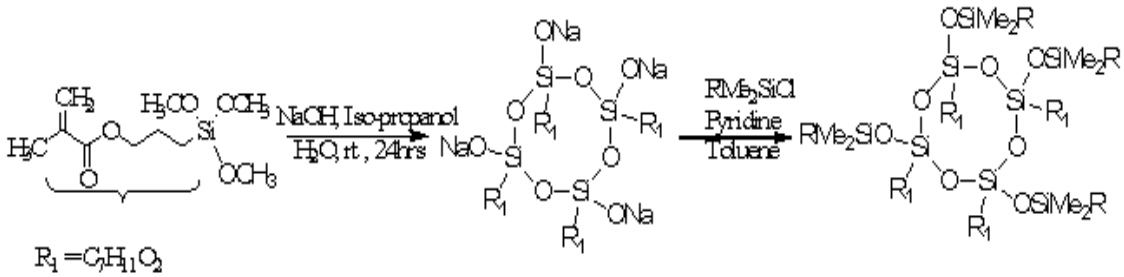

Scheme 5.3. Equation for the synthesis of cyclic tetramer.

This was carried out to see if there were any cyclic molecules present in the silsesquioxane mixture. This was also not successful but rather resulted in a complex mixture.

c) Using the MPTMS dimer to obtain a linear/branched tetramer silsesquioxane resin

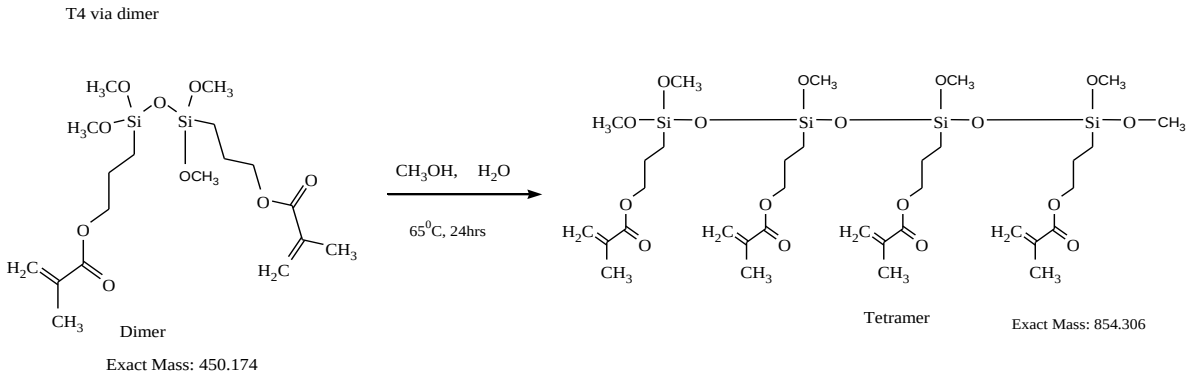

Scheme 5.4. Equation for the synthesis of linear MPTMS tetramer

5.3.2.2 Characterisation of the tetramers

After the tetramers were synthesised and the product obtained, it was characterised to identify the tetramer. However, the tetramer could not be distilled because of its very high boiling point, neither could it be separated by column chromatography as that was explored but no apparent separation occurred. Hence it was analysed as prepared.

5.3.2.2.1 ^{29}Si NMR result of the MPTMS tetramer

^{29}Si NMR was used to identify the tetramer.

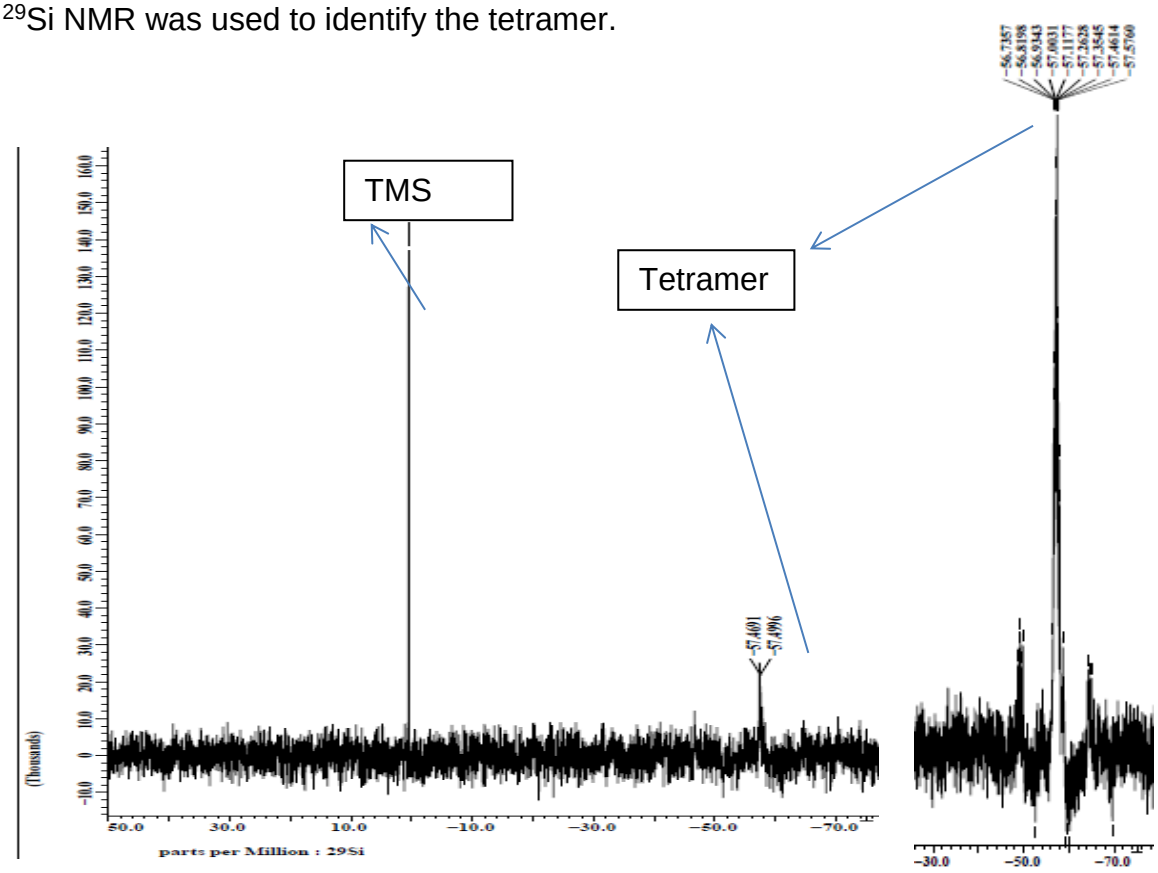

Figure 5.37. ^{29}Si-NMR (both spectra) of the synthesised MPTMS tetramer

The ^{29}Si-NMR spectrum (**Figure 5.37**) displayed a tetramer peak at -57.46ppm which could be a linear or cyclic tetramer. An expansion of the peak region shows a small presence of some other species which are other larger oligomers as the MALDI-ToF-MS also confirms in **Figure 5.38**.

5.3.2.2.2 MALDI-ToF MS of MPTMS tetramer

Maldi-Tof MS (**Figure 5.38**) exhibited five main peak regions corresponding to the tetramer (~100%), pentamer (~25%), hexamer (~35%), heptamer (10%) and octamer (10%). Very small fractions of other peak regions can be seen which could be nonamers and decamers.

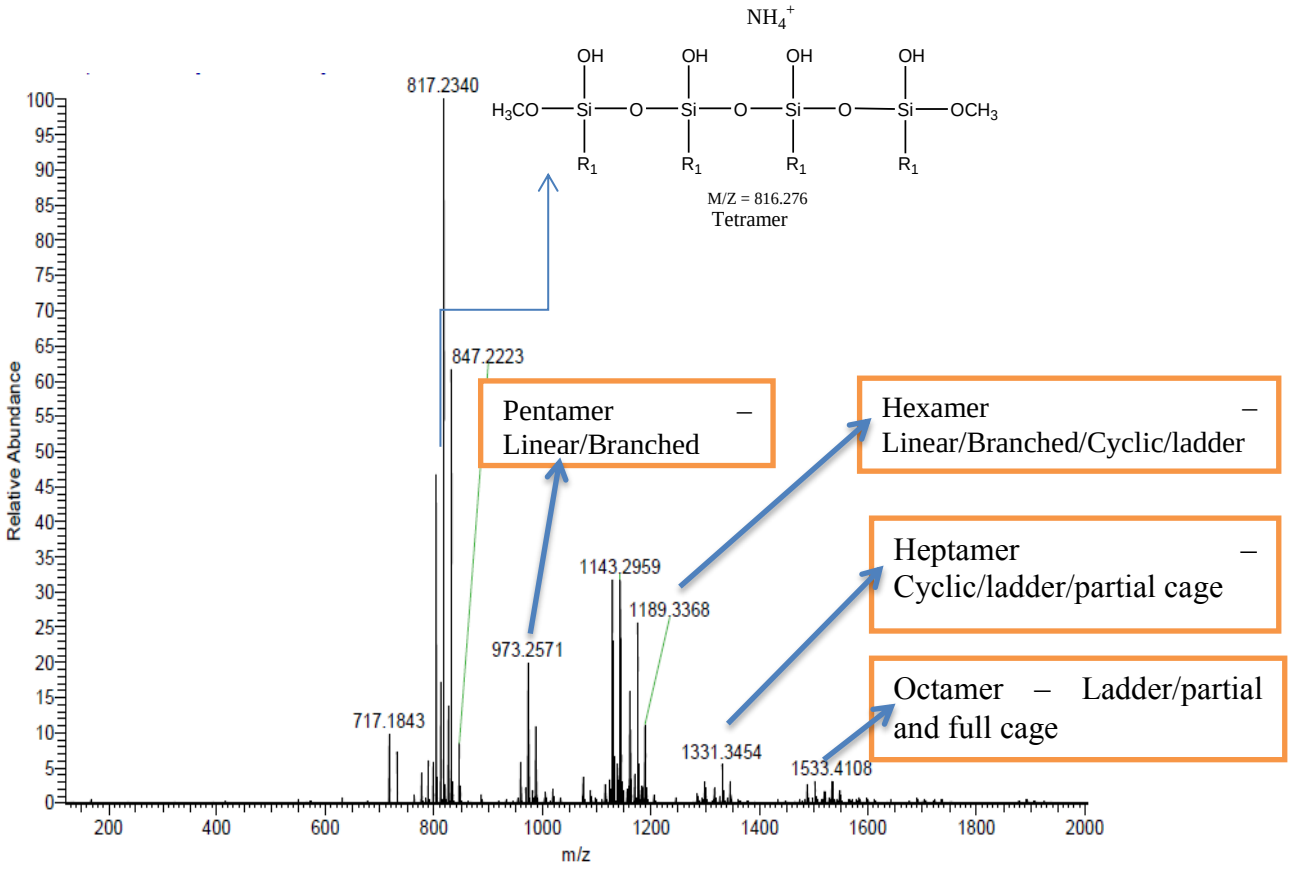

Figure 5.38. Maldi-ToF MS of the synthesised MPTMS tetramer

From **Figure 5.38,** it suggests that the hydrolysis of the dimer did not give the pure tetramer but a mixture of mainly the tetramer with higher oligomers (T_3 species as the ^{29}SiNMR showed).

5.3.2.2.3 LC-MS of the tetramer

On the LCMS, only the tetrameric region was scanned using single ion monitoring mode and the following spectra were obtained (**Figure 5.39**).

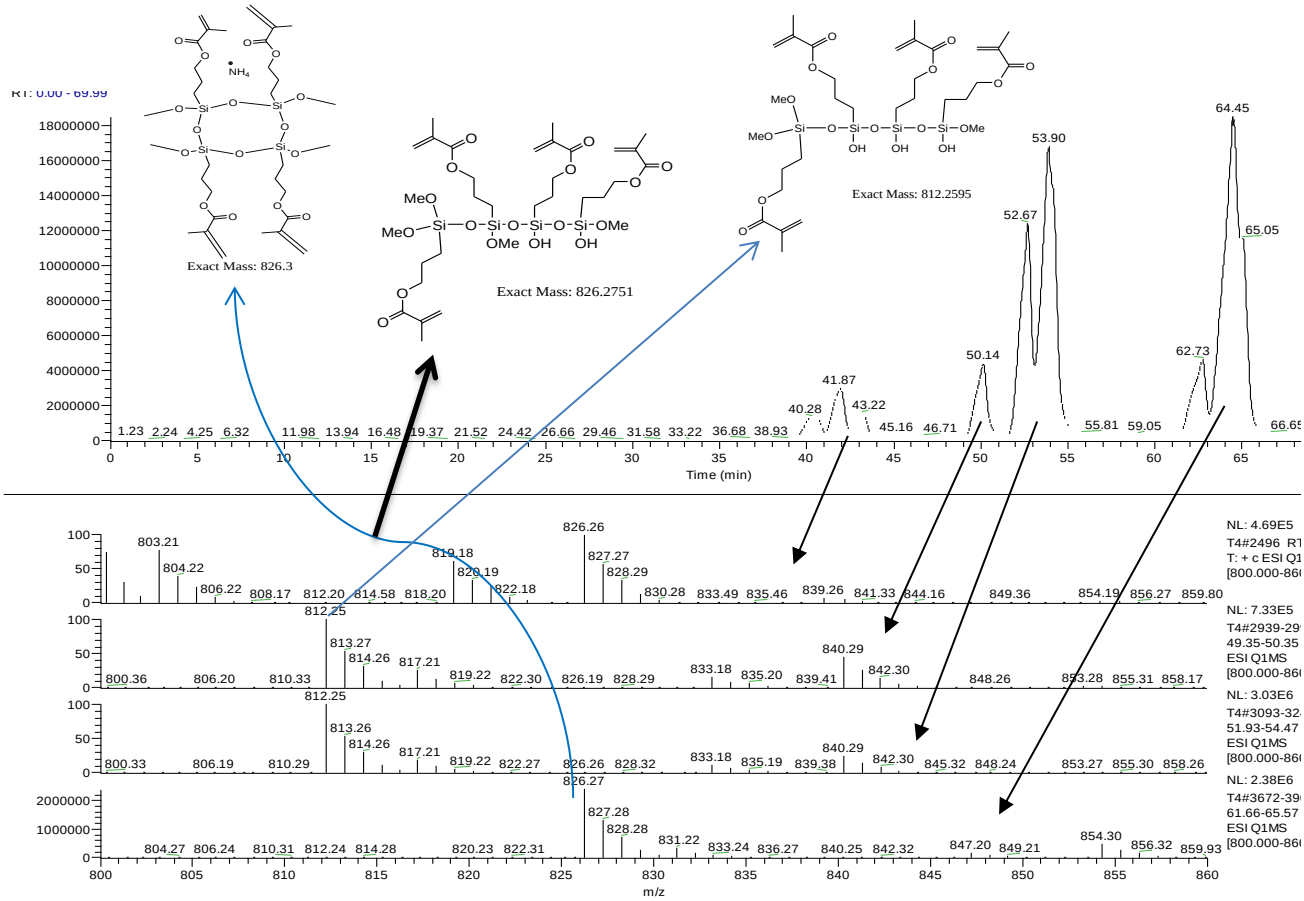

Figure 5.39. HPLC-MS chromatogram and mass spectrometry of the synthesised MPTMS tetramer showing tetrameric isomeric species as retention time increases (linears and cyclics) with arrows showing different chromatograms and structures.

The HPLC-MS results in **Figure 5.39** show all tetramers of different possible structural arrangements. The difference in retention times could be due to the different interaction of the different structures with the mobile phase. The peaks represent tetrameric species of different structures. Only the tetrameric region (800-860 m/z) were being looked at on the HPLC-MS hence the reason the high

molecular weight species were not observed on the mass spectrum, hydrolysis could have occurred in the HPLC.

5.3.2.2.4 GPC of the MPTMS tetramer

The GPC analysis of the tetramer to determine the range of the molecular weights of the species present in the tetrameric product mixture is shown in **Figure 5.40.**

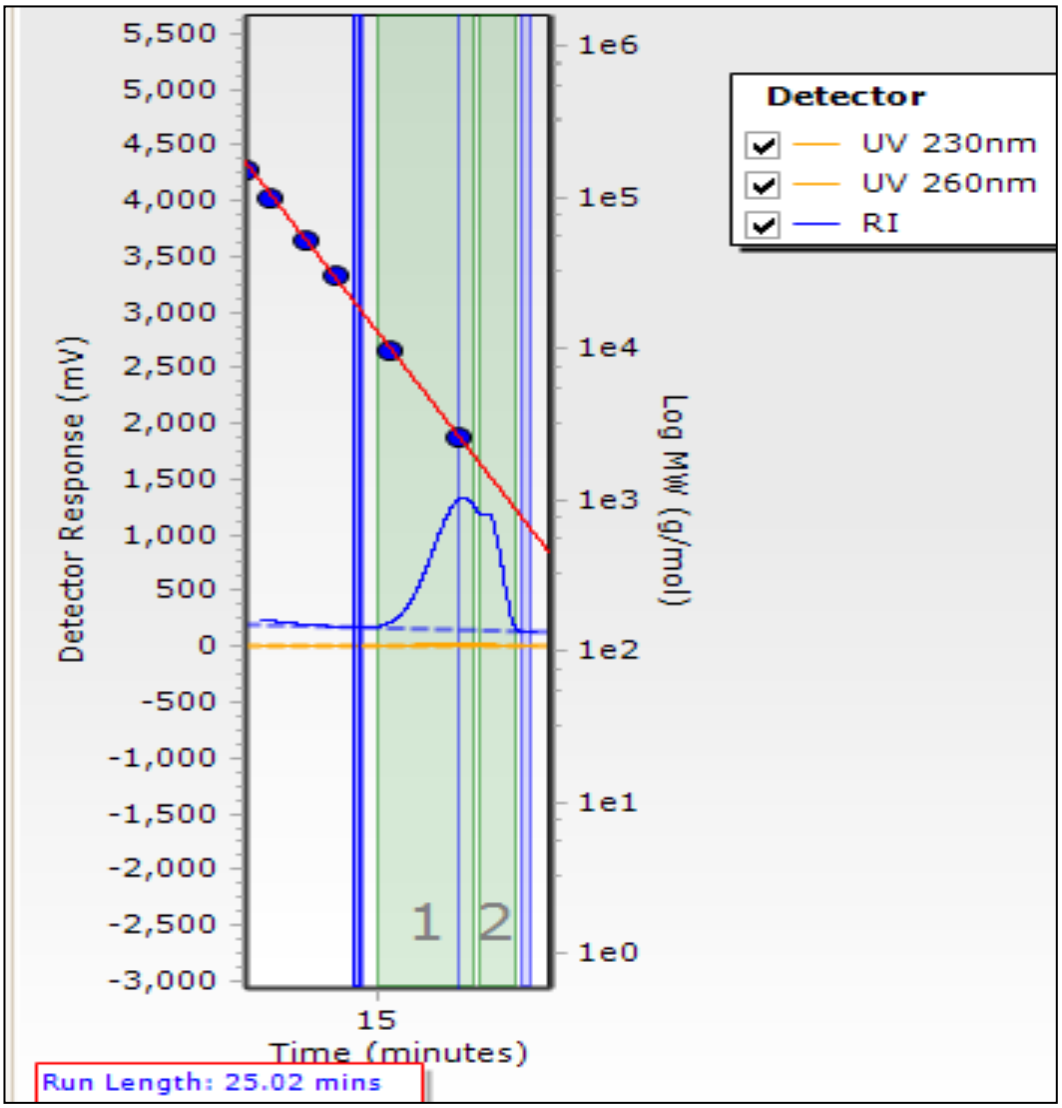

Figure 5.40. GPC chromatogram of the synthesised MPTMS tetramer

The GPC result in **Figure 5.40** suggests a slightly bimodal peak. This suggest the tetramer but also some possibilities of other higher oligomers. See **Appendix 21** for full GPC details of this GPC analysis. The molecular weight gave two regions; 1433g/mol and 5080g/mol. The molecular weight of the tetramer ~800, hence the GPC confirms the presence of the tetramer and other higher oligomers just as the silicon NMR, HPLC-MS and Maldi-Tof-MS suggested.

5.3.3 T_8 silsesquioxane cage

T_8 caged species was synthesised and isolated to use as a model compound to verify whether there are any cages in the silsesquioxane resin. The synthesis follows the method of Bassindale *et al.*[27a,27b] and El Aziz *et al* [92,28]. The synthesis and characterisation are as below.

5.4.3.1 T_8 cage synthesis

The synthesis follows the reaction shown in the equation below (**Scheme 5.5**) and the synthetic process is described in **Chapter 2.1.9**. The product is then characterized as shown in **Figure 5.41** to **Figure 5.43**.

a) Using MPTMS, TBAF and toluene to synthesise T_8 cages

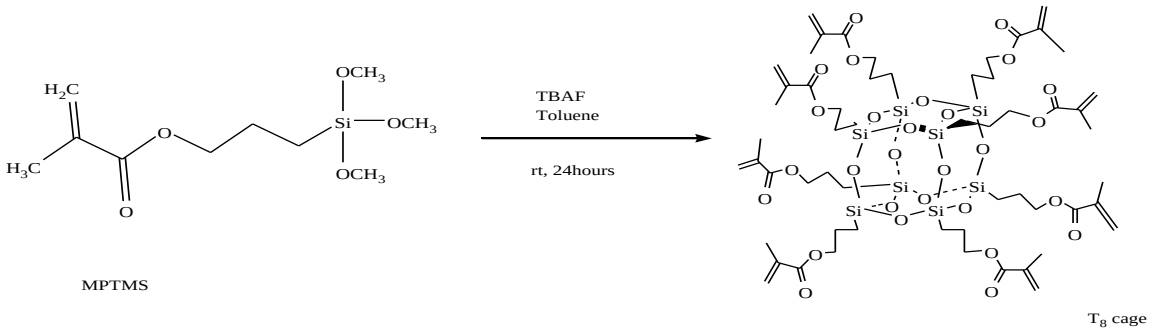

Scheme 5.5. Synthesis of T_8 cage[92]

5.4.3.2 X-Ray crystallography of the T_8 cage

Several recrystallization procedures were carried out using different solvents but there was no success even after using solvent ratios as in Taylor *et al*[280] and El Aziz *et al*[28]. Separation using column chromatography after several trials proved to be successful at least in one occasion. The crystals finally obtained following column chromatography, were analyzed by X-ray crystallography producing the crystal structure in **Figure 5.41**

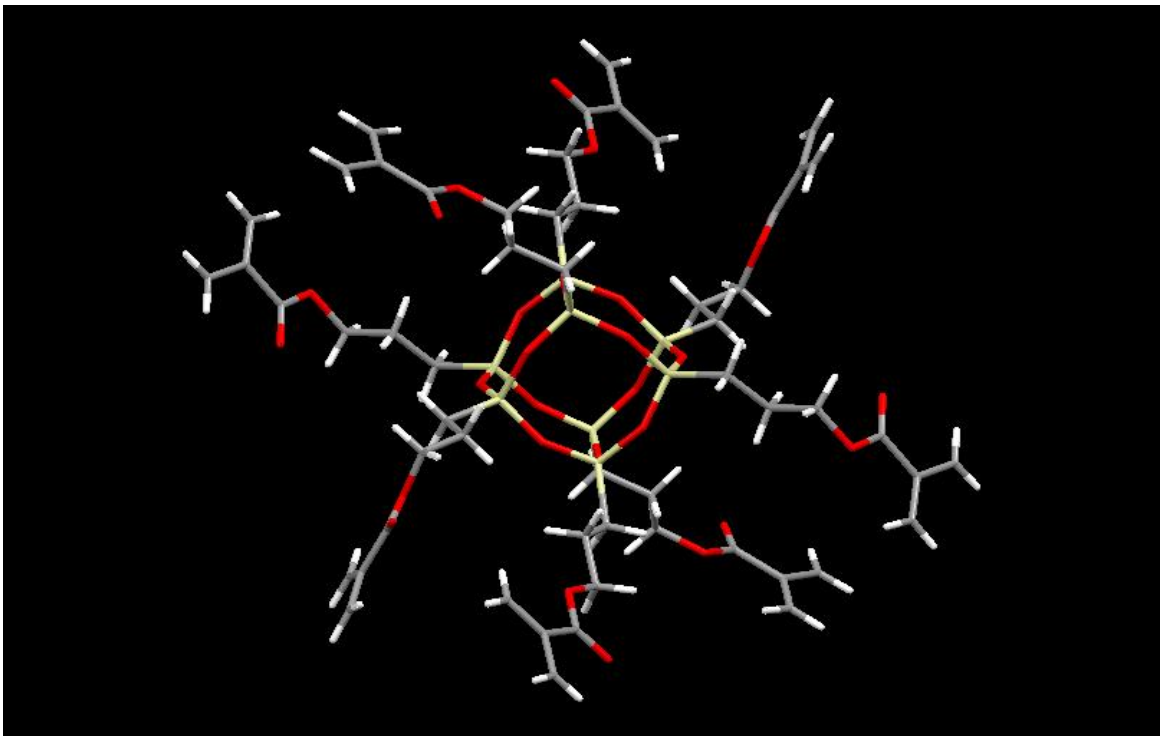

Figure 5.41. Crystal structure of T_8 cage from POSS showing the structure of a unit cell.

The crystal structure confirms the T8 cage and there was no solvent in the structure.

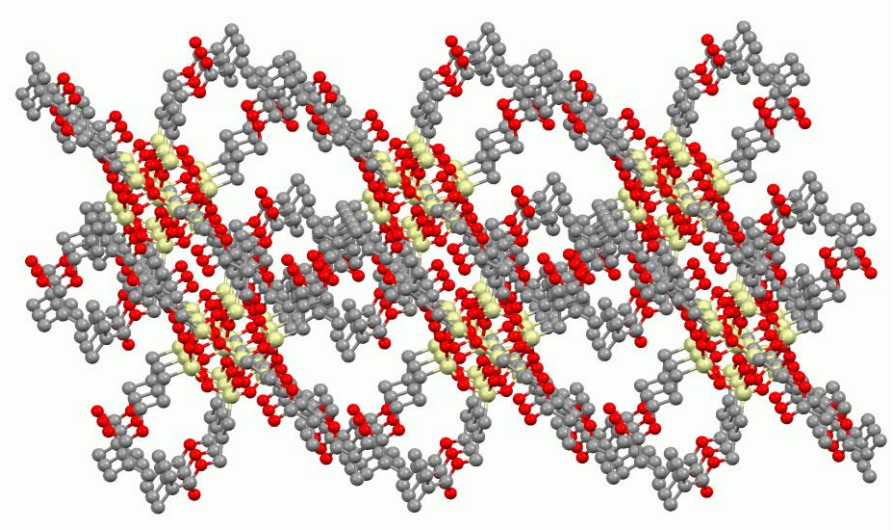

Figure 5.42. Packing diagram of the T_8 cage with only one symmetry independent molecule.

The packing range of the T_8 is very interesting showing the methacrylate arms extending outward. Selected bond lengths and angles are as recorded in **Table 5.6.**

Table 5.6. Selected bond angles and bond lengths of the T_8 cage.

	T_8 average bond lengths and angles [^{0}]
average bond lengths [Å]	
Si-O	1.818
Si-C	1.841
average bond angles [^{0}]	
Si-O-Si	148.78
C-Si-O	110.24
O-Si-O	108.70

Although the r factors cannot be trace back to the data from where the analysis were carried out, the r factors could be similar to that of Hursthouse *et al*[281] whose recorded r factors were: r factor (Obs) 0.0495, r factor (All) 0.0996, Weighted r factor (Obs) 0.1000, Weighted r factor (All) 0.1162 [281] prepared using a similar approach.

The ^{29}Si-NMR shows a single peak at -66.83ppm indicating the purity of the T_8 cage (**Figure 5.43b**). The proton NMR also (**Figure 5.43a**) confirms it is a T_8 cage.

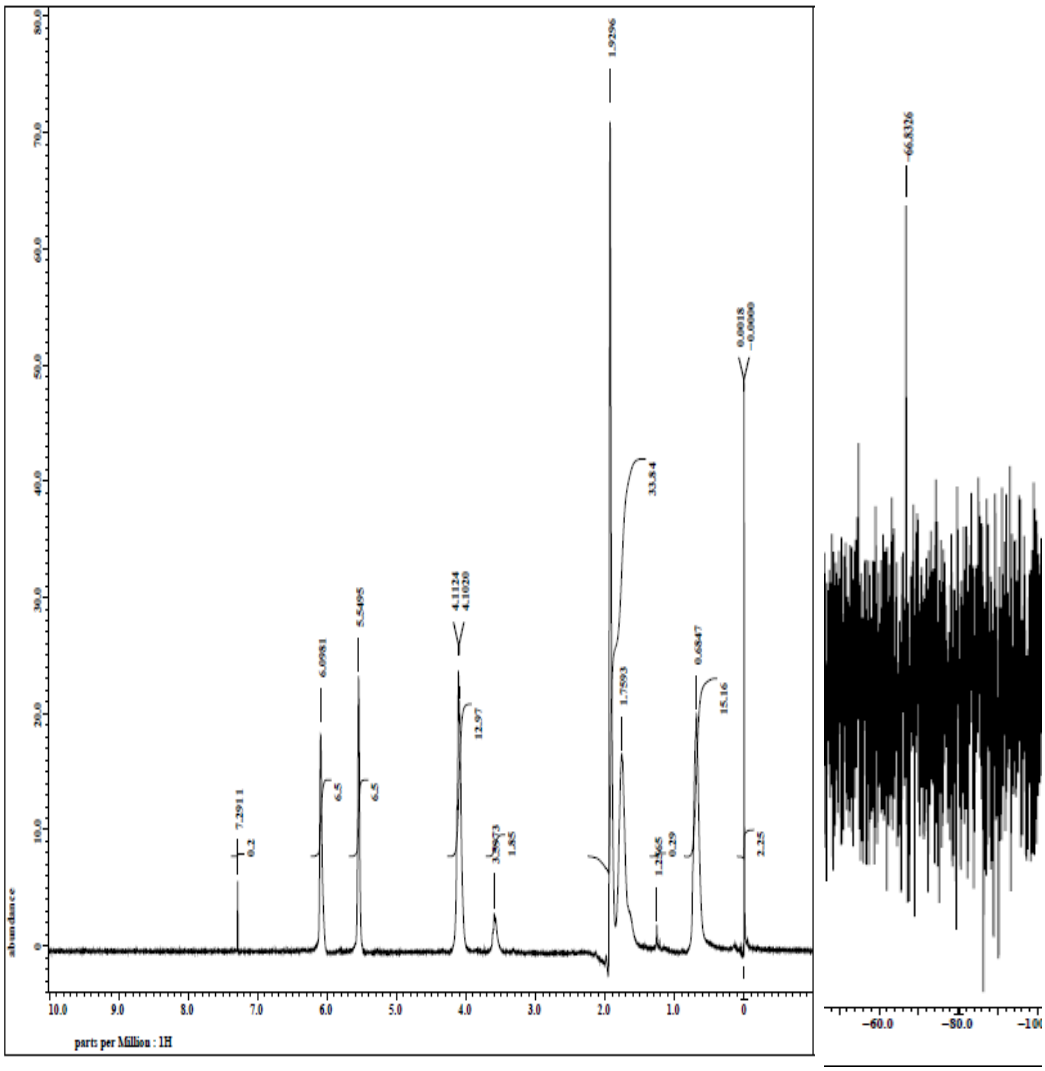

(a) **(b)**

Figure 5.43. ^{1}H-NMR (a) and ^{29}Si-NMR (b) of the T_8 cage

5.4.4 Using LCMS results of the various model compounds to characterize the silsesquioxane resin

After isolating and characterizing each of the species mentioned above, the LCMS was again used to analyze the two resin systems (A and AZ-systems) to further confirm the presence of the different species in their product mixture. The same conditions were applied here as for the individual model compound analysis. Due to the closeness of the peaks making them difficult to separate (**Figure 5.32**), a single ion monitoring mode was used to target the individual peaks from the retention times in the mixture. The results of the analysis are shown below in **Figure 5.44 – 5.53** using HPLC-MS. Note that the structures shown are just one of the options, there could be different isomeric structures for the same species in all cases. Also note that the retention times could be different from those of the individual species isolated in seen in **Figure 5.11**. This is because, each species being in a mixture, will exhibit a slightly different retention time from the profile of a pure compound. The individual species study was useful to determine the range of molecular mass from which to analyse individual species in the vitolane mixture.

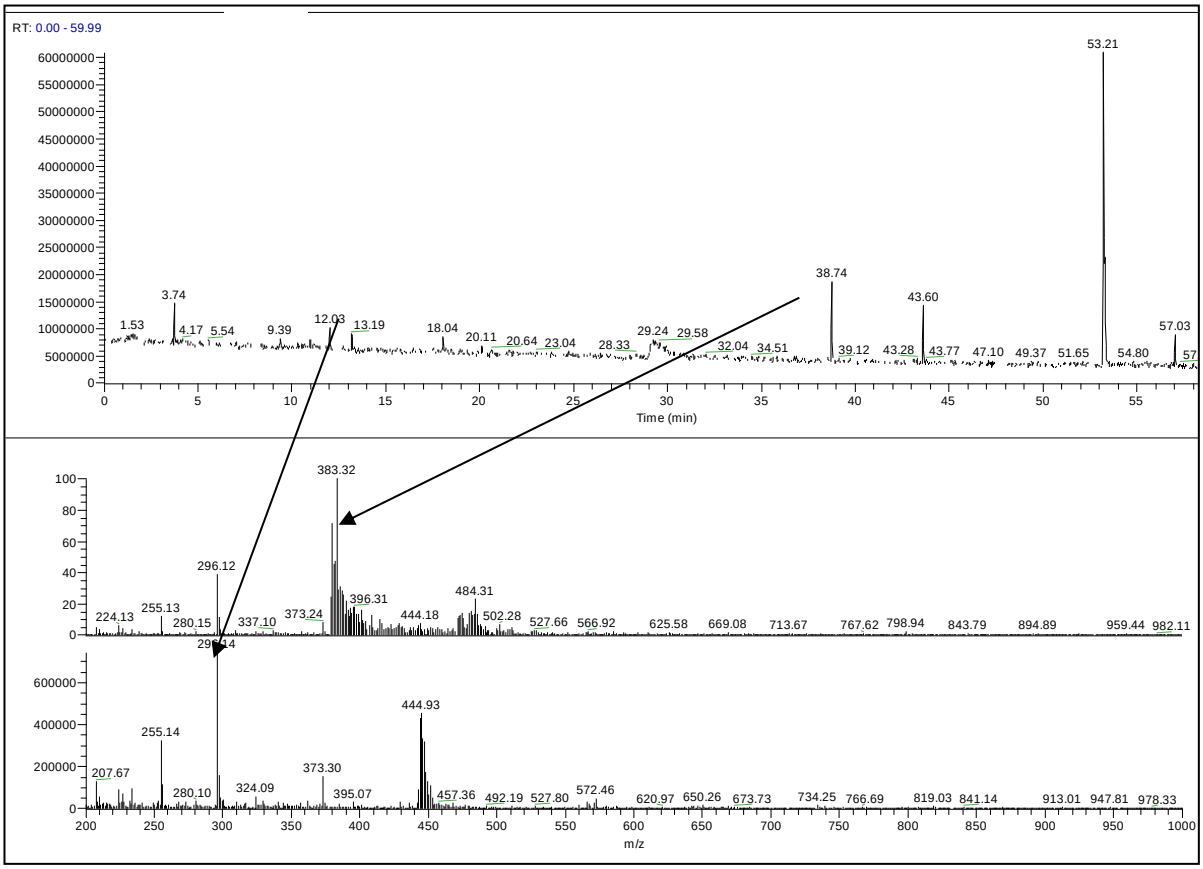

Figure 5.44. HPLC-MS showing the full chromatogram of silsesquioxanes and randomly selected two mass spectra from the chromatogram.

Identifying the dimer in the silsesquioxane resins (A & AZ-systems)

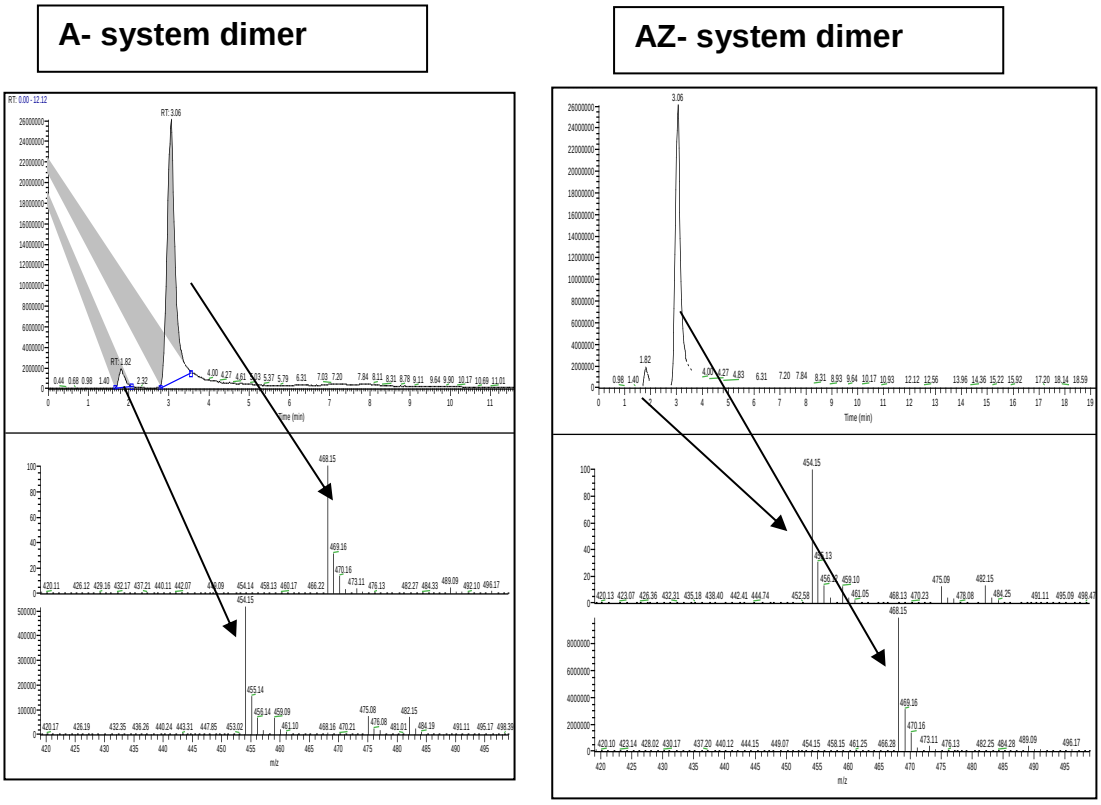

Figure 5.45. LCMS showing the dimers of silsesquioxanes

Comparing the above silsesquioxane dimers to that of the pure synthesized dimer in **Figure 5.35** gave similar dimer peaks though there is a difference in the retention time. This is not a major difference because the interaction of a pure dimer with the LC column is different from the interaction of the dimer in a mixture with the LC column, hence the difference in the retention times.

Identifying the trimers in the silsesquioxane resins (A and AZ-systems)

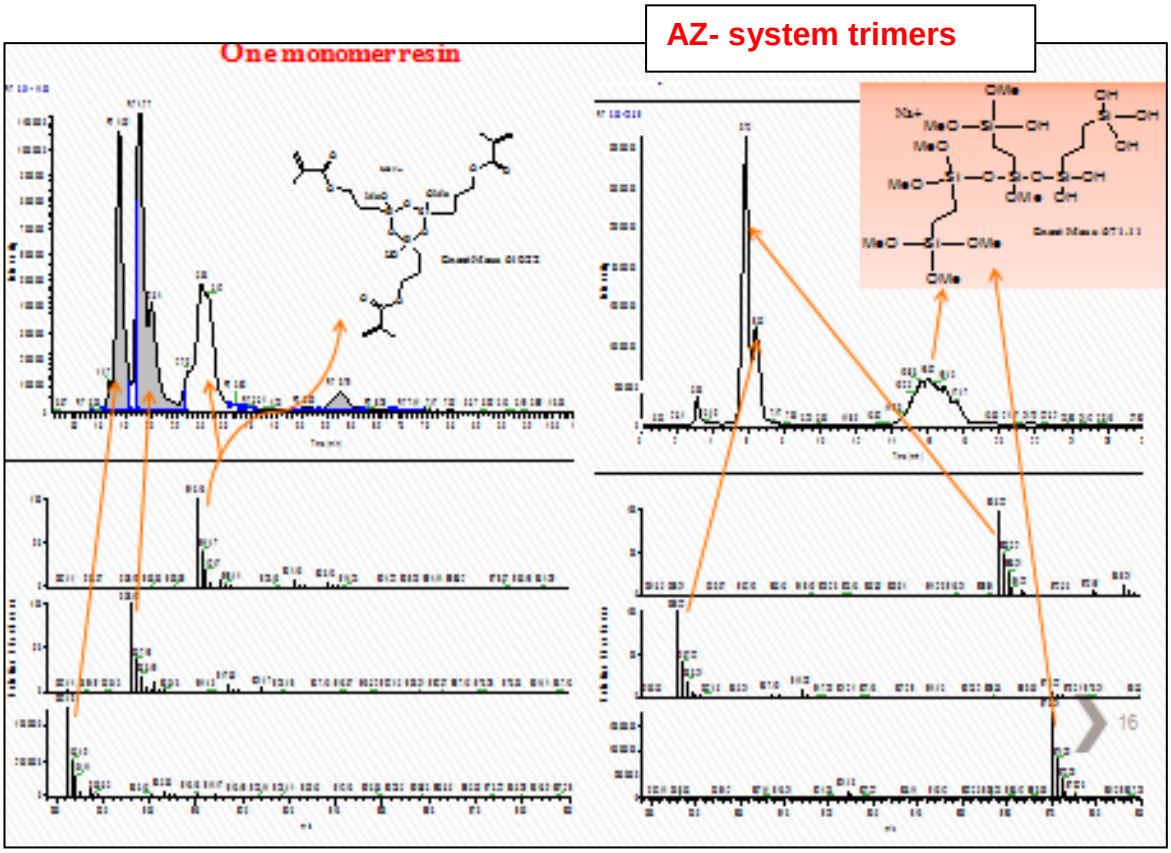

Figure 5.46. LCMS showing the trimers of silsesquioxanes

Figure 5.46 show that the trimers obtained from both systems were of variable structures (linears and cyclics).

Identifying the tetramers in the silsesquioxane resins (A and AZ-systems)

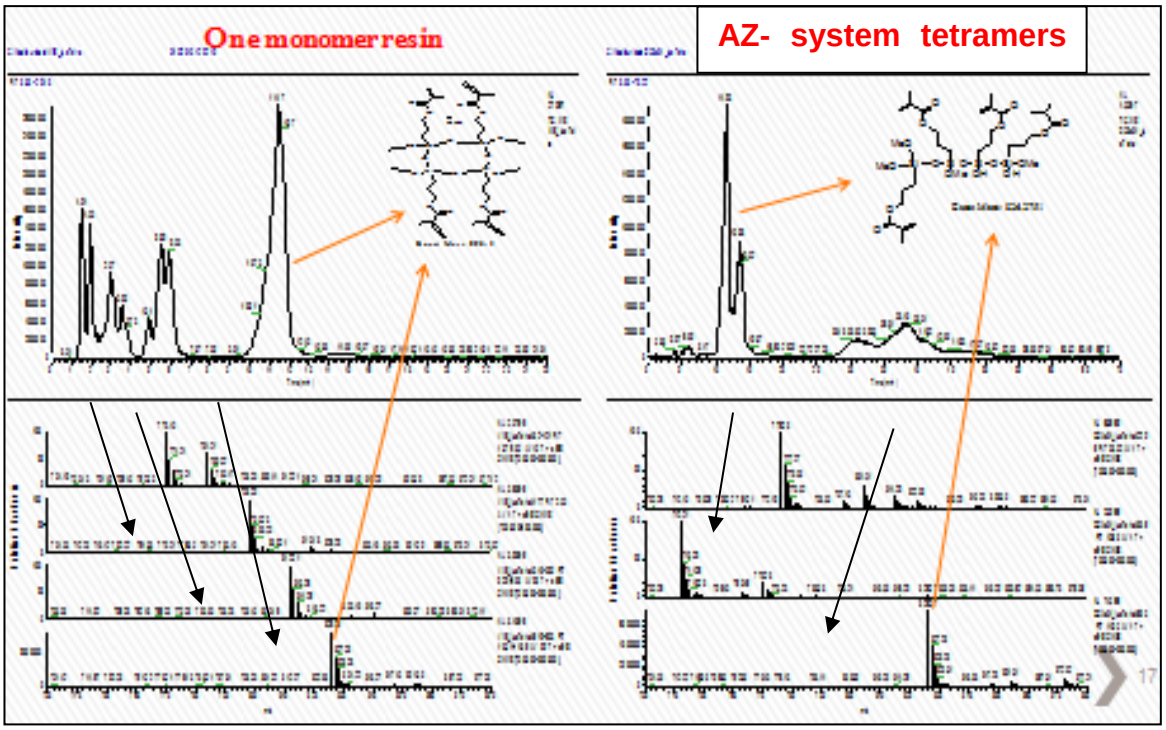

Figure 5.47. LCMS showing tetramers of silsesquioxanes

Figure 5.47 show that the tetramers obtained from both systems were of variable structures (linears and cyclics).

Identifying the pentamers in the silsesquioxane resins

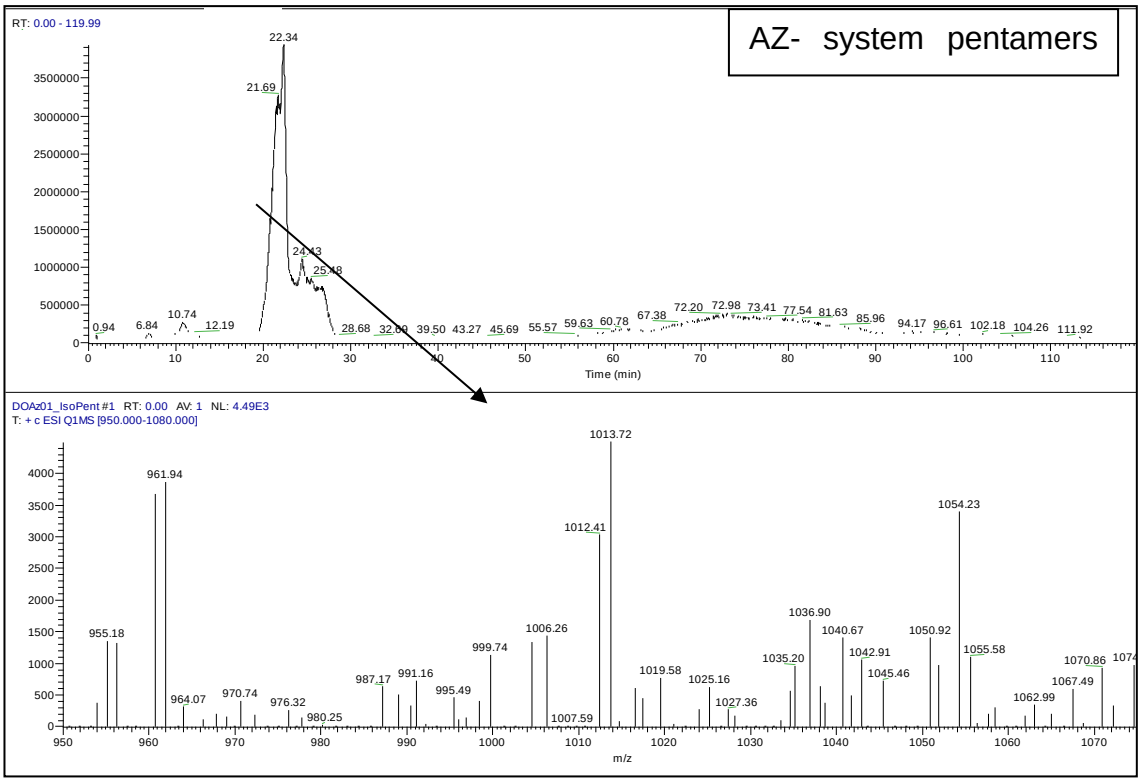

Figure 5.48. LCMS showing the pentamers of Silsesquioxanes

Figure 5.48 show a large pentameric peak on the chromatogram confirming the presence of pentamers in the AZ-vitolane resin.

Identifying the hexamers in the silsesquioxane resins

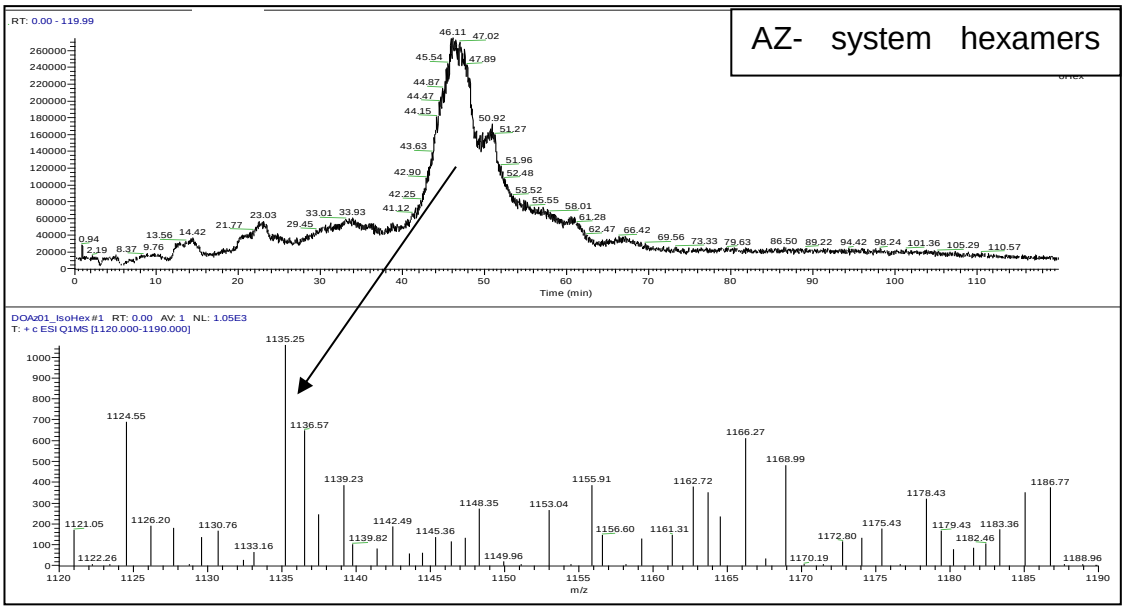

Figure 5.49. LCMS showing the hexamers of silsesquioxanes

Figure 5.49 show a large hexameric peak on the chromatogram and the mass spectrum represented below the chromatogram.

Identifying the heptamers in the silsesquioxane resins

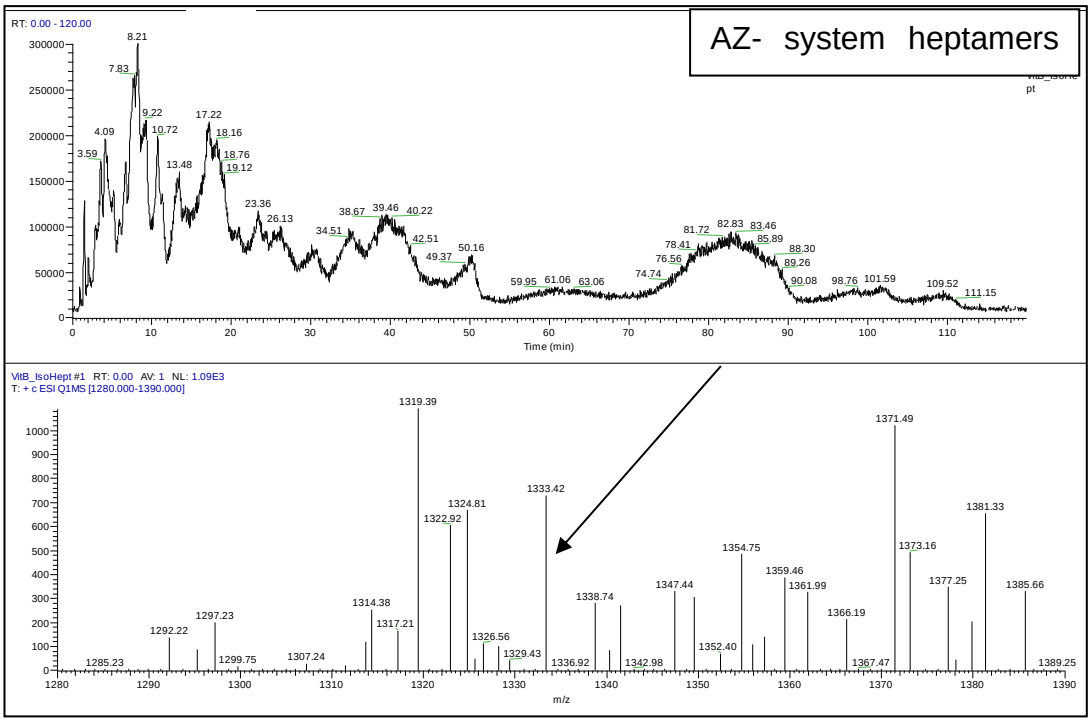

Figure 5.50. LCMS showing the heptamers of silsesquioxanes

The heptamers in **Figure 5.50** also show very many peaks which is indicative of many structures (linears, ladders, cyclics) within the resin.

Identifying the octamers in the silsesquioxane resins

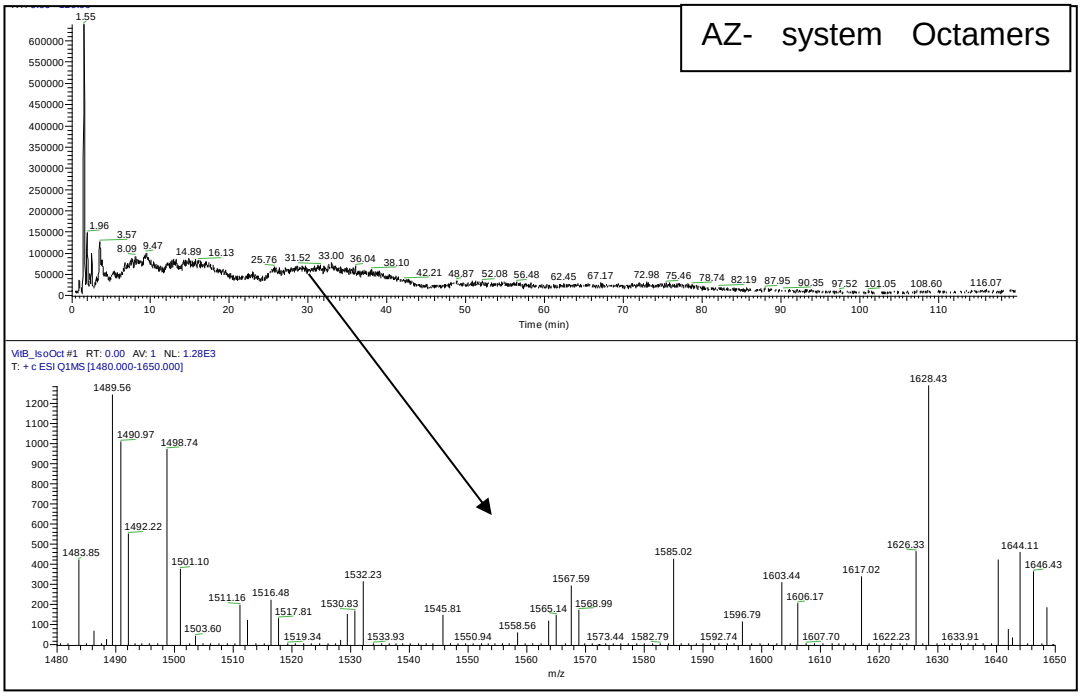

Figure 5.51. LCMS showing the Octamers of silsesquioxanes

Figure 5.51 show few broad peaks close to the baseline which confirm the earlier prediction of a very small amount of octamers present.

Identifying the nonamers in the silsesquioxane resins

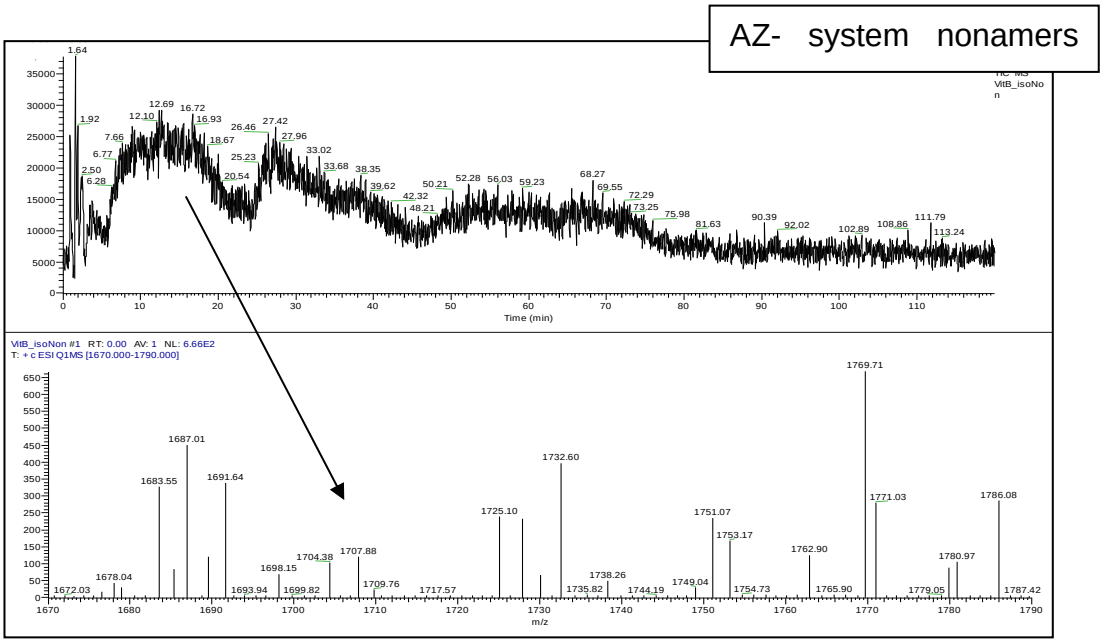

Figure 5.52. LCMS showing the nonamers of silsesquioxanes

Figure 5.52 confirms the presence of nonamers in very small amounts.

Identifying the decamers in the silsesquioxane resins

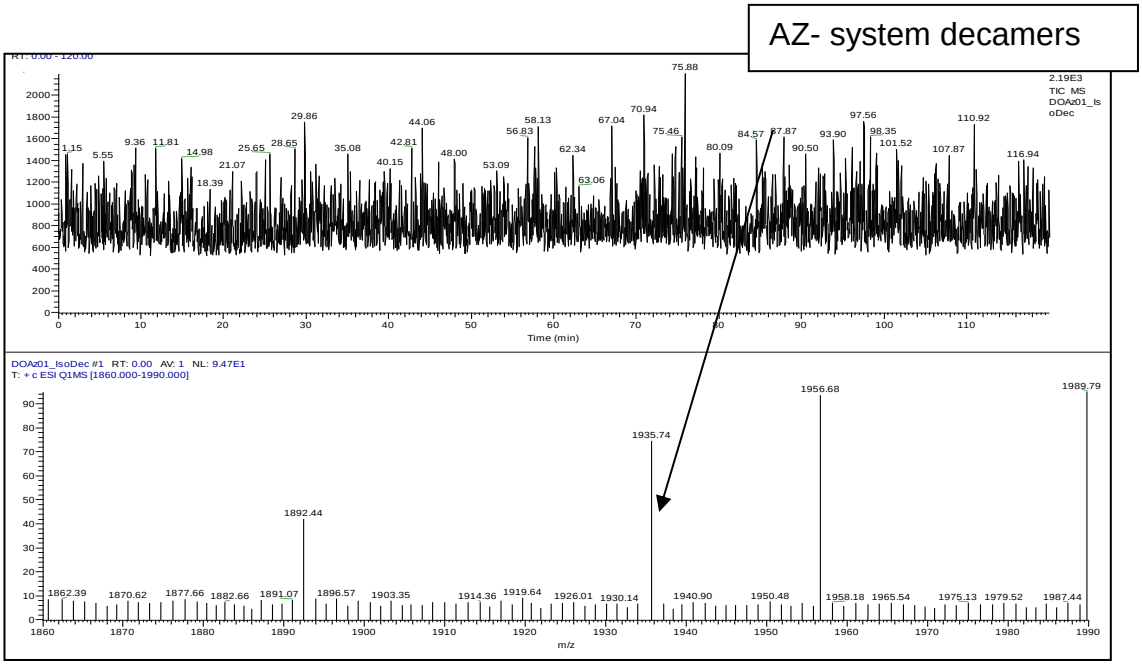

Figure 5.53. LCMS showing the decamers of silsesquioxanes

Figure 5.53 show very few peaks which also confirm the earlier prediction of a very small amount of decamers.

5.4.4.2 Discussion of the HPLC-MS results of the mixture compared to the isolated compounds.

From the HPLC-MS results above, the silsesquioxane resin exhibit each of the species from dimer to higher oligomers. Similar masses in the mixture match the individual peaks of the isolated compounds although not in a very large abundance. See **Appendix 14** for structural representation of the species.

5.5 Summary and Conclusion

The present study has focused on the synthesis; optimization and characterization of a silsesquioxane resin formed using two different methods, a single component (A-system) and the two component system (AZ-system). The resin was synthesized by hydrolytic polycondensation as described in this thesis. The key findings can be summarised as below.

Firstly, the silsesquioxane resin from both systems has been synthesized successfully several times making it very repeatable and reproducible. We have also identified that the silsesquioxane resin obtained consists of a mixture of various structures; linears, ladder, cyclic and very little cages as proven by GC-MS, ESI-MS, MALDI-ToF-MS, and HPLC-MS See **Appendix 14** for structures.

Secondly, the dimer (disiloxane), tetramer and T_8 cage have been successfully isolated from the vitolane reaction confirming some of the structures of the silsesquioxane resin as shown by the LCMS results. This has been proven by the kinetic study that has been carried out, thereby achieving one of the purposes of this research.

Finally, DSC and TGA results confirm that the thermal stability of the silsesquioxane resin are very similar (A-system resin and the AZ-system). Also, the resin obtained following the A-system contains incompletely condensed silsesquioxane structures similar to the AZ-system resin as confirmed by the ^{29}Si NMR, GPC, LCMS and MALDI-ToF MS results. These results also suggest that the silsesquioxane resin in general ranges from dimers to higher oligomers. Identifying the species and structures is another important finding from this research.

To conclude, this chapter confirms that silsesquioxane resin can be fully identified using the following instrumentations; ^{29}Si NMR, Maldi-ToF MS, LCMS and GPC. Other techniques like TGA and DSC can be use to study the thermal properties of the resin.

Chapter 6 – Stöber sphere silica nanoparticles

The aim here is to use the understanding of hydrolysis and condensation of TEOS in Chapter three, to device Stöber silica nanoparticles of various sizes for the purpose of developing a pre polymerised liquid precursor with a high silica content (up to 60%). The understanding of the condition for a complete hydrolyses, partial condensation and functionalisation bring a level of control of the reaction to obtain a precursor with a high level of silica with a manageable viscosity. This precursor (advanced hybrid nanomaterial) is a very useful industrial (TWI) and European material which aim at developing a high silica content precursor for the fabrication of a robust aerogel and superhydrophic nanomaterials.

Introduction

Stöber spheres are silica nanoparticles made through the Stöber process[2]. They are currently being added to coating materials where they improves properties such as

extreme strength, toughness and hardness[282, 283, 284]. In particular they are used to create superhydrophobic (very high water repellence) coatings property that mimics the lotus leaf effect, **Figure 6.1** [285, 286, 287, 288, 289. 99, 290]. The cause of the superhydrophobicity in the lotus leaf is as a result of the roughness at the nanoscale on the surface of the lotus leaf that causes water and other fluids to roll off. The lotus leaf effect arises from this "roughness'' by the creation of nano pillars (shown in **Figure 6.1**) of about 100nm on the surfaces of materials. This layer of pillars trap air between the surface of the leaf and the water droplets hence prevents the water from wetting the surface and the water rolls off[291, 292, 293]. The Stöber spheres are therefore added to coating materials to create this surface "roughness". Developing a coating material that will exhibit such properties is of great interest to TWI therefore, synthesizing Stöber spheres has been explored in this thesis. Size variation, functionalization and characterisation of the Stöber spheres have all been studied in the past [294, 295, 296, 297,298].

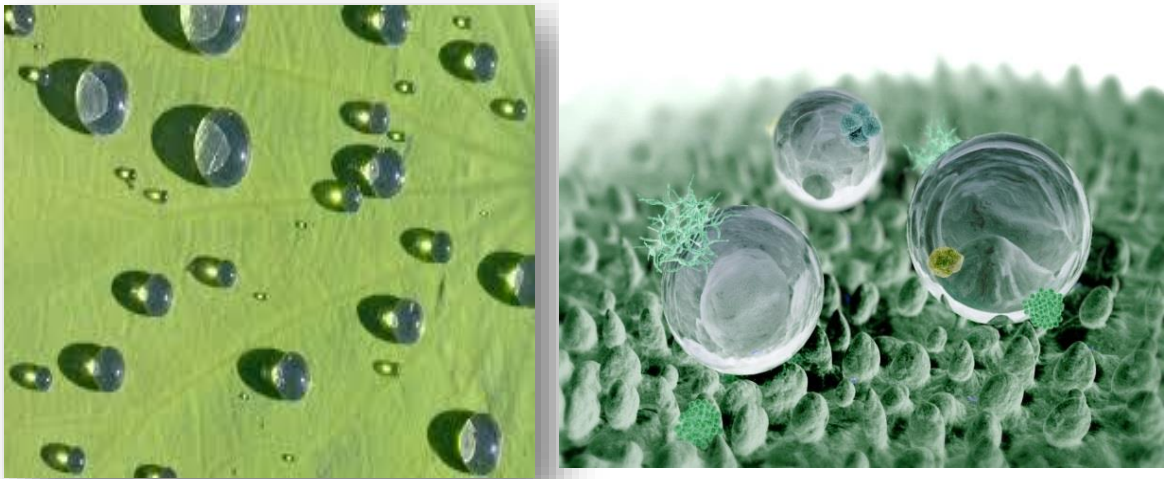

Figure 6.1. Nature's superhydrophobicity of the lotus leaf (TWI copyright)[23]. Notice the protrusions from the leaf covered in a rough material that creates its superhydrophobic surface.

Understanding the preparation of different sized nanoparticles and their application in different industries is very important[75,299]. In the preparation of nanoparticles for this thesis,TEOS was used as the main structural building block. A very careful study of the hydrolysis and condensation of TEOS has been discussed in chapter 3.

Stöber silica nanoparticle size is dependent on the rate of hydrolysis leading to condensation and hence nucleation (the development of small oligomeric particles), and the rate of condensation leading to growth (the development of larger particles[300, 301 302]. Therefore, by controlling these two factors, particle size can be controlled [82, 303,157, 228]. There will be a large amount of unhydrolysed or partially hydrolysed species formed depending on the reaction conditions used, especially the amounts of water. It is clear that the hydrolysis of TEOS does not produce only fully hydrolysed intermediates ($Si(OH)_4$) even if the right equivalent molar amounts of water to TEOS are being used. This has been demonstrated by Sanchez, Stöber and Hsu[122,2,230]. Lu *et al.*[114a] also demonstrated that as hydrolysis occurs, TEOS concentration decreases and other intermediate hydrolysed TEOS species develop leading to the various stages of Stöber sphere formation[24, 243, 242, 240,245].

Green *et al.*[125] have reported that on varying the amounts of the reagents, including the catalyst, the structure, properties and most importantly the size of the nanoparticle formed vary quite substantially. These results are consistent with earlier results reported for the Stöber sol-gel process[2] and are also consistent with the findings in this research. We have observed that between 1-2 molar ratios of water to TEOS the solution becomes opaque and goes white, but becomes less opaque as the water or TEOS becomes deficient in the reaction mixture [304].

Some scientists including: Rao *et al*.[140], Bogush 1991 [157], Buckley *et al.*[305], Flory-Huggins [158] and Tanaka and co-workers[159] have made spherical particles using the Stöber process but under different conditions. Bogush 1991, was able to achieve sizes of between 1-10nm using the Stöber process. The size of the particles is important especially in the coating industry. Coatings made from large particles could easily cause flaking whereas small sized particles of 1-10nm provide a durable, good reflectant and transparent coating, hence the reason for size control that is at the heart of this research [306, 307, 308, 309].

Also, if the particle is too big, it will not exhibit superhydrophobicity. If the particles are too big the coating will not be transparent. The particle size needs to be less than 30nm to not interfere with the colour of the coating.

Synthesis of Stöber silica nanoparticles

The Stöber method of synthesising Stöber silica nanoparticles has been discussed in **Chapter 2.1.9**. A slightly different sol-gel process, applying different conditions called the microwave method (**Chapter 2.1.10**) has also been used as a comparison, to see if it was a quicker or a more suitable method. The conditions used to obtain different sizes and morphology of the particles has also been addressed. The general equation of the sol-gel synthetic route is as shown below in **Scheme 6.1**.

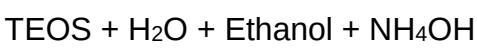

Scheme 6.1. Synthetic route for making Stöber silica nanoparticles

Functionalization of silica nanoparticles

Functionalization of silica nanoparticles involves the addition of a functionalising agent e.g. attaching a silane to the surface of the particles to improve the functionality of the particle[310, 311, 312, 313, 314]. In coating, functionalization helps to improve the chemical and physical properties such as its hydrophobic or hydrophilic properties, also its miscibility with solvents and coatings polymers. Some functionalising silsesquioxane agents that could be used to functionalise Stöber spheres as seen in **Table 1.3**. The greater the functionalization or coverage of the functionalising agents on the surface of silica nanoparticles, the better the material developed[285,315] . **Figure 6.16** below is a picture of a super hydrophobic coating that TWI Ltd has developed based on some of our research to achieve a contact angle of 150^0.

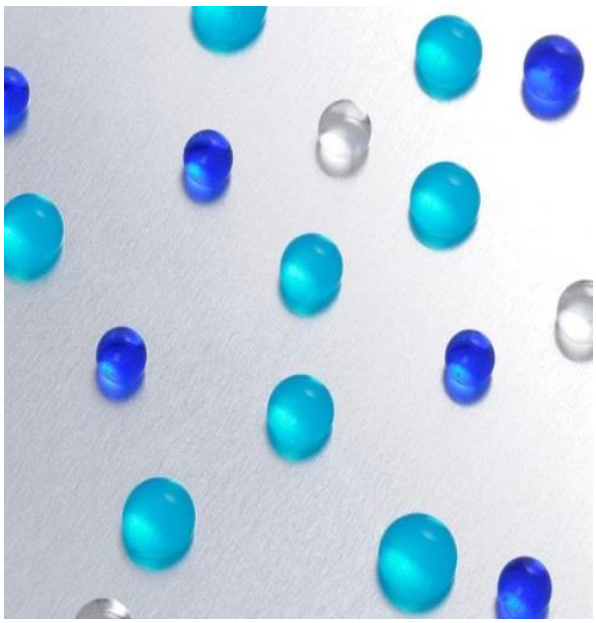

Figure 6.16. Pictures of a glass coated silica surface that repels different types of liquid. Contact angle of 150^0. This advanced coating was achieved following our collaborative research work with our industrial counterpart, TWI Ltd[23].

6.1.1 Functionalization process

The procedure used in this thesis to functionalise particles follows the method of Chi-Hwan *et al.* [212] and Jafarzadeh *et al.* [213] and are described in **Chapter 2.1.5** and **2.1.11**. A range of other functionalising agents were used as shown in **Table 2.6** and characterised by TEM and DLS below in section 6.5. **Figure 6.17** below shows the chemical representation for the functionalization using one of the functionalising agents (APTES).

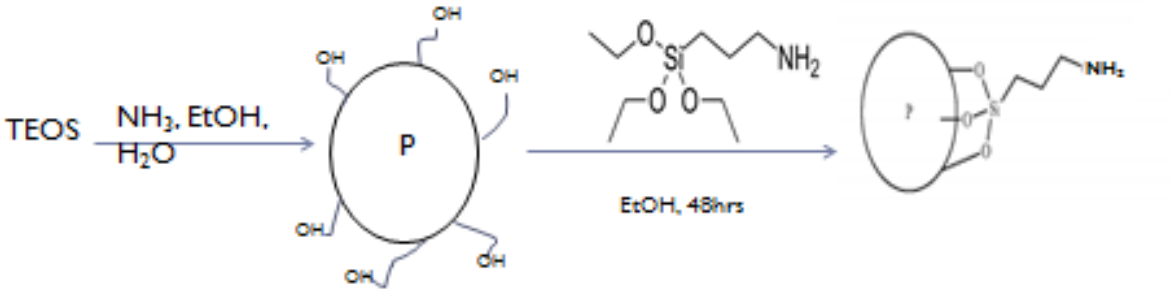

Figure 6.17. Synthesis of silica nanoparticles and functionalization using 3-aminopropyltriethoxysilane (APTES).

A schematic representation is shown below (**Figure 6.18**) showing the surface coverage of the amino silane bonding on the silica surface.

Schematic representation showing surface coverage

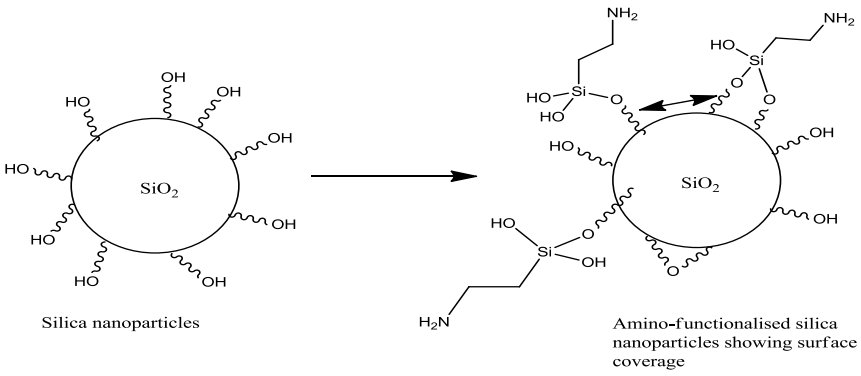

Figure 6.18. Diagram showing the surface coverage of amino silane on a particle surface.

6.1.2 Surface coverage calculation studies via back titration

Back titration is an in-house method that has been devised to measure percentage coverage[316, 317, 318]. This has been validated by comparing its results with other published methods and has been proven to work accurately.

Titration and calculation of percentage surface coverage of Stöber spheres

The back titration experiment of amino functionalised Stöber silica nanoparticles (using 3-aminopropyltriethoxysilane) is described in Chapter 2.1.6. We can calculate the percentage surface coverage as below: [319,215]

Density of silica particles, D = 2.5g/cm^3 = 2500000g/m^3 as in literature [320, 321]

Diameter of my particles = 115nm, =1.15X10^{-7}m

Radius of my particles, r = 5.75x10^{-8}m

Surface area of a sphere, $\mathbf{S_1}$ = 4πr^2 = 4.15x10^{-14}m^2

Volume of a sphere, **V** = 4/3πr^3 = 7.96x10^{-22}m^3

Mass of a particle = Density.Vol = 2500000g/m^3 . 7.96x10^{-22}m^3 =1.99x10^{-15}g

Surface area of single particle: 4.15 × 10^{-14} m^2

Surface to mass: 4.15 × 10^{-14} m^2 / 1.99 × 10^{-15} g = 20.85 m^2/g, or *ca*. 21 m^2/g.

Therefore, the calculated surface area of our silica is = 21 m^2/g (assuming that the particles are completely spherical and are non-porous).

From our titration results, 0.09mmol/g of amine was found from the titration as mentioned in experimental, chapter 2.1.6.

This implies, for coverage, if 21m^2/g uses 0.09mmol/g of -NH_2

Therefore, 1m^2/g uses Xmmol/g

X = 0.09mmol/g/21

X =0.0043mmol/m^2

X = 0.0000043mol/m^2 or **4.3umol/m^2**

According to literature, a typical ligand (functionalizing agent) coverage on a nanoparticle is between 4.3-4.5 umol/m^2 [322] which is roughly 50% of available Si-OH (see later).This confirms the accuracy of my results. Therefore, assuming a surface coverage of my results (surface concentration of ~NH_2 silane) = 4.3 µmol/m^2. This implies, 4.3 µmol/m^2 of amine is bonded to 1 square meter of the SiO_2 surface [323, 324, 325].

However, 4.3 µmol/m^2 = 4.3 × 10^{-6} mol/m^2

1 mol of particle = 6.02 × 10^{23} ligands on the surface, so we have

4.3 × 10^{-6} mol/m^2× 6.02 × 10^{23}mol/ligand = 2.6 × 10^{18} ligands/m^2

1 m = 10^9 nm, or 1 m^2 = 10^{18} nm^2,

So we have 2.6 × 10^{18} / 10^{18} = 2.6 ligands/nm^2.

Therefore, there are **2.6** ligands per square nanometer.

Theoretical coverage (%)

Research suggest that there are **5-OH** groups per 100Å^2(Å^2 = Angstroms)for 100% coverage based on literature [323,319 326].

Therefore**, 2.6 ligands** based on my results implies **50%** coverage of the ~NH functionalised Stöber silica nanoparticles. 50% is what has been achieved and published by most other researchers in the literature[319, 327]. That is, there is one NH_2 group for every two OH groups.

Characterisation of functionalised and unfunctionalised Stöber silica nanoparticles

A range of techniques have been used for characterising the silica nanoparticles and for examining at various aspects of the particle surface. Some of the techniques include: NMR, FTIR, TEM, DLS, XPS, TGA and DSC. TEM and DLS are the two most important ones used in this thesis for the size measurements. The results of the instrumental analysis are discussed in **Section 6.8**.

6.1.3 Dynamic Light Scattering

Dynamic light scattering (DLS) experiments were performed to determine the weighted mean particle size and the breadth of the particle size distribution (polydispersity index, PDI). This was achieved using a Zetasizer Nano (Malvern UK) instrument. A full description of how these were measured can be found in **Chapter 2.2.** The DLS results of the Stöber silica nanoparticles are shown in **Figure 6.2 i-iv** for unimodal particles, bimodal and even trimodal functionalised particles (**Table**

2.5 and **2.6**). The Stöber nanoparticles were prepared using 1:1 molar amounts of TEOS:water as in **Table 2.5** and functionalised using the procedure in section 2.1.11 and different functionalising agents as on **Table 2.6.**

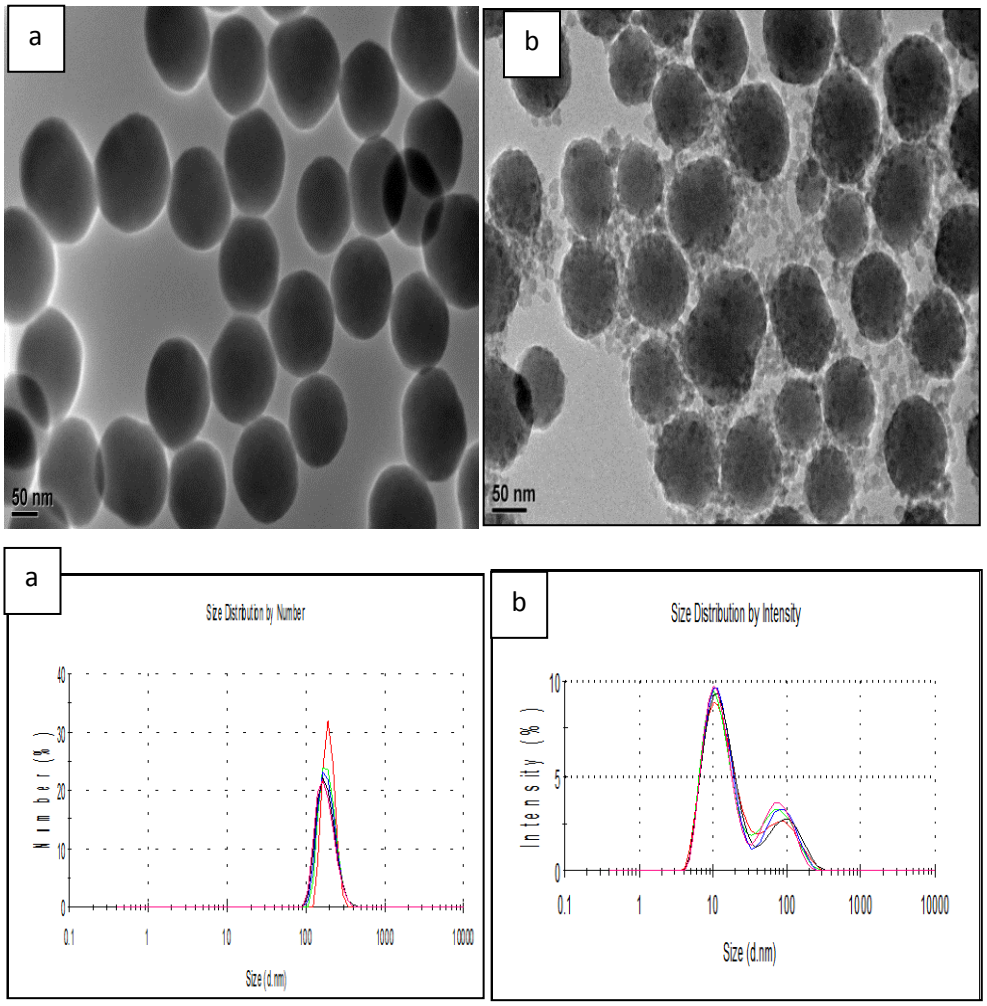

Figure 6.2i. Stöber silica nanoparticles showing the sizes and distribution of the particles formed (a) TEM (top) and DLS (monomodal) nanoparticles, (b) TEM (top) and DLS (bimodal) using 1:1 molar ratio of TEOS:water.

A B

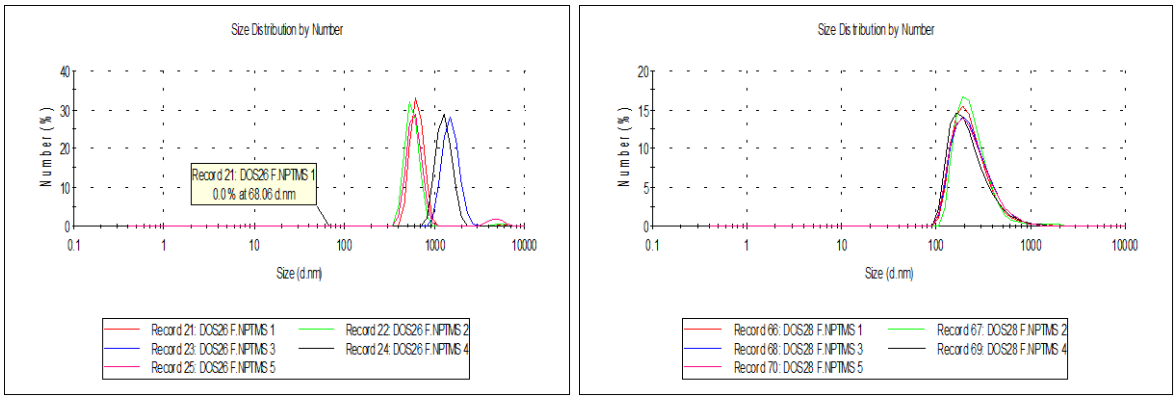

Figure 6.2.ii. DLS of NPTMS functionalised nanoparticles prepared showing different size distribution

A) NPTMS functionalised Stober nanoparticles (Average size = 990nm) at room temperature (bimodal).

B) Imidasol before NPTMS functionalised Stober nanoparticles (Average size = 255nm) at room temperature (Unimodal).

A B

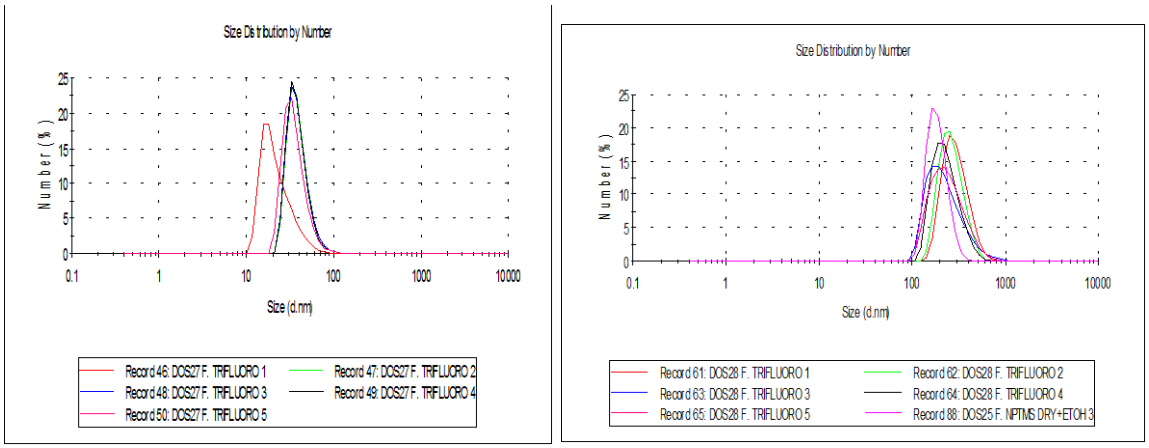

Figure 6.2.iii. DLS of 2,2,2 trifluoropropyl trimethoxysilane functionalised nanoparticles showing different particles size distribution

A) Using 3,3,3-trifluoropropyltrimethoxysilane to functionalised Stober nanoparticles (Average size = 35nm) at room temperature (partially unimodal).

B) Using imidazole before addition of 3,3,3-trifluoropropyltrimethoxysilane to functionalised Stober nanoparticles (Average size = 262nm) at room temperature (Unimodal).

A B

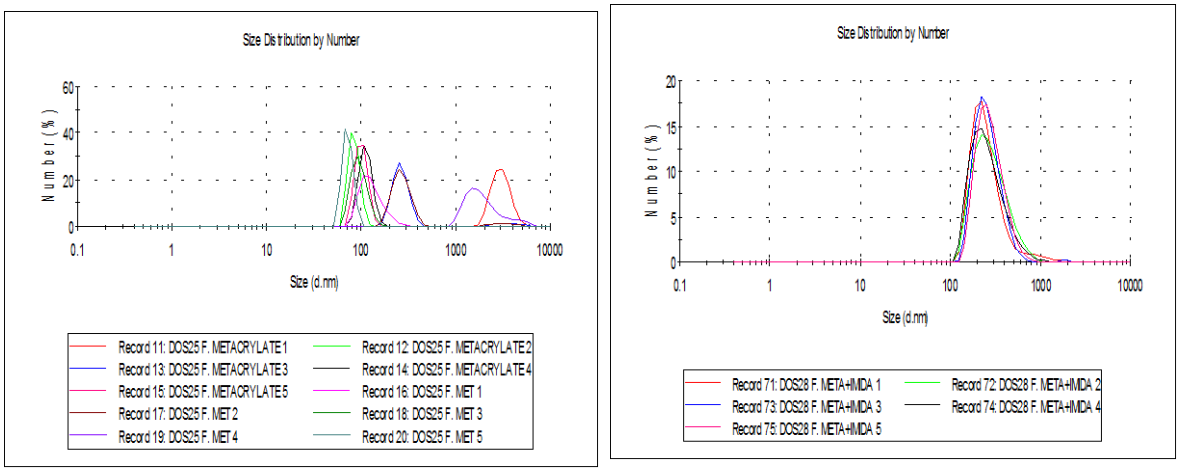

Figure 6.2.iv. DLS of MPTMS functionalised nanoparticles showing different particles size distribution

A) MPTMS functionalised Stober nanoparticles (Average size = 675nm) at room temperature (trimodal),

B) Imidasol followed by MPTMS functionalised Stober nanoparticles (Average size = 284nm) at room temperature (Unimodal).

Using different types of functionalising agents (as in **Table 2.6**), the sizes of particles formed are different as shown in **Figure 6.2i-iv**. These results also show that using imidazole catalyst prior to functionalisation, the particles that results are more unimodal (**Figure 6.2ii-iv**).

6.1.4 TEM-EDX

Particle size measurements using transmission electron microscopy energy dispersive X-ray spectroscopy (TEM-EDX) were carried out using a JEOL, JEM 2100, TEM running a LaB_6 (lanthanum hexaboride crystal) emitter. The instrument's description and reason for using it is discussed in section 2.2.11. The results were processed using imagej software and the EDX results shown in **Figure 6.3** and discussed below.

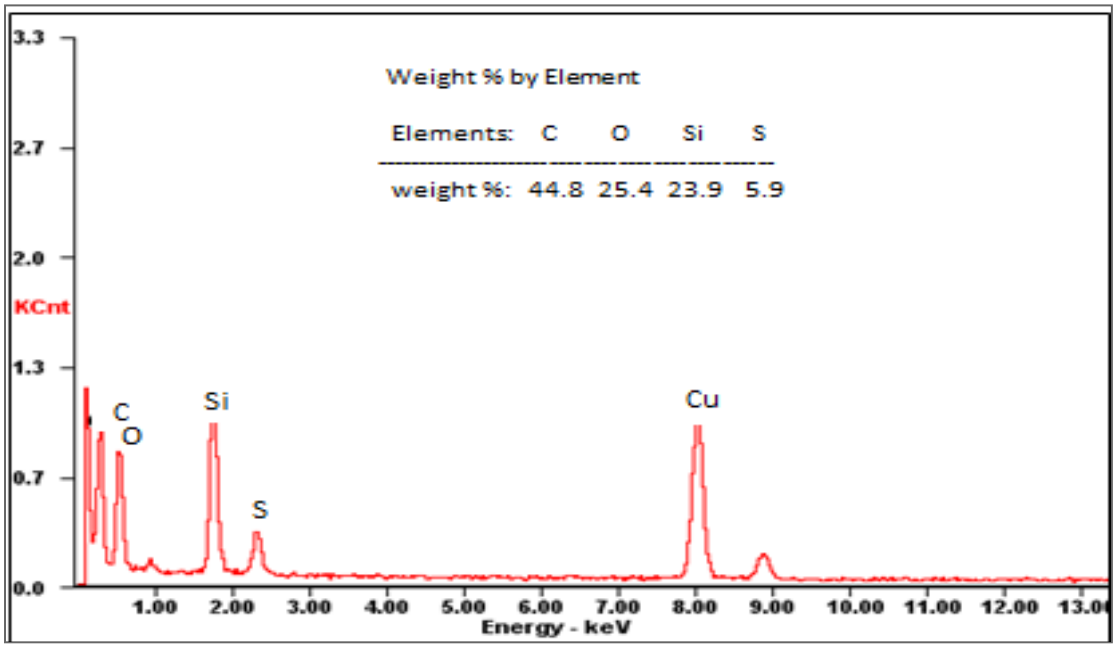

Figure 6.3. TEM-EDX of the functionalised Stöber silica nanoparticles showing the functionalization with thiol 3-mercaptopropyltrimethoxysilane on the silica nanoparticle surfaces.

The particles analysed by TEM-EDX in **Figure 6.3** were functionalised using a thiol functionalising silane. As the **Figure 6.3** shows, the presence of sulphur and carbon is an indication that the silane is attached to the surface of the Stöber nanoparticles[228, 328,329, 330]. Weight % by element is the percentage of each of the

elements present on the particle surface. That is, the silica and the surface on the surface and the thiol functional group. Normal unfunctionalised silica will only show silicon and oxygen which is the constituent of silica (SiO_2). This confirms the success of the functionalization of the Stöber silica nanoparticles formed. TEM-EDX of the thiol functional group was the main focus.

6.1.5 ^{29}Si NMR of functionalized silica nanoparticles

The ^{29}silicon NMR spectra were carried out using ^{29}Si CP MAS described in Chapter 2.2.1 and a result for the functionalised silica nanoparticles is shown in **Figure 6.4**.

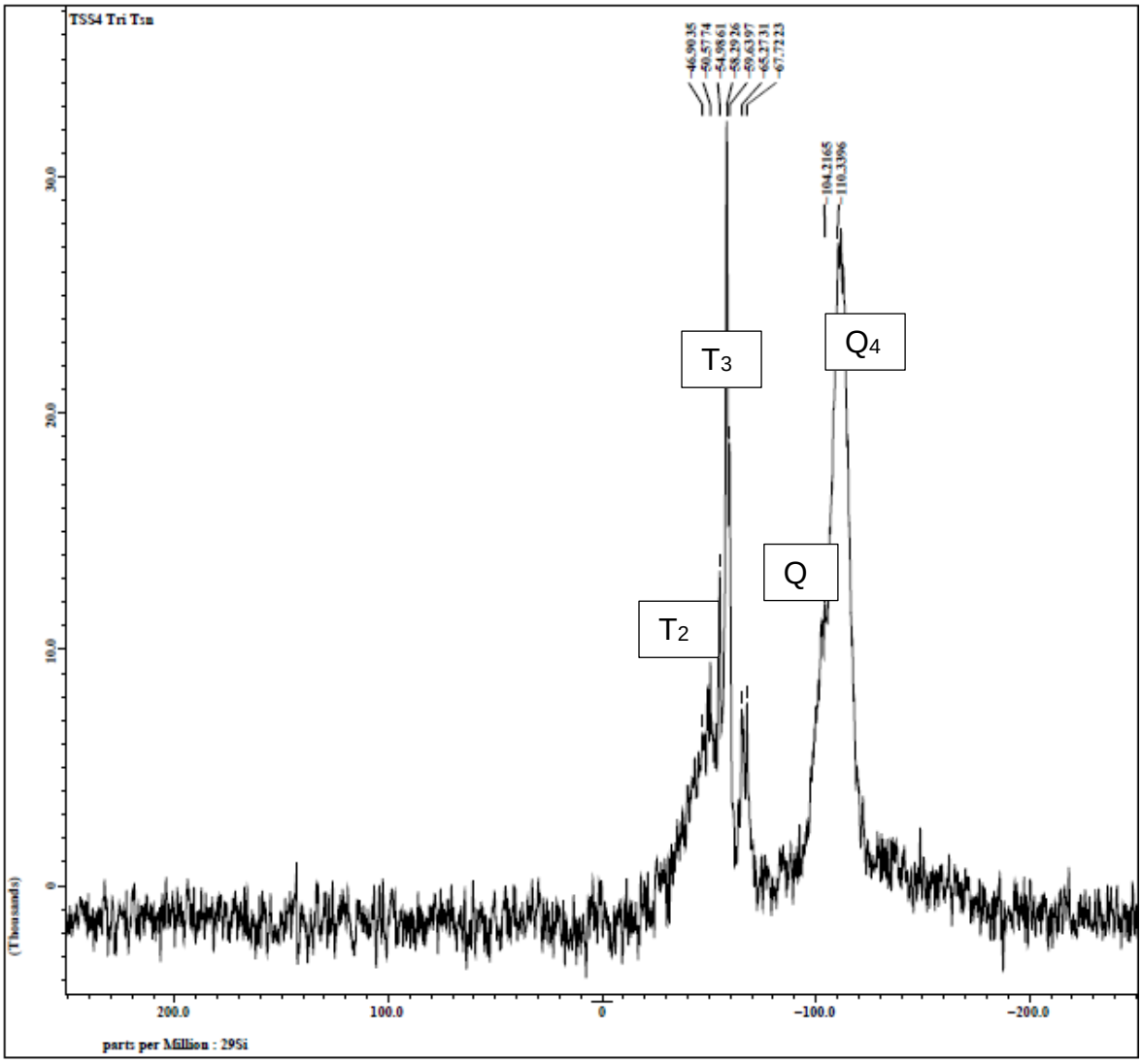

Figure 6.4. ^{29}Si CP MAS spectrum of functionalised silica nanoparticles.

The above result in **Figure 6.4** is a clear indication that the silane functionalising agent (represented in the T peaks) is attached to the surface of the Stöber nanoparticles (Q peaks). ^{29}Si NMR is a suitable technique to determine whether the particles are functionalised or not, which is another aspect of interest to this research. Literature found the same results, that is, with functionalisation on silica surface, there are the presence of T-species depending on what the functionalising agent is or are. Song *et al*[185] in Figure 1.26 show the presence of APTES on the surface of silica nanoparticles using the same ^{29}SiNMR CP MAS analysis approach.

6.1.6 XPS

X-ray photoelectron spectroscopy (XPS) measures the elemental composition of the elements that exist on a material [310]. A description of the instrument has been written in Chapter 2.2.14. The XPS results for the amino functionalised Stöber silica nanoparticles are as shown in **Figure 6.5** and discussed below.

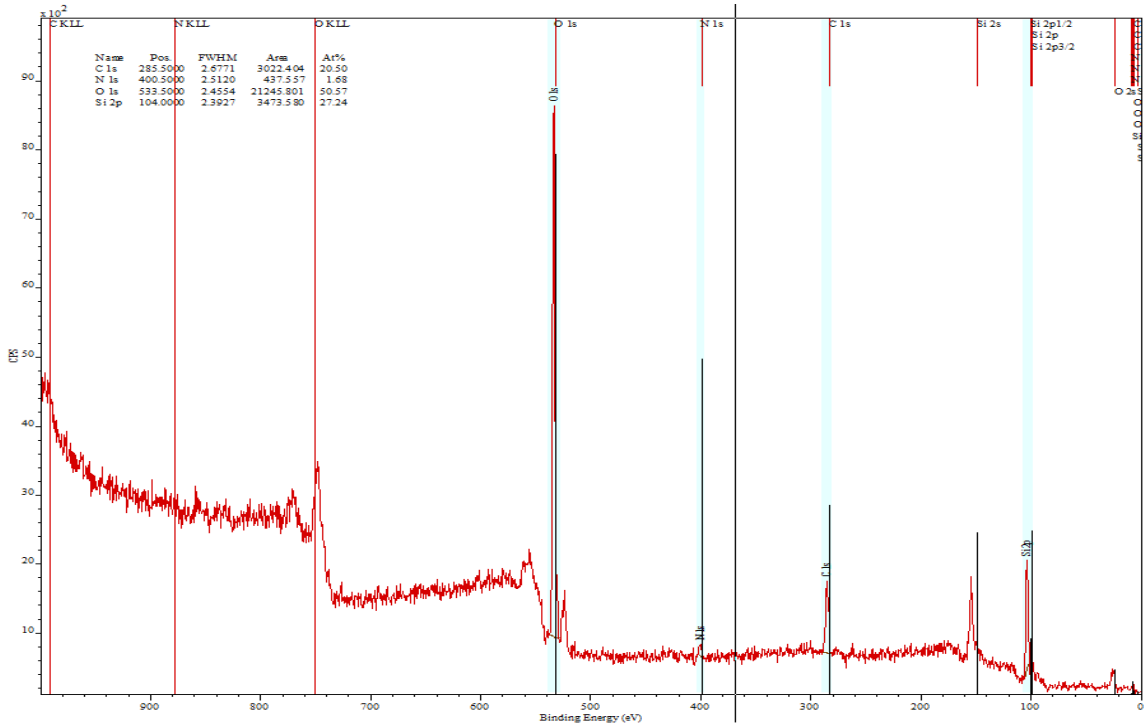

Figure 6.5. XPS of functionalised Stöber silica nanoparticles using 3-aminopropyltriethoxysilane (APTES)

In **Figure 6.5**, the carbon and nitrogen peaks are a strong indication of the presence of the amino group on the surface of the Stöber silica nanoparticles. This indicates the attachment of the amino group to the surface of the Stöber particle was successful.

Thermal stability of functionalised and unfunctionalised Stöber silica nanoparticles

The Stöber silica nanoparticles prepared using a 1:1 mol ratio TEOS:water as in **Table 2.5** were heated and cooled (unfunctionalised and functionalised nanoparticles) in the DLS instrument between 5^{o}C to 70^{o}C. The characterisation approach follows the same as a normal DLS approach describe in **section 2.2.10** with different temperature program 20 – 80^{o}C and vice versa upon cooling. The results are shown in **Figure 6.6** and discussed below.

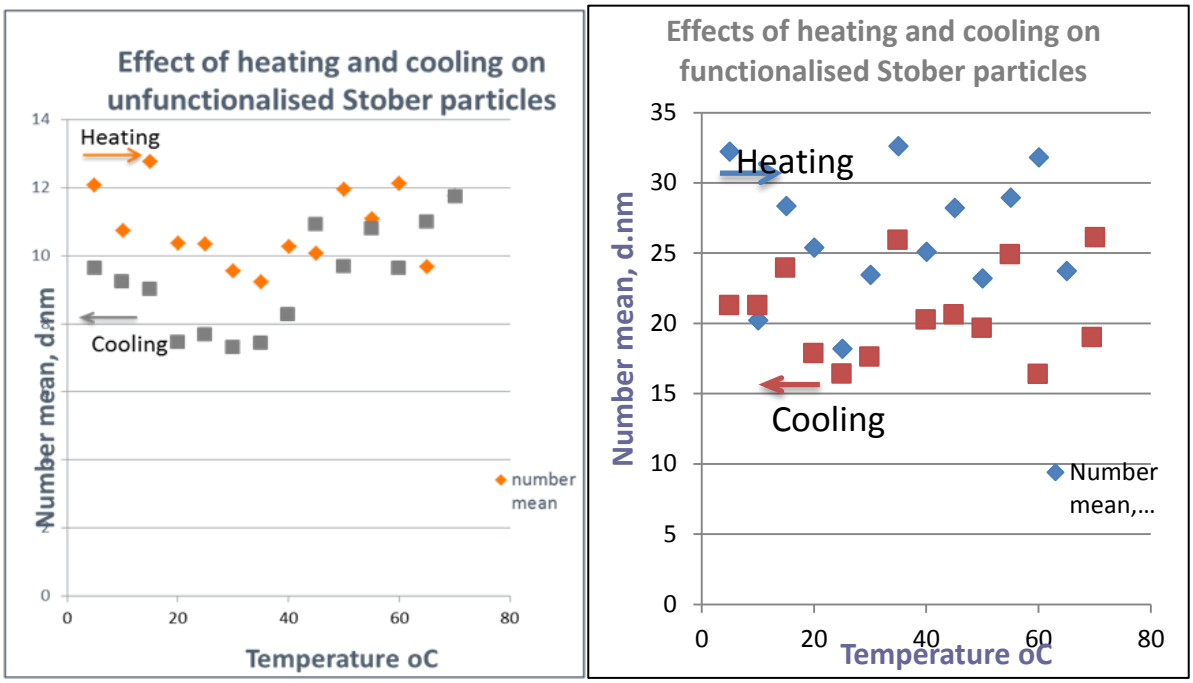

A B

Figure 6.6. Conformational and phase transition of unfunctionalised Stöber silica particles (A) and functionalised (B) as a result of increasing/decrease in temperature. Where ◇represent heating cycles and □ represent cooling cycles.

In **Figures 6.6**, the arrows show the directions of heating and cooling of the Stöber particles. **Figure 6.6A** shows that the particles remain roughly the same size (10-12nm) upon heating from 0-80^{0}C. It also shows that the sizes do not return to their original size upon cooling. There is a very similar behaviour with **Figure 6.6B**. For the functionalised samples, the particles are almost stable and reversible upon heating and cooling with slight difference in temperature. This is a novel finding as literature has not reported any result on this.

Factors that affects the Stöber nanoparticles size variation

The concentration of TEOS, water and ammonia all affect the size of the silica nanoparticles formed [7, 160,82]. Below are the findings of how each affects nanoparticle sizes compared to the findings of other researchers.

6.1.7 Effect of TEOS concentration.

As mentioned in the introduction, Stöber *et al.*[2] reported that size does not increase with increasing TEOS concentration. However, Bogush *et al*.[157] and Raman *et al*.[148] discovered that the particle size gets larger as the TEOS concentration increases. On the other hand, Van Helden *et al.* [161] reported that the size gets smaller as the TEOS concentration increases. Other studies have also said that size increases with an increase in TEOS concentrations. More recent studies by Rao *et al.*[140] have shown that the size decreases with increasing TEOS concentration. Rao explained that since the rate of hydrolysis is a function of water concentration, the rate will increase with increasing water concentration.

The research findings in this thesis (**Figure 6.7)** disagree with Rao and agree with Bogush and Rahman *et al*[177]. Following an experimental procedure as conducted in section 2.1.9 and Table 2.3 the results following TEM analysis as discussed earlier are as explained below.

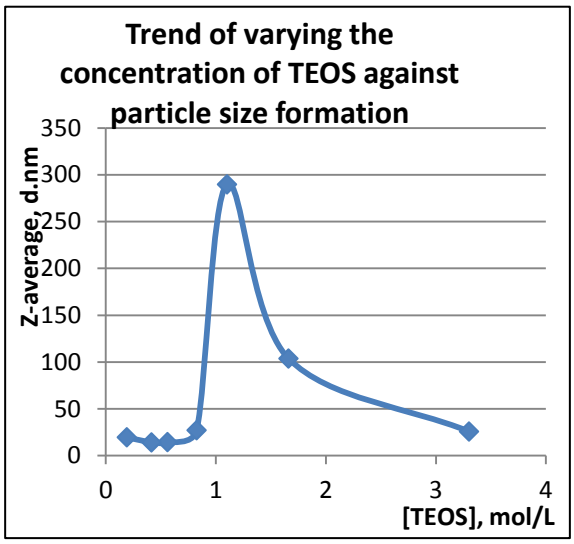

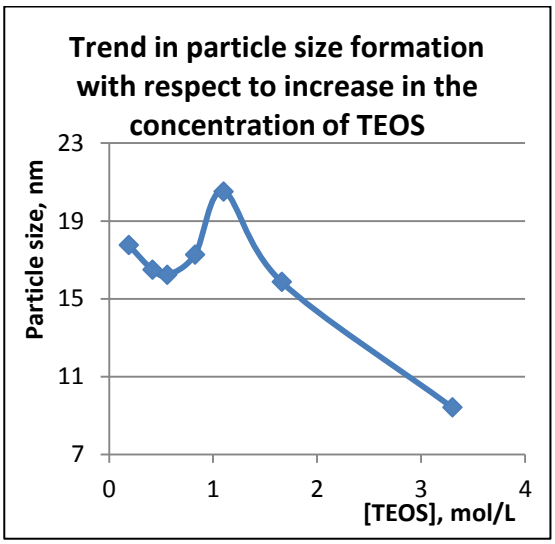

DLS TEM

Figure 6.7. Effect of TEOS concentration on particle size (a) DLS (b) TEM

According to the data in **Figure 6.7**, as the concentration of TEOS increases, more nucleation occurs i.e. more growing sites and the particle size increases until a maximum is reached at about 1.2mol/L TEOS concentration . After the maximum, any further addition of TEOS leads to no further increase because there is not enough water left in the system to react to promote nucleation and hence growth of the particles, hence the reason for a decrease in particle size once higher amounts of TEOS are used. A pictorial representation of the results is shown in **Figure 6.8** showing the size variation with respect to increasing the concentration of TEOS. There is a difference in particle size between the two instruments; DLS and TEM. DLS analyses are carried out in solution hence the size appears bigger than in TEM where dried samples are used and the actual particle sizes are measured. Regardless of which of the methods used, the trend of the particle size is the same hence the conclusion is accurate.

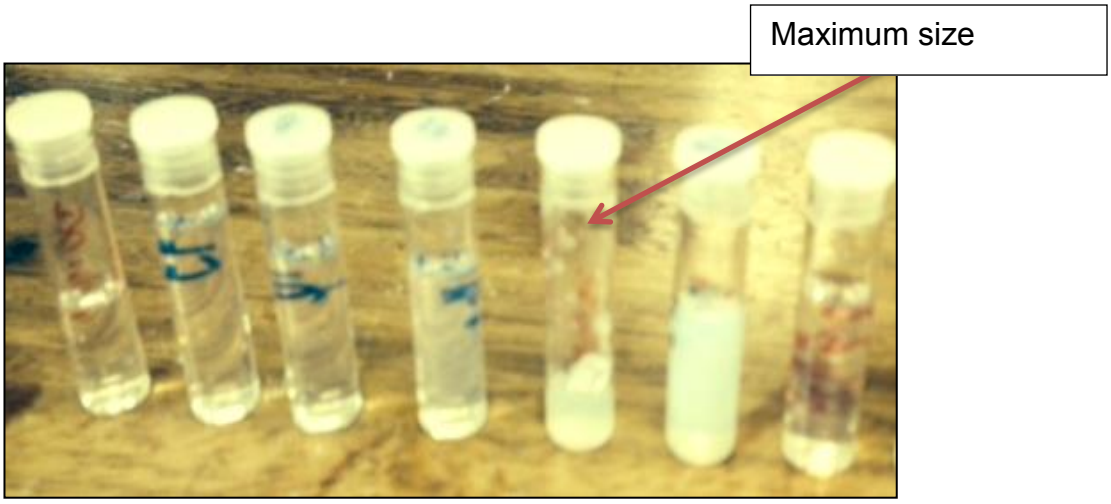

Figure 6.8. Picture showing particles with increasing [TEOS]. Different concentrations of TEOS from left to right: 0, 0.4, 0.6, 0.8, 1.1, 1.6, 3.3 mol/L (**Table 2.5**).From left to right, the samples become cloudier as the amount and size of nanoparticles increases with increase in TEOS concentration until a maximum point is reach at which there is no size nor amount increase irrespective of the concentration of TEOS added.

6.1.8 Effect of water concentration on particle size variation

Using the experimental procedure in Chapter 2.1.9 and Table 2.5 data, the effect of varying the water concentration are shown in **Figure 6.9** and **Figure 6.10** and the TEM images further shown in **Figure 6.12a-f.**

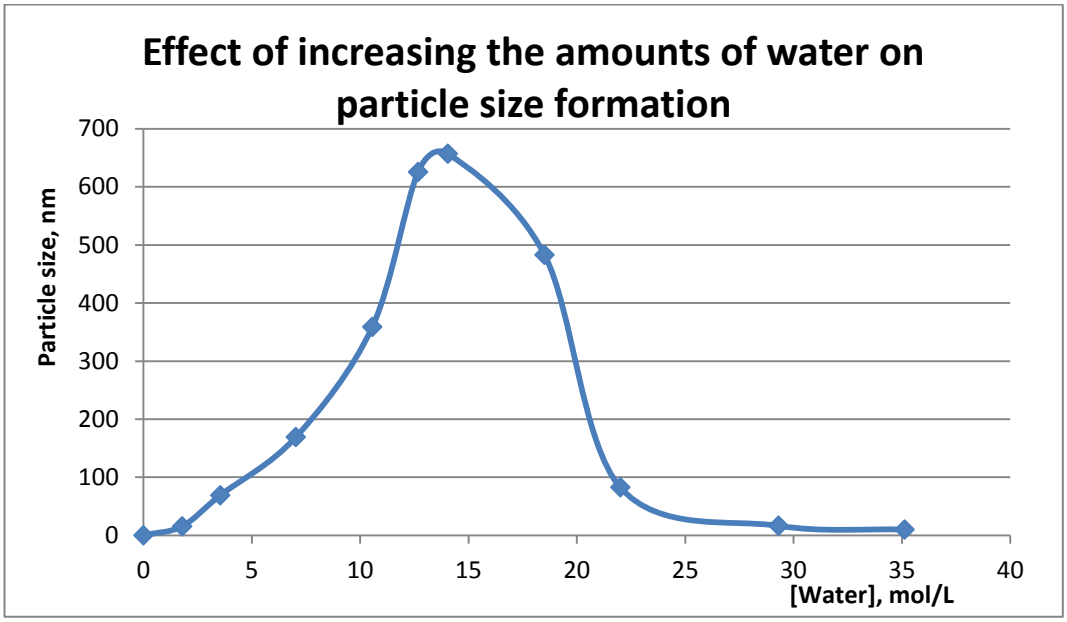

Figure 6.9. TEM results of TEOS hydrolysis showing the trends of particle size with increasing [H_2O]

Notice that in **Figure 6.9**, the calculation assumed a certain density of the mixture to be that of ethanol since it is the bulk of the solution in most of the individual mixtures.

NB: Increasing TEOS concentrations from left to right: 0, 1.78, 3.54, 7.03, 10.56, 12.67, 14.05, 22.00, 29.30, 35.15 mol/L (**Figure 2.7**)

Figure 6.10. Picture showing particles with increasing [water] from left to right

Figure 6.9 and **Figure 6.10** indicates that with fixed [TEOS], as you increase the [H_2O], the number of nucleation sites increases as hydrolysis and condensation increase. This is because, there is plenty of water for particle growth and so size increases (3-650nm). At high or excess [H_2O](>14mol/L), the number of nucleation sites increases but the reaction runs out of TEOS quickly and thus, they cannot grow to their full size hence particle size decreases (650-3nm) below a certain threshold of the [TEOS]. This agrees with the findings of Park *et al.*[162] and Wang *et al*[132] .

Another explanation of the relationship between water and particle size is that more water will lead to more hydrolysis and thus more silanols. Ionisation of these silanols leads to negative charge build up on the nuclei such that they repel each other and hence leading to less agglomeration. With a greater number of nuclei and a set amount of TEOS the particles will end up smaller. Thus the final size depends upon the number of nuclei which in turn depends upon amount of aggregation. If nuclei aggregate, there will be fewer particles and thus they grow to be bigger. Aggregation depends upon the negative charge on the nuclei. The more negative charge, the less aggregation occurs because of repulsion. Negative charge on nuclei depends upon the amount of silanol and the amount of silanol depends upon the extent of hydrolysis (nucleation). Also, as the amount of water increases, the polarity of the solvent increases and so the silanol dissociates into negative silanolate ions, $Si\text{-}O^-$, more readily. See **Figure 6.11** for the schematic

representation of the nucleation and growth process of a Stöber sphere nanoparticle. Notice also that more water leads to smaller particles, uniform and more spherical particles as confirmed in **Figure 6.12**.

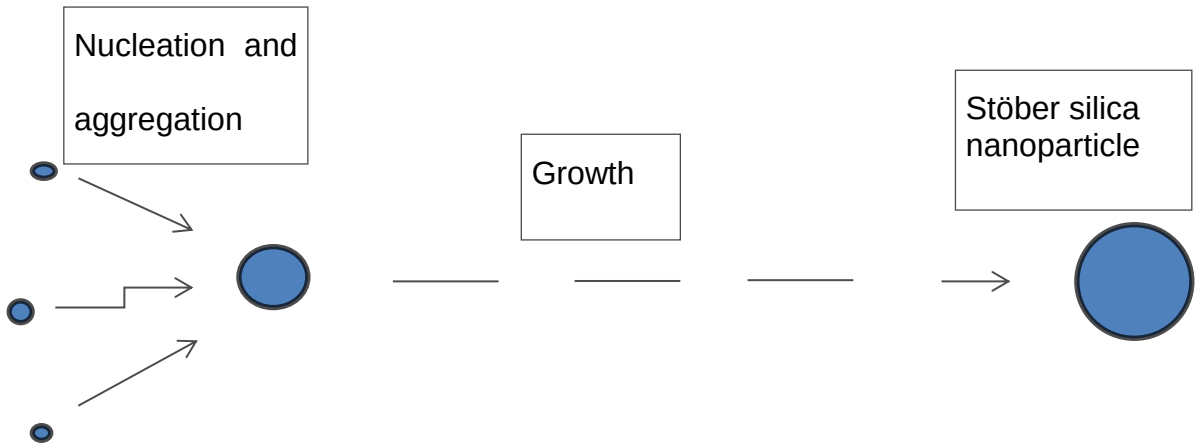

Figure 6.11. Schematic drawing showing the growth process of a nanoparticle

Initial studies by Matsouka *et al*. [155] mentioned that increasing the amount of water leads to an increase in particle size. Yet recent studies carried out by Matsouka *et al.*[190b] have found that increasing the amount of water leads to a decrease in the size of the particles formed. Park *et al.* [162] later reported that increasing the amount of water leads to an increase in the sizes of particles. Park ***et al's*** report was supported by the fact that, increasing water concentration leads to agglomeration of the particles hence larger sizes are observed. However, Park *et al.* then concluded that, with excess amount of water, the particles become smaller.

These thesis results agree with Park *et al.* and suggest Matsouka *et al.* must have studied only one phase of the reaction at a time (either before or after the maximum) hence their findings gave an incomplete report. If an extensive study was performed as in this case, they would have found that size increases and then decreases.

Increasing the amount of water increases the size until a point is reached where any further increase in [H_2O] leads to smaller particles as the reaction system becomes deficient of TEOS to react with. The size variation can be seen in **Figure 6.12(a-j)** which are the size representations of the same samples in **Figures 6.9**.

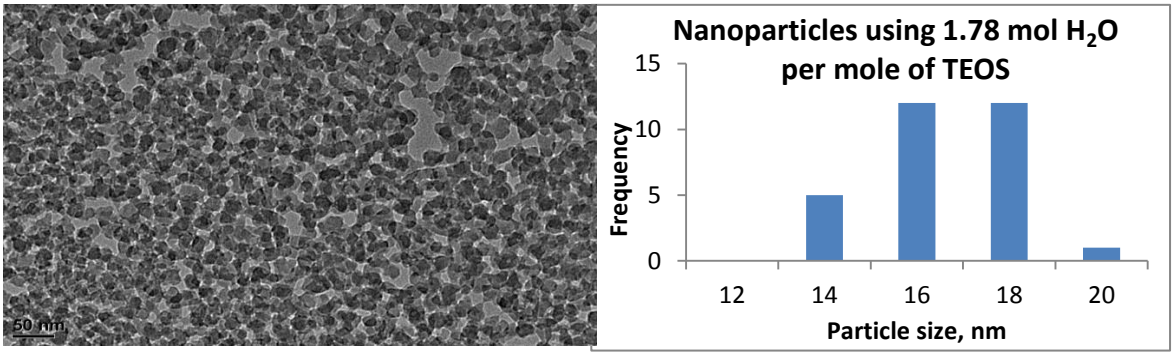

a

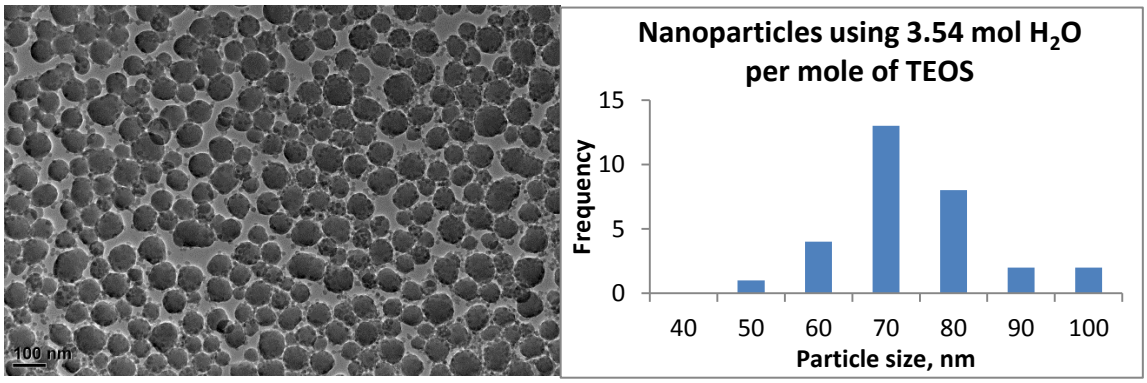

b

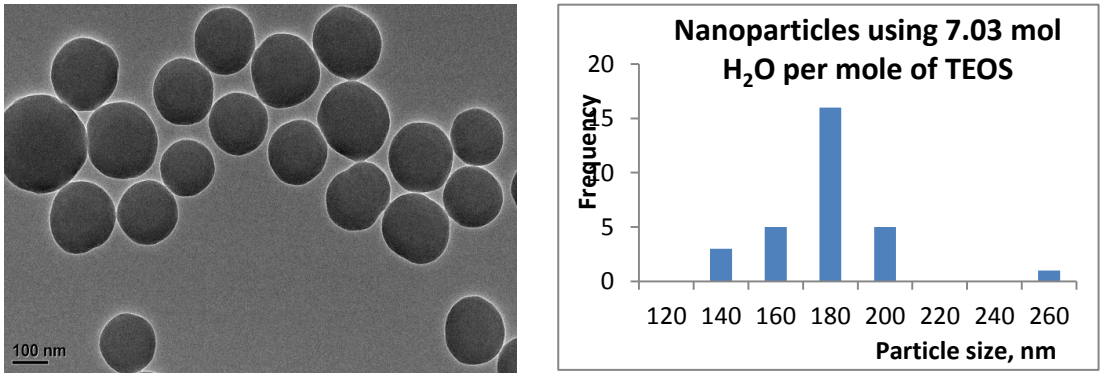

c

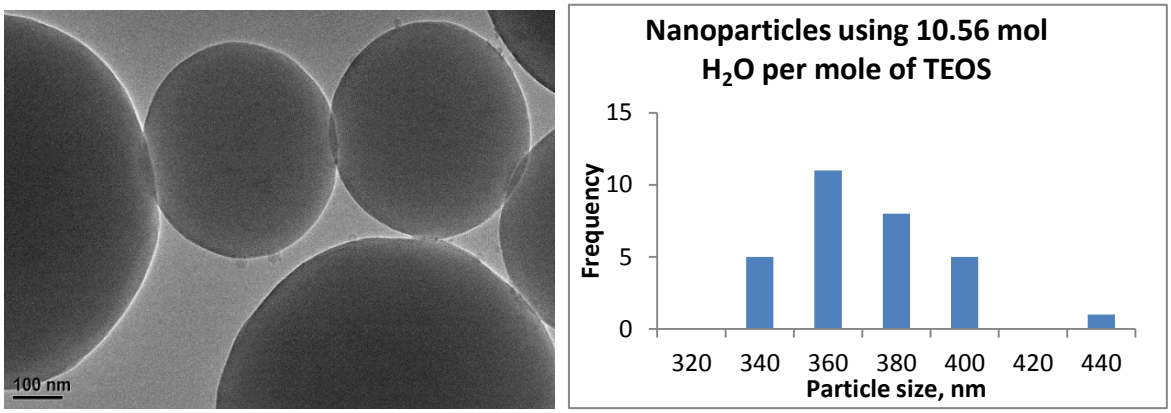
100 nm
Nanoparticles using 10.56 mol H_2O per mole of TEOS
Frequency
15
10
5
0
320
340
360
380
400
420
440
Particle size, nm

d

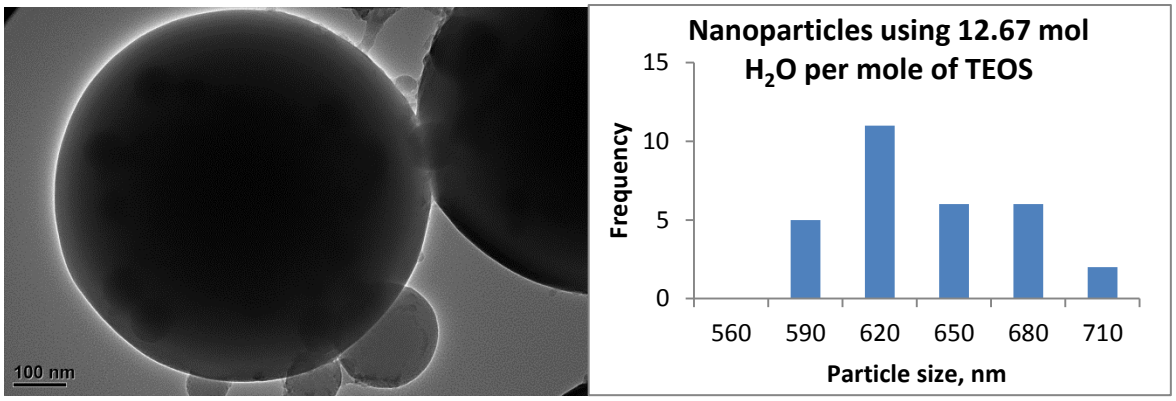
100 nm
Nanoparticles using 12.67 mol H_2O per mole of TEOS
Frequency
15
10
5
0
560
590
620
650
680
710
Particle size, nm

e

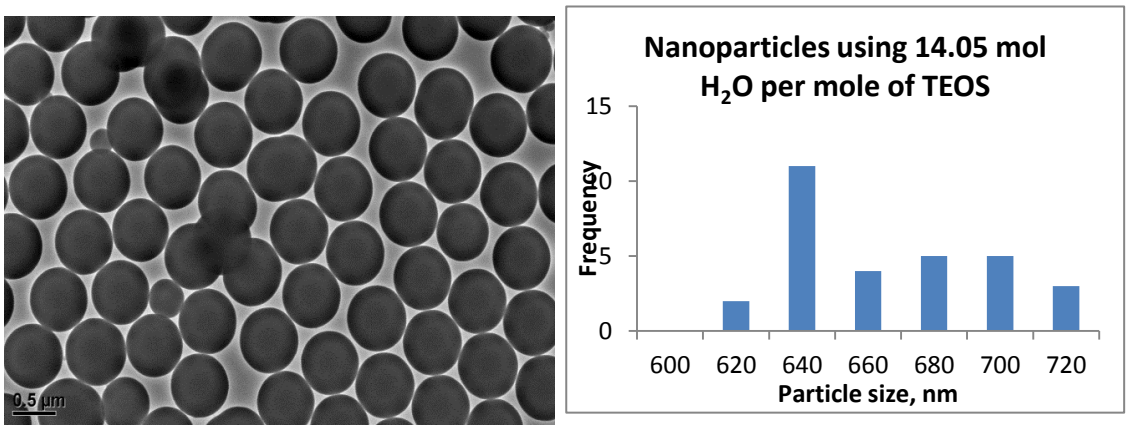
0.5 µm
Nanoparticles using 14.05 mol H_2O per mole of TEOS
Frequency
15
10
5
0
600
620
640
660
680
700
720
Particle size, nm

f

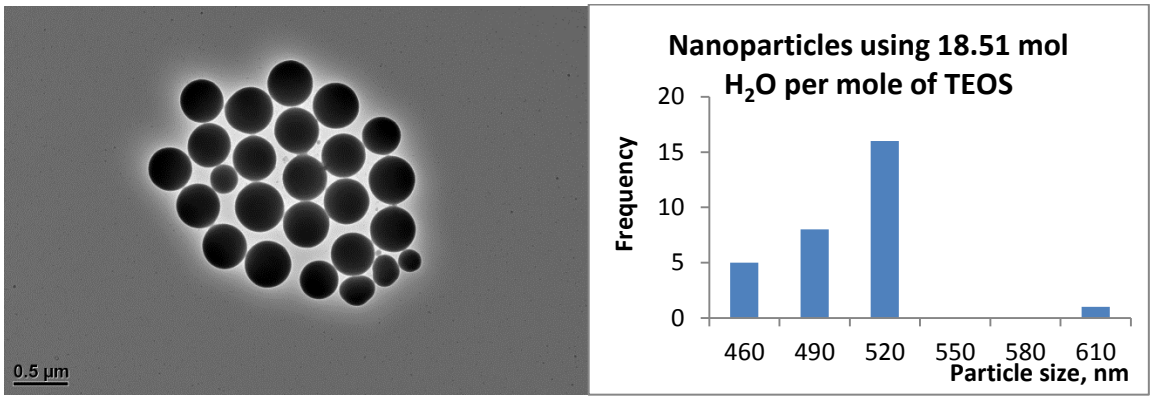
0.5 µm
Nanoparticles using 18.51 mol H_2O per mole of TEOS
Frequency
20
15
10
5
0
460
490
520
550
580
610
Particle size, nm

g

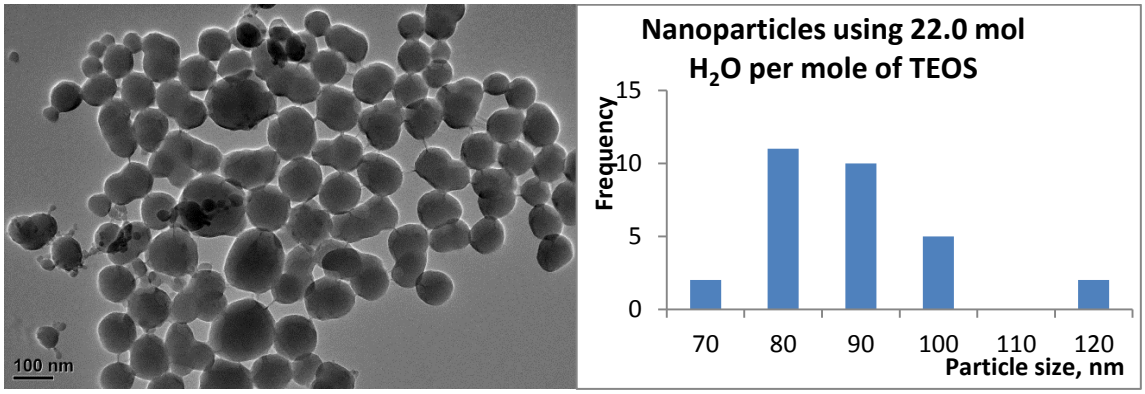
100 nm
Nanoparticles using 22.0 mol H_2O per mole of TEOS
Frequency
15
10
5
0
70
80
90
100
110
120
Particle size, nm

h

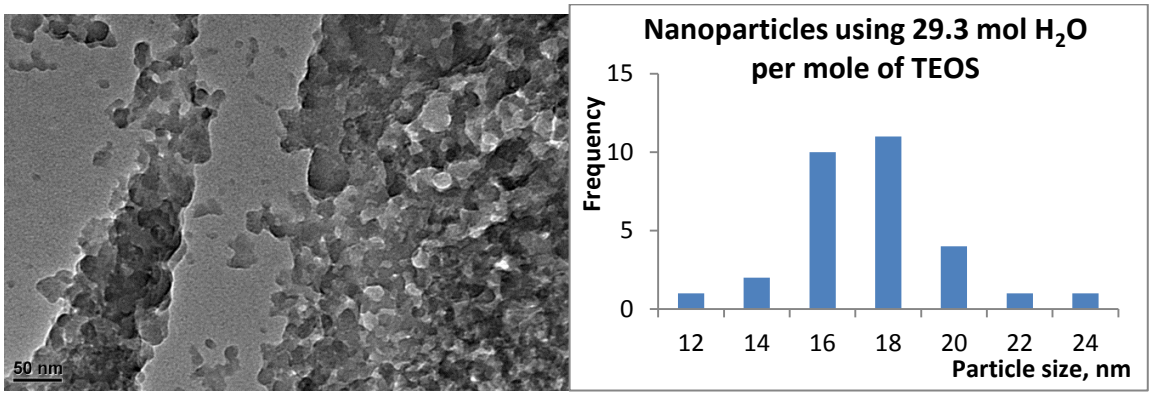
50 nm
Nanoparticles using 29.3 mol H_2O per mole of TEOS
Frequency
15
10
5
0
12
14
16
18
20
22
24
Particle size, nm

i

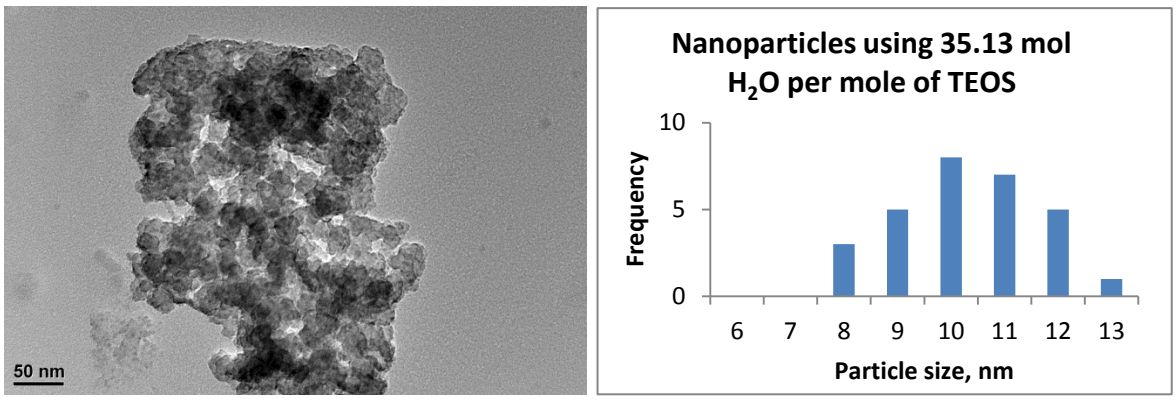

j

Figure 6.12. TEM images showing size distribution of SiO_2 nanoparticles synthesised using different concentrations of water (a-j).

6.1.9 Effect of the amount of ammonia solution on particle size

According to previous studies by Rahman and Green *et al.*, an increase in the amount of ammonia solution leads to a proportional increase in the sizes of the particles[148,125]. Ammonia acts as a catalyst by speeding up the rate of both the hydrolysis and condensation of TEOS. If the rate of hydrolysis and condensation are fast, the faster the particles nucleate and grow and the larger the particles will become. This was also confirmed by Stöber *et al* [2]. The growth could be because as the amount of ammonia ($NH_4^+OH^-$) increases, the amount of water also increases which as previously shown also affect the charge on the particles. Another factor that could be responsible maybe the fact that agglomeration could be occurring leading to the development of some charge difference. **Figure 6.13** and **Figure 6.14** show the findings of this research which proves that as the amount of ammonia solution increases, the sizes of the particles increase as explained above (experimental procedure in Chapter 2.1.9 and Table 2.4 data). Other scientists like

Rao *et al.* [140] have recently reported the opposite. Rahman *et al*.[148] reported that particles prepared at higher ammonia concentration are smooth, spherical and highly dispersed and are obtained in greater yield.

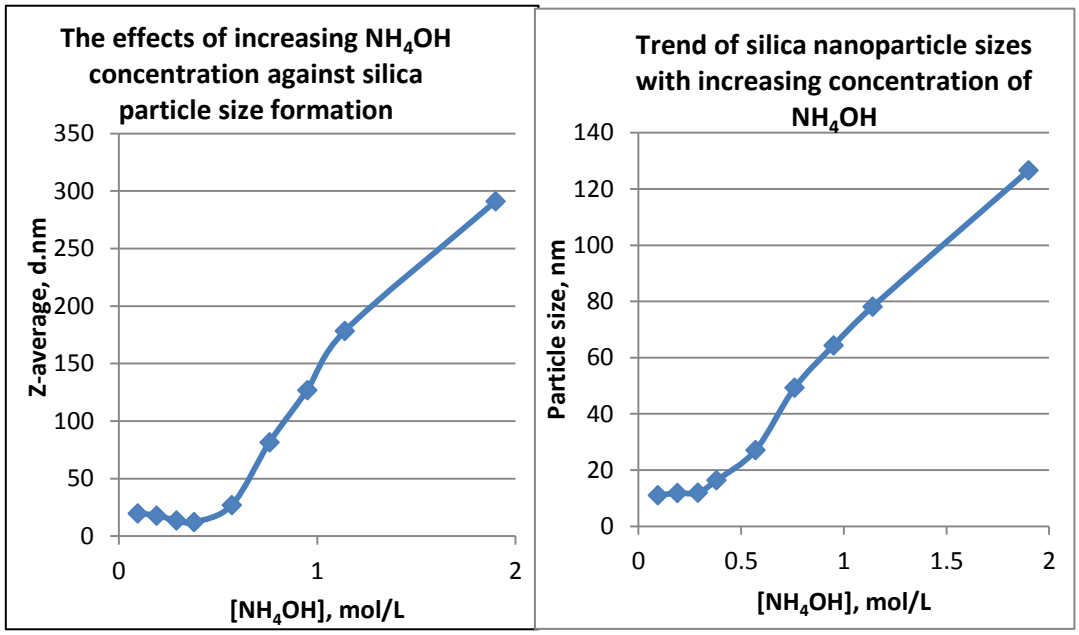

A B

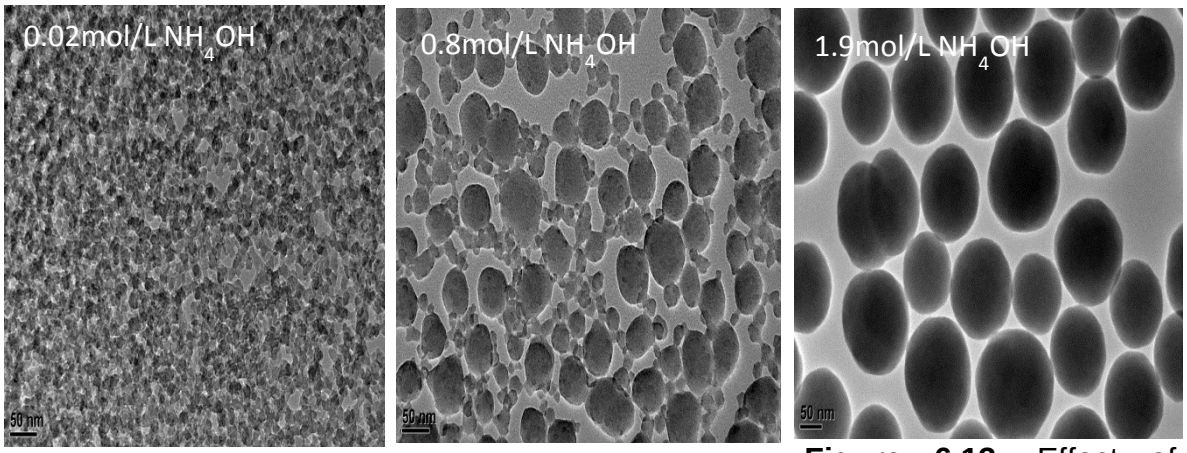

Figure 6.13. Effect of increasing the amount of ammonia solution on particle size (a) DLS (B)TEM.**Figure 6.14.** TEM images of SiO_2 nanoparticles synthesized using different concentrations of ammonia. Particle size increases with increasing concentration of catalyst (NH_4OH).

A pictorial image reflecting the size increase with increasing [NH_4OH] is shown in **Figure 6.15**.

NB Different ammonia concentrations from left to right: 0.1, 0.2, 0.3, 0.4, 0.8, 1.0, 1.1, 1.9 mol/L (**Table 2.6**)

Figure 6.15. Picture showing particles with increasing [NH_4OH]

Discussion of Stöber silica nanoparticles

From the results, one can clearly see that the TEM results show slightly different but broadly similar sizes compared to the DLS results (**Figures 6.6, 6.8, 6.12**). The reason being that DLS measures in solution hence it measures all the particles including the aggregates which are normally formed in solution as opposed to TEM where the samples are measured in their dried state. This was more pronounced for smaller particles because of the high level of aggregation. Ozge Malay *et al.* [265, 327] had the same findings. One can say that TEM gives the primary particle size while DLS gives the size of the particles with agglomeration. Also, when the particles

are being left in ammonia solution, they continue to react, which could be another reason for the DLS technique giving larger sizes.

6.1.10 Effects of water on Stöber particle size formation

There is a trend in the way the particle size changes from 0.5 to 4.0 molar ratio of water though not constant (**Figure 6.12a-f**). As the amount of water increases so the amount of hydrolysis and condensation increases. Hydrolysis leads to silanols but at lower concentrations of water the concentration of silanol is relatively low such that condensation is slow. As the amount of water increases more silanols are being formed leading to nucleation. Also, condensation is faster which leads to greater growth of particles. Small hydrolysable species are fairly stable at low water concentrations hence small particle sizes. At higher water concentrations, more complex species become dominant, as condensation is faster leading to more growth and hence larger particles. With excess water, more condensation is observed but this quickly becomes stable with little further condensation happening regardless of the amount of water added. At this stage, there is less TEOS available to react with the excess water hence particles formed are limited by the amounts of TEOS. That is, more nucleation occurs but low growth because the amount of TEOS is restricted.

6.1.11 Effects of the concentration of TEOS on the extent of condensation of the products formed

The effects of TEOS concentration are similar to that of water. As water and TEOS are both limiting reagents, the absence of one affects the rate of condensation hence the size of the particles formed.

6.1.12 Effects of ammonium hydroxide concentration on particle size formation

The graph (**Figure 6.12**) shows that the size of the particles increases with increases in the amounts of ammonium hydroxide catalyst and hence increase in the amount of water. As the amount of ammonium hydroxide increases, the rate of hydrolysis and condensation becomes fast. The faster the particles will nucleate and grow.

From the results, one can clearly see that water, TEOS and ammonia concentrations all have an effect on the size of the particles formed.

6.1.13 The success of the functionalization of different silanes on Stöber particle surfaces

Both the TEM and XPS give elemental information. From the **TEM** results (**Figure 6.2**), one can see the presence of carbon, oxygen; silicon and sulphur are detected with their percentage composition. Copper is shown as an artefact and hence an impurity that is constant in the instrument. For bare silica nanoparticles, only silicon and oxygen peaks would be detected. So the presence of carbon and sulphur is an indication that the functionalization using 3-mercaptopropyltriethoxysilane was successful.

The XPS results in **Figure 6.4** also give elemental information and their composition. Again, oxygen and silicon, carbon and nitrogen were equally detected indicating the

successful bonding of the APTES group on the surface of the Stöber silica nanoparticles.

The Silicon NMR spectra also confirm the bonding of a functionalising agent on the surface of Stöber nanoparticles. **Figure 6.3** shows two peaks, the T peaks arise from the silane on the surface and the Q peaks from the Stöber silica. This is a good preliminary test for functionalization before one can decide to proceed to obtain elemental information.

Summary and Conclusion

We have demonstrated that particle size can be controlled and this is important for applications such as the coatings with different properties or for making nanomaterials. Stöber particle size formation has been monitored using DLS and TEM. Water, TEOS and ammonia concentrations all have an effect on the sizes of Stöber nanoparticle formation.

The synthesis of coatings through the sol-gel process is simple and fast, making the process ideal for large scale industrial application. The main problem with silica nanoparticles is in controlling aggregation. Aggregation can be prevented by functionalising the silica particles' surface using different silanes, as shown in **Table 6.4**. Another way for silanes bonded on silica surface to affect properties is by improving the compatibility with the matrix. This is important and thus affects the structural properties of the final formulation and coatings.

Functionalization of Stöber nanoparticles has been successfully achieved and the percentage of surface coverage successfully calculated. This provide some control on how much silane can be put on the surface of particles depending on the type of coating or material to be made.

Techniques such as NMR, TEM, DLS and XPS all give very reliable and insightful results for the characterisation of Stöber nanoparticles and functionalization. Solid state ^{29}Si-NMR confirms that chemical bonds are formed between the silane and the nanoparticles. XPS revealed the presence of some elements hence an indication of bonding of the silane on the Stöber silica surface. TEM and DLS were useful to determine the relative sizes of the particles before and after functionalization. Surface bonding calculation following titration reported a 50% coverage which is a proven good coverage as literature report. Also, the DLS results suggest that there is no effect of temperature between 0-80^{o}C on the Stöber silica nanoparticles whether functionalised or unfunctionalised.

Chapter 7 – General summary, conclusion and future work

This chapter comprises the general conclusion of all the above chapters. It gives a general summary and then the conclusion. Future work proposals has also been provided here.

7.1 Summary and conclusion

To conclude, silsesquioxane and silica nanoparticle based materials form a fairly new family of inorganic-organic hybrid nanomaterials [331, 332, 333]. This study provides the basic understanding of the hydrolysis and condensation of silsesquioxanes and TEOS leading to the formation of hybrid materials for various applications such as aerogels and super-hydrophobic materials[334, 335, 336,] . In particular we are now able to understand their mechanism of formation and to be able to control the conditions to get the properties we desired from carrying out the water and silane concentration

studies. The results allowed us to understand the process of silsesquioxane and Stöber silica nanoparticle formation such as the initial chemical conditions and the structures formed. The results in this thesis further help us to clarify the key chemical parameters which may give rise to enhanced process management capability.

The key achievement so far is being able to follow the stepwise polymerization mechanism which has been fully exploited in chapters three and four. Knowledge gained from this understanding have been applied in chapters five and six to make and understand silsesquioxanes and Stöber silica nanoparticles and their properties such as size variation. Polymerization of both TEOS and silsesquioxanes using different instruments such as; NMR, GPC, HPLC and MS have equally been well exploited during this research. This has been investigated in chapters three and four and we can conclude that we have knowledge of how this happens and how it can be used to achieve different properties (structure, hardness, temperature resistance, durability) of the materials. First hydrolysis occur leading to silanol (Si-OH) formation and then condensation to form siloxane (Si-O-Si) bonds. Previous studies have shown that the hydrolysis and condensation of tri and tetraalkoxysilanes in acidic or basic medium yield polymeric products but there existed some discrepancies amongst the published findings some of which have been clarified in this research. That is, most silsesquioxanes are made under basic conditions, here an acid catalyst has been used which allows smaller structural evolution steps to be made which is novel.

The computational model is a significant discovery that was designed and used in chapters three and four and provides a major understanding of tri and tetra alkoxy

silane hydrolysis and condensation. This model could be used to predict other sol-gel mixtures even before trying them out in the laboratory. This will save a lot of time in the laboratory by avoiding unnecessary experiments.

Initially in the hydrolysis and condensation reaction, the broad Si-OH peaks on the FTIR spectra indicate a large degree of hydrolysis taking place. This confirms the presence of silanols (Si-OH). As hydrolysis proceeds leading to condensation, the smaller the OH peak become as seen in Figure 5.30 in chapter 5.3.3.6.

From the results obtained for both A and AZ systems, the silsesquioxanes formed are of variable structures and molecular weights of between 500-50,000. According to GC-MS, ESI-MS and MALDI-ToF-MS analysis, the silsesquioxane resin obtain contains a mixture of various structures: linears, random and some cyclic. Some of these structures can be found in **Appendix 14** and referenced at various parts in the thesis.

Another novel and technologically useful discovery in this research is the discovery that after a certain period of time, pseudo equilibrium is achieved where there are silanols present that do not condense any further (this helps with the shelf life of the material). The composition of this pseudo equilibrium depends upon the reaction conditions. Even studies beyond equilibrium have been performed to understand the stability or shelf life (**Chapter 4.6.3**) and the thermal stability of the materials.

The addition of Stöber spheres to resins is another way of optimising coating materials. Coating materials formed using different sizes and types of Stöber sphere give different superhydrophobicity to coating especially if the Stöber spheres are functionalised, as confirmed by TWI's products on **Figure 6.16** showing contact angles of up to150^{o}C. We have proven that the amount of water, acid and/or base and starting material are critical for the composition and the size of the Stöber spheres formed.

Another valuable finding in this thesis is that the dimer was achieved within the first one hour of the reaction. This is important because it provide information of when to stop the reaction depending on the type of resin/coating material we want to produce. This is key in coating formulation and hence another central principle of this thesis.

Timing is also one of the research aims that needed being addressed. The time taken for resin development determines the properties of the resin. According to the kinetic studies carried out, the time of the synthesis can be reduced from 24 hours to about 4-5 hours, hence reducing the resin production time. This does not only reduce the time but maintains the quality of the resin product. Reducing the time of production increases the robustness of the synthetic process from the current twenty four hours to just four hours.

Finally, the synthesis and characterisation of the resin showed that going from a one component system resin to a two components system resin improved the structural

properties of the resin product (**Chapter 5**). The ^{29}Si NMR, TEM, CHN analysis, DSC, GPC and TGA all show some differences between the two systems. For example, the DSC and TGA results showed no weight loss until around 308^{0}C for the one component system. The two component system showed weight loss at a slightly higher temperature greater than 400^{o}C. This finding indicates an increase in the chemical and physical properties and thermal stability of the coating material once different or multiple starting materials are used. In some cases, the two component system did not show any difference from the one component system. This means the two component system only enhances some properties of the resin, depending on the composition.

7.2 Future work

The functionalization of Stöber silica nanoparticles were mostly done using literature approaches which in most cases were not controlled. As this was an area of the research that developed later in the research process, more time is needed to explore the sol-gel method of controlling the functionalization of particles. This is important because knowing how much of the silanes has been functionalized on the surface is important (as explored in **Chapter 6.6**.), but knowing how to control how much is functionalized on the surface is essential.

Carrying out a BET instrumental analysis to study the surface porosity of the Stöber silica nanoparticles is another important factor to investigate further. Our research lab and colleagues did not have a BET instrument so knowing the surface porosity of the Stöber silica nanoparticles produced was not possible despite several trials. Knowing the surface porosity of the particles helps to control functionalization as one can determine whether all the silanes are on the surface have reacted and whether the ligand has penetrated the pores. This analysis will help with the functionalization control studies.

Similarly in the future it would be useful to analyse the hydrolysis and condensation product of nPTMS using Maldi-ToF-MS in order to determine the reason why there appears to be a reduced amount of it in the AZ-system resin.

On the other hand, in the future other silane hydrolysis and condensation such as nPTES, dimethyltriethoxysilane and TMOS need to be studied as part of improving the process.

Measuring the amount of water in the resin needs to be conducted once they are formed. This will give more information on whether it is silanol left after the process is complete or if it is residual water. This will give more information on the understanding of the process and especially the situation at pseudo-equilibrium.

A final future piece of work would be to continue to develop chapter 6. Also, information from Chapter 4 needs to be used to prepare different silsesquioxane resins using different amounts of water. That way, a large variety of silsesquioxanes will be obtained that will be useful for different types of coating material applications.

References

1. Han, Y.-H.; Taylor, A.; Mantle, M. D.; Knowles, K. M., Sol–gel-derived organic–inorganic hybrid materials. *Journal of Non-Crystalline Solids* **2007,** *353* (3), 313-320.
2. Stöber, W.; Fink, A.; Bohn, E., Controlled growth of monodisperse silica spheres in the micron size range. *Journal of Colloid and Interface Science* **1968,** *26* (1), 62-69.
3. Naito, T.; Yokoyama, Y.; Konno, N.; Tokunaga, T.; Itoh, T., Characteristics of Silicon Films Deposited by Atmospheric-Pressure Plasma-Enhanced Chemical Transport. *Electronics & Communications in Japan* **2013,** *96* (8), 26-31.
4. Henke, T.; Bartha, J. W.; Rebohle, L.; Merkel, U.; Hübner, R.; Albert, M.; Skorupa, W., Formation of regularly arranged large grain silicon islands by using embedded micro mirrors in the flash crystallization of amorphous silicon. *Journal of Applied Physics* **2014,** *115* (3), 1-14.
5. Qi, C.; Striemer, C. C.; Gaborski, T. R.; McGrath, J. L.; Fauchet, P. M., Highly porous silicon membranes fabricated from silicon nitride/silicon stacks. *Small (Weinheim An Der Bergstrasse, Germany)* **2014,** *10* (14), 2946-2953.
6. Sylwester, B.; Phillips, K.; Sylwester, J.; Kępa, A., Silicon Abundance from RESIK Solar Flare Observations. *Solar Physics* **2013,** *283* (2), 453-461.
7. Sinkó, K., Influence of Chemical Conditions on the Nanoporous Structure of Silicate Aerogels. *Materials (1996-1944)* **2010,** *3* (1), 704-740.
8. Jiang, H.; Zheng, Z.; Li, Z.; Wang, X., Effects of Temperature and Solvent on the Hydrolysis of Alkoxysilane under Alkaline Conditions. *Industrial & Engineering Chemistry Research* **2006,** *45* (25), 8617-8622.
9. Shaltout, A. M. K. B., M. M.; Bakry, A.; Ichimoto, K., , The abundance of silicon in the solar atmosphere. . *Oxford Univeristy press: 2013;* **2013,** *430* (4), p2979-p2985, 7p.
10. De La Rocha, C. L.; Brzezinski, M. A.; DeNiro, M. J.; Shemesh, A., Silicon-isotope composition of diatoms as an indicator of past oceanic change. *Nature* **1998,** *395* (6703), 680.
11. Petri, W.; Jaakko, E. L., Manufacture of resin-free fiberboards from wood fibers activated with Fenton's reagent (H2O2/Fe2+). In *Silanes and Other Coupling Agents, Volume 3*, CRC Press: 2004; pp 241-256.
12. Corriu, R., Organosilicon chemistry and nanoscience. *Journal of Organometallic Chemistry* **2003,** *686* (1–2), 32-41.
13. New horizon of organosilicon chemistry. *Dalton Transactions* **2010,** *39* (39), 9175-9175.
14. Burkhard, C. A.; Rochow, E. G.; Booth, H. S.; Hartt, J., The Present State of Organosilicon Chemistry. *Chemical Reviews* **1947,** *41* (1), 97-149.
15. Torsten, T.; Dierk, K.; Thomas, B.; Eckhard, S., Inorganic-organic hybrid polymers based on silanes for coating textile substrates. In *Silanes and Other Coupling Agents, Volume 3*, CRC Press: 2004; pp 193-203.
16. Vignesh, P.; Wim, J. V. O., Modified silane coatings as an alternative to chromates for corrosion protection of aluminum alloys. In *Silanes and Other Coupling Agents, Volume 3*, CRC Press: 2004; pp 119-159.
17. Chang, K. C.; Hsu, C. H.; Lu, H. I.; Ji, W. F.; Chang, C. H.; Li, W. Y.; Chuang, T. L.; Yeh, J. M.; Liu, W. R.; Tsai, M. H., Advanced anticorrosive coatings prepared from electroactive polyimide/graphene nanocomposites with synergistic effects of

redox catalytic capability and gas barrier properties. *Express Polymer Letters* **2014,** *8* (4), 243-255.
18. Zhou, J. F.; Wang, L.; Dong, X. C.; Yang, Q.; Deng, L.; Huo, J.; Tan, Q. H.; Liu, Q. Q., *Preparation of organic/inorganic hybrid nanomaterials using aggregates of star block copolymer consisting of poly(stearyl methacrylate) and poly(3-(trimethoxysilyl) propyl methacrylate) as precursor*. 2008.
19. Zhou, H. J.; Rong, M. Z.; Zhang, M. Q.; Lehmann, B.; Friedrich, K., Grafting of Poly(glycidyl methacrylate) onto Nano-SiO2 and Its Reactivity in Polymers. *Polym J* **2005,** *37* (9), 677-685.
20. Rong, M. Z.; Zhang, M. Q.; Zheng, Y. X.; Zeng, H. M.; Walter, R.; Friedrich, K., Structure–property relationships of irradiation grafted nano-inorganic particle filled polypropylene composites. *Polymer* **2001,** *42* (1), 167-183.
21. Urata, C.; Yamada, H.; Wakabayashi, R.; Aoyama, Y.; Hirosawa, S.; Arai, S.; Takeoka, S.; Yamauchi, Y.; Kuroda, K., Aqueous Colloidal Mesoporous Nanoparticles with Ethenylene-Bridged Silsesquioxane Frameworks. *Journal of the American Chemical Society* **2011,** *133* (21), 8102-8105.
22. A., T., United State Patent. **2011**.
23. Taylor, A., "Process for the Production of Organosilsequioxanes"

Alan Taylor, US7910216 Publication Date: 31 May 2007. *United state Patent* **2007**.
24. Bauer, F.; Sauerland, V.; Ernst, H.; Gläsel, H.-J.; Naumov, S.; Mehnert, R., Preparation of Scratch- and Abrasion-Resistant Polymeric Nanocomposites by Monomer Grafting onto Nanoparticles, 4. *Macromolecular Chemistry and Physics* **2003,** *204* (3), 375-383.
25. Sanchez, J.; Rankin, S. E.; McCormick, A. V., 29Si NMR Kinetic Study of Tetraethoxysilane and Ethyl-Substituted Ethoxysilane Polymerization in Acidic Conditions. *Industrial & Engineering Chemistry Research* **1996,** *35* (1), 117-129.
26. Sinirlioglu, D.; Muftuoglu, A. E., Synthesis of an Inorganic-Organic Hybrid Material Based on Polyhedral Oligomeric Silsesquioxane and Polystyrene via Nitroxide-Mediated Polymerization and Click Reactions. *Designed Monomers & Polymers* **2011,** *14* (3), 273-286.
27. (a) Bassindale, A. R.; Pourny, M.; Taylor, P. G.; Hursthouse, M. B.; Light, M. E., Fluoride-Ion Encapsulation within a Silsesquioxane Cage. *Angewandte Chemie International Edition* **2003,** *42* (30), 3488-3490; (b) Bassindale, A. R.; Chen, H.; Liu, Z.; MacKinnon, I. A.; Parker, D. J.; Taylor, P. G.; Yang, Y.; Light, M. E.; Horton, P. N.; Hursthouse, M. B., A higher yielding route to octasilsesquioxane cages using tetrabutylammonium fluoride, Part 2: further synthetic advances, mechanistic investigations and X-ray crystal structure studies into the factors that determine cage geometry in the solid state. *Journal of Organometallic Chemistry* **2004,** *689* (21), 3287-3300.
28. El Aziz, Y.; Bassindale, A. R.; Taylor, P. G.; Stephenson, R. A.; Hursthouse, M. B.; Harrington, R. W.; Clegg, W., X-ray Crystal Structures, Packing Behavior, and Thermal Stability Studies of a Homologous Series of n-Alkyl-Substituted Polyhedral Oligomeric Silsesquioxanes. *Macromolecules* **2013,** *46* (3), 988-1001.
29. Kwon, S. J.; Hwang, C. R.; Jang, A. R.; Bae, J.; Chae, B.; Won, J. C.; Lee, S. W., Preparation and Characterization of Transparent Polyimide/Silica Composite Films by a Sol-Gel Reaction. *Molecular Crystals and Liquid Crystals* **2013,** *584* (1), 9-17.
30. Kaneko, Y.; Coughlin, E. B.; Gunji, T.; Itoh, M.; Matsukawa, K.; Naka, K., Silsesquioxanes: Recent Advancement and Novel Applications. *International Journal of Polymer Science* **2012,** *2012*, 2.

31. Itoh, M., Polyhedral Oligomeric Silsesquioxanes (POSS). In *Encyclopedia of Polymeric Nanomaterials*, Kobayashi, S.; Müllen, K., Eds. Springer Berlin Heidelberg: 2014; pp 1-8.
32. Liles, D. T., The fascinating world of silicones. *Dow Corning Corporation. http://www.dowcorning.com/content/publishedlit/The_Fascinating_World_of_SiliconesPart1.pdf* **2012**.
33. Silane Coupling Agents. In *Silanes and Other Coupling Agents, Volume 3*, CRC Press: 2004; pp 1-1.
34. Helmut, M., Silane oligomers. In *Silanes and Other Coupling Agents, Volume 3*, CRC Press: 2004; pp 11-20.
35. Pohl, E. R.; Chaves, A., Sterically hindered silanes for waterborne systems. In *Silanes and Other Coupling Agents, Volume 3*, CRC Press: 2004; pp 3-9.
36. Anuj, S.; Wim, J. V. O., Silane coupling agents as corrosion fatigue inhibitors. In *Silanes and Other Coupling Agents, Volume 3*, CRC Press: 2004; pp 119-117.
37. Joshi, M.; Bhattacharyya, A.; Agarwal, N.; Parmar, S., Nanostructured coatings for super hydrophobic textiles. *Bulletin of Materials Science* **2012,** *35* (6), 933-938.
38. Philipp, M.; Müller, U.; Gervais, P.-C.; Wehlack, C.; Possart, W.; Sanctuary, R.; Klee, J. E.; Krüger, J. K., Influence of Nanoparticles on the Coupling Between Optical Dipoles in Epoxy-Silica Nanocomposites During Network Formation. *Journal of Adhesion* **2012,** *88* (7), 566.
39. Hybrid Polymeric Nanoparticles Containing Inorganic Nanostructures. In *Polymer and Polymer-Hybrid Nanoparticles*, CRC Press: 2013; pp 303-368.
40. AmandaEvelynRiderKostyaKen, O., Assembly and Self-Organization of Nanomaterials. In *Plasma Processing of Nanomaterials*, CRC Press: 2011; pp 371-392.
41. (a) Cyrill, B.; Alberto, B.; Maurizio, P.; Kostas, K., Biodegradation of Carbon-Based Nanomaterials. In *Handbook of Safety Assessment of Nanomaterials*, Pan Stanford: 2014; pp 319-339; (b) Haghi, A. K.; Hamrang, A., Nanomaterials. In *Foundations of High Performance Polymers*, Apple Academic Press: 2013; pp 195-270.
42. LeVier, R. R.; Harrison, M. C.; Cook, R. R.; Lane, T. H., What is silicone? *Journal of Clinical Epidemiology* **1995,** *48* (4), 513-517.
43. Cha, J. N.; Shimizu, K.; Zhou, Y.; Christiansen, S. C.; Chmelka, B. F.; Stucky, G. D.; Morse, D. E., Silicatein filaments and subunits from a marine sponge direct the polymerization of silica and silicones in vitro. *Proceedings of the National Academy of Sciences* **1999,** *96* (2), 361-365.
44. Rodrigues, E. M.; Souza, E. R.; Monteiro, J. H. S. K.; Gaspar, R. D. L.; Mazali, I. O.; Sigoli, F. A., Non-stabilized europium-doped lanthanum oxyfluoride and fluoride nanoparticles well dispersed in thin silica films. *Journal of Materials Chemistry* **2012,** *22* (45), 24109-24123.
45. Cha, J. N.; Stucky, G. D.; Morse, D. E.; Deming, T. J., Biomimetic synthesis of ordered silica structures mediated by block copolypeptides. *Nature* **2000,** *403* (6767), 289-292.
46. Iler, R. K., The Chemistry of silica: solubility, polymerisation, colloid and surface properties and biochemistry, . *John Wiley and Sons, Ney York* **1979**.
47. Célérier, S.; Laberty-Robert, C.; Long, J. W.; Pettigrew, K. A.; Stroud, R. M.; Rolison, D. R.; Ansart, F.; Stevens, P., Synthesis of La9.33Si6O26 Pore–Solid Nanoarchitectures via Epoxide-Driven Sol–Gel Chemistry. *Advanced Materials* **2006,** *18* (5), 615-618.
48. Malfatti, L.; Innocenzi, P., Sol–gel chemistry: from self-assembly to complex materials. *Journal of Sol-Gel Science and Technology* **2011,** *60* (3), 226-235.

49. Sanchez, C.; Ribot, F.; Lebeau, B., Molecular design of hybrid organic-inorganic nanocomposites synthesized via sol-gel chemistry. *Journal of Materials Chemistry* **1999,** *9* (1), 35-44.
50. Weinhold, F.; West, R., Hyperconjugative Interactions in Permethylated Siloxanes and Ethers: The Nature of the SiO Bond. *Journal of the American Chemical Society* **2013,** *135* (15), 5762-5767.
51. Karapanagiotis, I.; Manoudis, P. N.; Zurba, A.; Lampakis, D., From Hydrophobic to Superhydrophobic and Superhydrophilic Siloxanes by Thermal Treatment. *Langmuir* **2014,** *30* (44), 13235-13243.
52. (a) Ghosh, A.; Seeley, S. K.; Nartker, S. R.; Seeley, J. V., Analysis of siloxanes in hydrocarbon mixtures using comprehensive two-dimensional gas chromatography. *Journal of Chromatography A* **2014,** *1360* (0), 258-263; (b) Xu, L.; Shi, Y.; Cai, Y., Occurrence and fate of volatile siloxanes in a municipal Wastewater Treatment Plant of Beijing, China. *Water Research* **2013,** *47* (2), 715-724.
53. Girardi, F.; Cappelletto, E.; Sandak, J.; Bochicchio, G.; Tessadri, B.; Palanti, S.; Feci, E.; Di Maggio, R., Hybrid organic–inorganic materials as coatings for protecting wood. *Progress in Organic Coatings* **2014,** *77* (2), 449-457.
54. Giessmann, S.; Fischer, A.; Edelmann, F. T., - Silyl-functionalized silsesquioxanes: New building blocks for larger Si-O-assemblies, including the first Si-Si-bonded silsesquioxanes. **2004**.
55. dell' Erba, I. E.; Fasce, D. P.; Williams, R. J. J.; Erra-Balsells, R.; Fukuyama, Y.; Nonami, H., - Poly(silsesquioxanes) derived from the hydrolytic condensation of organotrialkoxysilanes containing hydroxyl groups. **2003**.
56. Vautravers, N.; Andre, P.; Slawin, A. M.; Cole-Hamilton, D., Synthesis and characterization of photoluminescent vinylbiphenyl decorated polyhedral oligomeric silsesquioxanes. *Organic and biomolecular Chemistry* **2009,** *7* (4), 717-724.
57. Helling, R.; Seifried, P.; Fritzsche, D.; Simat, T. J., Characterisation and migration properties of silicone materials during typical long-term commercial and household use applications: a combined case study. *Food Additives & Contaminants. Part A: Chemistry, Analysis, Control, Exposure & Risk Assessment* **2012,** *29* (9), 1489-1500.
58. Narisawa, M., Silicone Resin Applications for Ceramic Precursors and Composites. *Materials (1996-1944)* **2010,** *3* (6), 3518-3536.
59. Marks, D. J.; Jones, R. R., Optimising the adhesion of glass fibres to an epoxy resin using plasma copolymers. In *Silanes and Other Coupling Agents, Volume 3*, CRC Press: 2004; pp 205-223.
60. Matinlinna, J. P.; Laajalehto, K.; Lassila, L. J.; Yli-urpo, A.; Vallittu, P. K., FT-IR and XPS surface characterization of allyltrimethoxysilane and 3-methacryloxypropyltrimethoxysilane mixture adsorbed onto titanium substrate. In *Silanes and Other Coupling Agents, Volume 3*, CRC Press: 2004; pp 21-37.
61. Nagarale, R. K.; Gohil, G. S.; Shahi, V. K., Recent developments on ion-exchange membranes and electro-membrane processes. *Advances in Colloid and Interface Science* **2006,** *119* (2–3), 97-130.
62. Derouet, D.; Ha Thuc, C. N., Synthesis and characterization of poly(methyl methacrylate)-grafted silica microparticles. *Journal of Applied Polymer Science* **2008,** *109* (4), 2113-2127.
63. Bhosle, T., Trialkoxysilane grafting onto nanoparticles for the preparation of clear coat polyacrylate systems with excellent scratch performance. *Paintindia* **2010,** *60* (7), 57-64.
64. Martinelli, A., Effects of a Protic Ionic Liquid on the Reaction Pathway during Non-Aqueous Sol-Gel Synthesis of Silica: A Raman Spectroscopic Investigation. *International Journal of Molecular Sciences* **2014,** *15* (4), 6488-6503.

65. Wakabayashi, R.; Kuroda, K., Siloxane-Bond Formation Promoted by Lewis Acids: A Nonhydrolytic Sol-Gel Process and the Piers-Rubinsztajn Reaction. *ChemPlusChem* **2013,** *78* (8), 764-774.
66. Canton, G.; Riccò, R.; Marinello, F.; Carmignato, S.; Enrichi, F., Modified Stöber synthesis of highly luminescent dye-doped silica nanoparticles. *Journal of Nanoparticle Research* **2011,** *13* (9), 4349-4356.
67. Takeda, Y.; Komori, Y.; Yoshitake, H., Direct stöber synthesis of monodisperse silica particles functionalized with mercapto-, vinyl- and aminopropylsilanes in alcohol–water mixed solvents. *Colloids and Surfaces A: Physicochemical and Engineering Aspects* **2013,** *422* (0), 68-74.
68. Labéguerie-Egéa, J.; McEvoy, H.; McDonagh, C., Synthesis, characterisation and functionalisation of luminescent silica nanoparticles. *Journal of Nanoparticle Research* **2011,** *13* (12), 6455-6465.
69. English, M.; Waclawik, E., A novel method for the synthesis of monodisperse gold-coated silica nanoparticles. *Journal of Nanoparticle Research* **2012,** *14* (1), 1-10.
70. San, T. H.; Daud, W. R. W.; Kadhum, A. A. H.; Mohamad, A. B.; Kamarudin, S. K.; Shyuan, L. K.; Majlan, E. H., Synthesis of palladium-doped silica nanofibers by sol-gel reaction and electrospinning process. *AIP Conference Proceedings* **2012,** *1455* (1), 109-113.
71. Koebel, M.; Rigacci, A.; Achard, P., Aerogel-based thermal superinsulation: an overview. *Journal of Sol-Gel Science and Technology* **2012,** *63* (3), 315-339.
72. Dudása, Z.; Chiriac, A.; Preda, G., Simple entrapment of alcalase in different silica xerogels using the two steps sol-gel method. . *Annals of West University of Timisoara: Series of Chemistry* **2011,** *20* (4), 97-104.
73. Green, J. W.; Rubal, M. J.; Osman, B. M.; Welsch, R. L.; Cassidy, P. E.; Fitch, J. W.; Blanda, M. T., Silicon-organic hybrid polymers and composites prepared in supercritical carbon dioxide. *Polymers for Advanced Technologies* **2000,** *11* (8-12), 820-825.
74. 25th anniversary advanced materials. *Advanced Materials* **2014,** *26* (14), 2116-2118.
75. Téllez, L.; Rubio, J.; Rubio, F.; Morales, E.; Oteo, J. L., FT-IR Study of the Hydrolysis and Polymerization of Tetraethyl Orthosilicate and Polydimethyl Siloxane in the Presence of Tetrabutyl Orthotitanate. *Spectroscopy Letters* **2004,** *37* (1), 11-31.
76. Van Tendeloo, G.; Bals, S.; Van Aert, S.; Verbeeck, J.; Van Dyck, D., Advanced Electron Microscopy for Advanced Materials. *Advanced Materials* **2012,** *24* (42), 5655-5675.
77. Myers, R. M.; Fitzpatrick, D. E.; Turner, R. M.; Ley, S. V., Flow Chemistry Meets Advanced Functional Materials. *Chemistry – A European Journal* **2014,** *20* (39), 12348-12366.
78. Kraytsberg, A.; Ein-Eli, Y., Review of Advanced Materials for Proton Exchange Membrane Fuel Cells. *Energy & Fuels* **2014,** *28* (12), 7303-7330.
79. Li, W.; Wang, F.; Feng, S.; Wang, J.; Sun, Z.; Li, B.; Li, Y.; Yang, J.; Elzatahry, A. A.; Xia, Y.; Zhao, D., Sol–Gel Design Strategy for Ultradispersed TiO2 Nanoparticles on Graphene for High-Performance Lithium Ion Batteries. *Journal of the American Chemical Society* **2013,** *135* (49), 18300-18303.
80. Peng, J.; Xu, K.; Cai, H.; Wu, J.; Lin, W.; Yu, Z.; Chen, M., Can an intact and crystalline octakis(methacryloxypropyl) silsesquioxane be prepared by hydrolysis-condensation of a trimethoxysilane precursor? *RSC Advances* **2014,** *4* (14), 7124-7131.

81. Peng, J.; Xu, K.; Cai, H. L.; Wu, J. C.; Lin, W. H.; Yu, Z. W.; Chen, M. C., *Can an intact and crystalline octakis(methacryloxypropyl) silsesquioxane be prepared by hydrolysis-condensation of a trimethoxysilane precursor?* Royal society of Chemistry: 2014.
82. Shimura, N.; Ogawa, M., Preparation of surfactant templated nanoporous silica spherical particles by the Stöber method. Effect of solvent composition on the particle size. *Journal of Materials Science* **2007,** *42* (14), 5299-5306.
83. Ervithayasuporn, V.; Chimjarn, S., Synthesis and Isolation of Methacrylate- and Acrylate-Functionalized Polyhedral Oligomeric Silsesquioxanes (T8, T10, and T12) and Characterization of the Relationship between Their Chemical Structures and Physical Properties. *Inorganic Chemistry* **2013,** *52* (22), 13108-13112.
84. Assink, R. A.; Kay, B. D., *The Chemical-Kinetics of Silicate Sol-Gels - Functional-Group Kinetics of Tetraethoxysilane*. colloids and surfaces A:Physicochemical and engineering aspects: 1992; Vol. 74.
85. Hemali, R.; John, F., Donor and Acceptor Functionalized Silsesquioxane Nanostructures for Organic-Based Photovoltaic Devices. In *Organic Solar Cells*, CRC Press: 2015; pp 19-42.
86. Bogdana, S.; Irina-Elena, B.; Magdalena, A.; Florica, D.; Corneliu, C.; Mihaela, O., Protective Coatings Based on Silsesquioxane Nanocomposite Materials. In *Polymer Nanocomposite Coatings*, CRC Press: 2013; pp 213-244.
87. Costela, A.; García-Moreno, I.; Cerdán, L.; Martín, V.; Pérez-Ojeda, M. E.; García, O.; Sastre, R., Solid-state Scatty Lasers Based on Nanohybrid POSS Composites. In *Polymer Processing and Characterization*, Apple Academic Press: 2012; pp 91-108.
88. Panov, A. A.; Zaikov, G. E.; Panov, A. K., Nanotechnologies in Polymer Processing. In *Multicomponent Polymeric Materials*, Apple Academic Press: 2013; pp 49-53.
89. Roberto, J. J. W.; Jean-Pierre, P., Phase Morphology of Nanostructured Thermosetting Multiphase Blends. In *Micro- and Nanostructured Multiphase Polymer Blend Systems*, CRC Press: 2005; pp 359-390.
90. Arguello, J.; Magosso, H. A.; Landers, R.; Pimentel, V. L.; Gushikem, Y., Synthesis, characterization and electroanalytical application of a new SiO2/SnO2 carbon ceramic electrode. *Electrochimica Acta* **2010,** *56* (1), 340-345.
91. Sahoo, S.; Chakraborti, C. K.; Mishra, S. C.; Naik, S., Analytical Characterization of a Gelling Biodegradable Polymer. *Drug Invention Today* **2011,** *3* (6), 78-82.
92. El Aziz, Y.; Bassindale, A. R.; Taylor, P. G.; Horton, P. N.; Stephenson, R. A.; Hursthouse, M. B., *Facile synthesis of novel functionalized silsesquioxane nanostructures containing an encapsulated fluoride anion*. 2012.
93. Wu, M.; Wu, R. a.; Li, R.; Qin, H.; Dong, J.; Zhang, Z.; Zou, H., Polyhedral Oligomeric Silsesquioxane as a Cross-linker for Preparation of Inorganic−Organic Hybrid Monolithic Columns. *Analytical Chemistry* **2010,** *82* (13), 5447-5454.
94. Cordes, D. B.; Lickiss, P. D.; Rataboul, F., Recent developments in the chemistry of cubic polyhedral oligosilsesquioxanes. *Chemical Reviews* **2010,** *110* (4), 2081-2173.
95. Wu, J.; Mather, P. T., POSS Polymers: Physical Properties and Biomaterials Applications. *Polymer Reviews* **2009,** *49* (1), 25-63.
96. Poinescu, A. A.; Doncea, S.-M.; Ion, R. M., Characterization of Hydroxyapatite Materials by FTIR Spectroscopy. *Caracterizarea hydroxyapatitei prin spectroscopie FTIR.* **2010,** *62* (3A), 149-154.

97. Simone, G.; Perozziello, G., UV/Vis visible optical waveguides fabricated using organic-inorganic nanocomposite layers. *Journal Of Nanoscience And Nanotechnology* **2011,** *11* (3), 2057-2063.
98. Wallace, W. E.; Guttman, C. M.; Antonucci, J. M., Molecular structure of silsesquioxanes determined by matrix-assisted laser desorption/ionization time-of-flight mass spectrometry. *Journal of the American Society for Mass Spectrometry* **1999,** *10* (3), 224-230.
99. Yasmin, F.; Aaron, T.; Alexander, M. S., POSS-Containing Nanocomposite Polymer Coatings. In *Polymer Nanocomposite Coatings*, CRC Press: 2013; pp 245-276.
100. Yiu-Wing, M.; Shing-Chung, W., Performance Synergism in Polymer-Based Hybrid Materials. In *Advanced Polymeric Materials*, CRC Press: 2003.
101. Zotou, A., An overview of recent advances in HPLC instrumentation. *Central European Journal of Chemistry* **2012,** *10* (3), 554.
102. Kotler, P. and Levy, S.J. (1969), Broadening the concept of marketing, Journal of Marketing, 33(1), pp.10-15.
103. Mishra, A. K.; Bose, S.; Kuila, T.; Kim, N. H.; Lee, J. H., Silicate-based polymer-nanocomposite membranes for polymer electrolyte membrane fuel cells. *Progress in Polymer Science* **2012,** *37* (6), 842-869.
104. Wang, L.; Lu, S.; Zhou, Y.; Guo, X.; Lu, Y.; He, J.; Evans, D. G., Facile synthesis of metal–organic cobalt hydroxide nanorods exhibiting a reversible structural transitionElectronic supplementary information (ESI) available: Instrumentation, FT-IR, PXRD, TGA, UV-visible diffuse reflectance and EDX spectra, and. *Chemical Communications* **2011,** *47* (39), 11002-11004.
105. Nørgaard, A. W.; Wolkoff, P.; Lauritsen, F. R., Characterization of nanofilm spray products by mass spectrometry. *Chemosphere* **2010,** *80* (11), 1377-1386.
106. Baumgaertel, A.; Altuntaş, E.; Schubert, U. S., Recent developments in the detailed characterization of polymers by multidimensional chromatography. *Journal of Chromatography A* **2012,** *1240*, 1-20.
107. Nunes, M.; Gushikem, Y.; Landers, R.; Dupont, J.; Costa, T.; Benvenutti, E., Charged silsesquioxane used as a vehicle for gold nanoparticles to perform the synthesis of catalyst xerogels. *Journal of Sol-Gel Science and Technology*, 1-8.
108. Silva, P. R.; Almeida, V. O.; Machado, G. B.; Benvenutti, E. V.; Costa, T. M. H.; Gallas, M. R., Surfactant-Based Dispersant for Multiwall Carbon Nanotubes to Prepare Ceramic Composites by a Sol–Gel Method. *Langmuir* **2011,** *28* (2), 1447-1452.
109. Hosseini Nejad, E.; Paoniasari, A.; Koning, C. E.; Duchateau, R., Semi-aromatic polyesters by alternating ring-opening copolymerisation of styrene oxide and anhydrides. *Polymer Chemistry* **2012,** *3* (5), 1308-1313.
110. Fang, M.; Wang, K.; Lu, H.; Yang, Y.; Nutt, S., Single-layer graphene nanosheets with controlled grafting of polymer chains. *Journal of Materials Chemistry* **2010,** *20* (10), 1982-1992.
111. Kato, K.; Uchida, E.; Kang, E.-T.; Uyama, Y.; Ikada, Y., Polymer surface with graft chains. *Progress in Polymer Science* **2003,** *28* (2), 209-259.
112. Brevett, C. S.; Cagle, P. C.; Klemperer, W. G.; Millar, D. M.; Ruben, G. C., Synthesis and sol-gel polymerization. *Journal of Inorganic and Organometallic Polymers* **1991,** *1* (3), 335-342.
113. Maegawa, Y.; Mizoshita, N.; Tani, T.; Shimada, T.; Inagaki, S., Enhanced sol-gel polymerization of organoallylsilanes by solvent effect. *Journal of Materials Chemistry* **2011,** *21* (36), 14020-14024.
114. (a) Lu, T.; Cui, F., Synthesis and Properties of Non-functional Cubic Silsesquioxane Macromonomers. *Designed Monomers & Polymers* **2010,** *13*

(1), 73-85; (b) Matějka, L.; Dukh, O.; Brus, J.; Simonsick Jr, W. J.; Meissner, B., Cage-like structure formation during sol–gel polymerization of glycidyloxypropyltrimethoxysilane. *Journal of Non-Crystalline Solids* **2000,** *270* (1–3), 34-47.
115. Izunobi, J. U.; Higginbotham, C. L., Polymer Molecular Weight Analysis by 1H NMR Spectroscopy. *Journal of Chemical Education* **2011,** *88* (8), 1098-1104.
116. Lucenti, E.; Feher, F. J.; Ziller, J. W., Synthesis and Characterization of Osmium-Containing Silsesquioxanes: High-Yield Routes. *Organometallics* **2006,** *26* (1), 75-82.
117. Lee, D. W.; Kawakami, Y., Incompletely Condensed Silsesquioxanes: Formation and Reactivity. *Polym. J* **2007,** *39* (3), 230-238.
118. He, Y.; Wang, J.-A.; Pei, C.-L.; Song, J.-Z.; Zhu, D.; Chen, J., Novel epoxy-silicone thermolytic transparent packaging adhesives chemical modified by ZnO nanowires for HB LEDs. *Journal of Nanoparticle Research* **2010,** *12* (8), 3019-3024.
119. Joshi, M.; Butola, B. S., Polymeric Nanocomposites—Polyhedral Oligomeric Silsesquioxanes(POSS) as Hybrid Nanofiller. *Journal of Macromolecular Science: Polymer Reviews* **2004,** *44* (4), 389-410.
120. Sugahara, Y.; Okada, S.; Kuroda, K.; Kato, C., *Si-29-Nmr Study of Hydrolysis and Initial Polycondensation Processes of Organoalkoxysilanes .1. Dimethyldiethoxysilane*. 1992.
121. Schmidt, H.; Scholze, H.; Kaiser, A., Principles of hydrolysis and condensation reaction of alkoxysilanes. *Journal of Non-Crystalline Solids* **1984,** *63* (1–2), 1-11.
122. Sanchez, J.; McCormick, A., Kinetic and thermodynamic study of the hydrolysis of silicon alkoxides in acidic alcohol solutions. *The Journal of Physical Chemistry* **1992,** *96* (22), 8973-8979.
123. Malay, O.; Yilgor, I.; Menceloglu, Y., Effects of solvent on TEOS hydrolysis kinetics and silica particle size under basic conditions. *J Sol-Gel Sci Technol* **2013,** *67* (2), 351-361.
124. Dickson, D.; Ely, R., Silica sol-gel encapsulation of cyanobacteria: lessons for academic and applied research. *Applied Microbiology & Biotechnology* **2013,** *97* (5), 1809-1819.
125. Green, D. L.; Lin, J. S.; Lam, Y.-F.; Hu, M. Z. C.; Schaefer, D. W.; Harris, M. T., Size, volume fraction, and nucleation of Stober silica nanoparticles. *Journal of Colloid and Interface Science* **2003,** *266* (2), 346-358.
126. Brinker, C. J.; Assink, R. A., *Spinnability of Silica Sols - Structural and Rheological Criteria*. ELSEVIER SCIENCE BV: 1989.
127. Kelts, L. W.; Armstrong, N. J., *A Si-29 Nmr-Study of the Structural Intermediates in Low Ph Sol-Gel Reactions*. Journal of materials research; Mar-Apr, 1989, 4 2, p423-p433, 11p. : 1989.
128. Bauer, F.; Sauerland, V.; Ernst, H.; Glasel, H. A.; Naumov, S.; Mehnert, R., *Preparation of scratch- and abrasion-resistant polymeric nanocomposites by monomer grafting onto nanoparticles, 4 - Application of MALDI-TOF mass spectrometry to the characterization of surface modified nanoparticles*.
129. Terracciano, R.; Casadonte, F.; Pasqua, L.; Candeloro, P.; Di Fabrizio, E.; Urbani, A.; Savino, R., Enhancing plasma peptide MALDI-TOF-MS profiling by mesoporous silica assisted crystallization. *Talanta* **2010,** *80* (4), 1532-1538.
130. Tadanaga, K.; Morita, K.; Mori, K.; Tatsumisago, M., Synthesis of monodispersed silica nanoparticles with high concentration by the Stöber process. *Journal of Sol-Gel Science and Technology* **2013,** *68* (2), 341-345.

131. Lee, K.; Sathyagal, A. N.; McCormick, A. V., A closer look at an aggregation model of the Stöber process. *Colloids and Surfaces A: Physicochemical and Engineering Aspects* **1998,** *144* (1–3), 115-125.
132. Wang, X.-D.; Shen, Z.-X.; Sang, T.; Cheng, X.-B.; Li, M.-F.; Chen, L.-Y.; Wang, Z.-S., Preparation of spherical silica particles by Stöber process with high concentration of tetra-ethyl-orthosilicate. *Journal of Colloid and Interface Science* **2010,** *341* (1), 23-29.
133. Kust, P. R.; Hendel, R. A.; Markowitz, M. A.; Schoen, P. E.; Gaber, B. P., Effect of surfactant and oil type on the solution synthesis of nanosized silica. *Colloids and Surfaces A: Physicochemical and Engineering Aspects* **2000,** *168* (3), 207-214.
134. Bazuła, P. A.; Arnal, P. M.; Galeano, C.; Zibrowius, B.; Schmidt, W.; Schüth, F., Highly microporous monodisperse silica spheres synthesized by the Stöber process. *Microporous and Mesoporous Materials* **2014,** *200* (0), 317-325.
135. Goodarzi, K.; Ramezani, S. R.; Hajati, S., Reducing thermal contact resistance using nanocoating. *Applied Thermal Engineering* **2014,** *70* (1), 641-646.
136. Raul, A.; Das, D.; Timande, S. M., Nanotechnology -A new vision of coating technology. *Paintindia* **2010,** *60* (9), 61-74.
137. Chen, H.; Bujalski, D.; Su, K., Characterization of low molecular weight components of silsesquioxanes by electrospray ionization fourier transform mass spectrometry (ESI-FTMS). *Journal of The American Society for Mass Spectrometry* **2005,** *16* (4), 524-534.
138. Gholami, T.; Salavati-Niasari, M.; Bazarganipour, M.; Noori, E., Synthesis and characterization of spherical silica nanoparticles by modified Stöber process assisted by organic ligand. *Superlattices and Microstructures* **2013,** *61* (0), 33-41.
139. Yan, L.; Yang, Y.; Zhang, W.; Chen, X., Nanotechnology: Advanced Materials and Nanotechnology for Drug Delivery (Adv. Mater. 31/2014). *Advanced Materials* **2014,** *26* (31), 5576-5576.
140. Rao, K. S.; El-Hami, K.; Kodaki, T.; Matsushige, K.; Makino, K., A novel method for synthesis of silica nanoparticles. *Journal of Colloid and Interface Science* **2005,** *289* (1), 125-131.
141. Libermana, A.; , N. M.; , W. C. T.; , A. C. K., n, Synthesis and surface functionalization of silica nanoparticles for nanomedicine. *Surface Science Reports* **2015,** *70* (3), IFC.
142. Aikawa, K.; Kaneko, K.; Tamura, T.; Fujitsu, M.; Ohbu, K., Formation of fractal porous silica by hydrolysis of TEOS in a bicontinuous microemulsion. *Colloids and Surfaces A: Physicochemical and Engineering Aspects* **1999,** *150* (1–3), 95-104.
143. Yu, K.; Guo, Y.; Ding, X.; Zhao, J.; Wang, Z., Synthesis of silica nanocubes by sol–gel method. *Materials Letters* **2005,** *59* (29–30), 4013-4015.
144. Romero, A. I.; Parentis, M. L.; Habert, A. C.; Gonzo, E. E., Synthesis of polyetherimide/silica hybrid membranes by the sol-gel process: influence of the reaction conditions on the membrane properties. *Journal of Materials Science* **2011,** *46* (13), 4701-4709.
145. Nils, P.; Niklas, S.; Gabi, S.; Ralf, T.; Benedikt, S.; Martin, S. B.; Christian, H.; Christof, S.; Hartmut, W., Plasma synthesis of nanostructures for improved thermoelectric properties. *Journal of Physics: D Applied Physics* **2011,** *44* (17), 174034-174034.
146. Tarn, D.; Ashley, C. E.; Xue, M.; Carnes, E. C.; Zink, J. I.; Brinker, C. J., *Mesoporous Silica Nanoparticle Nanocarriers: Biofunctionality and Biocompatibility*. AMER CHEMICAL SOC: 2013.

147. Blanco, I.; Abate, L.; Bottino, F.; Bottino, P.; Chiacchio, M., Thermal degradation of differently substituted Cyclopentyl Polyhedral Oligomeric Silsesquioxane (CP-POSS) nanoparticles. *Journal of Thermal Analysis & Calorimetry* **2012,** *107* (3), 1083-1091.
148. Rahman, I. A.; Padavettan, V., Synthesis of Silica Nanoparticles by Sol-Gel: Size-Dependent Properties, Surface Modification, and Applications in Silica-Polymer Nanocomposites-A Review. *Journal of Nanomaterials* **2012**, 1-15.
149. Plumeré, N.; Ruff, A.; Speiser, B.; Feldmann, V.; Mayer, H. A., Stöber silica particles as basis for redox modifications: Particle shape, size, polydispersity, and porosity. *Journal of Colloid and Interface Science* **2012,** *368* (1), 208-219.
150. Jafarzadeh, M.; Rahman, I. A.; Sipaut, C. S., Synthesis of silica nanoparticles by modified sol–gel process: the effect of mixing modes of the reactants and drying techniques. *Journal of Sol-Gel Science and Technology* **2009,** *50* (3), 328-336.
151. Liu, H.; Li, H.; Ding, Z.; Fu, A.; wang, H.; Guo, P.; Yu, J.; Wang, C.; Zhao, X., Preparation of Porous Hollow SiO2 Spheres by a Modified Stöber Process Using MF Microspheres as Templates. *J Clust Sci* **2012,** *23* (2), 273-285.
152. Rahman, I. A.; Vejayakumaran, P.; Sipaut, C. S.; Ismail, J.; Bakar, M. A.; Adnan, R.; Chee, C. K., An optimized sol–gel synthesis of stable primary equivalent silica particles. *Colloids and Surfaces A: Physicochemical and Engineering Aspects* **2007,** *294* (1–3), 102-110.
153. Trofimova, E.; Aleksenskii, A.; Grudinkin, S.; Korkin, I.; Kurdyukov, D.; Golubev, V., Effect of tetraethoxysilane pretreatment on synthesis of colloidal particles of amorphous silicon dioxide. *Colloid Journal* **2011,** *73* (4), 546-550.
154. Yang, Y.; Yan, X. H.; Cui, Y.; He, Q.; Li, D. X.; Wang, A. H.; Fei, J. B.; Li, J. B., *Preparation of polymer-coated mesoporous silica nanoparticles used for cellular imaging by a "graft-from" method*.
155. Matsoukas, T.; Gulari, E., *Self-Sharpening Distributions Revisited Polydispersity in Growth by Monomer Addition*. 1998.
156. Arantes, T. M.; Pinto, A. H.; Leite, E. R.; Longo, E.; Camargo, E. R., Synthesis and optimization of colloidal silica nanoparticles and their functionalization with methacrylic acid. *Colloids and Surfaces A: Physicochemical and Engineering Aspects* **2012,** *415* (0), 209-217.
157. Bogush, G. H.; Tracy, M. A.; Zukoski Iv, C. F., Preparation of monodisperse silica particles: Control of size and mass fraction. *Journal of Non-Crystalline Solids* **1988,** *104* (1), 95-106.
158. Flory, P. J., Principles of Polymer Chemistry. *Cornell University Press* **1953**.
159. Tanaka, T., Fillmore, D.J., , Kinetics of swelling of gels. *J. Chem. Phys* **1979,** *70* (3), 1214-1218.
160. Howard, A. G.; Khdary, N. H., Spray synthesis of monodisperse sub-micron spherical silica particles. *Materials Letters* **2007,** *61* (8–9), 1951-1954.
161. Van Helden, A. K.; Jansen, J. W.; Vrij, A., Preparation and characterization of spherical monodisperse silica dispersions in nonaqueous solvents. *Journal of Colloid and Interface Science* **1981,** *81* (2), 354-368.
162. Park, J.-H.; Kim, Y.-G.; Oh, C.; Shin, S.-I.; Kim, Y.-C.; Oh, S.-G.; Kong, S.-H., Fabrication of hollow silver spheres by MPTMS-functionalized hollow silica spheres as templates. *Materials Research Bulletin* **2005,** *40* (2), 271-280.
163. Roberto Sato-Berrú1, J. M. S., José Flores-Flores1 and María Sanchez-Espíndola2, Simple Method for the Controlled Growth of SiO_2 Spheres. *Journal of Materials Science and Engineering* **2013,** *3* (4), 237-242.
164. Yang, Y.; Song, W.; Wang, A.; Zhu, P.; Fei, J.; Li, J., Lipid coated mesoporous silica nanoparticles as photosensitive drug carriers. *Physical Chemistry Chemical Physics* **2010,** *12* (17), 4418-4422.

165. Terashima, T.; Sugita, T.; Fukae, K.; Sawamoto, M., Synthesis and Single-Chain Folding of AmphiphilicRandom Copolymers in Water. *Macromolecules* **2014,** *47* (2), 589-600.
166. Perruchot, C.; Khan, M. A.; Kamitsi, A.; Armes, S. P.; Watts, J. F.; von Werne, T.; Patten, T. E., XPS characterisation of core–shell silica–polymer composite particles synthesised by atom transfer radical polymerisation in aqueous media. *European Polymer Journal* **2004,** *40* (9), 2129-2141.
167. Mai, T.; Tran, T.; Rafiqul Islam, M.; Park, J.; Lim, K., Covalent functionalization of silica nanoparticles with poly(N-isopropylacrylamide) employing thiol-ene chemistry and activator regenerated by electron transfer ATRP protocol. *Journal of Materials Science* **2014,** *49* (4), 1519-1526.
168. Ou, B.; Yang, G.; Xiao, Y.; Zeng, X.; Zhou, Z.; Liu, Q.; Zhang, X.; Li, D., Covalent Functionalization of Silica Nanoparticle with Poly(glycidyl methacrylate) via ATRP at Ambient Temperature. *Journal of Macromolecular Science: Pure & Applied Chemistry* **2013,** *50* (1), 25-28.
169. Boday, D. J.; Keng, P. Y.; Muriithi, B.; Pyun, J.; Loy, D. A., *Mechanically reinforced silica aerogel nanocomposites via surface initiated atom transfer radical polymerizations*.
170. Matyjaszewski, K.; Tsarevsky, N. V., Nanostructured functional materials prepared by atom transfer radical polymerization. *Nature Chemistry* **2009,** *1* (4), 276-288.
171. Strauss, M.; Damasceno, J. P. V.; Maroneze, C. M.; Costa, L. P.; Sigoli, F. A.; Gushikem, Y.; Mazali, I. O., Exploring the functionalization ratio of mesoporous silica glass with imidazolium entities on the synthesis of supported gold nanoparticles. *Journal of Nanoparticle Research* **2013,** *15* (3), 1-10.
172. Yu, H.; Wenlong, G.; Hong, Y.; You, W.; Loy, D. A., Modification of a Phenolic Resin with Epoxy- and Methacrylate-Functionalized Silica Sols to Improve the Ablation Resistance of Their Glass Fiber-Reinforced Composites. *Polymers (20734360)* **2014,** *6* (1), 105-113.
173. Chiang, C.-L.; Ma, C.-C. M., Synthesis, characterization, thermal properties and flame retardance of novel phenolic resin/silica nanocomposites. *Polymer Degradation and Stability* **2004,** *83* (2), 207-214.
174. Bywalez, R.; Karacuban, H.; Nienhaus, H.; Schulz, C.; Wiggers, H., Stabilization of mid-sized silicon nanoparticles by functionalization with acrylic acid. *Nanoscale Research Letters* **2012,** *7* (1), 76-76.
175. Woods, R.; Feldbacher, S.; Langer, G.; Satzinger, V.; Schmidt, V.; Kern, W., Epoxy silicone based matrix materials for two-photon patterning of optical waveguides. *Polymer* **2011,** *52*, 3031-3037.
176. Hermida, L.; Abdullah, A. Z.; Mohamed, A. R., Synthesis and Characterization of Mesostructured Cellular Foam (MCF) Silica Loaded with Nickel Nanoparticles as a Novel Catalyst. *Materials Sciences & Applications* **2013,** *4* (1), 52-62.
177. Rahman, I. A.; Padavettan, V., Synthesis of Silica Nanoparticles by Sol-Gel: Size-Dependent Properties, Surface Modification, and Applications in Silica-Polymer Nanocomposites—A Review. *Journal of Nanomaterials* **2012,** *2012*, 15.
178. Van Doren, E. A. F.; De Temmerman, P.-J. R. H.; Francisco, M. A. D.; Mast, J., Determination of the volume-specific surface area by using transmission electron tomography for characterization and definition of nanomaterials. *Journal of Nanobiotechnology* **2011,** *9* (1), 17-24.
179. Szekeres, M.; Tóth, J.; Dékány, I., Specific Surface Area of Stoeber Silica Determined by Various Experimental Methods. *Langmuir* **2002,** *18* (7), 2678-2685.

180. (a) Achatz, D. E.; Heiligtag, F. J.; Li, X.; Link, M.; Wolfbeis, O. S., Colloidal silica nanoparticles for use in click chemistry-based conjugations and fluorescent affinity assays. *Sensors and Actuators B: Chemical* **2010,** *150* (1), 211-219; (b) Bexell, U.; Berger, R.; Olsson, M.; Grehk, T. M.; Sundell, P. E.; Johansson, M., Bonding of vegetable oils to mercapto silane treated metal surfaces: Surface engineering on the nano scale. *Thin Solid Films* **2006,** *515* (2), 838-841.
181. Luo, J. J.; Chu, W.; Sall, S.; Petit, C., *Facile synthesis of monodispersed Au nanoparticles-coated on Stober silica*. Colloids and surfaces a-physicochemical and engineering aspects:, MAY 20, 2013, ; Vol. 425 p83-p91, 9p.
182. (a) Marjorie, S.; Sophie, B.; Khalil, J., Friction of Graphite against Silane-Functionalized Silicon Wafers. In *Surfactants in Tribology, Volume 2*, CRC Press: 2011; pp 47-84; (b) Wilma, K. D.; Louis, A. E. M. R.; Annemieke, J. W. T. B.; Jacques, W. M. N., Silane coupling agents for silica-filled tire-tread compounds. In *Silanes and Other Coupling Agents, Volume 3*, CRC Press: 2004; pp 89-103.
183. Tang, P.; Ritter, T., Silver-mediated fluorination of aryl silanes. *Tetrahedron* **2011,** *67* (24), 4449-4454.
184. Delafosse, G.; Merlen, A.; Clair, S.; Patrone, L., A surface enhanced Raman spectroscopy study of aminothiophenol and aminothiophenol-C60 self-assembled monolayers: Evolution of Raman modes with experimental parameters. *Journal of Chemical Physics* **2012,** *136* (19), 194704.
185. Song, C.; Hayakawa, S.; Shirosaki, Y.; Fujii, E.; Kawabata, K.; Tsuru, K.; Osaka, A., Sol–Gel Synthesis and Microstructure Analysis of Amino-Modified Hybrid Silica Nanoparticles from Aminopropyltriethoxysilane and Tetraethoxysilane. *Journal of the American Ceramic Society* **2009,** *92* (9), 2074-2082.
186. Brus, J.; Dybal, J., Copolymerization of tetraethoxysilane and dimethyl(diethoxy)silane studied by 29Si NMR and ab initio calculations of 29Si NMR chemical shifts. *Polymer* **1999,** *40* (25), 6933-6945.
187. Bounor-Legaré, V.; Angelloz, C.; Blanc, P.; Cassagnau, P.; Michel, A., A new route for organic–inorganic hybrid material synthesis through reactive processing without solvent. *Polymer* **2004,** *45* (5), 1485-1493.
188. Ruff, A.; Schuler, P.; Speiser, B., Redox-active silica nanoparticles. Part 6. Synthesis and spectroscopic and electrochemical characterization of viologen-modified Stöber silica particles with diameters of approximately 125 nm. *J Solid State Electrochem* **2013,** *17* (1), 79-97.
189. Pattanayak, A.; Subramanian, A., Impact of Porogens on the Pore Characteristics of Zirconia Particles Made by Polymer-Induced Colloid Aggregation. *International Journal of Applied Ceramic Technology* **2011,** *8* (1), 94-111.
190. (a) Mao, P.; Zhangjie, L.; Zhongming, Z.; Honglei, G.; Huijun, W., Fumed silica/polymer hybrid nanoparticles prepared by redox-initiated graft polymerization in emulsions. *Journal of Materials Science* **2009,** *44* (23), 6286-6293; (b) Cao, J.; Matsoukas, T., Deposition kinetics on particles in a dusty plasma reactor. *Journal of Applied Physics* **2002,** *92* (5), 2916.
191. Baer, D. R.; Gaspar, D. J.; Nachimuthu, P.; Techane, S. D.; Castner, D. G., Application of surface chemical analysis tools for characterization of nanoparticles. *Analytical & Bioanalytical Chemistry* **2010,** *396* (3), 983-1002.
192. Ayrat, M.; Sebastian, G.; Kay, N., Measurement of element mass distributions in particle ensembles applying ICP-OESResearch has been performed within the network Plasma-Analyte Interaction Working Group (PAIWG). PAIWG is a collaborative effort of the University of Florida (Gainesville. *JAAS (Journal of Analytical Atomic Spectrometry)* **2010,** *25* (9), 1395-1401.
193. Lijun, Z.; Yunhui, Z.; XijunChang; Qun, H.; Xinping, H.; Zheng, H., Determination of trace metals in natural samples by ICP-OES after preconcentration

on modified silica gel and on modified silica nanoparticles. *Microchimica Acta* **2009,** *165* (3/4), 319-327.
194. Ogoshi, T.; Chujo, Y., Organic–inorganic polymer hybrids prepared by the sol-gel method. *Composite Interfaces* **2005,** *11* (8/9), 539-566.
195. Aneli, J.; Mukbaniani, O.; Markarashvili, E.; Zaikov, G. E.; Klodzinska, E., A Study on Physical Properties of Composites Based on Epoxy Resin. In *Key Elements in Polymers for Engineers and Chemists*, Apple Academic Press: 2014; pp 333-342.
196. (a) LoïcLe, P., Epoxy-Based Nanocomposites. In *Recent Advances in Polymer Nanocomposites*, CRC Press: 2010; pp 75-136; (b) Ying-ling, L.; Yu-Jane, C.; Yao-Hsuan, W.; Chuan-shao, W., Preparation and properties of epoxy/maleimide compounds and their cured resins. In *Polyimides and Other High Temperature Polymers*, CRC Press: 2005; pp 141-154.
197. Zaragoza, S.; lvarez, A.; Tarrío-Saavedra, J.; lvarez, B.; Naya, S.; Gómez, S., Thermal stability of epoxies for recreational crafts. In *Developments in Maritime Transportation and Exploitation of Sea Resources*, CRC Press: 2013; pp 435-440.
198. Gu, J.; Wu, Y.; Wang, J.; Lu, Y.; Ren, X., In situ assembly of ZSM-5 nanocrystals into micro-sized single-crystal-like aggregates via acid-catalyzed hydrolysis of tetraethylorthosilicate. *Journal of Materials Science* **2009,** *44* (14), 3777-3783.
199. Cattoën, X.; Noureddine, A.; Croissant, J.; Moitra, N.; Bürglová, K.; Hodačová, J.; de los Cobos, O.; Lejeune, M.; Rossignol, F.; Toulemon, D.; Bégin-Colin, S.; Pichon, B.; Raehm, L.; Durand, J.-O.; Wong Chi Man, M., Click approaches in sol–gel chemistry. *Journal of Sol-Gel Science and Technology* **2014,** *70* (2), 245-253.
200. Laughlin, J. B.; Sarquis, J. L.; Jones, V. M.; Cox, J. A., Using Sol-Gel Chemistry to Synthesize a Material with Properties Suited for Chemical Sensing. Development and Implementation of a Materials Science Experiment for the Undergraduate Curriculum. *Journal of Chemical Education* **2000,** *77* (1), 77.
201. Poole, C. F., Advanced materials for separation science. *Journal of Chromatography A* **2014,** *1357* (0), 1.
202. Türe, H.; Blomfeldt, T. O. J.; Gällstedt, M.; Hedenqvist, M. S.; Farris, S., Nanostructured Silica/Wheat Gluten Hybrid Materials Prepared by Catalytic Sol–Gel Chemistry. *Macromolecular Chemistry and Physics* **2013,** *214* (10), 1131-1139.
203. Ponyrko, S.; Kobera, L.; Brus, J.; Matějka, L., Epoxy-silica hybrids by nonaqueous sol–gel process. *Polymer* **2013,** *54* (23), 6271-6282.
204. Liu, C.; Li, F.; Ma, L.-P.; Cheng, H.-M., Advanced Materials for Energy Storage. *Advanced Materials* **2010,** *22* (8), E28-E62.
205. Jeong, B.; Kim, S. W.; Bae, Y. H., Thermosensitive sol–gel reversible hydrogels. *Advanced Drug Delivery Reviews* **2012,** *64, Supplement* (0), 154-162.
206. Lakshmi, R. V.; Bharathidasan, T.; Basu, B. J., Superhydrophobic sol–gel nanocomposite coatings with enhanced hardness. *Applied Surface Science* **2011,** *257* (24), 10421-10426.
207. Wang, J.; Hu, M.; Fang, J.; Gao, H., Synthesis and Characterization of Copolymerized Vinyl/phenylsilsesquioxane Microspheres. *Journal of Macromolecular Science: Pure & Applied Chemistry* **2011,** *48* (11), 947-951.
208. Other Polymeric Applications in Photovoltaic Modules. In *Solar Module Packaging*, CRC Press: 2011; pp 181-206.
209. Keld, A. J.; Anne, T. S., Case Study: Paints and Lacquers with Silica Nanoparticles. In *Safety of Nanomaterials along Their Lifecycle*, CRC Press: 2014; pp 381-398.

210. Min, Z., Effects of Micro- and Nanoscale Texturing on Surface Adhesion and Friction. In *Micro- and Nanoscale Phenomena in Tribology*, CRC Press: 2011; pp 103-152.
211. Lukowiak, A.; Lao, J.; Lacroix, J.; Nedelec, J.-M., Bioactive glass nanoparticles obtained through sol-gel chemistry. *Chemical Communications* **2013,** *49* (59), 6620-6622.
212. Chi-Hwan Han, T.-y. C., Sang-Hoon Bae, Kwan-Woo Ko, Jae-Hyung Bak, Nanoparticle having Imidazolium salt Chemically bound thereto, method of preparing nanogel electrolyte for dye-sensitive solar cell. **2013**.
213. Jafarzadeh, M.; Adnan, R.; Mazlan, M. K. N., Thermal stability and optical property of ormocers (organically modified ceramics) nanoparticles produced from copolymerization between amino-silanes and tetraethoxysilane. *Journal of Non-Crystalline Solids* **2012,** *358* (22), 2981-2987.
214. Wang, N.; Guo, Y.; Wang, L.; Liang, X.; Liu, S.; Jiang, S., Preparation of an aminopropyl imidazole-modified silica gel as a sorbent for solid-phase extraction of carboxylic acid compounds and polycyclic aromatic hydrocarbons. *Analyst* **2014,** *139* (10), 2531-2537.
215. Van Der Voort, P.; Vrancken, K. C.; Vansant, E. F., Gas-phase chlorosilylation of silica gel: effectiveness, surface coverage and stoichiometry. *Journal of the Chemical Society, Faraday Transactions* **1995,** *91* (2), 353-357.
216. Belam, W., Sol–gel chemistry synthesis and DTA–TGA, XRPD, SIC and 7Li, 31P, 29Si MAS–NMR studies on the Li-NASICON Li3Zr2−ySi2−4yP1+4yO12 system. *Journal of Alloys and Compounds* **2013,** *551* (0), 267-273.
217. Kurajica, S.; Tkalčec, E.; Gržeta, B.; Iveković, D.; Mandić, V.; Popović, J.; Kranzelić, D., Evolution of structural and optical properties in the course of thermal evolution of sol–gel derived cobalt-doped gahnite. *Journal of Alloys and Compounds* **2011,** *509* (7), 3223-3228.
218. Martini, F.; Borsacchi, S.; Geppi, M.; Pilati, F.; Toselli, M., Structure, dynamics and interactions of complex sol–gel hybrid materials through SSNMR and DSC: Part I, binary systems based on PE-PEG block copolymer, PHS and silica. *Polymer* **2011,** *52* (20), 4536-4544.
219. Queiroz, D. P. R.; Fraïsse, F.; Fayolle, B.; Kuntz, M.; Verdu, J., Radiochemical ageing of epoxy coating for nuclear plants. *Radiation Physics and Chemistry* **2010,** *79* (3), 362-364.
220. Gallardo, J.; Galliano, P.; Durán, A., Thermal Evolution of Hybrid Sol-Gel Silica Coatings: A Structural Analysis. *Journal of Sol-Gel Science and Technology* **2000,** *19* (1-3), 393-397.
221. Bittner, A.; Schmitt, A.; Jahn, R.; Löbmann, P., Characterization of stacked sol–gel films: Comparison of results derived from scanning electron microscopy, UV–vis spectroscopy and ellipsometric porosimetry. *Thin Solid Films* **2012,** *520* (6), 1880-1884.
222. Vera-Avila, L. E.; Márquez-Lira, B. P.; Villanueva, M.; Covarrubias, R.; Zelada, G.; Thibert, V., Determination of carbofuran in surface water and biological tissue by sol–gel immunoaffinity extraction and on-line preconcentration/HPLC/UV analysis. *Talanta* **2012,** *88* (0), 553-560.
223. Bagheri, H.; Piri-Moghadam, H.; Ahdi, T., Role of precursors and coating polymers in sol–gel chemistry toward enhanced selectivity and efficiency in solid phase microextraction. *Analytica Chimica Acta* **2012,** *742* (0), 45-53.
224. Careri, M.; Elviri, L.; Lorenzi, A.; Mangia, A.; Penna, A.; Predieri, G., Improved silica xerogel film processing for MALDI-TOF–MS quantitative analysis of peptides and small molecules. *Journal of Sol-Gel Science and Technology* **2011,** *60* (3), 359-365.

225. Dudarko, O. A.; Gunathilake, C.; Wickramaratne, N. P.; Sliesarenko, V. V.; Zub, Y. L.; Górka, J.; Dai, S.; Jaroniec, M., Synthesis of mesoporous silica-tethered phosphonic acid sorbents for uranium species from aqueous solutions. *Colloids and Surfaces A: Physicochemical and Engineering Aspects* **2015,** *482* (0), 1-8.
226. Kumarathasan, P.; Mohottalage, S.; Goegan, P.; Vincent, R., An optimized protein in-gel digest method for reliable proteome characterization by MALDI–TOF–MS analysis. *Analytical Biochemistry* **2005,** *346* (1), 85-89.
227. Bouanani, F.; Bendedouch, D.; Teixeira, J.; Marx, L.; Hemery, P., Characterization of a miniemulsion by DLS and SANS. *Colloids and Surfaces A: Physicochemical and Engineering Aspects* **2012,** *404* (0), 47-51.
228. Chen, Z. H.; Kim, C.; Zeng, X.-b.; Hwang, S. H.; Jang, J.; Ungar, G., Characterizing Size and Porosity of Hollow Nanoparticles: SAXS, SANS, TEM, DLS, and Adsorption Isotherms Compared. *Langmuir* **2012,** *28* (43), 15350-15361.
229. Meseguer, F.; Fenollosa, R.; Rodriguez, I.; Xifré-Pérez, E.; Ramiro-Manzano, F.; Garín, M.; Tymczenko, M., Silicon colloids: A new enabling nanomaterial. *Journal of Applied Physics* **2011,** *109* (10), 102424.
230. Hsu, C.-C.; Lan, W.-L.; Chen, N.-P.; Wu, C.-C., The hydrophobic and omnidirectional antireflection coating of SiO2 nanospheres with C18-TEOS. *Optics & Laser Technology* **2014,** *58* (0), 202-206.
231. Du, H.; Hamilton, P. D.; Reilly, M. A.; d'Avignon, A.; Biswas, P.; Ravi, N., A facile synthesis of highly water-soluble, core–shell organo-silica nanoparticles with controllable size via sol–gel process. *Journal of Colloid and Interface Science* **2009,** *340* (2), 202-208.
232. Rutherford, E., High Frequency Radiation of the X-Ray Type. *Science* **1929,** *69* (1784), 259-263.
233. Hale, G. E., National Academies and the Progress of Research. *Science* **1914,** *40* (1043), 907-919.
234. Nesbitt, H. W.; Dalby, K. N., High resolution O 1s XPS spectral, NMR, and thermodynamic evidence bearing on anionic silicate moieties (units) in PbO-SiO2 and Na2O-SiO2 glasses. *Canadian Journal of Chemistry* **2007,** *85* (10), 782-792.
235. Bo, Z.; Nieuwoudt, M.; Easteal, A. J., Sol–Gel Route to Nanocrystalline Lithium Metasilicate Particles. *Journal of the American Ceramic Society* **2008,** *91* (6), 1927-1932.
236. Matsuura, Y.; Miura, S.; Naito, H.; Inoue, H.; Matsukawa, K., Nanostructured polysilane–titania hybrids and their application to porous titania thin films. *Journal of Organometallic Chemistry* **2003,** *685* (1–2), 230-234.
237. Chen, M.-A.; Lu, X.-B.; Guo, Z.-H.; Huang, R., Influence of hydrolysis time on the structure and corrosion protective performance of (3-mercaptopropyl)triethoxysilane film on copper. *Corrosion Science* **2011,** *53* (9), 2793-2802.
238. Xie, Z.; Dao, B.; Hodgkin, J.; Hoang, M.; Hill, A.; Gray, S., Synthesis and characterization of hybrid organic-inorganic materials based on sulphonated polyamideimide and silica. *Journal of Polymer Research* **2011,** *18* (5), 965-973.
239. Karmakar, B.; De, G.; Ganguli, D., Dense silica microspheres from organic and inorganic acid hydrolysis of TEOS. *Journal of Non-Crystalline Solids* **2000,** *272* (2–3), 119-126.
240. Kameneva, O.; Kuznetsov, A.; Smirnova, L.; Rosez, L.; Sanchez, C.; Kanaev, A.; Alexandrov, A.; Bityurin, N., New hybrid organic-inorganic materials based on a poly(titanium oxide) gel with efficient UV-induced separation of charges. *Doklady Physics* **2006,** *51* (3), 103-105.
241. (a) Pfeifer, S.; Schwarzer, A.; Schmidt, D.; Brendler, E.; Veith, M.; Kroke, E., Precursors for pyromellit-bridged silica sol-gel hybrid materials. *New Journal of*

Chemistry **2013,** *37* (1), 169-180; (b) Oubaha, M.; Smaïhi, M.; Etienne, P.; Coudray, P.; Moreau, Y., Spectroscopic characterization of intrinsic losses in an organic–inorganic hybrid waveguide synthesized by the sol–gel process. *Journal of Non-Crystalline Solids* **2003,** *318* (3), 305-313.
242. Donatti, D. A.; Vollet, D. R., Study of the hydrolysis of TEOS-TMOS mixtures under ultrasound stimulation. *Journal of Non-Crystalline Solids* **1996,** *204* (3), 301-304.
243. Afonina, G.; Leonov, V.; Popova, O., Effect of the conditions of hydrolysis of tetraethoxysilane on the synthesis of forsterite. *Glass & Ceramics* **2008,** *65* (11/12), 447-451.
244. Brunet, F., Polymerization reactions in methyltriethoxysilane studied through 29Si NMR with polarization transfer. *Journal of Non-Crystalline Solids* **1998,** *231* (1–2), 58-77.
245. Kim, K.; Kim, H., Formation of Silica Nanoparticles by Hydrolysis of TEOS Using a Mixed Semi-Batch/Batch Method. *Journal of Sol-Gel Science and Technology* **2002,** *25* (3), 183-189.
246. Mori, H., Design and Synthesis of Functional Silsesquioxane-Based Hybrids by Hydrolytic Condensation of Bulky Triethoxysilanes. *International Journal of Polymer Science* **2012,** *2012*, 17.
247. Mauritz, K. A.; Hassan, M. K., Nanophase Separated Perfluorinated Ionomers as Sol-Gel Polymerization Templates for Functional Inorganic Oxide Nanoparticles. *Polymer Reviews* **2007,** *47* (4), 543-565.
248. Green, D. L.; Jayasundara, S.; Lam, Y.-F.; Harris, M. T., Chemical reaction kinetics leading to the first Stober silica nanoparticles – NMR and SAXS investigation. *Journal of Non-Crystalline Solids* **2003,** *315* (1–2), 166-179.
249. Depla, A.; Verheyen, E.; Veyfeyken, A.; Van Houteghem, M.; Houthoofd, K.; Van Speybroeck, V.; Waroquier, M.; Kirschhock, C. E. A.; Martens, J. A., UV-Raman and 29Si NMR Spectroscopy Investigation of the Nature of Silicate Oligomers Formed by Acid Catalyzed Hydrolysis and Polycondensation of Tetramethylorthosilicate. *The Journal of Physical Chemistry C* **2011,** *115* (22), 11077-11088.
250. dell' Erba, I. E.; Fasce, D. P.; Williams, R. J. J.; Erra-Balsells, R.; Fukuyama, Y.; Nonami, H., *Poly(silsesquioxanes) derived from the hydrolytic condensation of organotrialkoxysilanes containing hydroxyl groups*.
251. (a) Wang, Y. Y.; Qiu, F. X.; Lv, Y. F.; Xu, J. C.; Yang, D. Y., Preparation and properties of waterborne poly(urethane acrylate)/silica dispersions and hybrid composites. *Plastics, Rubber & Composites* **2012,** *41* (10), 418-424; (b) Wei, W.; Baohua, G.; Liang, L., Effect of Surfactants on the Formation, Morphology, and Surface Property of Synthesized SiO2 Nanoparticles. *Journal of Dispersion Science & Technology* **2004,** *25* (5), 593-601.
252. Sun, X.; Xu, Y.; Jiang, D.; Yang, D.; Wu, D.; Sun, Y.; Yang, Y.; Yuan, H.; Deng, F., Study on the ammonia-catalyzed hydrolysis kinetics of single phenyltriethoxysilane and mixed phenyltriethoxysilane/tetraethoxysilane systems by liquid-state 29Si NMR. *Colloids and Surfaces A: Physicochemical and Engineering Aspects* **2006,** *289* (1–3), 149-157.
253. Arantes, T. M.; Pinto, A. H.; Leite, E. R.; Longo, E.; Camargo, E. R., Synthesis and optimization of colloidal silica nanoparticles and their functionalization with methacrylic acid. *Colloids & Surfaces A: Phys. Eng. Asp.* **2012,** *415*, 209-217.
254. Abdali, A.; Moritz, B.; Gupta, A.; Wiggers, H.; Schulz, C., Hybrid microwave-plasma hot-wall reactor for synthesis of silica nanoparticles under well-controlled conditions. 2010.

255. Yanjun, X.; Callum, A. S. H.; Dongyang, S.; Zaihan, J.; Qingwen, W.; Carsten, M., Effects of dynamic aging (hydrolysis and condensation) behaviour of organofunctional silanes in the aqueous solution on their penetrability into the cell walls of wood. . *BioResources* **2011,** *6* (3), 2323-2339.
256. Nakamura, Y.; Gotoh, T.; Honda, H.; Fujii, S.; Nagata, K., AFM Observation of a Mica Surface Treated with Silane Coupling Agent Having a Mercapto Group. *Composite Interfaces* **2010,** *17* (4), 395-404.
257. Ramezanzadeh, B.; Mohseni, M.; Karbasi, A., Preparation of sol-gel-based nanostructured hybrid coatings; part 1: morphological and mechanical studies. *Journal of Materials Science* **2012,** *47* (1), 440-454.
258. Sutra, P.; Fajula, F.; Brunel, D.; Lentz, P.; Daelen, G.; Nagy, J. B., 29Si and 13C MAS-NMR characterization of surface modification of micelle-templated silicas during the grafting of organic moieties and end-capping. *Colloids and Surfaces A: Physicochemical and Engineering Aspects* **1999,** *158* (1–2), 21-27.
259. Zhang, X.; Kong, L.; Dai, L.; Zhang, X.; Wang, Q.; Tan, Y.; Zhang, Z., Synthesis, characterization, and thermal properties of poly(siloxane-carborane)s. *Polymer* **2011,** *52* (21), 4777-4784.
260. Jiucun, C.; Jiming, X.; Zhengwang, C. A. I.; Huang, Y.; Haodong, W.; Lihui, Z.; Wenqian, L. U. O.; Hu, M. I. N., Synthesis of Hydrophobic Polymer Brushes on Silica Nanoparticles Via the Combination of Surface-Initiated ATRP, ROP and Click Chemistry. *Journal of Macromolecular Science: Pure & Applied Chemistry* **2010,** *47* (7), 655-662.
261. Zhou, T.; Wang, X.; Cheng, P.; Wang, T.; Xiong, D., Improving the thermal conductivity of epoxy resin by the addition of a mixture of graphite nanoplatelets and silicon carbide microparticles. *Express Polymer Letters* **2013,** *7* (7), 585-594.
262. Pouxviel, J. C.; Boilot, J. P., Kinetic simulations and mechanisms of the sol-gel polymerization. *Journal of Non-Crystalline Solids* **1987,** *94* (3), 374-386.
263. Ro, J. C. C. J., Sol-gel kinetics of tetraethylorthosilicate (TEOS) in acid catalyst. *Journal of Non-Crystalline Solids* **1989,** *110*, 26-32.
264. Yang, H.; Ding, Z. S.; Jiang, Z. H.; Xu, X. P., *Sol-Gel Process Kinetics for Si(Oet)4*. 1989.
265. Hook, R. J., A 29Si NMR study of the sol-gel polymerisation rates of substituted ethoxysilanes. *Journal of Non-Crystalline Solids* **1996,** *195* (1–2), 1-15.
266. Nam, K.-H.; Lee, T.-H.; Bae, B.-S.; Popall, M., Condensation reaction of 3-(methacryloxypropyl)-trimethoxysilane and diisobutylsilanediol in non-hydrolytic sol-gel process. *Journal of Sol-Gel Science and Technology* **2006,** *39* (3), 255-260.
267. Zhang, L.; Xu, J.; Hou, G.; Tang, H.; Deng, F., Interactions between Nafion resin and protonated dodecylamine modified montmorillonite: A solid state NMR study. *Journal of Colloid and Interface Science* **2007,** *311* (1), 38-44.
268. B. Arkles, J. R. S., J. Zazyczny, P. Mehta, Factors contributing to the stability of alkoxysilanes in aqueous solution. **1991**, 91 - 104.
269. Mel, S., Coatings (Thermal Spray Processes). In *Innovations in Materials Manufacturing, Fabrication, and Environmental Safety*, CRC Press: 2010; pp 385-444.
270. Nordstrom, J. D., Polymers For Coatings For Plastics. In *Coatings Of Polymers And Plastics*, CRC Press: 2003.
271. Patrick, G., Thermal barrier coatings. In *Aerospace Materials*, Taylor & Francis: 2001.
272. Richard, G. W., Thermal Barrier Coating Systems: Multilayer Multifunctional Surface Engineering. In *Multifunctional Materials for Tribological Applications*, Pan Stanford: 2015; pp 59-86.

273. SinemCevik, U., Corrosion and Oxidation in Thermal Barrier Coatings. In *Corrosion and Materials in the Oil and Gas Industries*, CRC Press: 2013; pp 129-146.
274. Su Kim, M.; Kim, S.; Leem, J.-Y., Laser-assisted sol-gel growth and characteristics of ZnO thin films. *Applied Physics Letters* **2012,** *100* (25), 252108.
275. Schwarzinger, C.; Gabriel, S.; Beißmann, S.; Buchberger, W., Quantitative Analysis of Polymer Additives with MALDI-TOF MS Using an Internal Standard Approach. *Journal of the American Society for Mass Spectrometry* **2012,** *23* (6), 1120.
276. Dekker, B.; Keen, H.; Shaw, D.; Disley, L.; Hastings, D.; Hadfield, J.; Reader, A.; Allan, D.; Julyan, P.; Watson, A.; Zweit, J., Functional comparison of annexin V analogues labeled indirectly and directly with iodine-124. *Nuclear Medicine and Biology* **2005,** *32* (4), 403-413.
277. Kodba, Z.; Vončina, D., A Rapid Method for the Determination of Organochlorine, Pyrethroid Pesticides and Polychlorobiphenyls in Fatty Foods Using GC with Electron Capture Detection. *Chroma* **2007,** *66* (7-8), 619-624.
278. Dai, X.; Kramer-Tremblay, S., Five-Column Chromatography Separation for Simultaneous Determination of Hard-to-Detect Radionuclides in Water and Swipe Samples. *Analytical Chemistry* **2014,** *86* (11), 5441-5447.
279. Joseph M. Antonucci, S. H. D., Bruce O. Fowler, Hockin H. K. Xu, Walter G. McDonough, Chemistry of Silanes: Interfaces in Dental

Polymers and Composites1. *Journal of Research of the National Institute of Standards and Technology* **2005,** *110* (5), 110, 541-558.
280. Taylor, P. G.; Bassindale, A. R.; El Aziz, Y.; Pourny, M.; Stevenson, R.; Hursthouse, M. B.; Coles, S. J., Further studies of fluoride ion entrapment in octasilsesquioxane cages; X-ray crystal structure studies and factors that affect their formation. *Dalton Transactions* **2012,** *41* (7), 2048-2059.
281. Hursthouse, M. B. a. H., Peter N. and Light, Mark E. and Yang, Y. and Taylor, P. G. and MacKinnon, I. A. and Liu, Z. and Bassindale, A. R. , octakis(4-Methoxycarbonyl)-3,3-dimethyl-n-butyl)octasilsesquioxane. *University of Southampton, Crystal Structure Report Archive.* **2001**.
282. Keith Morton1, O. K. C. T., Chih-Kuan Tung3, James C Sturm4, Stephen Y Chou4 and Robert Austin5,6,7, The anti-lotus leaf effect in nanohydrodynamic bump arrays *New Journal of Physics* **2010,** *12*.
283. Marks, P., Lotus leaf effect ramps up the power of solar cells. *New Scientist* **2009,** *204* (2736), 25-25.
284. Meng, Z.; Wang, Q.; Qu, X.; Zhang, C.; Li, J.; Liu, J.; Yang, Z., Papillae mimetic hairy composite spheres towards lotus leaf effect coatings. *Polymer* **2011,** *52* (3), 597-601.
285. von Baeyer, H. C., The lotus effect. *Sciences* **2000,** *40* (1), 12.
286. Gu, Z.-Z.; Uetsuka, H.; Takahashi, K.; Nakajima, R.; Onishi, H.; Fujishima, A.; Sato, O., Structural Color and the Lotus Effect. *Angewandte Chemie International Edition* **2003,** *42* (8), 894-897.
287. Bittoun, E.; Marmur, A., The Role of Multiscale Roughness in the Lotus Effect: Is It Essential for Super-Hydrophobicity? *Langmuir* **2012,** *28* (39), 13933-13942.
288. Li, J.; Wang, G.; Meng, Q.; Ding, C.; Jiang, H.; Fang, Y., A biomimetic nano hybrid coating based on the lotus effect and its anti-biofouling behaviors. *Applied Surface Science* **2014,** *315* (0), 407-414.
289. Marmur, A., The Lotus Effect: Superhydrophobicity and Metastability. *Langmuir* **2004,** *20* (9), 3517-3519.

290. Yoshino, M.; Willy, K.; Yamanaka, A.; Matsumura, T.; Aravindan, S.; Rao, P. V., Micro- and Nanostructured Surface Development by Nano Plastic Forming and Roller Imprinting. In *Micromanufacturing Processes*, CRC Press: 2012; pp 243-261.
291. Boreyko, J. B.; Chen, C.-H., Restoring Superhydrophobicity of Lotus Leaves with Vibration-Induced Dewetting. *Physical Review Letters* **2009,** *103* (17), 174502.
292. Dawood, M. K.; Zheng, H.; Liew, T. H.; Leong, K. C.; Foo, Y. L.; Rajagopalan, R.; Khan, S. A.; Choi, W. K., Mimicking Both Petal and Lotus Effects on a Single Silicon Substrate by Tuning the Wettability of Nanostructured Surfaces. *Langmuir* **2011,** *27* (7), 4126-4133.
293. Karmouch, R.; Ross, G. G., Superhydrophobic wind turbine blade surfaces obtained by a simple deposition of silica nanoparticles embedded in epoxy. *Applied Surface Science* **2010,** *257* (3), 665-669.
294. Mohanta, V.; Patil, S., Enhancing Surface Coverage and Growth in Layer-by-Layer Assembly of Protein Nanoparticles. *Langmuir* **2013,** *29* (43), 13123-13128.
295. Shi, X.; Bertóti, I.; Pukánszky, B.; Rosa, R.; Lazzeri, A., Structure and surface coverage of water-based stearate coatings on calcium carbonate nanoparticles. *Journal of Colloid and Interface Science* **2011,** *362* (1), 67-73.
296. Budijono, S. J.; Russ, B.; Saad, W.; Adamson, D. H.; Prud'homme, R. K., Block copolymer surface coverage on nanoparticles. *Colloids and Surfaces A: Physicochemical and Engineering Aspects* **2010,** *360* (1–3), 105-110.
297. Pease, L. F.; Tsai, D.-H.; Zangmeister, R. A.; Zachariah, M. R.; Tarlov, M. J., Quantifying the Surface Coverage of Conjugate Molecules on Functionalized Nanoparticles. *The Journal of Physical Chemistry C* **2007,** *111* (46), 17155-17157.
298. Yu, Q.; Wang, P.; Hu, S.; Hui, J.; Zhuang, J.; Wang, X., Hydrothermal Synthesis of Hollow Silica Spheres under Acidic Conditions. *Langmuir* **2011,** *27* (11), 7185-7191.
299. Mguni, L.; Mukenga, M.; Muzenda, E.; Jalama, K.; Meijboom, R., Expanding the synthesis of Stöber spheres: towards the synthesis of nano-magnesium oxide and nano-zinc oxide. *Journal of Sol-Gel Science and Technology* **2013,** *66* (1), 91-99.
300. Kobayashi, Y.; Nozawa, T.; Nakagawa, T.; Gonda, K.; Takeda, M.; Ohuchi, N., Fabrication and fluorescence properties of multilayered core-shell particles composed of quantum dot, gadolinium compound, and silica. *Journal of Materials Science* **2012,** *47* (4), 1852-1859.
301. Sasaki, Y.; Konishi, N.; Kasuya, M.; Kohri, M.; Taniguchi, T.; Kishikawa, K., Preparation of size-controlled polymer particles by polymerization of O/W emulsion monomer droplets obtained through phase inversion temperature emulsification using amphiphilic comb-like block polymers. *Colloids and Surfaces A: Physicochemical and Engineering Aspects* **2015,** *482* (0), 68-78.
302. Ki Do, K.; Hee Taik, K., New Process for the Preparation of Monodispersed, Spherical Silica Particles. *Journal of the American Ceramic Society* **2002,** *85* (5), 1107.
303. (a) Sarawade, P. B.; Quang, D. V.; Hilonga, A.; Jeon, S. J.; Kim, H. T., Synthesis and characterization of micrometer-sized silica aerogel nanoporous beads. *Materials Letters* **2012,** *81* (0), 37-40; (b) Czarnobaj, K., Preparation and Characterization of Silica Xerogels as Carriers for Drugs. *Drug Delivery* **2008,** *15* (8), 485-492.
304. Soleimani Dorcheh, A.; Abbasi, M. H., Silica aerogel; synthesis, properties and characterization. *Journal of Materials Processing Technology* **2008,** *199* (1–3), 10-26.
305. Buckley, A. M.; Greenblatt, M., The Sol-Gel Preparation of Silica Gels. *Journal of Chemical Education* **1994,** *71* (7), 599.

306. Meera, K. M. S.; Sankar, R. M.; Jaisankar, S. N.; Mandal, A. B., Mesoporous and biocompatible surface active silica aerogel synthesis using choline formate ionic liquid. *Colloids and Surfaces B: Biointerfaces* **2011,** *86* (2), 292-297.
307. Metal Coatings. In *Steelwork Corrosion Control*, Taylor & Francis: 2002.
308. Chang-Jiu, L.; Guan-Jun, Y.; Özge, A., Thermal Spray Coatings for Aeronautical and Aerospace Applications. In *Aerospace Materials Handbook*, CRC Press: 2012; pp 281-358.
309. Klaus-Werner, R.; Hans Christian, G., Automotive Plastic Coatings In Europe. In *Coatings Of Polymers And Plastics*, CRC Press: 2003.
310. Viswanathan, K.; Ozhalici, H.; Elkins, C. L.; Heisey, C.; Ward, T. C.; Long, T. E., Multiple Hydrogen Bonding for Reversible Polymer Surface Adhesion. *Langmuir* **2006,** *22* (3), 1099-1105.
311. Andersen, M. Ø.; Lichawska, A.; Arpanaei, A.; Rask Jensen, S. M.; Kaur, H.; Oupicky, D.; Besenbacher, F.; Kingshott, P.; Kjems, J.; Howard, K. A., Surface functionalisation of PLGA nanoparticles for gene silencing. *Biomaterials* **2010,** *31* (21), 5671-5677.
312. Henry, C. A., The Incorporation of Nanomaterials into Polymer Media. In *Polymer Nanocomposites Handbook*, CRC Press: 2009.
313. Nidhin, M.; Sreeram, K. J.; Nair, B. U.; Jakubowicz, J.; Adamek, G.; Karekar, S. E.; Bhanvase, B. A.; Sonawane, S. H.; Suman, S.; Meena, V. K.; Jain, D. V. S.; Singla, M. L., Complexities in Nanomaterials. In *Engineering of Polymers and Chemical Complexity, Volume I*, Apple Academic Press: 2014; pp 317-423.
314. Prashant, K.; Gary, J. C., Laser-Based Manufacturing Systems for Nanomaterials and Nanostructures. In *Laser and Photonic Systems*, CRC Press: 2014; pp 23-52.
315. Prado, L. A. S. A.; Sriyai, M.; Ghislandi, M.; Barros-Timmons, A.; Schulte, K., Surface modification of alumina nanoparticles with silane coupling agents. *Journal of the Brazilian Chemical Society* **2010,** *21*, 2238-2245.
316. Saha, B.; Evers, T. H.; Prins, M. W. J., How Antibody Surface Coverage on Nanoparticles Determines the Activity and Kinetics of Antigen Capturing for Biosensing. *Analytical Chemistry* **2014,** *86* (16), 8158-8166.
317. Orchard, K. L.; Shaffer, M. S. P.; Williams, C. K., Organometallic Route to Surface-Modified ZnO Nanoparticles Suitable for In Situ Nanocomposite Synthesis: Bound Carboxylate Stoichiometry Controls Particle Size or Surface Coverage. *Chemistry of Materials* **2012,** *24* (13), 2443-2448.
318. Helgason, T.; Awad, T. S.; Kristbergsson, K.; McClements, D. J.; Weiss, J., Effect of surfactant surface coverage on formation of solid lipid nanoparticles (SLN). *Journal of Colloid and Interface Science* **2009,** *334* (1), 75-81.
319. Jean-Paul Gallas, J.-M. G., Alexandre Vimont, Jean-Claude Lavalley, Barbara Gil, Jean-Pierre Gilson, Olivier Miserque, Quantification of water and silanol species on various silicas by coupling IR spectroscopy and in-situ thermogravimetry. *Langmuir* **2009 May 19,** (25(10): 5825–5834.).
320. Jabbari-Hichri, A.; Bennici, S.; Auroux, A., Enhancing the heat storage density of silica–alumina by addition of hygroscopic salts (CaCl2, Ba(OH)2, and LiNO3). *Solar Energy Materials and Solar Cells* **2015,** *140*, 351-360.
321. Kucheyev, S. O.; Stadermann, M.; Shin, S. J.; Satcher, J. H.; Gammon, S. A.; Letts, S. A.; van Buuren, T.; Hamza, A. V., Super-Compressibility of Ultralow-Density Nanoporous Silica. *Advanced Materials* **2012,** *24* (6), 776-780.
322. Zhang, Y.; Luo, H.; Carr, P. W., Silica-based, hyper-crosslinked acid stable stationary phases for high performance liquid chromatography. *Journal of Chromatography A* **2012,** *1228* (0), 110-124.

323. Beredensen GE, D. G. L., Pikaart, Chromatographic retention behaviour, modelling and separation optimisation of the quaternary ammonium salt isometamidium chloride and related compounds on a range of reversed-phase liquid chromatographic stationary phases. *Journal of Liquid Chromatogry* **1978),** (36), 561-586
324. De Galan L, Chromatographic retention behaviour, modelling and separation optimisation of the quaternary ammonium salt isometamidium chloride and related compounds on a range of reversed-phase liquid chromatographic stationary phases *Journay of Liquid Chromatography* **1980,** *3* (37), 1437-1464.
325. Huang, Y.; Classics, T. U. o. A., *Study of Pore Size Effect in Chromatography by Vibrational Spectroscopy and Colloidal Arrays*. University of Arizona: 2008.
326. Bouchard G, C. P., Testa B, Gobry V, Girault HH, Chromatographic retention behaviour, modelling and separation optimisation of the quaternary ammonium salt isometamidium chloride and related compounds on a range of reversed-phase liquid chromatographic stationary phases *Journal of Pharmaceutical Research* **2001,** *18* (5), 702-708 (38).
327. Friederici, M.; Angurell, I.; Seco, M.; Rossell, O.; Llorca, J., Synthetic strategies for the surface functionalisation of gold nanoparticles with metals and metal clusters. *Dalton Transactions* **2011,** *40* (31), 7934-7940.
328. Andy, B.; Antonio, A. C., Fingermark Detection Using Nanoparticles. In *Lee and Gaensslen's Advances in Fingerprint Technology, Third Edition*, CRC Press: 2012; pp 307-380.
329. Harald, B.; Bernhard, W.; Burkhard, L.; Christina, G.; Eckart, R. h., Elastic Scattering of Soft X-rays from Free Size-Selected Nanoparticles. In *Fundamentals and Applications in Aerosol Spectroscopy*, CRC Press: 2010; pp 401-417.
330. Ignacio Del, V.; Javier, G.; Carlos, R. Z.; Jesus, M. C., Nano-Materials and Nano-Structures for Chemical and Biological Optical Sensors. In *Optochemical Nanosensors*, Taylor & Francis: 2012; pp 307-384.
331. Coating Smart Polymers and Nanomaterials. In *Coated Textiles*, CRC Press: 2007; pp 203-209.
332. Hybrid Nanomaterials. In *Nanomaterials for Chemical Sensors and Biotechnology*, Pan Stanford Publishing: 2009; pp 37-68.
333. Nanomedicine Applications of Nanomaterials. In *Nanomaterials for Chemical Sensors and Biotechnology*, Pan Stanford Publishing: 2009; pp 85-112.
334. Fricke, J., http://www.nature.com.libezproxy.open.ac.uk/scientificamerican/journal/v258/n5/pdf/scientificamerican0588-92.pdf. *scientific america* **1988**.
335. Mohanan, J. L.; Arachchige, I. U.; Brock, S. L., Porous Semiconductor Chalcogenide Aerogels. *Science* **2005,** *307* (5708), 397-400.
336. Burchell, M. J. M., J. Creighton, J.A. Kearsley, A.T., Graham, G. Franchi, I.A., Identification of minerals and meteoritic materials via Raman techniques after capture in hypervelocity impacts on aerogel *Journal of Meteoritics and Planetary Science* **2006,** *2*, P 217-232.

APPENDICES

1 Appendix – TEOS/Water Kinetic study

NB; All ^{29}Si NMR files for Appendix 1 are found in cd attached (TEOS kinetics)

0.5 water

(From Chapter 3 –TEOS, Figure 3.3, Graph 1).

Species/time	**0**	**4**	**8**	**12**	**16**	**20**	**34**	**204**	**408**
Q_0^2	0	5	4	4	3	3	2	0	0
Q_0^1	0	32	35	35	33	31	26	15	10
Q_0^0	100	63	59	59	59	60	55	46	37
Q_1^1	0	0	1	2	2	2	4	6	7
Q_1^0	0	0	0	1	3	5	12	30	41
Q_2^0	0	0	0	0	0	0	0	3	5

1.0 water

Time/Species	Q_0^3	Q_0^2	Q_0^1	Q_0^0	Q_1^2	Q_1^1	Q_1^0	Q_2^2	Q_2^1	Q_2^0
0	0	0	0	100	0	0	0	0	0	0
2	3	15	25	57	0	0	0	0	0	0
4	0	18	44	36	0	3	0	0	0	0
6	0	14	43	34	0	7	1	0	0	0
10	0	13	40	32	0	11	5	0	0	0
14	0	12	38	33	0	10	7	0	0	0
20	0	10	37	31	0	13	10	0	0	0
36	0	9	34	31	0	14	12	0	0	0
48	0	7	28	25	2	17	17	2	2	0
60	0	6	25	23	3	19	21	1	1	0
72	0	6	23	23	2	20	24	1	0	3
84	0	5	21	21	2	20	26	1	1	4
96	0	4	19	19	2	21	27	1	1	5
108	0	5	20	19	0	21	31	0	0	4
144	0	15	16	1	0	24	36	0	2	6
216	0	12	14	1	0	19	40	0	9	8
288	0	2	10	13	2	22	32	2	7	9

1.5 water

Time/Species	Q_0^3	Q_0^2	Q_0^1	Q_0^0	Q_1^2	Q_1^1	Q_1^0	Q_2^2	Q_2^1	Q_2^0
0	0	0	0	100	0	0	0	0	0	0
2	4	8	14	74	0	0	0	0	0	0
4	7	24	24	46	0	0	0	0	0	0
6	7	28	33	31	0	2	0	0	0	0
10	4	26	40	20	2	7	0	0	0	0
14	5	25	41	17	2	10	0	0	0	0
20	3	24	40	16	3	12	2	0	0	0
132	0	12	24	8	5	31	14	0	2	3

2.0 water

Time/Species	Q_0^3	Q_0^2	Q_0^1	Q_0^0	Q_1^2	Q_1^1	Q_1^0	Q_2^2	Q_2^1	Q_2^0	Q_3^1
0	0	0	0	100	0	0	0	0	0	0	0
20	5	8	15	73	0	0	0	0	0	0	0
40	12	28	25	35	0	0	0	0	0	0	0
60	10	32	31	19	3	4	0	0	0	0	0
80	9	32	34	13	4	8	0	0	0	0	0
100	8	30	35	12	4	11	0	0	0	0	0
120	7	26	29	10	8	17	4	0	0	0	0
140	6	24	28	9	9	17	8	0	0	0	0
160	6	22	26	8	10	20	7	0	0	0	0
180	5	22	25	9	10	22	7	0	0	0	0
200	5	19	26	8	12	23	8	0	0	0	0
220	5	19	23	7	11	26	9	0	0	0	0

240	3	18	23	9	13	25	10	0	0	0	0
260	5	17	22	8	12	26	10	0	0	0	0
280	5	17	20	8	11	27	10	4	0	0	0
300	4	16	20	7	13	25	11	4	0	0	0
320	5	16	19	5	11	27	13	4	0	0	0
340	4	16	17	6	13	29	10	4	0	0	0
360	4	16	17	7	10	28	13	5	0	0	0
380	5	16	18	7	14	28	9	4	0	0	0
400	4	13	16	7	12	27	11	5	0	0	5
420	5	11	15	7	13	30	13	6	0	0	0
440	4	15	16	7	12	27	14	6	0	0	0
460	4	17	23	7	10	27	10	3	0	0	0
480	4	18	22	7	10	27	10	3	0	0	0
500	3	16	21	8	10	29	10	3	0	0	0
660	0	13	16	5	10	30	10	4	4	4	0

2.5 water

Time/Species	**Q_0^3**	**Q_0^2**	**Q_0^1**	**Q_0^0**	**Q_1^2**	**Q_1^1**	**Q_1^0**	**Q_2^2**
0	0	0	0	100	0	0	0	0
1	0	0	12	88	0	0	0	0
2	3	6	16	75	0	0	0	0
3	8	12	17	62	0	0	0	0
4	11	18	19	53	0	0	0	0
6	14	26	21	39	0	0	0	0
8	15	32	25	28	0	0	0	0
12	16	37	26	21	0	0	0	0

16	16	39	28	13	2	3	0	0
32	13	36	28	4	6	13	0	0
184	0	25	19	0	15	41	0	0
384	0	14	8	0	19	39	9	12

3.0water

Time/Species	**Q_0^3**	**Q_0^2**	**Q_0^1**	**Q_0^0**	**Q_1^2**	**Q_1^1**	**Q_1^0**	**Q_2^2**	**Q_2^1**
0	0	0	0	100	0	0	0	0	0
1	0	0	8	92	0	0	0	0	0
2	0	0	13	87	0	0	0	0	0
3	0	6	15	80	0	0	0	0	0
4	4	11	19	67	0	0	0	0	0
6	10	17	17	55	0	0	0	0	0
8	14	22	18	46	0	0	0	0	0
12	16	26	19	39	0	0	0	0	0
16	14	29	19	38	0	0	0	0	0
32	18	37	23	16	4	3	0	0	0
180	13	35	23	4	12	12	0	0	0
612	8	36	22	0	11	20	0	0	3

3.5 water

Time/Species	Q_0^3	Q_0^2	Q_0^1	Q_0^0	Q_1^2	Q_1^1	Q_1^0	Q_2^2	Q_2^1
0	0	0	0	100	0	0	0	0	0
0.5	9	12	15	63	0	0	0	0	0
1.5	19	29	19	33	0	0	0	0	0
2.5	21	42	21	16	0	0	0	0	0
4.5	22	45	24	7	0	2	0	0	0
6.5	20	45	26	2	3	4	0	0	0
8.5	21	40	19	5	6	9	0	0	0
10.5	22	42	18	0	8	10	0	0	0
12.5	20	41	15	4	9	12	0	0	0
48	13	36	0	0	25	26	0	0	0
96	0	11	0	0	27	37	0	21	4
336	0	0	0	0	14	19	0	53	14

4.0water

Time/Species	Q_0^4	Q_0^3	Q_0^2	Q_0^1	Q_0^0	Q_1^2	Q_1^1	Q_1^0	Q_2^2	Q_2^1	Q_2^0	Q_3^1
0	0	0	0	0	100	0	0	0	0	0	0	0
2	0	0	0	16	84	0	0	0	0	0	0	0
4	0	10	15	20	55	0	0	0	0	0	0	0
6	0	19	26	16	38	0	0	0	0	0	0	0
10	4	22	31	18	25	0	0	0	0	0	0	0
14	0	25	39	21	15	0	0	0	0	0	0	0
20	0	25	43	19	11	3	0	0	0	0	0	0
24	0	28	51	16	5	0	0	0	0	0	0	0
84	0	19	36	14	2	9	17	2	0	0	0	0
252	0	11	21	11	0	19	25	0	5	5	0	4

See appendix 1&2 on usb for spectra using different ratios of water to TEOS.

2 Appendix – Initial reaction rate profile (TEOS)

(From Chapter 3 –TEOS, Figure 3.5, Initial rate profile)

Initial rate against [TEOS]

Initial rate graph
Tangent to the TEOS graph at time zero for each
Rate = change in [TEOS]/change in time hrs.
Then plot rate vs molar ratio of TEOS to water (0.5-4)

Ratio of TEOS to water, mol	Rate (%L-1hr-1)	Rate(molL-1hr-1)	[TEOS]	Rate(molL-1hr-1)x[TEOS]
1	22.73	0.2273	1.66	0.377318
1.5	13.51	0.1351	1.13	0.152663
2	15.87	0.1587	0.78	0.123786
2.5	12.82	0.1282	0.66	0.084612
3	8.33	0.0833	0.53	0.044149
3.5	76.92	0.7692	0.47	0.361524
4	11.36	0.1136	0.4	0.04544

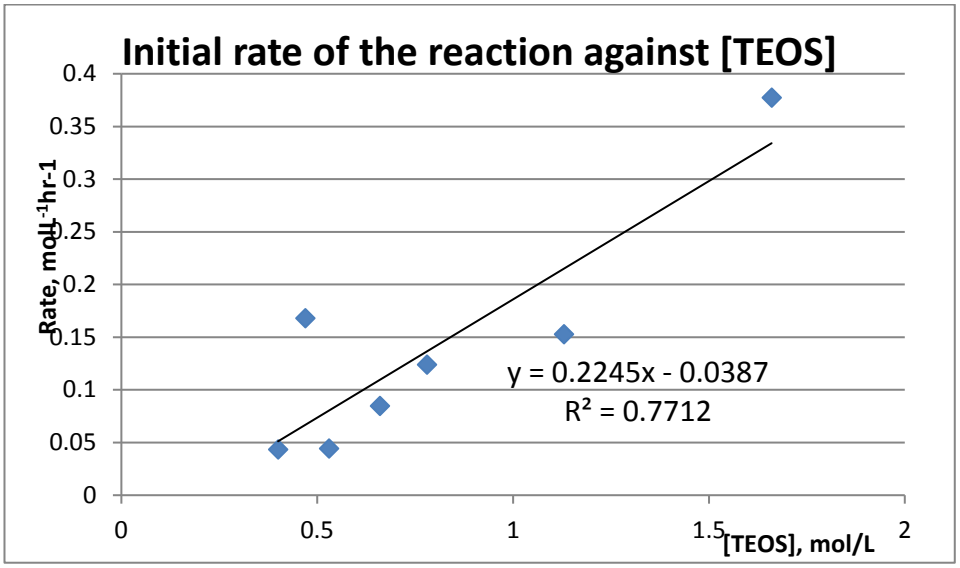

See Appendix 2 –USB for the individual rate profiles.

See Appendix 2 for - USB for TEOS (validation) hydrolysis and condensation worksheet.

3 Appendix – Initial reaction rate profile (acid)

(From Chapter 3 –TEOS, Figure 3.6, Initial rate profile)

X1 acid

Time/Species	**Q_0^3**	**Q_0^2**	**Q_0^1**	**Q_0**
0	0	0	0	100
1	0	0	0	100
2	0	0	6	94
3	0	0	11	89
4	0	0	11	89
5	0	3	16	81
7	2	4	15	79
9	3	7	18	72
13	7	12	20	61
17	8	14	20	58

X2 acid

Time/Species	Q_0^3	Q_0^2	Q_0^1	Q_0^0
0	0	0	0	100
1	0	0	3	97
2	0	0	9	91
3	0	4	15	81
4	3	7	17	73
5	6	10	18	67
7	8	13	20	59
9	11	18	20	51

X3 acid

Time/Species	Q_0^3	Q_0^2	Q_0^1	Q_0^0	Q_1^2	Q_1^1
0	0	0	0	100	0	0
1	2	4	15	79	0	0
2	10	20	20	51	0	0
3	12	31	23	34	0	0
4	12	38	29	22	0	0
5	11	38	32	18	2	0
7	9	37	33	11	4	6
9	8	36	35	9	4	8
13	9	34	34	8	4	11
17	7	36	41	8	0	8

X4 acid

Time/Species	Q_0^3	Q_0^2	Q_0^1	Q_0^0	Q_1^2	Q_1^1
0	0	0	0	100	0	0
1	2	4	15	79	0	0
2	10	20	20	51	0	0
3	12	31	23	34	0	0
4	12	38	29	22	0	0
5	11	38	32	18	2	0
7	9	37	33	11	4	6
9	8	36	35	9	4	8
13	9	34	34	8	4	11
17	7	36	41	8	0	8

X5 acid

Time/Species	Q_0^3	Q_0^2	Q_0^1	Q_0	Q_1^2	Q_1^1	Q_1	Q_2^2
0	0	0	0	100	0	0	0	0
1	8	15	18	58	0	0	0	0
2	5	33	26	27	0	0	0	0
3	12	37	32	16	0	2	0	0
4	11	36	33	10	3	5	0	2
5	9	36	35	8	5	7	0	1
7	9	35	33	7	4	11	0	0
9	7	39	38	4	0	11	2	0

See Appendix 3 –USB for the individual rate profiles.

4 Appendix 4 – Initial reaction rate profile (acid Figure 3.7)

From Chapter 3 –TEOS, Figure 3.7, Initial rate profile (acid)

Figure 3.7

Initial rate profile by varying the concentration of Acid

Acid amounts	Rate (%$L^{-1}h^{-1}$)	Rate (mol$L^{-1}h^{-1}$)	[Acid] x 10^{-5} M	Rate(mol$L^{-1}h^{-1}$) x [CF_3SO_3H] x 10^{-5}
1	3.85	0.0385	4.8	0.1848
2	6.71	0.0671	9.6	0.64416
3	24.39	0.2439	14	3.4146
4	28.57	0.2857	19	5.4283
5	46.51	0.4651	24	11.1624

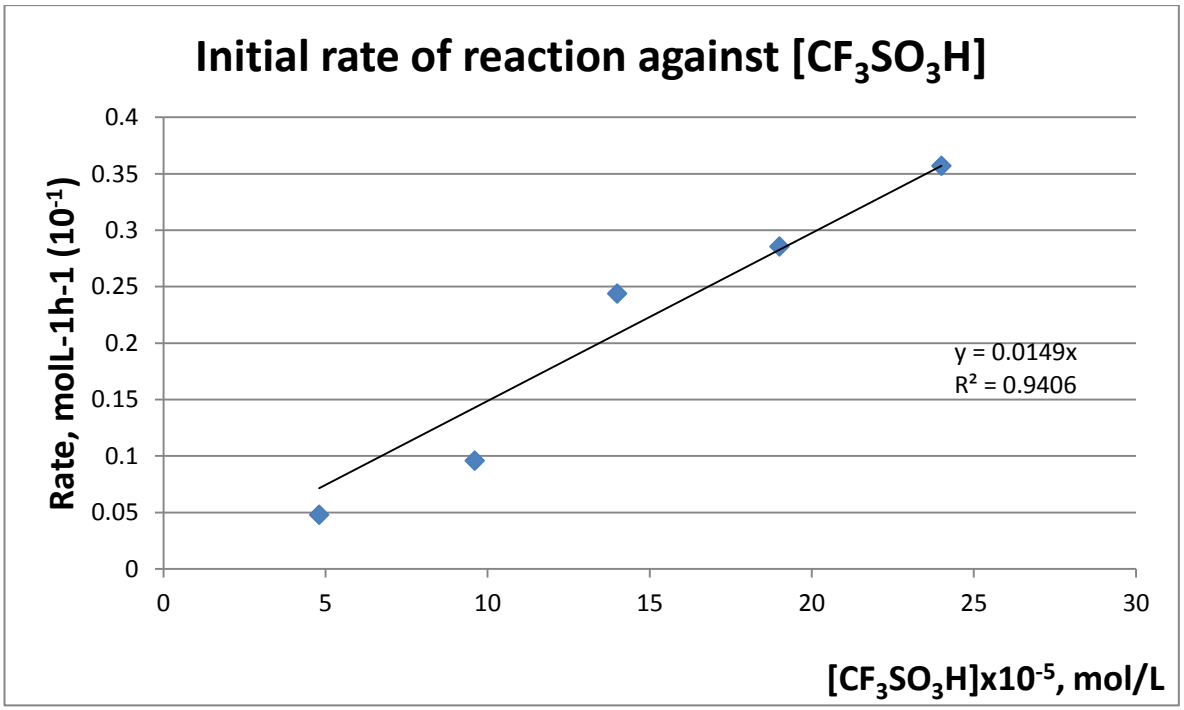

5 Appendix – Rate constant spreadsheet of TEOS hydrolysis

See appendix 2 -USB attached

6 Appendix – Hydrolysis and condensation of MPTES varying [MPTES]

Trend of species at pseudo equilibrium

Ratio of MPTES to water, mol	Rate ($\%L^{-1}hr^{-1}$)	Rate ($molL^{-1}hr^{-1}$)	[MPTES]	Rate ($molL^{-1}hr^{-1}$) x [MPTES]
1	111.1	1.11	1.66	1.8426
1.5	76.9	0.76	1.11	0.8436
2	125	1.25	0.83	1.0375
2.5	125	1.25	0.67	0.8375
3	125	1.25	0.53	0.6625

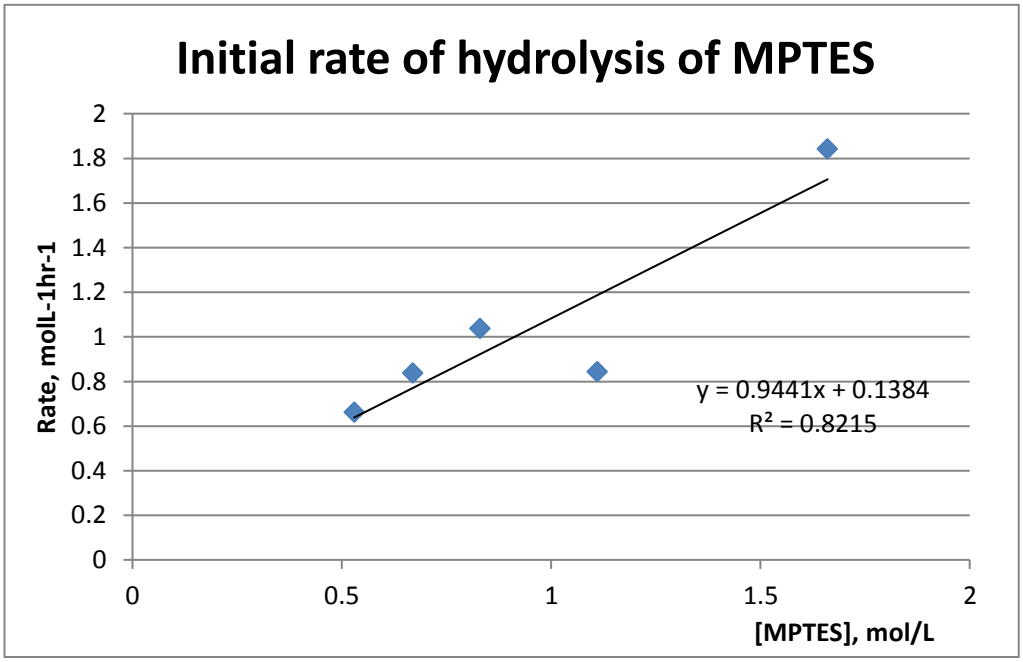

See Appendix 6 ^{29}SiNMR spectra (MPTES kinetic study) on raw data in USB attached

7 Appendix – MPTES acid reaction rate studies

Relative rates with increasing amounts of acid

Ratio of MPTES to water, mol	**Rate (%L-1hr^{-1})**	**Rate(molL-1hr^{-1})**	**Acid conc x10^{-5} M**	**Rate const, molL-1hr^{-1}) x[Acid]**
1	8	0.08	4.8	0.082
2	31.28	0.31	9.6	0.44
3	52.63	0.52	14	0.681
4	58.82	0.58	19	0.733
5	76.9	0.76	24	0.949

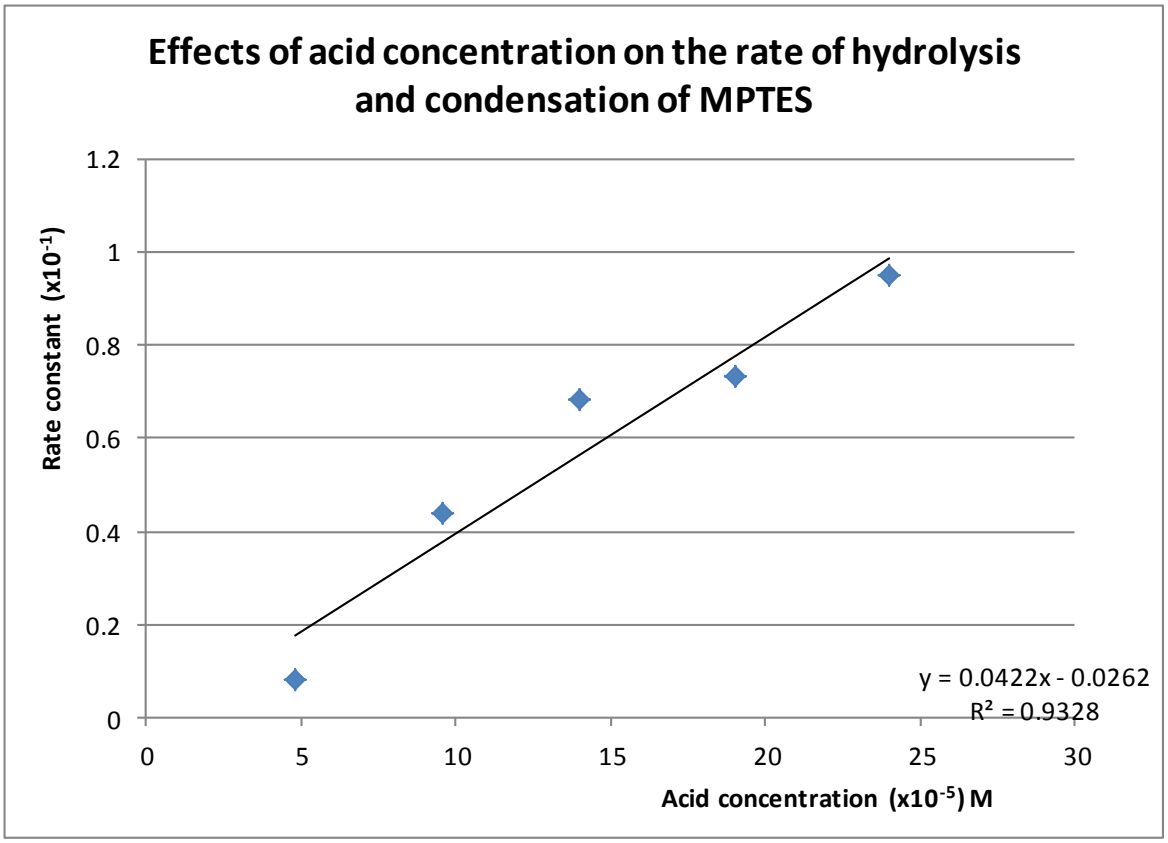

See Appendix 7, ^{29}SiNMR spectra of MPTES hydrolysis (acid study) on raw data in USB attached

8 Appendix - nPTMS spectra Interpretation and initial rate profile

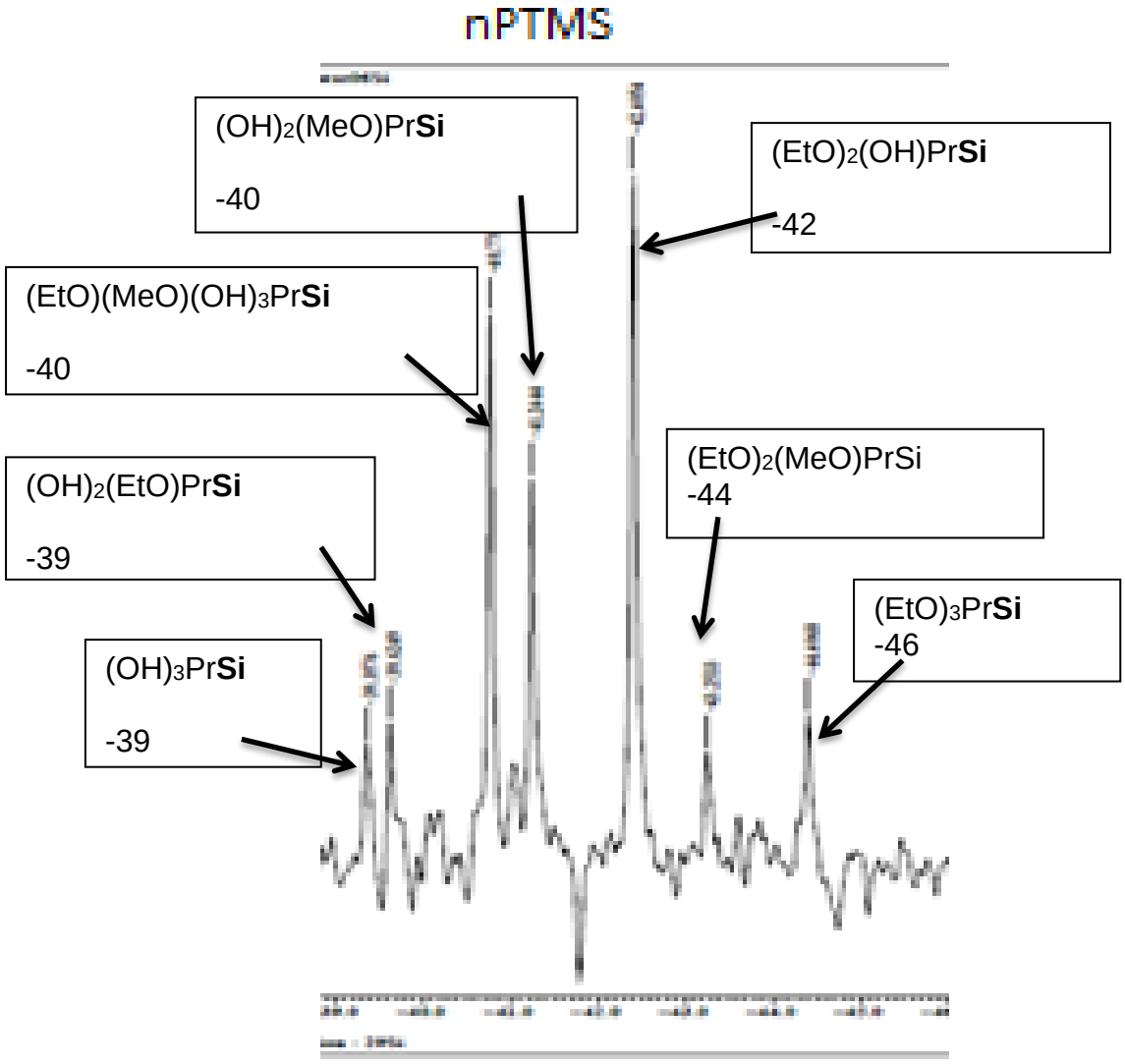

See the rest of the kinetic profile on the USB (nPTMS)

9 Appendix - MPTMS spectra Interpretation and initial rate profile

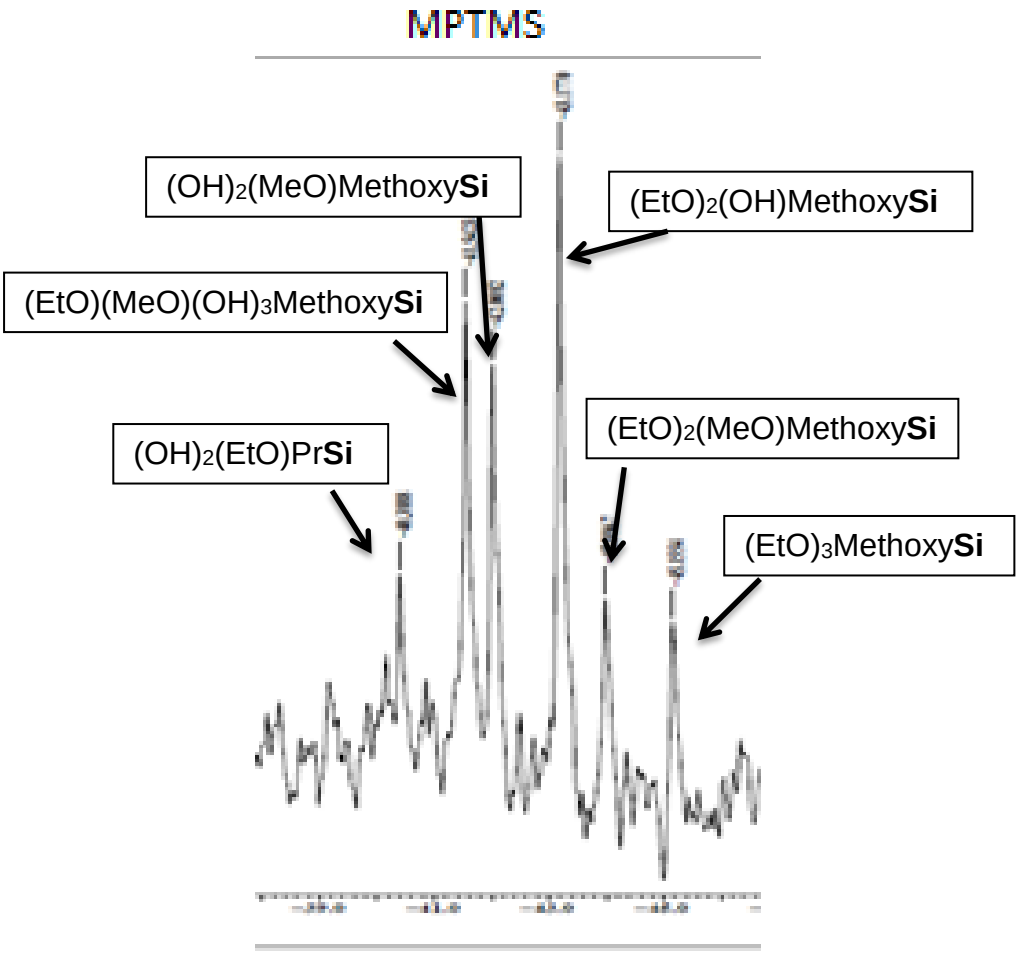

See the rest of the reaction rate profile spectras on the USB (MPTMS**)**

10 Appendix - MPTES spectra Interpretation and initial rate profile

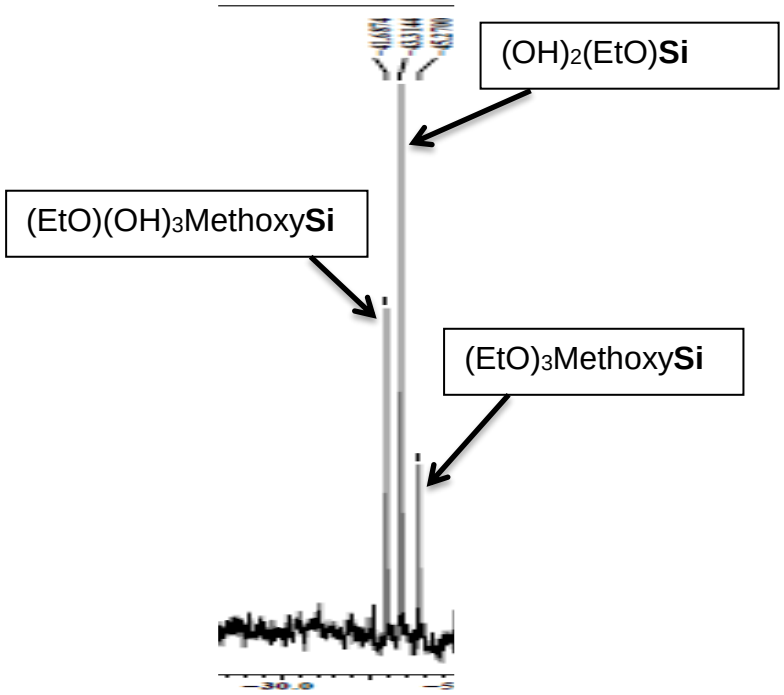

11 Appendix – Equilibrium studies (MPTES)

See USB for spectra's

12 Appendix - MPTMS.nPTMS mixing pattern

See USB for spectra's

13 Appendix – MPTMS.nPTMS

See USB for spectra's

14 Appendix - Possible MALDI-ToF-MS/ESI-MS structures

14.1 Possible MALDI-ToF-MS structures 1

Ions	Ions + (Na^+) Possible structures	Ions + (NH_4^+)
Dimer Linear	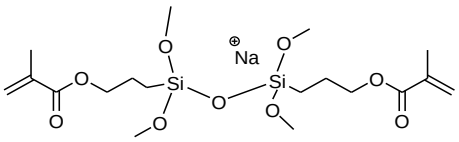 $C_{18}H_{34}NaO_9Si_2^+$ Exact Mass: 473.16 Mol. Wt.: 473.62	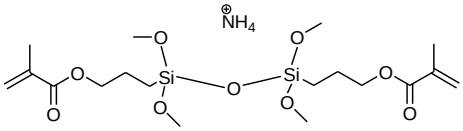 $C_{18}H_{38}NO_9Si_2^+$ Exact Mass: 468.21 Mol. Wt.: 468.67
Trimer linear	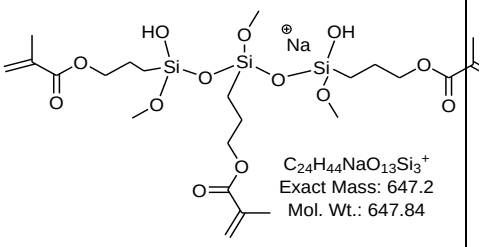 $C_{24}H_{44}NaO_{13}Si_3^+$ Exact Mass: 647.2 Mol. Wt.: 647.84 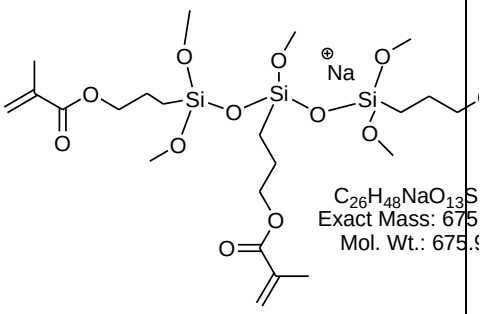 $C_{26}H_{48}NaO_{13}S$ Exact Mass: 675 Mol. Wt.: 675.9	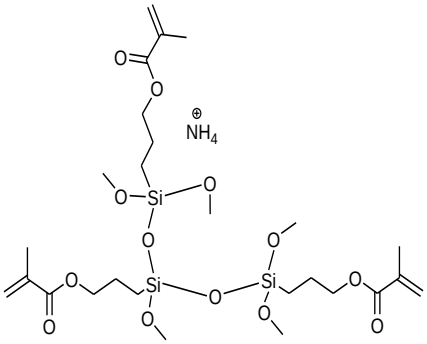 $C_{26}H_{52}NO_{13}Si_3^+$ Exact Mass: 670.27 Mol. Wt.: 670.95
Tetramer linear	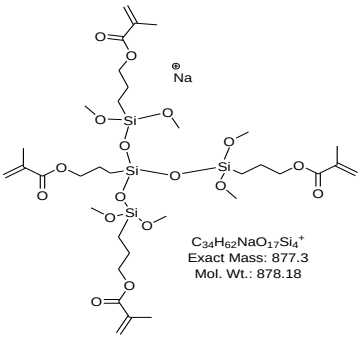 $C_{34}H_{62}NaO_{17}Si_4^+$ Exact Mass: 877.3 Mol. Wt.: 878.18	

	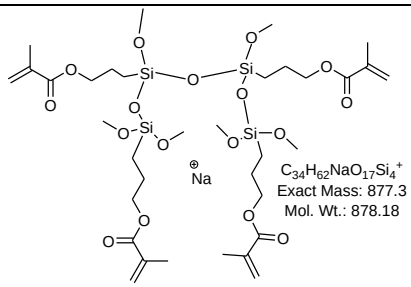	
Tetramer cyclic	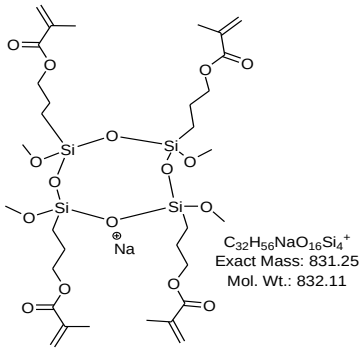	

a. Possible MALDI-ToF-MS structures 2

Ions	Possible structures	Ions + (Na^+)	Ions + (NH_4^+)
Pentamer branched			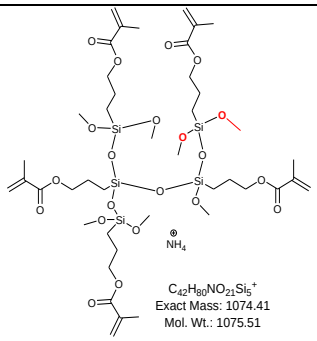

Pentamer Cyclic		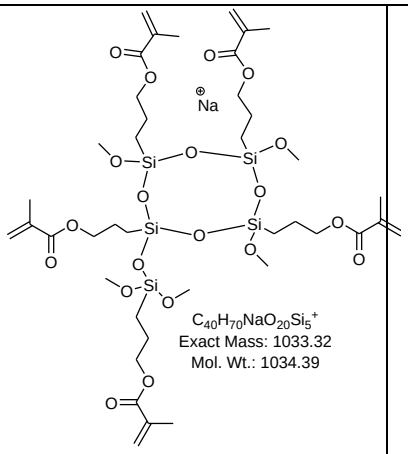 $C_{40}H_{70}NaO_{20}Si_5^+$ Exact Mass: 1033.32 Mol. Wt.: 1034.39 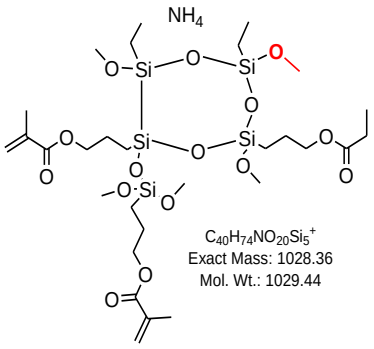 $C_{40}H_{74}NO_{20}Si_5^+$ Exact Mass: 1028.36 Mol. Wt.: 1029.44	
Hexamer Ladder and semi-ladder			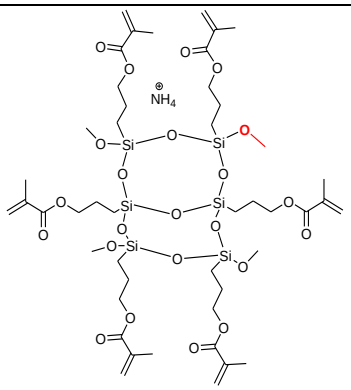 $C_{46}H_{82}NO_{23}Si_6^+$ Exact Mass: 1184.39 Mol. Wt.: 1185.65

			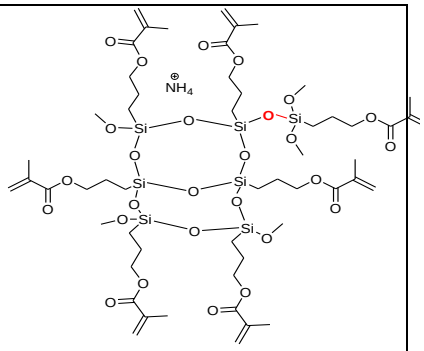 $C_{54}H_{96}NO_{27}Si_7^+$ Exact Mass: 1386.45 Mol. Wt.: 1387.93
Heptamer Partial cage			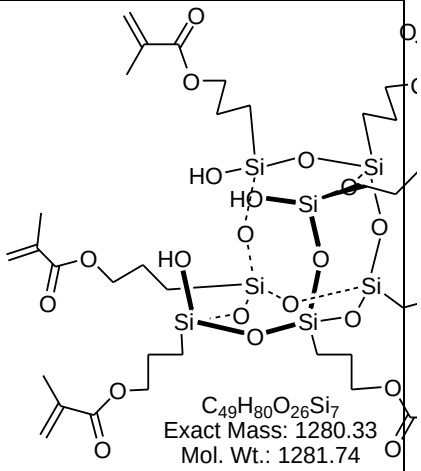 $C_{49}H_{80}O_{26}Si_7$ Exact Mass: 1280.33 Mol. Wt.: 1281.74

b. 14.2 Possible MALDI-ToF-MS structures 3

Vitolane (A-system)	Vitolane (AZ-system)
Dimers 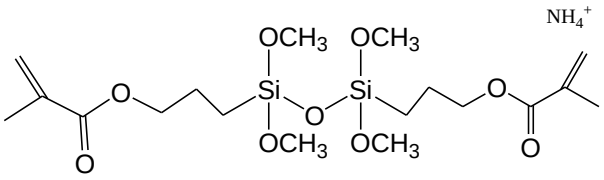 Exact Mass: 468.21 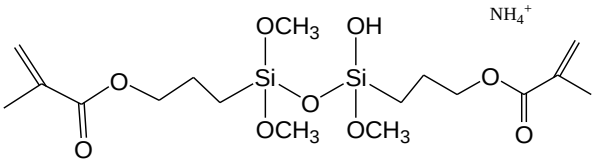 Exact Mass: 454.19 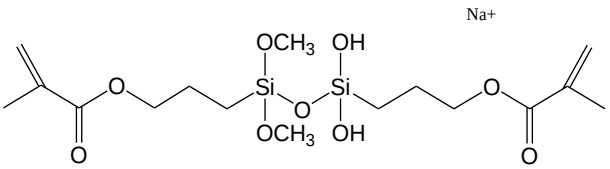 Exact Mass: 445.1321	Dimers 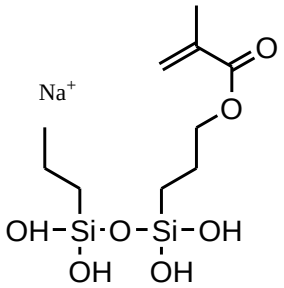 Exact Mass: 333.0796

Trimers	Trimers
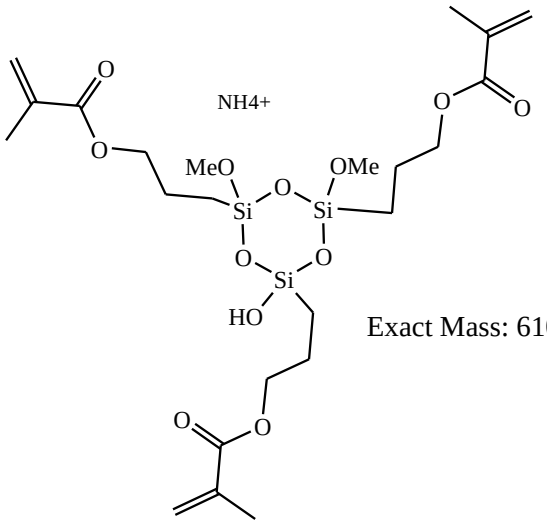 Exact Mass: 610.22	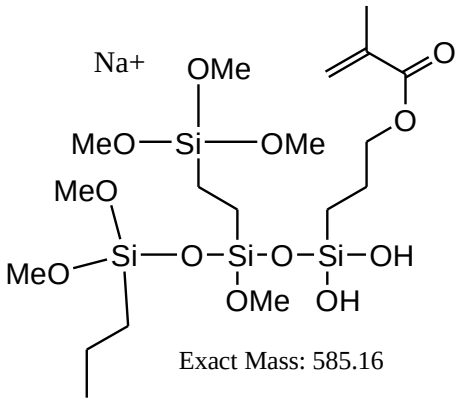 Exact Mass: 585.16
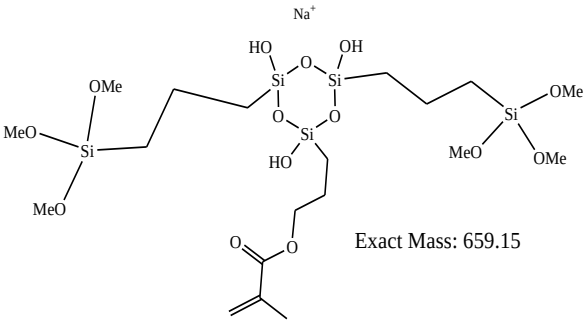 Exact Mass: 659.15	
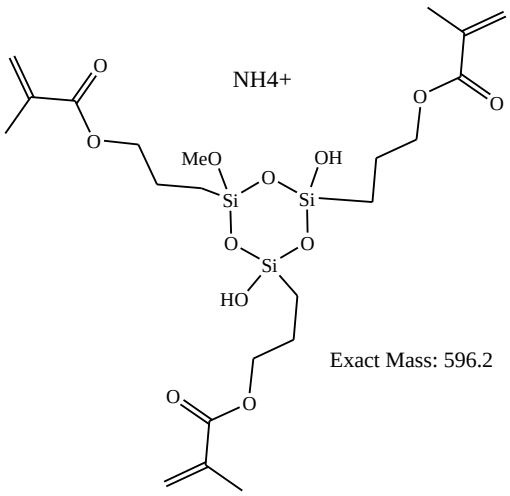 Exact Mass: 596.2	
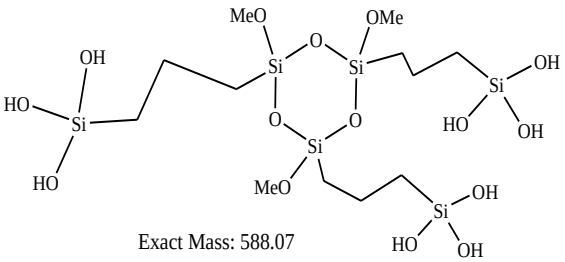 Exact Mass: 588.07	

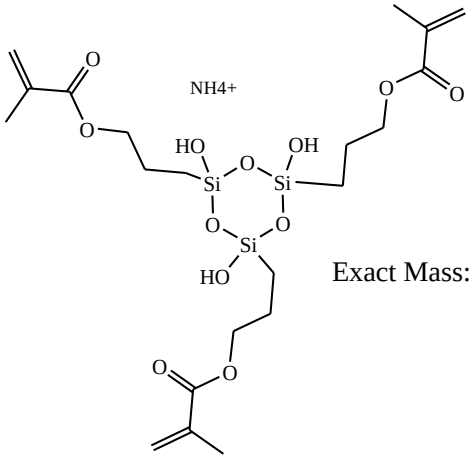

Exact Mass: 582.19

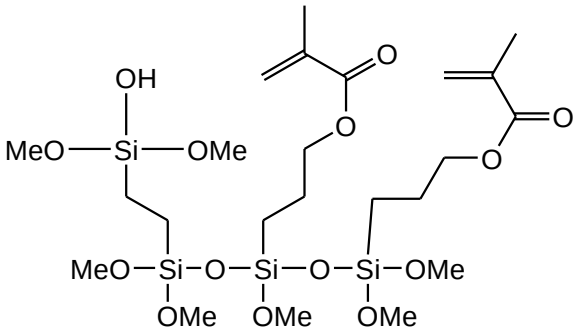

Exact Mass: 660.21

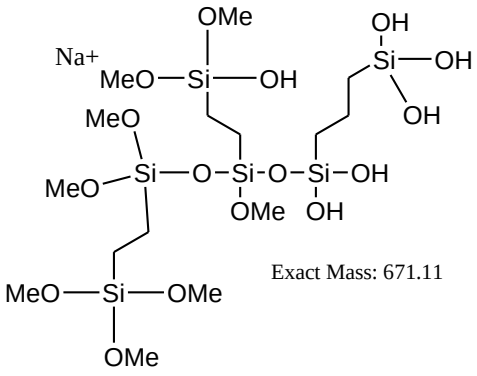

Exact Mass: 671.11

Tetramers

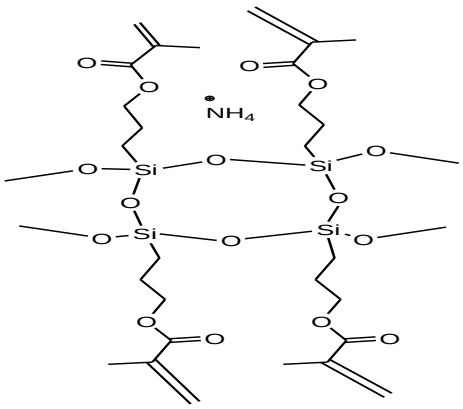

Exact Mass: 826.3

Tetramers

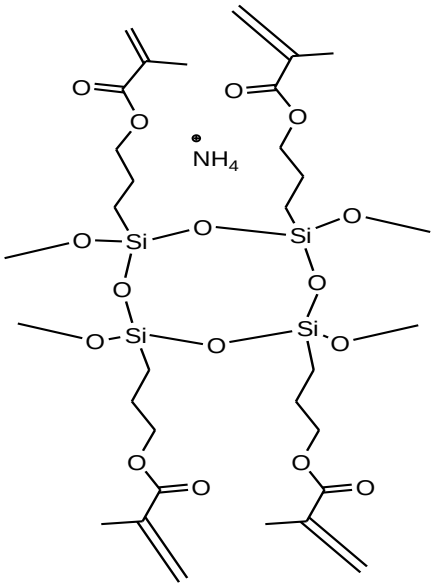

Exact Mass: 826.3

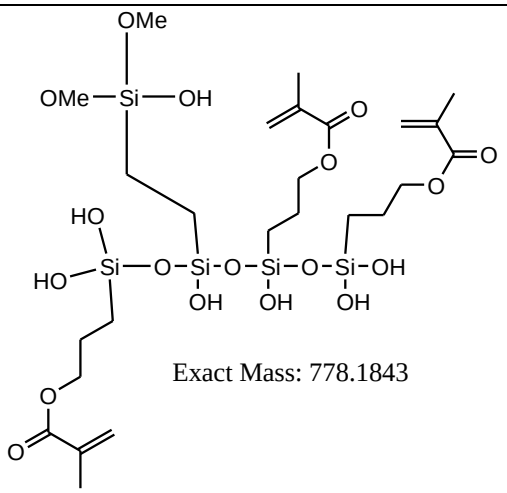

Exact Mass: 778.1843

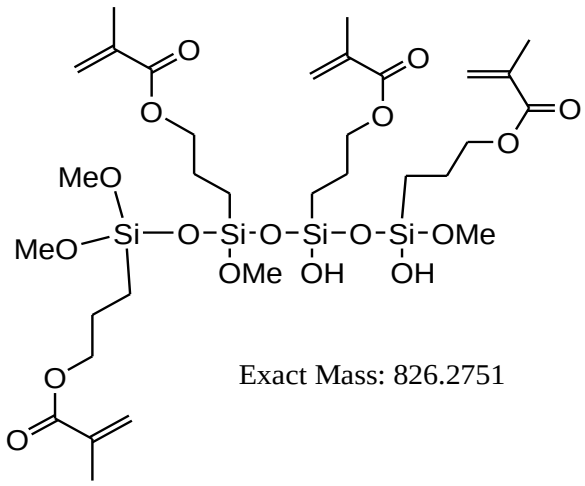

Exact Mass: 826.2751

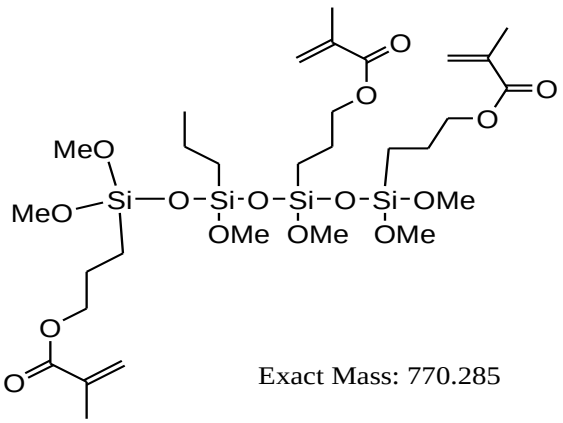

Exact Mass: 770.285

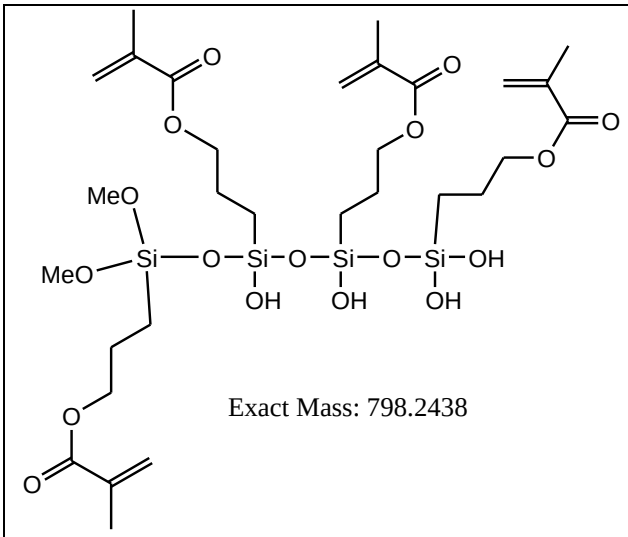

Exact Mass: 798.2438

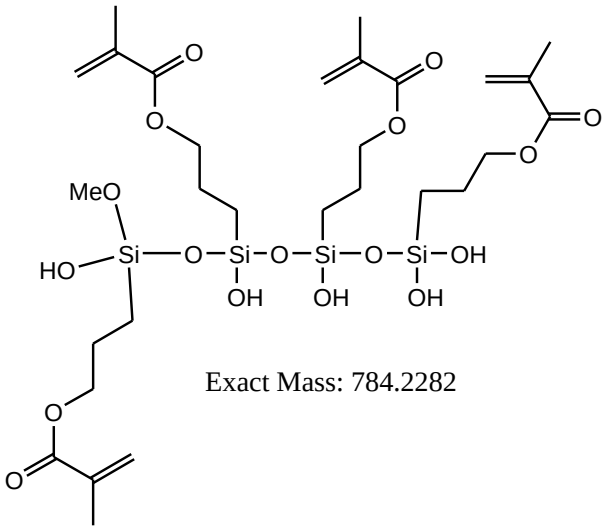

Exact Mass: 784.2282

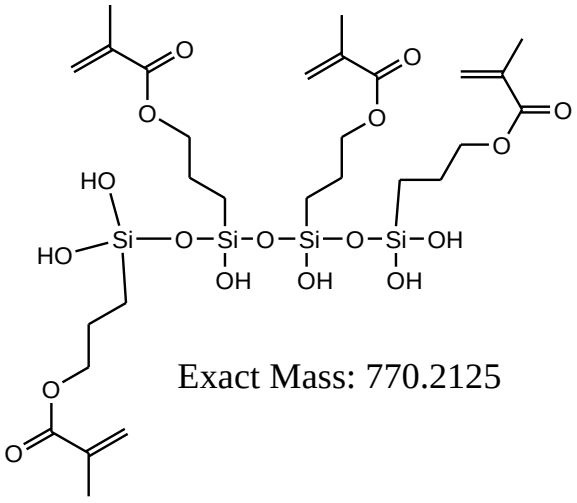

Exact Mass: 770.2125

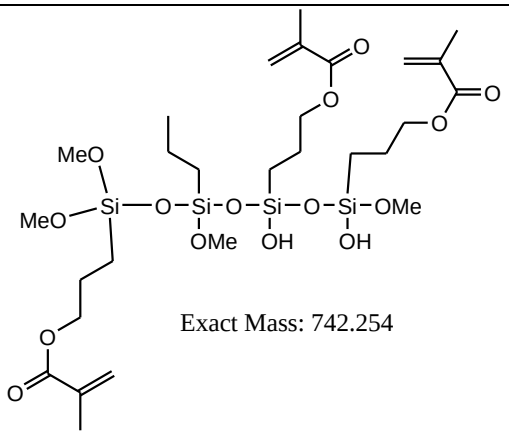

Exact Mass: 742.254

Pentamers	Pentamers

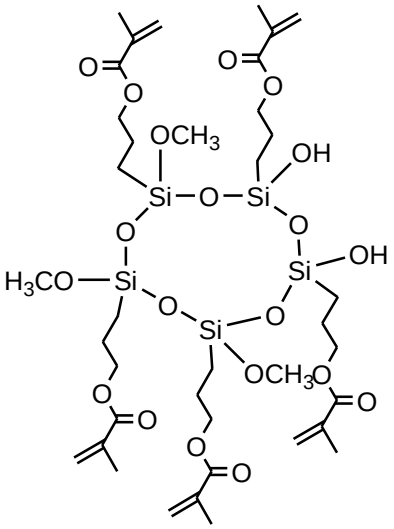

Exact Mass: 982.3

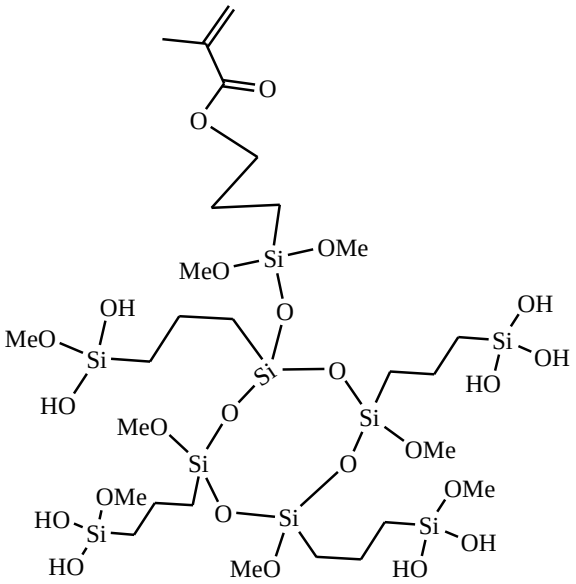

Exact Mass: 1028.2

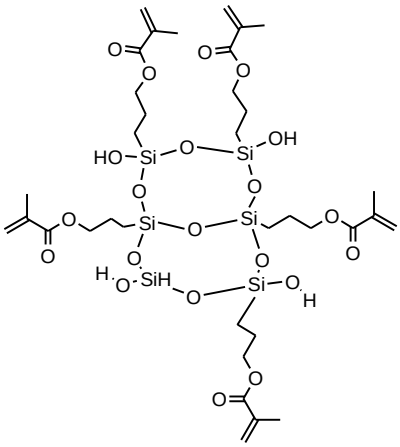

Exact Mass: 984.22

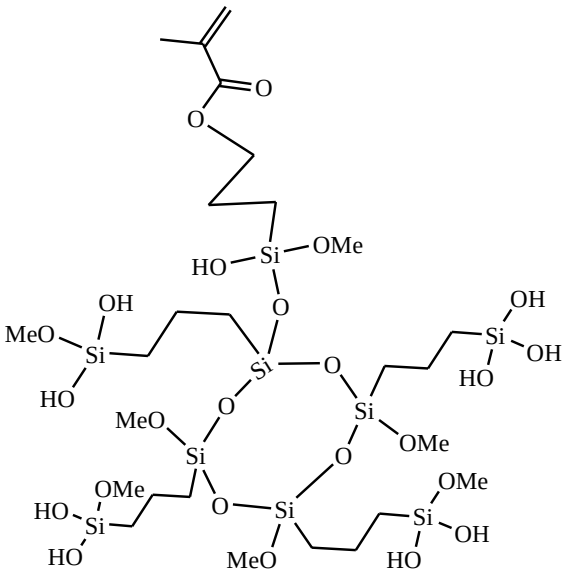

Exact Mass: 1014.19

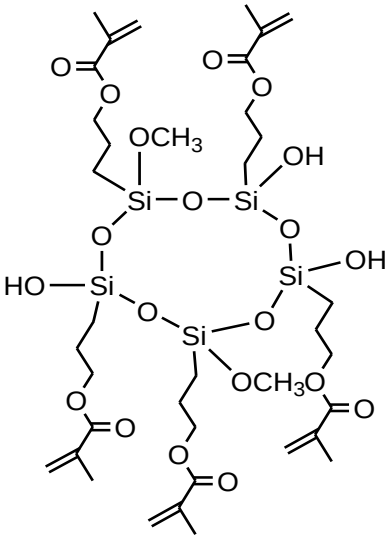

Exact Mass: 968.28

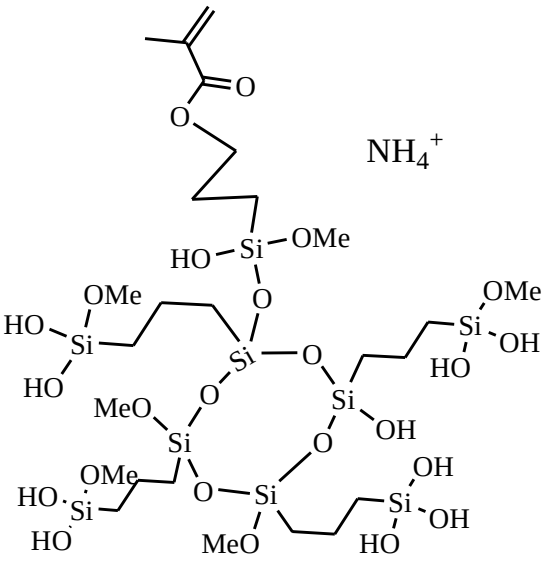

Exact Mass: 1018.2

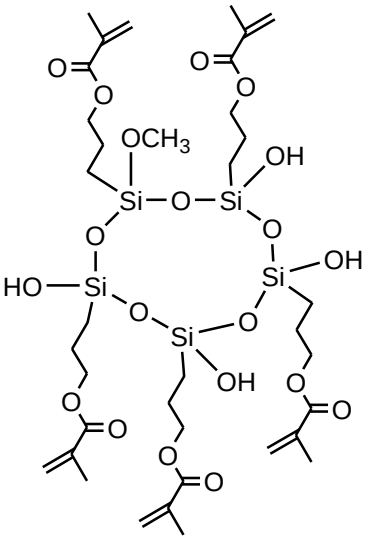

Exact Mass: 954.27

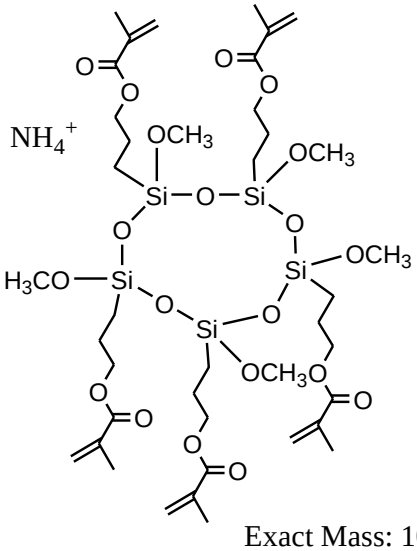 Exact Mass: 1028.36	
Hexamers 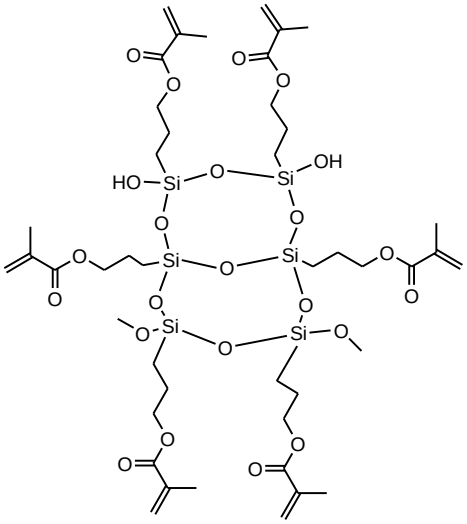 Exact Mass: 1138.32	Hexamers

15 Appendix - 13C NMR of the pure dimer isolated from distillation

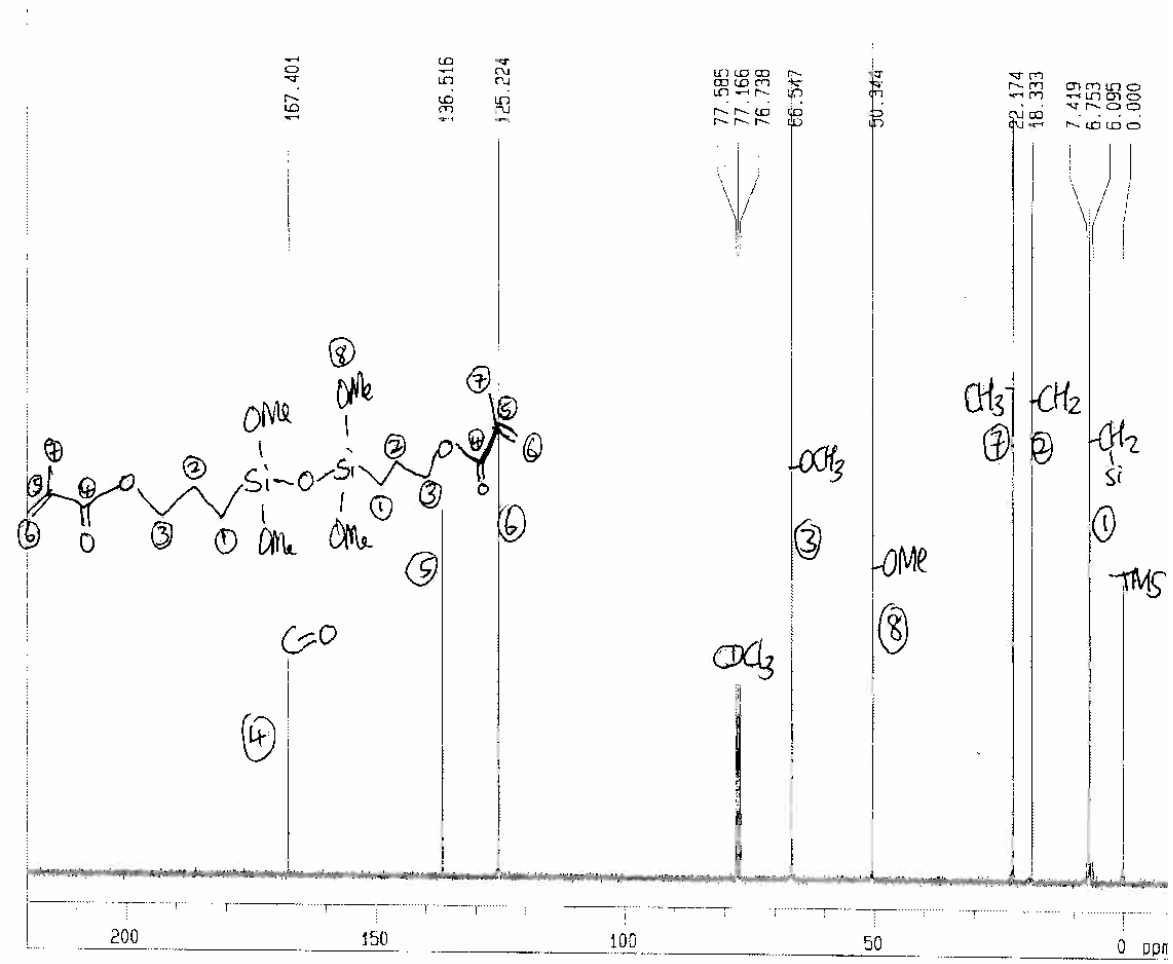

16 Appendix – GC-MS spectra of the pure dimer from distillation

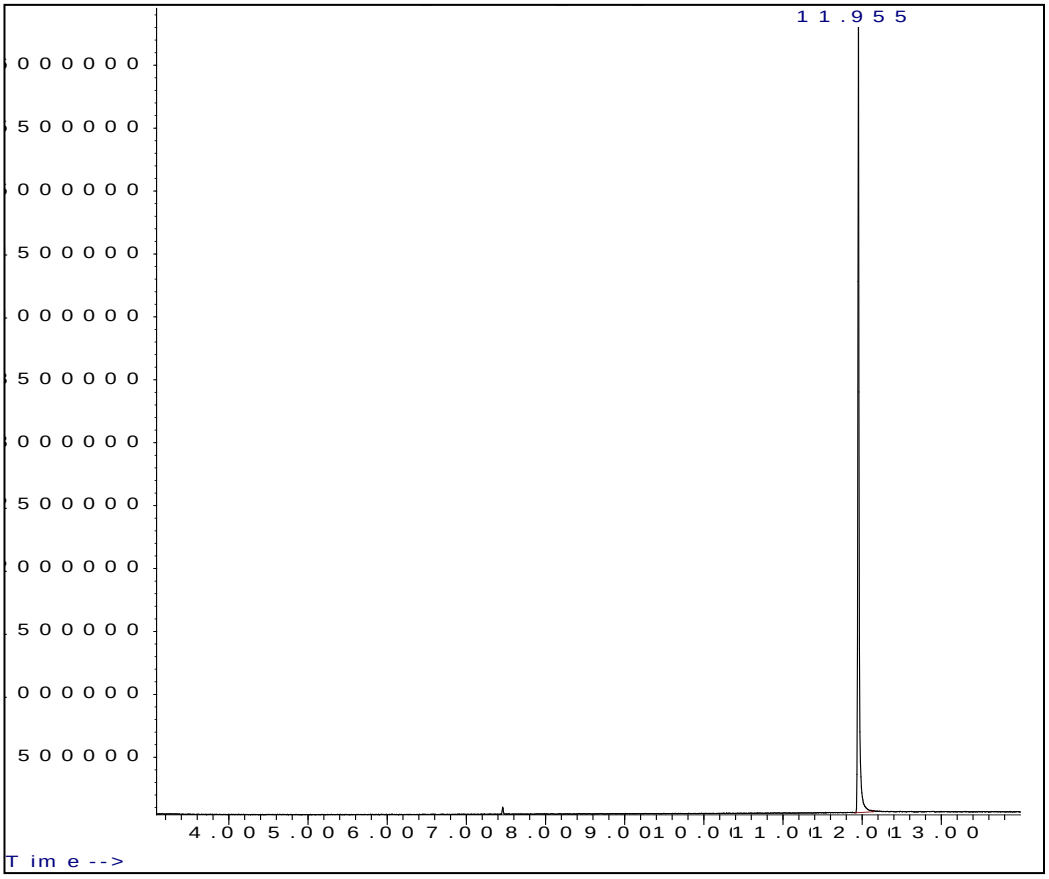

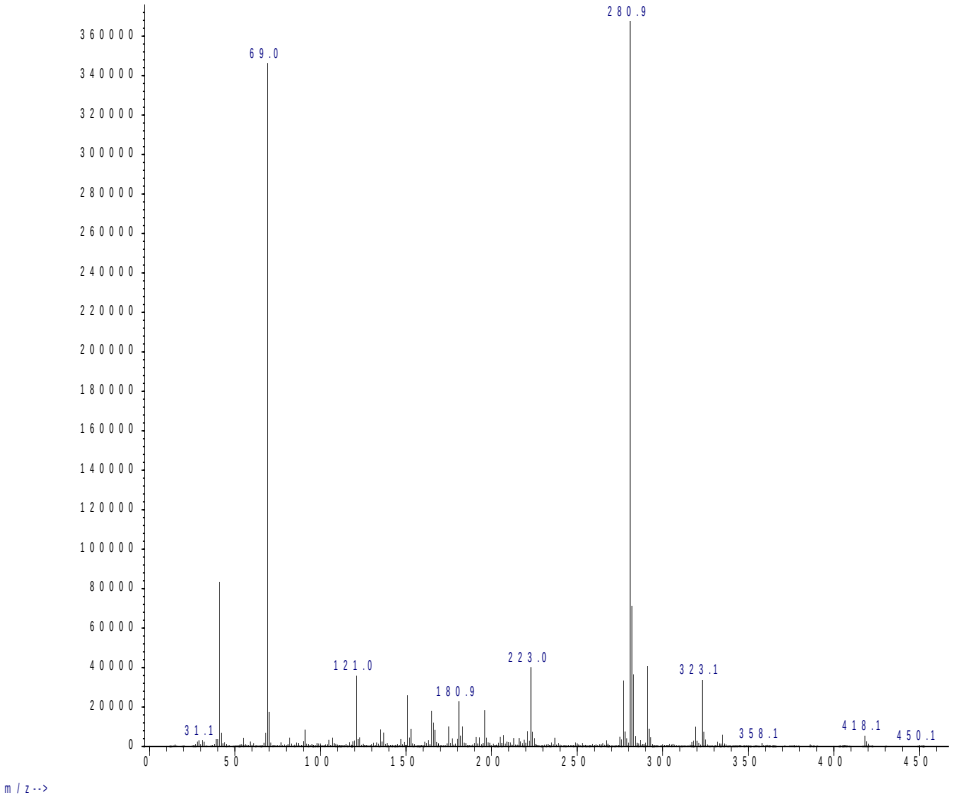

Gas chromatography mass spectrometry of the pure dimer

17 Appendix – GPC spectra of the single-component system resin (A)

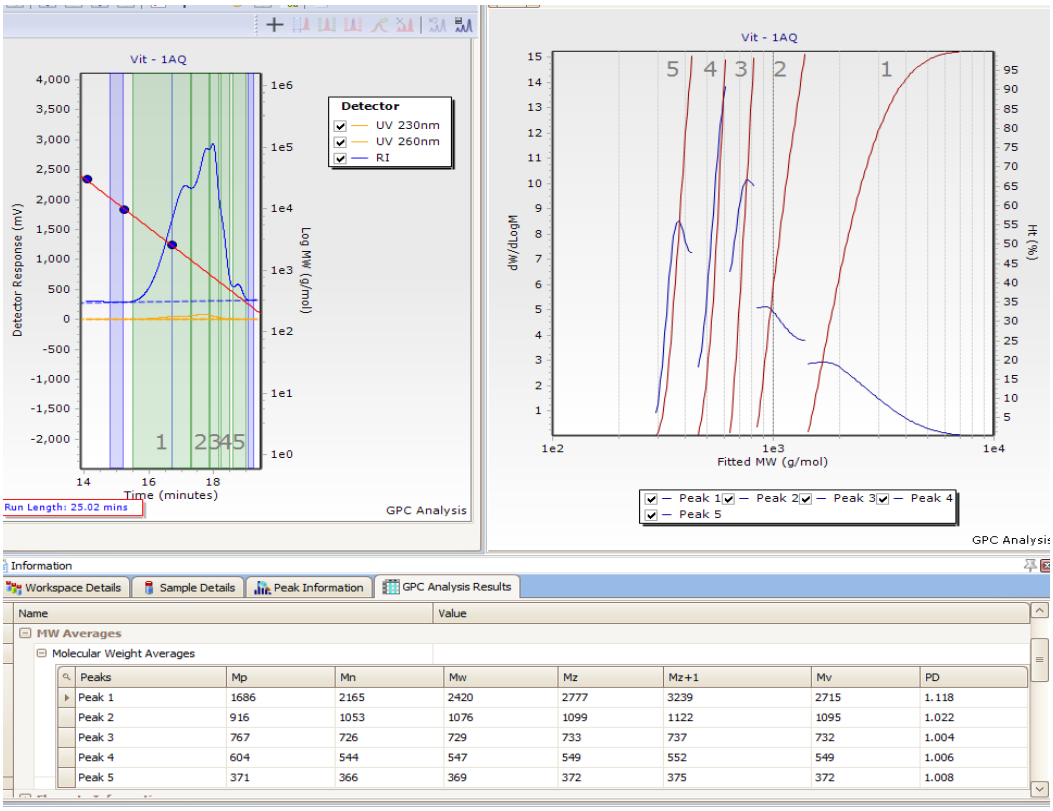

Peaks	Mp	Mn	Mw	Mz	Mz+1	Mv	PD
Peak 1	1686	2165	2420	2777	3239	2715	1.118
Peak 2	916	1053	1076	1099	1122	1095	1.022
Peak 3	767	726	729	733	737	732	1.004
Peak 4	604	544	547	549	552	549	1.006
Peak 5	371	366	369	372	375	372	1.008

18 Appendix – GPC spectra of the two-component system resin (AZ)

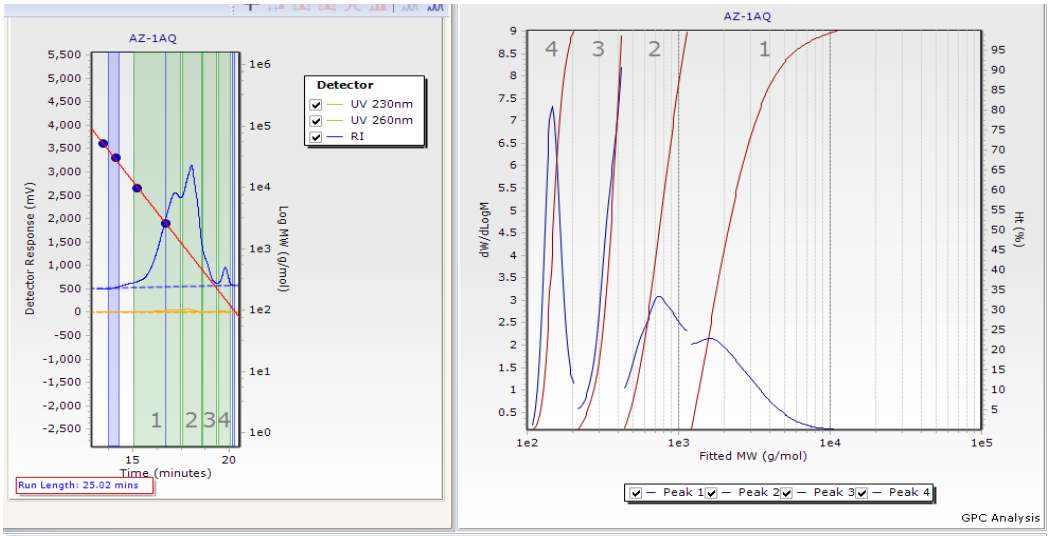

Peaks	Mp	Mn	Mw	Mz	Mz+1	Mv	PD
Peak 1	1610	2112	2655	3652	5147	3464	1.257
Peak 2	744	716	762	807	850	801	1.064
Peak 3	420	341	349	356	362	355	1.023
Peak 4	147	148	151	153	155	153	1.02

19 Appendix – Maldi-ToF MS of the two-component system resin (DOAZ-6 and DOAZ-9)

DOAZ-6

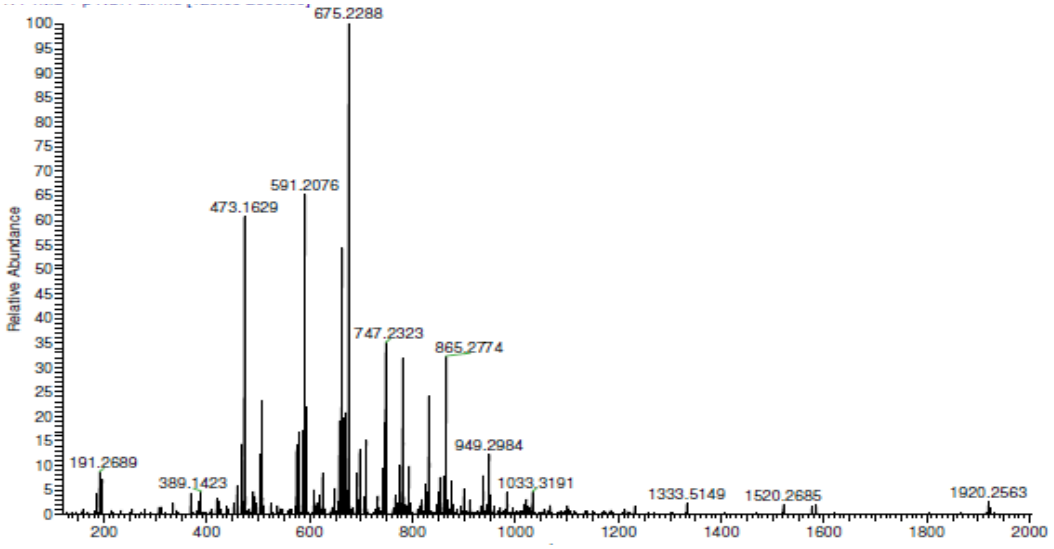

DOAZ-9

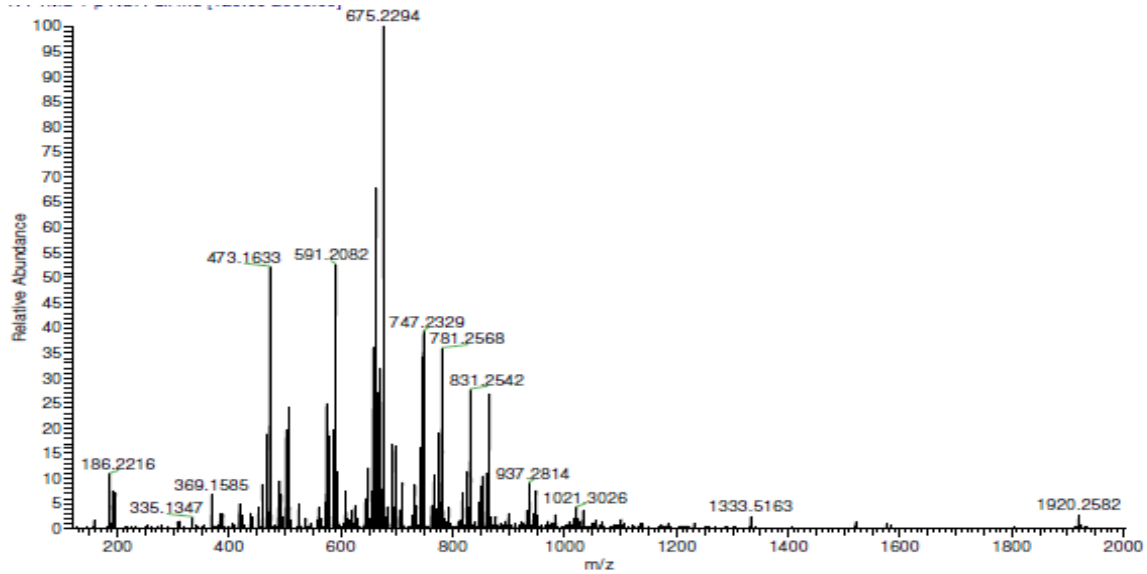

20 Appendix – GPC chromatograms of the one monomer system (A) and the two-monomers (AZ) system from another instrument

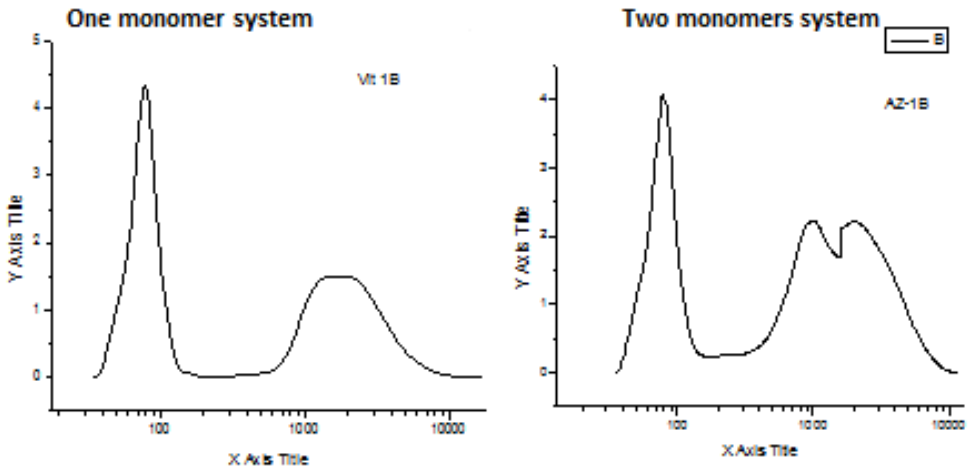

21 Appendix – GPC chromatograms of MPTMS tetramer

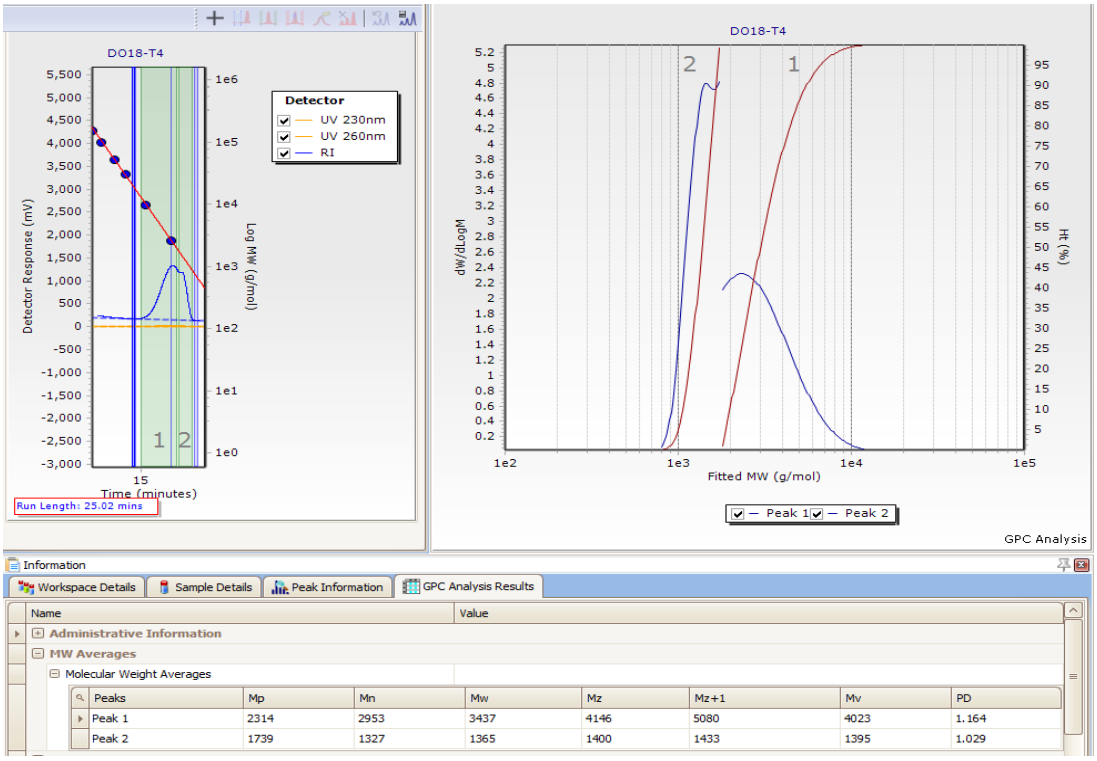

Peaks	Mp	Mn	Mw	Mz	Mz+1	Mv	PD
Peak 1	2314	2953	3437	4146	5080	4023	1.164
Peak 2	1739	1327	1365	1400	1433	1395	1.029

22 Appendix – GPC chromatograms of MPTMS dimer

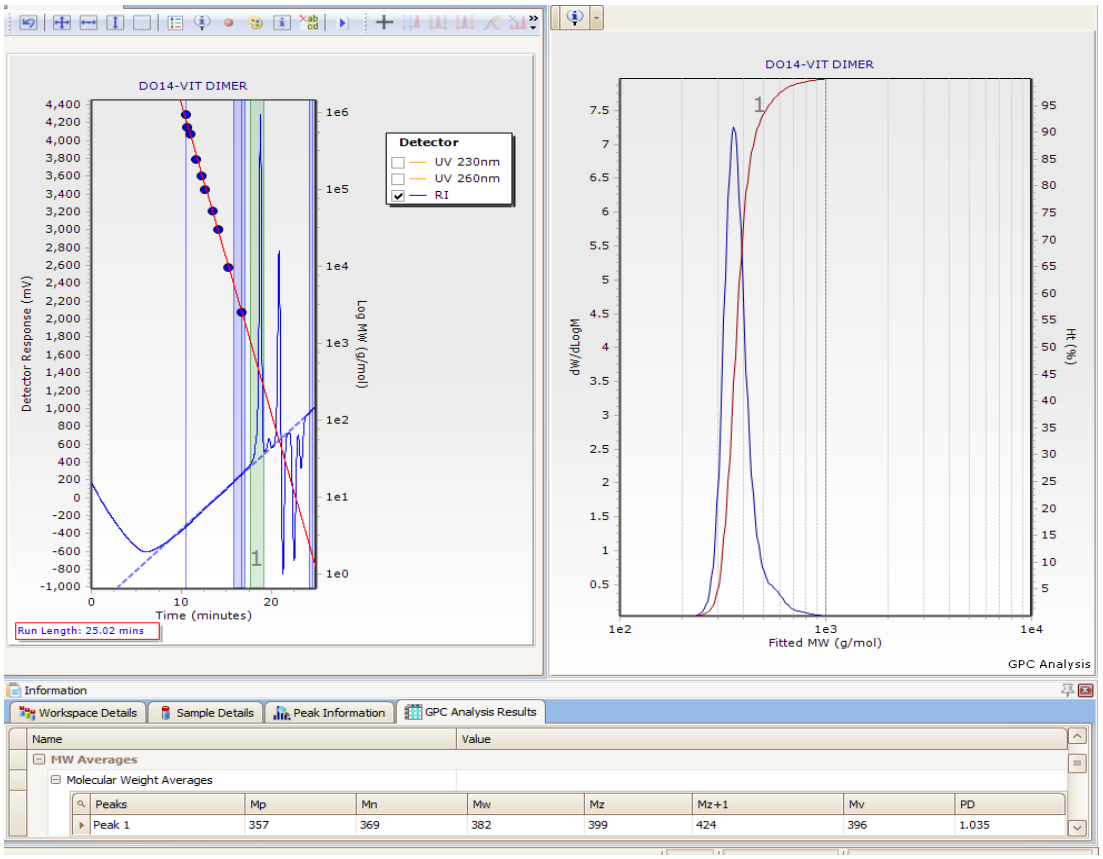

23 LCMS chromatogram of DOAZ -6B and DOAZ-9B

LCMS of DOAZ-6B

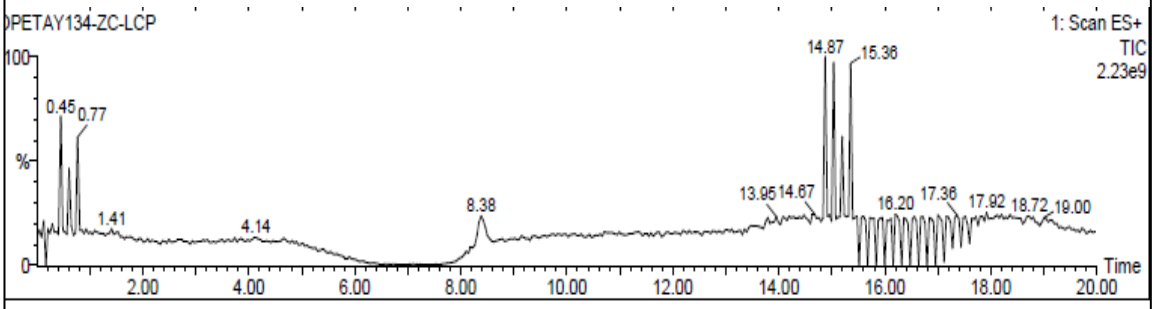

LCMS of DOAZ-9B

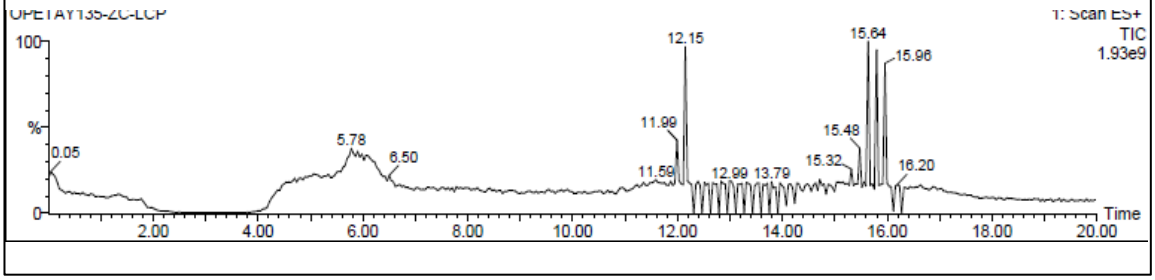

24 Licence 1

Title:	An optimized sol–gel synthesis of stable primary equivalent silica particles
Author:	I.A. Rahman,P. Vejayakumaran,C.S. Sipaut,J. Ismail,M. Abu Bakar,R. Adnan,C.K. Chee
Publication:	Colloids and Surfaces A: Physicochemical and Engineering Aspects
Publisher:	Elsevier
Date:	15 February 2007

Logged in as:

Delphine Delphine

LOGOUT

Order Completed

Thank you very much for your order.
This is a License Agreement between Delphine Delphine ("You") and Elsevier ("Elsevier"). The license consists of your order details, the terms and conditions provided by Elsevier, and the payment terms and conditions.

Get the printable license.

License Number	3674170213621
License date	Jul 22, 2015
Licensed content publisher	Elsevier
Licensed content publication	Colloids and Surfaces A: Physicochemical and Engineering Aspects
Licensed content title	An optimized sol–gel synthesis of stable primary equivalent silica particles
Licensed content author	I.A. Rahman,P. Vejayakumaran,C.S. Sipaut,J. Ismail,M. Abu Bakar,R. Adnan,C.K. Chee
Licensed content date	15 February 2007
Licensed content volume number	294
Licensed content issue number	1-3
Number of pages	9
Type of Use	reuse in a thesis/dissertation
Portion	figures/tables/illustrations
Number of figures/tables/illustrations	8
Format	both print and electronic
Are you the author of this Elsevier article?	No
Will you be translating?	No
Original figure numbers	Figs; 2,3,4,5,6,7,10,11
Title of your thesis/dissertation	Synthesis of Advanced Hybrid Polymeric Nanomaterials and Characterization of Novel Silsesquioxanes
Expected completion date	Aug 2015
Estimated size (number of pages)	350
Elsevier VAT number	GB 494 6272 12
Permissions price	0.00 GBP
VAT/Local Sales Tax	0.00 GBP / 0.00 GBP

25 Licence 2

26 License 3